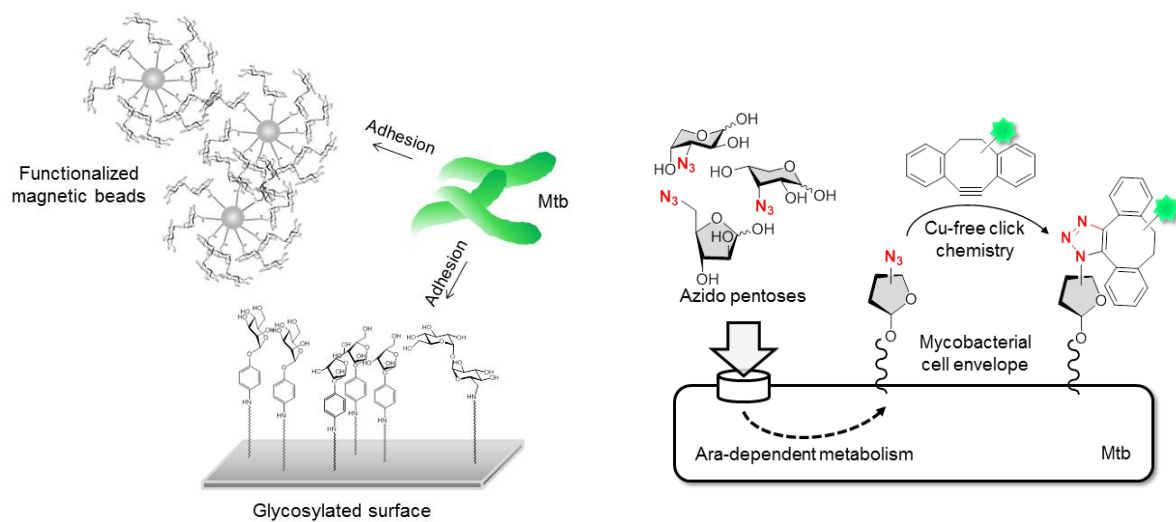


# New carbohydrate derivatives as tools to bind and metabolically label strains of the *Mycobacterium tuberculosis* complex



Dissertation

Submitted in fulfillment of the  
requirements for the degree of  
Doctor rerum naturalium

by

Katharina Kolbe

Kiel 2016

1. reviewer: Prof. Dr. Thisbe K. Lindhorst
2. reviewer: PD Dr. Norbert Reiling

Date of the oral examination: 28. April 2016

Sgd. Prof. Dr. Wolfgang J. Duschl, Dekan

Supervisor

Prof. Dr. Thisbe K. Lindhorst

Organic Chemistry

Otto Diels Institute of Organic Chemistry

Christiana Albertina University of Kiel

Co-supervisor

PD Dr. Norbert Reiling

Microbial Interface Biology

Research Center Borstel

Leibniz-Center for Medicine and Biosciences

K. Kolbe thanks

the Verband der Chemischen Industrie for a doctoral fellowship

and

the VolkswagenStiftung and the collaborative research center SFB 677 for financial support

PhD thesis

March 2012 - March 2016

Eidesstattliche Erklärung:

Hiermit erkläre ich, Katharina Kolbe, dass ich die vorliegende Dissertation selbständig verfasst und keine weiteren als die angegebenen Quellen und Hilfsmittel verwendet habe. Inhalt und Form dieser Arbeit sind eigenständig erarbeitet und verfasst worden. Die Arbeit entstand unter der Einhaltung der Regeln guter wissenschaftlicher Praxis der Deutschen Forschungsgemeinschaft. Weder die gesamte Arbeit noch Teile davon habe ich an anderer Stelle im Rahmen eines Prüfungsverfahrens eingereicht. Dies ist mein erster Promotionsversuch.

Kiel, den 14. 03. 2016

Katharina Kolbe

(Katharina Kolbe)



## Meinen Eltern

“A scientist in his laboratory is not only a technician; he is also a child placed before natural phenomena which impress him like a fairy tale”

„Ein Gelehrter in seinem Laboratorium ist nicht nur ein Techniker; er steht auch vor den Naturgesetzen wie ein Kind vor der Märchenwelt.“

(Marie Curie)

## Kurzfassung

Tuberkulose (Tb), hervorgerufen durch das *Mycobacterium tuberculosis* (Mtb), ist weltweit die am häufigsten zum Tode führende bakterielle Infektionskrankheit. Erschwert wird die Therapie dieser Erkrankung durch das zunehmende Auftreten antibiotikaresistenter Mtb-Stämme und dem Mangel an Testsystemen, die eine schnelle und spezifische Diagnose der Tb ermöglichen. Die Zellhülle der Mtb-Bakterien trägt dabei wesentlich zur Virulenz des Erregers bei und stellt bislang ein besonderes Hindernis bei der Tb-Bekämpfung dar. Die Einzigartigkeit dieser mykobakteriellen Zellhülle kann jedoch auch als Vorteil verstanden werden und dazu beitragen, neue Methoden für die spezifische Diagnostik und gezielte Therapie von Tb zu entwickeln. In der hier vorliegenden Arbeit wurden die besonderen Eigenschaften der Mtb-Zellhülle gezielt ausgenutzt, um Mykobakterien aus einer Lösung anzureichern und verschiedene klinische Mtb-Isolate metabolisch zu markieren.

Bei der Untersuchung der bislang kaum erforschten kohlenhydratbindenden Eigenschaften der Mykobakterien stellte sich heraus, dass die Adhäsion sowohl vom verwendeten Kohlenhydrat, als auch von der Konfiguration der glykosidischen Bindung und von der Struktur des Aglykons beeinflusst wird. In einem Mikrotiterplatten-basierten Testsystem zeigte der Mykobakterien-Impfstamm *Bacillus Calmette Guérin* (BCG) eine starke Adhäsion an Oberflächen, die mit dem  $\alpha$ -D-Arabinofuranosid **1**, dem  $\alpha$ -D-Mannopyranosid **4** oder dem  $\beta$ -D-Glucopyranosid **7** beschichtet waren. Für den pathogenen Mtb-Stamm H37Rv wurde hingegen eine starke Bindung an *p*-Aminophenyl- $\alpha$ -D-galactopyranosid (**8**) und 6-Amino-6-desoxy- $\alpha,\alpha$ -D-trehalose (**3**) nachgewiesen. Magnetische Mikropartikel, die mit *p*-Aminophenyl- $\alpha$ -D-mannopyranosid (**4**) oder dem Trehalose-Derivat **3** funktionalisiert waren, wurden erfolgreich eingesetzt, um Mtb-Bakterien aus einer Lösung anzureichern. Mikropartikel, die mit dem Lipid-Liganden **36** oder dem zum Trehalose-Monomykolat analogen Derivat **37** modifiziert waren, zeigten jedoch deutlich höhere Bindungseffizienzen, die sich auf die hydrophoben Eigenschaften der mykobakteriellen Zellhülle zurückführen lassen. Die Ergebnisse dieser Adhäsionsstudien sollen zukünftig zur Entwicklung einer neuen Methode beitragen, die eine Anreicherung der Mtb-Bakterien aus Patientenproben (z.B. aus Speichel) ermöglicht und zur verbesserten Detektion des Erregers beiträgt.

Die einzigartigen Kohlenhydrate der mykobakteriellen Zellhülle bilden die Grundlage für eine spezifische Markierung des Erregers. Synthetisierte Kohlenhydrat-Derivate können aufgenommen, metabolisiert und in die Zellhülle der Bakterien eingebaut werden. In der hier vorliegenden Arbeit wurden drei neue Azido-Pentosen, 3-Azido-3-desoxy- $\alpha,\beta$ -D-arabinose (3AraAz, **38**), 3-Azido-3-desoxy- $\alpha,\beta$ -D-ribose (3RiboAz, **39**) und 5-Azido-5-desoxy- $\alpha,\beta$ -D-arabinofuranose (5AraAz, **40**), synthetisiert und erfolgreich für die metabolische Markierung von Mtb eingesetzt. Der Einbau der Kohlenhydrat-Derivate in die mykobakterielle

Zellhülle ermöglicht völlig neue Einblicke in bisher unerforschte Bereiche der Biologie des Erregers. Die Ergebnisse der metabolischen Markierung deuten stark auf das Vorhandensein von Transportmolekülen für Arabinosen und Ribosen in der Mtb-Zellhülle und auf die Existenz bisher unbekannter Biosynthesewege für Arabinose-Derivate hin. Die eingesetzten Azido-Zucker, insbesondere 5AraAz, zeigten keine toxischen Eigenschaften und eine hohe Markierungseffizienz, auch in klinischen Mtb-Isolaten. Diese Methode auf Grundlage metabolischer Prozesse ermöglichte die Fluoreszenzmarkierung verschiedener Mtb-Stämme ohne zeitaufwendige genetische Modifikationen. Die markierten Mtb-Bakterien wurden in Infektionsstudien mit humanen Makrophagen verwendet. Hierbei zeigten sich vergleichbare erregerspezifische Virulenzeigenschaften für 5AraAz-markierte und unmarkierte Mtb-Bakterien. Die neuen Azido-Pentosen können zukünftig zur Aufklärung noch unbekannter Mechanismen der Kohlenhydrataufnahme und -biosynthese beitragen. Ferner ermöglichen sie die Untersuchung der stammspezifischen Pathogenität in Wirtszellen, die mit dem klinischen Verlauf einer Tuberkuloseerkrankung in engem Zusammenhang steht. Des Weiteren kann der Einbau der Kohlenhydrat-Derivate auch die Grundlage für die Entwicklung einer neuartigen Methode darstellen, die es ermöglicht, Mtb-Bakterien gezielt anzugreifen und zu markieren. Es ist zu hoffen, dass die metabolische Markierung der Mtb-Zellhülle zukünftig zu einer Verbesserung der Tb-Therapie beitragen wird.

## Abstract

Tuberculosis (Tb), caused by *Mycobacterium tuberculosis* (Mtb), is the single leading bacterial cause of death from infectious diseases worldwide. Tb therapy is complicated by an increase in antibiotic resistant Mtb strains and the lack of fast and specific diagnostic tools. The cell envelope of Mtb bacteria represents a major virulence factor and contributes to the intrinsic difficulties of eradicating the pathogen. However, the uniqueness of the Mtb cell envelope can also be seen as an advantage and could bear the chance to develop novel tuberculosis-specific diagnostic and therapeutic tools. In this thesis the unique features of the Mtb cell envelope were utilized to enrich mycobacteria from solution and to metabolically label different Mtb clinical isolates.

The widely unknown carbohydrate-binding characteristics of mycobacteria were investigated showing different adhesion efficiencies dependent on the applied sugar, the configuration of the glycosidic linkage and the structure of the aglycon. While the vaccine strain *Bacillus Calmette-Guérin* (BCG) strongly adhered to surfaces functionalized with  $\alpha$ -D-arabinofuranoside **1**,  $\alpha$ -D-mannopyranoside **4** and  $\beta$ -D-glucopyranoside **7** containing an aromatic aglycon, the pathogenic Mtb strain H37Rv showed strong binding to *p*-aminophenyl  $\alpha$ -D-galactopyranoside (**8**) and 6-amino-6-deoxy- $\alpha,\alpha$ -D-trehalose (**3**) in a microtiter plate-based assay system. Magnetic beads functionalized with *p*-aminophenyl  $\alpha$ -D-mannopyranoside (**4**) and the trehalose derivative **3**, respectively, could be used to capture Mtb bacteria from solution. However, binding efficiencies were strongly surpassed by beads functionalized with the lipid ligand **36** and the trehalose 6-monomycolate-analog derivative **37** addressing the high hydrophobicity of the Mtb cell envelope. The results of these adhesion studies will prospectively contribute to the development of a novel tool to enrich and more easily detect Mtb bacteria in patient specimen (e.g. in easy accessible saliva).

The unique carbohydrate constituents of the mycobacterial cell envelope provide the possibility to specifically target Mtb. Synthesized derivatives of selected carbohydrates can be taken up, metabolized and subsequently be introduced into the cell envelope of Mtb bacteria. In this thesis three new azido pentoses, 3-azido-3-deoxy- $\alpha,\beta$ -D-arabinose (3AraAz, **38**), 3-azido-3-deoxy- $\alpha,\beta$ -D-ribose (3RiboAz, **39**) and 5-azido-5-deoxy- $\alpha,\beta$ -D-arabinofuranose (5AraAz, **40**), were synthesized and successfully used for metabolic labeling, thus shedding light on so far unknown Mtb biology. The data strongly suggest the presence of arabinose and ribose transporters in the Mtb cell envelope and as well the existence of yet unknown biosynthetic pathways for arabinose derivatives. The investigated azido sugars, in particular 5AraAz, exhibited no toxicity and high labeling efficiency, also in Mtb clinical isolates. This metabolic method enables to fluorescently label different Mtb strains without time consuming genetic modifications. Metabolically labeled Mtb bacteria were further used in infection studies with

human macrophages, showing comparable pathogen-specific virulence characteristics to untreated Mtb bacteria. The new azido pentoses can now be employed to identify unknown uptake and metabolic mechanisms of Mtb bacteria and to study strain-specific pathogenicity in host cells, which is strongly associated with the clinical outcome of tuberculosis. In addition, the introduced carbohydrate derivatives may form the basis for a new and unexpected way to specifically reach and target Mtb bacteria, which might hopefully facilitate the improvement of tuberculosis therapy in future.

## **A guide to this thesis**

The work described in this thesis was carried out at the interface of chemistry and biology. New carbohydrate derivatives were synthesized and analyzed in the group of Prof. Dr. Thisbe K. Lindhorst (Organic Chemistry, Christiana Albertina University of Kiel, Germany). The synthesized compounds were further applied in the group of PD Dr. Norbert Reiling (Microbial Interface Biology, Research Center Borstel, Germany) to facilitate the development of new tools to specifically capture and target *Mycobacterium tuberculosis* (Mtb), the main causative agent of tuberculosis.

The thesis starts with a general introduction on current challenges in the fight against this infectious disease and on the uniqueness and relevancy of the mycobacterial cell envelope in this context. The following first part of this thesis focuses on the enrichment of mycobacteria from solution using carbohydrate derivatives or lipid ligands. The second part of this thesis deals with the application of carbohydrate derivatives as tools to metabolically label different Mtb clinical isolates. Both chapters are structured into a short specific introduction, the objectives of the study, a description of the obtained results and a subsequent detailed discussion of the results. The used methods are listed at the end of each part. NMR spectra of new compounds and known molecules, which were used for metabolic labeling, are depicted in the appendix.

## Table of contents

<b>1. Introduction.....</b>	<b>1</b>
1.1 Tuberculosis – a global emergency .....	1
1.2 Tuberculosis diagnostics .....	1
1.3 Tuberculosis therapy .....	3
1.4 <i>Mycobacterium tuberculosis</i> .....	5
1.4.1 The bacterium .....	5
1.4.2 The unique cell envelope of Mtb bacteria.....	6
1.4.3 The rare carbohydrates of the mycobacterial cell envelope .....	11
1.4.4 Mycobacterial carbohydrates connected to Mtb pathogenicity .....	15
1.4.5 Mycobacterial lectins .....	19
<b>2 Exploitation of mycobacterial adhesion characteristics to improve detection of <i>Mycobacterium tuberculosis</i>.....</b>	<b>21</b>
2.1 Introduction .....	21
2.2 Objectives .....	22
2.3 Results.....	23
2.3.1 Syntheses.....	24
2.3.2 Mycobacterial adhesion assay .....	28
2.3.3 Adhesion characteristics of <i>M. bovis Bacillus Calmette-Guérin</i> bacteria.....	29
2.3.4 Adhesion characteristics of Mtb H37Rv bacteria.....	35
2.3.5 Capture of Mtb with beads functionalized with carbohydrate derivatives .....	37
2.3.6 Adhesion of Mtb to magnetic PEG beads functionalized with lipid ligands .....	41
2.3.7 Verifying adhesion of Mtb bacteria by polymerase chain reaction.....	44
2.4 Discussion.....	48
2.4.1 Carbohydrate-specific adhesion characteristics of mycobacteria.....	48
2.4.2 Capture of Mtb bacteria with functionalized magnetic beads .....	52
2.4.3 Development of a diagnostic mouth rinse or chewing gum .....	54
2.5 Concluding remarks.....	57
2.6 Materials and methods.....	58
2.6.1 Reagents .....	58
2.6.2 Buffer and media .....	60
2.6.3 Biological assays.....	61
2.6.4 Syntheses.....	65
<b>3 Azido pentoses, a new tool for specific labeling of <i>Mycobacterium tuberculosis</i> .</b>	<b>79</b>
3.1 Introduction .....	79
3.1.1 Metabolic oligosaccharide engineering.....	79
3.1.2 Bioorthogonal reactions.....	80
3.1.3 Metabolic labeling of bacteria .....	82

3.2	Objectives .....	84
3.3	Results.....	85
3.3.1	Syntheses.....	86
3.3.2	Metabolic labeling of Mtb bacteria .....	89
3.3.3	Microscopic analysis of metabolic labeled Mtb bacteria.....	92
3.3.4	Influence of azido sugars on mycobacterial growth .....	93
3.3.5	Stability of Mtb labeling with 5AraAz .....	94
3.3.6	Incorporation of 5AraAz into lipoglycans of the Mtb cell envelope .....	95
3.3.7	5AraAz labeling of Mtb bacteria in the presence of D-arabinose .....	98
3.3.8	Labeling of Mtb clinical isolates with azido pentoses.....	98
3.3.9	Infection of human macrophages with metabolically labeled Mtb bacteria .....	100
3.3.10	Analysis of putative cytotoxic effects of the azido pentoses on epithelial cells.....	103
3.3.11	Metabolic labeling of epithelial cells with the new azido pentoses .....	104
3.3.12	Metabolic labeling of Mtb bacteria with 5AraI .....	107
3.3.13	Cysteamine derivatives and their influence on mycobacterial growth.....	108
3.4	Discussion.....	114
3.4.1	Arabinose uptake mechanisms.....	114
3.4.2	Arabinose metabolism .....	115
3.4.3	Arabinose derivatives used for MOE.....	117
3.4.4	Applications of MOE .....	121
3.5	Concluding remarks.....	126
3.6	Materials and methods.....	127
3.6.1	Reagents .....	127
3.6.2	Buffer and media .....	128
3.6.3	Biological assays.....	131
3.6.4	Syntheses.....	140
<b>4</b>	<b>References .....</b>	<b>159</b>
<b>5</b>	<b>Appendix.....</b>	<b>I</b>
5.1	NMR spectra.....	I
5.2	Abbreviations.....	XXIX
<b>6</b>	<b>Curriculum vitae</b>	
<b>7</b>	<b>Danksagung</b>	



## 1. Introduction

### 1.1 Tuberculosis – a global emergency

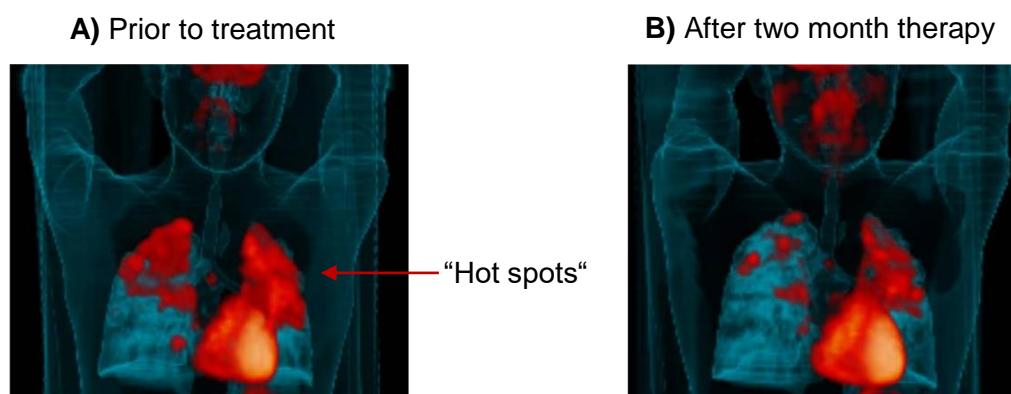
Tuberculosis (Tb) is an infectious bacterial disease mainly caused by *Mycobacterium tuberculosis* (Mtb), which typically affects the lung (pulmonary Tb), but can also be present in other parts of the body (extra pulmonary Tb). It remains one of the world's deadliest communicable diseases and was responsible for an estimated 1.5 million fatalities in 2014. The World Health Organization (WHO) reports almost 10 million new cases every year and overall more than 2 billion infected people.<sup>1</sup> In the majority of infected people the bacterium is controlled by the immune system and does not cause disease (latent Tb). Only 10% of the infected individuals develop clinical symptoms (active Tb). However, the quantity of latent infections is a major risk. Compromised immune functions can result in a re-emergence of an active, transmittable disease. A STOP TB initiative organized by the WHO was initiated in the early 1990's to provide standardized treatment and supervision and expand diagnostic tools and therapies. Furthermore, an overall goal of worldwide reduction of deaths due to Tb by 50% until 2015 and total elimination of disease by 2050 was envisaged.<sup>2</sup> Because of these efforts, worldwide Tb is slowly declining each year and it is estimated that 43 million lives were saved between 2000 and 2014. However, the annual case rate remains unacceptably high.<sup>1</sup> The fact that the amount of multi-drug resistant (MDR) and extensively-drug resistant (XDR) strains increases rapidly represents a severe problem in the fight against Tb and underlines the necessity to identify new drug targets and to come up with new anti-Mtb strategies. Furthermore, the development of rapid, accurate and inexpensive diagnostic tools is essential to fully reach the goals set by the STOP TB global initiative.

### 1.2 Tuberculosis diagnostics

Early detection of Tb infections and identification of drug resistances are crucial for tuberculosis prevention and control, but global case detection rates still remain low. In 2014 only 63% of the estimated 10 million people, who developed Tb, were registered as newly diagnosed cases before.<sup>1</sup> The most common methods for detection of active Tb are direct microscopy of patient sputa and culturing of Mtb.<sup>3</sup> In high burden countries the "gold standard" of Tb diagnosis is the direct microscopic examination of non-concentrated sputum samples.<sup>4</sup> The bacteria are visualized by acid-fast staining procedures, such as the Ziehl-Neelsen stain or the auramine fluorescence stain. The microscopic analysis is not as sensitive as culture-based techniques. Less than 50% of cases detected as positive by culture are also positive by smear microscopy.<sup>1</sup> However, culturing the bacteria from sputum is more costly, requires specialized biosafety infrastructure and takes weeks to obtain results, because of the extremely slow growth rate of Mtb bacteria. In addition, high sensitivity can also be reached by nucleic acid-based diagnostic

strategies. With an Mtb-specific polymerase chain reaction (PCR) it is thought that Tb can be diagnosed with 98% reliability.<sup>5,6</sup> Genetic methods further allow more precise detection of drug resistances<sup>7-9</sup> and mutations correlating with Tb pathogenicity. However, they require a high technical competence. New methods increasing sensitivity and being at the same time cheap and easy applicable would strongly improve detection of active Tb.

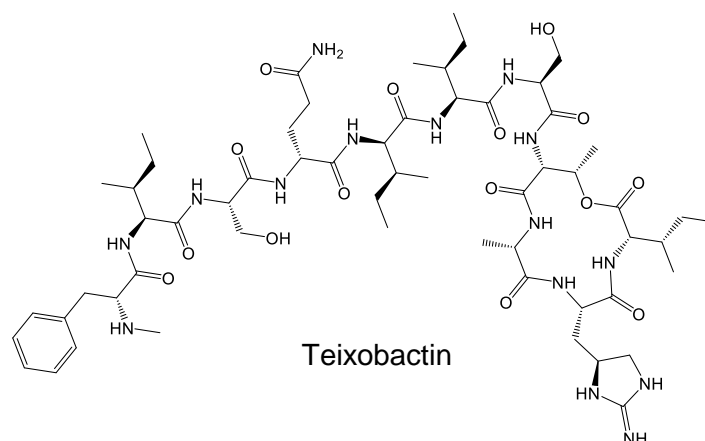
Beside the diagnosis of active Tb, detection of latent infected people is extremely important being aware of the fact that at least one half of all tuberculosis cases are the result of reactivation.<sup>1</sup> Immunological-based strategies, like the tuberculin skin test (TST) and blood-based interferon- $\gamma$  (IFN- $\gamma$ ) release assays (IGRAs), are currently applied.<sup>10</sup> While in the TST the immune response to a protein mixture, purified from the filtrate of a mycobacteria culture, is visualized by skin induration,<sup>11</sup> IGRAs are based on immune responses of isolated T-lymphocytes to Mtb-specific antigens.<sup>12,13</sup> These antigens are absent in most non-tuberculosis mycobacteria. Thus, IGRAs, in contrast to the tuberculin assay, can distinguish between Mtb infected and *Bacillus Calmette-Guérin* (BCG) vaccinated people. However, both TST and IGRAs have limitations as they cannot distinguish between latent infected people and successfully cured individuals. Therefore, much work has been done on discovery of specific biomarkers in Tb infection<sup>14</sup> that might provide an indication of treatment efficacy. Components of the mycobacterial cell envelope, for example, were directly detected in sputum or urine during active and latent infection, showed a treatment-dependent concentration in- or decrease and vanished after successful therapy.<sup>15-18</sup> However, poor sensitivity has led to limited use of biomarker-based diagnostic tools.<sup>19</sup> In addition, a new strategy was recently developed to analyze treatment efficacy by direct visualization of infected regions within the lung.<sup>20,21</sup> This imaging method relies on an increased uptake of radiolabeled tracers, like 2-deoxy-2-(<sup>18</sup>F)fluoro-D-glucose (FDG), by activated inflammatory cells.<sup>20</sup> Accumulation of radioactivity is detected by positron emission tomography (PET), while morphological information is obtained by computed tomography (CT) high resolution X-ray images. Simultaneously performing PET/CT scans can monitor Mtb infections over time (Figure 1).<sup>21</sup> This method gives the possibility to quantitatively measure drug efficacy and will further enable to explain why some Tb lesions do not respond to certain drugs. PET/CT scans are a major step forward in Tb diagnostics and will hopefully lead to an improvement of Tb therapy. However, both the currently used PET/CT scans and the biomarker-based methods do not directly detect Mtb bacteria. Thus, novel strategies that might allow to specifically visualize the bacterium within the body would strongly improve detection of latent Tb and analysis of drug efficacy. Furthermore, Mtb-specific labeling methods will lead to deeper insights into Mtb pathogenicity, which will facilitate the development of novel diagnostic and therapeutic tools.



**Figure 1. PET/CT images of a patient's lung prior and two months after antibiotic treatment.** PET/CT is a promising method, which enables live imaging of infected regions within the lung. In a non-treated patient's lung intense FDG uptake in regions with activated inflammatory cells ("hot spots") is visualized (A). Disease improvement after two months of antibiotic therapy is shown by a reduction of radioactivity within the lung. However, response to antibiotic therapy is lesion dependent (B). The images underline the potential application of PET/CT as a diagnostic tool to study drug efficiency and therapy outcomes. These PET/CT images were originally published in Russell, D. G. et al. *Science* **328**, 852-856 (2010) and was adapted by permission from *Science*.<sup>22</sup>

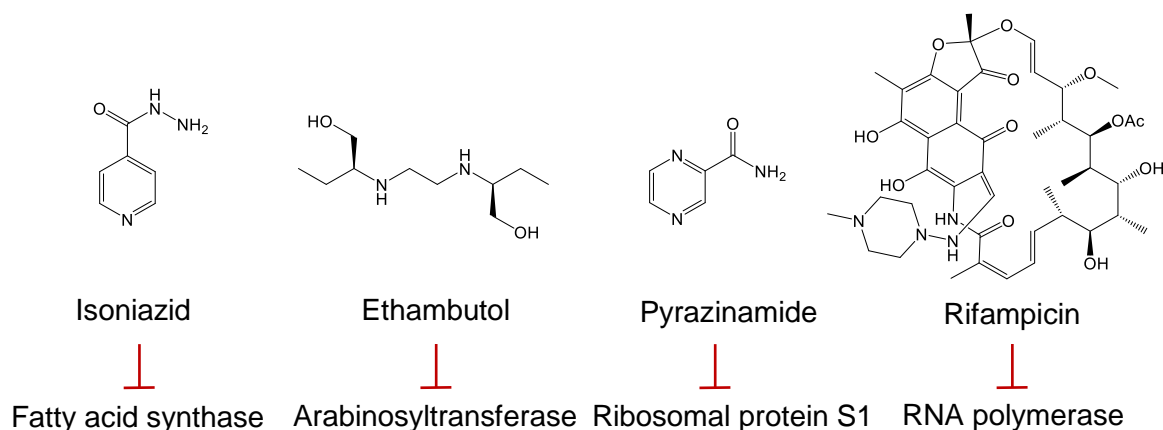
### 1.3 Tuberculosis therapy

The major problem in Tb control is the fact that more and more strains develop resistances to the drugs used for therapy. The emergence of drug resistance was first observed in the 1940's.<sup>23</sup> Ultimately the use of antibiotic monotherapy was replaced by a four-drug (isoniazid, rifampicin, pyrazinamide and ethambutol) regimen for two months, followed by four months of therapy with rifampin and isoniazid (for chemical structures see Figure 3). However, non-compliance and relatively limited availability of drugs have resulted in the major problems of today. 480 000 new cases of MDR Tb, resistant to at least isoniazid and rifampin, were notified in 2014 and even 10% of them were detected as extensively drug-resistant (XDR) strains, which are not only resistant to first- but also to second-line drugs.<sup>1</sup> In high burden regions (e.g. Russian Federation, Latvia and China) between 20% and 30% of the new Tb cases and 50% of the retreated cases are infected by MDR strains.<sup>1</sup> Clinical outcomes of MDR/XDR Tb are largely suboptimal and their treatment is very long, toxic and expensive.<sup>24</sup> Especially in developing countries increasing resistances are a particular dilemma, because the susceptibility testing and second-line agents are usually insufficient. Fortunately, 2015 a novel drug was described, where preliminary data indicate high antibacterial activity in the absence of resistance development. Teixobactin (Figure 2) was obtained as a natural product from uncultured soil bacteria and is a multistep inhibitor of the bacterial cell envelope biosynthesis.<sup>25</sup> Although teixobactin still has to pass the clinical trials, the first results make it reasonable that antibiotics might be developed, which do not lead to resistance formation.



**Figure 2: Chemical structure of the novel antibiotic teixobactin.** First data indicate high antibacterial activity in the absence of resistance development.

In addition to the increasing prevalence of MDR/XDR cases caused by genetic resistance mechanisms, drug therapy is complicated due to changes in the physiological and metabolic state of the bacterium. The ability of Mtb bacteria to enter into a non-replicating dormant lifestyle leads to an additional challenge.<sup>26,27</sup> Currently applied drugs (Figure 3) can mainly attack bacteria, which are actively replicating and are metabolically active.<sup>28</sup> Isoniazid and ethambutol are inhibitors of the cell envelope biosynthesis. Isoniazid is a prodrug that is activated by the mycobacterial catalase-peroxidase KatG forming the isonicotinic acyl-NADH complex. This complex competitively inhibits the fatty acid synthase and therefore the mycolic acid formation, an essential fatty acid of the Mtb cell envelope.<sup>29</sup> Ethambutol inhibits the arabinosyltransferase disrupting the arabinogalactan synthesis.<sup>30</sup> This heteropolysaccharide is essential for the structure of the mycobacterial cell envelope. Beside inhibition of cell envelope formation, anti-Tb drugs interrupt, for example, the RNA synthesis by inhibition of bacterial DNA-dependent RNA polymerase (rifampicin)<sup>31</sup> and protein translation by inhibition of the ribosomal protein S1 (pyrazinamide).<sup>32</sup> New drugs or even novel antibacterial strategies, which act against Tb during varying physiological stages and show limited resistance formation, are urgently required.



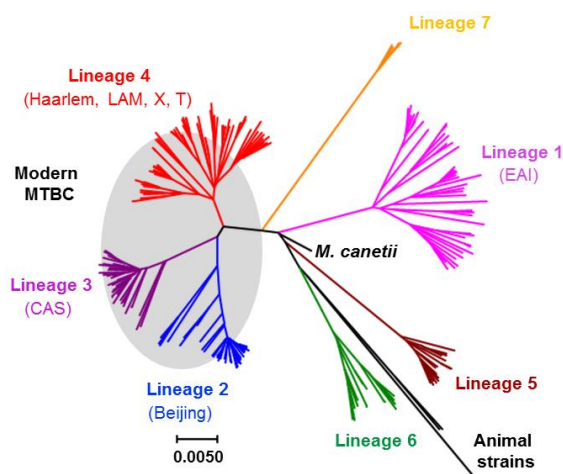
**Figure 3. Chemical structures of first-line drugs used for Tb therapy.**

## 1.4 *Mycobacterium tuberculosis*

### 1.4.1 The bacterium

Mtb was already discovered 1882 by Robert Koch<sup>33</sup> as the causative agent of Tb. Since then a group of phylogenetically closely related mycobacteria, collectively known as the *Mycobacterium tuberculosis* complex (MTBC), were identified to cause Tb.<sup>34</sup> The MTBC comprises seven closely related species. Tb in humans is primarily caused by Mtb and *Mycobacterium africanum*, which is currently limited to West Africa.<sup>35</sup> Furthermore, *Mycobacterium canettii* can also infect humans. However, this pathogen widely differs from the other members of the MTBC.<sup>36</sup> *M. canettii* mainly leads to extra pulmonary forms of Tb and seems to lack the capability of human-to-human transmission. The rare clinical cases caused by this species are confined to the Horn of Africa.<sup>37</sup> In addition to human pathogens, several animal-adapted members of MTBC exist, including *Mycobacterium bovis* (bovine), *Mycobacterium caprae* (sheep and goats), *Mycobacterium microti* (rodents) and *Mycobacterium pinnipedii* (seals).<sup>38</sup> Human Tb infections caused by *M. bovis* were detected.<sup>39</sup> However, there is currently no evidence of transmission between humans. The different members of MTBC appear to be strongly adapted to their particular host species.<sup>40</sup>

Mtb comprises a large amount of different strains, which can be classified into families and further into five lineages (lineage 1, 2, 3, 4, 7) based on phylogenetic studies (Figure 4).<sup>41</sup> These lineages are grouped based on their ancientness into “modern” lineages (Clade 1) and “ancient” lineages (Clade 2).<sup>42,43</sup> The major Mtb families (Beijing, Central Asian (CAS), Haarlem, Latin American Mediterranean (LAM), T and X) belong to lineages identified as “modern”.<sup>44,45</sup> Strains of the Mtb family East African Indian (EAI) are ancient strains and deviate genetically from modern strains. The pathogenicity of Mtb bacteria differs between the two Clades, the different lineages and even the strains, which is strongly associated with the clinical outcome of Tb.<sup>41,46,47</sup>



**Figure 4. Phylogeny of the MTBC based on genome analysis.** The eight human pathogenic lineages are represented including the five Mtb lineages (lineages 1, 2, 3, 4 and 7), the two lines of *M. africanum* (lineages 5 and 6) and *M. canettii*. The animal lineages represent a monophyletic branch in the complex. The “modern” lineages are located in the grey oval, as opposed to all the other lineages, which are called “ancient”. The major Mtb families are assigned to the lineages and shown in brackets. (scale bar: nucleotide substitutions per site) This phylogenetic tree was originally published in Comas, I. et al. *Nat Genet* **45**, 1176-1182 (2013) and was adapted by permission from *Nature*.<sup>48</sup>

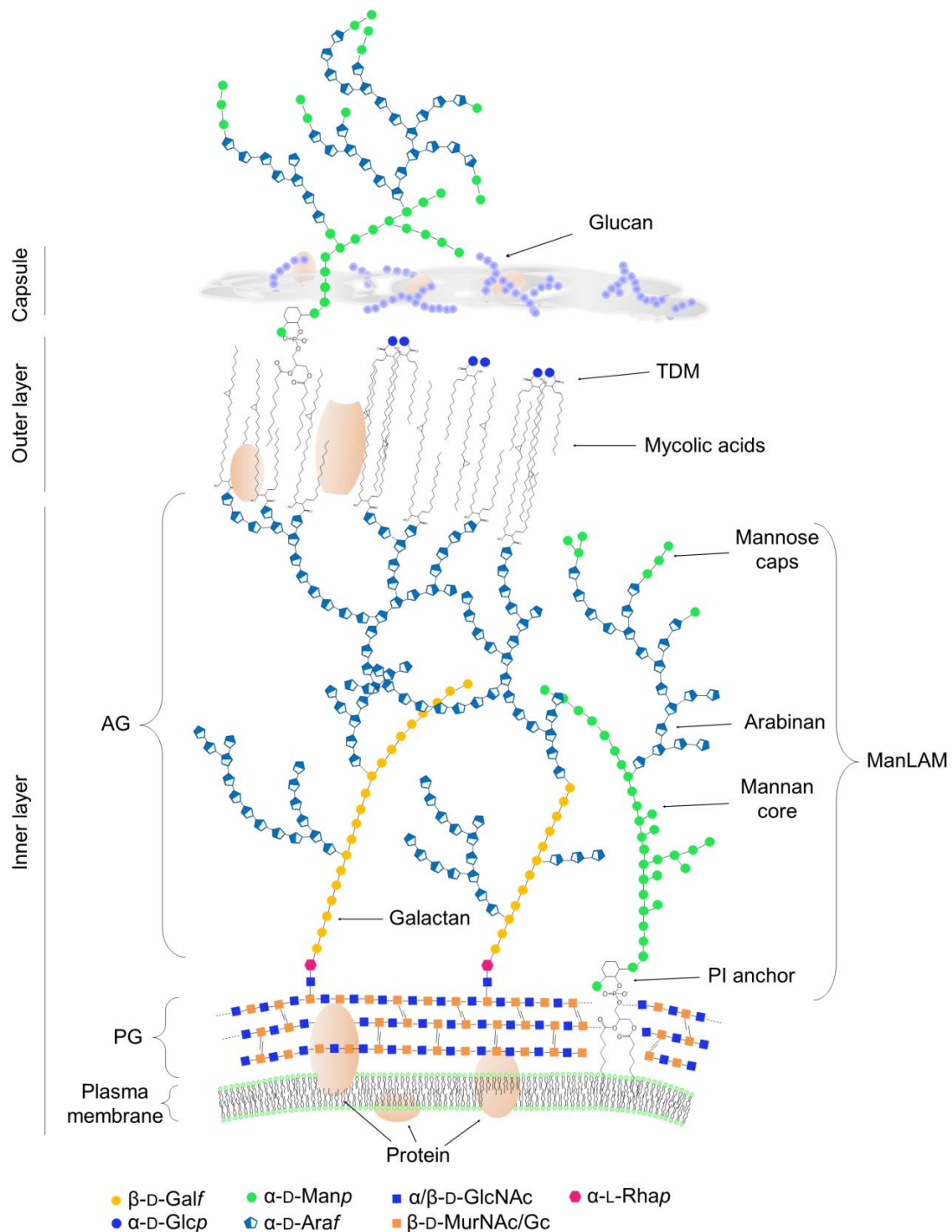
Despite distinct genetic differences between the various species, all mycobacteria share a rod shaped appearance, long lifecycles up to 24 hours and an idiosyncratic hydrophobic cell envelope. Mycobacteria withstand weak disinfectants and can survive in a dry state for weeks. Its unusual cell envelope, rich in lipids, is likely responsible for this resistance, the failure of many antibiotics and is a key virulence factor.<sup>49</sup> Since the mycobacterial cell envelope is essential for viability and virulence of Mtb, it is an important drug target.<sup>28</sup> Understanding the uniqueness of the cell envelope structures in further detail will provide the basis for the development of new diagnostic tools and novel antibacterial strategies.

#### 1.4.2 The unique cell envelope of Mtb bacteria

Mycobacteria were classified as Gram-positive bacteria based on 16S ribosomal RNA sequence comparison<sup>50,51</sup> and a weakly positive Gram stain.<sup>52</sup> The cell envelope of Gram-positive bacteria is composed of a plasma membrane followed by a thick layer of peptidoglycan and membrane- or peptidoglycan-attached glycopolymers. The mycobacterial cell envelope, however, contains an outer lipid layer<sup>53,54</sup> and is more reminiscent of Gram-negative bacteria whose thinner peptidoglycan layer is followed by an outer membrane. Although there are some structural similarities to Gram-positive and Gram-negative bacteria, the structure in detail contains many unique features only found in the bacterial suborder of the *Corynebacterineae*, to which the mycobacteria belong. The mycobacterial cell envelope (Figure 5) consists of three major compartments:

1. The “**inner layer**” is localized beyond a typical plasma membrane. This “inner layer” consists of proteins, lipid linked polysaccharides, like lipoarabinomannan (LAM) and its precursors lipomannan (LM) and phosphatidylinositol mannosides (PIM), and a mycolyl-arabinogalactan-peptidoglycan (mAGP) complex composed of a peptidoglycan (PG)-layer connected to arabinogalactan (AG), which is further conjugated with mycolic acids (MA). These long fatty acids are responsible for the connection to the second compartment, the “outer layer”.
2. The “**outer layer**” consists of lipids and proteins. The lipids are freely associated with the “inner layer” by hydrophobic interactions. The lipid-linked polysaccharides consist of LAM and LM. Additional glycolipids are present like phenolic glycolipids (PGL), sulfolipids (SL) and mycolic acid containing glycolipids (e.g. trehalose 6-monomycolate (TMM) and trehalose 6,6'-dimycolate (TDM)).
3. The “**capsule**” is loosely attached and mainly composed of the glycogen-like polysaccharide  $\alpha$ -D-glucan, few lipids and proteins, including lipases and proteases.

Subsequently the chemical structures and biological roles of the polysaccharides AG, LM and LAM and the glycolipids TMM and TDM are described in further detail.

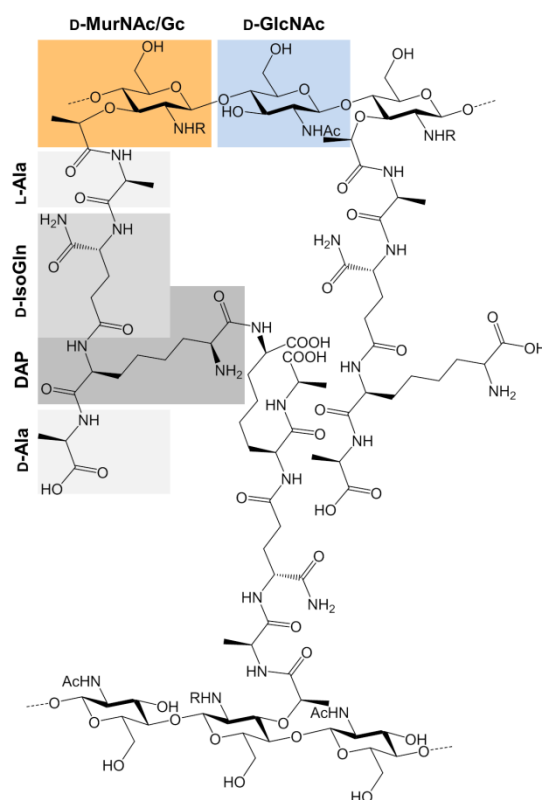


**Figure 5. Illustration of the unique mycobacterial cell envelope.** The cell envelope consists of three major compartments: “inner layer”, “outer layer” and “capsule”. The “outer layer” sticks to the “inner layer” through hydrophobic interactions supported by the enormous length (C60-90) of mycolic acids. While bacteria-specific D-arabinofuranosides are located in the “inner layer” and “outer layer” as a component of lipoarabinomannan (LAM) and arabinogalactan (AG), trehalose is mainly a constituent of trehalose 6,6'-dimycolate (TDM) and trehalose 6-monomycolate (TMM), which are intercalated into the “outer layer”.  $\beta$ -D-Galf:  $\beta$ -D-galactofuranoside,  $\alpha$ -D-Glcp:  $\alpha$ -D-glucopyranoside,  $\alpha$ -D-Manp:  $\alpha$ -D-mannopyranoside,  $\alpha$ -D-Araf:  $\alpha$ -D-arabinofuranoside,  $\alpha/\beta$ -D-GlcNAc: *N*-acetyl- $\alpha/\beta$ -D-glucosamine,  $\beta$ -D-MurNAc/Gc: *N*-acetyl-/*N*-glycolyl- $\beta$ -D-muramic acid,  $\alpha$ -L-Rhap:  $\alpha$ -L-rhamnopyranoside. Figure based on Brennan, P. J. et al. *Curr Top Med Chem* **7**, 475-488 (2007).<sup>55</sup>



### Mycolyl-arabinogalactan-peptidoglycan complex

The peptidoglycan (PG) in mycobacteria (Figure 6) follows the structure of the most common type of peptidoglycan in bacteria, the A1 $\gamma$  class. The glycan chains of PG consist of alternating subunits of *N*-acetyl- $\beta$ -D-glucosamine (GlcNAc) and *N*-acetyl- or *N*-glycolyl- $\beta$ -D-muramic acid (MurNAc/Gc).<sup>56</sup> Two glycan chains are cross-linked by tetrapeptides consisting of L-alanine, D-isoglutamine, meso-diaminopimelate and D-alanine.<sup>57</sup> The cross-linking occurs between two meso-diaminopimelic acid units either by an alanine or directly.

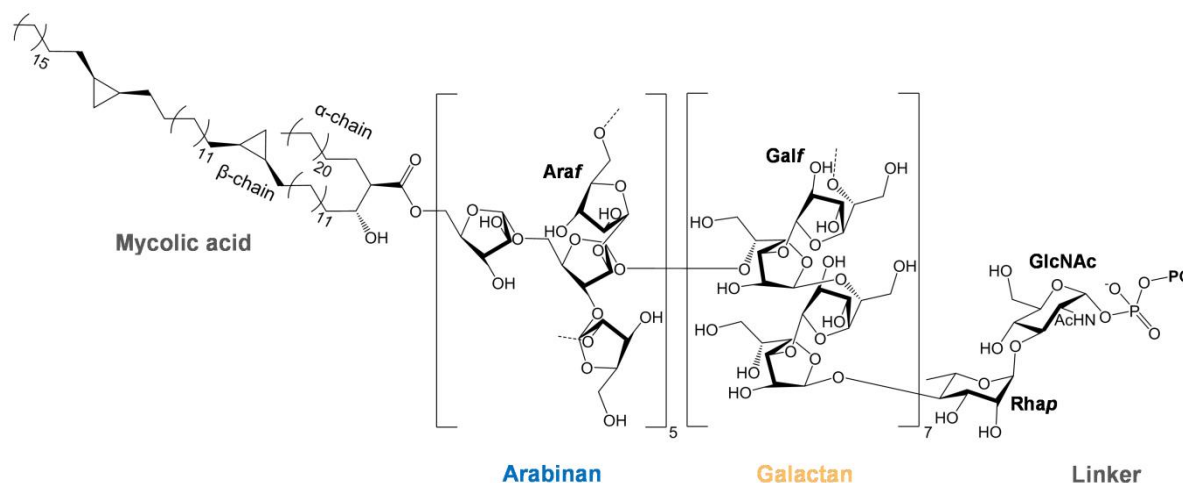


**Figure 6. Chemical structure of the peptidoglycan in mycobacteria.** The glycan chains of PG consist of alternating *N*-acetyl- $\beta$ -D-glucosamine (GlcNAc) and *N*-acetyl- or *N*-glycolyl- $\beta$ -D-muramic acid (MurNAc/Gc). MurNAc/Gc is connected to a tetrapeptide. The peptides of two glycan chains are cross-linked between two meso-diaminopimelic acids either by an alanine or directly, as depicted. (R: acetyl (Ac)/ glycolyl (Gc), L-Ala: L-alanine, D-IsoGln: D-isoglutamine, DAP: meso-diaminopimelate, D-Ala: D-alanine)

The peptidoglycan is covalently linked to the galactan chain of arabinogalactan (AG) by a unique linker (Figure 7) consisting of a phosphodiester,  $\alpha$ -D-GlcNAc and  $\alpha$ -L-rhamnopyranoside (Rhap).<sup>58</sup> AG (Figure 7) is the major polysaccharide of the mycobacterial cell envelope and connects the PG layer to the mycolic acid layer. AG is composed of D-arabinose and D-galactose, both in the relatively uncommon furanose form. The galactofuranosyl (D-Galf) residues are connected in alternating  $\beta$ (1 $\rightarrow$ 5) and  $\beta$ (1 $\rightarrow$ 3) linkages of approximately 30 residues forming the galactan polysaccharide. Galactan is attached to three arabinan polysaccharides by  $\alpha$ (1 $\rightarrow$ 5) linkages.<sup>59</sup> The  $\alpha$ -D-arabinofuranosyl ( $\alpha$ -D-Araf) residues of arabinan are connected by (1 $\rightarrow$ 2), (1 $\rightarrow$ 3) and (1 $\rightarrow$ 5) linkages. Terminal



Araf residues are functionalized with mycolic acids (MA) forming an ester bond between the acid and the primary hydroxyl group of Araf.<sup>59,60</sup> MAs are  $\alpha$ -alkyl- $\beta$ -hydroxyl-fatty acids ranging from 60 to 90 carbons per chain and representing the longest fatty acids produced by an organism to date.<sup>61</sup> While the short  $\alpha$ -chain is saturated, the longer  $\beta$ -chain can be modified with different functional units, such as double bonds, methoxy or keto groups, cyclopropanes and epoxides, which vary in different Tb strains.<sup>62,63</sup> MAs contribute to the intercalation of further glycolipids forming the “outer layer”.<sup>64</sup>

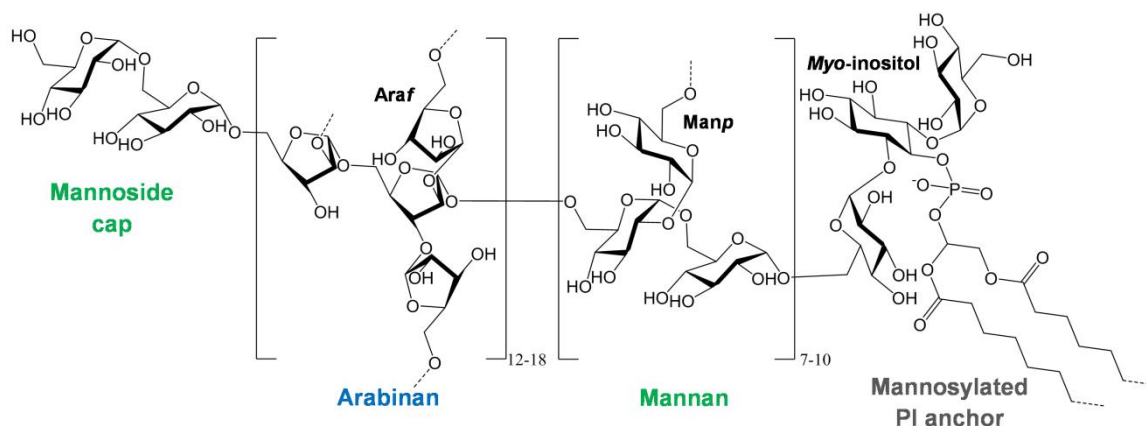


**Figure 7. Chemical structure of the mycolyl-arabinogalactan-peptidoglycan complex.** The mAGP consists of peptidoglycan, which is covalently attached to galactan of the AG heteropolysaccharide by a unique linker. The arabinofuranosyl residues are terminally functionalized with mycolic acids.  $\beta$ -D-Galf:  $\beta$ -D-galactofuranoside,  $\alpha$ -D-Araf:  $\alpha$ -D-arabinofuranoside,  $\alpha$ -D-GlcNAc: *N*-acetyl- $\alpha$ -D-glucosamine,  $\alpha$ -L-Rhap:  $\alpha$ -L-rhamnopyranoside.

### Mycobacterial lipoglycans and glycolipids

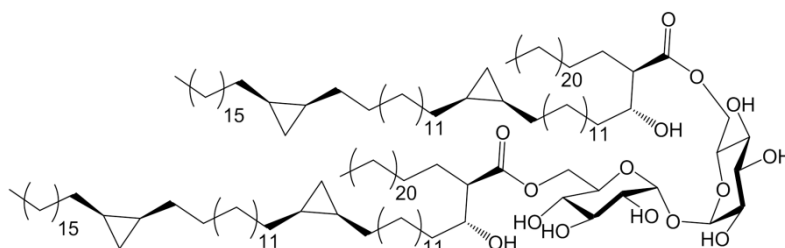
LAM (Figure 8) and its precursor LM are the major lipoglycans found in the mycobacterial cell envelope. They contain a phosphatidyl-*myo*-inositol moiety (PI), which is connected to a diacylglyceride attaching the molecule non-covalently to the plasma membrane or to the “outer layer”.<sup>65</sup> The smallest glycolipid precursor of LAM is PIM<sub>1</sub>, which has one  $\alpha$ -D-mannopyranosyl (Man<sub>p</sub>) residue bound to the 2-position of *myo*-inositol.<sup>66,67</sup> Addition of another Man<sub>p</sub> residue to the 6-position of the *myo*-inositol ring of PIM<sub>1</sub> results in the formation of PIM<sub>2</sub>, which can be further elongated forming PIM<sub>6</sub>.<sup>68</sup> If the backbone is extended with additional 20-30 Man<sub>p</sub> residues the polysaccharide is called LM. The mannan core of LM consists of linear  $\alpha(1\rightarrow6)$ -linked Man<sub>p</sub> residues and is further supplemented by  $\alpha(1\rightarrow2)$ -Man<sub>p</sub> side branches. LAM, based on the structure of LM, has a highly branched arabinan polymer attached to mannan by  $\alpha(1\rightarrow6)$  linkage.<sup>69</sup> The  $\alpha$ -D-arabinofuranosyl ( $\alpha$ -D-Araf) residues of arabinan are connected by (1 $\rightarrow$ 2), (1 $\rightarrow$ 3) and (1 $\rightarrow$ 5) linkages. LAM is classified based on peripheral attachment of further molecules, “capping”. In pathogenic species, such as Mtb, LAM is capped to various degrees with short mannopyranosyl chains consisting of one to three residues,<sup>70</sup> inositol phosphate-capped LAM (PILAM) is found in fast growing non-pathogenic

*Mycobacterium smegmatis*, and AraLAM,<sup>71</sup> which has neither mannoside nor inositol phosphate caps, could be detected in *Mycobacterium chelonae*.<sup>72</sup>



**Figure 8. Chemical structure of lipoarabinomannan.** The lipoglycan LAM is attached to the plasma membrane or the “outer layer” by the diacylglyceride moiety of the PI anchor. Myo-inositol of the PI anchor is glycosylated at the 2- and 6-position and thereby connected to mannan. Terminal mannosides of this polysaccharide are linked to arabinan. In pathogenic mycobacteria (e.g. Mtb) arabinofuranosides of arabinan are terminally connected to mannosides by  $\alpha$ -(1→5) linkages.  $\alpha$ -D-Manp:  $\alpha$ -D-mannopyranoside,  $\alpha$ -D-Araf:  $\alpha$ -D-arabinofuranoside, PI: phosphatidyl-*myo*-inositol.

Various free, noncovalently associated glycolipids are present in the mycobacterial cell envelope. The mycolic acid diester TDM and its precursor TMM were ubiquitous detected among mycobacterial species.<sup>73</sup> TDM (Figure 9) is composed of trehalose functionalized with mycolic acids at the primary hydroxyl groups. The mycolic acids can possess different Tb strain-dependent modifications and chain lengths.<sup>62</sup>



**Figure 9. Chemical structure of a trehalose 6,6'-dimycolate molecule.** TDM is a mycolic acid diester of trehalose. The depicted mycolic acids are only an example for a variety of mycolic acids present in mycobacteria. The 60 to 90 carbon long fatty acids exhibit Mtb strain-dependent functional units (double bonds, methoxy or keto groups, cyclopropanes and epoxides) and chain lengths.

The described lipoglycans and glycolipids are only a part of the free lipids forming the “outer layer” of the Mtb cell envelope. The high amount of lipids has a strong impact on cell envelope fluidity and permeability. While hydrophobic molecules can pass through the thick and dense cell envelope, hydrophilic substances have to be actively transported or can passively diffuse through porins. The thickness and hydrophobicity of the mycobacterial cell envelope are linked to the considerable resistance of Mtb bacteria to many drugs.<sup>74</sup>

The carbohydrates of the lipoglycans and glycolipids contribute to the pathogenicity of Mtb<sup>68</sup> and are part of the uniqueness of the mycobacterial cell envelope. While some of the carbohydrate components, such as mannopyranosides and glucopyranosides, are widely prevalent in cell envelopes of bacteria and eukaryotic cells, D-trehalose and D-arabinofuranosides are mainly found in the cell envelope of *Corynebacterineae*.<sup>75,76</sup> These unique sugars have the potential to promote the development of novel specific diagnostic and therapeutic strategies and are the focus of this thesis.

### 1.4.3 The rare carbohydrates of the mycobacterial cell envelope

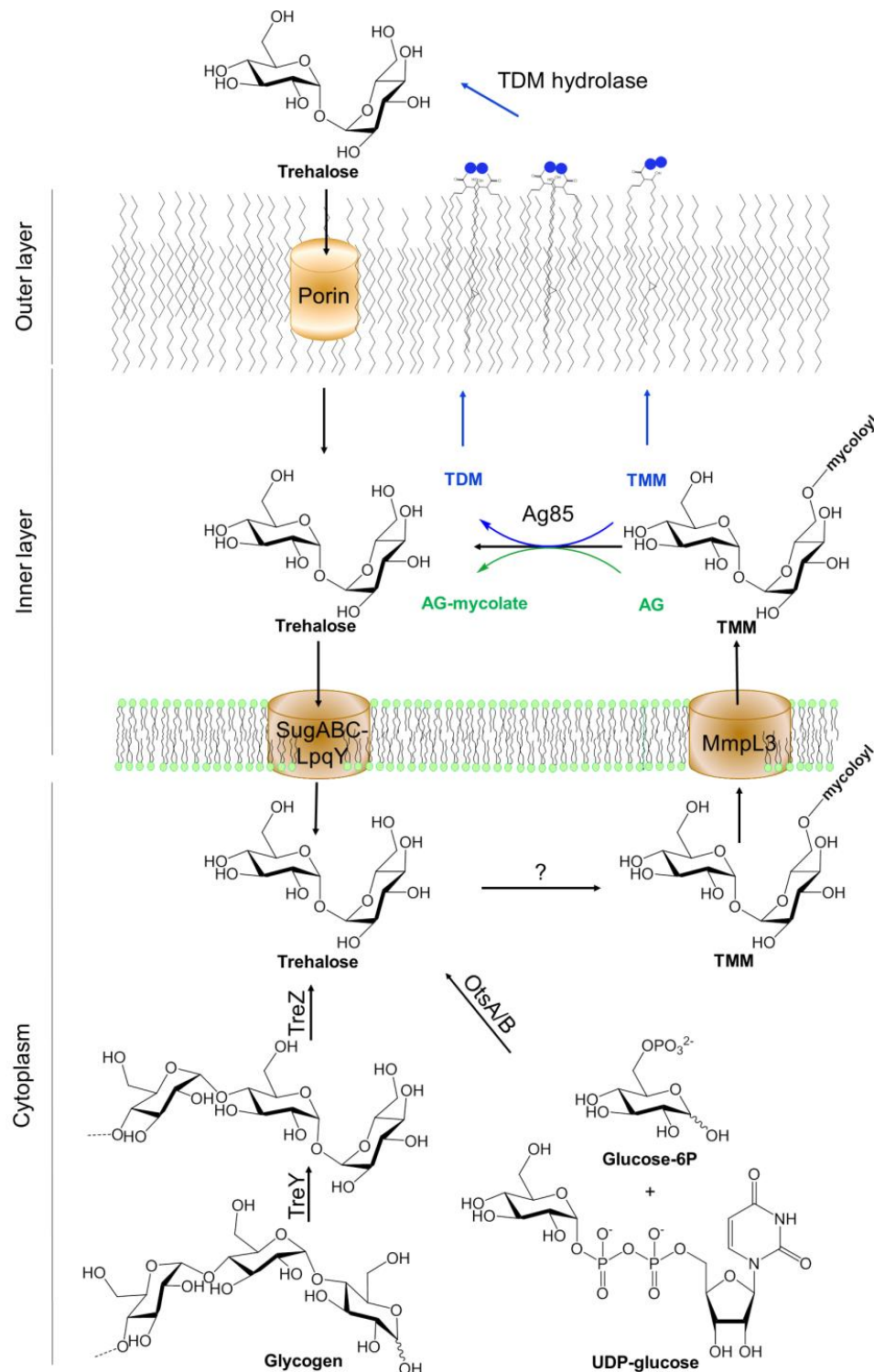
#### D-Trehalose

Trehalose is a non-reducing disaccharide of  $\alpha(1\rightarrow1)$ -linked glucose. It is present in several eukaryotic organisms (e.g. fungi, insects and plants, but not in mammals) and in both Gram-positive bacteria (e.g. *Propionibacterium freudenreichii*) and Gram-negative bacteria (e.g. *Pseudomonas aeruginosa*, *Escherichia coli*).<sup>75</sup> In these organisms trehalose is mainly located in the cytoplasm. Intracellular trehalose is considered to act as a stress protector molecule, as it was shown to shield proteins, membranes or whole cells from heat-induced denaturation, freezing or  $\gamma$ -radiation.<sup>77-79</sup> In mycobacteria trehalose is not only present as a free disaccharide in the cytoplasm but is also a prominent constituent of several cell envelope glycolipids, such as TDM and TMM. While the essential role of membrane-bound trehalose for cell envelope integrity and pathogenicity of Mtb is proven,<sup>80</sup> the contribution of intracellular trehalose on dehydration tolerance is only hypothetical.<sup>81</sup>

#### Biosynthesis of trehalose 6,6'-dimycolate

The biosynthesis (Figure 10) of the unique trehalose-containing glycolipids is localized in the cytoplasm, where free trehalose is mainly synthesized from activated glucose derivatives. Uracil-diphosphate(UDP)-glucose and glucose-6-phosphate are converted into trehalose-6-phosphate (T6P), catalyzed by the trehalose-6-phosphate synthase (OtsA). This intermediate is subsequently dephosphorylated into trehalose by the specific trehalose-6-phosphate phosphatase (OtsB).<sup>82,83</sup> Beside the biosynthesis from glucose, trehalose can also be generated from glycogen. Maltooligosyltrehalose synthase (TreY) catalyzes the isomerization of the  $\alpha(1\rightarrow4)$ -linkage of the terminal disaccharide at the reducing end of glycogen into a  $\alpha(1\rightarrow1)$ -linkage, followed by the release of trehalose by maltooligosyltrehalose trehalohydrolase (TreZ).<sup>75</sup> If trehalose-6-phosphate or trehalose is the substrate for the TMM synthesis remains to be confirmed. TMM is translocated across the plasma membrane by the mycobacterial membrane protein large 3 (MmpL3).<sup>84,85</sup> The antigen 85 (Ag85) complex is essential to transfer mycolate from TMM to either AG or another molecule of TMM generating TDM.<sup>86</sup> Both transesterification processes release free trehalose, which is recycled by a

trehalose-specific ATP-dependent transporter SugABC-LpqY.<sup>87</sup> While mycolated arabinogalactan connected with the PG layer is a constituent of the “inner layer” of the Mtb cell envelope, TMM and TDM are intercalated into the “outer layer”.



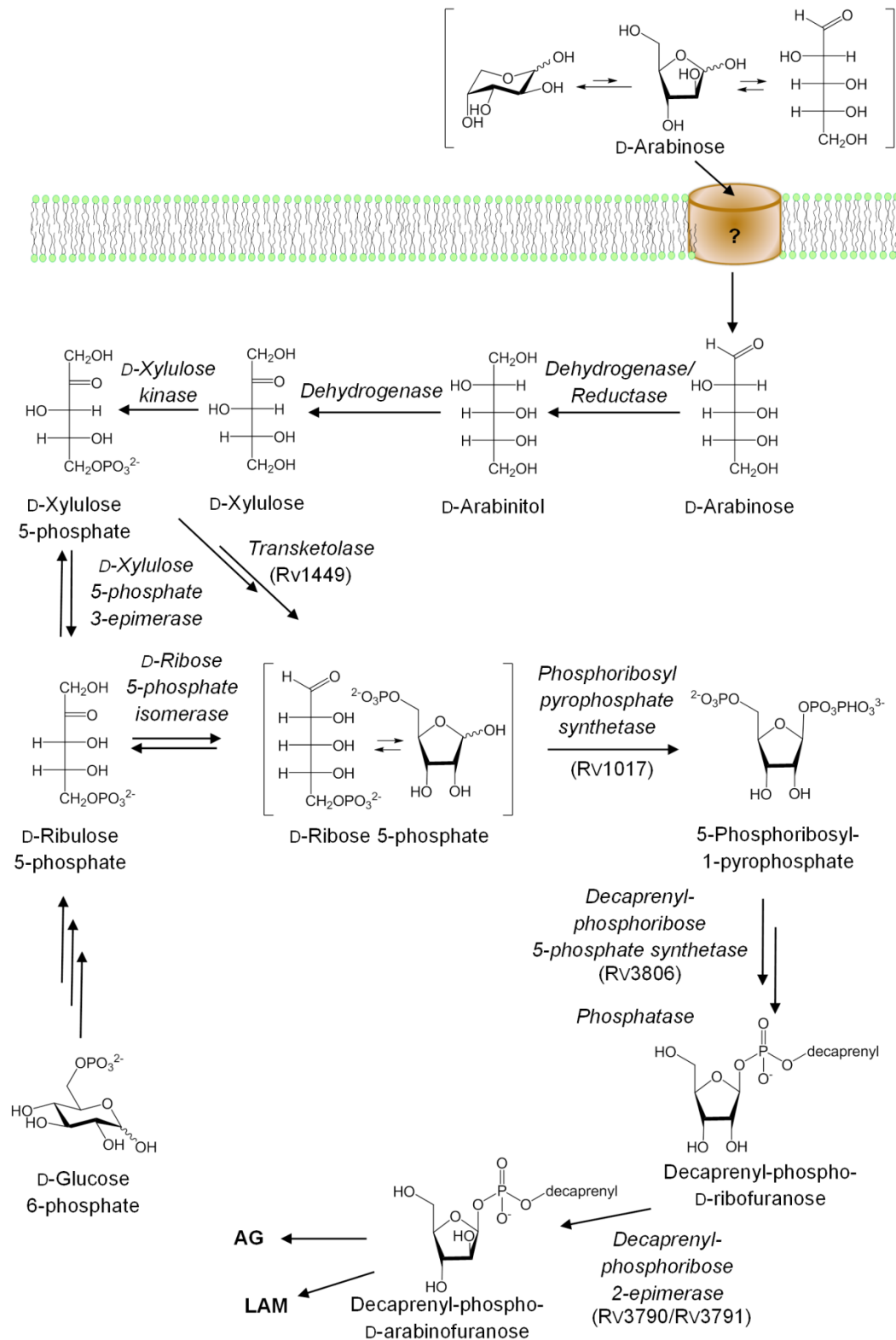
**Figure 10. Illustration of the TDM metabolism.** Trehalose is either derived from activated glucose derivatives or through glycogen degradation. Cytosolic trehalose can be acylated forming TMM, which is a precursor for TDM. TDM is obtained by mycolic acid transfer in the “inner layer”. Trehalose derivatives located in the cell envelope are unique constituents of mycobacteria. (● :  $\alpha$ -D-glucopyranoside ( $\alpha$ -D-Glcp)) Figure based on Swarts, B. M. et al. *J Am Chem Soc* **134**, 16123-15126 (2012).<sup>88</sup>

### D-Arabinofuranoside

D-Arabinose is a very rare sugar in nature. While D-arabinopyranose (Arap) occurs in some eukaryotes, such as plants<sup>89</sup> and some parasitic protozoa like the trypanosomatid parasite *Leishmania major*,<sup>90–94</sup> D-arabinofuranose (Araf) can only be found in prokaryotes. Araf is a cytoplasmic intermediate in the biosynthesis of 3-deoxy-D-manno-octulosonic acid (Kdo),<sup>95</sup> an essential carbohydrate of the lipopolysaccharide (LPS) in Gram-negative bacteria. In addition Araf is a unique component of cell surface polysaccharides and glycolipids of mainly *Corynebacterineae*.<sup>96</sup> In mycobacteria, including pathogenic Mtb, Araf is a prominent constituent of the two major cell envelope polysaccharides AG and LAM.

### Biosynthesis of the arabinofuranosyl components of AG and LAM

The biosynthesis of arabinose-containing polysaccharides (Figure 11) has been characterized in detail for *Mycobacterium smegmatis* (Msg), while for Mtb several steps remain uncertain.<sup>97</sup> In the LAM/AG-metabolism activated D-glucose-6-phosphate is transformed to D-ribulose-5-phosphate catalyzed by two dehydrogenases and a lactonase. This intermediate can also be derived from exogenous D-arabinose via a fungal-like pathway.<sup>97–99</sup> D-Arabinose is taken up and reduced to D-arabinitol, which is further oxidized to D-xylulose. This pentose is phosphorylated to D-xylulose-5-phosphate and epimerized to D-ribulose-5-phosphate. D-ribose-5-phosphate is either obtained by an isomerization of activated D-ribulose or directly from D-xylulose-5-phosphate with sedoheptulose-7-phosphate as an intermediate. Subsequently activated D-ribose is further converted to decaprenyl-phospho-ribose. The last metabolic steps contain a 2-epimerization of decaprenyl-phospho-ribose to decaprenyl-phospho-arabinose, which serves as the donor of D-arabinofuranosyl residues for the LAM and AG formation.<sup>97</sup> In contrast to Msg, for which the biosynthesis of arabinan from external D-arabinose was described and a specific ATP-dependent (ABC) arabinose transporter is known, in Mtb only a few enzymes of the arabinan metabolism have been defined to date<sup>97</sup> and the carbohydrate transport systems are poorly characterized.<sup>100</sup>



**Figure 11. Illustration of the arabinan metabolism.** The biosynthetic pathway for LAM and AG is mainly studied for *Msg*. For *Mtb* a few genes (shown in brackets) encoding for metabolic enzymes were identified to be essential for the arabinan metabolism. While the uptake of environmental arabinose is described for *Msg* and an ABC-transporter is known, no pentose transport systems were identified for *Mtb* to date. The donor for the arabinan synthesis is decaprenyl-phospho-D-arabinose, other precursors have never been identified. D-Arabinofuranosides are mainly present in the cell envelopes of *Corynebacterineae*. Figure based on Wolucka, B. A. *FEBS J* **275**, 2691-2711 (2008).<sup>97</sup>

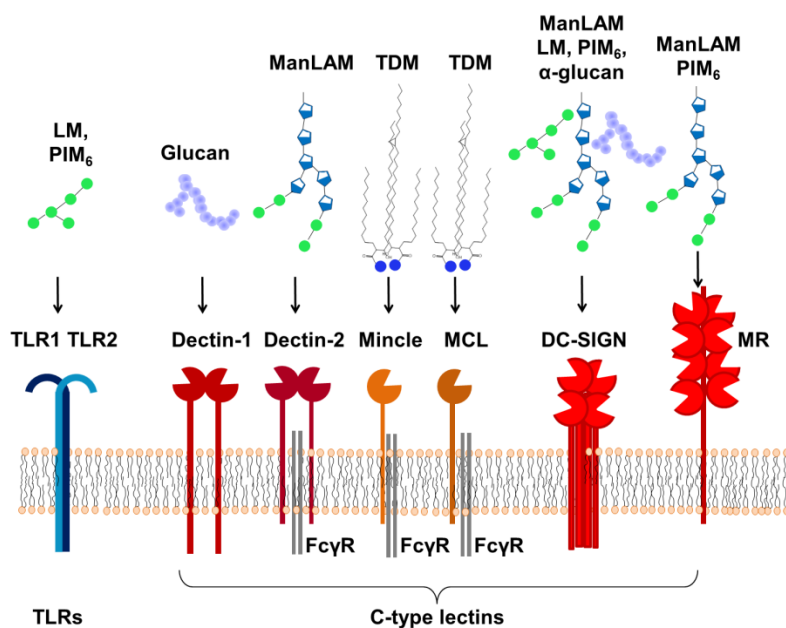
#### 1.4.4 Mycobacterial carbohydrates connected to Mtb pathogenicity

The carbohydrates of the Mtb cell envelope are strongly associated with mycobacterial pathogenicity. Mtb bacteria are mainly transmitted by inhalation of aerosolized droplets released from infected patients by coughing. The initial step in the infection process is the contact between inhaled bacteria and primarily alveolar macrophages, which internalize the bacterium through phagocytosis. Following recognition and uptake the host cell initiates a number of responses to limit bacteria replication and spread with the ultimate goal of eradicating the pathogen. Mtb, however, has evolved successful strategies to survive, replicate and persist within macrophages for days, months or years and needs host cells for nutrient acquisition and protection against the immune system. The polysaccharides and glycolipids of the Mtb cell envelope strongly contribute to the manipulation of host cells and the survival of Mtb bacteria within phagosomes.<sup>68,101,102</sup>

Initial recognition of mycobacteria by the innate immune system is triggered by several pattern recognition receptors (PRRs).<sup>103,104</sup> These PRRs comprise humoral receptors, such as surfactant proteins<sup>105</sup> and the mannose-binding lectin (MBL).<sup>106</sup> In addition a variety of membranous receptors belong to the PRRs including toll-like receptors (TLRs) and C-type lectins, such as the DC-specific intercellular adhesion molecule 3-grabbing nonintegrin (DC-SIGN),<sup>107,108</sup> the dendritic cell-specific C-type lectins (Dectin-1, Dectin-2),<sup>109–111</sup> the macrophage inducible C-type lectin (Mincle),<sup>80,112</sup> the macrophage C-type lectin (MCL)<sup>113,114</sup> and the mannose receptor (MR)<sup>115,116</sup> (Figure 12). Several of the PRRs are lectins, which recognize carbohydrate structures on the mycobacterial cell surface. The soluble collectin surfactant proteins A (SP-A), for example, interacts with ManLAM and LM and acts as an opsonin, enhancing binding and uptake of Mtb bacteria by macrophages.<sup>105</sup> The most prominent membranous receptor involved in phagocytosis of Mtb bacteria by macrophages is the MR.<sup>115,116</sup> The main ligand of MR is ManLAM.<sup>115</sup> The binding affinity of the MR to LAM depends on mannosylation.<sup>117</sup> While ManLAM from pathogenic Mtb strains show intense binding, PILAM from Mmsg does not bind to the MR. Higher-order PIMs (PIM<sub>5</sub> and PIM<sub>6</sub>) were identified as additional ligands.<sup>118</sup> The MR is distinguished by the fact that it mediates internalization without triggering pro-inflammatory response.<sup>119</sup> Thus, phagocytosis via the MR can be regarded as a strategy of Mtb to escape immune surveillance.<sup>119</sup> In addition to direct pathogen uptake, other classes of PRRs, such as TLRs, play essential roles in activating signal transduction pathways.<sup>104</sup> The TLR1/TLR2 complex was identified to recognize LM and to a lesser degree PIM<sub>6</sub>.<sup>120,121</sup> This interaction, in contrast to the MR, leads to an activation of the macrophage resulting in the transcription of pro-inflammatory cytokines.<sup>121</sup> However, the importance of TLRs in immunity to tuberculosis is controversially discussed and might be less significant than originally assigned.<sup>122</sup> Additional carbohydrates involved in host-pathogen interactions are the  $\alpha$ -glucan of the capsule and trehalose of the unique TDM of the “outer



layer". While  $\alpha$ -glucan is one of the variety of ligands recognized by DC-SIGN<sup>123–125</sup> and might also interact with Dectin-1,<sup>126</sup> TDM is the main mycobacterial ligand for Mincle and MCL and strongly contributes to the survival of Mtb bacteria within phagosomes.<sup>80,112–114</sup>

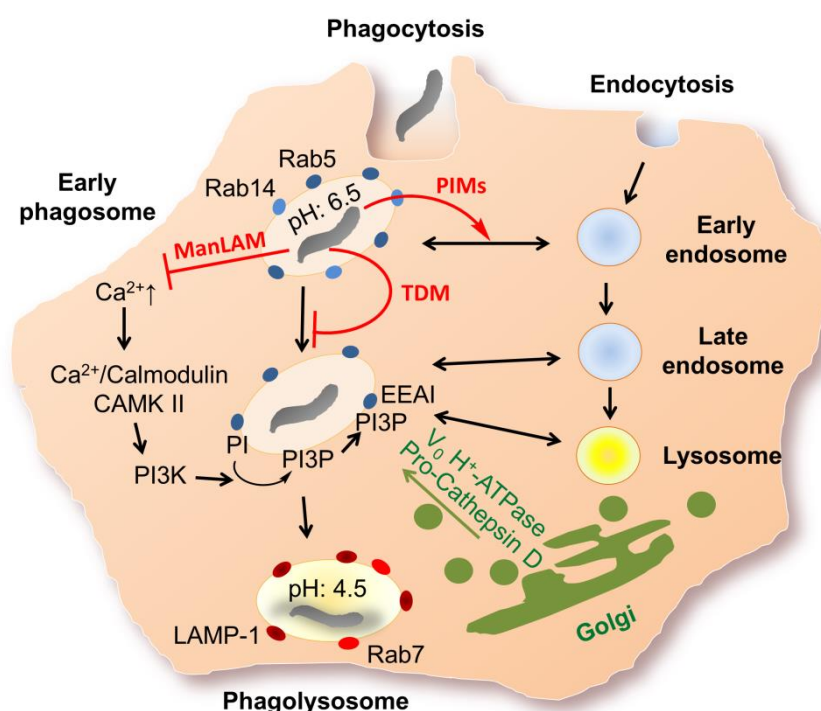


**Figure 12. Illustration of the pattern recognition receptors present on the cell surface of macrophages, which recognize carbohydrate structures of the Mtb cell envelope.** Several C-type lectins (DC-specific intercellular adhesion molecule 3-grabbing nonintegrin (DC-SIGN), dendritic cell-specific C-type lectins (Dectin-1, Dectin-2), macrophage inducible C-type lectin (Mincle), macrophage C-type lectin (MCL), mannose receptor (MR)) and the toll-like receptor 1 (TLR1)/TLR2 complex were identified as receptors for polysaccharides ( $\alpha$ -glucan), glycolipids (TDM, PIM) and lipoglycans (LM, ManLAM) of the Mtb cell envelope.

Mycobacterial glycolipids and lipoglycans play an important role in regulating phagocytosis (Figure 13). Macrophages engulf pathogens forming a phagosome, which then matures into a phagolysosome involving a series of fusion reactions with the endocytic and secretory pathways and ultimately fusion with lysosomes. Phagolysosomes have an acidic pH of 4.5, hydrolase activities through lysosomal enzymes (e.g. proteases, lipases and glycoside hydrolases) and contain antimicrobial peptides. Phagosome maturation is crucial for killing of engulfed microbes as well as for antigen presentation to T-lymphocytes. Mtb bacteria are able to inhibit phagosome maturation triggered by different cell envelope carbohydrate structures.<sup>127,128</sup> ManLAM limits influx of calcium ions ( $\text{Ca}^{2+}$ ) into the cytosol presumably by binding to the MR.<sup>129</sup> A decreased  $\text{Ca}^{2+}$  concentration reduces the binding of  $\text{Ca}^{2+}$ /calmodulin to  $\text{Ca}^{2+}$ /calmodulin-dependent protein kinase (CAMK II), a serine-threonine kinase, which activates the phosphatidylinositol 3 kinase (PI3K).<sup>130,131</sup> PI3K catalyzes the phosphorylation of phosphatidylinositol at the 3-position of the inositol ring leading to the formation of phosphatidylinositol 3-phosphate (PI3P) on the phagosomal membrane. PI3P and the GTPase Ras-related in brain 5 (Rab5), which is an important marker of early endosomes and involved in endosomal fusion, are important mediators of the recruitment of the early endosome



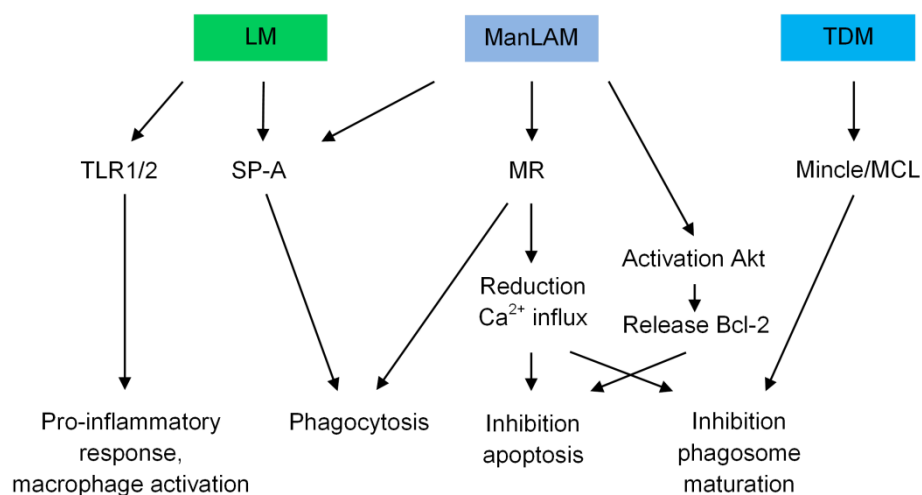
antigene 1 (EEA1) to the phagosomal membrane. EEA1 is necessary to deliver hydrolases such as cathepsin D and H<sup>+</sup>-ATPase subunit Vo from the trans-Golgi network (TGN) to the phagosome and promotes the fusion of phagosomes with vesicles of the endosomal-lysosomal pathway.<sup>132</sup> Therefore, inhibition of Ca<sup>2+</sup> influx directly correlates with inhibition of phagosome maturation. In addition, PIMs can also inhibit phagosome acidification, not by preventing EEA1 recruitment, but by promoting fusion between the phagosome and early endosomes.<sup>133</sup> Other host receptors that are involved are the TDM recognizing lectins Mincle<sup>112</sup> and MCL.<sup>113</sup> TDM-coated beads are sufficient to delay phagosome maturation in macrophages.<sup>134</sup> Different carbohydrate-lectin interactions contribute to the fact that Mtb bacteria reside in phagosomes with incomplete luminal acidification (pH 6.5) and absence of mature lysosomal hydrolases, containing early endosomal markers like Rab5, only a transient localization of the late endosomal marker Rab7 and low levels of the lysosome-associated membrane protein 1 (LAMP-1).<sup>127,135,136</sup>



**Figure 13. Illustration how glycolipids and lipoglycans of the Mtb cell envelope contribute to the inhibition of the phagosome maturation.** ManLAM contributes to the inhibition of the phagosome maturation by reduction of the influx of calcium ions (Ca<sup>2+</sup>) into the cytosol. A limited Ca<sup>2+</sup> concentration results ultimately in a reduced phosphorylation of phosphatidylinositol (PI). Phosphatidylinositol 3-phosphate (PI3P) and the GTPase Ras-related in brain 5 (Rab5) are important mediators of the recruitment of the early endosome antigen 1 (EEA1) to the phagosomal membrane, which induces the delivery of hydrolases such as cathepsin D and H<sup>+</sup>-ATPase subunit Vo from the golgi to the phagosome and promotes the fusion of phagosomes with vesicles of the endosomal-lysosomal pathway leading to a phagosome maturation. PIMs induce fusion with early endosomes. In addition TDM contributes to the fact that Mtb resides in phagosomes with incomplete luminal acidification (pH 6.5) and absence of mature lysosomal hydrolases. (CAMK II: Ca<sup>2+</sup>/calmodulin-dependent protein kinase, PI3K: the phosphatidylinositol 3 kinase, LAMP-1: lysosome-associated membrane protein 1)

Mtb bacteria can also regulate processes of cell death in macrophages. Inhibition of apoptosis is regarded to be beneficial for the pathogen during early stage of infection for maintaining its replicative niche, while lysis of the host cell at a later stage reaching a certain bacterial load enables spreading and entering new host cells. Apoptosis inhibition can be induced by ManLAM. Reduction of  $\text{Ca}^{2+}$  signaling, as described for inhibition of phagosome maturation, appears to be an important step in blocking infection-induced apoptosis.<sup>137</sup> Beside regulation of the cytosolic  $\text{Ca}^{2+}$  concentration, ManLAM can activate the serine-threonine kinase Akt leading to a phosphorylation of Bcl-2-associated death promoter (Bad) and release of the anti-apoptotic protein B-cell lymphoma 2 (Bcl-2).<sup>138</sup>

While ManLAM strongly reduces phagosome maturation and apoptosis,<sup>119</sup> LM binds to TLR2 and induces pro-inflammatory responses<sup>139,140</sup> and an activation of the macrophage<sup>121</sup> (Figure 14). As LAM and LM are both part of the mycobacterial cell envelope, one might expect a direct correlation between mycobacterial virulence and a LAM/LM ratio.<sup>68</sup> However, the biological significance of the LAM/LM balance or even more importantly of the whole carbohydrate composition of the mycobacterial cell envelope are only rarely studied<sup>119,141</sup> and remain to be investigated in further detail. Therefore, a fast and easy tool that might allow to visualize the carbohydrate composition on cell surfaces of different Mtb strains will facilitate the identification of the strain-specific cell envelope heterogeneity, which might further enable to correlate carbohydrate composition to Mtb pathogenicity.



**Figure 14. Illustration of the immunomodulative properties of the carbohydrate structures of the mycobacterial cell envelope.** While ManLAM and PIMs show mainly anti-inflammatory activity, LM can induce the secretion of pro-inflammatory cytokines. This figure shows only a part of functions induced by mycobacterial glycolipids and lipoglycans. (TLR: toll-like receptor, SP-A: surfactant protein-A, MR: mannose receptor, Mincle: macrophage inducible C-type lectin, Akt is a serine-threonine kinase, Bcl-2: B-cell lymphoma-2).

The unique carbohydrates of the Mtb cell envelope, trehalose and arabinofuranoside, contribute to a varying extent to the virulence of Mtb bacteria. Trehalose as a constituent of

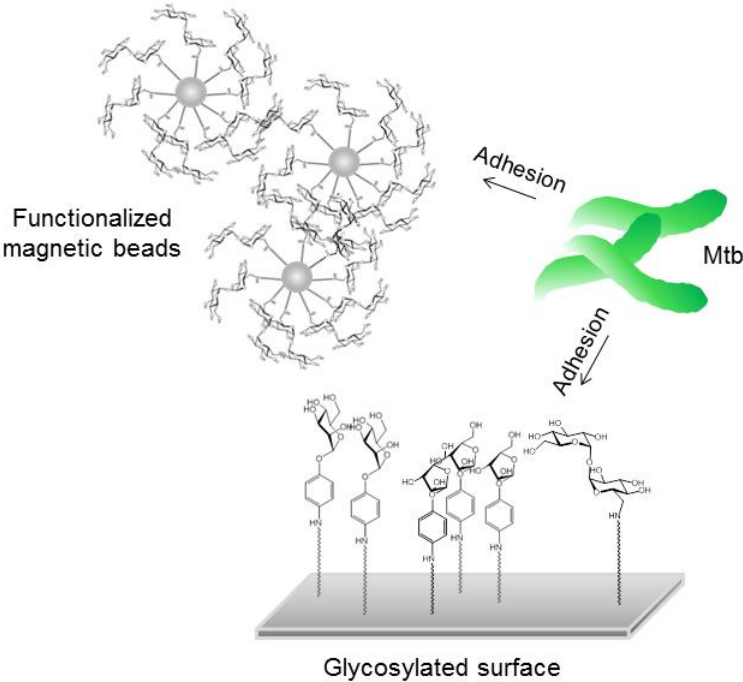
TDM is strongly involved in inhibition of phagosome maturation.<sup>134</sup> The physiological role of arabinans was thought to be exclusively structural.<sup>97</sup> However, the arabinofuranosides are essential, since inhibition of the arabinan synthesis is lethal in Mtb.<sup>142,143</sup> Unconsidered their biological functions, both carbohydrates represent good targets for new diagnostic and therapeutic tools, since they are not synthesized in mammals and seldom localized on cell surfaces of other microorganisms.

#### 1.4.5 Mycobacterial lectins

Lectins on host cells recognizing carbohydrates of the Mtb cell envelope strongly contribute to mycobacteria recognition and uptake and have an influence on the immune response. The importance of bacterial lectins for adhesion, pathogenicity and biofilm formation is known for many Gram-positive and Gram-negative bacteria.<sup>144</sup> However, there is very little information available about mycobacterial lectins. Their impact on host-pathogen interactions and the adhesion among mycobacteria is rarely studied. In 1989 an extracellular lectin, “mycotin”, was isolated from Msm, which was able to agglutinate human A, B and O erythrocytes.<sup>145</sup> This agglutination could be inhibited by different carbohydrates. Apart from D-arabinose, mannan and *p*-nitrophenyl  $\alpha$ -D-mannopyranoside showed high inhibitory potency. Other mycobacteria, like Mtb, were found to contain molecules immunologically related to mycotin.<sup>146</sup> However, the potential lectin of Mtb was not isolated until now and it is still unclear where it is encoded in the bacterial genome. That lectins are involved in mycobacterial aggregation was shown by V. Anton et al..<sup>147</sup> In this case D-arabinose was identified to inhibit aggregation of Mtb bacteria. The arabinose-specific lectin, which mediates self-aggregation, has also not been isolated or further characterized to date. After the genome of Mtb was completely deciphered a few years ago, D. D. Singh et al. identified ten potential lectins present in the mycobacterial genome by bioinformatic analysis.<sup>148</sup> Those proteins span a wide range in length and functional annotations and can be classified to belong to families like haemagglutinins, mannose-sensitive agglutinins or C-type lectins, which bind carbohydrates in a calcium-dependent manner.<sup>148,149</sup> Although this genetic analysis strongly indicates that mycobacterial lectins are present, little is known about carbohydrate specificity, localization and biological functions. Identification of membranous mycobacterial lectins and their biological role might give new insights into Mtb pathogenicity. Carbohydrate-lectin interactions might further be utilized to develop new diagnostic tools.

In this thesis the presence of rare carbohydrates and possibly of specific mycobacterial lectins in the Mtb cell envelope and the high hydrophobicity of the mycobacterial cell surface formed the basis for the development of new tools to enrich mycobacteria from solution (part 1) and to specifically label different Mtb clinical isolates (part 2) - firsts steps towards new diagnostic and therapeutic tools.

**Exploitation of mycobacterial adhesion characteristics to improve detection of *Mycobacterium tuberculosis***



## 2 Exploitation of mycobacterial adhesion characteristics to improve detection of *Mycobacterium tuberculosis*

The concentration of mycobacteria in patient specimen is a limiting factor in Tb diagnostics. The first part of the thesis focuses on enrichment of mycobacteria from solution.

### 2.1 Introduction

Low bacteria numbers contribute to false negative results from sputum samples.<sup>150</sup> In addition an alternative patient specimen, such as saliva, was excluded for diagnostics, because it contains even lower amounts of mycobacteria compared to the commonly used sputum.<sup>151</sup> Sputum, however, has several disadvantages. Children and cachectic patients usually cannot cough up enough phlegm to allow laboratory evaluations. Furthermore, children tend to swallow the specimen rather than expectorate it. In order to enrich samples, sputum induction, where a child inhales a saline solution to help them cough up sputum, and gastric or nasopharyngeal aspiration, where a tube is inserted into the stomach or nose to suction out a sputum sample, are applied.<sup>152–154</sup> These procedures are very unpleasant and may also require hospitalization and trained personnel, which can be hard to come by in resource-limited settings. Saliva might represent a good alternative, because of its easy accessibility. Recent visualization of Mtb bacteria in saliva using auramine rhodamine as staining method instead of the common Ziehl-Neelsen stain underlines the potency of saliva as an alternative biological sample for diagnosis.<sup>155,156</sup> Detection of Mtb bacteria in saliva by PCR is also possible as recently proven.<sup>157</sup> Although Mtb bacteria were detected in saliva, development of diagnostic tests based on oral samples remained unsuccessful due to the low bacteria numbers.<sup>158,159</sup> Thus, mycobacteria enrichment is necessary to increase the detection rate.

The development of a new tool to capture Mtb bacteria from solution might enable to use saliva as an alternative specimen for detection of Mtb. Therefore, a ligand, which binds Mtb bacteria with high efficiency, has to be identified. Previously surfaces functionalized with peptides, proteins or antibodies have been used to capture mycobacteria with high specificity.<sup>160–165</sup> However, such ligands are quite susceptible to proteolytic degradation and denaturation and are too expensive for extensive use. A more promising approach was published 2010 by Microsens Medtech Ltd.<sup>166</sup> The “Tb-Beads” are paramagnetic beads coated with the hydrophobic poly-diallyldimethyl ammonium chloride (pDADMAC). The “Tb-Beads” are applied to capture Mtb bacteria from sputum facilitating existing laboratory practice, such as microscopy and cultivation.<sup>167,168</sup> In addition to hydrophobic interactions, diagnostic tools can be based on carbohydrate-lectin interactions. Recently, magnetic nanobeads coated with the mannose-binding lectin (MBL) were used to clean blood from

pathogens, an extracorporeal device for sepsis therapy.<sup>169</sup> Furthermore, beads functionalized with carbohydrate derivatives were used as ligands for microbial lectins leading to bacteria detection in water, food, urine or even saliva.<sup>170–173</sup> Carbohydrate derivatives and lipid-based ligands are cheaper to produce and more stable than proteins and antibodies. Thus, they represent good ligands to develop a new diagnostic tool. While the use of hydrophobic ligands to capture Mtb bacteria is based on the high hydrophobicity of the mycobacterial cell envelope, carbohydrate derivatives are targeted on mycobacterial lectins, which are rarely studied. Previous results indicate that mycobacteria contain lectins, which recognize carbohydrate structures of the Mtb cell envelope and are involved in mycobacterial aggregation. A lectin specific for the rare arabinofuranoside was suggested.<sup>147</sup> Only a limited number of D-trehalose- or D-arabinofuranoside-specific lectins are described in other organisms to date.<sup>114,174–176</sup> Thus, capture of Mtb bacteria with derivatives of the unique trehalose or arabinofuranoside might allow to preferentially enrich mycobacteria from patient specimen.

## 2.2 Objectives

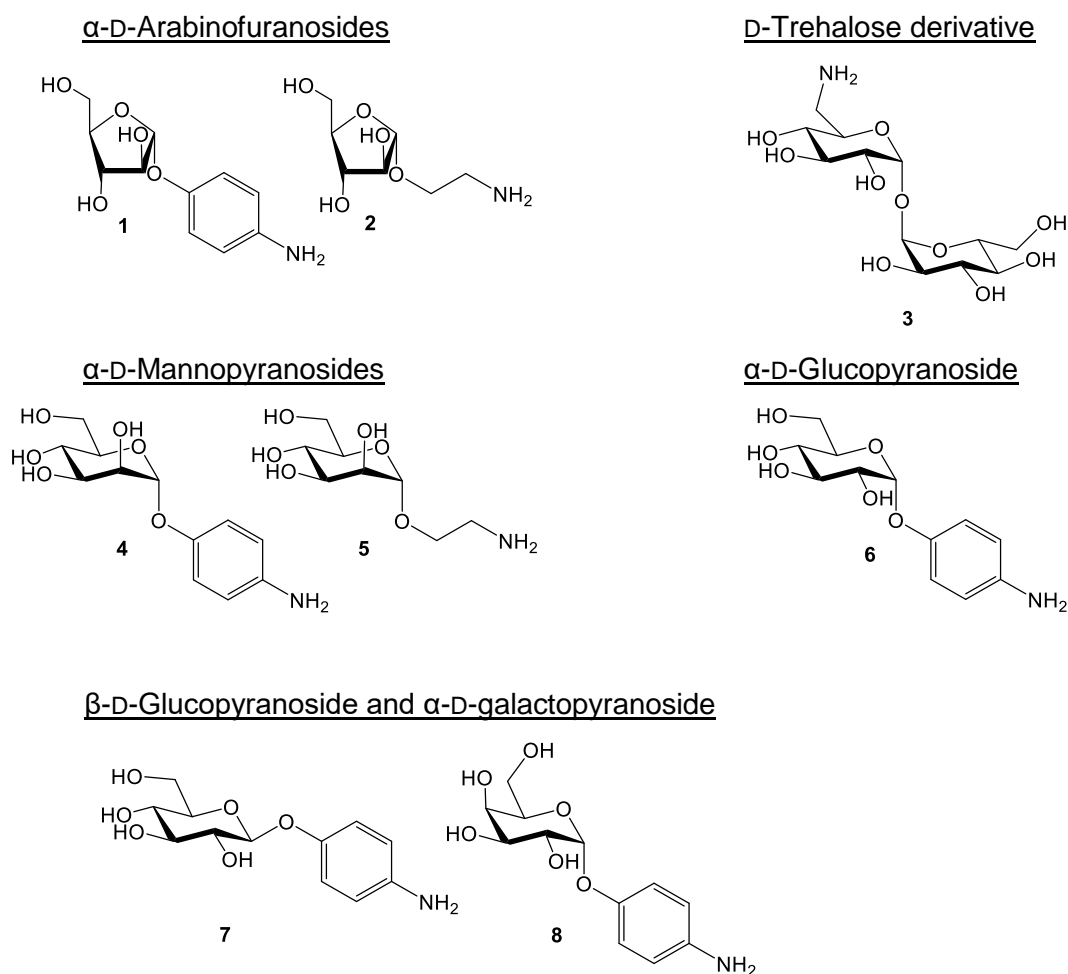
In order to develop a new tool to enrich Mtb bacteria from solution, adhesion characteristics of mycobacteria have to be analyzed. In the current study different carbohydrate derivatives and lipid ligands were chosen as potential ligands to bind Mtb bacteria. The molecules were immobilized on microtiter plates and magnetic beads. Adhesion of mycobacteria to the functionalized surfaces was studied to address the following questions:

1. Do Mtb bacteria have carbohydrate-specific adhesion characteristics?
2. Can carbohydrates be applied to capture Mtb bacteria from solution?
3. Can ligands with a hydrophobic moiety be applied to capture Mtb bacteria from solution?

The adhesion studies might prospectively contribute to the development of a mouth rinse or chewing gum to enrich and diagnose Mtb from easy accessible saliva as envisaged in the project “Development of a sorbent chewing gum for the detection of pulmonary tuberculosis”. This project was supported by a grant of the VolkswagenStiftung given to Dr. Christian Herzmann of the Research Center Borstel, Germany.

## 2.3 Results

Prior to the analysis of the adhesion characteristics of mycobacteria suitable ligands (Figure 15) had to be synthesized. Different carbohydrate derivatives were synthesized based on the sugar constituents of the mycobacterial lipoglycans LM and ManLAM ( $\alpha$ -D-arabinofuranosides,  $\alpha$ -D-mannopyranosides), glycolipids TMM and TDM (trehalose) and the polysaccharide  $\alpha$ -glucan ( $\alpha$ -D-glucopyranoside). Lectins recognizing these carbohydrates might be involved in mycobacterial aggregation.  $\alpha$ -D-Mannopyranosides and  $\alpha$ -D-glucopyranosides are also present in the glycocalyx of host cells. Therefore, lectins recognizing these two glycosides might also be involved in adhesion of mycobacteria to host cells. Additional glycoside derivatives based on host carbohydrates<sup>177</sup> ( $\alpha$ -D-galactopyranoside,  $\beta$ -D-glucopyranoside) were synthesized to further address host-pathogen interactions and to study the influence of the configuration of the hydroxyl groups at the sugar ring and of the glycosidic linkage on mycobacterial adhesion.

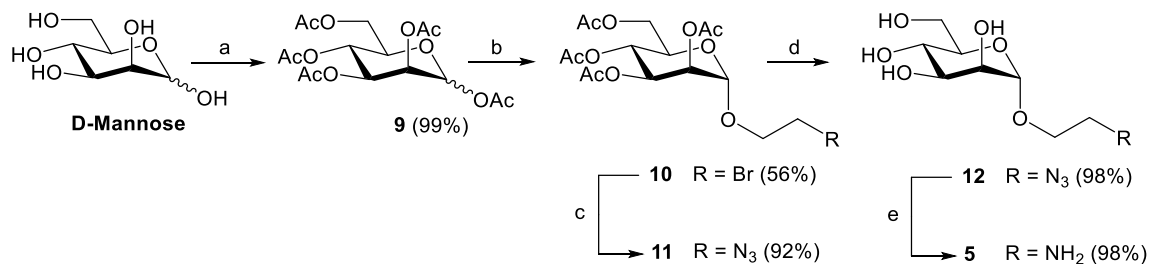


**Figure 15.** Chemical structures of the synthesized carbohydrate derivatives, which were used to study the adhesion characteristics of mycobacteria.

The nature of the aglycon of the glycoside ligands may further affect the strength of the glycoside-lectin interaction. As previously shown for many lectins, such as the fimbrial lectin FimH of *Escherichia coli* (*E. coli*),<sup>178,179</sup> aromatic aglycons contribute to a stronger adhesion of the glycoside to the lectin. This increased adhesion is based on the structure of the lectin containing aromatic amino acids near the carbohydrate binding side. Since no crystal structure of any membranous mycobacterial lectin is analyzed to date, an optimal aglycon could not be predicted. Thus, the arabinosides **1** and **2** and the mannosides **4** and **5** with aliphatic and aromatic aglycons, respectively, were synthesized. All synthesized sugar derivatives contained an amino group, which enabled covalent immobilization of the respective ligands on microtiter plates or magnetic beads. Functionalization of the surfaces with the carbohydrate derivatives **1-8** could be achieved for instance via amide coupling. In all glycosides the amino group was part of the aglycon leaving the carbohydrate unaffected by the immobilization process. In the case of the trehalose derivative **3** one primary hydroxyl group was replaced by an amino group due to the fact that in the mycobacterial cell envelope trehalose is a constituent of TMM and TDM. These glycolipids are trehalose derivatives, which are esterified with mycolic acids at one or at both primary hydroxyl groups of the disaccharide. Thus, lectins recognizing TMM or TDM might most likely tolerate functionalization at the 6-position of trehalose.

### 2.3.1 Syntheses

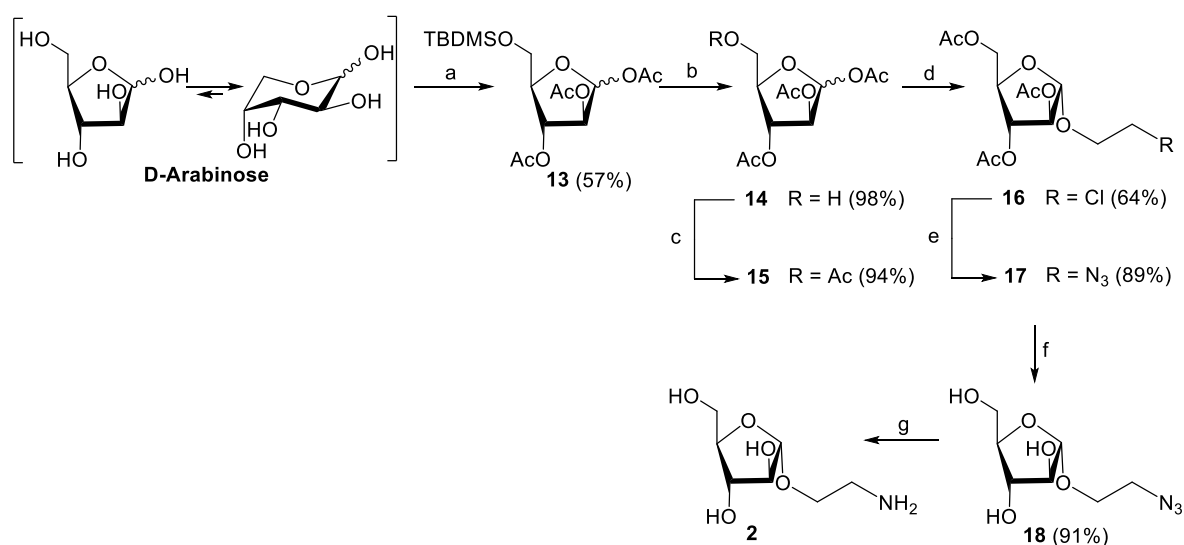
In analogy to the carbohydrate constituents of ManLAM, present in the Mtb cell envelope, (2-aminoethyl)  $\alpha$ -D-mannopyranoside (**5**)<sup>180</sup> and (2-aminoethyl)  $\alpha$ -D-arabinofuranoside (**2**) were synthesized. D-Mannose was acetylated<sup>181</sup> and subsequently functionalized at the anomeric position mediated by the Lewis acid boron trifluoride ( $\text{BF}_3$ ) giving the  $\alpha$ -glycoside **10** in 56% yield.<sup>182</sup> The bromoethyl mannoside **10** was converted into the iodoethyl derivative as an intermediate. Iodine represents a better leaving group for the following nucleophilic substitution with sodium azide leading to the glycoside **11**.<sup>180</sup> This acetylated azidoethyl mannoside was deprotected according to Zemplén's method.<sup>183</sup> The desired product **5** was received by palladium-catalyzed reduction (Scheme 1).<sup>180</sup>



**Scheme 1. Synthesis of the mannopyranoside 5.** a) NaOAc, Ac<sub>2</sub>O, reflux, 1 h, 99%; b) HOEtBr, BF<sub>3</sub>·Et<sub>2</sub>O, DCM, ice-cooling, 30 min → rt, overnight, 56%; c) NaN<sub>3</sub>, TBAI, DMF, 70°C, 8 h → rt, overnight, 92%; d) NaOMe, MeOH, rt, overnight, 98%; e) H<sub>2</sub>, Pd/C, MeOH, rt, overnight, 98%.



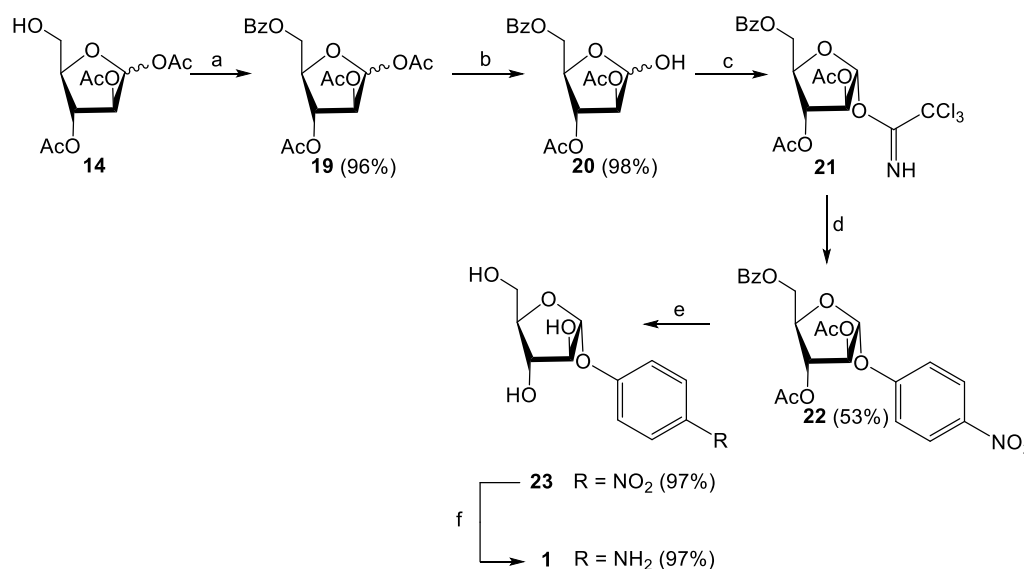
The arabinose derivative **2** was synthesized similarly to the mannopyranoside **5**. D-Arabinose, which was used as starting material, is present in two isomeric forms, as D-arabinopyranose (Arap) and D-arabinofuranose (Araf). To avoid pyranosides, previous fixation of the sugar in its furanose form was required. Therefore, D-arabinose was reacted with *tert*-butyl-dimethylsilyl chloride (TBDMSCl), which due to its steric hindrance selectively protects primary hydroxyl groups, only present in the furanose form. After fixation of the furanose isomer, unprotected secondary hydroxyl groups were acetylated giving the product **13** in 57% yield.<sup>184</sup> Under acidic conditions TBDMS was removed and the primary hydroxyl group was also acetylated. The tetraacetate **15**<sup>185</sup> was used as a glycosyl donor and was converted with 2-chloroethanol catalyzed by tin tetrachloride (SnCl<sub>4</sub>) to give the  $\alpha$ -glycoside **16** in 64% yield.<sup>186</sup> Separation of the anomers could only be accomplished by column chromatography using a solvent composition of n-hexane and ethyl acetate, mixtures of cyclohexane/ethyl acetate and methylene chloride/methanol were ineffective. Subsequently, nucleophilic substitution with sodium azide gave the glycoside **17** in 89% yield.<sup>186</sup> Deacetylation followed by azide reduction resulted in the desired aminoethyl derivative **2**. This amino sugar was not stable enough to store probably forming a cyclic amine, thus it was directly used without further characterization (Scheme 2).



**Scheme 2. Synthesis of the arabinofuranoside 2.** a) TBDMSCl, pyridine, rt, 4 h, Ac<sub>2</sub>O, rt, overnight, 57%; b) HOAc/dH<sub>2</sub>O, rt, overnight, 98%; c) Ac<sub>2</sub>O, pyridine, rt, overnight, 94%; d) SnCl<sub>4</sub>, acetonitrile, rt, 30 min, HOEtCl, rt, 45 min, 64%; e) NaN<sub>3</sub>, TBAI, DMF, 70°C, 7 h → rt, overnight, 89%; f) NaOMe, MeOH, rt, overnight; 91% g) H<sub>2</sub>, Pd/C, MeOH, rt, 2.5 h.

Beside glycosides with aliphatic aglycons, carbohydrates carrying aromatic aglycons were synthesized. While the *p*-aminophenyl mannoside **4**<sup>187</sup> was directly obtained by palladium-catalyzed reduction of the commercial available nitrophenyl derivative, *p*-aminophenyl  $\alpha$ -D-arabinofuranoside (**1**) was synthesized with D-arabinose as starting material. As

mentioned before the C-5-deprotected arabinofuranose **14**<sup>188</sup> was received in two synthetic steps (Scheme 2). Subsequently, the primary hydroxyl group was protected with benzoylchloride under basic conditions resulting in the arabinofuranose derivative **19**. Anomeric deprotection was carried out by synthesizing the classical glycosyl donor of the Koenigs Knorr reaction,<sup>189</sup> a glycosyl bromide, which was immediately converted to the reducing sugar **20** due to its high reactivity even with low quantities of water. Reaction of **20** with trichloroacetonitrile and 1,8-diazabicycloundec-7-ene (DBU) as a base yielded the arabinofuranosyl trichloroacetimidate **21**, which was directly employed for glycosylation of *p*-nitrophenol, because of its low stability. *p*-Nitrophenyl  $\alpha$ -D-arabinofuranoside **22** was obtained over two steps from the reducing sugar **20** in 53% yield. The arabinofuranoside **22** was deprotected according to Zemplén's method<sup>183</sup> and reduced with hydrogen catalyzed by palladium giving the product **1** (Scheme 3).

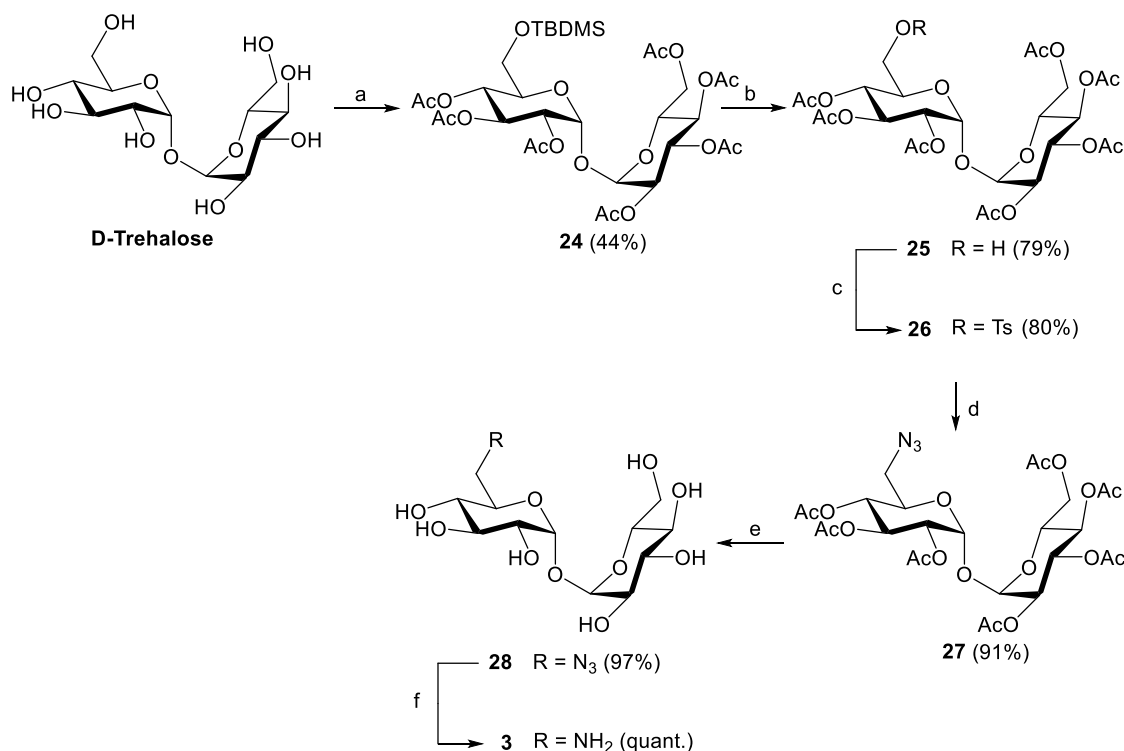


**Scheme 3. Synthesis of the arabinofuranoside 1.** a) BzCl, pyridine, rt, overnight, 96%; b) HBr, Ac<sub>2</sub>O, DCM, ice cooling, 30 min → rt, overnight, dH<sub>2</sub>O, 98%; c,d) Cl<sub>3</sub>CN, DBU, DCM, ice cooling, 15 min; pNO<sub>2</sub>PhOH, BF<sub>3</sub>·Et<sub>2</sub>O, DCM, ice cooling, 30 min → rt, overnight, 53%; e) NaOMe, MeOH, rt, overnight, 97%; f) H<sub>2</sub>, Pd/C, MeOH, rt, 3 h.

Beside the arabinose and mannose derivatives **1**, **2**, **4**<sup>187</sup> and **5**<sup>180</sup> the glucosides **6** and **7** and the galactoside **8** with *p*-aminophenyl as aglycon were synthesized. Derivatives of those carbohydrates address mainly bacteria-host interactions instead of adhesion among mycobacteria. All three compounds were directly obtained by palladium-catalyzed reduction of the respective commercially available nitrophenyl glycosides.

Another important carbohydrate, solely found in mycobacterial cell envelopes, is trehalose. The trehalose mycolic acid ester TDM is also named cord factor and was previously related to the cording process of Mtb.<sup>190</sup> Although nowadays it is assumed that the presence of

cyclopropane rings in mycolic acids is responsible for the cord-like appearance of Mtb bacteria,<sup>191</sup> trehalose might also be involved in adhesion processes between mycobacteria. To analyze whether mycobacteria have trehalose-specific adhesion characteristics, amino trehalose **3** was synthesized.  $\alpha,\alpha$ -D-Trehalose was protected with TBDMSCl and acetic anhydride under basic conditions resulting in the desired product **24** containing one TBDMS group (44%) and the byproducts, where none or both primary hydroxyl groups were functionalized with bulky silyl ethers.<sup>192</sup> TBDMS was removed under acidic conditions.<sup>192</sup> The unprotected hydroxyl group of the trehalose derivative **25** was activated by tosylation, followed by a nucleophilic substitution with sodium azide. Azido trehalose **27**<sup>193,194</sup> was deprotected using sodium methoxide and subsequently reduced giving the trehalose derivative **3** in 97% yield over the final two steps (Scheme 4).<sup>195</sup>



**Scheme 4. Synthesis of the trehalose derivative 3.** a) 1. TBDMSCl, pyridine, ice cooling  $\rightarrow$  rt, overnight; 2. Ac<sub>2</sub>O, rt, 6 h, 44%; b) DMF/dH<sub>2</sub>O/AcOH: 1:1:4, rt, overnight, 79%; c) TsCl, pyridine, rt, overnight, 80%; d) NaN<sub>3</sub>, DMF, 80°C, 6 h, 91%; e) NaOMe, MeOH, rt, overnight, 97%; f) H<sub>2</sub>, Pd/C, MeOH, rt, 3 h, quant.

### Results 2.3.1: Summary

- The carbohydrate derivatives **2-8** were synthesized according to literature including minor synthetic modifications.
- *p*-Aminophenyl  $\alpha$ -D-arabinofuranoside (**1**) was synthesized as a new compound.
- All final products contained an amino group facilitating immobilization on microtiter plates or magnetic beads.

### 2.3.2 Mycobacterial adhesion assay

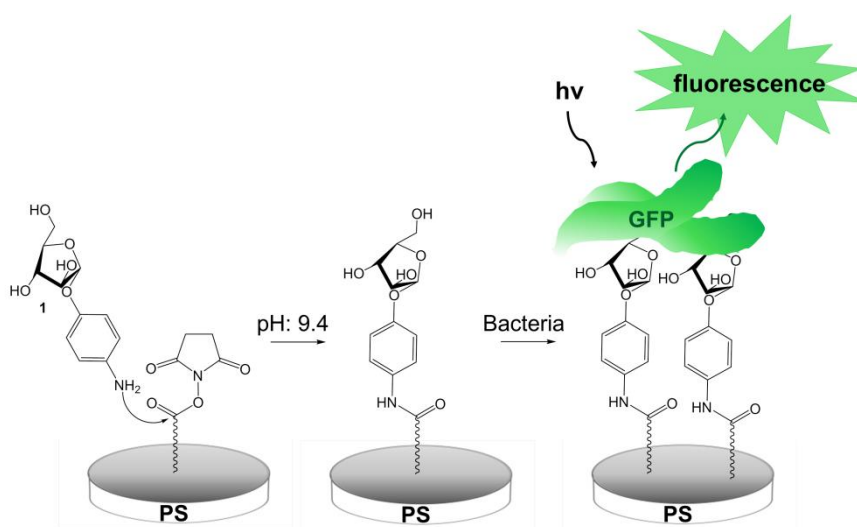
An adhesion assay on microtiter plates was established in order to study mycobacterial adhesion to the synthesized carbohydrate derivatives.

#### Immobilization of the synthesized carbohydrate derivatives on microtiter plates

Initially the ligands were immobilized on microtiter plates. All sugar derivatives contained an amino group, which enabled functionalization of Nunc Immobilizer Amino 96 well microtiter plates under basic conditions. The reactive groups on the surface of the microtiter plates are not declared by the company. However, it can be assumed that epoxides, isothiocyanates or, even more likely, active esters, as depicted in Figure 16, are present. The functionalization method applied is commonly used in the Lindhorst group to study adhesion characteristics of *E. coli*, as previously published.<sup>196</sup> Therefore, no further control experiments demonstrating successful immobilization were implemented.

#### Adhesion assay

Serially diluted concentrations of GFP-expressing mycobacteria, with  $4 \cdot 10^8$  bacteria/ml as the highest and  $2 \cdot 10^5$  bacteria/ml as the lowest concentration, were incubated in functionalized microtiter plates for one hour at  $37^\circ\text{C}$  while gently shaking. After two washing steps the adhered bacteria were detected using a fluorescence reader (Figure 16).



**Figure 16. Illustration of the microtiter plate-based adhesion assay.** The synthesized carbohydrate derivatives were immobilized via the amino group. GFP-expressing mycobacteria were added to the functionalized surfaces and adhered bacteria were detected by fluorescence-based read-out systems.

#### Data analysis

In all adhesion assays the mannoside **4** was used as a reference substance. Differences between fluorescence intensity of adhered bacteria to functionalized wells and fluorescence intensity of adhered bacteria to non-modified wells are depicted in the graphs (Figure 17-21). Data are normalized with measured relative fluorescence intensity 125 000 set as 100.

### 2.3.3 Adhesion characteristics of *M. bovis* *Bacillus Calmette-Guérin* bacteria

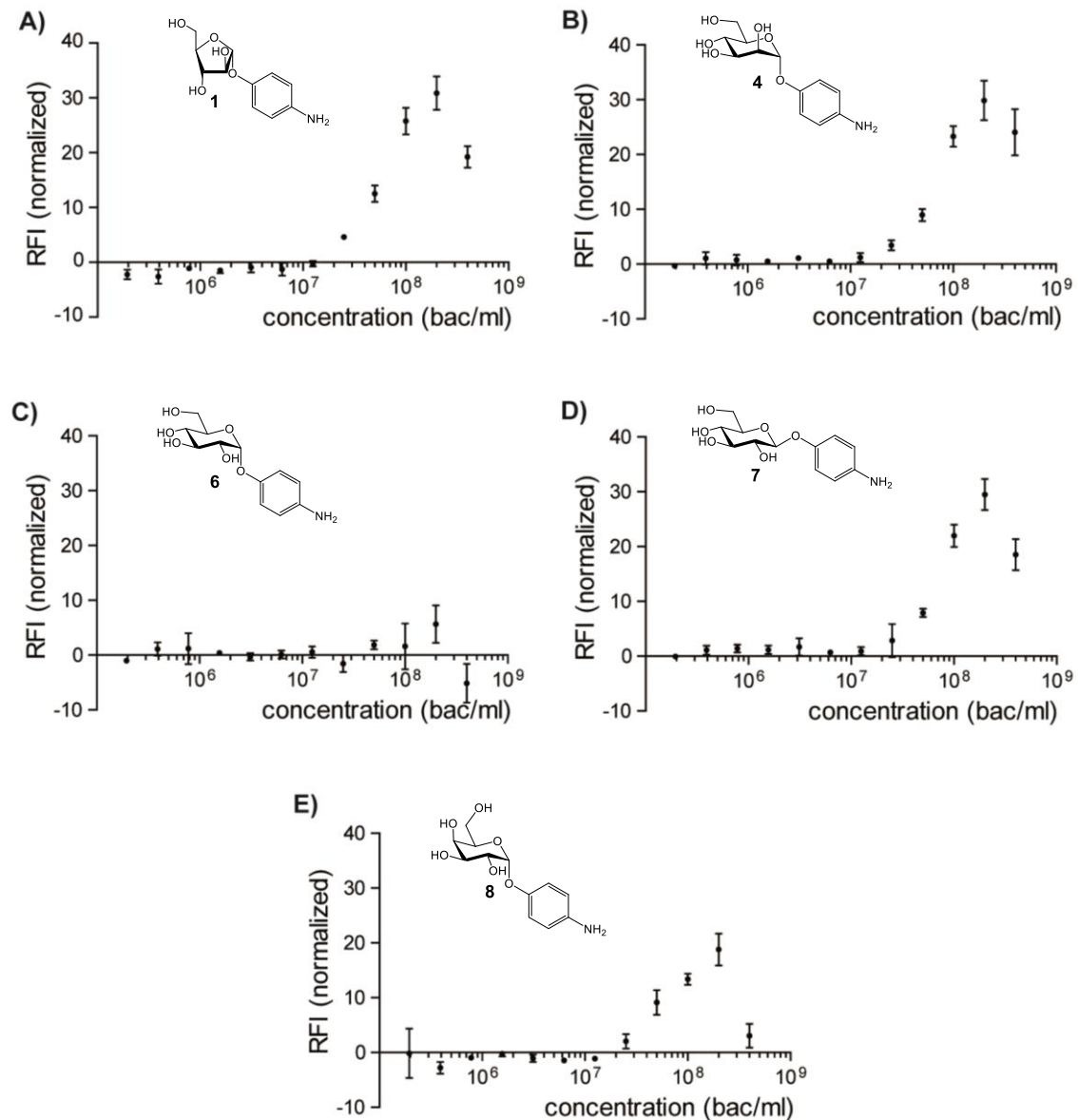
First adhesion assays were carried out using *M. bovis* *Bacillus Calmette-Guérin* (BCG) bacteria. *M. bovis* BCG is a Tb vaccine strain derived from an attenuated *M. bovis* strain by subculturing.<sup>1,197</sup> Here it is used as an avirulent mycobacterial model system simplifying the establishment of an adhesion assay for mycobacteria.

#### Adhesion of *M. bovis* BCG bacteria to sugar derivatives containing an aromatic aglycon

The synthesized and immobilized glycosides **1**, **4**, **6**, **7** and **8** with aromatic aglycons were tested regarding their potency to bind *M. bovis* BCG bacteria (Figure 17) using the adhesion assay in microtiter plates, as described before.

Incubation with *M. bovis* BCG bacteria resulted in an enhanced fluorescence intensity in wells functionalized with the  $\alpha$ -glycosides **1**, **4** and **8**, respectively, or the  $\beta$ -glycoside **7** compared to non-modified wells at a concentration of  $2 \cdot 10^7$  bacteria/ml. Wells functionalized with the  $\alpha$ -arabinofuranoside **1**, the  $\alpha$ -mannopyranoside **4** or the  $\beta$ -glucopyranoside **7** showed stronger signals than wells functionalized with the  $\alpha$ -galactopyranoside **8** after incubation with mycobacteria. The fluorescence intensities in wells functionalized with the glycosides **1**, **4** or **7** were 1.5fold higher (Figure 17 A, B and D) compared to the galactoside **8** (Figure 17 E) at a concentration of  $2 \cdot 10^8$  bacteria/ml. In all cases an increase of the bacteria concentration, up to  $2 \cdot 10^8$  bacteria/ml, was in line with an increase of fluorescence intensity. At the highest *M. bovis* BCG concentration ( $4 \cdot 10^8$  bacteria/ml) a lower fluorescence intensity was measured compared to the second highest bacteria concentration. Supplementation of *M. bovis* BCG bacteria to wells functionalized with the  $\alpha$ -glucopyranoside **6** led to similar fluorescence intensities as measured for non-modified surfaces (Figure 17 C).

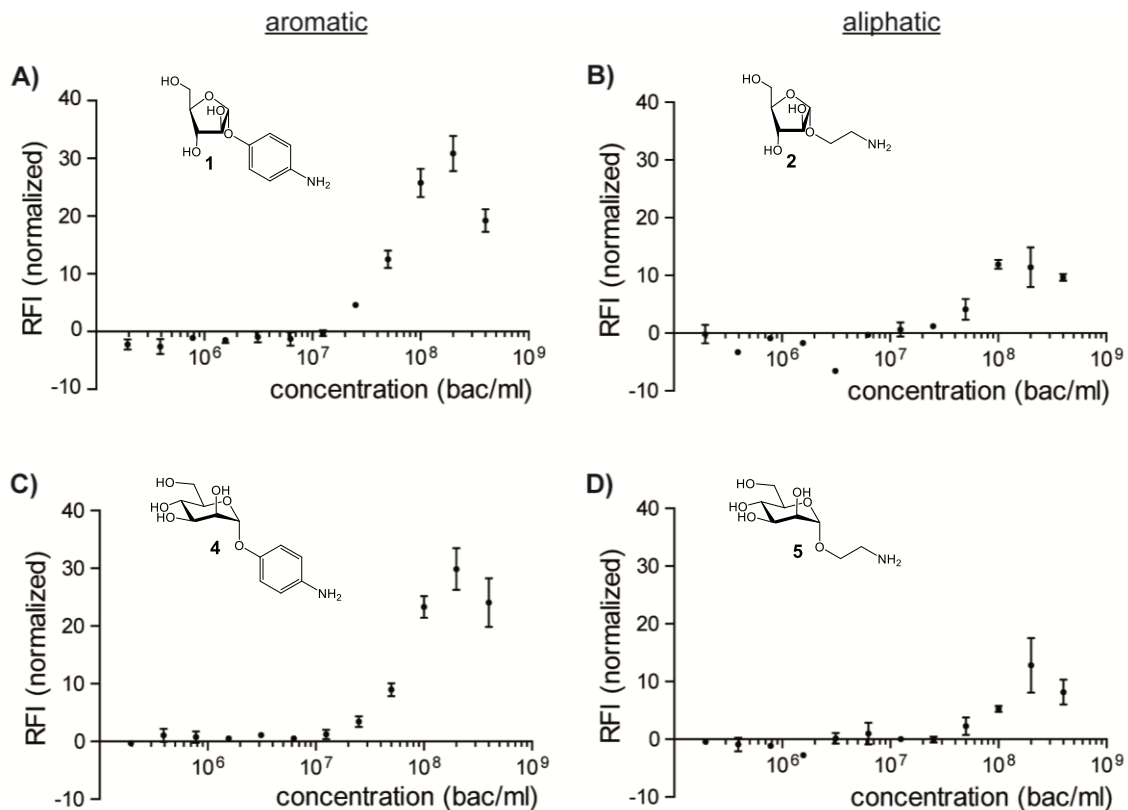
Since fluorescence signals correlate with adhered bacteria, the results indicate that *M. bovis* BCG bacteria have carbohydrate-dependent adhesion characteristics. *M. bovis* BCG bacteria adhered to surfaces functionalized with the  $\alpha$ -arabinofuranoside **1**, the  $\alpha$ -mannopyranoside **4**, the  $\beta$ -glucopyranoside **7** or the  $\alpha$ -galactopyranoside **8**. Mycobacterial adhesion is influenced by the configuration of the hydroxyl groups at the sugar ring and also by the configuration of the anomeric linkage of the aglycon.



**Figure 17. Adhesion of *M. bovis* BCG bacteria to surfaces functionalized with carbohydrate derivatives, which contain an aromatic aglycon.** Microtiter plates were functionalized with the carbohydrate derivatives 1, 4, 6, 7 and 8. Serially diluted suspensions of GFP-expressing *M. bovis* BCG bacteria ( $4 \cdot 10^8$  bacteria/ml  $\rightarrow$   $2 \cdot 10^5$  bacteria/ml) were incubated for 1 h,  $37^\circ\text{C}$ , gentle agitation. Adhered bacteria were detected using a fluorescence reader. Data represent differences between fluorescence intensity of adhered bacteria to functionalized wells and fluorescence intensity of adhered bacteria to non-modified wells; three technical replicates (+/- SD); one of at least two independent experiments shown; relative fluorescence intensity normalized with measured relative fluorescence intensity of  $125\,000 = 100$ . (RFI: relative fluorescence intensity).

### Adhesion of *M. bovis* BCG bacteria to sugar derivatives containing an aliphatic aglycon

Beside the glycon moiety of a glycoside its aglycon might be involved in interactions with mycobacterial lectins. To address this question mannopyranosides and arabinofuranosides containing aromatic and aliphatic aglycons, respectively, were tested. Microtiter plates were modified with the glycosides **1**, **2**, **4** and **5** and applied for mycobacterial adhesion assays (Figure 18).



**Figure 18. Adhesion of *M. bovis* BCG bacteria to surfaces functionalized with carbohydrate derivatives, which contain aromatic and aliphatic aglycons, respectively.** Microtiter plates were functionalized with the carbohydrates derivatives **1** and **4**, which contain aromatic aglycons, and the glycosides **2** and **5** with aliphatic aglycons. Serially diluted suspensions of GFP-expressing *M. bovis* BCG bacteria ( $4 \cdot 10^8$  bacteria/ml  $\rightarrow$   $2 \cdot 10^5$  bacteria/ml) were incubated for 1 h,  $37^\circ\text{C}$ , gentle agitation. Adhered bacteria were detected using a fluorescence reader. Data represent differences between fluorescence intensity of adhered bacteria to functionalized wells and fluorescence intensity of adhered bacteria to non-modified wells; three technical replicates ( $\pm$  SD); one of at least two independent experiments shown; relative fluorescence intensity normalized with measured relative fluorescence intensity of  $125\,000 = 100$ . (RFI: relative fluorescence intensity).

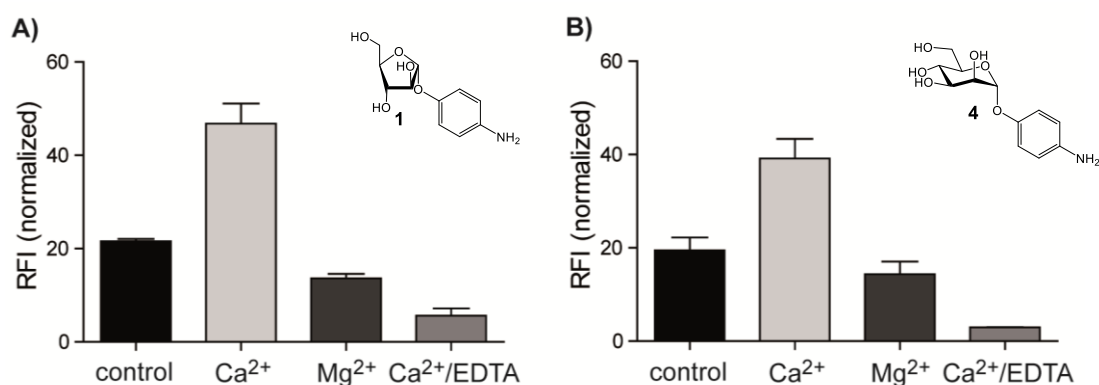
After incubation with *M. bovis* BCG bacteria enhanced fluorescence intensity was measured in wells functionalized with the glycosides **2** or **5** compared to non-modified wells at a concentration of  $5 \cdot 10^7$  bacteria/ml. Increased bacteria concentrations, up to  $2 \cdot 10^8$  bacteria/ml, were in line with an increase in fluorescence intensity. At the highest bacteria concentration ( $4 \cdot 10^8$  bacteria/ml) the fluorescence intensity was lower compared to the second highest

concentration ( $2 \cdot 10^8$  bacteria/ml) (Figure 18 B and D). The overall fluorescence in wells functionalized with the glycosides **2** or **5**, which have aliphatic aglycons, (Figure 18 B and D) was lower compared to wells modified with the derivatives **1** or **4** with aromatic aglycons (Figure 18 A and C). At a concentration of  $2 \cdot 10^8$  bacteria/ml the fluorescence signals derived from adhered bacteria were roughly three times more intense in the case of the derivatives **1** and **4**.

These results indicate that the adhesion of *M. bovis* BCG bacteria is influenced by the structure of the aglycon.

#### Ca<sup>2+</sup>-dependency of the adhesion of *M. bovis* BCG bacteria

Carbohydrate-lectin interactions can be influenced by calcium ions. Lectins, which show Ca<sup>2+</sup>-dependent binding efficiencies, are C-type lectins. Previous comparative genome analysis indicates that mycobacteria might express C-type lectins.<sup>149</sup> Thus, it was tested if Ca<sup>2+</sup> influences the adhesion of *M. bovis* BCG bacteria to surfaces functionalized with the arabinofuranoside **1** or the mannopyranoside **4**. GFP-expressing *M. bovis* BCG bacteria were incubated in functionalized microtiter plates in the presence or absence of Ca<sup>2+</sup>. Adhered bacteria were detected using a fluorescence reader. Normalized fluorescence at a mycobacteria concentration of  $4 \cdot 10^8$  bacteria/ml shown (Figure 19).



**Figure 19. Ca<sup>2+</sup>-dependency of *M. bovis* BCG adhesion.** Microtiter plates were functionalized with the glycosides **1** and **4**. GFP-expressing *M. bovis* BCG bacteria were incubated in functionalized microtiter plates in the presence or absence of Ca<sup>2+</sup> (5 mM), Mg<sup>2+</sup> (5 mM) or Ca<sup>2+</sup> (5 mM)/EDTA (15 mM) for 1 h, 37°C, gentle agitation. Adhered bacteria were detected using a fluorescence reader. Data represent differences between fluorescence intensity of adhered bacteria ( $4 \cdot 10^8$  bacteria/ml) to functionalized wells and fluorescence intensity of adhered bacteria ( $4 \cdot 10^8$  bacteria/ml) to non-modified wells; two technical replicates (+SD); one of at least two independent experiments shown; relative fluorescence intensity normalized with measured relative fluorescence intensity of 125 000 = 100. (RFI: relative fluorescence intensity).

In both cases, surfaces functionalized with the arabinofuranoside **1** (Figure 19 A) or the mannopyranoside **4** (Figure 19 B), Ca<sup>2+</sup> supplementation to the *M. bovis* BCG bacteria

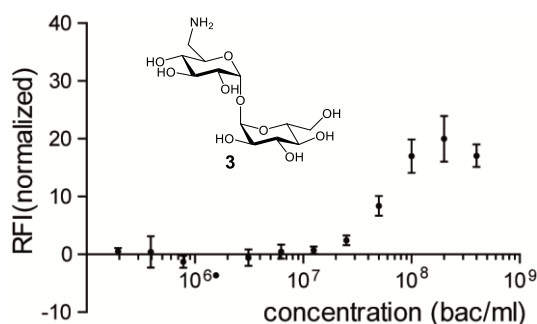


suspension resulted in two times higher fluorescence intensity compared to the untreated bacteria. In contrast addition of magnesium ions ( $Mg^{2+}$ ) had only minor effect on the fluorescence signal. Supplementation of  $Ca^{2+}$  and ethylenediaminetetraacetate (EDTA) led to no increased fluorescence intensity. In fact, the fluorescence signal was even lower compared to untreated bacteria.

These data suggest that the adhesion of *M. bovis* BCG bacteria to surfaces functionalized with the arabinofuranoside **1** or the mannopyranoside **4** is  $Ca^{2+}$ -dependent.

#### Adhesion of *M. bovis* BCG bacteria to the disaccharide trehalose

So far, monosaccharides were examined regarding their mycobacterial binding efficiency, but frequently di- or oligosaccharides represent the optimal ligands for lectins. A unique disaccharide of the mycobacterial cell envelope is trehalose. Beside its immunomodulative properties<sup>80</sup> it might also be involved in adhesion among mycobacteria. To address whether *M. bovis* BCG bacteria bind to the mycobacterial disaccharide trehalose, amino trehalose **3** was immobilized and incubated with GFP-expressing *M. bovis* BCG bacteria (Figure 20) as described before.



**Figure 20. Adhesion of *M. bovis* BCG bacteria to surfaces functionalized with the trehalose derivative 3.**

Microtiter plates were functionalized with the disaccharide **3**. Serially diluted suspensions of GFP-expressing *M. bovis* BCG bacteria ( $4 \cdot 10^8$  bacteria/ml  $\rightarrow$   $2 \cdot 10^5$  bacteria/ml) were incubated for 1 h, 37°C, gentle agitation. Adhered bacteria were detected using a fluorescence reader. Data represent differences between fluorescence intensity of adhered bacteria to functionalized wells and fluorescence intensity of adhered bacteria to non-modified wells; three technical replicates (+/- SD); one of two independent experiments shown; relative fluorescence intensity normalized with measured relative fluorescence intensity of  $125\,000 = 100$ . (RFI: relative fluorescence intensity).

Similar to the glycosides **1**, **4**, **7** and **8** (Figure 17) increased fluorescence intensity was detectable in wells functionalized with the trehalose derivative **3** at a concentration of  $2 \cdot 10^7$  bacteria/ml and the highest fluorescence intensity was measured at a concentration of  $2 \cdot 10^8$  bacteria/ml. At the highest bacteria concentration ( $4 \cdot 10^8$  bacteria/ml) the fluorescence intensity was lower than at the second highest concentration.

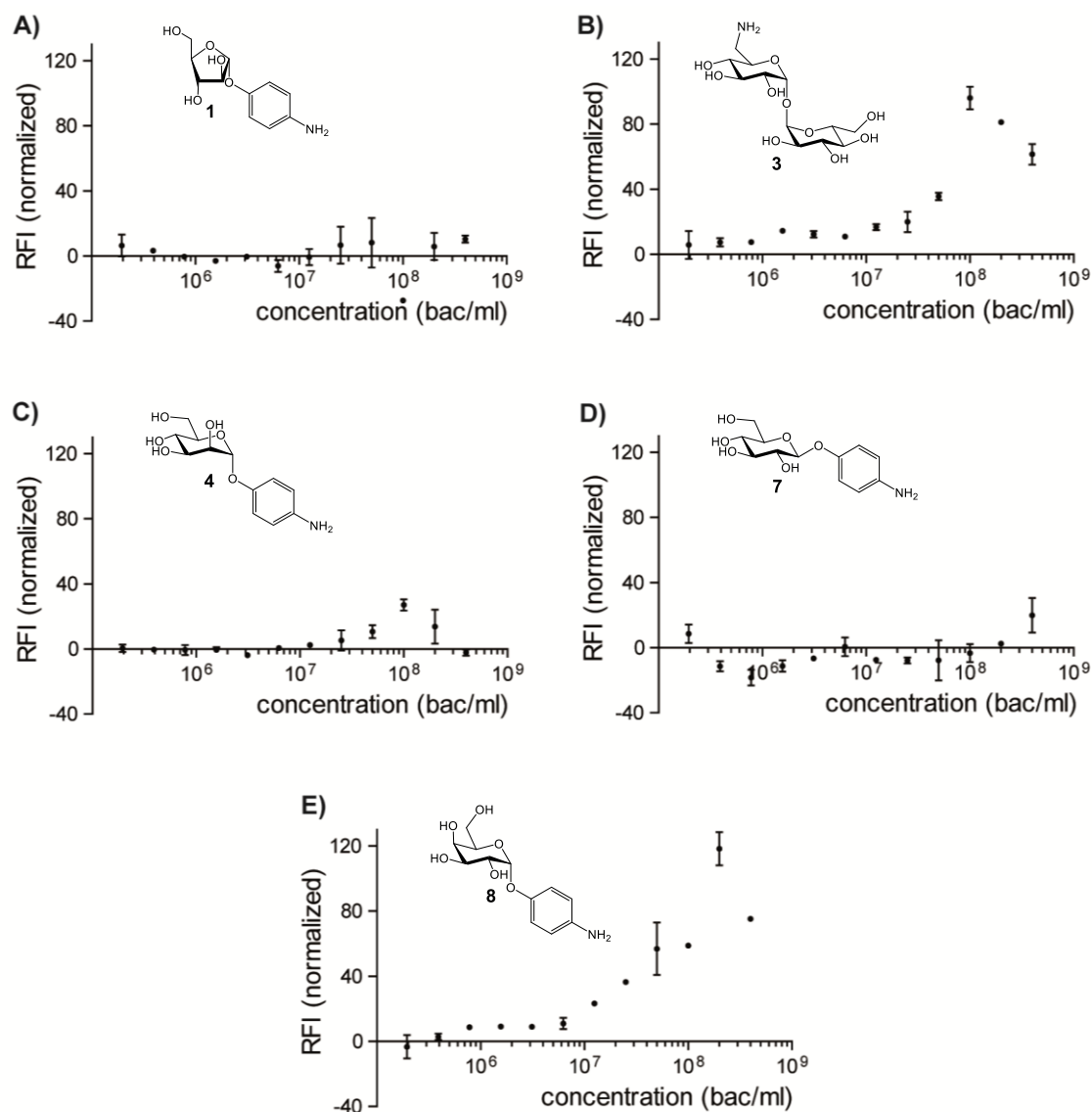
These results suggest trehalose-specific adhesion characteristics of *M. bovis* BCG bacteria.

**Results 2.3.3: Summary**

- A mycobacterial adhesion assay in microtiter plates was established using GFP-expressing *M. bovis* BCG bacteria.
- Carbohydrate-dependent adhesion of *M. bovis* BCG bacteria was detected.
- The arabinofuranoside **1**, the mannopyranoside **4** and the glucopyranoside **7** were the most potent glycosides of the tested ligands resulting in adhesion of *M. bovis* BCG bacteria.
- Adhesion of *M. bovis* BCG bacteria to surfaces functionalized with the arabinofuranoside **1** or the mannopyranoside **4** was Ca<sup>2+</sup>-dependent.

### 2.3.4 Adhesion characteristics of Mtb H37Rv bacteria

In the case of *M. bovis* BCG three different carbohydrate derivatives were identified as most potent ligands to bind mycobacteria: the arabinofuranoside **1**, the mannopyranoside **4** and the glucopyranoside **7**. Furthermore, the trehalose derivative **3** and the galactopyranoside **8** showed promising influence on the adhesion of *M. bovis* BCG bacteria (Figure 17 and Figure 20). These five compounds were further applied to investigate adhesion characteristics of the pathogenic Mtb strain H37Rv. Adhesion assays were carried out as described before for *M. bovis* BCG bacteria.



**Figure 21. Adhesion of Mtb H37Rv bacteria to surfaces functionalized with carbohydrate derivatives, which were identified as effective ligands for adhesion of *M. bovis* BCG bacteria.** Microtiter plates were functionalized with the carbohydrate derivatives **1**, **3**, **4**, **7** and **8**. Serially diluted suspensions of GFP-expressing Mtb H37Rv ( $4 \cdot 10^8$  bacteria/ml  $\rightarrow$   $2 \cdot 10^5$  bacteria/ml) were incubated for 1 h, 37°C, gentle agitation. Adhered bacteria were detected using a fluorescence reader. Data represent differences between fluorescence intensity of adhered bacteria to functionalized wells and fluorescence intensity of adhered bacteria to non-modified wells; two technical replicates (+/- SD); one of two independent experiments shown; relative fluorescence intensity normalized with measured relative fluorescence intensity of 125 000 = 100. (RFI: relative fluorescence intensity).

Incubation with Mtb H37Rv bacteria resulted in higher fluorescence intensities in wells functionalized with the carbohydrate derivatives **3**, **4** or **8** compared to non-modified wells (Figure 21). Surfaces functionalized with the glycoside **4** showed enhanced fluorescence signals at a concentration of  $5 \cdot 10^7$  bacteria/ml. Increase of the bacteria concentration was in line with an increase of fluorescence intensity. However, at high bacteria concentrations a fluorescence decrease was measured. In the case of the galactopyranoside **8** fluorescence derived from adhered mycobacteria increased at a concentration of  $5 \cdot 10^6$  bacteria/ml and reached a fluorescence maximum at  $2 \cdot 10^8$  bacteria/ml, which was almost nine times stronger compared to the mannopyranoside **4**. Functionalization with the trehalose derivative **3** resulted in detectable fluorescence signals at a concentration of  $1 \cdot 10^6$  bacteria/ml and led to as high fluorescence intensities as measured on surfaces functionalized with the derivative **8**, but already at a lower concentration ( $1 \cdot 10^8$  bacteria/ml). In both cases the fluorescence intensity increased with higher mycobacteria concentrations followed by a decrease at the highest concentrations. The overall fluorescence intensity detected in wells modified with the galactoside **8** or the trehalose derivative **3** was higher compared to fluorescence signals detected after incubation with *M. bovis* BCG bacteria (trehalose derivative **3**: 5.5fold at  $1 \cdot 10^8$  bacteria/ml; galactoside **8**: 6fold at  $2 \cdot 10^8$  bacteria/ml) (Figure 20; Figure 17).

These data indicate that Mtb H37Rv bacteria have carbohydrate-dependent adhesion characteristics. Binding intensities varied compared to *M. bovis* BCG bacteria. Most intense adhesion was detected on surfaces functionalized with the trehalose derivative **3** and the galactoside **8**. Therefore, these two compounds were identified as promising candidates to capture Mtb bacteria.

#### Results 2.3.4: Summary

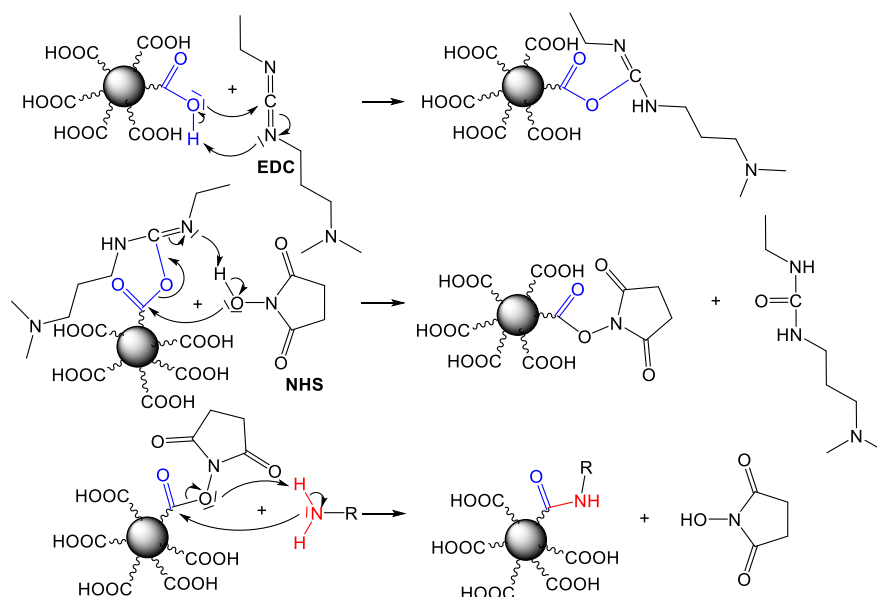
- Carbohydrate-dependent adhesion of the pathogenic Mtb strain H37Rv was detected.
- The trehalose derivative **3** and the galactopyranoside **8** were the most potent carbohydrate derivatives of the tested ligands resulting in adhesion of Mtb bacteria.
- Mtb H37Rv bacteria showed stronger adhesion to surfaces functionalized with the carbohydrate derivatives **3** and **8** compared to *M. bovis* BCG bacteria.

### 2.3.5 Capture of Mtb with beads functionalized with carbohydrate derivatives

To develop a diagnostic tool binding of Mtb bacteria has to work out not only in microtiter plates but also with a more applicable system. Here magnetic polyethylene glycol (PEG) beads, suitable for a mouth rinse, were used to capture Mtb bacteria from solution. The magnetic properties of the beads facilitate fast and easy extraction of the beads from solutions avoiding time consuming centrifugation. The pegylation of the beads is beneficial due to its bio-repulsive properties and prevents unspecific adhesion of mycobacteria. Thus, the detected adhesion is ligand-dependent, which is necessary in order to identify a new potential ligand to capture Mtb bacteria. Furthermore, carboxyl functional groups enable to easily immobilize amino-functionalized molecules on the bead surface.

#### Functionalization of the beads with the synthesized carbohydrate derivatives

Formally, a carboxylic acid can react with an amine forming an amide with the release of one equivalent of water. However, this nucleophilic substitution reaction competes with the acid-base reaction resulting in unreactive carboxylate and ammonium groups. To facilitate the formation of an amide the carboxyl group was converted to an active ester. Carbodiimides are widely used to activate carboxyl groups by the formation of highly reactive *O*-acylisourea intermediates. Here the water soluble 1-ethyl-3-(3-dimethylaminopropyl)-carbodiimide (EDC) was applied. To avoid undesirable side reactions of the *O*-acylisourea intermediates, *N*-hydroxysuccinimide (NHS) was added to form the more stable NHS ester derivative. NHS ester-activated beads were reacted with the primary amino groups of the synthesized ligands resulting in a covalent immobilization of the carbohydrate derivatives via amide bonds (Figure 22).

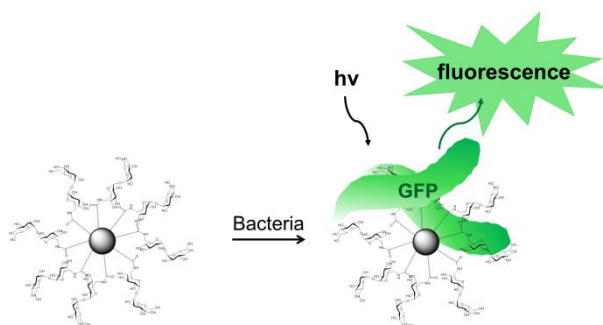


**Figure 22. Functionalization of magnetic PEG beads with the synthesized carbohydrate derivatives.**

Functionalization of the beads is based on EDC/NHS activation of the carboxyl groups forming NHS-esters. These active esters can react with amino groups of the synthesized carbohydrate derivatives leading to a covalent immobilization of the ligands by an amide bond. (R = carbohydrate derivatives)

### Bead-based adhesion assay

Functionalized beads ( $2 \cdot 10^7$  beads) were added to GFP-expressing Mtb H37Rv bacteria, which were suspended in PBS in desired concentrations. After incubation for one hour at 37°C while gently shaking beads were extracted and washed. Adhered bacteria were detected using a fluorescence reader (Figure 23).



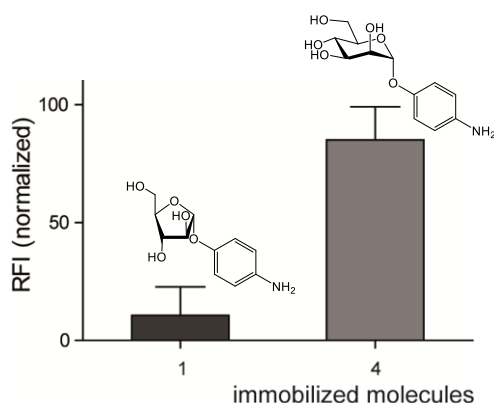
**Figure 23. Illustration of the bead-based adhesion assay.** GFP-expressing Mtb H37Rv bacteria were added to the functionalized beads. Subsequently, adhered bacteria were detected by a fluorescence-based read-out systems.

### Data analysis

In all adhesion assays the mannoside **4** was used as a reference substance. Normalized fluorescence intensity shown (auto-fluorescence of beads subtracted). Fluorescence intensity of non-modified beads, incubated with GFP-expressing Mtb H37Rv bacteria, shown in order to quantify the amount of unspecific adhesion.

### Verification of a successful bead functionalization

To verify bead functionalization, beads modified with the mannosopyranoside **4**, as positive control, and beads functionalized with the arabinofuranoside **1**, as a negative control, were incubated with Concanavalin A (ConA). ConA is a  $\alpha$ -mannoside and  $\alpha$ -glucoside specific lectin, originally extracted from the jack-bean *Canavalia ensiformis*.<sup>198</sup> The ConA applied carries fluorescein, which enables visualization of bound lectins. Functionalized beads were incubated with ConA. Bound ConA was detected using a fluorescence reader (Figure 24).



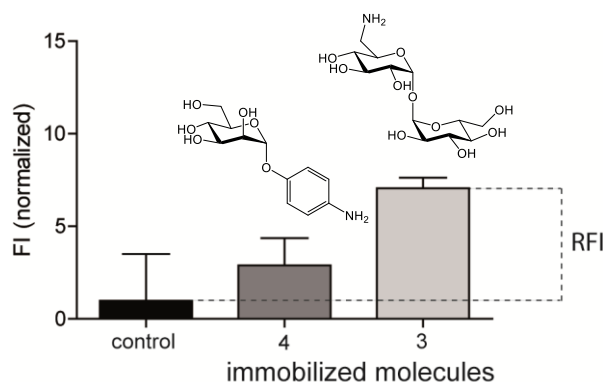
**Figure 24. Verifying bead functionalization using the lectin ConA.** Magnetic PEG beads were functionalized with the carbohydrate derivatives **1** and **4**. Beads were incubated with ConA-fluorescein (250  $\mu$ g/ml) for 1.5 h, rt, gentle agitation. Bound ConA was detected using a fluorescence reader. Data represent difference between fluorescence intensity of bound ConA to functionalized beads and fluorescence intensity of bound ConA to non-modified beads; three technical replicates (+SD); one of two independent experiments shown; fluorescence normalized with measured highest fluorescence of the derivative **4** = 100. (RFI: relative fluorescence intensity).

Beads functionalized with the mannopyranoside **4** showed an eight times stronger fluorescence intensity compared to beads functionalized with the arabinofuranoside **1**.

Fluorescence directly correlates with the amount of bound ConA. Since ConA specifically interacts with mannopyranosides, these results verify the presence of mannoses on the bead surface and thereby a successful functionalization of the PEG beads.

#### Adhesion of Mtb bacteria to magnetic PEG beads, which were functionalized with carbohydrate derivatives

In order to analyze whether beads functionalized with carbohydrate derivatives can be used to capture Mtb bacteria from solution, magnetic beads were modified with the carbohydrate derivatives **3** and **4**, respectively, and subsequently applied in the bead-based adhesion assay with GFP-expressing Mtb H37Rv bacteria (Figure 25).



**Figure 25. Adhesion characteristics of Mtb H37Rv bacteria to PEG beads functionalized with the carbohydrate derivatives 3 and 4.** Magnetic PEG beads were functionalized with the carbohydrate derivatives **3** and **4**. Functionalized and non-modified (control) beads were incubated with GFP-expressing Mtb H37Rv bacteria ( $1 \cdot 10^8$  bacteria/ml) for 1 h,  $37^\circ\text{C}$ , gentle agitation. Adhered bacteria were detected using a fluorescence reader. Data represent differences between fluorescence intensity of adhered bacteria ( $1 \cdot 10^8$  bacteria/ml) to functionalized beads and auto-fluorescence of non-modified beads (+SEM); duplicates of at least three independent experiments; fluorescence intensity normalized with measured fluorescence intensity of 125 000 = 100. (FI: fluorescence intensity).

Non-modified beads incubated with GFP-expressing Mtb H37Rv bacteria showed slightly increased fluorescence signals compared to beads, which were not incubated with mycobacteria. Addition of Mtb H37Rv bacteria to magnetic beads functionalized with carbohydrate derivatives, led to three times and seven times higher fluorescence intensities, respectively, compared to non-modified beads. Beads functionalized with the trehalose derivative **3** showed about two times higher fluorescence intensity after incubation with mycobacteria compared to beads functionalized with the mannopyranoside **4**. The fluorescence difference (RFI) between beads functionalized with the trehalose derivative **3** and

non-modified beads (control) was 14 times lower compared to the microtiter plate-based system at the same bacteria concentration ( $1 \cdot 10^8$  bacteria/ml).

These results indicate that beads functionalized with the carbohydrate derivatives **3** and **4**, respectively, can be used to capture Mtb bacteria from solution. However, the modified beads show lower binding efficiencies compared to microtiter plates, which were functionalized with the same carbohydrate derivatives.

#### **Results 2.3.5: Summary**

- Magnetic beads functionalized with the carbohydrate derivatives **3** and **4**, respectively, can be used to capture Mtb H37Rv bacteria from solution.
- Lower amounts of Mtb H37Rv bacteria adhered to the functionalized magnetic beads compared to the microtiter plate-based system.

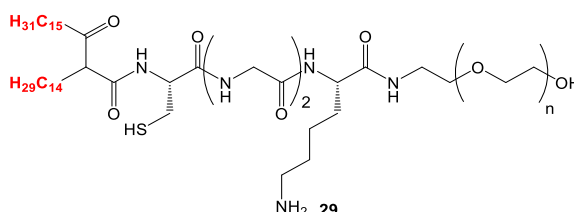


### 2.3.6 Adhesion of Mtb to magnetic PEG beads functionalized with lipid ligands

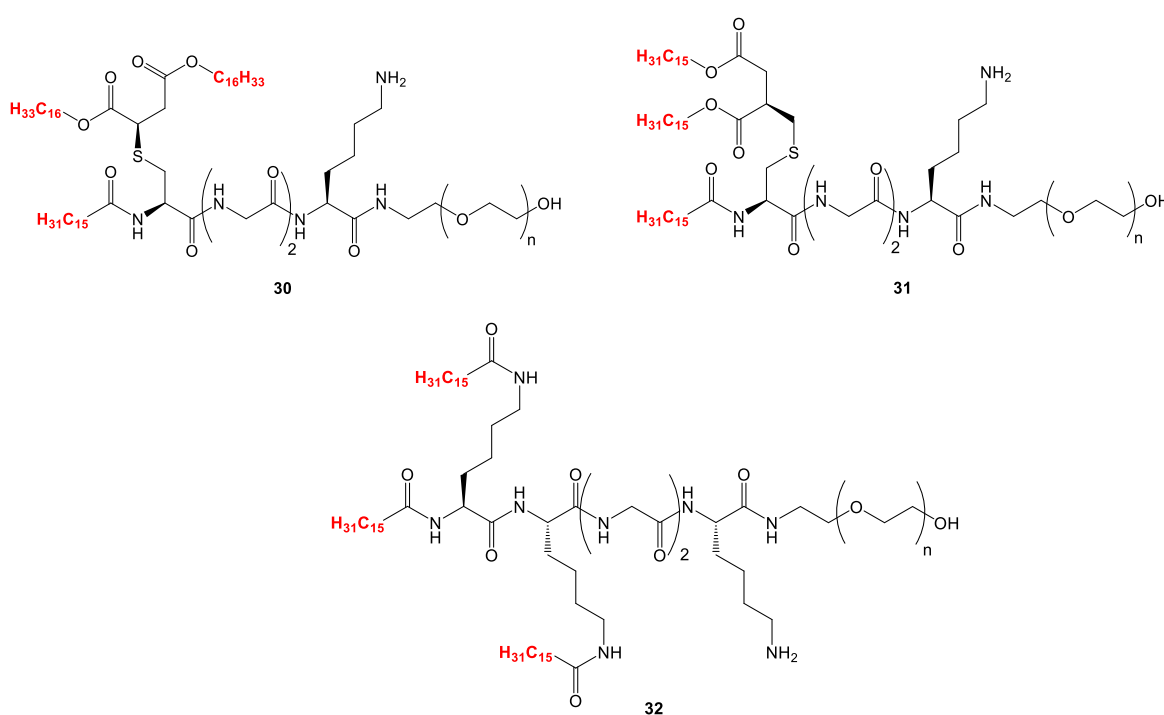
Beside carbohydrate derivatives, molecules with long chain alkyl groups were considered as appropriate ligands to capture Mtb bacteria from solution. Using hydrophobic ligands for mycobacteria enrichment is based on the high hydrophobicity of the Mtb cell envelope. Eight different ligands, containing two to eight alkyl chains (red), were obtained from Prof. Dr. Karl-Heinz Wiesmüller of the EMC Microcollections GmbH, Germany. Water solubility, necessary for surface functionalization, was either achieved by pegylation (ligand **29-35**) or positively charged lysines (ligand **36**). In addition, a TMM-analog derivative was synthesized by the group of Prof. Dr. Mark S. Baird from Bangor University, UK. This molecule combines both types of potential Mtb ligands, carbohydrate and fatty acid.

#### PEG-containing ligands

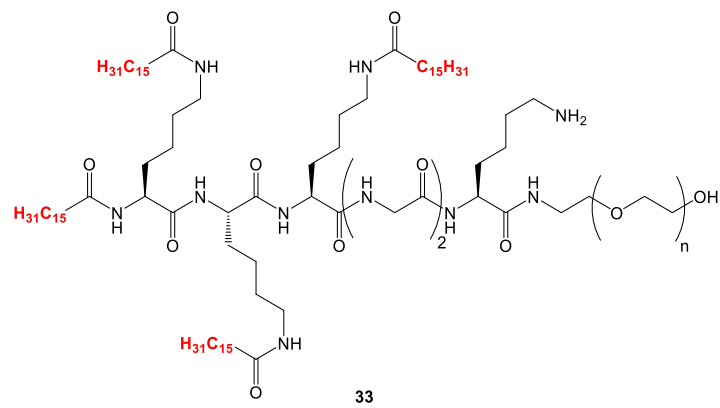
##### *2 alkyl chains*



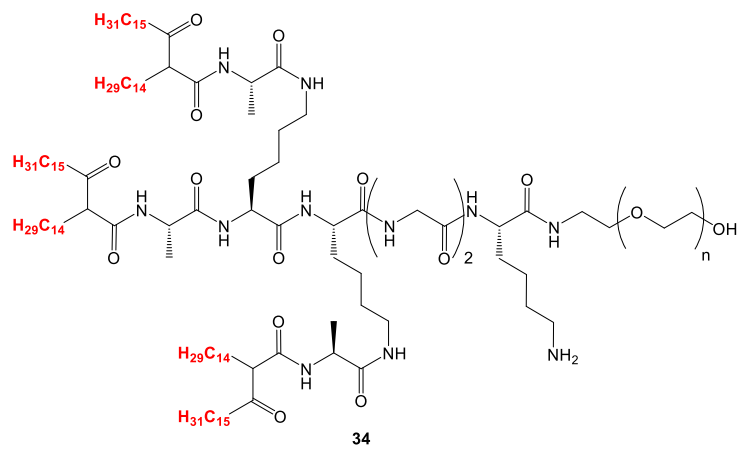
##### *3 alkyl chains*



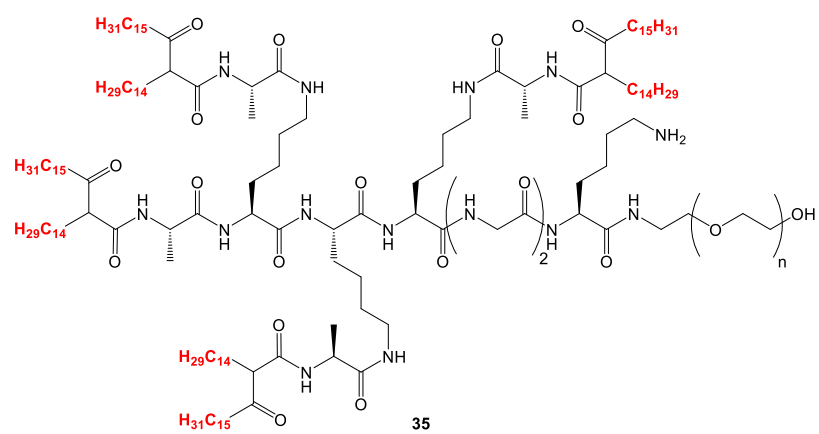
4 alkyl chains



6 alkyl chains

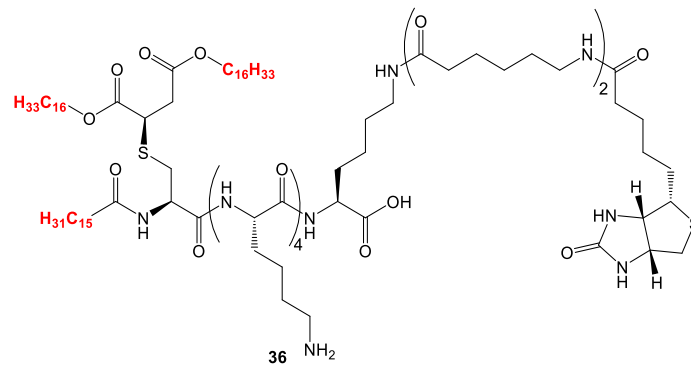


8 alkyl chains

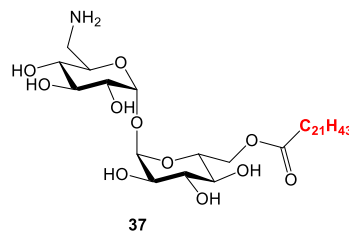


### Lysine-rich ligand

#### 3 alkyl chains

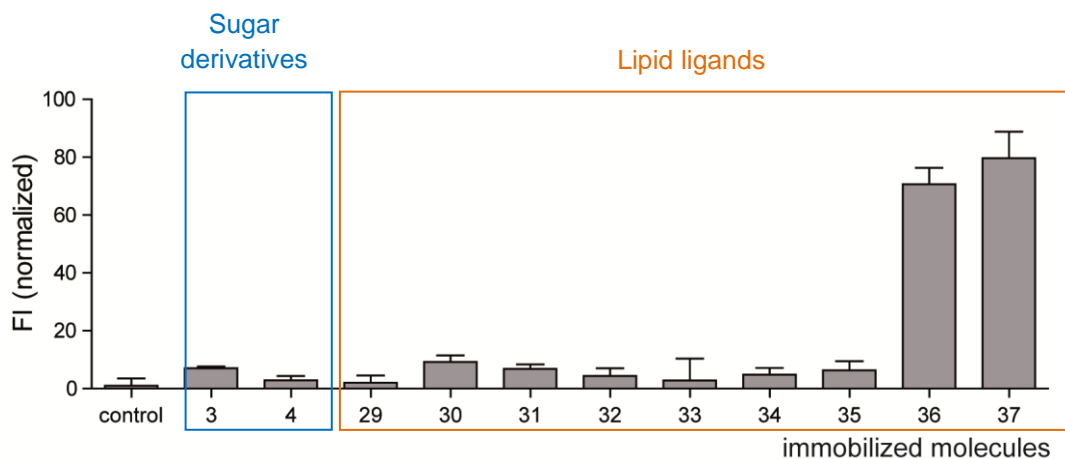


### TMM-analog derivative



**Figure 26. Lipid ligands applied to capture Mtb bacteria from solution.** Nine ligands, containing one to eight alkyl chains, were immobilized on magnetic beads by an amino group. Functionalized beads were used in a bead-based adhesion assay with Mtb H37Rv bacteria. (n: 2700-3300)

The nine different lipid ligands contained one or more amino groups, which enabled immobilization of the molecules on magnetic PEG beads, as described for the carbohydrate derivatives. Functionalized beads were applied in the bead-based adhesion assay.



**Figure 27. Adhesion of Mtb H37Rv bacteria to PEG beads functionalized with lipid ligands.** Magnetic PEG beads were functionalized with the derivatives 29-37. Functionalized and non-modified (control) beads were incubated with GFP-expressing Mtb H37Rv bacteria for 1 h, 37°C, gentle agitation. Adhered bacteria were detected using a fluorescence reader. Data represent differences between fluorescence intensity of adhered bacteria ( $1 \cdot 10^8$  bacteria/ml) to functionalized beads and auto-fluorescence of non-modified beads (+SEM); duplicates of at least three independent experiments; fluorescence intensity normalized with measured fluorescence intensity of 125 000 = 100. (FI: relative fluorescence intensity). (For comparison glycosylated beads 3 and 4 included from Figure 25)

Incubation of the beads, which were functionalized with the ligands **29-35**, with Mtb H37Rv bacteria resulted in enhanced fluorescence signals compared to non-modified beads. While fluorescence intensity was increased fivefold using ligand **29**, ligand **33** led to seven times, ligand **32** and **34** to twelve times, ligand **31** and **35** to 17 times and ligand **30** to 24 times higher fluorescence signals. The detected fluorescence enhancement was in range with the increased fluorescence signals measured for the beads functionalized with the carbohydrate derivatives **3** and **4**. On the other hand after incubation of the beads functionalized with the ligand **36** or the TMM-analog ligand **37** with the mycobacteria much more intensive fluorescence was detected with an 180fold and 220fold increase, respectively, compared to non-modified beads.

Based on these data the ligand **36** and the TMM-analog derivative **37** were identified as potent ligands to capture Mtb bacteria from solution using functionalized magnetic beads.

### **2.3.7 Verifying adhesion of Mtb bacteria by polymerase chain reaction**

To detect captured Mtb bacteria by a system applicable for Tb diagnostics, mycobacteria enrichment was analyzed by PCR. Therefore, DNA was extracted from captured Mtb bacteria and quantified by real-time PCR (RT-PCR). RT-PCR studies were carried out in cooperation with Daniela Sievert from the group of Prof. Dr. Katharina Kranzer, National Reference Center (NRC) for Mycobacteria of the Research Center Borstel, Germany.

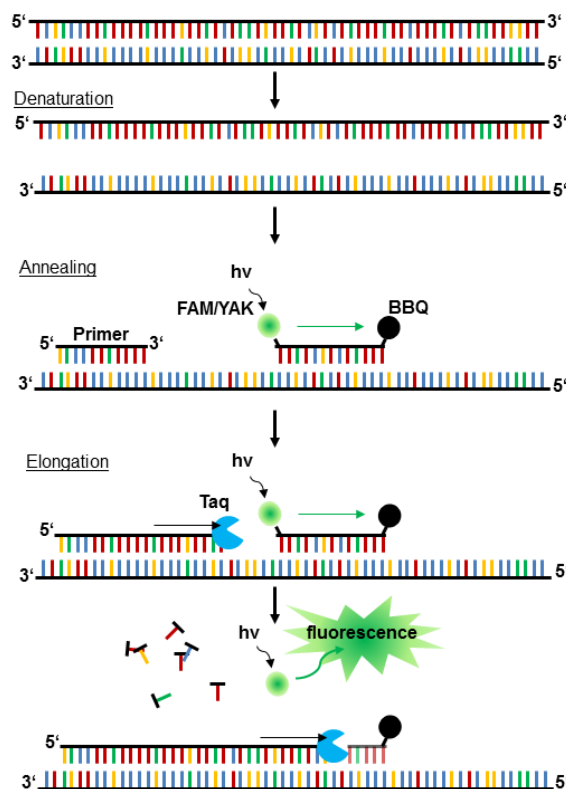
#### Extraction of mycobacterial DNA

The bead-based adhesion assay with Mtb H37Rv bacteria was carried out as described before. Subsequently, beads were suspended in TRIzol, which contains phenol and guanidine isothiocyanate and leads to cell lysis and DNA release. After addition of ethanol, mycobacterial DNA was isolated using the DirectZol RNA MiniPrep kit (Zymo Research) excluding the DNase step.

#### Real-time PCR

An RT-PCR (Figure 28) enables to amplify and detect specific mycobacterial DNA regions and to quantify the initial concentration of mycobacterial DNA. In a first step, the denaturation, the DNA-containing sample is heated to 95°C, which causes disruption of the hydrogen bonds between complementary bases within double-stranded DNA and yielding single-stranded DNA molecules. Subsequently, in the annealing step the reaction temperature is lowered to 55°C allowing annealing of the primers, specific for mycobacterial DNA, to the single-stranded DNA template. In a real-time PCR, additionally, fluorescence resonance energy transfer (FRET) probes are used, which are oligonucleotides linked to a fluorescent molecule (e.g. fluorescein (FAM) or YakimaYellow (YAK)) and a quencher (e.g. BlackBerry (BBQ)), which absorbs the fluorescence of the fluorophore. The close proximity of the fluorescent molecule to the

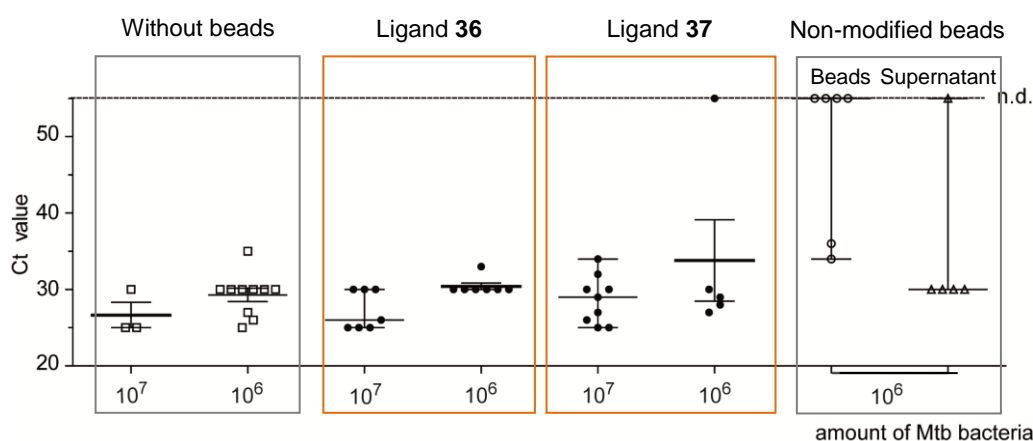
quencher prevents detection of the fluorescence. The FRET probe binds to a complementary DNA region within the target DNA that is to be amplified. After annealing of primer and FRET-probe the DNA-elongation step is started. The DNA polymerase of the bacterium *Thermus aquaticus* (Taq polymerase) is commonly used to catalyze the linkage of deoxynucleoside triphosphates (dNTPs) and thereby the synthesis of a new DNA strand complementary to the DNA template strand. During DNA elongation the Taq polymerase, which further contains exonuclease activity, removes the FRET-probe. Cleavage of the FRET-probe results in a disruption of the reporter-quencher proximity and a detectable fluorescence emission. The denaturation, annealing and elongation steps are repeated several times leading to an amplification of the DNA and a proportional breakdown of the FRET-probe. An increase in the targeted DNA by each PCR cycle causes an increase in fluorescence intensity. The amount of PCR cycles (cycle threshold (ct)), necessary to induce a detectable fluorescence signal, depends on the initial concentration of the mycobacterial DNA. Thus, ct values correlate inversely proportional with the concentration of the target DNA and can be used to quantify mycobacterial DNA.



**Figure 28. Illustration of RT-PCR, which was used to quantify DNA of captured mycobacteria.** In a PCR mycobacterial DNA is specifically amplified. A FRET-probe, containing a fluorescent dye and a quencher, binds to a complementary DNA region within the target DNA that is to be amplified. The Taq polymerase catalyzes the synthesis of a new DNA strand complementary to the DNA template strand and thereby removes the FRET-probe. Disruption of the reporter-quencher proximity results in a detectable fluorescence emission. The measured fluorescence intensity correlates with the amount of amplification cycles and the initial concentration of mycobacterial DNA. (FAM: fluorescein; YAK: YakimaYellow (fluorescent dyes); BBQ: BlackBerry (quencher); Taq: *Thermus aquaticus* polymerase)

### Detection of captured Mtb bacteria by RT-PCR

Magnetic beads functionalized with the ligand **36** and the ligand **37**, respectively, and non-modified beads were incubated with Mtb H37Rv bacteria as described in the bead-based adhesion assay. DNA was extracted from captured mycobacteria and quantified by RT-PCR. For comparison DNA was also isolated from determined amounts of mycobacteria and analyzed by RT-PCR.



**Figure 29. Detection of captured Mtb bacteria by real-time PCR.** DNA was isolated from captured Mtb H37Rv bacteria and quantified by real-time PCR. Data represent ct values (median with range) of at least three independent experiments; one to three technical replicates each. Ct values also determined of known bacteria concentrations. (n.d.: no DNA detected)

DNA extracted from 10<sup>7</sup> bacteria resulted in an averaged ct value of 27 and from 10<sup>6</sup> bacteria in a ct value of roughly 29. Deviations of up to 4 ct values were detected. DNA quantification of mycobacteria captured by beads functionalized with the ligand **36** showed similar ct values: DNA isolated from the beads, after incubation with 10<sup>7</sup> bacteria, led to a ct value of roughly 26 and after incubation with 10<sup>6</sup> bacteria to a ct value of roughly 30. While deviations of up to 5 ct values were measured for the higher bacteria concentration, almost homogeneous data were detected for 10<sup>6</sup> bacteria. Analysis of isolated DNA of Mtb bacteria captured with beads coated with the TMM-analog derivative **37** resulted in mean ct values slightly higher as those detected for the beads modified with the ligand **36**. Also in this case mycobacteria concentration and ct values were inversely proportional. Adhesion assays with unmodified beads led in most of the cases to no DNA detection in the bead fractions. The related supernatant showed ct values of 29, which were identical with those detected for DNA isolated from 10<sup>6</sup> bacteria alone. In the control experiments with unmodified beads strong variations of ct values were measured for a couple of samples.

These data demonstrate that DNA isolated from mycobacteria, which were captured by functionalized beads, can be detected by RT-PCR in a concentration-dependent manner.

### **Results 2.3.6 and Results 2.3.7: Summary**

- The lysine-rich ligand **36** and the TMM-analog derivative **37** were identified as potent lipid ligands to capture Mtb bacteria from solution.
- DNA of adhered mycobacteria was detected by RT-PCR in a concentration-dependent manner.

## 2.4 Discussion

Tb diagnostic is complicated by limited concentrations of Mtb bacteria in patient specimen. In this thesis it was envisaged to identify new ligands to enrich mycobacteria from solution. A potential existence of lectins on the mycobacterial cell surface and the highly hydrophobic character of the mycobacterial cell envelope led to the synthesis of (i) different carbohydrate derivatives and the application of (ii) several lipid ligands. The different molecules were immobilized on microtiter plates or on magnetic PEG-beads and tested for their ability to capture Mtb bacteria.

### 2.4.1 Carbohydrate-specific adhesion characteristics of mycobacteria

Capturing bacteria with carbohydrate-functionalized surfaces presume the presence of lectins in the bacterial cell envelope. So far, there were only minor indications that mycobacteria might express carbohydrate-binding proteins.<sup>145,147–149,199</sup> From one single Mtb lectin<sup>200</sup> and a Msg lectin domain<sup>201</sup> crystallization and preliminary X-ray studies were reported. The crystallized 13 kDa large lectin from Mtb, sMTL-13, is a secreted protein, which natural ligand was not identified yet. Although this lectin was detected in patients during Mtb infections,<sup>199</sup> it cannot be addressed for mycobacteria enrichment from patient specimen, since it is not membranous. Indications for membranous mycobacterial lectins and their corresponding ligands were received from previous studies of V. Anton et al..<sup>147</sup> Several monosaccharides were identified as inhibitors for mycobacterial aggregation. Mycobacteria are known to form large clumps, especially in stationary liquid culture. In the case of Mtb H37Rv bacteria these aggregates were dispersed by addition of D-arabinose, while D-glucose, D-mannose and D-xylose were ineffective. In contrast adhesion among Msg bacteria was not only inhibited by D-arabinose, but also by D-xylose, inositol and D-glucose. The impact of D-glucose was studied even more precisely showing an inhibitory effect of methyl- $\beta$ -D-glucoside but not methyl- $\alpha$ -D-glucoside.<sup>147</sup> Further indications for potential ligands for mycobacterial lectins were obtained from M. Kundu et al., who isolated a lectin from Msg, mycotin, which was able to agglutinate human A, B and O erythrocytes. This haemagglutination could be inhibited by D-arabinose, mannan and *p*-nitrophenyl  $\alpha$ -D-mannopyranoside.<sup>145</sup>

Based on these first indications the mannosides **4** and **5**, the arabinosides **1** and **2**, the  $\beta$ -glucoside **7** and the  $\alpha$ -glucoside **6** were synthesized and applied in adhesion assays with *M. bovis* BCG bacteria and Mtb H37Rv bacteria. Since mycobacterial aggregation is probably based on lectin binding to carbohydrates present in the mycobacterial cell envelope, a derivative of the rare disaccharide, trehalose, was also included. Furthermore, *p*-aminophenyl  $\alpha$ -D-galactopyranoside (**8**) was synthesized to expand the configurational variety of the hydroxyl groups at the sugar scaffold and to address pathogen-host interactions.



In contrast to the results described by V. Anton et al., Mtb H37Rv bacteria did not adhere to surfaces functionalized with the arabinoside derivative **1**. However, in this synthesized molecule arabinose is fixed in the furanose form, while the unmodified D-arabinose, applied by V. Anton et al., is mainly present in the pyranose form. Thus, the results might not be contradictory, but rather suggest that an arabinopyranose-, but not arabinofuranoside-binding lectin might be present in the mycobacterial cell envelope. While Mtb H37Rv bacteria showed no adhesion, *M. bovis* BCG bacteria strongly adhered to microtiter plates functionalized with the D-arabinofuranoside **1**. Carbohydrate-dependent adhesion of *M. bovis* BCG has never been addressed before. In accordance to the inhibitory results of Msg aggregation, *M. bovis* BCG bacteria adhered to surfaces functionalized with the  $\beta$ -glucopyranoside **7**, but not to the immobilized  $\alpha$ -glucopyranoside **6**. Thus, a similar lectin might be present in Msg and *M. bovis* BCG. Adhesion to wells modified with the trehalose derivative **3** or the galactopyranoside **8** was detected for both, *M. bovis* BCG bacteria and Mtb H37Rv bacteria. However, adhesion efficiency was much higher for Mtb H37Rv bacteria. This stronger adhesion might either be based on a larger number of lectins present on the Mtb surface or might be based on higher affinity of the addressed Mtb lectins to the carbohydrate derivatives **3** and **8** compared to the lectins of *M. bovis* BCG. None of the two carbohydrates were analyzed regarding their capability to bind these two mycobacterial species before. Taken together, the adhesion experiments, implemented in the current study, unambiguously verified carbohydrate-dependent adhesion characteristics of *M. bovis* BCG bacteria and Mtb H37Rv bacteria. Specific adhesion to both mycobacterial and host carbohydrates was detected indicating that lectins involved in interactions among the bacteria and also between pathogen and host cells might be present in the mycobacterial cell envelope. The carbohydrate specificity strongly varied between the two investigated mycobacterial species. Thus, the lectin composition might be species or even strain dependent. This heterogeneity is in line with the results reported by V. Anton et al., as described before, and is further supported by previous computer-based genome analysis. A computational search of lectins in all fully or partially sequenced mycobacterial genomes identified 94 potential carbohydrate-binding proteins. The number of detected lectins and their potential association to lectin families strongly varied dependent on the analyzed strain.<sup>149</sup> This carbohydrate specificity bears the chance to distinguish between different mycobacteria and to preferentially capture Mtb bacteria.

Trehalose, detected as a potent ligand for Mtb H37Rv bacteria, is absent in non-mycobacterial cell envelopes. Thus, trehalose-dependent adhesion might be involved in mycobacterial aggregation. This presumption is further supported by the fact that the amount of adhered mycobacteria increased with the use of higher mycobacteria concentrations, but then decreased when the concentration exceeds a threshold of approximately  $2 \cdot 10^8$  bacteria/ml. This reduction might be explained by a competitive process, where Mtb bacteria either binds

to the glycosylated surface or to surrounding mycobacteria. Lower adhesion at the highest bacteria load was determined for all tested carbohydrate derivatives. Thus, carbohydrate-dependent binding, investigated in this study, might mainly address lectins involved in mycobacteria aggregation. Although the  $\beta$ -D-glucopyranoside **7** and the  $\alpha$ -D-galactopyranoside derivative **8** do not represent glycosides present in the mycobacterial cell envelope, they seem to interact with mycobacterial lectins involved in aggregation processes. This might be based on a broad ligand tolerance by the addressed lectins.

As described the configuration of the hydroxyl groups at the sugar scaffold and the configuration of the linkage at the anomeric centre strongly influence mycobacterial adhesion. Furthermore, also the aglycon itself had an impact on the binding efficiency of *M. bovis* BCG bacteria. While the derivatives **2** and **5** with aliphatic aglycons led to low amounts of adhered mycobacteria, the derivatives **1** and **4** with aromatic aglycons increased the bacterial load by a factor of three. These results are similar to previous observations with other lectins. Adhesion and inhibition studies with the fimbrial lectin FimH of *E. coli* bacteria, for example, also revealed higher binding efficiencies of carbohydrates carrying an aromatic aglycon compared to derivatives with aliphatic aglycons.<sup>178,179</sup> These findings can be explained by the protein structure of FimH. Increased adhesion is based on  $\pi$ - $\pi$  interactions between the aromatic aglycon and tyrosine residues located at the outer region of the carbohydrate binding pocket.<sup>178,179</sup> Although no structure of a membranous mycobacterial lectin is known to date, aglycon-dependent adhesion variations might give first indications about the binding pocket of a potential mycobacterial lectin. Hydrophobic or aromatic amino acids might be localized in or close to the sugar binding region of arabinofuranoside- and mannopyranoside-specific mycobacterial lectins. Only two of four carbohydrates were analyzed regarding the influence of the aglycon so far. Thus, experiments should be extended including galactoside and glucoside derivatives to get deeper insights into mycobacterial adhesion characteristics.

Adhesion of *M. bovis* BCG bacteria to the arabinoside derivative **1** and the mannoside **4** could be further increased by addition of calcium ions. This increase was not observed when  $\text{Ca}^{2+}$  was previously complexed by EDTA. The amount of adhered bacteria was even reduced by EDTA supplementation, which can be explained by additional complexation of ions, naturally present on the mycobacterial surface and relevant for binding processes. These results suggest that C-type lectins might be involved in mycobacterial adhesion to surfaces functionalized with mannoside and arabinoside derivatives, respectively. Mycobacterial lectins identified by computer-based genome analysis showed homologies to  $\beta$ -prism-II lectins present in plants, R-type lectins, a unique lectin from cyanobacterium *Microcystis viridis* (MVL) and also C-type lectins.<sup>149</sup> Gene sequences similar to those encoding for C-type lectins were detected in all analyzed strains of Mtb, *M. marinum* and *M. canettii*, but not *M. bovis* BCG. Therefore, calcium-dependent adhesion of *M. bovis* BCG bacteria, as shown in the current

study, is not in line with the results received by K. V. Abhinav et al.<sup>149</sup> and no potent gene region could be associated so far. Furthermore,  $\text{Ca}^{2+}$ -depend binding of mycobacterial lectins might be a disadvantage for diagnostic applications. Human saliva mainly consists of water (99.5%), but also contains mucus, enzymes, immunoglobulins, such as IgA, and ions.  $\text{Ca}^{2+}$  is present in a 1 mM concentration.<sup>202</sup> Therefore, capturing Mtb bacteria based on mycobacterial C-type lectins might be possible but not favorable, since patient-specific ion concentrations might have a strong impact on binding efficiencies.

In the microtiter plate-based adhesion assay bacteria concentrations of at least  $1 \cdot 10^6$  bacteria/ml were necessary to detect carbohydrate-dependent adhesion. This might be explained by a limited detection level of fluorescent bacteria (ca.  $1 \cdot 10^5$  bacteria) using a fluorescence reader. However, the synthesized molecules might also not represent the optimal ligands and therefore exhibit low binding affinities. It is conceivable that the natural ligand is not even a monosaccharide, but a di- or oligosaccharide. To address this question it might be necessary to identify and characterize the related protein. Single knockdown of the ten potential Mtb lectins, detected by genome analysis, will help to identify the related gene region of a mycobacterial lectin.<sup>148</sup> Furthermore, transformation of a selected gene region into Mgs bacteria followed by overexpression of the related protein might enable to construct a less pathogenic model organism to study lectin-dependent adhesion or to isolate and characterize the mycobacterial lectin. Beside these biological approaches, it might also be convenient to apply photoaffinity labeling (PAL) to target mycobacterial lectins.<sup>203–206</sup> For PAL carbohydrate derivatives can be designed carrying a diazirine group.<sup>207–213</sup> This nitrogen containing cyclopropene-like ring is activated at a wavelength of light ( $\sim 355$  nm) that is not damaging to proteins. Upon photo-activation of the diazirine moiety a carbene intermediate is formed, which rapidly inserts into X-H bonds ( $X = \text{C}, \text{N}, \text{S}, \text{O}$ ) in the near proximity forming stable covalent insertion products.<sup>207,209</sup> In the case of sugar-lectin interactions, amino acids near the carbohydrate binding pocket of the lectin will react with the carbene of the sugar derivative.<sup>210</sup> Thereby, carbohydrate ligands will be covalently connected to the target protein, which can subsequently be identified by mass spectrometry.<sup>214</sup> PAL represents a useful method for target identification in complex protein mixtures or even within whole cells.<sup>208,210–213</sup> Here, it might be used to identify potential mycobacterial lectins.

In this thesis new carbohydrate derivatives were identified as potential ligands to bind Mtb bacteria, thus shedding light on the so far barely studied carbohydrate-binding characteristics of mycobacteria. Based on these results it will be highly fascinating not only to characterize the structure and natural ligand of the potential lectin, but also to analyze distribution and function of mycobacterial lectins. A largely unexplored area, that might allow deeper insights into virulence characteristics of the pathogen and will hopefully help to develop new specific diagnostic tools for tuberculosis infections.

### 2.4.2 Capture of Mtb bacteria with functionalized magnetic beads

Carbohydrate-dependent mycobacterial adhesion was unambiguously detected in a microtiter plate-based assay. Especially the trehalose **3**-specific adhesion was highly promising. The uniqueness of trehalose as a cell envelopes constituent might correlate with a limited number of membranous trehalose-specific lectins in other organisms. Thus, trehalose derivatives might represent potent molecules to specifically capture mycobacteria. To develop a diagnostic tool, based on trehalose-specific adhesion of mycobacteria, binding of Mtb has to work out not only in microtiter plates but also with a system applicable for Tb diagnostics. Therefore, beads were functionalized suitable for a mouth rinse. However, the magnetic PEG beads functionalized with the trehalose derivative **3** did not show high binding efficiency. This drawback might be caused by carbohydrate arrangement and accessibility. Bead size and ligand density should be varied in future studies in order to possibly enhance binding affinity of Mtb bacteria towards the functionalized beads. In addition, the low binding efficiency might also be a consequence of the structural properties of the related mycobacterial lectin. Catch bond characteristics of the lectin would explain the higher affinity to static compared to mobile surfaces. In case of static surfaces shear forces can be provoked for example by solvent flow, which normally would reduce adhesion (slip bond). Proteins with catch bond characteristics do not show weaker but even stronger binding under increased flow conditions.<sup>215</sup> This untypical binding behavior was previously detected for the von Willebrand factor, cadherins, selectins and the mannose-specific lectin FimH.<sup>215-219</sup> In the case of FimH change of binding efficiency is based on a lengthening of the protein structure combined with a conformational change of a  $\beta$ -sheet in the binding pocket due to shear-originated mechanical force.<sup>216,220</sup> A catch-bond character of mycobacterial lectins might be an advantage for the bacterium to attach to the lung surface or to already adhered bacteria within the lung resisting the strong air flow through. However, here it would be a disadvantage for the development of a diagnostic mouth rinse.

While beads functionalized with carbohydrate derivatives failed to effectively capture Mtb bacteria from solution, strong mycobacterial adhesion could be obtained by the application of beads functionalized with the lipid ligands **36** and **37**, respectively. Although the other ligands, received from Prof. Dr. Karl-Heinz Wiesmüller, had hydrophobic regions comparable to the ligand **36**, minor binding affinities were detected. This might be explained by the fact that the lysines, which were important for immobilization, are located between the hydrophobic moiety and the hydrophilic-PEG region. Therefore, functionalized beads might have alternating hydrophobic and hydrophilic parts instead of a complete hydrophobic surface. Furthermore, an insufficient functionalization of the beads using the ligands **29-35** might be the reason for the low Mtb affinity. Thus, in future studies functionalization efficiency should be examined. Successful ligand immobilization can be detected by investigating changes in surface charge between functionalized and non-modified beads using Zeta potential analysis.<sup>221</sup> In addition,

the amount of unreacted carboxyl groups and thereby functionalization degree can be quantified by UV titration with toluidine blue O (TBO).<sup>222</sup>

Capturing mycobacteria due to hydrophobic interactions was previously shown by Microsens Medtech Ltd..<sup>166</sup> The developed “Tb-Beads” are paramagnetic particles coated with pDADMAC, a charged and hydrophobic ligand, which is believed to have a high affinity for LAM and mycolic acids. The beads were applied to enrich Mtb bacteria from sputum and subsequently analyze bound bacteria by microscopy, cultivation or PCR.<sup>167,168,223</sup> Beside this diagnostic tool, Steinhäuser et al. exploited the hydrophobic character of the mycobacterial cell envelope to label Mtb bacteria with magnetic nanoparticles. This magnetic tag enabled a specific isolation and investigation of mycobacteria-containing phagosomes.<sup>136</sup> The magnetic nanoparticles were immobilized in the mycobacterial cell envelope using the same lipid ligand **36**, as applied in the current study. Thus, successful capturing of Mtb bacteria by this molecule was expectable. The TMM-analog molecule **37**, synthesized by the group of Prof. Dr. Mark S. Baird, has never been applied for binding studies with Mtb bacteria before. The high binding affinity of ligand **37** might be based on hydrophobic interactions, but can also be explained by lectin-dependent adhesion. A mycobacterial lectin similar to Mincle is conceivable. This macrophage inducible C-type lectin is assumed to be involved in mycobacteria-dependent inhibition of phagosome maturation.<sup>80</sup> The main ligand of Mincle is TDM.<sup>112</sup> X-ray crystallography and mutagenesis studies have revealed an extended ligand-binding site that interacts with both trehalose and one mycolic acid of the glycolipid.<sup>224</sup> Binding affinity of 6-octanoyl-trehalose was up to 50 times higher compared to trehalose.<sup>224</sup> In analogy, adhesion of Mtb H37Rv bacteria to beads functionalized with the TMM-analog ligand **37** compared to beads modified with the trehalose derivative **3** was increased by roughly twelvefold. This enhancement could be based on a mycobacterial lectin with a binding pocket recognizing trehalose and a neighboring hydrophobic binding site. However, since no membranous lectin has been published to date, an Mtb lectin similar to Mincle is only speculation.

Binding of mycobacteria due to carbohydrate-lectin interactions would enable to specifically capture Mtb bacteria, while hydrophobic ligands might target a wide range of different bacteria or apoptotic host cells. The low specificity of the ligand **36** was already shown by Steinhäuser et al. This lipid ligand could not only be used to magnetically tag Mtb bacteria, but also other mycobacteria (e.g. *M. avium*), Gram-positive bacteria (e.g. *Listeria monocytogenes*) and Gram-negative bacteria (e.g. *E. coli*).<sup>136</sup> Thus, capturing Mtb bacteria using a mouth rinse with hydrophobic particles might also result in binding of commensal oral bacteria and fungi. However, analytical methods like PCR will enable the specific detection of Mtb bacteria even within a mixture of isolated microorganisms. High binding selectivity is favorable, but not obligatory necessary.

In this study, RT-PCR was used to verify and quantify mycobacterial adhesion to hydrophobic beads. It was shown that the ligand **36** and the TMM-analog derivative **37** bind Mtb bacteria with high efficiency. Similar numbers of amplification cycles were necessary to detect mycobacterial DNA isolated from either ligand **36**-captured Mtb bacteria or from the total bacteria amount. Thus, a comparable DNA concentration must have been present. It can be assumed that beads functionalized with the ligand **36** capture nearly all mycobacteria from solution. Slightly higher mean ct values were detected for beads functionalized with the ligand **37**. This might not be due to minor binding efficiency, but can rather be explained by strong variations of detected ct values. Differences of up to five ct values were measured for DNA isolates from Mtb bacteria captured by functionalized beads or untreated bacteria. This limited accuracy might be caused by a loss of sample material during the adhesion assay or by the DNA-extraction procedure. Detection of ct values in experiments with unmodified beads might be based on insufficient washing steps. To obtain more reliable data, the current method should be further optimized. However, concentration dependent detection of Mtb bacteria by PCR verified that both, ligands **36** and **37**, are suitable to effectively extract mycobacteria from solution.

Comparison of the three hydrophobic ligands, derivative **36**, **37** and pDADMAC, revealed a strong Mtb binding efficiency for all of them. However, while pDADMAC is immobilized by ionic interactions, the other two molecules are covalently attached, which might be an advantage for the stability of the functionalization. The primary amino groups of ligand **36** and **37** facilitate a fast and easy immobilization by peptide-coupling or thiourea formation to a variety of surfaces. The TMM-analog derivative **37** has a big advantage over the ligand **36**. The carbohydrate scaffold will enable easy modifications of this molecule. Further structures can be selectively introduced at any position of the six unmodified hydroxyl groups. Derivatization might help to optimize the ligand and further increase binding efficiency. Also the functional amino group can be easily replaced facilitating alternative immobilization methods and prospective polymerization reactions. It might be conceivable to attach butadiene to the molecule **37** and then include this new ligand by radical or anionic polymerization into a polybutadiene structure suitable for a chewing gum. The potential structural variety based on the TMM-analog derivative **37** will positively contribute to finally reach the goal of developing a diagnostic mouth rinse or chewing gum.

### **2.4.3 Development of a diagnostic mouth rinse or chewing gum**

The most common methods for Tb detection are direct microscopy of patient sputa and culturing of Mtb bacteria.<sup>3,4</sup> However, children and cachectic patients usually cannot cough up enough phlegm to allow laboratory evaluations. One of the most important advantages for using saliva as a diagnostic tool is its simple, non-invasive sampling process. Mycobacteria were detected in saliva earlier, but the development of a diagnostic test remained unsuccessful

due to the low bacteria numbers.<sup>158,159</sup> The amount of mycobacteria in saliva is between 100 and 5000 times lower compared to sputum.<sup>151</sup> However, A. G. Holani et al. successfully visualized Mtb bacteria from oral samples using fluorochrome staining.<sup>156</sup> Additionally, detection of Mtb bacteria in saliva using PCR was recently shown by G. G. Mediero et al..<sup>157</sup> These results identified saliva as an alternative biological sample for rapid diagnosis of pulmonary Tb.

Nevertheless, bacteria enrichment is necessary to increase the detection rate. Methods to capture mycobacteria to solid surfaces have previously been proposed, including immobilized phage or phage derived binding peptides,<sup>160,162</sup> antibody coated beads<sup>161,163–165</sup> or the hydrophobic Tb-Beads described before.<sup>166</sup> Finally, only the Tb-Beads found their way into a diagnostic application. Antibodies are highly specific, but too expensive for extensive use, especially in less developed countries, and are susceptible to denaturation. Tb-Beads were designed to isolate mycobacteria from sputum, applications in saliva have not been described so far. The hydrophobic beads, investigated in the current study, might be used in analogy to the known Tb-Beads. The newly identified ligands **36** and **37** show high affinity for Mtb bacteria and high stability, are good to immobilize and cheap and easy to synthesize. Moreover, binding capacity of the applied beads might be further improved by an increase of the surface area. As shown by M. Behra et al. porous magnetic PEG beads have three times higher bacteria binding efficiency than nonporous particles.<sup>225</sup> However, to develop a mouth rinse further biomedical standards have to be fulfilled. The oral rinse should not be toxic and has to be applicable also for children and cachectic patients, which are the main target group. Oral solutions for dental health are mainly approved for children older than six years. Thus, a diagnostic mouth rinse might not be suitable for babies and children younger than six, because they may swallow the rinse.

Alternatively, a chewing gum or even better a non-dissolving lollipop could be designed. Chewing gums have been used for therapeutic applications since decades.<sup>226</sup> Already during the late 19th century Dr. Edward Beeman incorporated pepsin powder into a chewing gum and 1924 aspirin containing chewing gums were introduced in the US.<sup>227</sup> One of the best known examples is the nicotine containing chewing gum used to help patients break the smoking habit.<sup>226</sup> However, diagnostic chewing gums have only been rarely studied. Prof. Dr. Lorenz Meinel from the Julius Maximilian University of Würzburg developed a chewing gum detecting biomarkers of pathogens present in the mouth cavity. Thereby, a peptide is released from the gum matrix and cleaved by a pathogen-specific protease resulting in a bitter taste. This diagnostic system was designed for patient self-monitoring.<sup>228</sup> Another diagnostic chewing gum is currently under investigation by Andrew Fung. He combines both magnetic particles and a gum matrix to isolate Malaria-specific proteins from saliva.<sup>229</sup> Neither an Mtb-specific chewing gum nor mouth rinse have ever been developed before.

In analogy to the described diagnostic chewing gums, mycobacteria might also be detected in saliva by Mtb-specific molecules. Much work has been done on discovery of biomarkers in active and latent Tb infections.<sup>14</sup> One of the most promising antigens that were evaluated is LAM. It is known that this lipoglycan is shedded from the Mtb cell envelope and released by exocytosis.<sup>230</sup> Enzyme-linked immunosorbent (ELISA)-based assays were used to reveal LAM in sputum and urine.<sup>16-18</sup> Furthermore, Ag85 was directly measured in sputum.<sup>15</sup> Mtb-specific biomarkers in saliva were not investigated so far.

To finally analyze bead- or chewing gum-captured mycobacteria, even in less developed countries, microscopy, cultivation or PCR can be applied. All three methods were successfully tested using the known Tb-Beads.<sup>167,168,223</sup> Microscopy is not as sensitive as culture-based techniques.<sup>1</sup> At least 3000 bacteria/ml are required, whereas Mtb concentrations of 10 bacteria/ml can be detected by liquid culture. However, culturing bacteria is more costly, requires specialized biosafety infrastructure and takes weeks to obtain results, because of the extremely slow growth rate of Mtb bacteria. Nucleic acid-based diagnostic strategies can detect approximately 100 bacteria/ml, making them less sensitive than culture, but significantly more sensitive than microscopy. With DNA amplification systems it is thought that Tb can be diagnosed from sputum with 98% reliability.<sup>5,6</sup> Genetic methods further allow more precise detection of drug resistances<sup>7-9</sup> and mutations correlating with Tb pathogenicity. However, they require a high technical competence. Alternatively, a fast and easy method is conceivable, that might enable patient self-monitoring. A novel method for sensitive and rapid Mtb detection was recently developed by the chemist Jianghong Rao and the microbiologist Jeffrey Cirillo.<sup>231-233</sup> They took advantage of the high specificity of the  $\beta$ -lactamase BlaC, naturally surface-localized and secreted by Mtb bacteria. The  $\beta$ -lactamase activity was used to cleave cephalosporin-based fluorogenic substrates generating fluorescence and leading to direct and rapid detection of mycobacteria. By this chemical method 90% of cases detected as positive by culture were identified correctly.<sup>231-233</sup> Based on this strategy a new method can be developed, which might combine capturing of mycobacteria and Mtb detection by color appearance. After capture of Mtb bacteria by a diagnostic chewing gum or lollipop this diagnostic tool might be placed into a solution containing a cephalosporin-based substrate. This substrate should be cleaved by mycobacterial BlaC activity realizing a molecule, which turns the solvent colorful. This color appearance might be directly detected by patients and might allow patient self-monitoring.

Although two potent ligands for enrichment of Mtb bacteria, the lipid ligands **36** and **37**, were identified in this study, for the development of a diagnostic tool it is still a long way to go. A perfectly applicable material, a suitable chemistry for ligand introduction, a strategy for subsequent Mtb bacteria release and a cheap and easy, but highly sensitive analytical method need to be investigated. However, developing a chewing gum, lollipop or mouth rinse for detection Mtb bacteria will certainly contribute to improved Tb diagnostics in future.



## 2.5 Concluding remarks

In order to develop a new tool to enrich and detect Mtb bacteria, carbohydrate derivatives and lipid ligands were applied to capture Mtb bacteria from solution. With the synthesized sugar derivatives **1-8** a largely unexplored area of mycobacterial lectins was addressed. Findings of the current study revealed carbohydrate-specific adhesion of *M. bovis* BCG bacteria and Mtb H37Rv bacteria indicating that lectins might indeed be present in the mycobacterial cell envelope. Lectin composition seems to vary between the two investigated species, which might be utilized to distinguish between different mycobacteria and preferentially capture Mtb bacteria. Microtiter plates and magnetic PEG-beads functionalized with the carbohydrate derivatives **1-8** could be used to enrich Mtb bacteria from solution. However, the adhesion efficiency of the Mtb strain H37Rv to beads functionalized with the  $\alpha$ -D-mannopyranoside **4** and amino trehalose **3** was strongly surpassed by beads carrying the lipid ligands **36** and **37**, respectively. These adhesion studies will prospectively contribute to the development of a chewing gum or mouth rinse for Tb diagnostics.

## 2.6 Materials and methods

### 2.6.1 Reagents

Acetic acid	Merck KGaA, Darmstadt, Germany
Acetic anhydride	Thermo Fisher Scientific, Waltham, USA
Acetone	Thermo Fisher Scientific, Waltham, USA
Acetonitrile	Sigma-Aldrich, St. Louis, USA
Amberlite IR120 ion exchange resin	Sigma-Aldrich, St. Louis, USA
D-Arabinose	VWR International, Radnor, USA
Benzoylchloride	Thermo Fisher Scientific, Waltham, USA
2-Bromoethanol	Sigma-Aldrich, St. Louis, USA
Boron trifluoride diethyl etherate	abcr GmbH, Karlsruhe, Germany
Calcium chloride	Sigma-Aldrich, St. Louis, USA
Calcium hydride	Thermo Fisher Scientific, Waltham, USA
Celite 545	Thermo Fisher Scientific, Waltham, USA
2-Chloroethanol	Sigma-Aldrich, St. Louis, USA
Chloroform- <i>d</i> <sub>1</sub>	Deutero GmbH, Kastellaun, Germany
Concanavalin A, FITC-labeled	Sigma-Aldrich, St. Louis, USA
Cyclohexane	Sigma-Aldrich, St. Louis, USA
Deuterium oxide	Deutero GmbH, Kastellaun, Germany
1,8-Diazabicycloundec-7-ene (DBU)	Alfa Aesar, Ward Hill, USA
Dichloromethane (DCM)	Merck KGaA, Darmstadt, Germany
Diethyl ether	Merck KGaA, Darmstadt, Germany
Dimethylformamide (anhydrous) (DMF)	Thermo Fisher Scientific, Waltham, USA
Dulbecco's PBS (10x)	Merck KGaA, Darmstadt, Germany
Dimethyl sulfoxide (DMSO)	Sigma-Aldrich, St. Louis, USA
Ethanol	VWR International, Radnor, USA
Ethanolamine	TOKYO CHEMICAL INDUSTRY CO., Tokyo, Japan
Ethyl acetate	Merck KGaA, Darmstadt, Germany
1-Ethyl-3-(3-dimethylaminopropyl)carbodiimide (EDC)	Sigma-Aldrich, St. Louis, USA
Ethylenediaminetetraacetic acid (EDTA)	Sigma-Aldrich, St. Louis, USA
Glycerol	Serva Electrophoresis GmbH, Heidelberg, Germany
n-Hexane	Thermo Fisher Scientific, Waltham, USA
Hydrochloric acid, 37%	Sigma-Aldrich, St. Louis, USA
Hydrogen bromide/ glacial acetic acid, 33%	Sigma-Aldrich, St. Louis, USA
4-(2-Hydroxyethyl)-1-piperazineethanesulfonic acid (HEPES)	Sigma-Aldrich, St. Louis, USA
Lithium aluminium hydride	Thermo Fisher Scientific, Waltham, USA
Manganese chloride	Alfa Aesar, Ward Hill, USA
Magnesium chloride	Sigma-Aldrich, St. Louis, USA
Magnesium sulfate	Thermo Fisher Scientific, Waltham, USA
Magnesium turnings	Sigma-Aldrich, St. Louis, USA

D-Mannose	Thermo Fisher Scientific, Waltham, USA
Methanol (MeOH)	Sigma-Aldrich, St. Louis, USA
Methanol- <i>d</i> <sub>4</sub>	Deutero GmbH, Kastellaun, Germany
Middlebrook 7H9 broth	Becton Dickinson, Franklin Lakes, USA
<i>N</i> -Hydroxysuccinimide (NHS)	Sigma-Aldrich, St. Louis, USA
<i>p</i> -Nitrophenol	Alfa Aesar, Ward Hill, USA
<i>p</i> -Nitrophenyl $\alpha$ -D-galactopyranoside	abcr GmbH, Karlsruhe, Germany
<i>p</i> -Nitrophenyl $\alpha$ -D-glucopyranoside	TOKYO CHEMICAL INDUSTRY CO., Tokyo, Japan
<i>p</i> -Nitrophenyl $\alpha$ -D-manopyranoside	Iris Biotech GmbH, Marktredwitz, Germany
2-( <i>N</i> -morpholino)ethanesulfonic acid (MES)	VWR International, Radnor, USA
OADC (oleic acid, albumin, dextrose, catalase)	Becton Dickinson, Franklin Lakes, USA
Palladium/charcoal activated, 10%	Sigma-Aldrich, St. Louis, USA
Phosphorus pentoxide	Sigma-Aldrich, St. Louis, USA
Potassium hydroxide	Merck KGaA, Darmstadt, Germany
Pyridine	Thermo Fisher Scientific, Waltham, USA
Sodium acetate	Merck KGaA, Darmstadt, Germany
Sodium azide	Sigma-Aldrich, St. Louis, USA
Sodium carbonate	Sigma-Aldrich, St. Louis, USA
Sodium chloride	Sigma-Aldrich, St. Louis, USA
Sodium hydrogen carbonate	Sigma-Aldrich, St. Louis, USA
Sodium hydroxide	Sigma-Aldrich, St. Louis, USA
Sodium methoxide	Thermo Fisher Scientific, Waltham, USA
TaqMan Universal PCR Master Mix	Thermo Fisher Scientific, Waltham, USA
Tetrahydrofuran (THF)	Merck KGaA, Darmstadt, Germany
<i>tert</i> -Butyldimethylsilyl chloride (TBDMSCl)	Sigma-Aldrich, St. Louis, USA
Tetrabutylammonium iodide (TBAI)	Sigma-Aldrich, St. Louis, USA
Tin tetrachloride	Sigma-Aldrich, St. Louis, USA
Toluene	Thermo Fisher Scientific, Waltham, USA
<i>p</i> -Toluenesulfonyl chloride	Sigma-Aldrich, St. Louis, USA
Trichloroacetonitrile	Alfa Aesar, Ward Hill, USA
Triethylamine	Thermo Fisher Scientific, Waltham, USA
Tris(hydroxymethyl)aminomethane (Tris)	Serva Electrophoresis GmbH, Heidelberg, Germany
TRizol	Thermo Fisher Scientific, Waltham, USA
Tween 80	Carl Roth GmbH & Co. KG, Karlsruhe, Germany

## 2.6.2 Buffer and media

pH-Values were adjusted with aqueous HCl (100 mM) or NaOH (100 mM) solutions, respectively, unless otherwise described. All buffer and media were autoclaved prior use.

Carbonate buffer, pH 9.4	Sodium carbonate (1.59 g, 15.0 mmol) and sodium hydrogen carbonate (2.52 g, 30.0 mmol) were dissolved in double dist. water (1.00 l) with subsequent pH adjustment.
Lectin binding buffer (LBB), pH 7.0	HEPES (238 mg, 1.00 mmol), sodium chloride (292 mg, 5.00 mmol), manganese chloride (12.6 mg, 100 $\mu$ mol) and calcium chloride (11.1 mg, 100 $\mu$ mol) were dissolved in double dist. water (100 ml) with subsequent pH adjustment.
2-( <i>N</i> -morpholino)ethanesulfonic acid(MES) buffer, pH 6.3	MES (9.76 g, 50.0 mmol) was dissolved in double dist. water (100 ml) with subsequent pH adjustment using a sodium carbonate solution (2.5 M).
Middlebrook 7H9 medium	Middlebrook 7H9 broth (4.70 g) were dissolved in double dist. water (900 ml) and Tween 80 (500 $\mu$ l, 412 $\mu$ mol) and glycerol (2.00 ml, 27.4 mmol) were added.
Phosphate-buffered saline (PBS), pH 7.0	Dulbecco's PBS (10x) was diluted 1:10 with double dist. water
Tris-buffered saline (TBS), pH 7.6 (adhesion assay)	Tris (2.42 g, 20.0 mmol) and sodium chloride (8.00 g, 137 mmol) were dissolved in double dist. water (1.00 l) with subsequent pH adjustment.

### 2.6.3 Biological assays

#### Mycobacterial strains used in this study

All bacterial strains (Table 1) were grown in Middlebrook 7H9 medium containing oleic acid-albumin-dextrose-catalase (OADC, 10%), Tween 80 (0.05%) and glycerol (0.2%). At mid-log phase ( $OD_{600} = 0.4$ ) cultures were harvested and frozen at  $-80^{\circ}\text{C}$  as previously described.<sup>46</sup> For adhesion assays frozen stocks ( $2.5 \cdot 10^8$  bacteria/ml) were thawed ( $37^{\circ}\text{C}$ ) and centrifuged ( $3629 \times g$ ,  $4^{\circ}\text{C}$ , 10 min). Bacteria were re-suspended in PBS or TBS (with or without supplementation of  $\text{Ca}^{2+}$  (5 mM),  $\text{Mg}^{2+}$  (5 mM) or  $\text{Ca}^{2+}$  (5 mM)/ EDTA (15 mM)), the concentration was adjusted to  $4 \cdot 10^8$  bacteria/ml and the bacterial suspension homogenized using a sterile 1 ml syringe with a 26 gauge needle.

**Table 1: Mycobacterial strains used in this study.**

<u>Sample name</u>	<u>Description</u>	<u>Source</u>
GFP-expressing <i>M. bovis</i> BCG	<i>M. bovis</i> BCG Pasteur strain (1173P2)  Strain carrying a GFP-expressing plasmid (pMN437) <sup>234</sup>	Plasmid (pMN437) <sup>234</sup> kindly provided by Prof. Dr. M. Niederweis, University of Alabama at Birmingham, USA
GFP-expressing Mtb H37Rv	In order to obtain stable GFP expression in Mtb H37Rv, codon usage, fluorescence and folding optimized <i>gfpm2+</i> from pMN437 <sup>234</sup> was cloned into the integrative mycobacterial plasmid pMV306 <sup>235</sup> giving pSvM4 which was used to transform Mtb H37Rv (ATCC 27294).	Plasmid (pMN437) <sup>234</sup> kindly provided by Prof. Dr. M. Niederweis, University of Alabama at Birmingham, USA

#### Functionalization of microtiter plates<sup>196</sup>

Black Immobilizer Amino™ F96 MicroWell™ plates (Nunc) were incubated with a solution of the carbohydrate derivatives **1-8** (10 mM in carbonate buffer, pH 9.4, 100  $\mu\text{l}$ /well) overnight at rt and under gentle agitation (100 rpm). Wells were washed with PBS (2·150  $\mu\text{l}$ /well) and unreacted functional groups on the microtiter plate surface were blocked with ethanolamine (10 mM in carbonate buffer, pH 9.4, 120  $\mu\text{l}$ /well) for 2 h at rt under gentle agitation (100 rpm). The wells were washed with PBS (2·150  $\mu\text{l}$ /well) and the microtiter plates were directly applied to adhesion assays or stored overnight at  $4^{\circ}\text{C}$ .

#### Functionalization of magnetic PEG beads

Beads (micromer-M, polystyrol core, surface: PEG-COOH, 5  $\mu\text{m}$ , micromod; 800  $\mu\text{l}$ ,  $5.6 \cdot 10^8$  beads) were supplemented with *N*-hydroxysuccinimide (NHS, 12.8 mg) and 1-ethyl-3-(3-dimethylaminopropyl)carbodiimide (EDC, 6.40 mg) dissolved in MES buffer (pH 6.3, 200  $\mu\text{l}$ ) and incubated for 1.5 h at rt while intensely shaking (600 rpm). The activated beads were washed twice with PBS (1.00 ml each) and partitioned (3 batches,  $1.87 \cdot 10^8$  beads each). Each

batch was incubated with a solution of the carbohydrate derivatives **1**, **3** or **4** (10 mM in carbonate buffer, pH 9.4, 1.00 ml) or the lipid ligands **29-37** (1.00 mg/ml carbonate buffer, pH 9.4; lipid **37**: 1.00 mg/ 200  $\mu$ l DMSO, 20.0  $\mu$ l Et<sub>3</sub>N, 780  $\mu$ l carbonate buffer, pH 9.4 (in the described order)) for 4.5 h at rt while intensely shaking (600 rpm). The functionalized beads were washed twice with PBS (1.00 ml/batch each) and unreacted NHS esters on the bead surface were blocked with ethanolamine (10 mM in carbonate buffer, pH 9.4, 1.00 ml/batch) for 1 h at rt, intense shaking (600 rpm). The beads were washed twice with PBS (1.00 ml/batch each), re-suspended in PBS (1.00 ml) and stored at 4°C. All steps were carried out in eppendorf tubes. A magnetic rack (DynaMag-2 magnet, Life technologies) was used for bead extraction.

### ConA-assay

The beads were functionalized as described before in the method “Functionalization of magnetic PEG beads”. ConA-fluorescein was dissolved in LBB (250  $\mu$ g/ml). The beads ( $2 \cdot 10^7$  beads) were removed from PBS, suspended in the ConA-fluorescein solution (200  $\mu$ l) and incubated for 1.5 h at rt while gently shaking (100 rpm) in the dark. The beads were washed twice with PBS (200  $\mu$ l/batch each), re-suspended in PBS (100  $\mu$ l), transferred to black microtiter plates (Nunc Maxisorp) and analyzed using a fluorescence microplate reader (Synergy 2, Biotek, excitation: 485 nm /emission: 528 nm). All steps were carried out in eppendorf tubes. A magnetic rack (DynaMag-2 magnet, Life technologies) was used for bead extraction.

### Mycobacterial adhesion assay on microtiter plates

GFP-expressing mycobacteria (Mtb H37Rv or *M. bovis* BCG,  $4 \cdot 10^8$  bacteria/ml in PBS) were serially diluted (1:2) with PBS in functionalized microtiter plates (100  $\mu$ l/well, highest concentration:  $4 \cdot 10^8$  bacteria/ml, lowest concentration:  $2 \cdot 10^5$  bacteria/ml) and incubated for 1 h at 37°C while gently shaking (100 rpm) in the dark. Wells were washed twice with PBS (150  $\mu$ l/well each) followed by addition of PBS (100  $\mu$ l/well). The bacterial adhesion was analyzed using a fluorescence microplate reader (Synergy 2, Biotek, excitation: 485 nm/emission: 528 nm).

### Mycobacterial adhesion assay studying Ca<sup>2+</sup> dependency

The adhesion assay was carried out analog as described before in method “Mycobacterial adhesion assay on microtiter plates”. Variations: Bacteria were suspended and diluted in TBS (with or without supplementation of Ca<sup>2+</sup> (5 mM), Mg<sup>2+</sup> (5 mM) or Ca<sup>2+</sup> (5 mM)/EDTA (15 mM)); for washing steps the same TBS buffer was used.

### Mycobacterial adhesion assay using functionalized magnetic PEG beads

The beads were functionalized as described before in the method “Functionalization of magnetic PEG beads”. Functionalized or unmodified beads ( $2 \cdot 10^7$  beads, 100  $\mu$ l), PBS (300  $\mu$ l) and GFP-expressing Mtb H37Rv bacteria ( $4 \cdot 10^8$  bacteria/ml, 100  $\mu$ l) were incubated for 1 h at rt while gently shaking in the dark. The beads were washed twice (500  $\mu$ l/batch) and re-suspended in PBS (100  $\mu$ l). The suspension was transferred to black microtiter plates (Nunc Maxisorp) and analyzed using a fluorescence microplate reader (Synergy 2, Biotek, excitation: 485 nm/emission: 528 nm).

### Verifying mycobacterial adhesion by PCR

The beads were functionalized as described before in method “Functionalization of magnetic PEG beads”. Functionalized or unmodified beads ( $5 \cdot 10^6$  beads, 25.0  $\mu$ l), PBS (375  $\mu$ l) and Mtb H37Rv bacteria in desired concentrations (100  $\mu$ l) were combined and incubated for 1 h at rt while gently shaking in the dark. Beads were washed twice (500  $\mu$ l/batch), centrifuged and re-suspended in PBS (50.0  $\mu$ l). For comparison Mtb H37Rv bacteria in desired concentrations were centrifuged and re-suspended in PBS (50.0  $\mu$ l). All samples were equally treated in the following steps.

TRIzol (250  $\mu$ l) and ethanol (250  $\mu$ l) were added and mixed. The suspension was transferred to a spin column in a collection tube of the DirectZol RNA MiniPrep kit (Zymo Research) followed by centrifugation (13000 x g, 1 min). The column was transferred into a new collection tube and the flow-through discarded. Pre-washing buffer (400  $\mu$ l) was added to the column, which was subsequently centrifuged (13000 x g, 1 min). Flow-through was discarded and the pre-washing step was repeated. Washing buffer (700  $\mu$ l) was added to the column followed by centrifugation (13000 x g, 2 min). The column was transferred into an RNase-free tube. To elute DNA, DNase/RNase-free water (50  $\mu$ l) was added and finally centrifuged (13000 x g, 1 min). Isolated DNA was stored at  $-80^\circ\text{C}$ .

For quantitative real-time PCR (qRT-PCR) analysis TaqMan Universal PCR Master Mix (10.0  $\mu$ l), Beijing primer (sense and antisense, 200  $\mu$ M, 1.0  $\mu$ l each), non-Beijing primer (sense and antisense, 200  $\mu$ M, 1.0  $\mu$ l each), fluorescein (FAM)-BlackBerry (BBQ) non-Beijing probe (4  $\mu$ M, 1.0  $\mu$ l), YakimaYellow (YAK)-BlackBerry (BBQ) Beijing probe (4  $\mu$ M, 1.0  $\mu$ l), double dist. water (2.0  $\mu$ l) and isolated DNA (2.0  $\mu$ l) were combined. The samples were transferred to a white 96 well plate, which was sealed, centrifuged (180 x g, 2 min,  $4^\circ\text{C}$ ) and subjected to the Rotor-Gene system (Qiagen). The used qRT-PCR protocol is given in table 4.

**Table 2: Primers used in this study.<sup>236</sup>**

<u>Primer pair</u>	<u>Name</u>	<u>Forward primer</u>	<u>Reverse primer</u>
Non-Beijing	nBjF/nBjR	5'-aagcattcccttgacagtcgaa	5'-ggcgcgatgactcgaaagaag
Beijing	BjF/BjR	5'-ctcggcagcttctcgat	5'-cgaactcgaggctgcctactac

**Table 3: FRET-probes used in this study.<sup>236</sup>**

<u>FRET-probe</u>	<u>Sequence</u>
Non-Beijing	5'-6FAM-tcatcaaagaccctcttgaaggccc-BBQ
Beijing	5'-YAK-aacgccagagaccagccgccggct-BBQ

**Table 4: qRT-PCR protocol (55 cycles)**

<u>Program</u>	<u>Temperature</u>	<u>Time</u>
Denaturation	95°C	15 min
Annealing	55°C	60 sec
Elongation	72°C	20 sec
End	25°C	5 min



## 2.6.4 Syntheses

### General methods for synthesis

Commercially available starting materials and reagents were used without further purification. Anhydrous dimethylformamide (DMF) was purchased, all other solvents used were dried for reactions (acetone over phosphorus pentoxide, acetonitrile over calcium hydride, dichloromethane (DCM) over calcium hydride, methanol (MeOH) over magnesium turnings, pyridine over potassium hydroxide, tetrahydrofuran (THF) over lithium aluminium hydride). Air- and/or moisture-sensitive reactions were carried out under an atmosphere of nitrogen. Thin layer chromatography (TLC) was performed on silica gel plates (GF 254, Merck). Detection was effected by UV irradiation and/or charring with sulfuric acid in ethanol (10%) followed by heat treatment. Flash chromatography was performed on silica gel 60 (particle size 0.040-0.063 mm, Merck).  $^1\text{H}$  and  $^{13}\text{C}$  NMR spectra were recorded on a DRX-500 or AV-600 instrument (Bruker). Chemical shifts are referenced to internal tetramethylsilane (TMS,  $^1\text{H}$ :  $\delta$  0.00 ppm) or to the residual proton of the NMR solvent:  $\text{CDCl}_3$  ( $^1\text{H}$ :  $\delta$  7.26 ppm,  $^{13}\text{C}$ :  $\delta$  77.00 ppm),  $\text{MeOH-}d_4$  ( $^1\text{H}$ :  $\delta$  3.31 ppm;  $^{13}\text{C}$ :  $\delta$  49.05 ppm) or  $\text{D}_2\text{O}$  ( $^1\text{H}$ :  $\delta$  4.65 ppm). Data are presented as follows: chemical shift, multiplicity (s: singlet, d: doublet, t: triplet, q: quartet, m: multiplet), coupling constant in Hertz (Hz) and integration of the respective signals. Full assignment was achieved with 2D NMR techniques ( $^1\text{H}$ - $^1\text{H}$  COSY,  $^1\text{H}$ - $^{13}\text{C}$  HSQC and  $^1\text{H}$ - $^{13}\text{C}$  HMBC). ESI-MS measurements were recorded on a LCQ Classic (Thermo Finnigan) and HRMS ESI spectra on an Agilent 6224 ESI-TOF. Optical rotation was measured on a polarimeter 341 (Perkin-Elmer) (Na-D-line: 589 nm, length of cell 1 dm, concentration listed: g/100ml). IR spectra were recorded on a Paragon 1000 FT-IR instrument (Perkin-Elmer). Melting points (m.p.) were determined on a Büchi 510 apparatus (Flawil).

### *p*-Aminophenyl $\alpha$ -D-arabinofuranoside (**1**)

*p*-Nitrophenyl  $\alpha$ -D-arabinofuranoside (**23**, 700 mg, 2.56 mmol) was dissolved in methanol (50.0 ml) and 10% palladium on charcoal (spatula tip) was added. The reaction was stirred for 3 h at rt under a hydrogen atmosphere, purified using a syringe filter (Satorius), concentrated in vacuo and lyophilized. The product **1** was obtained as a colorless solid (600 mg, 2.49 mmol, 97%). TLC (cyclohexane/ethyl acetate/methanol, 1:1:0.25):  $R_f$  = 0.07; rotation value:  $[\alpha]_D^{22} = +176.0^\circ$  ( $c = 1.0$ , MeOH); m.p.: 158.5-160.2°C;  $^1\text{H}$  NMR (500 MHz, MeOH- $d_4$ , 300 K):  $\delta$  = 6.91-6.88 (m, 2H, aryl- $\text{H}_{\text{meta}}$ ), 6.73-6.70 (m, 2H, aryl- $\text{H}_{\text{ortho}}$ ), 5.39 (d,  $^3J_{1,2} = 1.9$  Hz, 1H, H-1), 4.22 (dd,  $^3J_{1,2} = 2.0$  Hz,  $^3J_{2,3} = 4.1$  Hz, 1H, H-2), 4.09 (ddd,  $^3J_{3,4} = 6.5$  Hz,  $^3J_{4,5a} = 3.2$  Hz,  $^3J_{4,5b} = 5.1$  Hz, 1H, H-4), 3.97 (dd,  $^3J_{2,3} = 4.0$  Hz,  $^3J_{3,4} = 6.5$  Hz, 1H, H-3), 3.80 (dd,  $^3J_{4,5a} = 3.2$  Hz,  $^2J_{5a,5b} = 12.0$  Hz, 1H, H-5a), 3.69 (dd,  $^3J_{4,5b} = 5.1$  Hz,  $^2J_{5a,5b} = 12.0$  Hz, 1H, H-5b) ppm;  $^{13}\text{C}$  NMR (125 MHz, MeOH- $d_4$ , 300 K):  $\delta$  = 151.4 (aryl- $\text{C}_{\text{ipso}}$ ), 143.2 (aryl- $\text{C}_{\text{para}}$ ), 119.4 (aryl- $\text{C}_{\text{meta}}$ ), 117.8 (aryl- $\text{C}_{\text{ortho}}$ ), 109.0 (C-1), 85.9 (C-4), 83.8 (C-2), 78.4 (C-3), 62.9 (C-5) ppm; HRMS (ESI-MS):  $m/z$  = 264.0886,  $[\text{M}+\text{Na}]^+$  (calc. 264.0848 for  $\text{C}_{11}\text{H}_{15}\text{NO}_5+\text{Na}$ ).

### (2-Aminoethyl) $\alpha$ -D-arabinofuranoside (2)

The arabinofuranoside derivative **18** (11.0 mg, 50.2  $\mu$ mol) was dissolved in methanol (3.00 ml) and 10% palladium on charcoal (spatula tip) was added. The reaction was stirred for 2.5 h at rt under a hydrogen atmosphere, purified using a syringe filter (Satorius) and concentrated in vacuo. TLC (methanol/ethyl acetate, 5:1):  $R_f$  = 0.07. The instable product **2** was not further analyzed and directly used for surface functionalization.

### 6-Amino-6-deoxy- $\alpha,\alpha$ -D-trehalose (3)<sup>195</sup>

The trehalose derivative **28** (120 mg, 323  $\mu$ mol) was dissolved in methanol (25.0 ml) and 10% palladium on charcoal (spatula tip) was added. The reaction was stirred for 3 h at rt under a hydrogen atmosphere, purified using a syringe filter (Satorius), concentrated in vacuo and lyophilized. The product **3** was obtained as a white solid (110 mg, 323  $\mu$ mol, quant.). TLC (methanol/H<sub>2</sub>O/Et<sub>3</sub>N, 4:1:0.1):  $R_f$  = 0.12.; <sup>1</sup>H NMR (500 MHz, D<sub>2</sub>O, 300 K):  $\delta$  = 5.14 (d, <sup>3</sup> $J_{1',2'}$  = 4.0 Hz, 1H, H-1'), 5.13 (d, <sup>3</sup> $J_{1,2}$  = 3.9 Hz, 1H, H-1), 3.82-3.68 (m, 4H, H-4, H-4', H-5', H-6'a), 3.70 (ddd, <sup>3</sup> $J_{4,5}$  = 6.5 Hz, <sup>3</sup> $J_{5,6a}$  = 2.5 Hz, <sup>3</sup> $J_{5,6b}$  = 7.3 Hz, 1H, H-5), 3.70 (dd, <sup>3</sup> $J_{5',6'b}$  = 5.2 Hz, <sup>2</sup> $J_{6'a,6'b}$  = 12.0 Hz, 1H, H-6'b), 3.59 (dd, <sup>3</sup> $J_{1,2}$  = 3.9 Hz, <sup>3</sup> $J_{2,3}$  = 9.9 Hz, <sup>3</sup> $J_{1',2'}$  = 3.9 Hz, <sup>3</sup> $J_{2',3'}$  = 9.9 Hz, 2H, H-2, H-2'), 3.39 (dd~t, <sup>3</sup> $J_{2',3'}$  = 9.5 Hz, <sup>3</sup> $J_{3',4'}$  = 9.5 Hz, 1H, H-3'), 3.28 (dd~t, <sup>3</sup> $J_{2,3}$  = 9.5 Hz, <sup>3</sup> $J_{3,4}$  = 9.5 Hz, 1H, H-3), 2.95 (dd, <sup>3</sup> $J_{5,6a}$  = 2.7 Hz, <sup>2</sup> $J_{6a,6b}$  = 13.7 Hz, 1H, H-6a), 2.70 (dd, <sup>3</sup> $J_{5,6b}$  = 7.8 Hz, <sup>2</sup> $J_{6a,6b}$  = 13.7 Hz, 1H, H-6b) ppm.

### *p*-Aminophenyl $\alpha$ -D-mannopyranoside (4)<sup>187</sup>

*p*-Nitrophenyl  $\alpha$ -D-mannopyranoside (1.00 g, 3.32 mmol) was dissolved in methanol (50.0 ml) and 10% palladium on charcoal (spatula tip) was added. The reaction was stirred for 4 h at rt under a hydrogen atmosphere, purified using a syringe filter (Satorius), concentrated in vacuo and lyophilized. The product **4** was obtained as a white solid (900 mg, 3.32 mmol, quant.). TLC (cyclohexane/ethyl acetate/methanol, 1:1:0.2):  $R_f$  = 0.10; <sup>1</sup>H NMR (500 MHz, MeOH-*d*<sub>4</sub>, 300 K):  $\delta$  = 6.92-6.88 (m, 2H, aryl-H<sub>meta</sub>), 6.70-6.67 (m, 2H, aryl-H<sub>ortho</sub>), 5.28 (d, <sup>3</sup> $J_{1,2}$  = 1.8 Hz, 1H, H-1), 3.97 (dd, <sup>3</sup> $J_{1,2}$  = 1.9 Hz, <sup>3</sup> $J_{2,3}$  = 3.4 Hz, 1H, H-2), 3.87 (dd, <sup>3</sup> $J_{2,3}$  = 3.4 Hz, <sup>3</sup> $J_{3,4}$  = 9.2 Hz, 1H, H-3), 3.78 (dd, <sup>3</sup> $J_{5,6a}$  = 2.4 Hz, <sup>2</sup> $J_{6a,6b}$  = 11.9 Hz, 1H, H-6a), 3.73 (dd, <sup>3</sup> $J_{3,4}$  = 8.0 Hz, <sup>3</sup> $J_{4,5}$  = 10.9 Hz, 1H, H-4), 3.72 (dd, <sup>3</sup> $J_{5,6b}$  = 5.1 Hz, <sup>2</sup> $J_{6a,6b}$  = 12.0 Hz, 1H, H-6b), 3.67 (ddd, <sup>3</sup> $J_{4,5}$  = 9.8 Hz, <sup>3</sup> $J_{5,6a}$  = 2.3 Hz, <sup>3</sup> $J_{5,6b}$  = 4.8 Hz, 1H, H-5) ppm.

### (2-Aminoethyl) $\alpha$ -D-mannopyranoside (5)<sup>180</sup>

The azido sugar **12** (900 mg, 3.61 mmol) was dissolved in methanol (50.0 ml) and 10% palladium on charcoal (spatula tip) was added. The reaction was stirred overnight at rt under a hydrogen atmosphere, purified using a syringe filter (Satorius) and concentrated in vacuo. The product **5** was obtained as a white foam (790 mg, 3.54 mmol, 98%).

TLC (methanol/ethyl acetate, 5:1):  $R_f = 0.06$ ;  $^1\text{H NMR}$  (500 MHz,  $\text{MeOH-}d_4$ , 300 K):  $\delta = 4.77$  (d,  $^3J_{1,2} = 1.7$  Hz, 1H, H-1), 3.84 (dd,  $^3J_{5,6a} = 2.4$  Hz,  $^2J_{6a,6b} = 11.7$  Hz, 1H, H-6a), 3.83 (dd,  $^3J_{1,2} = 1.8$  Hz,  $^3J_{2,3} = 3.2$  Hz, 1H, H-2), 3.77 (ddd,  $^3J = 4.8$  Hz,  $^3J = 6.0$  Hz,  $^2J = 10.1$  Hz, 1H,  $\text{OCH}_2\text{CH}_2\text{NH}_2$ ), 3.71 (dd,  $^3J_{2,3} = 3.4$  Hz,  $^3J_{3,4} = 9.2$  Hz, 1H, H-3), 3.70 (dd,  $^3J_{5,6b} = 6.0$  Hz,  $^2J_{6a,6b} = 11.7$  Hz, 1H, H-6b), 3.60 (dd-t,  $^3J_{3,4} = 9.5$  Hz,  $^3J_{4,5} = 9.5$  Hz, 1H, H-4), 3.54 (ddd,  $^3J = 2.1$  Hz,  $^3J = 6.0$  Hz,  $^2J = 9.7$  Hz, 1H,  $\text{OCH}_2\text{CH}_2\text{NH}_2$ ), 3.46 (ddd,  $^3J_{4,5} = 10.0$  Hz,  $^3J_{5,6a} = 4.7$  Hz,  $^3J_{5,6b} = 6.1$  Hz, 1H, H-5), 2.86-3.77 (m, 2H,  $\text{OCH}_2\text{CH}_2\text{NH}_2$ ) ppm.

#### *p*-Aminophenyl $\alpha$ -D-glucopyranoside (**6**)<sup>237</sup>

*p*-Nitrophenyl  $\alpha$ -D-glucopyranoside (1.00 g, 3.32 mmol) was dissolved in methanol (50.0 ml) and 10% palladium on charcoal (spatula tip) was added. The reaction was stirred overnight at rt under a hydrogen atmosphere, purified using a syringe filter (Satorius), concentrated in vacuo and lyophilized. The product **6** was obtained as a colorless foam (890 mg, 3.28 mmol, 99%). TLC (ethyl acetate/methanol, 2:1):  $R_f = 0.36$ ;  $^1\text{H NMR}$  (500 MHz,  $\text{MeOH-}d_4$ , 300 K):  $\delta = 6.98$ -6.94 (m, 2H, aryl-H<sub>meta</sub>), 6.71-6.67 (m, 2H, aryl-H<sub>ortho</sub>), 5.27 (d,  $^3J_{1,2} = 3.7$  Hz, 1H, H-1), 3.82 (dd-t,  $^3J_{2,3} = 9.4$  Hz,  $^3J_{3,4} = 9.4$  Hz, 1H, H-3), 3.76 (dd,  $^3J_{5,6a} = 1.8$  Hz,  $^2J_{6a,6b} = 12.6$  Hz, 1H, H-6a), 3.76-3.71 (m, 1H, H-5), 3.70 (dd,  $^3J_{5,6b} = 6.1$  Hz,  $^2J_{6a,6b} = 12.5$  Hz, 1H, H-6b), 3.51 (dd,  $^3J_{1,2} = 3.7$  Hz,  $^3J_{2,3} = 9.7$  Hz, 1H, H-2), 3.41 (dd-t,  $^3J_{3,4} = 9.1$  Hz,  $^3J_{4,5} = 9.1$  Hz, 1H, H-4) ppm.

#### *p*-Aminophenyl $\beta$ -D-glucopyranoside (**7**)<sup>237</sup>

*p*-Nitrophenyl  $\beta$ -D-glucopyranoside (260 mg, 864  $\mu\text{mol}$ ) was dissolved in methanol (13.0 ml) and 10% palladium on charcoal (spatula tip) was added. The reaction was stirred overnight at rt under a hydrogen atmosphere, purified using a syringe filter (Satorius), concentrated in vacuo and lyophilized. The product **7** was obtained as a colorless foam (224 mg, 827  $\mu\text{mol}$ , 96%). TLC (ethyl acetate/methanol, 2:1):  $R_f = 0.35$ ;  $^1\text{H NMR}$  (500 MHz,  $\text{MeOH-}d_4$ , 300 K):  $\delta = 6.94$ -6.91 (m, 2H, aryl-H<sub>meta</sub>), 6.70-6.67 (m, 2H, aryl-H<sub>ortho</sub>), 4.72 (d,  $^3J_{1,2} = 7.4$  Hz, 1H, H-1), 3.88 (dd,  $^3J_{5,6a} = 1.6$  Hz,  $^2J_{6a,6b} = 12.0$  Hz, 1H, H-6a), 3.69 (dd,  $^3J_{5,6b} = 5.2$  Hz,  $^2J_{6a,6b} = 12.0$  Hz, 1H, H-6b), 3.48-3.39 (m, 3H, H-3, H-4, H-5), 3.40 (dd,  $^3J_{1,2} = 7.3$  Hz,  $^3J_{2,3} = 2.7$  Hz, 1H, H-2) ppm.

#### *p*-Aminophenyl $\alpha$ -D-galactopyranoside (**8**)<sup>187</sup>

*p*-Nitrophenyl  $\alpha$ -D-galactopyranoside (1.00 g, 3.32 mmol) was dissolved in methanol (50.0 ml) and 10% palladium on charcoal (spatula tip) was added. The reaction was stirred for 2.5 h at rt under a hydrogen atmosphere, purified using a syringe filter (Satorius), concentrated in vacuo and lyophilized. The product **8** was obtained as a colorless solid (897 mg, 3.31 mmol, quant.). TLC (ethyl acetate/methanol, 2:1):  $R_f = 0.38$ ;  $^1\text{H NMR}$  (200 MHz,  $\text{MeOH-}d_4$ , 300 K):

$\delta = 7.06\text{-}6.97$  (m, 2H, aryl- $H_{\text{meta}}$ ),  $6.78\text{-}6.69$  (m, 2H, aryl- $H_{\text{ortho}}$ ),  $5.33$  (d,  ${}^3J_{1,2} = 2.7$  Hz, 1H, H-1),  $4.10\text{-}3.93$  (m, 4H, H-3, H-5, H-6a, H-6b),  $3.78\text{-}3.70$  (m, 2H, H-2, H-4) ppm.

#### 1,2,3,4,6-Penta-O-acetyl- $\alpha,\beta$ -D-mannopyranose (**9**)<sup>181</sup>

A suspension of sodium acetate (4.10 g, 50.0 mmol) in acetic anhydride ( $\text{Ac}_2\text{O}$ , 45 ml) was refluxed. The heating source was removed and D-mannose (9.00 g, 50.0 mmol, 1 eq.) was slowly added. The reaction mixture was stirred for 30 min at rt and for 30 min under reflux. After addition of ice (200 ml) it was stirred 1 h and extracted with DCM. The organic phases were dried over  $\text{MgSO}_4$ , filtered and concentrated in vacuo. The product **9** was co-evaporated with toluene and a colorless oil was obtained (19.2 g, 49.3 mmol, 99%) ( $\alpha:\beta$  ratio = 3:1 by integration of the  ${}^1\text{H}$  NMR spectrum). TLC (cyclohexane/acetone, 3:2):  $R_f = 0.35$ ;  ${}^1\text{H}$  NMR (200 MHz,  $\text{CDCl}_3$ , 300 K, TMS):  $\delta = 6.09$  (d,  ${}^3J_{1,2} = 1.9$  Hz, 1H, H-1 ( $\alpha$ )),  $5.86$  (d,  ${}^3J_{1,2} = 1.2$  Hz, 1H, H-1 ( $\beta$ )),  $5.49$  (dd,  ${}^3J_{1,2} = 1.2$  Hz,  ${}^3J_{2,3} = 3.2$  Hz, 1H, H-2 ( $\beta$ )),  $5.38\text{-}5.24$  (m, 4H, H-2 ( $\alpha$ ), H-3 ( $\alpha$ ), H-4 ( $\alpha$ ), H-4 ( $\beta$ )),  $5.13$  (dd,  ${}^3J_{2,3} = 3.2$  Hz,  ${}^3J_{3,4} = 10.0$  Hz, 1H, H-3 ( $\beta$ )),  $4.31$  (dd,  ${}^3J_{5,6a} = 5.4$  Hz,  ${}^2J_{6a,6b} = 12.4$  Hz, 1H, H-6a ( $\alpha$ )),  $4.29$  (dd,  ${}^3J_{5,6b} = 4.9$  Hz,  ${}^2J_{6a,6b} = 12.3$  Hz, 1H, H-6b ( $\alpha$ )),  $4.16$  (dd,  ${}^3J_{5,6a} = 2.5$  Hz,  ${}^2J_{6a,6b} = 8.0$  Hz, 1H, H-6a ( $\beta$ )),  $4.18\text{-}4.00$  (m, 2H, H-5 $\alpha$ , H-6b ( $\beta$ )),  $3.81$  (ddd,  ${}^3J_{4,5} = 9.7$  Hz,  ${}^3J_{5,6a} = 5.3$  Hz,  ${}^3J_{5,6b} = 2.5$  Hz, 1H, H-5 ( $\beta$ )),  $2.18, 2.17, 2.09, 2.06, 2.01$  (s each, 3H each, 5  $\text{COCH}_3$  ( $\alpha,\beta$ )) ppm.

#### (2-Bromoethyl) 2,3,4,6-tetra-O-acetyl- $\alpha$ -D-mannopyranoside (**10**)<sup>182</sup>

Acetyl protected mannose **9** (1.50 g, 3.85 mmol) and 2-bromoethanol (330  $\mu\text{l}$ , 4.64 mmol, 1.2 eq.) were dissolved in dry DCM (15.0 ml). Boron trifluoride diethyl etherate ( $\text{BF}_3 \cdot \text{Et}_2\text{O}$ , 2.70 ml, 21.3 mmol, 5.5 eq.) was added slowly within 30 min under cooling with an ice bath and the reaction was stirred overnight at rt. Dist. water was added and the aqueous phase extracted with DCM. The combined organic phases were dried over  $\text{MgSO}_4$ , filtered and concentrated in vacuo. The crude product was chromatographed on silica gel (cyclohexane/ethyl acetate, 2:1) and recrystallized from diethyl ether to give the pure  $\alpha$ -anomere **10** as colorless solid (986 mg, 2.16 mmol, 56%). TLC (cyclohexane/ethyl acetate, 1:1):  $R_f = 0.48$ ;  ${}^1\text{H}$  NMR (500 MHz,  $\text{CDCl}_3$ , 300 K, TMS):  $\delta = 5.35$  (dd,  ${}^3J_{2,3} = 3.4$  Hz,  ${}^3J_{3,4} = 10.1$  Hz, 1H, H-3),  $5.31\text{-}5.27$  (m, 2H, H-2, H-4),  $4.88$  (d,  ${}^3J_{1,2} = 1.7$  Hz, 1H, H-1),  $4.27$  (dd,  ${}^3J_{5,6a} = 6.0$  Hz,  ${}^2J_{6a,6b} = 12.7$  Hz, 1H, H-6a),  $4.16\text{-}4.12$  (m, 2H, H-5, H-6b),  $3.98$  (dt,  ${}^3J = 6.3$  Hz,  ${}^2J = 11.2$  Hz, 1H,  $\text{OCH}_2\text{CH}_2\text{Br}$ ),  $3.89$  (dt,  ${}^3J = 5.8$  Hz,  ${}^2J = 11.3$  Hz, 1H,  $\text{OCH}_2\text{CH}_2\text{Br}$ ),  $3.52$  (t,  ${}^3J = 6.0$  Hz,  ${}^3J = 6.0$  Hz, 2H,  $\text{OCH}_2\text{CH}_2\text{Br}$ ),  $2.16, 2.11, 2.05, 2.00$  (s each, 3H each, 4  $\text{COCH}_3$ ) ppm.

(2-Azidoethyl) 2,3,4,6-tetra-O-acetyl- $\alpha$ -D-mannopyranoside (**11**)<sup>180</sup>

To a solution of bromoethyl mannopyranoside **10** (3.00 g, 6.59 mmol) in dry DMF (50.0 ml) sodium azide (2.13 g, 32.7 mmol, 5 eq.) and tetrabutylammonium iodide (TBAI, 490 mg, 1.32 mmol, 0.2 eq.) were added. The reaction mixture was stirred under a nitrogen atmosphere for 8 h at 70°C and overnight at rt. Dist. water was added and the aqueous phase was extracted with DCM. The combined organic layers were dried over MgSO<sub>4</sub>, filtered and concentrated in vacuo. The crude product was chromatographed on silica gel (cyclohexane/ethyl acetate, 2:1) to give the azido sugar **11** (2.54 g, 6.09 mmol, 92%) as colorless crystals. TLC (cyclohexane/ethyl acetate, 2:1): R<sub>f</sub> = 0.16; <sup>1</sup>H NMR (500 MHz, CDCl<sub>3</sub>, 300 K, TMS):  $\delta$  = 5.37 (dd, <sup>3</sup>J<sub>2,3</sub> = 3.5 Hz, <sup>3</sup>J<sub>3,4</sub> = 10.0 Hz, 1H, H-3), 5.30 (dd~t, <sup>3</sup>J<sub>3,4</sub> = 10.0 Hz, <sup>3</sup>J<sub>4,5</sub> = 10.0 Hz, 1H, H-4), 5.28 (dd, <sup>3</sup>J<sub>1,2</sub> = 1.8 Hz, <sup>3</sup>J<sub>2,3</sub> = 3.4 Hz, 1H, H-2), 4.87 (d, <sup>3</sup>J<sub>1,2</sub> = 1.7 Hz, 1H, H-1), 4.29 (dd, <sup>3</sup>J<sub>5,6a</sub> = 5.4 Hz, <sup>2</sup>J<sub>6a,6b</sub> = 12.3 Hz, 1H, H-6a), 4.13 (dd, <sup>3</sup>J<sub>5,6b</sub> = 2.4 Hz, <sup>2</sup>J<sub>6a,6b</sub> = 12.3 Hz, 1H, H-6b), 4.05 (ddd, <sup>3</sup>J<sub>4,5</sub> = 9.9 Hz, <sup>3</sup>J<sub>5,6a</sub> = 5.3 Hz, <sup>3</sup>J<sub>5,6b</sub> = 2.4 Hz, 1H, H-5), 3.87 (ddd, <sup>3</sup>J = 3.8 Hz, <sup>3</sup>J = 6.9 Hz, <sup>2</sup>J = 10.7 Hz, 1H, OCH<sub>2</sub>CH<sub>2</sub>N<sub>3</sub>), 3.68 (ddd, <sup>3</sup>J = 3.7 Hz, <sup>3</sup>J = 6.0 Hz, <sup>2</sup>J = 10.6 Hz, 1H, OCH<sub>2</sub>CH<sub>2</sub>N<sub>3</sub>), 3.50 (ddd, <sup>3</sup>J = 3.6 Hz, <sup>3</sup>J = 6.9 Hz, <sup>2</sup>J = 13.3 Hz, 1H, OCH<sub>2</sub>CH<sub>2</sub>N<sub>3</sub>), 3.45 (ddd, <sup>3</sup>J = 3.8 Hz, <sup>3</sup>J = 6.0 Hz, <sup>2</sup>J = 13.3 Hz, 1H, OCH<sub>2</sub>CH<sub>2</sub>N<sub>3</sub>), 2.16, 2.10, 2.05, 1.99 (s each, 3H each, 4 COCH<sub>3</sub>) ppm.

(2-Azidoethyl)  $\alpha$ -D-mannopyranoside (**12**)<sup>180</sup>

The acetyl-protected mannopyranoside derivative **11** (2.10 g, 5.04 mmol) was suspended in dry methanol and sodium methoxide (spatula tip) was added. The reaction mixture was stirred overnight at rt under a nitrogen atmosphere. After neutralization with Amberlite IR120 ion exchange resin and concentration in vacuo, the crude product was chromatographed on silica gel (ethyl acetate/methanol, 7:1) and lyophilized to give the product **12** (1.23 g, 4.93 mmol, 98%) as a white solid. TLC (ethyl acetate/methanol, 2:1): R<sub>f</sub> = 0.50; <sup>1</sup>H NMR (500 MHz, MeOH-*d*<sub>4</sub>, 300 K):  $\delta$  = 4.85 (d, <sup>3</sup>J<sub>1,2</sub> = 1.7 Hz, 1H, H-1), 3.95 (ddd, <sup>3</sup>J = 4.6 Hz, <sup>3</sup>J = 4.6 Hz, <sup>2</sup>J = 9.8 Hz, 1H, OCH<sub>2</sub>CH<sub>2</sub>N<sub>3</sub>), 3.87 (dd, <sup>3</sup>J<sub>1,2</sub> = 1.7 Hz, <sup>3</sup>J<sub>2,3</sub> = 3.5 Hz, 1H, H-2), 3.88 (dd, <sup>3</sup>J<sub>5,6a</sub> = 2.4 Hz, <sup>2</sup>J<sub>6a,6b</sub> = 11.6 Hz, 1H, H-6a), 3.76 (dd, <sup>3</sup>J<sub>2,3</sub> = 3.4 Hz, <sup>3</sup>J<sub>3,4</sub> = 9.1 Hz, 1H, H-3), 3.75 (dd, <sup>3</sup>J<sub>5,6b</sub> = 5.7 Hz, <sup>2</sup>J<sub>6a,6b</sub> = 11.8 Hz, 1H, H-6b), 3.69-3.63 (m, 2H, H-4, H-5), 3.60 (ddd, <sup>3</sup>J = 2.3 Hz, <sup>3</sup>J = 5.8 Hz, <sup>2</sup>J = 9.8 Hz, 1H, OCH<sub>2</sub>CH<sub>2</sub>N<sub>3</sub>), 3.46-3.42 (m, 2H, OCH<sub>2</sub>CH<sub>2</sub>N<sub>3</sub>) ppm.

5-O-*tert*-Butyldimethylsilyl-1,2,3-tri-O-acetyl- $\alpha$ , $\beta$ -D-arabinofurose (**13**)<sup>184</sup>

D-Arabinose (5.00 g, 33.3 mmol) was suspended in dry pyridine (50.0 ml) and *tert*-butyldimethylsilyl chloride (TBDMSCl, 5.50 g, 36.5 mmol, 1.1 eq.) was added. The reaction mixture was stirred for 4 h at rt under a nitrogen atmosphere. Acetic anhydride (Ac<sub>2</sub>O, 15.0 ml, 136 mmol, 4 eq.) was added and the reaction was stirred overnight. After addition of a saturated aqueous NaHCO<sub>3</sub> solution (150 ml) the resulting mixture was extracted with DCM.

The combined organic layers were dried over  $\text{MgSO}_4$ , filtered and concentrated in vacuo. The crude product was chromatographed on silica gel (cyclohexane/ethyl acetate 4:1) to give the arabinofuranose derivative **13** (7.32 g, 18.8 mmol, 57%) as a colorless oil ( $\alpha$ : $\beta$  ratio = 2:1 by integration of the  $^1\text{H}$  NMR spectrum). TLC (cyclohexane/ethyl acetate, 2:1):  $R_f$  = 0.50; rotation value:  $[\alpha]_D^{22} = +12.8^\circ$  ( $c = 0.5$ ,  $\text{CH}_2\text{Cl}_2$ );  $^1\text{H}$  NMR (500 MHz,  $\text{CDCl}_3$ , 300 K):  $\delta$  = 6.34 (d,  $^3J_{1,2} = 4.7$  Hz, 1H, H-1 ( $\beta$ )), 6.16 (d~s, 1H, H-1 ( $\alpha$ )), 5.48 (dd,  $^3J_{3,4} = 5.9$  Hz,  $^3J_{2,3} = 7.1$  Hz, 1H, H-3 ( $\beta$ )), 5.33 (dd,  $^3J_{1,2} = 4.7$  Hz,  $^3J_{2,3} = 7.1$  Hz, 1H, H-2 ( $\beta$ )), 5.20 (dd,  $^3J_{2,3} = 1.7$  Hz,  $^3J_{3,4} = 4.9$  Hz, 1H, H-3 ( $\alpha$ )), 5.18 (dd~d,  $^3J_{2,3} = 1.7$  Hz, 1H, H-2 ( $\alpha$ )), 4.20 (ddd~q,  $^3J_{3,4} = 4.3$  Hz,  $^3J_{4,5a} = 4.3$  Hz,  $^3J_{4,5b} = 4.3$  Hz, 1H, H-4 ( $\alpha$ )), 4.06 (ddd~q,  $^3J_{3,4} = 5.7$  Hz,  $^3J_{4,5a} = 5.7$  Hz,  $^3J_{4,5b} = 5.7$  Hz, 1H, H-4 ( $\beta$ )), 3.85 (dd,  $^3J_{4,5a} = 4.2$  Hz,  $^2J_{5a,5b} = 11.2$  Hz, 1H, H-5a ( $\alpha$ )), 3.81 (dd,  $^3J_{4,5b} = 4.3$  Hz,  $^2J_{5a,5b} = 11.2$  Hz, 1H, H-5b ( $\alpha$ )), 3.79 (dd,  $^3J_{4,5a} = 5.7$  Hz,  $^2J_{5a,5b} = 12.0$  Hz, 1H, H-5a ( $\beta$ )), 3.77 (dd,  $^3J_{4,5b} = 5.7$  Hz,  $^2J_{5a,5b} = 12.1$  Hz, 1H, H-5b ( $\beta$ )), 2.11, 2.10, 2.09 (s each, 3H each, 3  $\text{COCH}_3$  ( $\alpha$ )), 2.08, 2.07, 2.06 (s each, 3H each, 3  $\text{COCH}_3$  ( $\beta$ )), 0.90 (s, 9H,  $\text{OSi}(\text{CH}_3)_2\text{C}(\text{CH}_3)_3$  ( $\alpha$ )), 0.89 (s, 9H,  $\text{OSi}(\text{CH}_3)_2\text{C}(\text{CH}_3)_3$  ( $\beta$ )), 0.07, 0.067, 0.065, 0.06 (s each, 3H each,  $\text{OSi}(\text{CH}_3)_2\text{C}(\text{CH}_3)_3$  ( $\alpha,\beta$ )) ppm;  $^{13}\text{C}$  NMR (125 MHz,  $\text{CDCl}_3$ , 300 K):  $\delta$  = 169.7, 169.6, 169.6, 169.3, 169.1, 169.1 (6  $\text{COCH}_3$  ( $\alpha,\beta$ )), 99.3 (C-1 ( $\alpha$ )), 93.5 (C-1 ( $\beta$ )), 84.6 (C-4 ( $\alpha$ )), 81.6 (C-4 ( $\beta$ )), 81.0 (C-2 ( $\alpha$ )), 76.5 (C-3 ( $\alpha$ )), 75.4 (C-2 ( $\beta$ )), 74.2 (C-3 ( $\beta$ )), 63.7 (C-5 ( $\beta$ )), 61.9 (C-5 ( $\alpha$ )), 25.5 (2  $\text{OSi}(\text{CH}_3)_2\text{C}(\text{CH}_3)_3$  ( $\alpha,\beta$ )), 20.8, 20.5, 20.2 (3  $\text{COCH}_3$  ( $\beta$ )), 20.8, 20.5, 20.4 (3  $\text{COCH}_3$  ( $\alpha$ )), 18.0 ( $\text{OSi}(\text{CH}_3)_2\text{C}(\text{CH}_3)_3$  ( $\alpha,\beta$ )), -5.6 ( $\text{OSi}(\text{CH}_3)_2\text{C}(\text{CH}_3)_3$  ( $\beta$ )), -5.7 ( $\text{OSi}(\text{CH}_3)_2\text{C}(\text{CH}_3)_3$  ( $\alpha$ )) ppm; ESI-MS:  $m/z$  = 413.078,  $[\text{M}+\text{Na}]^+$  (calc. 413.161 for  $\text{C}_{17}\text{H}_{30}\text{O}_5\text{Si}+\text{Na}$ ).

#### 1,2,3-Tri-O-acetyl- $\alpha,\beta$ -D-arabinofurose (14)

The product **14** was obtained by a different synthetic route as described in literature:<sup>188</sup> The arabinofuranose derivative **13** (10.7 g, 27.4 mmol) was stirred in acetic acid (120 ml) and distilled water (60.0 ml) overnight at rt. A saturated aqueous  $\text{NaHCO}_3$  solution was added and the resulting mixture was extracted with DCM. The combined organic layers were dried over  $\text{MgSO}_4$ , filtered and concentrated in vacuo. The crude product was chromatographed on silica gel (cyclohexane/ethyl acetate, 1:1) to give **14** (7.41 g, 26.8 mmol, 98%) as a colorless oil. ( $\alpha$ : $\beta$  ratio = 2:1 by integration of the  $^1\text{H}$  NMR spectrum). TLC (cyclohexane/ethyl acetate, 2:1):  $R_f$  = 0.08;  $^1\text{H}$  NMR (500 MHz,  $\text{CDCl}_3$ , 300 K, TMS):  $\delta$  = 6.39-6.38 (m, 1H, H-1 ( $\beta$ )), 6.18 (d~s, 1H, H-1 ( $\alpha$ )), 5.40-5.39 (m, 2H, H-2 ( $\beta$ ), H-3 ( $\beta$ )), 5.25 (dd~d,  $^3J_{2,3} = 1.9$  Hz, 1H, H-2 ( $\alpha$ )), 5.12 (dd,  $^3J_{2,3} = 1.8$  Hz,  $^3J_{3,4} = 5.2$  Hz, 1H, H-3 ( $\alpha$ )), 4.23 (ddd,  $^3J_{3,4} = 5.2$  Hz,  $^3J_{4,5a} = 3.4$  Hz,  $^3J_{4,5b} = 4.2$  Hz, 1H, H-4 ( $\alpha$ )), 4.11-4.07 (m, 1H, H-4 ( $\beta$ )), 3.89 (dd,  $^3J_{4,5a} = 3.4$  Hz,  $^2J_{5a,5b} = 12.3$  Hz, 1H, H-5a ( $\alpha$ )), 3.86 (dd,  $^3J_{4,5a} = 4.4$  Hz,  $^2J_{5a,5b} = 12.2$  Hz, 1H, H-5a ( $\beta$ )), 3.81 (dd,  $^3J_{4,5b} = 4.2$  Hz,  $^2J_{5a,5b} = 12.3$  Hz, 1H, H-5b ( $\alpha$ )), 3.74 (dd,  $^3J_{4,5b} = 5.3$  Hz,

$^2J_{5a,5b} = 12.2$  Hz, 1H, H-5b ( $\beta$ ), 2.14, 2.13, 2.12 (s each, 3H each, 3 COCH<sub>3</sub> ( $\alpha$ )), 2.12, 2.10, 2.00 (s each, 3H each, 3 COCH<sub>3</sub> ( $\beta$ )) ppm.

#### 1,2,3,5-Tetra-O-acetyl- $\alpha,\beta$ -D-arabinofurose (15)

The product **15** was obtained by a different synthetic route as described in literature.<sup>185</sup> The arabinofurose derivative **14** (4.00 g, 14.5 mmol) was dissolved in dry pyridine (40.0 ml) and acetic anhydride (2.80 ml, 29.6 mmol, 2 eq.) was added. The reaction mixture was stirred overnight at rt under a nitrogen atmosphere. After addition of a saturated aqueous NaHCO<sub>3</sub> solution (100 ml) the resulting mixture was extracted with DCM. The combined organic layers were washed with dist. water, dried over MgSO<sub>4</sub>, filtered and concentrated in vacuo. The crude product was co-evaporated with toluene and chromatographed on silica gel (cyclohexane/ethyl acetate, 2:1) to give the tetraacetylated sugar **15** (4.32 g, 13.6 mmol, 94%) as a colorless oil ( $\alpha:\beta$  ratio = 2:1 by integration of the <sup>1</sup>H NMR spectrum). TLC (cyclohexane/ethyl acetate, 2:1): R<sub>f</sub> = 0.20; <sup>1</sup>H NMR (500 MHz, CDCl<sub>3</sub>, 300 K, TMS):  $\delta$  = 6.39 (d,  $^3J_{1,2} = 3.9$  Hz, 1H, H-1 ( $\beta$ )), 6.20 (d~s, 1H, H-1 ( $\alpha$ )), 5.36-5.35 (m, 2H, H-2 ( $\beta$ ), H-3 ( $\beta$ )), 5.22 (dd,  $^3J_{1,2} = 0.5$  Hz,  $^3J_{2,3} = 1.3$  Hz, 1H, H-2 ( $\alpha$ )), 5.07-5.04 (ddd,  $^3J_{2,3} = 1.8$  Hz,  $^3J_{3,4} = 4.6$  Hz,  $^4J = 0.6$  Hz, 1H, H-3 ( $\alpha$ )), 4.40 (dd,  $^3J_{4,5a} = 4.0$  Hz,  $^2J_{5a,5b} = 14.6$  Hz, 1H, H-5a ( $\alpha$ )), 4.40-4.36 (m, 1H, H-4 ( $\alpha$ )), 4.36 (dd,  $^3J_{4,5a} = 4.2$  Hz,  $^2J_{5a,5b} = 11.7$  Hz, 1H, H-5a ( $\beta$ )), 4.27 (dd,  $^3J_{4,5b} = 7.2$  Hz,  $^2J_{5a,5b} = 11.6$  Hz, 1H, H-5b ( $\beta$ )), 4.25-4.20 (m, 2H, H-5b ( $\alpha$ ), H-4 ( $\beta$ )), 2.13 (s, 6H, 2 COCH<sub>3</sub> ( $\alpha$ )), 2.12, 2.10 (s each, 3H each, 2 COCH<sub>3</sub> ( $\alpha$ )), 2.11, 2.10, 2.09, 2.08 (s each, 3H each, 4 COCH<sub>3</sub> ( $\beta$ )) ppm.

#### (2-Chloroethyl) 2,3,5-tri-O-acetyl- $\alpha$ -D-arabinofuranoside (16)<sup>186</sup>

Acetyl protected arabinofuranose derivative **15** (500 mg, 1.57 mmol) was dissolved in dry acetonitrile (15.0 ml), tin tetrachloride (1 M in DCM, 6.00 ml, 6.00 mmol, 4 eq.) was slowly added and the reaction mixture was stirred for 30 min at rt. 2-Chloroethanol was diluted in dry acetonitrile (3.00 ml) and added dropwise. The reaction was stirred 45 min at rt, followed by ice-cooling and slowly supplementation of a saturated aqueous NaHCO<sub>3</sub> solution. The crude product was filtrated through celite, extracted with DCM and washed with brine and dist. water. It was further purified by silica gel-chromatography (n-hexane/ethyl acetate, 3:1) giving the arabinofuranoside derivative **16** (340 mg, 1.01 mmol, 64%) as colorless oil. TLC (n-hexane/ethyl acetate, 2:1): R<sub>f</sub> = 0.21; <sup>1</sup>H NMR (500 MHz, CDCl<sub>3</sub>, 300 K, TMS):  $\delta$  = 5.12 (dd~d,  $^3J_{2,3} = 1.6$  Hz, 1H, H-2), 5.09 (d~s, 1H, H-1), 4.99 (dd,  $^3J_{2,3} = 1.5$  Hz,  $^3J_{3,4} = 5.1$  Hz, 1H, H-3), 4.44 (dd,  $^3J_{4,5a} = 3.4$  Hz,  $^2J_{5a,5b} = 11.8$  Hz, 1H, H-5a), 4.30 (ddd,  $^3J_{3,4} = 5.3$  Hz,  $^3J_{4,5a} = 3.4$  Hz,  $^3J_{4,5b} = 5.4$  Hz, 1H, H-4), 4.23 (dd,  $^3J_{4,5b} = 5.7$  Hz,  $^2J_{5a,5b} = 11.8$  Hz, 1H, H-5b), 3.94 (dt,  $^3J = 5.9$  Hz,  $^3J = 5.9$  Hz,  $^2J = 11.2$  Hz, 1H, OCH<sub>2</sub>CH<sub>2</sub>Cl), 3.78 (dt,  $^3J = 5.7$  Hz,

$^3J = 5.7$  Hz,  $^2J = 11.0$  Hz, 1H, OCH<sub>2</sub>CH<sub>2</sub>Cl), 3.66 (t,  $^3J = 5.8$  Hz,  $^3J = 5.8$  Hz, 2H, OCH<sub>2</sub>CH<sub>2</sub>Cl), 2.12, 2.11, 2.10 (s each, 3H each, 3 COCH<sub>3</sub>) ppm.

(2-Azidoethyl) 2,3,5-tri-O-acetyl- $\alpha$ -D-arabinofuranoside (**17**)<sup>186</sup>

The reported synthesis<sup>186</sup> was modified according to the following procedure: To a solution of chloroethyl arabinofuranoside **16** (300 mg, 888  $\mu$ mol) in dry DMF (20.0 ml) sodium azide (287 mg, 4.41 mmol, 5 eq.) and TBAI (66.0 mg, 179  $\mu$ mol, 0.2 eq.) was added. The reaction mixture was stirred under a nitrogen atmosphere for 7 h at 70°C and overnight at rt. Dist. water was added and the aqueous phase was extracted with DCM. The combined organic layers were dried over MgSO<sub>4</sub>, filtered and concentrated in vacuo. The crude product was chromatographed on silica gel (cyclohexane/ethyl acetate, 2:1) to give the azido sugar **17** (273 mg, 791  $\mu$ mol, 89%) as colorless oil. TLC (cyclohexane/ethyl acetate, 2:1):  $R_f = 0.22$ ; <sup>1</sup>H NMR (500 MHz, CDCl<sub>3</sub>, 300 K, TMS):  $\delta = 5.11$  (dd~d,  $^3J_{2,3} = 1.5$  Hz, 1H, H-2), 5.07 (d~s, 1H, H-1), 4.99 (ddd,  $^3J_{2,3} = 1.5$  Hz,  $^3J_{3,4} = 5.1$  Hz,  $^4J = 0.6$  Hz, 1H, H-3), 4.45 (dd,  $^3J_{4,5a} = 3.4$  Hz,  $^2J_{5a,5b} = 11.8$  Hz, 1H, H-5a), 4.32-4.29 (m, 1H, H-4), 4.24 (dd,  $^3J_{4,5b} = 5.7$  Hz,  $^2J_{5a,5b} = 11.8$  Hz, 1H, H-5b), 3.92 (ddd,  $^3J = 3.4$  Hz,  $^3J = 7.0$  Hz,  $^2J = 10.5$  Hz, 1H, OCH<sub>2</sub>CH<sub>2</sub>N<sub>3</sub>), 3.66 (ddd,  $^3J = 3.4$  Hz,  $^3J = 6.2$  Hz,  $^2J = 10.6$  Hz, 1H, OCH<sub>2</sub>CH<sub>2</sub>N<sub>3</sub>), 3.44 (ddd,  $^3J = 3.4$  Hz,  $^3J = 7.0$  Hz,  $^2J = 13.3$  Hz, 1H, OCH<sub>2</sub>CH<sub>2</sub>N<sub>3</sub>), 3.36 (ddd,  $^3J = 3.4$  Hz,  $^3J = 6.2$  Hz,  $^2J = 13.3$  Hz, 1H, OCH<sub>2</sub>CH<sub>2</sub>N<sub>3</sub>), 2.12, 2.11, 2.10 (s each, 3H each, 3 COCH<sub>3</sub>) ppm.

(2-Azidoethyl)  $\alpha$ -D-arabinofuranoside (**18**)<sup>186</sup>

The reported synthesis<sup>186</sup> was modified according to the following procedure: The acetyl-protected arabinofuranoside derivative **17** (250 mg, 725  $\mu$ mol) was dissolved in dry methanol (10.0 ml) and sodium methoxide (a spatula tip) was added. The reaction mixture was stirred overnight at rt under a nitrogen atmosphere. The reaction mixture was neutralized with Amberlite IR120 ion exchange resin, it was filtered and the solvent removed under reduced pressure. Purification of the crude product on silica gel (ethyl acetate/methanol, 8:1) gave the product **18** (145 mg, 662  $\mu$ mol, 91%) as a colorless oil. TLC (ethyl acetate/methanol, 4:1):  $R_f = 0.51$ ; <sup>1</sup>H NMR (500 MHz, MeOH-*d*<sub>4</sub>, 300 K):  $\delta = 4.91$  (d,  $^3J_{1,2} = 1.7$  Hz, 1H, H-1), 4.00 (dd,  $^3J_{1,2} = 1.7$  Hz,  $^3J_{2,3} = 3.9$  Hz, 1H, H-2), 3.96 (ddd,  $^3J_{3,4} = 6.5$  Hz,  $^3J_{4,5a} = 3.2$  Hz,  $^3J_{4,5b} = 5.3$  Hz, 1H, H-4), 3.88 (ddd,  $^3J = 3.6$  Hz,  $^3J = 6.0$  Hz,  $^2J = 10.9$  Hz, 1H, OCH<sub>2</sub>CH<sub>2</sub>N<sub>3</sub>), 3.85 (dd,  $^3J_{2,3} = 3.8$  Hz,  $^3J_{3,4} = 6.4$  Hz, 1H, H-3), 3.76 (dd,  $^3J_{4,5a} = 3.2$  Hz,  $^2J_{5a,5b} = 11.9$  Hz, 1H, H-5a), 3.64 (dd,  $^3J_{4,5b} = 5.3$  Hz,  $^2J_{5a,5b} = 11.9$  Hz, 1H, H-5b), 3.63 (ddd,  $^3J = 2.6$  Hz,  $^3J = 5.4$  Hz,  $^2J = 10.9$  Hz, 1H, OCH<sub>2</sub>CH<sub>2</sub>N<sub>3</sub>), 3.46 (ddd,  $^3J = 3.6$  Hz,  $^3J = 7.1$  Hz,  $^2J = 13.2$  Hz, 1H, OCH<sub>2</sub>CH<sub>2</sub>N<sub>3</sub>), 3.38 (ddd,  $^3J = 3.7$  Hz,  $^3J = 5.9$  Hz,  $^2J = 13.2$  Hz, 1H, OCH<sub>2</sub>CH<sub>2</sub>N<sub>3</sub>) ppm.



### 5-O-Benzoyl-1,2,3-tri-O-acetyl- $\alpha,\beta$ -D-arabinofurose (19)

The triacetyl-arabinofuranose derivative **14** (450 mg, 1.63 mmol) was dissolved in dry pyridine (10.0 ml), supplemented with benzoylchloride (400  $\mu$ l, 3.45 mmol, 2 eq.) and stirred overnight at rt under a nitrogen atmosphere. A saturated aqueous NaHCO<sub>3</sub> solution was added and the aqueous phase was extracted with DCM. The combined organic layers were washed with dist. water, dried over MgSO<sub>4</sub>, filtered and concentrated in vacuo. The crude product was chromatographed on silica gel (cyclohexane/ethyl acetate, 2:1) giving the arabinofuranose derivative **19** (595 mg, 1.57 mmol, 96%) as a colorless oil ( $\alpha:\beta$  ratio = 2:1 by integration of the <sup>1</sup>H NMR spectrum) TLC (cyclohexane/ethyl acetate, 2:1): R<sub>f</sub> = 0.40; rotation value:  $[\alpha]_D^{22} = + 10.4^\circ$  (c = 1.8, CH<sub>2</sub>Cl<sub>2</sub>); <sup>1</sup>H NMR (500 MHz, CDCl<sub>3</sub>, 300 K, TMS):  $\delta$  = 8.04-7.99 (m, 2H, aryl-H<sub>ortho</sub> ( $\alpha,\beta$ )), 7.56-7.48 (m, 1H, aryl-H<sub>para</sub> ( $\alpha,\beta$ )), 7.42-7.35 (m, 2H, aryl-H<sub>meta</sub> ( $\alpha,\beta$ )), 6.34 (d, <sup>3</sup>J<sub>1,2</sub> = 4.7 Hz, 1H, H-1 ( $\beta$ )), 6.16 (d-s, 1H, H-1 ( $\alpha$ )), 5.47 (dd, <sup>3</sup>J<sub>2,3</sub> = 6.9 Hz, <sup>3</sup>J<sub>3,4</sub> = 5.8 Hz, 1H, H-3 ( $\beta$ )), 5.34 (dd, <sup>3</sup>J<sub>1,2</sub> = 4.7 Hz, <sup>3</sup>J<sub>2,3</sub> = 7.0 Hz, 1H, H-2 ( $\beta$ )), 5.18 (dd-d, <sup>3</sup>J<sub>1,2</sub> = 1.4 Hz, 1H, H-2 ( $\alpha$ )), 5.14-5.13 (m, 1H, H-3 ( $\alpha$ )), 4.58 (dd, <sup>3</sup>J<sub>4,5a</sub> = 3.8 Hz, <sup>2</sup>J<sub>5a,5b</sub> = 11.9 Hz, 1H, H-5a ( $\alpha,\beta$ )), 4.48 (dd, <sup>3</sup>J<sub>4,5b</sub> = 4.9 Hz, <sup>2</sup>J<sub>5a,5b</sub> = 11.9 Hz, 1H, H-5b ( $\alpha$ )), 4.45-4.41 (m, 2H, H-4 ( $\alpha$ ), H-5b ( $\beta$ )), 4.28 (dt, <sup>3</sup>J<sub>3,4</sub> = 6.0 Hz, <sup>3</sup>J<sub>4,5a</sub> = 4.2 Hz, <sup>3</sup>J<sub>4,5b</sub> = 6.0 Hz, 1H, H-4 ( $\beta$ )), 2.06, 2.07, 1.99 (s each, 3H each, 3 COCH<sub>3</sub> ( $\alpha$ )), 2.03, 2.04, 1.92 (s each, 3H each, 3 COCH<sub>3</sub> ( $\beta$ )) ppm; <sup>13</sup>C NMR (125 MHz, CDCl<sub>3</sub>, 300 K):  $\delta$  = 170.3, 169.8, 169.3 (3  $\underline{\text{C}}\text{OCH}_3$  ( $\alpha$ )), 170.0, 169.5, 169.3 (3  $\underline{\text{C}}\text{OCH}_3$  ( $\beta$ )), 166.1 ( $\underline{\text{C}}\text{Oaryl}$  ( $\alpha$ )), 166.0 ( $\underline{\text{C}}\text{Oaryl}$  ( $\beta$ )), 133.3 (aryl-C<sub>para</sub> ( $\alpha,\beta$ )), 129.8 (aryl-C<sub>ortho</sub>, aryl-C<sub>ipso</sub> ( $\alpha,\beta$ )), 128.4 (aryl-C<sub>meta</sub> ( $\beta$ )), 128.4 (aryl-C<sub>meta</sub> ( $\alpha$ )), 99.4 (C-1 ( $\alpha$ )), 93.7 (C-1 ( $\beta$ )), 82.8 (C-4 ( $\alpha$ )), 80.8 (C-2 ( $\alpha$ )), 79.7 (C-4 ( $\beta$ )), 77.1 (C-3 ( $\alpha$ )), 75.3 (C-2 ( $\beta$ )), 74.6 (C-3 ( $\beta$ )), 64.5 (C-5 ( $\beta$ )), 63.4 (C-5 ( $\alpha$ )), 21.1, 20.7, 20.6 (3 COCH<sub>3</sub> ( $\alpha$ )), 20.9, 20.7, 20.5 (3 COCH<sub>3</sub> ( $\beta$ )) ppm; ESI-MS:  $m/z$  = 403.105, [M+Na]<sup>+</sup> (calc. 403.101 for C<sub>18</sub>H<sub>20</sub>O<sub>9</sub>+Na).

### 5-O-Benzoyl-2,3-di-O-acetyl- $\alpha,\beta$ -D-arabinofurose (20)

The arabinofuranose derivative **19** (980 mg, 2.58 mmol) was dissolved in dry DCM (50.0 ml), cooled with ice and HBr/glacial acetic acid (33%, 2.50 ml, 37.2 mmol HBr, 14 eq.) and acetic anhydride (30.0  $\mu$ l, 272  $\mu$ mol, 0.1 eq.) were added slowly. The reaction was stirred in the dark for half an hour under cooling with an ice bath and overnight at rt. Ice (20.0 ml) was added and the mixture was extracted with DCM. The combined organic layers were washed with a saturated aqueous NaHCO<sub>3</sub> solution and dist. water, dried over MgSO<sub>4</sub>, filtered and concentrated in vacuo. The crude product was chromatographed on silica gel (cyclohexane/ethyl acetate, 2:1) to give the C-1-deprotected arabinofuranose derivative **20** (851 mg, 2.52 mmol, 98%) as a colorless oil ( $\alpha:\beta$  ratio = 2.5:1 by integration of the <sup>1</sup>H NMR spectrum). TLC (cyclohexane/ethyl acetate, 2:1): R<sub>f</sub> = 0.18, 0.12; rotation value:  $[\alpha]_D^{22} = + 16.9^\circ$  (c = 0.4, CH<sub>2</sub>Cl<sub>2</sub>); <sup>1</sup>H NMR (500 MHz, CDCl<sub>3</sub>, 300 K, TMS):  $\delta$  = 8.10-8.05 (m, 2H, aryl-H<sub>ortho</sub>

( $\alpha,\beta$ ), 7.59-7.54 (m, 1H, aryl-H<sub>para</sub> ( $\alpha,\beta$ )), 7.46-7.42 (m, 2H, aryl-H<sub>meta</sub> ( $\alpha,\beta$ )), 5.60 (d,  $^3J_{1,2} = 4.3$  Hz, 1H, H-1 ( $\beta$ )), 5.45 (d~s, 1H, H-1 ( $\alpha$ )), 5.43-5.41 (m, 1H, H-3 ( $\beta$ )), 5.18-5.16 (m, 1H, H-3 ( $\alpha$ )), 5.15 (dd,  $^3J_{1,2} = 4.3$  Hz,  $^3J_{2,3} = 8.9$  Hz, 1H, H-2 ( $\beta$ )), 5.14 (dd,  $^3J_{1,2} = 1.3$  Hz,  $^3J_{2,3} = 4.3$  Hz, 1H, H-2 ( $\alpha$ )), 4.69 (dd,  $^3J_{4,5a} = 3.1$  Hz,  $^2J_{5a,5b} = 11.4$  Hz, 1H, H-5a ( $\alpha$ )), 4.66 (dd,  $^3J_{4,5a} = 6.9$  Hz,  $^2J_{5a,5b} = 12.2$  Hz, 1H, H-5a ( $\beta$ )), 4.59 (dd,  $^3J_{4,5b} = 4.2$  Hz,  $^2J_{5a,5b} = 11.7$  Hz, 1H, H-5b ( $\beta$ )), 4.57-4.53 (m, 1H, H-4 ( $\alpha$ )), 4.51 (dd,  $^3J_{4,5b} = 5.3$  Hz,  $^2J_{5a,5b} = 11.4$  Hz, 1H, H-5b ( $\alpha$ )), 4.23 (dt,  $^3J_{3,4} = 4.4$  Hz,  $^3J_{4,5a} = 7.0$  Hz,  $^3J_{4,5b} = 4.4$  Hz, 1H, H-4 ( $\beta$ )), 3.50 (s, 1H, OH ( $\beta$ )), 3.18 (s, 1H, OH ( $\alpha$ )), 2.14, 2.10 (s each, 3H each, COCH<sub>3</sub> ( $\beta$ )), 2.13, 2.04 (s each, 3H each, 2 COCH<sub>3</sub> ( $\alpha$ )) ppm;  $^{13}\text{C}$  NMR (125 MHz, CDCl<sub>3</sub>, 300 K):  $\delta = 170.3, 170.1$  (2 COCH<sub>3</sub> ( $\beta$ )), 170.2, 169.8 (2 COCH<sub>3</sub> ( $\alpha$ )), 166.5 (COaryl ( $\beta$ )), 166.2 (COaryl ( $\alpha$ )), 133.2 (aryl-C<sub>para</sub> ( $\alpha,\beta$ )), 129.8 (aryl-C<sub>ortho</sub>, aryl-C<sub>ipso</sub> ( $\alpha$ )), 129.8 (aryl-C<sub>ortho</sub>, aryl-C<sub>ipso</sub> ( $\beta$ )), 128.4 (aryl-C<sub>meta</sub> ( $\beta$ )), 128.4 (aryl-C<sub>meta</sub> ( $\alpha$ )), 100.8 (C-1 ( $\alpha$ )), 95.3 (C-1 ( $\beta$ )), 81.8 (C-2 ( $\alpha$ )), 81.4 (C-4 ( $\alpha$ )), 79.0 (C-4 ( $\beta$ )), 77.4 (C-3 ( $\alpha$ )), 77.0 (C-2 ( $\beta$ )), 76.0 (C-3 ( $\beta$ )), 65.6 (C-5 ( $\beta$ )), 63.7 (C-5 ( $\alpha$ )), 20.8, 20.7 (2 COCH<sub>3</sub> ( $\alpha$ )), 20.8, 20.6 (2 COCH<sub>3</sub> ( $\beta$ )) ppm; ESI-MS:  $m/z = 361.088$ , [M+Na]<sup>+</sup> (calc. 361.090 for C<sub>16</sub>H<sub>18</sub>O<sub>8</sub>+Na).

#### *p*-Nitrophenyl 5-O-benzoyl-2,3-di-O-acetyl- $\alpha$ -D-arabinofuranoside (22)

The C-1-deprotected arabinofuranose derivative **20** (845 mg, 2.18 mmol) was dissolved in dry DCM (10.0 ml), cooled with an ice bath and trichloroacetonitrile (2.60 ml, 26.0 mmol, 12 eq.) and 1,8-diazabicycloundec-7-ene (DBU, 26.0  $\mu\text{l}$ , 174  $\mu\text{mol}$ , 0.08 eq.) were added slowly. The reaction was stirred 15 min under cooling with an ice bath and concentrated in vacuo at a low heat (max. 30°C). The crude product was chromatographed on silica gel (cyclohexane/ethyl acetate, 4:1) to give the instable product **21** (1.00 g, 2.08 mmol) as a colorless oil. The intermediate and *p*-nitrophenol (350 mg, 2.52 mmol, 1.2 eq.) were dissolved in dry DCM (30.0 ml). Boron trifluoride diethyl etherate (BF<sub>3</sub>·Et<sub>2</sub>O, 450  $\mu\text{l}$ , 3.91 mmol, 1.8 eq.) was added slowly within 30 min under cooling with an ice bath and the reaction was stirred overnight at rt. DCM was added and the organic layer was washed with a saturated aqueous NaHCO<sub>3</sub> solution and dist. water, dried over MgSO<sub>4</sub>, filtered and concentrated in vacuo. The crude product was chromatographed on silica gel (cyclohexane/ethyl acetate, 7:1) to give the arabinofuranose derivative **22** (534 mg, 1.16 mmol, 53% over two steps) as colorless crystals. TLC (cyclohexane/ethyl acetate, 2:1): R<sub>f</sub> = 0.28; rotation value:  $[\alpha]_D^{22} = +59.7^\circ$  (c = 1.0, CH<sub>2</sub>Cl<sub>2</sub>);  $^1\text{H}$  NMR (500 MHz, CDCl<sub>3</sub>, 300 K, TMS):  $\delta = 8.22$ -8.18 (m, 2H, PhNO<sub>2meta</sub>), 8.09-8.07 (m, 2H, COPh<sub>ortho</sub>), 7.60-7.56 (m, 1H, COPh<sub>para</sub>), 7.47-7.43 (m, 2H, COPh<sub>meta</sub>), 7.18-7.14 (m, 2H, PhNO<sub>2ortho</sub>), 5.80 (d~s, 1H, H-1), 5.42 (dd~d,  $^3J_{2,3} = 1.1$  Hz, 1H, H-2), 5.29 (ddd,  $^3J_{2,3} = 1.4$  Hz,  $^3J_{3,4} = 4.7$  Hz,  $^4J = 0.6$  Hz, 1H, H-3), 4.70 (dd,  $^3J_{4,5a} = 3.4$  Hz,  $^2J_{5a,5b} = 12.1$  Hz, 1H, H-5a), 4.58 (dd,  $^3J_{4,5a} = 4.7$  Hz,  $^2J_{5a,5b} = 12.1$  Hz, 1H, H-5b), 4.51 (dt,  $^3J_{3,4} = 4.7$  Hz,  $^3J_{4,5a} = 3.5$  Hz,  $^3J_{4,5b} = 4.7$  Hz, 1H, H-4), 2.16, 2.07 (s each, 3H each, 2 COCH<sub>3</sub>) ppm;  $^{13}\text{C}$  NMR

(125 MHz, CDCl<sub>3</sub>, 300 K):  $\delta$  = 170.2, 169.6 (2 C=OCH<sub>3</sub>), 166.0 (COPh), 160.8 (PhNO<sub>2</sub>-C<sub>ipso</sub>), 142.8 (PhNO<sub>2</sub>-C<sub>para</sub>), 133.3 (COPh-C<sub>para</sub>), 129.8 (COPh-C<sub>ortho</sub>), 129.7 (COPh-C<sub>ipso</sub>), 128.4 (COPh-C<sub>meta</sub>), 125.8 (PhNO<sub>2</sub>-C<sub>meta</sub>), 116.6 (PhNO<sub>2</sub>-C<sub>ortho</sub>), 100.8 (C-1), 82.5 (C-4), 81.3 (C-2), 77.0 (C-3), 63.1 (C-5), 20.7, 20.6 (2 COCH<sub>3</sub>) ppm; ESI-MS:  $m/z$  = 482.1, [M+Na]<sup>+</sup> (calc. 482.1 for C<sub>22</sub>H<sub>21</sub>NO<sub>10</sub>+Na).

### *p*-Nitrophenyl $\alpha$ -D-arabinofuranoside (**23**)

The Arabinofuranoside derivative **22** (700 mg, 1.53 mmol) was dissolved in dry methanol and sodium methoxide (spatula tip) was added. The reaction mixture was stirred overnight at rt under a nitrogen atmosphere. After neutralization with Amberlite IR120 ion exchange resin and concentration in vacuo, the crude product was chromatographed on silica gel (cyclohexane/ethyl acetate/methanol, 1:1:0.25) to give the product **23** (400 mg, 1.48 mmol, 97%) as colorless crystals. TLC (cyclohexane/ethyl acetate/methanol, 1:1:0.5): R<sub>f</sub> = 0.29; rotation value:  $[\alpha]_D^{22} = +210.7^\circ$  (c = 1.0, MeOH); m.p.: 158.5-160.2°C; <sup>1</sup>H NMR (500 MHz, MeOH-*d*<sub>4</sub>, 300 K):  $\delta$  = 8.22-8.19 (m, 2H, aryl-H<sub>meta</sub>), 7.23-7.20 (m, 2H, aryl-H<sub>ortho</sub>), 5.67 (d, <sup>3</sup>J<sub>1,2</sub> = 1.7 Hz, 1H, H-1), 4.30 (dd, <sup>3</sup>J<sub>1,2</sub> = 1.8 Hz, <sup>3</sup>J<sub>2,3</sub> = 3.8 Hz, 1H, H-2), 4.06 (ddd, <sup>3</sup>J<sub>3,4</sub> = 6.2 Hz, <sup>3</sup>J<sub>4,5a</sub> = 3.2 Hz, <sup>3</sup>J<sub>4,5b</sub> = 5.0 Hz, 1H, H-4), 4.02 (ddd, <sup>3</sup>J<sub>2,3</sub> = 3.8 Hz, <sup>3</sup>J<sub>3,4</sub> = 6.4 Hz, <sup>4</sup>J = 0.5 Hz, 1H, H-3), 3.78 (dd, <sup>3</sup>J<sub>4,5a</sub> = 3.2 Hz, <sup>2</sup>J<sub>5a,5b</sub> = 12.1 Hz, 1H, H-5a), 3.68 (dd, <sup>3</sup>J<sub>4,5b</sub> = 5.0 Hz, <sup>2</sup>J<sub>5a,5b</sub> = 12.1 Hz, 1H, H-5b) ppm; <sup>13</sup>C NMR (125 MHz, MeOH-*d*<sub>4</sub>, 300 K):  $\delta$  = 163.5 (aryl-C<sub>ipso</sub>), 143.6 (aryl-C<sub>para</sub>), 126.6 (aryl-C<sub>meta</sub>), 117.7 (aryl-C<sub>ortho</sub>), 107.8 (C-1), 87.0 (C-4), 83.6 (C-2), 78.2 (C-3), 62.7 (C-5) ppm; HRMS (ESI-MS):  $m/z$  = 294.0643, [M+Na]<sup>+</sup> (calc. 294.0590 for C<sub>11</sub>H<sub>13</sub>NO<sub>7</sub>+Na).

### 6-O-*tert*-Butyldimethylsilyl-2,3,4,2',3',4',6'-hepta-O-acetyl- $\alpha,\alpha$ -D-trehalose (**24**)<sup>192</sup>

The reported synthesis<sup>192</sup> was modified according to the following procedure: D-Trehalose (2.00 g, 5.85 mmol) was suspended in dry pyridine (20.0 ml), cooled with an ice bath and supplemented with TBDMSCl (1.00 g, 6.63 mmol, 1.1 eq.). The reaction was stirred overnight at rt under a nitrogen atmosphere. Ac<sub>2</sub>O (6.00 ml, 63.6 mmol, 10 eq.) was added and stirring was continued for 6 h at rt. After addition of a saturated aqueous NaHCO<sub>3</sub> solution the resulting mixture was extracted with DCM. The combined organic layers were dried over MgSO<sub>4</sub>, filtered and concentrated in vacuo. The crude product was chromatographed on silica gel (cyclohexane/ethyl acetate, 4:1 → 2:1) to give **24** (1.94 g, 2.59 mmol, 44%) as a white solid. TLC (cyclohexane/ethyl acetate, 1:1): R<sub>f</sub> = 0.29; <sup>1</sup>H NMR (500 MHz, CDCl<sub>3</sub>, 300 K):  $\delta$  = 5.49 (dd~d, <sup>3</sup>J<sub>3,4</sub> = 9.4 Hz, 1H, H-3), 5.47 (dd~d, <sup>3</sup>J<sub>3',4'</sub> = 9.4 Hz, 1H, H-3'), 5.28 (d, <sup>3</sup>J<sub>1,2</sub> = 3.9 Hz, 1H, H-1), 5.25 (d, <sup>3</sup>J<sub>1',2'</sub> = 3.9 Hz, 1H, H-1'), 5.08 (dd, <sup>3</sup>J<sub>1,2</sub> = 3.9 Hz, <sup>3</sup>J<sub>2,3</sub> = 10.2 Hz, 1H, H-2), 5.07-5.01 (m, 2H, H-4, H-4'), 4.98 (dd, <sup>3</sup>J<sub>1',2'</sub> = 3.9 Hz, <sup>3</sup>J<sub>2',3'</sub> = 10.3 Hz, 1H, H-2'), 4.23 (dd, <sup>3</sup>J<sub>5,6a</sub> = 5.7 Hz, <sup>2</sup>J<sub>6a,6b</sub> = 12.2 Hz, 1H, H-6a), 4.06 (ddd, <sup>3</sup>J<sub>4,5</sub> = 10.3 Hz, <sup>3</sup>J<sub>5,6a</sub> = 5.7 Hz,

$^3J_{5,6b} = 2.1$  Hz, 1H, H-5), 4.00 (dd,  $^3J_{5,6b} = 2.2$  Hz,  $^2J_{6a,6b} = 12.2$  Hz, 1H, H-6b), 3.93 (ddd,  $^3J_{4',5'} = 10.2$  Hz,  $^3J_{5',6'a} = 4.6$  Hz,  $^3J_{5',6'b} = 2.9$  Hz, 1H, H-5'), 3.63 (dd,  $^3J_{5',6'a} = 4.7$  Hz,  $^2J_{6'a,6'b} = 11.3$  Hz, 1H, H-6'a), 3.61 (dd,  $^3J_{5',6'b} = 2.7$  Hz,  $^2J_{6'a,6'b} = 11.3$  Hz, 1H, H-6'b), 2.08, 2.07, 2.04, 2.03, 2.02, 2.01 (s each, 1·6H, 5·3H, COCH<sub>3</sub>), 0.86 (s, 9H, OSi(CH<sub>3</sub>)<sub>2</sub>C(CH<sub>3</sub>)<sub>3</sub>), 0.02, 0.00 (s each, 3H each, OSi(CH<sub>3</sub>)<sub>2</sub>C(CH<sub>3</sub>)<sub>3</sub>) ppm.

### 2,3,4,2',3',4',6'-Hepta-O-acetyl- $\alpha,\alpha$ -D-trehalose (25)<sup>192</sup>

The reported synthesis<sup>192</sup> was modified according to the following procedure: The trehalose derivative **24** (1.30 g, 1.73 mmol) was dissolved in DMF (30.0 ml), supplemented with dist. water (30.0 ml) and conc. acetic acid (120 ml). The reaction mixture was stirred overnight at rt. After addition of a saturated aqueous NaHCO<sub>3</sub> solution the resulting mixture was extracted with diethyl ether. The combined organic layers were washed with dist. water, dried over MgSO<sub>4</sub>, filtered and concentrated in vacuo. The crude product was chromatographed on silica gel (cyclohexane/ethyl acetate, 1:1 → 1:3) to give **25** (864 mg, 1.36 mmol, 79%) as a white solid. TLC (cyclohexane/ethyl acetate, 1:1): R<sub>f</sub> = 0.07; <sup>1</sup>H NMR (500 MHz, CDCl<sub>3</sub>, 300 K):  $\delta = 5.53$  (dd~d,  $^3J_{3,4} = 9.5$  Hz, 1H, H-3), 5.49 (dd~d,  $^3J_{3',4'} = 9.5$  Hz, 1H, H-3'), 5.30 (d,  $^3J_{1,2} = 3.4$  Hz, 1H, H-1), 5.29 (d,  $^3J_{1',2'} = 3.4$  Hz, 1H, H-1'), 5.05 (dd,  $^3J_{3,4} = 9.4$  Hz,  $^3J_{4,5} = 10.3$  Hz, 1H, H-4), 5.03-4.99 (m, 3H, H-2, H-2', H-4'), 4.26 (dd,  $^3J_{5,6a} = 5.7$  Hz,  $^2J_{6a,6b} = 12.2$  Hz, 1H, H-6a), 4.09 (ddd,  $^3J_{4,5} = 10.4$  Hz,  $^3J_{5,6a} = 5.5$  Hz,  $^3J_{5,6b} = 2.1$  Hz, 1H, H-5), 3.99 (dd,  $^3J_{5,6b} = 2.2$  Hz,  $^2J_{6a,6b} = 12.2$  Hz, 1H, H-6b), 3.91 (ddd,  $^3J_{4',5'} = 10.3$  Hz,  $^3J_{5',6'a} = 5.7$  Hz,  $^3J_{5',6'b} = 2.4$  Hz, 1H, H-5'), 3.65-3.59 (m, 2H, H-6a', H-6b'), 2.08, 2.07, 2.06, 2.04, 2.03, 2.02, 2.01 (s each, 3H each, COCH<sub>3</sub>) ppm.

### 2,3,4,2',3',4',6'-Hepta-O-acetyl-6-O-tosyl- $\alpha,\alpha$ -D-trehalose (26)

The product **26** was obtained by a different synthetic route as described in literature.<sup>194</sup> The trehalose derivative **25** (2.00 g, 3.15 mmol) was dissolved in dry pyridine (50.0 ml). Tosyl chloride (TsCl, 1.70 g, 8.93 mmol, 2.8 eq.) was added slowly. The reaction was stirred overnight at rt under a nitrogen atmosphere and was concentrated in vacuo. The crude product was chromatographed on silica gel (cyclohexane/ethyl acetate, 1:1) to give the the tosylated sugar **26** (2.01 g, 2.52 mmol, 80%) as a white solid. TLC (cyclohexane/ethyl acetate, 1:1): R<sub>f</sub> = 0.17; <sup>1</sup>H NMR (500 MHz, CDCl<sub>3</sub>, 300 K):  $\delta = 7.74$  (dt,  $^3J_{\text{meta,ortho}} = 8.3$  Hz,  $^4J_{\text{meta,CH}_3} = 1.7$  Hz, 2H, aryl-H<sub>meta</sub>), 7.34 (d,  $^3J_{\text{meta,ortho}} = 8.0$  Hz, 2H, aryl-H<sub>ortho</sub>), 5.45 (dd,  $^3J_{2',3'} = 9.3$  Hz,  $^3J_{3',4'} = 10.2$  Hz, 1H, H-3'), 5.40 (dd,  $^3J_{2,3} = 8.7$  Hz,  $^3J_{3,4} = 9.5$  Hz, 1H, H-3), 5.15 (d,  $^3J_{1',2'} = 3.8$  Hz, 1H, H-1'), 5.06 (d,  $^3J_{1,2} = 3.8$  Hz, 1H, H-1), 5.05-5.01 (m, 2H, H-2, H-2'), 4.93 (dd,  $^3J_{3,4} = 9.3$  Hz,  $^3J_{4,5} = 10.3$  Hz, 1H, H-4), 4.92 (dd,  $^3J_{3',4'} = 10.3$  Hz,  $^3J_{4',5'} = 3.9$  Hz, 1H, H-4'), 4.22 (dd,  $^3J_{5,6a} = 5.4$  Hz,  $^2J_{6a,6b} = 12.0$  Hz, 1H, H-6a), 4.13 (ddd,  $^3J_{4',5'} = 4.3$  Hz,  $^3J_{5',6'a} = 5.4$  Hz,  $^3J_{5',6'b} = 2.6$  Hz, 1H, H-5'), 4.11-4.04 (m, 2H, H-6'a, H-6'b), 4.02 (ddd,  $^3J_{4,5} = 10.2$  Hz,

$^3J_{5,6a} = 5.4$  Hz,  $^3J_{5,6b} = 2.2$  Hz, 1H, H-5), 3.98 (dd,  $^3J_{5,6b} = 2.2$  Hz,  $^2J_{6a,6b} = 12.0$  Hz, 1H, H-6b), 2.45 (s, 3H, aryl-CH<sub>3</sub>), 2.10, 2.07, 2.05, 2.04, 2.03, 2.02, 2.01 (s each, 3H each, COCH<sub>3</sub>) ppm.

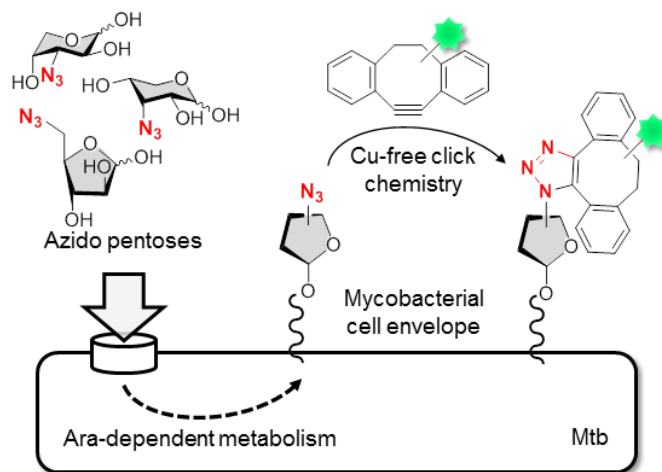
#### 6-Azido-6-deoxy-2,3,4,2',3',4',6'-hepta-O-acetyl- $\alpha,\alpha$ -D-trehalose (**27**)

The product **27** was obtained by a different synthetic route as described in literature:<sup>193,194</sup> To a stirring solution of the tosylated molecule **26** (100 mg, 125  $\mu$ mol) in dry DMF (12.0 ml) sodium azide (33.0 mg, 508  $\mu$ mol, 4 eq.) was added. The reaction mixture was heated to 80°C and stirred for 6 h under a nitrogen atmosphere. Dist. water was added and the reaction mixture was extracted with diethyl ether. The combined organic layers were dried over MgSO<sub>4</sub>, filtered and concentrated in vacuo. The crude product was chromatographed on silica gel (cyclohexane/ethyl acetate, 1:1) to give the azido sugar **27** (75.0 mg, 114  $\mu$ mol, 91%) as a white solid. TLC (cyclohexane/ethyl acetate, 1:1): R<sub>f</sub> = 0.175; <sup>1</sup>H NMR (500 MHz, CDCl<sub>3</sub>, 300 K):  $\delta$  = 5.49 (dd,  $^3J_{2',3'} = 10.2$  Hz,  $^3J_{3',4'} = 9.4$  Hz, 1H, H-3'), 5.47 (dd,  $^3J_{2,3} = 10.2$  Hz,  $^3J_{3,4} = 9.5$  Hz, 1H, H-3), 5.33 (d,  $^3J_{1',2'} = 4.0$  Hz, 1H, H-1'), 5.31 (d,  $^3J_{1,2} = 3.9$  Hz, 1H, H-1), 5.08 (dd,  $^3J_{1',2'} = 3.9$  Hz,  $^3J_{2',3'} = 10.3$  Hz, 1H, H-2'), 5.06 (dd,  $^3J_{3',4'} = 9.5$  Hz,  $^3J_{4',5'} = 10.3$  Hz, 1H, H-4'), 5.03 (dd,  $^3J_{1,2} = 3.9$  Hz,  $^3J_{2,3} = 10.4$  Hz, 1H, H-2), 4.98 (dd,  $^3J_{3,4} = 9.3$  Hz,  $^3J_{4,5} = 10.4$  Hz, 1H, H-4), 4.25 (dd,  $^3J_{5,6a} = 5.7$  Hz,  $^2J_{6a,6b} = 12.2$  Hz, 1H, H-6a), 4.10-4.04 (m, 2H, H-5, H-5'), 4.00 (dd,  $^3J_{5,6b} = 2.2$  Hz,  $^2J_{6a,6b} = 12.2$  Hz, 1H, H-6b), 3.35 (dd,  $^3J_{5',6'a} = 7.2$  Hz,  $^2J_{6'a,6'b} = 13.4$  Hz, 1H, H-6'a), 3.16 (dd,  $^3J_{5',6'b} = 2.5$  Hz,  $^2J_{6'a,6'b} = 13.3$  Hz, 1H, H-6'b), 2.12, 2.09, 2.08, 2.06, 2.05, 2.03, 2.02 (s each, 3H each, COCH<sub>3</sub>) ppm.

#### 6-Azido-6-deoxy- $\alpha,\alpha$ -D-trehalose (**28**)<sup>193</sup>

The heptaacetate **27** (50.0 mg, 75.8  $\mu$ mol) was dissolved in dry methanol (8.00 ml). Sodium methoxide (spatula tip) was added and the reaction mixture was stirred overnight at rt under a nitrogen atmosphere. The reaction was neutralized with Amberlite IR120 ion exchange resin and the solvent was removed in vacuo. After lyophilization the product **28** was obtained (27.0 mg, 74.6  $\mu$ mol, 97%) as a white solid. TLC (cyclohexane/ethyl acetate/ methanol, 1:1:0.5): R<sub>f</sub> = 0.07; <sup>1</sup>H NMR (500 MHz, D<sub>2</sub>O, 300 K):  $\delta$  = 5.14 (d,  $^3J_{1',2'} = 4.1$  Hz, 1H, H-1'), 5.13 (d,  $^3J_{1,2} = 4.0$  Hz, 1H, H-1), 3.92 (dd,  $^3J_{3',4'} = 5.9$  Hz,  $^3J_{4',5'} = 9.8$  Hz, 1H, H-4'), 3.91 (dd,  $^3J_{3,4} = 5.9$  Hz,  $^3J_{4,5} = 9.9$  Hz, 1H, H-4), 3.82-3.75 (m, 3H, H-3, H-3', H-6'a), 3.70 (dd,  $^3J_{5',6'b} = 5.1$  Hz,  $^2J_{6'a,6'b} = 12.1$  Hz, 1H, H-6'b), 3.62 (dd,  $^3J_{5,6a} = 2.6$  Hz,  $^2J_{6a,6b} = 13.6$  Hz, 1H, H-6a), 3.61 (dd,  $^3J_{1',2'} = 3.9$  Hz,  $^3J_{2',3'} = 10.4$  Hz, 1H, H-2'), 3.59 (dd,  $^3J_{1,2} = 3.8$  Hz,  $^3J_{2,3} = 10.3$  Hz, 1H, H-2), 3.50 (dd,  $^3J_{5,6b} = 5.9$  Hz,  $^2J_{6a,6b} = 13.6$  Hz, 1H, H-6b), 3.42-3.37 (m, 2H, H-5, H-5') ppm.

**Azido pentoses, a new tool for specific labeling of  
*Mycobacterium tuberculosis***



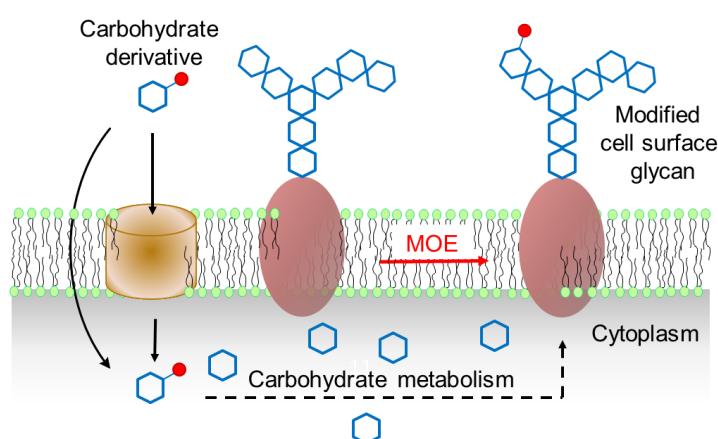
**Part 2**

### 3 Azido pentoses, a new tool for specific labeling of *Mycobacterium tuberculosis*

A major challenge in Tb therapy is the lack of specific probes that can be used to diagnose and treat Mtb bacteria in a selective manner while leaving many other microorganisms and eukaryotic host cells unaffected. The second part of the thesis focuses on the development of a new tool to specifically label Mtb bacteria.

#### 3.1 Introduction

Recently, first efforts have been made to selectively target bacteria based on the presence of unique carbohydrates in the bacterial cell envelope and the broad substrate tolerance of enzymes of the carbohydrate metabolism.<sup>88,192,238–240</sup> Chemically modified carbohydrate derivatives were added to the bacterial environment to be specifically taken up, pass through the natural carbohydrate metabolism and subsequently be incorporated into the bacterial cell envelope replacing endogenous sugars (Figure 30).<sup>241,242</sup> This strategy enabled to distinguish between bacteria and host cells and also between different bacteria classes. This metabolic labeling method is also referred to as metabolic oligosaccharide engineering (MOE).<sup>241,242</sup>



**Figure 30. Illustration of metabolic oligosaccharide engineering (MOE).** Environmental carbohydrate derivatives are transported to the cytoplasm, metabolized and introduced into structures of the cell envelope.

##### 3.1.1 Metabolic oligosaccharide engineering

MOE was pioneered by C. R. Bertozzi,<sup>243,244</sup> W. Reutter<sup>245,246</sup> and colleagues to study and target eukaryotic glycans. Only recently, it was extended to bacterial cell envelope structures.<sup>88,192,238,239</sup> The carbohydrate derivatives, used for metabolic labeling, can directly carry the whole diagnostic or therapeutic probe or only a small functional group, which can be further modified on the cell surface by a selective reaction. Chemical reactions that can occur on the cell surface or even within living organisms without interfering with native biochemical processes are termed bioorthogonal, as coined by C. R. Bertozzi.<sup>247,248</sup> Carbohydrates carrying a large functional group are only rarely incorporated into cell envelope structures due to the substrate specificity of the metabolic enzymes. Small modifications, however, are often tolerated. Furthermore, a two-step approach, based on the incorporation of an unnatural sugar

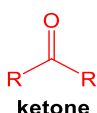
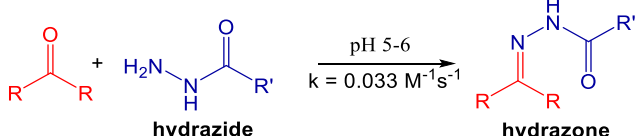
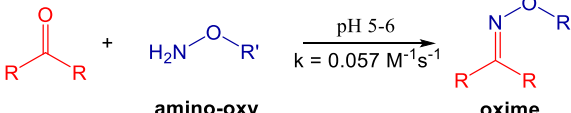
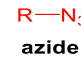
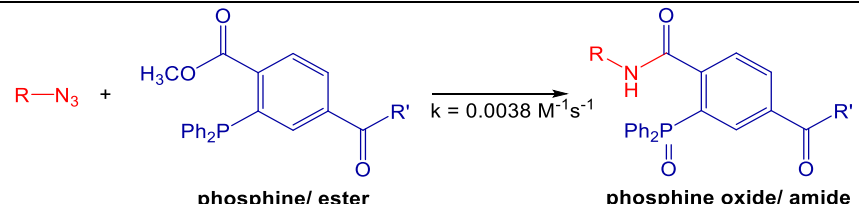
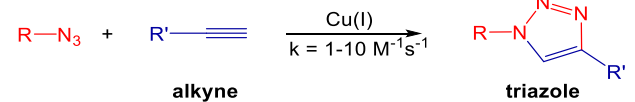
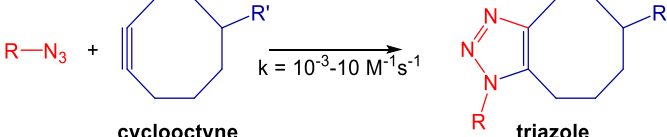

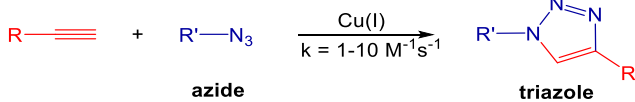
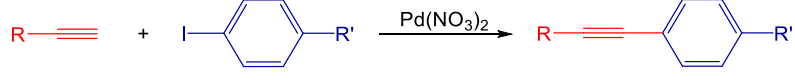
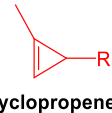
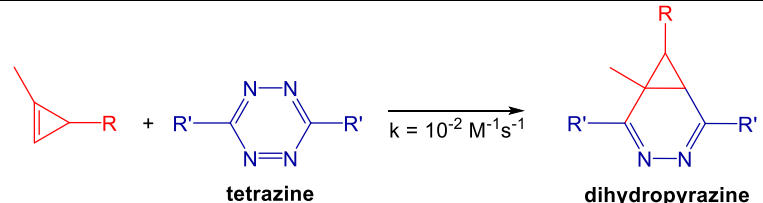
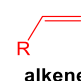
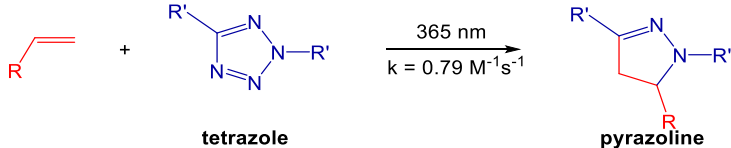
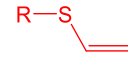
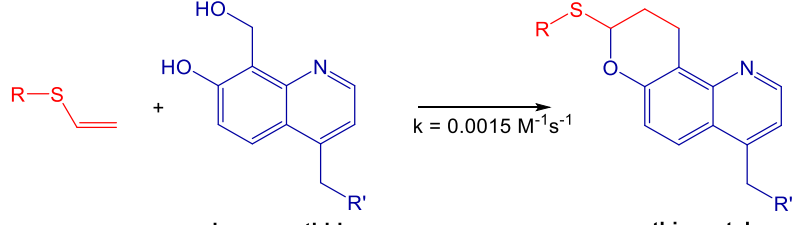
derivative carrying a small function group and a subsequent selective biorthogonal reaction, allows to covalently immobilize a large variety of molecules differing in size, charge and function.

### 3.1.2 Bioorthogonal reactions

Synthetic sugar derivatives incorporated into the bacterial cell envelope should exhibit functional groups that are naturally absent from biological systems, stable in water, nonreactive with functional groups, which are naturally present on the cell surface, and capable to undergo covalent modifications with selective reaction partners under physiological conditions. Therefore, several bioorthogonal chemical strategies have been developed (Table 5).<sup>249–251</sup> Ketone-, azide- or alkyne-containing carbohydrates have been used to label bacterial glycans.<sup>88,238,239</sup> Originally, ketones were explored as chemical reporters being almost absent on cell surfaces.<sup>243</sup> Ketones specifically react with hydrazide or amino-oxy probes in near neutral environment (pH 5-6) forming hydrazone and oxime products, respectively.<sup>248</sup> Ketone-hydrazide chemistry has been successfully used to label both Gram-positive and Gram-negative bacteria.<sup>239</sup> This biorthogonal reaction is even suitable to target bacteria within a host. Unlike ketones, azides are truly absent from biological systems.<sup>247</sup> Azides react with triarylphosphines via Staudinger ligation to yield amides.<sup>252</sup> This selective reaction has already been successfully used within mice without unintended side reactions.<sup>247</sup> However, triarylphosphines are easily inactivated through oxidation and have slow reaction kinetics, which can be a drawback for targeting bacteria *in vivo*.<sup>247</sup> An alternative selective azide-based reaction was developed by M. Meldal, K. B. Sharpless and coworkers. They demonstrated that azides react with alkynes regioselectively at moderate temperature under copper(I) (Cu(I)) catalysis forming triazoles.<sup>253,254</sup> Although this cycloaddition is highly selective and especially fast ( $k = 1-10 \text{ M}^{-1}\cdot\text{s}^{-1}$ ),<sup>255</sup> *in vivo* applications are limited due to the high toxicity profile of copper.<sup>256,257</sup> This disadvantage could be minimized by copper chelators limiting Cu(II) formation and oxidative damage of biomolecules.<sup>258–263</sup> C. R. Bertozzi and coworkers developed the “strain promoted azide-alkyne cycloaddition” (SPAAC) which works completely without any catalysis. In SPAAC the azide reacts with a tensioned alkyne, a cyclooctyne.<sup>264,265</sup> The fact that copper is no longer necessary is based on the tension of the alkyne which leads to reduction of activation energy of the cycloaddition. This reaction was primarily discovered by G. Wittig and A. Krebs in 1961,<sup>266</sup> but only recently used for biological applications by the Bertozzi group. Most recently developed reagents for SPAAC have reaction rates comparable to that of Cu(I)-catalyzed chemistry<sup>250,267</sup> and show only minor side reactions.<sup>268,269</sup> Furthermore, this biorthogonal chemistry was successfully used in living animals, such as zebrafish,<sup>270–272</sup> nematodes<sup>273</sup> and mice.<sup>274</sup> Taken together, SPAAC offers an attractive choice for targeting bacterial glycans.



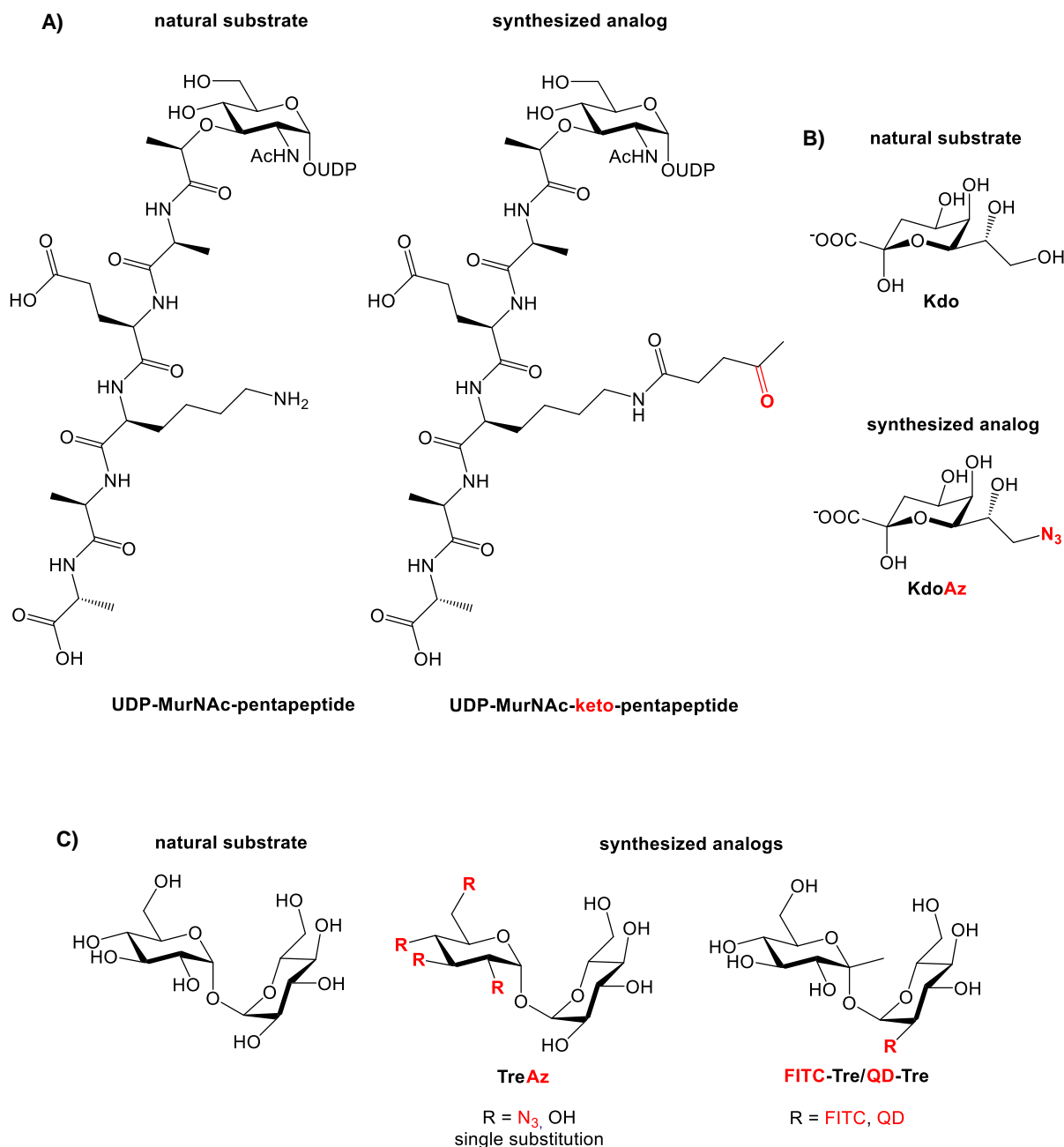
**Table 5. Some of the reported bioorthogonal chemistries, which can be used for covalent targeting of bacterial glycans.** k: reaction rate constant (second order rate), R: rest; based on Tra, V. N. et al. *Chem Commun* **50**, 4659-4673 (2014).<sup>240</sup>

Function group of the sugar derivative		Biorthogonal reaction
 ketone	a) <sup>275</sup>	 hydrazide → hydrazone
	b) <sup>276</sup>	 amino-oxy → oxime
 azide	c) <sup>252</sup>	 phosphine/ ester → phosphine oxide/ amide
	d) <sup>255</sup>	 alkyne → triazole
	e) <sup>250</sup>	 cyclooctyne → triazole
 alkyne	f) <sup>255</sup>	 azide → triazole
	g) <sup>277</sup>	 iodobenzene → phenylacetylene
 cyclopropene	h) <sup>278</sup>	 tetrazine → dihydropyrazine
 alkene	i) <sup>279</sup>	 tetrazole → pyrazoline
 vinyl sulfide	j) <sup>280</sup>	 o-quinone methide precursor → thioacetal

Beside metabolic labeling methods using specific reactions of keto and azido groups, additional bioorthogonal reactions (Table 5) have been developed. Terminal alkynes are rarely detectable in biological systems and can react with azides as described before,<sup>248</sup> but can also undergo covalent modification with indobenzene derivatives in the presence of catalytic palladium(II) nitrate ( $\text{Pd}(\text{NO}_3)_2$ ) via Sonogashira cross coupling.<sup>277</sup> Furthermore, cyclopropenes are tolerated by biosynthetic pathways in mammalian cells and react in an inverse electron demand Diels-Alder reaction with tetrazine conjugates on the cell surface leading to dihydropyrazines.<sup>278</sup> To date several new bioorthogonal reactions, such as alkene/tetrazole<sup>279</sup> and vinyl sulfide/o-quinone methide<sup>280</sup>, expand the repertoire of chemical reporters that could be used for probing bacterial glycans. Nevertheless, azide-cyclooctyne reactions are still the most commonly used bioorthogonal reactions and extremely well established.

### 3.1.3 Metabolic labeling of bacteria

The discovery of unique carbohydrates for specific targeting of bacteria remains the bottleneck in MOE. Ketone-modified uridine diphosphate *N*-acetylmuramic acid ((UDP)-MurNAc) (Figure 31 A), an analogue of a natural occurring peptidoglycan precursor, enabled metabolic labeling of many bacterial but not human cells.<sup>239</sup> More specifically, a derivative of 3-deoxy-D-manno-oct-2-ulosonic acid (Kdo), containing an azido group, (Figure 31 B) was used to discriminate between Gram-positive and Gram-negative bacteria. Kdo is a monosaccharide present in the inner core of the lipopolysaccharide (LPS), thus azide-modified Kdo (KdoAz) is incorporated into Gram-negative bacteria (e.g. *E. coli*, *Salmonella typhimurium*, *Legionella pneumophila*) but not Gram-positive bacteria (e.g. *Staphylococcus aureus*, *Bacillus subtilis*).<sup>238</sup> Only recently, mycobacteria could be selectively labeled by trehalose derivatives (Figure 31 C).<sup>88,192</sup> Trehalose is part of unique mycobacterial cell envelope components, such as TMM and TDM, and absent in cell envelopes of Gram-negative and Gram-positive bacteria. Azide-modified trehalose (TreAz) analogues are tolerated in mycobacterial biosynthesis anchoring the disaccharide into the mycobacterial cell envelope as mycolic acid esters. The small azido functional group was visualized in a subsequent bioorthogonal reaction, employing copper-free click chemistry with fluorescent cyclooctyne derivatives.<sup>88</sup> Beside this two-step approach, the mycobacterial cell envelope was directly modified by trehalose derivatives carrying a large fluorescein molecule or even quantum dots (QD).<sup>192</sup> The possibility to enter these impressively large carbohydrate derivatives is based on a broad substrate tolerance of the trehalose mycolyltransferase enzymes (Ag85A, Ag85B, Ag85C). Fluorescein isothiocyanate (FITC)-modified trehalose and quantum dots functionalized with trehalose derivatives could be used to label Mtb bacteria even within macrophages.<sup>192</sup> These results make it reasonable that carbohydrate derivatives can be used to specifically image and target Mtb bacteria and might prospectively be applied in Tb diagnostic and therapy.



**Figure 31. Carbohydrate derivatives used for metabolic labeling of bacteria.** UDP-MurNAc-keto-pentapeptide was metabolically incorporated into peptidoglycan structures of both Gram-positive and Gram-negative bacteria (A).<sup>239</sup> Azido Kdo was used to specifically target Gram-negative bacteria (B).<sup>238</sup> Different trehalose derivatives bearing an azido group (C) were incorporated into the cell envelope of *Msg* bacteria and *Mtb* bacteria and visualized by copper-free click chemistry.<sup>88</sup> *Mtb* bacteria could be fluorescently labeled, in a one-step approach, using fluorescein isothiocyanate (FITC)-modified trehalose or quantum dots (QD) functionalized with trehalose derivatives (C).<sup>192</sup>

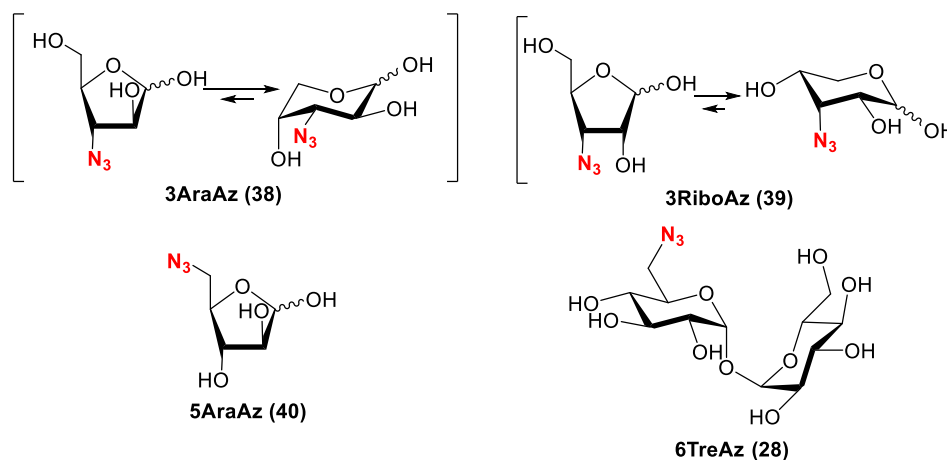
### 3.2 Objectives

To facilitate the development of Mtb-specific diagnostic and therapeutic tools, new carbohydrate derivatives, applicable for MOE, are of special interest. D-Arabinose is a non-mammalian sugar and especially rare in nature, but a major component of the mycobacterial cell envelope heteropolysaccharides LAM and AG. These features led to the following questions:

1. Can Mtb bacteria be labeled based on the arabinan metabolism?
2. Does arabinose-dependent MOE show unwanted side effects like bacteriostasis, cytotoxicity or labeling of host cells?
3. What can arabinose-dependent MOE be applied for?

### 3.3 Results

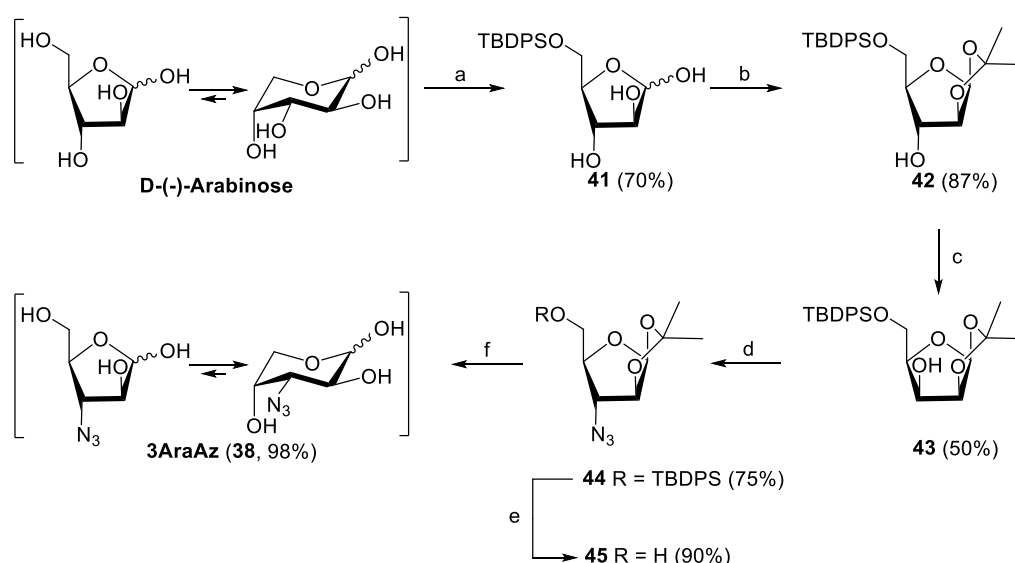
Developing new metabolic labeling strategies for Mtb bacteria is preceded by the synthesis of sugar derivatives tolerated by the carbohydrate metabolism and containing a functional group that can be addressed by bioorthogonal reactions. In this study three different carbohydrate derivatives were designed based on the arabinan metabolism of Mtb<sup>97</sup> (Figure 11) carrying an azido function. D-ribose-5-phosphate and 5-phospho-D-ribosylpyrophosphate are key intermediates of this metabolism. Thus, the 1- and 5-position of arabinose or ribose, respectively, were excluded from modifications. In a final biosynthetic step, 1-decaprenylphospho-D-ribofuranose is epimerized at position 2 to form the respective AraF substrate.<sup>97</sup> Consequently, also the 2-position of the sugar ring was not modified. Based on this analysis 3-azido-3-deoxy-D-arabinose (3AraAz, **38**) and 3-azido-3-deoxy-D-ribose (3RiboAz, **39**) were synthesized, with 5-azido-5-deoxy-D-arabinofuranose (5AraAz, **40**) as negative control compound (Figure 32). 6-Azido-6-deoxy-D-trehalose (6TreAz, **28**) was synthesized as a positive control compound based on the known metabolic labeling strategies for Mtb bacteria (Figure 31).<sup>88</sup>



**Figure 32. Azido compounds synthesized for bioorthogonal labeling of Mtb bacteria.** Three different azido pentoses (3-azido-3-deoxy- $\alpha,\beta$ -D-ribose (3RiboAz, **38**), 3-azido-3-deoxy- $\alpha,\beta$ -D-arabinose (3AraAz, **39**), 5-azido-5-deoxy- $\alpha,\beta$ -D-arabinofuranose (5AraAz, **40**)) and 6-azido-6-deoxy-trehalose (6TreAz, **28**) as a positive control compound were synthesized and applied for metabolic labeling of Mtb bacteria.

### 3.3.1 Syntheses

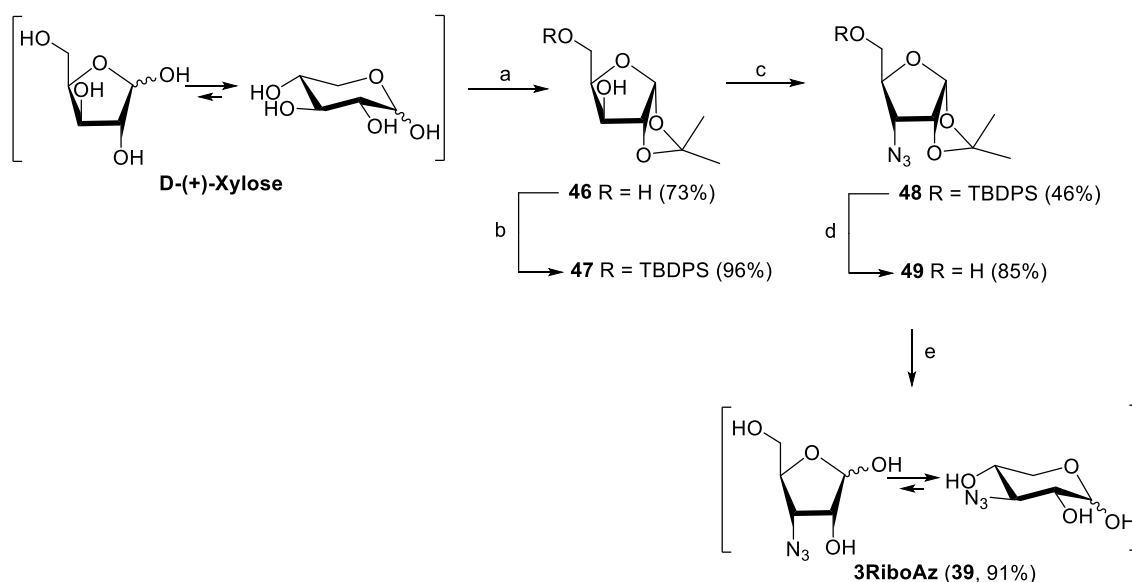
3AraAz was synthesized over six reaction steps with D-arabinose as starting material. Initially the primary hydroxyl group, only present in the furanose form of D-arabinose, was protected with *tert*-butyl-diphenylsilyl chloride (TBDPSCI) giving the arabinofuranose derivative **41** in 70% yield.<sup>281</sup> The *cis*-arranged hydroxyl groups at the 1- and 2-position of the sugar ring reacted with acetone under acid conditions leading to the formation of a 1,3-dioxolane. Consequently, only the hydroxyl group at the 3-position remained unprotected. Substitution of a hydroxyl group by an azido function is based on a nucleophilic substitution second order ( $S_N2$ ), thus is associated with an epimerization. To avoid the formation of a diastereomer, the hydroxyl group itself had to be epimerized prior substitution. The hydroxyl group at the 3-position was activated by trifluoromethanesulfonic anhydride ( $Tf_2O$ ) under basic conditions and subsequently reacted with sodium nitrite giving the epimerized product, 1,2,5-protected lyxofurose **43**,<sup>282</sup> in 50% yield. Finally, the azido function was introduced by activation of the unprotected hydroxyl group as a trifluoromethanesulfonic acid ester and a nucleophilic substitution with sodium azide.<sup>282</sup> The azido sugar **44** was stepwise deprotected. The silyl ether was removed by tetra-*N*-butylammonium fluoride (TBAF) and the isopropylidene group under acidic conditions giving 3AraAz (**38**) in an overall yield of 20% (Scheme 5).



**Scheme 5. Synthesis of the azido pentose 38 (3AraAz).** a) TBDPSCI, pyridine, rt, overnight, 70%; b) 2,2-dimethoxypropane, *p*-TsOH, acetone, rt, 3 h, 87%; c) 1.  $Tf_2O$ , pyridine, DCM, 0°C, 2 h; 2.  $NaNO_2$ , DMF, 70°C, overnight, 50%; d) 1.  $Tf_2O$ , pyridine, DCM, 0°C, 4.5 h; 2.  $NaN_3$ , DMF, 80°C, 5 h → rt, overnight, 75%; e) TBAF, THF, rt, 45 min, 90%; f) TFA,  $H_2O$ , DMF, 0°C, 2 h, 98%.

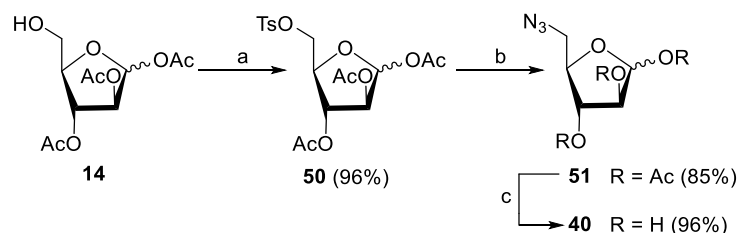
Based on the ribose intermediates in the arabinan metabolism of Msp 3RiboAz (**39**) was designed and synthesized. D-Xylose was protected with acetone under acidic conditions giving 1,2,3,5-di-*O*-isopropylidene- $\alpha$ -D-xylofuranose, which could be partially hydrolyzed with high selectivity leading to the 1,2-protected xylofuranose **46** in 73% yield.<sup>283</sup> The primary

hydroxyl group was protected by the sterically demanding TBDPS group, which resulted in the compound **47** containing only one unprotected hydroxyl group at the 3-position.<sup>284,285</sup> The hydroxyl group was activated by  $\text{Tf}_2\text{O}$  under basic conditions and subsequently reacted with sodium azide giving the azido ribose **48** in 46% yield.<sup>284,285</sup> The azido sugar **48** was stepwise deprotected. The silyl ether was removed by TBAF<sup>284,285</sup> and the isopropylidene group under acidic conditions yielding 3RiboAz (**39**) (Scheme 6).



**Scheme 6. Synthesis of the azido pentose 39 (3RiboAz).** a) 1. Acetone,  $\text{H}_2\text{SO}_4$ , rt, 30 min; 2.  $\text{Na}_2\text{CO}_3$ ,  $0^\circ\text{C} \rightarrow$  rt, 3 h, 73%; b) TBDPSCl, pyridine, rt, 3.5 h, 96%; c) 1.  $\text{Tf}_2\text{O}$ , pyridine, DCM,  $0^\circ\text{C}$ , 4.5 h; 2.  $\text{NaN}_3$ , DMF,  $80^\circ\text{C}$ , 5 h  $\rightarrow$  rt, overnight, 46%; d) TBAF, THF, rt, 45 min, 85%; e) TFA,  $\text{H}_2\text{O}$ , DMF,  $0^\circ\text{C}$ , 2 h, 91%.

While 3AraAz and 3RiboAz were regarded as promising candidates for metabolic labeling of Mtb bacteria, 5AraAz was synthesized as a negative control. The synthesis started from the arabinofuranose derivative **14**, which was prepared as described in the first part of this thesis (Scheme 2). The unprotected primary hydroxyl group was activated by tosylation followed by a nucleophilic substitution with sodium azide.<sup>286</sup> The azido arabinofuranose **51** was deprotected according to Zemplén's method<sup>183</sup> giving 5AraAz (**40**) in 78% yield over three steps (Scheme 7).<sup>286</sup>



**Scheme 7. Synthesis of the azido pentose 40 (5AraAz).** a) TsCl, pyridine, rt, overnight, 96%; b)  $\text{NaN}_3$ , DMF,  $70^\circ\text{C}$ , 5 h, 85%; c) NaOMe, MeOH, rt, overnight, 96%.

The azido trehalose **28** (6TreAz) was synthesized as a positive control compound based on the results recently published by B. M. Swarts et al..<sup>88</sup> The reaction pathway was the same as described for the amino trehalose **3** in the first part of this thesis (Scheme 4).

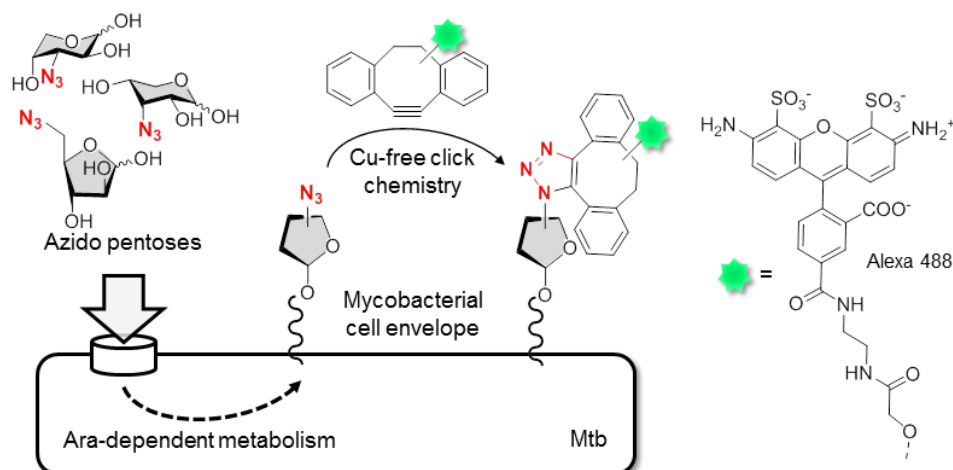
#### Results 3.3.1: Summary

- 3AraAz (**38**) and 3RiboAz (**39**) were successfully synthesized by protection group-based chemistry and specific epimerization steps.
- 5AraAz (**40**) was synthesized as a negative control based on the arabinan metabolism of Msp. 6TreAz (**28**) was synthesized as a positive control, as shown by B. M. Swarts et al..
- All derivatives carried an azido group, which can be addressed by cyclooctynes in a biorthogonal reaction.



### 3.3.2 Metabolic labeling of Mtb bacteria

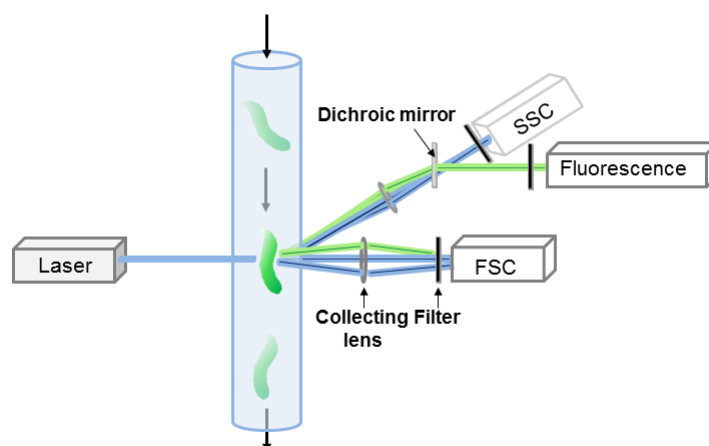
For metabolic labeling of Mtb (Figure 32), bacteria in the exponential growth phase were cultured in the presence of the azido sugars for three days. Incorporated azido groups in the mycobacterial cell envelope were detected using Cu-free click chemistry. Therefore, bacteria were incubated with dibenzocyclooctyne (DIBO)-Alexa 488 for one hour at 37°C while gently shaking.



**Figure 32. Illustration of the method to metabolically label Mtb bacteria using azido sugars and Cu-free click chemistry.** Mtb bacteria were cultured in the presence of azido sugars. Subsequently, bacteria were incubated with DIBO-Alexa 488, which led to azido group-dependent fluorescent labeling of Mtb bacteria.

### Detection of labeled Mtb bacteria by flow cytometry

Fluorescently labeled Mtb bacteria were detected by flow cytometry and labeling intensity quantified. Flow cytometry enables to simultaneously analyze the size (forward scatter) and the relative granularity (sideward scatter) of the bacteria<sup>287</sup> and to detect emitted fluorescence signals on a single cell level (Figure 33).

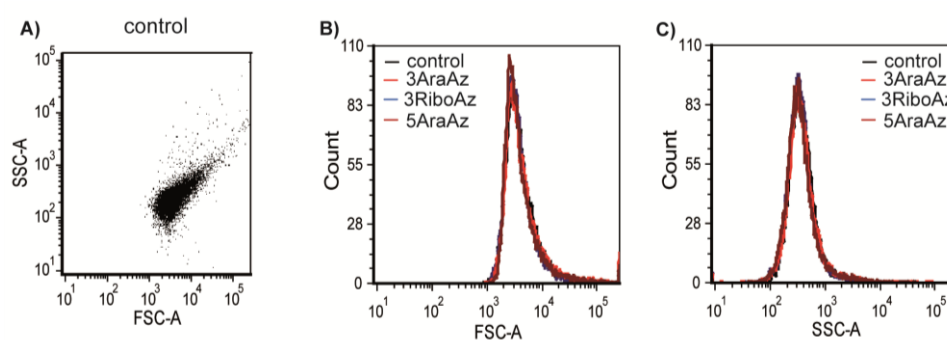


**Figure 33. Illustration of the flow cytometric analysis of metabolically labeled Mtb bacteria.** Flow cytometric analysis enables to detect fluorescence labeled bacteria on a single cell level and quantify fluorescence intensity. Beside detection of fluorescence signals, flow cytometry gives insights into size and granularity of the analyzed bacteria by detecting the scattered light. (FSC:forward scatter, SSC:sideward scatter)

In a flow cytometer bacteria in suspension are separated passing one at a time through a focused laser beam. The monochromatic light can be absorbed by a fluorescent dye (e.g. Alexa 488 linked to the bacterial cell envelope) re-emitting light of a specific wavelength. In addition, the excitation light is specifically scattered dependent on cell size, shape and granularity. Scattered and by a fluorochrome emitted light are collected via optics that direct the light to a series of filters and dichroic mirrors isolating particular desired wavelength bands. The light signals are detected by photomultiplier tubes and digitized for computer analysis.

#### Metabolic labeling of Mtb bacteria with the new azido pentoses

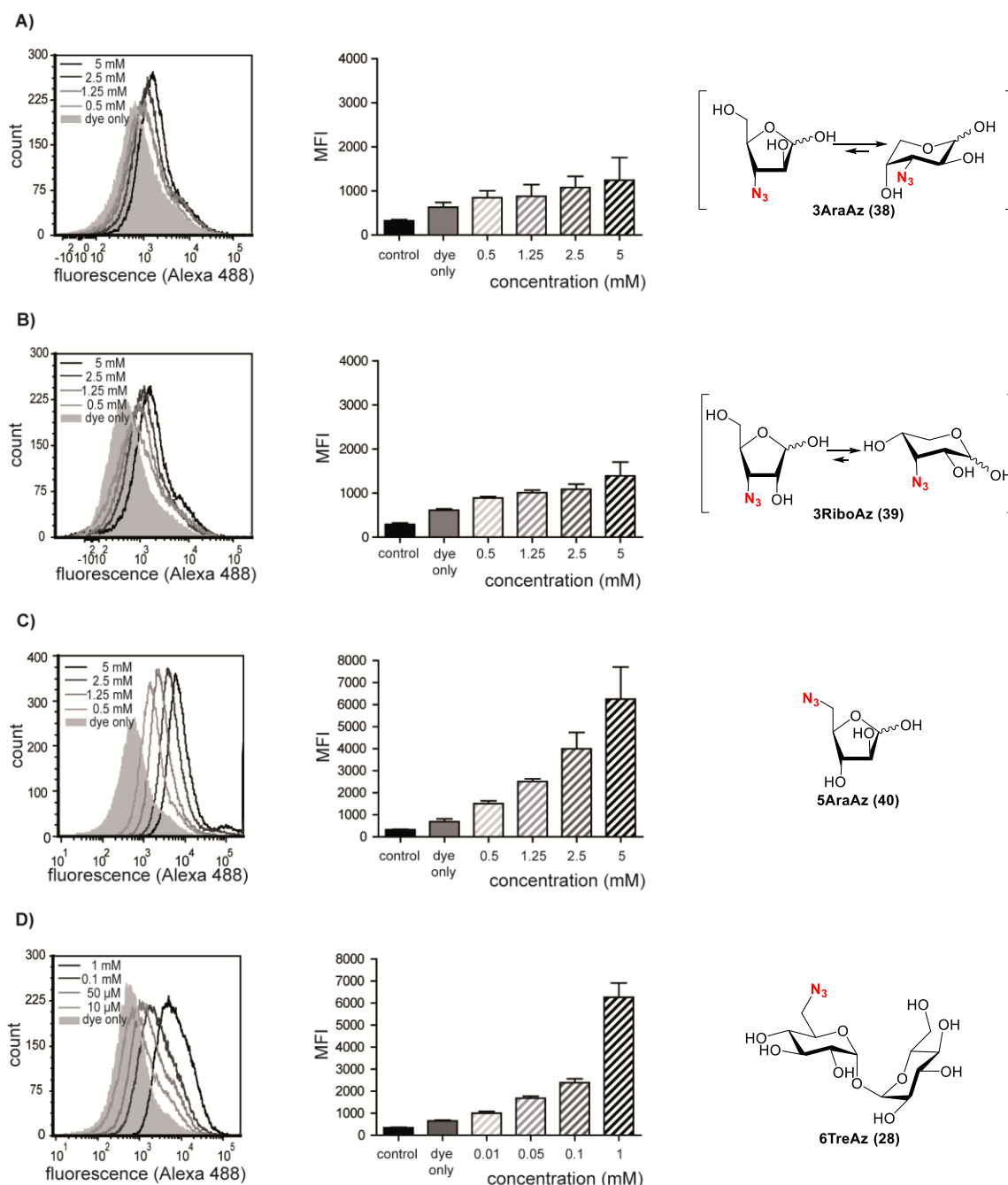
To test metabolic labeling of Mtb bacteria with the azido pentoses 3AraAz (**38**), 3RiboAz (**39**) and 5AraAz (**40**), and the known disaccharide 6TreAz (**28**) as control, the commonly used virulent Mtb strain H37Rv was cultured with the azido sugars at different concentrations, reacted with DIBO-Alexa 488 and labeled bacteria analyzed by flow cytometry (Figure 34 and Figure 35).



**Figure 34. Flow cytometric analysis shows the influence of metabolic labeling on the morphology of Mtb bacteria.** The Mtb strain H37Rv was cultured in the presence of different azido pentoses (3AraAz (**38**), 3RiboAz (**39**) and 5AraAz (**40**), concentrations: 5 mM each), reacted with DIBO-Alexa 488, fixed and analyzed by flow cytometry. Analysis shown includes 100% of detected events. Dot plot (A) shows the detected forward scatter (FSC-A) and sideward scatter (SSC-A) of the analyzed non-modified Mtb bacteria (control), each dot = one detected event; the histograms (B and C) show the FSC and SSC, respectively, of non-modified Mtb bacteria (control) and of labeled Mtb bacteria. One of two technical replicates of three independent experiments shown. (control: without azido sugar, without dye).

Culturing Mtb bacteria in the presence of azido pentoses, followed by click-reaction, led to similar forward scatter signals (FSC) and sideward scatter signals (SSC) as detected for cultured, but non-modified Mtb bacteria (control) (Figure 34). Supplementation of 3RiboAz (**39**) and 3AraAz (**38**), respectively, resulted in a dose dependent increase of fluorescence intensity reaching a twofold enhancement at a sugar concentration of 5 mM compared to Mtb bacteria cultured without azido sugar supplementation, but incubated with DIBO-Alexa 488 (dye only) (Figure 35 A and B). Whereas 3RiboAz (**39**) and 3AraAz (**38**) performed similarly, incubation with 5AraAz (**40**) resulted in highly intense signals and was about four times more efficient than the 3-azido derivatives **38** and **39** (Figure 35 C). The fluorescence increase obtained with

5AraAz (**40**) was similar to that observed with 6-azido-6-deoxy-D-trehalose (6TreAz, **28**)<sup>88</sup> (Figure 35 D). However, five times higher concentrations of 5AraAz (**40**) were required compared to 6TreAz (**28**) to reach fluorescence signals with similar intensity.

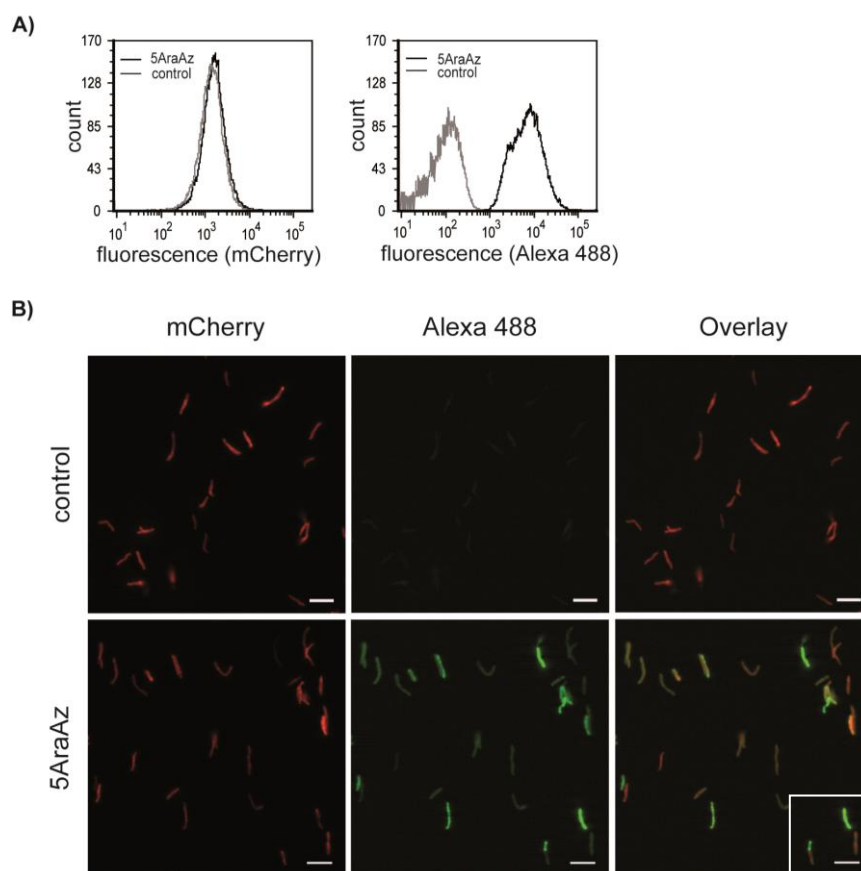


**Figure 35. Flow cytometric analysis of dose-dependent metabolic labeling of Mtb bacteria using the three synthesized azido pentoses (3AraAz (A), 3RiboAz (B), 5AraAz (C)) and 6TreAz (D).**<sup>88</sup> The Mtb strain H37Rv was cultured in the presence of the different azido pentoses **38**, **39** or **40** (concentrations: 0.5 mM, 1.25 mM, 2.5 mM, 5 mM) or 6TreAz (**28**) (concentrations: 0.01 mM, 0.05 mM, 0.1 mM, 1 mM), reacted with DIBO-Alexa 488, fixed and analyzed by flow cytometry. Analysis shown includes 100% of detected events. Bar diagram represent means (+SD) of duplicates of two independent experiments. (MFI: mean fluorescence intensity; control: without azido sugar, without dye; dye only: without azido sugar, with dye).

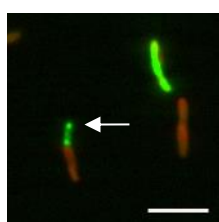
This flow cytometric analysis suggests that metabolic labeling of Mtb bacteria has no impact on the bacterial morphology and shows that a fluorescence staining can be observed with all three new azido pentoses **38**, **39** and **40**, but with different efficiencies. 5AraAz (**40**), which was originally synthesized as a negative control compound, was identified as the most potent pentose derivative for MOE.

### 3.3.3 Microscopic analysis of metabolic labeled Mtb bacteria

To microscopically document the labeling of Mtb bacteria, red fluorescent Mtb H37Rv bacteria expressing mCherry (Cherry 10) were cultured in the presence of 5AraAz (**40**), reacted with DIBO-Alexa 488 and analyzed by fluorescence microscopy.



**Figure 36. Flow cytometry and fluorescence microscopy of metabolically labeled Cherry 10.** mCherry expressing Mtb H37Rv bacteria (Cherry 10, red) were cultured in the absence (control) or presence of 5AraAz (**40**, 5 mM), reacted with DIBO-Alexa 488 (green) and analyzed by flow cytometry (A) and fluorescence microscopy (B). Shown is one representative experiment of at least three independent experiments performed as duplicates. Flow cytometric analysis includes 100% of detected events. (Control: without azido sugar, without dye; scale bar: 5  $\mu$ m).



**Figure 37. Enlarged view of a part (white box) of the fluorescence microscopic image of 5AraAz-labeled Mtb bacteria (overlay), as shown in Figure 36.** Intense green fluorescence at the bacterial poles (white arrow) shown.

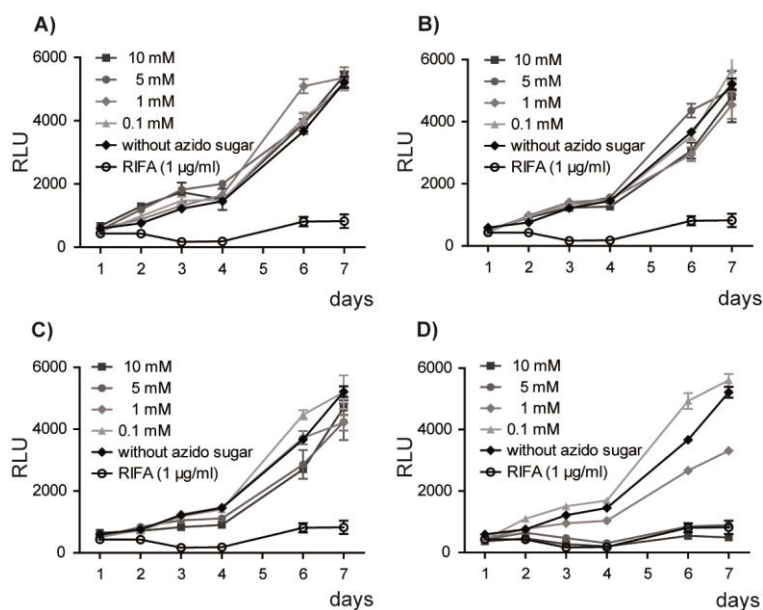
Flow cytometric analysis of 5AraAz (**40**)-labeled Mtb Cherry 10 bacteria showed a broad signal with roughly 100 times higher green fluorescence intensity compared to non-modified Mtb Cherry 10 bacteria (control). The red fluorescence intensity was similar between labeled and non-labeled Mtb bacteria (Figure 36 A). Microscopic analysis visualized green fluorescence signals for mycobacteria labeled with 5AraAz (**40**) and no green fluorescence signals for non-modified Mtb Cherry 10 bacteria. The detected green fluorescence was co-localization with the red fluorescence derived from the mCherry-expressing Mtb bacteria. The green fluorescence intensity was highly diverse. Approximately half of the bacteria show strong green fluorescence signals, whereas the other half of the visualized bacteria are less intensely green fluorescent or do not emit microscopically detectable green fluorescence. Some of the bacteria show more intense green fluorescence at the bacterial poles and less in mid sections (Figure 37). Few of the strongly green fluorescent mycobacteria show no detectable red fluorescence (Figure 36 B).

The flow cytometric analysis shows that Mtb Cherry 10 bacteria can be labeled similar to non-fluorescent Mtb H37Rv bacteria (Figure 36 A). Furthermore, MOE does not influence the fluorescence signal of the expressed mCherry protein. Microscopic analysis (Figure 36 B and Figure 37) verified the potency to label Mtb bacteria using 5AraAz (**40**) and gave first insights into surface distribution of the incorporated label. Microscopic analysis seemed to be less sensitive than flow cytometric analysis resulting probably in an absent visualization of weak fluorescence signals.

### 3.3.4 Influence of azido sugars on mycobacterial growth

As described before 5AraAz (**40**) has to be applied in five times higher concentrations compared to 6TreAz (**28**) to reach similar labeling efficiencies (Figure 35). Thus, it was analyzed whether these larger amounts of azido sugar have an impact on bacteria replication. Bacterial growth analysis performed in 96-well microtiter plates using GFP-expressing Mtb bacteria<sup>288</sup> was carried out with all three azido pentoses (3AraAz (**38**), 3RiboAz (**39**) and 5AraAz (**40**)) and 6TreAz (**28**) for seven days (Figure 38). In this assay bacteria replication is linked to an increase of fluorescence intensity, which was detected using a fluorescence reader.

A similar increase in fluorescence intensities over seven days was detected for bacteria cultured in the presence of the azido pentoses **38**, **39** and **40**, respectively, and untreated bacteria cultures (Figure 38 A-C). Addition of 6TreAz (**28**, 1 mM) led to a smaller increase and no change in fluorescence intensity was detected at 6TreAz (**28**) concentrations of 5 mM and 10 mM (Figure 38 D). The low fluorescence intensities measured for high concentrations (5 mM and 10 mM) of 6TreAz (**28**) were similar to those detected in wells containing the antibiotic rifampicin (RIFA).

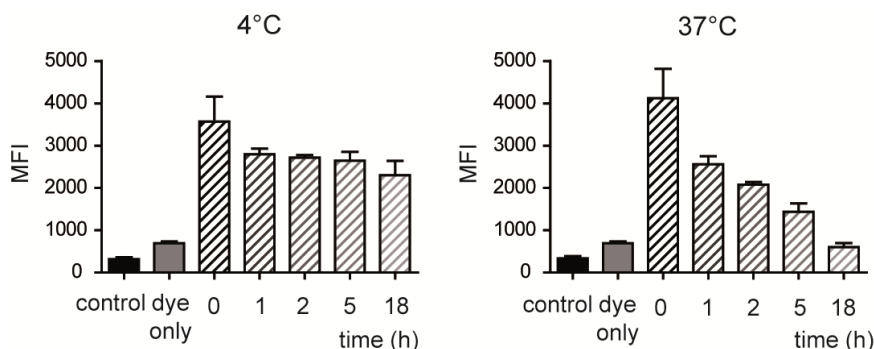


**Figure 38. Influence of the three synthesized azido pentoses (3AraAz (A), 3RiboAz (B) and 5AraAz (C) and 6TreAz (D) on growth of GFP-expressing Mtb bacteria.** Mtb growth analysis was performed as described elsewhere.<sup>288</sup> All four azido derivatives,<sup>28, 38, 39</sup> and <sup>40</sup>, were tested regarding their bacteriostatic effects in different concentrations (0.1 mM, 1 mM, 5 mM, 10 mM). Rifampicin (RIFA, 1 µg/ml) was used as positive control. Data represent means (+/-SD) of three technical replicates. One of three independent experiments shown. (RLU: relative light units)

Since fluorescence intensities correlate with mycobacteria quantity, the data indicate that neither 3AraAz (**38**), 3RiboAz (**39**) nor 5AraAz (**40**) influence bacteria replication up to a concentration of 10 mM. Thus, the toxicity profile of the new azido pentoses is highly favorable. In contrast 6TreAz (**28**) showed growth-limiting effects at a concentration of 1 mM.

### 3.3.5 Stability of Mtb labeling with 5AraAz

In order to address the stability of the labeling with 5AraAz (**40**), metabolically labeled Mtb bacteria were cultured for different time periods at 4°C and 37°C and analyzed by flow cytometry (Figure 39).

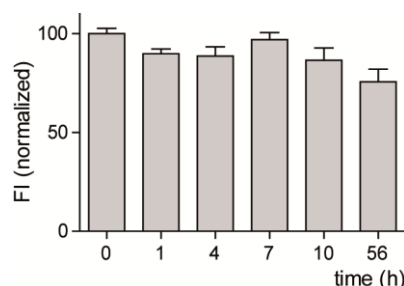


**Figure 39. Stability of Mtb labeling with 5AraAz (40).** 5AraAz (**40**)-labeled Mtb H37Rv bacteria were cultured for various time periods (1 h, 2 h, 5 h, 18 h) at 4°C and 37°C. Flow cytometric analysis includes 100% of detected events. Data represent means (+SD) of duplicates of at least two independent experiments. (MFI: mean fluorescence intensity; control: without azido sugar, without dye; dye only: without azido sugar, with dye).

At 4°C no major change in fluorescence intensity of the labeled mycobacteria was observed and even after 18 hours nearly 70% of the initial signal was detected. At 37°C, on the other hand, the fluorescence intensity of the labeled Mtb bacteria was reduced by half within the first two hours and vanished completely after 18 hours.

The results indicate a time- and temperature-dependent depletion of the incorporated label.

To analyze whether fluorescence degeneration is based on bleaching of the dye, DIBO-Alexa 488 was dissolved in 7H9 medium and incubated at 37°C for different time periods. Fluorescence intensity was detected (Figure 40) using a fluorescence reader.



**Figure 40. Stability of the dye DIBO-Alexa 488.** DIBO-Alexa 488 (final concentration 4  $\mu\text{M}$ ) was added to 7H9 medium and incubated for various time periods (1 h, 4 h, 7 h, 10 h, 56 h) at 37°C. Fluorescence intensity of the solution (100  $\mu\text{l}$  each) was analyzed using a fluorescence reader. Fluorescence intensity normalized with measured initial fluorescence intensity = 100. (FI: fluorescence intensity)

Incubation of the dye at 37°C resulted in no major change in fluorescence intensity. After 56 h roughly 75% of the initial signal was detected.

The observed depletion of the label, which was incorporated into the Mtb cell envelope, is not due to bleaching of the fluorescence dye Alexa 488.

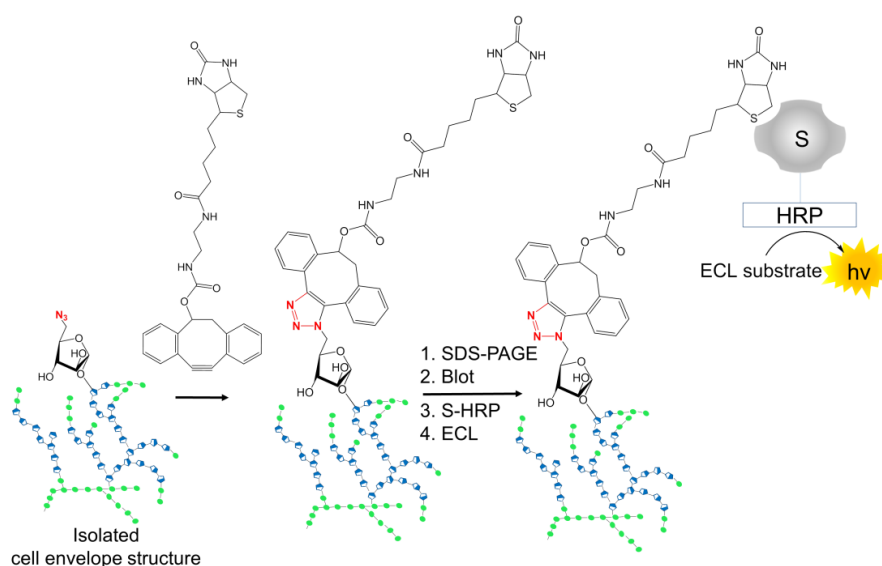
### 3.3.6 Incorporation of 5AraAz into lipoglycans of the Mtb cell envelope

5AraAz (**40**) was highly effective for metabolic labeling of Mtb bacteria (Figure 35). To prove that 5AraAz (**40**) indeed passes the biosynthetic pathway and is finally incorporated into mycobacterial cell envelope structures, Mtb lipoglycans and glycolipids were isolated from untreated (control) and 5AraAz (**40**)-treated Mtb H37Rv bacteria. The mycobacteria were cultured with or without supplementation of 5AraAz (**40**), washed and autoclaved. The resulting suspensions were further processed according to an established protocol to isolate ManLAM and its related precursors, LM and PIM, from the mycobacterial cell envelope.<sup>289</sup> The isolation of glycolipids and lipoglycans from the Mtb cell envelope was supported by Regina Engel from the group of Prof. Dr. Otto Holst of the Research Center Borstel, Germany. Both preparations, from 5AraAz (**40**)-treated and untreated bacteria, were denatured and the components separated by size using sodium dodecyl sulfate polyacrylamide gel electrophoresis



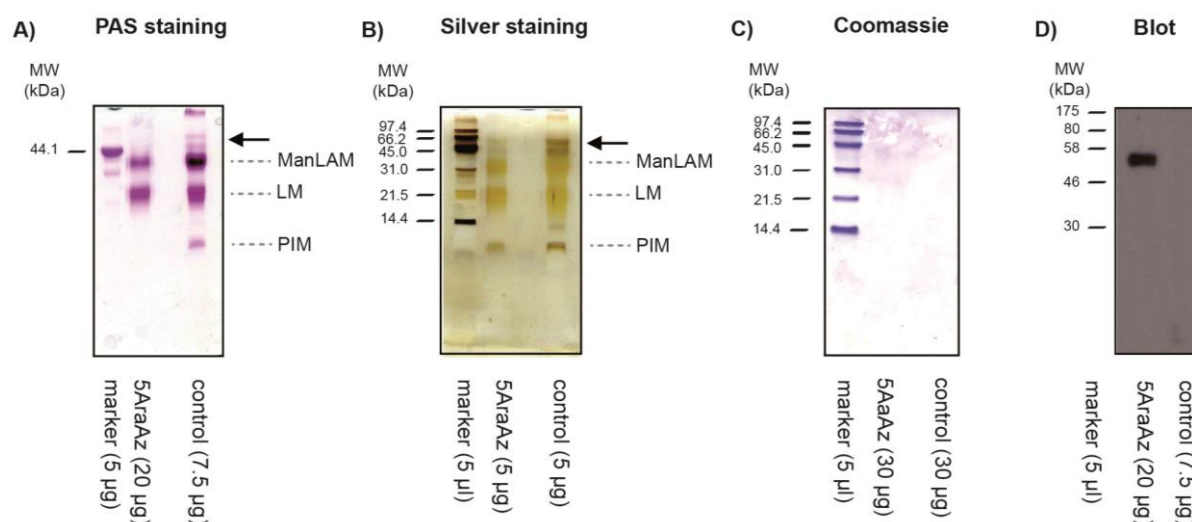
(SDS-PAGE, for additional information see method section). The separated cell envelope structures were analyzed by Periodic acid-Schiff reaction (PAS), coomassie staining and the more sensitive silver staining (Figure 42 A-C). PAS (Figure 42 A) was used to investigate, whether the isolated cell envelope structures contain carbohydrates and to estimate the sizes of the glycoconjugates. Vicinal diols of the sugar ring were oxidized by periodic acid resulting in two aldehyde groups. The aldehydes were reacted with Schiff's fuchsin-sulfite reagent to give a deep red-violet product. In a coomassie staining (Figure 42 C) a negative charged triphenylmethane dye, Coomassie Brilliant Blue, binds to positive charged molecules. Thereby proteins containing basic amino acids, such as arginine, lysine or histidine, can be visualized. The silver staining (Figure 42 B) is based on binding of silver ions to negative charged molecules. The attached silver ions are subsequently reduced by formaldehyde giving the visible elemental silver. To detect not only proteins, but also carbohydrates by this staining method the isolated and separated cell envelope structures were oxidized prior to the silver staining.

To analyze whether azido functions were integrated into the isolated cell envelope structures, both preparations were incubated with DIBO-biotin. After denaturation and separation by SDS-PAGE the cell envelope structures were transferred to a polyvinylidene fluoride (PVDF) membrane by wet electroblotting. The membrane was incubated with streptavidin-horseradish peroxidase (S-HRP), which specifically bound to biotin tagged and therefore azide containing cell envelope structures. The linked peroxidase enabled visualization of bound S-HRP via chemiluminescence (method Figure 41 and results Figure 42 D). The emitted light was detected on an X-ray film.



**Figure 41. Illustration of the used method to detect incorporated 5AraAz (40) in isolated cell envelope structures.** Isolated cell envelope structures (20  $\mu$ g) were incubated with DIBO-Biotin (4  $\mu$ M) for 1.5 h at rt, gentle agitation. SDS-PAGE, followed by blotting and incubation with streptavidin-horseradish peroxidase (S-HRP) enabled visualization of biotin tagged and therefore azide containing cell envelope structures via chemiluminescence. (ECL: enhanced chemiluminescence)





**Figure 42. Verification of the incorporation of 5AraAz (40) into glycolipids and lipoglycans of the Mtb cell envelope.** Mtb H37Rv bacteria were cultured in the presence of 5AraAz (40, 1 mM) or left untreated (control), followed by glycolipid and lipoglycan isolation. Analysis of the composition of the isolated fractions (5AraAz: from 5AraAz (40)-labeled Mtb H37Rv cultures; control: from unlabeled Mtb H37Rv cultures): Carbohydrates of mycobacterial cell envelope structures (lipoarabinomannan (ManLAM), lipomannan (LM) and phosphatidyl-*myo*-inositol mannosides (PIMs)) and two larger structures (arrows) were visualized with Periodic acid-Schiff reaction (PAS) (marker:  $\alpha$ -1-acid-glycoprotein) (A). Proteins were detected by coomassie staining (marker: low range marker (LRM)) (C). Silver staining was used to enrich the analytic sensitivity detecting proteins, carbohydrates or other negative charged molecules (marker: LRM) (B). To visualize incorporated azide functions isolated glycolipids were treated with DIBO-Biotin, separated by gel electrophoresis (marker: ColorPlus Prestained Protein Marker), blotted and incubated with streptavidine-HRP, followed by detection via chemiluminescence (D).

In both preparations, from 5AraAz-treated and untreated Mtb bacteria (control), bands were detected by PAS and silver staining (Figure 42 A and B) at molecular weights smaller than 14 kDa, between 18 and 22 kDa, between 31 and 35 kDa and two bands larger than 45 kDa (arrows Figure 42 A and B). No bands were visualized by coomassie staining (Figure 42 C).

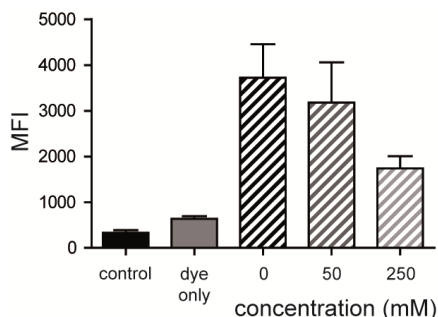
Bands visualized by PAS and silver staining were in line with molecular weights of the typical mycobacterial glycolipids and lipoglycans known from literature (PIM: < 12 kDa, LM: 15-20 kDa, ManLAM: 30-45 kDa).<sup>290-292</sup> No proteins were detected by coomassie staining. These results indicate a successful glycolipid and lipoglycan preparation from Mtb bacteria and suggest that 5AraAz (40) supplementation does not strongly influence cell envelope composition.

The blot showed only in the preparation from 5AraAz (40)-treated Mtb bacteria a specific band at around 50 kDa (Figure 42 D).

The band (~50 kDa) detected by chemiluminescence indicates that 5AraAz (40) is indeed incorporated into a cell envelope structure of Mtb. The fact that bands in this molecular size range were also detected in PAS and silver stain analysis suggests that 5AraAz (40) is introduced into a yet unknown non-protein glycoconjugate of the Mtb cell envelope.

### 3.3.7 5AraAz labeling of Mtb bacteria in the presence of D-arabinose

To investigate whether the incorporation of 5AraAz (**40**) depends on arabinose uptake mechanisms, 5AraAz (**40**) labeling of Mtb H37Rv bacteria was performed in the presence of increasing concentrations of D-arabinose (Figure 43).



**Figure 43. 5AraAz (**40**) labeling of Mtb bacteria in the presence of D-arabinose.** Mtb H37Rv bacteria were cultured in the presence of 5AraAz (**40**, 5 mM) and increasing concentrations of D-arabinose (50 mM, 250 mM), reacted with DIBO-Alexa 488, fixed and analyzed by flow cytometry. Analysis includes 100% of detected events. Data represent means (+SD) of duplicates of two independent experiments. (MFI: mean fluorescence intensity; control: without azido sugar, without dye; dye only: without azido sugar, with dye).

Flow cytometric analysis showed a reduction of the fluorescence intensity with increasing concentrations of D-arabinose.

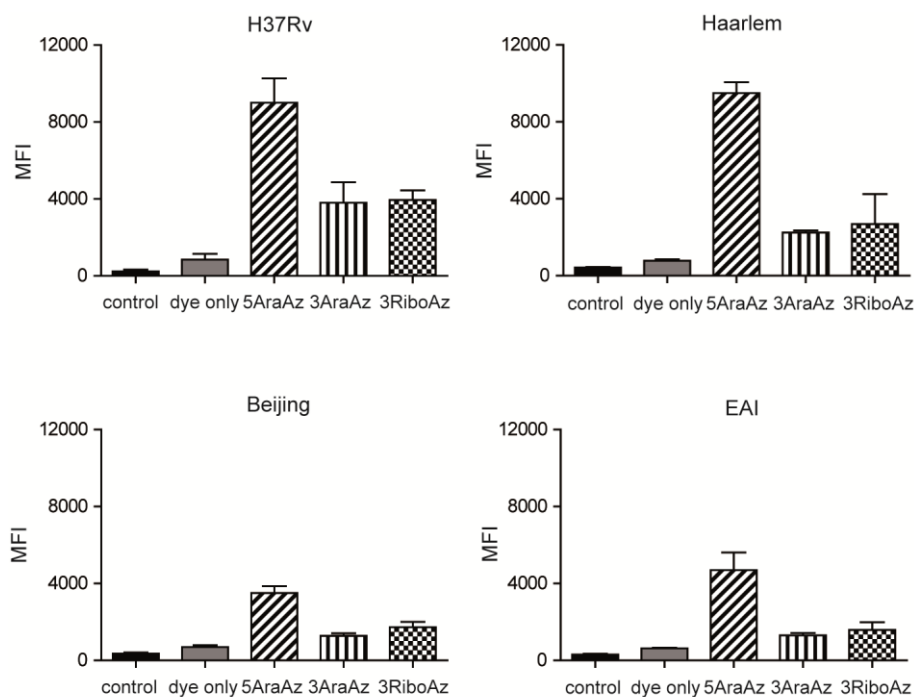
This observation strongly suggests that 5AraAz (**40**) is integrated into the mycobacterial cell envelope by an arabinose-dependent metabolism.

### 3.3.8 Labeling of Mtb clinical isolates with azido pentoses

To address whether carbohydrate-based metabolic labeling varies between Mtb clinical isolates, staining of four strains of the Mtb complex (H37Rv, Haarlem, Beijing and EAI) was carried out using the three new synthesized azido pentoses 5AraAz (**40**), 3AraAz (**38**) and 3RiboAz (**39**) (Figure 44).

In the case of Mtb H37Rv bacteria and the Mtb Haarlem strain roughly a tenfold increase in fluorescence intensity was obtained by addition of 5AraAz (**40**) and a three- or fourfold increase was detected after incubation with the 3-azido derivatives 3AraAz (**38**) and 3RiboAz (**39**). Fluorescence intensities measured for the Mtb Beijing strain and the Mtb EAI strain were lower, but clearly detectable. Similar to the results obtained with Mtb H37Rv bacteria also in these strains the addition of 5AraAz (**40**) led to higher signals compared to any other azido sugar applied, however the staining intensity was half as efficient as detected for the other strains.

The results show that all strains can be labeled with the three sugar derivatives **38**, **39** and **40**, but with different intensities dependent on the applied sugar and used strain.



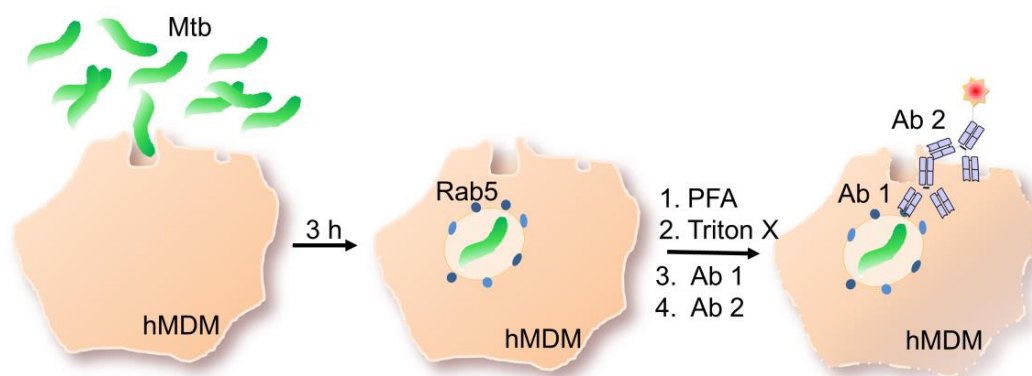
**Figure 44. Labeling of Mtb clinical isolates with azido pentoses.** Mtb H37Rv bacteria and three clinical isolates of the Haarlem (2336/02), Beijing (1934/03) and East African Indian (EAI, 1797/03) lineage were compared regarding the labeling efficiency of 5AraAz (**40**), 3AraAz (**38**) and 3RiboAz (**39**). Labeled bacteria were analyzed by flow cytometry. Analysis includes 100% of detected events. Data represent means (+SEM) of duplicates of three independent experiments. (MFI: mean fluorescence intensity; control: without azido sugar, without dye; dye only: without azido sugar, with dye).

### Results 3.3.2 – Results 3.3.8 Summary

- All three new azido pentoses (3AraAz (**38**), 3RiboAz (**39**) and 5AraAz (**40**)) were successfully used for metabolic labeling of different Mtb strains. Intensities varied dependent on the applied sugar and used strain.
- Culturing of Mtb bacteria in the presence of 5AraAz (**40**) led to most intense labeling.
- The results suggest that 5AraAz (**40**) is incorporated by an alternative arabinose-dependent metabolism into an unknown 50 kDa large glycostructure of the Mtb cell envelope.
- The three azido pentoses **38**, **39** and **40** had no influence on bacterial growth.
- The stability of the incorporated label was time- and temperature-dependent. Temperature dependency suggests that enzyme-catalyzed cellular processes of actively replicating bacteria may be involved in degradation of the incorporated label.

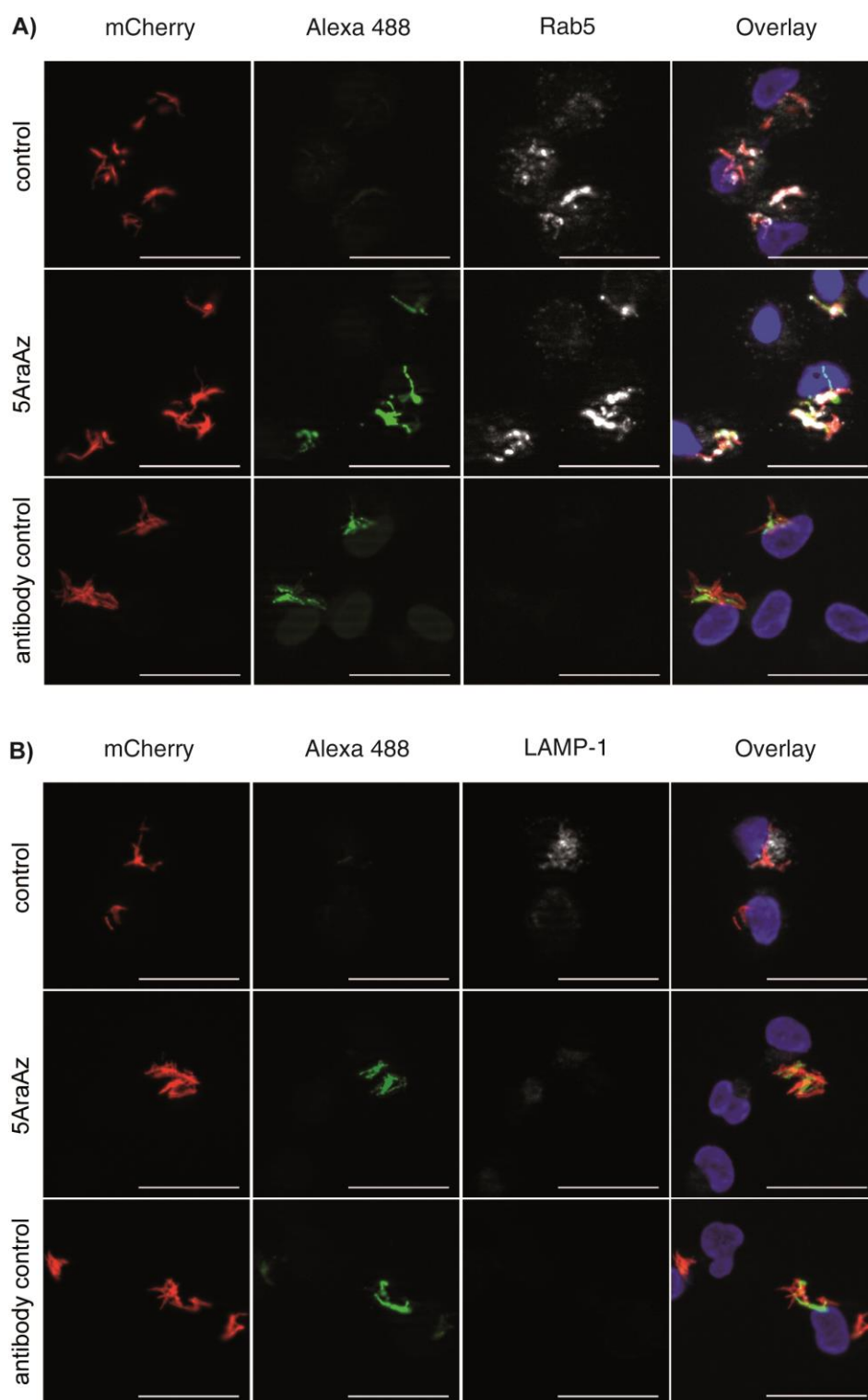
### 3.3.9 Infection of human macrophages with metabolically labeled Mtb bacteria

Mtb bacteria reside in phagosomes with incomplete luminal acidification (pH 6.5) and absence of mature lysosomal hydrolases, containing early endosomal markers like Rab5. Carbohydrate structures of the Mtb cell envelope contribute to the inhibition of the phagosome maturation (Figure 13). To address whether metabolically labeled Mtb bacteria would show the typical virulence characteristics of pathogenic Mtb bacteria, human monocyte-derived macrophages (hMDM) were infected with 5AraAz (40)-labeled or untreated red fluorescent Mtb bacteria with a multiplicity of infection (MOI) of ten for three hours. Infected hMDMs were fixed with paraformaldehyde (PFA) and permeabilized with Triton X. To study the maturation stage of Mtb containing phagosomes the cells were incubated with antibodies detecting the early endosomal marker protein Rab5 or the late endosomal and lysosomal marker protein LAMP-1.<sup>293,294</sup> Bound antibodies were detected by secondary antibodies carrying DyLight 680 and Cy5, respectively (Figure 45). Cells were analyzed by fluorescence microscopy (Figure 46) and co-localization of Mtb bacteria with Rab5 or LAMP-1 was quantified (Figure 47).

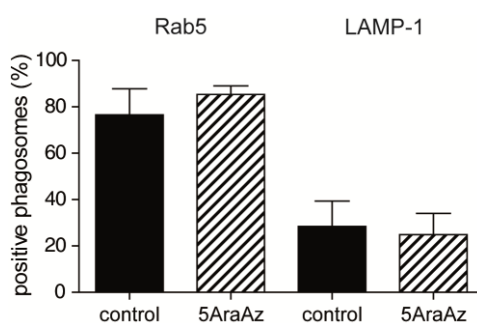


**Figure 45. Illustration of the infection of human macrophages with metabolically labeled Mtb bacteria and the subsequent antibody-based detection of phagosomal marker proteins.** Human monocyte-derived macrophages (hMDM) were infected with 5AraAz (40)-labeled (green) Mtb bacteria with a MOI of ten for three hours. During that time period bacteria are phagocytosed and first host-pathogen interactions take place. Infected cells were fixed with paraformaldehyde (PFA) and permeabilized with Triton X. Primary antibodies (Ab 1) bound to marker proteins on the phagosomal membrane. Secondary antibodies (Ab 2), which carried a fluorescent dye, bound to the primary antibodies. Fluorescence signals of labeled bacteria and secondary antibodies were visualized by fluorescence microscopy.

Three hours post infection the green fluorescence obtained by metabolic labeling was clearly detectable and unambiguously associated with red fluorescent Mtb bacteria within macrophages (Figure 46). Metabolically labeled Mtb bacteria were largely localized in compartments positive for the Rab5-specific antibody (ca. 80%). In addition, the majority of these compartments were not stained by an antibody detecting LAMP-1 (ca. 25%). Moreover, no differences were observed when labeled were compared to unlabeled Mtb bacteria (Figure 47).



**Figure 46. Detection of Rab5 and LAMP-1 proteins in human monocyte-derived macrophages infected with 5AraAz (40)-labeled and untreated Mtb bacteria, respectively.** mCherry expressing Mtb H37Rv bacteria (Cherry 10, red) were cultured in the presence of 5AraAz (40, 5 mM) and reacted with DIBO-Alexa 488 (green). Human monocyte-derived macrophages (hMDM) were infected with labeled and untreated Mtb (MOI: 10) for 3 h. Cells were fixed, permeabilized, blocked, incubated with anti-Rab5 or anti-LAMP-1 antibody and an appropriate fluorophore-conjugated secondary antibody (white). Nuclei were stained with 4',6-diamidino-2-phenylindole (DAPI) (blue). Microscopic pictures show Rab5 staining (A) and LAMP-1 staining (B) (antibody control: infected with 5AraAz (40)-labeled Cherry 10, without primary antibody, with secondary antibody; scale bar: 20  $\mu$ m).



**Figure 47. Quantification of Mtb co-localization with Rab5 and LAMP-1, respectively.** Microscopic pictures (representative pictures: Figure 25) were analyzed regarding co-localization of Mtb bacteria with fluorescence signals derived from anti-Rab5 or anti-LAMP-1 antibodies (blinded evaluation of > 200 phagosomes per condition). Bar diagram represents mean percentage (+SEM) of phagosomes positive for Rab5 and LAMP-1, respectively. Data of duplicates of three independent experiments analyzed. (Control: without azido sugar, without dye).

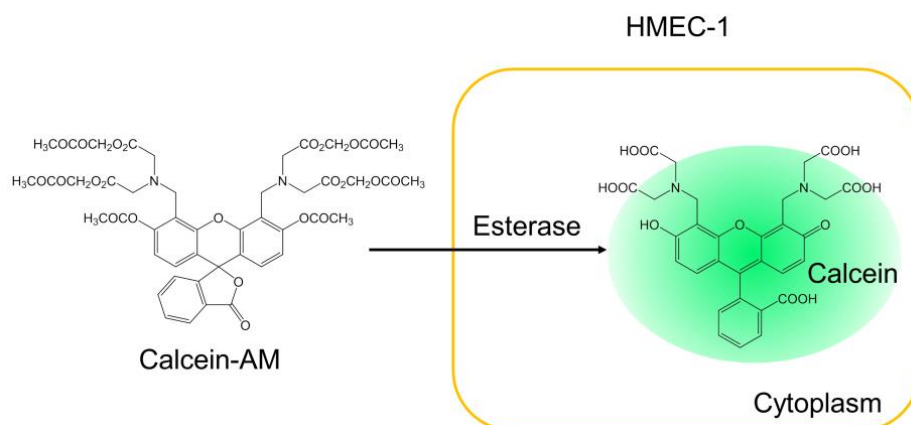
These data suggest that metabolic labeling of Mtb bacteria with 5AraAz (**40**) is stable during the early phase of infection experiments and it seems not to influence Mtb-induced phagosome arrest in primary macrophages.

#### Results 2.3.9: Summary

- Metabolic labeling of Mtb bacteria with 5AraAz (**40**) is stable during the early phase of infection experiments.
- Labeled as well as untreated Mtb bacteria reside in Rab5 positive early endosomal phagosomes.

### 3.3.10 Analysis of putative cytotoxic effects of the azido pentoses on epithelial cells

Carbohydrate derivatives can not only be used to specifically label bacteria in solution, but might also be applied to target bacteria within cells or even whole organisms.<sup>192</sup> Therefore, the sugar derivatives should neither be cytotoxic nor label mammalian cells, which was investigated in cooperation with Dr. Leonhard Möckl from the Ludwig Maximilian University of Munich, Germany. To investigate cytotoxic effects of the azido pentoses on mammalian cells, human mammary epithelial cells (HMEC-1) were cultured in the presence or absence of the new azido sugars **38**, **39** and **40**, respectively, or 6TreAz (**28**) at different concentrations and analyzed (Figure 49) by a calcein-dependent cell viability assay (Figure 48) using fluorescence microscopy. In live cells the non-fluorescent acetomethoxy derivate of calcein (calcein AM) can pass through the cellular membrane and is intracellularly converted into a green-fluorescent calcein after acetoxymethyl ester hydrolysis by esterases. Calcein in contrast to calcein AM cannot cross the plasma membrane and accumulates within the cytoplasm. Dead cells lack active esterases, thus, only live cells are labeled.<sup>295</sup>

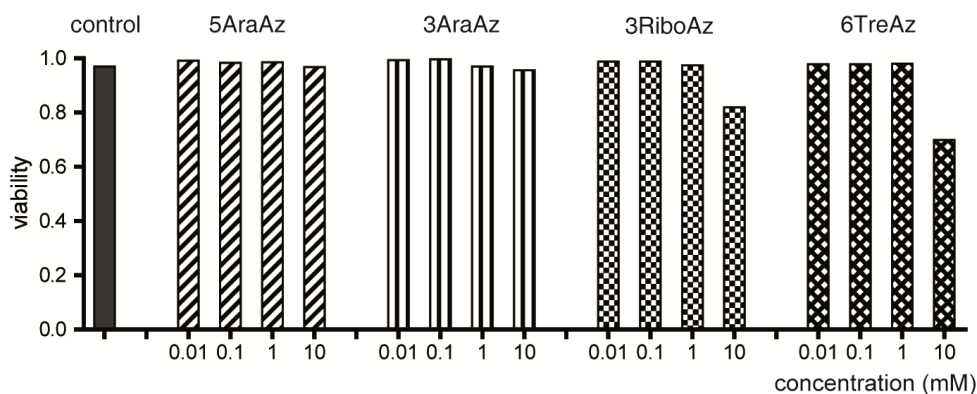


**Figure 48. Illustration of the calcein-dependent cell viability assay.** The non-fluorescent acetomethoxy derivate of calcein (Calcein-AM) can pass through the cellular membrane of human mammary epithelial cells (HMEC-1). In the cytoplasm the acetoxymethyl ester is hydrolyzed by esterases giving the fluorescent calcein. Dead cells lack active esterases, thus, only live cells are labeled.

98% of HMECs cultured without azido sugar supplementation and incubated with calcein-AM showed green fluorescence signals. The same amount of fluorescent cells was detected for HMECs cultured in the presence of azido arabinoses (5AraAz (**40**) and 3AraAz (**38**)) and for HMECs cultured in the presence of 3RiboAz (**39**) or 6TreAz (**28**) at concentrations of 0.01 mM, 0.1 mM and 1 mM. At a 3RiboAz (**39**) concentration of 10 mM 80% of the cells showed a green fluorescence. After addition of 6TreAz (**28**) in a final concentration of 10 mM 70% of the cells were fluorescent.

Since fluorescence correlates with cell viability the new azido pentoses, especially 5AraAz (**40**) and 3AraAz (**38**), show a highly favorable toxicity profile with regard to mammalian cells.

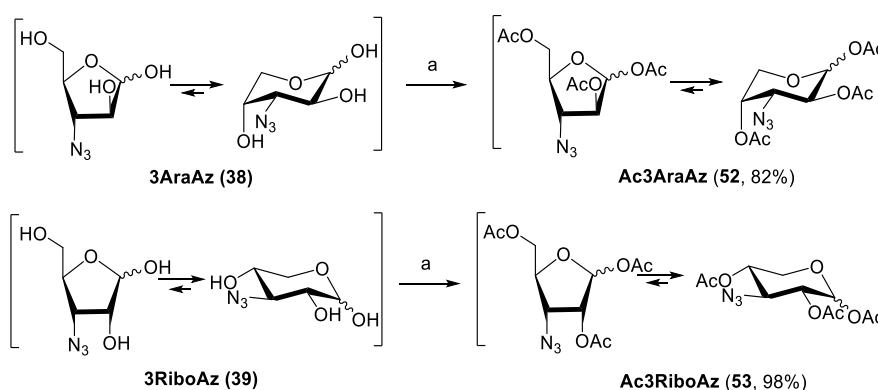




**Figure 49. Cytotoxic effects of the synthesized azido sugars were analyzed by a calcein-dependent cell viability assay.** HMEC were cultured in the presence of different carbohydrate concentrations (0.01 mM, 0.1 mM, 1 mM, 10 mM) or without azido sugar supplementation (control) for 2 d and treated with PBS+Ca<sup>2+</sup>/Mg<sup>2+</sup> containing calcein AM and ethidium homodimer. Fluorescence was analyzed by confocal microscopy. The viability was defined as the number of living cells divided by the total number of cells. Amount of analyzed cells (n): more than 1000 cells per condition. One of two independent experiments shown.

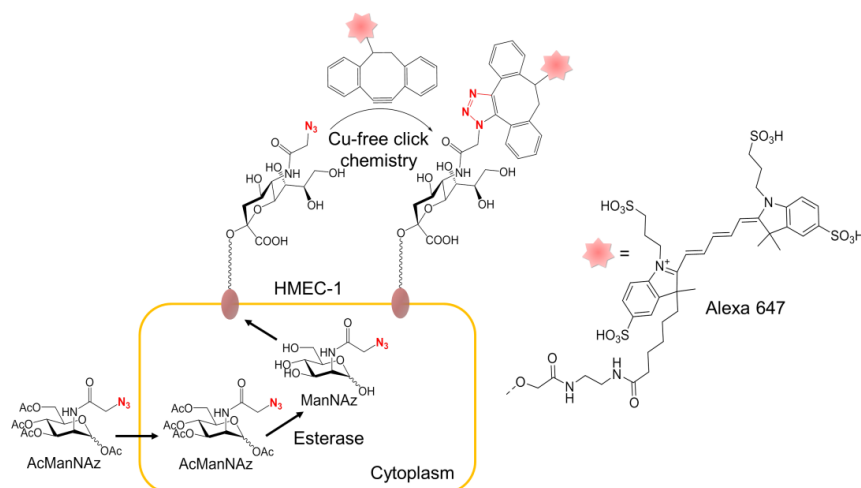
### 3.3.11 Metabolic labeling of epithelial cells with the new azido pentoses

To analyze whether the synthesized azido derivatives would label mammalian cells, HMEC-1 was incubated with the azido derivatives 5AraAz (**40**), 3AraAz (**38**), 3RiboAz (**39**) and 6TreAz (**28**) or the acetylated analogs Ac5AraAz (**51**), Ac3AraAz (**52**), Ac3RiboAz (**53**) and Ac6TreAz (**27**). Subsequently, cells were stained by Cu-free click chemistry using DIBO-Alexa 647 and analyzed by fluorescence microscopy (Figure 51). Acetylated compounds were synthesized (Scheme 8) and used for metabolic labeling of HMECs, based on the fact that azido sugars, which were previously developed for metabolic labeling of eukaryotic cells, are typically administered in the peracetylated form. This acetyl protection ensures entry by passive diffusion and is removed intracellularly by cytosolic esterases.<sup>242</sup> Acetylated *N*-azidoacetyl-mannosamine (AcManNAz) is known to be taken up, deprotected, metabolized and subsequently introduced into glycoproteins and glycolipids of HMECs forming azide-containing sialic acids on the cell surface (Figure 50).<sup>242,244</sup> Thus, AcManNAz was used as a positive control.

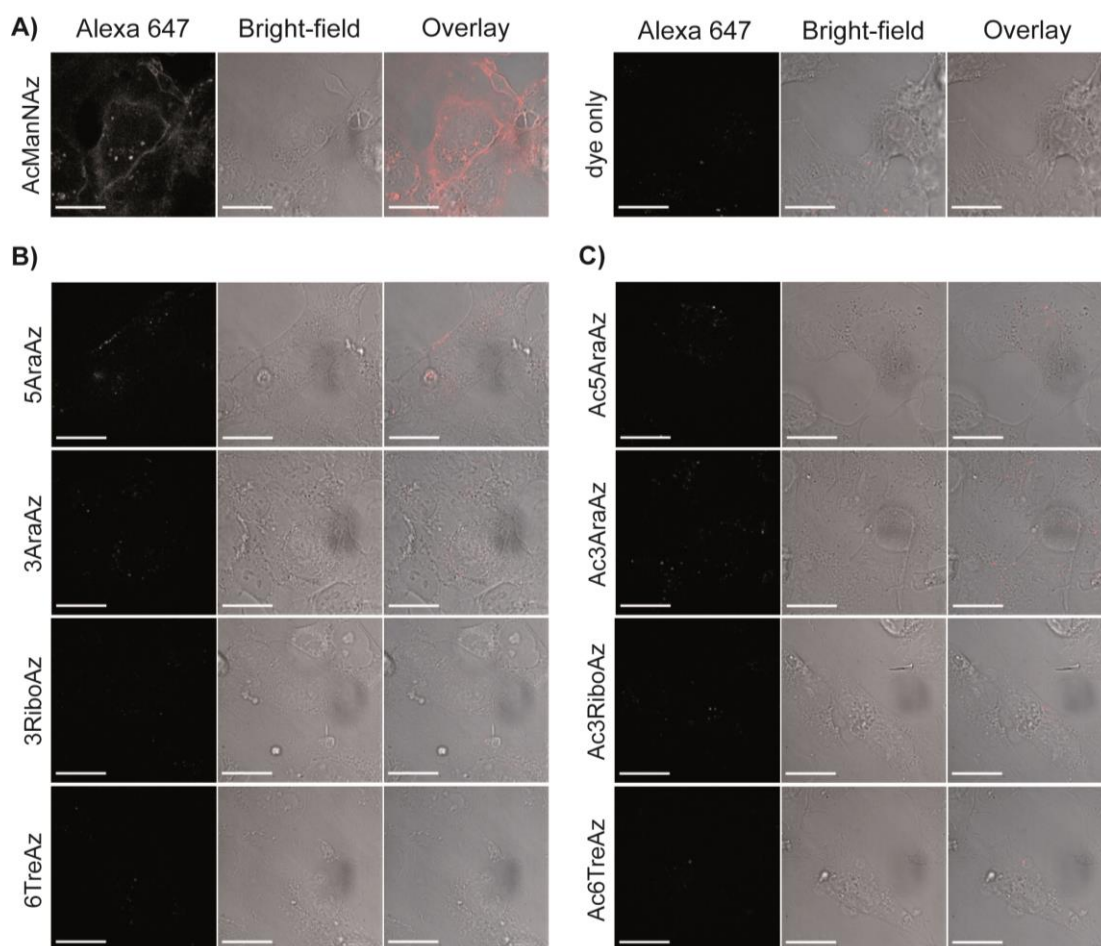


**Scheme 8. Acetylation of 3AraAz (38) and 3RiboAz (39).** a) Ac<sub>2</sub>O, pyridine, rt, 2 h, 82%; 98%.





**Figure 50. Illustration of a known method to metabolically label eukaryotic cells.**<sup>242,244</sup> AcManNAz is taken up, deprotected by cytosolic esterases, metabolized and subsequently introduced into glycoproteins and glycolipids of HMECs forming azide-containing sialic acids on the cell surface. The azido group can be visualized using fluorescent cyclooctyne derivatives (e.g. DIBO-Alexa 647).



**Figure 51. Metabolic labeling of HMECs using the synthesized azido derivatives and their acetylated analogs.** An epithelial cell line (HMEC-1) was incubated with 5AraAZ (**40**), 3AraAZ (**38**), 3RiboAZ (**39**) or 6TreAZ (**28**) (5 mM each), the acetylated derivatives Ac5AraAZ (**51**), Ac3AraAZ (**52**), Ac3RiboAZ (**53**) or Ac6TreAZ (**27**) (5 mM each) or AcManNAz (100  $\mu$ M).<sup>242,244</sup> After incubation with the azido sugars cells were stained with DIBO-Alexa 647 and analyzed by fluorescence microscopy. (dye only: without azido sugar, with dye; scale bar: 20  $\mu$ m).

Culturing HMECs in the presence of AcManNAz (100  $\mu$ M), followed by click-reaction, resulted in intense fluorescence signals located at the cell membranes. After the addition of the acetylated or unprotected azido pentoses **38**, **39**, **40**, **51**, **52** or **53** in even higher concentrations (5 mM instead of 100  $\mu$ M) almost no fluorescence was detectable. Neither 6TreAz (**28**) nor Ac6TreAz (**27**) supplementation led to detectable fluorescence signals.

These results show that AcManNAz, but none of the applied azido pentoses **38**, **39**, **40**, **51**, **52** and **53** or the trehalose derivatives **27** and **28**, can be used to metabolically label epithelial cells and underline the specificity of the azido pentose-based labeling of Mtb bacteria.

#### Results 3.3.9 - 3.3.11: Summary

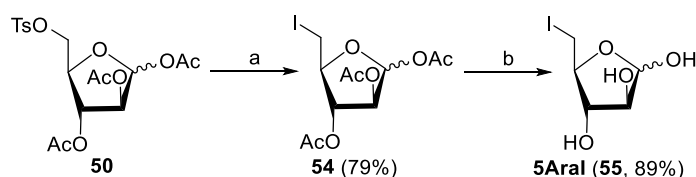
- The azido arabinoses (3AraAz (**38**), 5AraAz (**40**)) showed no cytotoxic effects.
- 3RiboAz (**39**) and 6TreAz (**28**) showed no cytotoxic effects up to 1 mM and had only minor effect on cell viability at the highest sugar concentration (10 mM).
- The tested azido pentoses **38**, **39** and **40** and 6TreAz (**28**) did not label mammalian cells, even not in the acetylated, membrane permeable form.

### 3.3.12 Metabolic labeling of Mtb bacteria with 5-deoxy-5-iodo- $\alpha,\beta$ -D-arabinofuranose

Fluorescent flow cytometry, as used in this study, is a highly sensitive method to analyze and quantify metabolically labeled bacteria at a single-cell level. However, limitations of this technique include photobleaching of the fluorescent dye and spectral overlap, when using several different fluorescent molecules in the same sample. Cytometry by time of flight (CyTOF) analysis combines flow cytometry and mass spectrometry (MS) facilitating multiparametric analysis of single cells. To investigate whether MOE can be used to label Mtb bacteria with heavy atoms suitable for CyTOF, an iodine analog (5Aral, **55**) of 5AraAz (**40**) (Scheme 9) was synthesized. 5Aral (**55**) was sent to Prof Dr. Niaz Banaei of Stanford University, USA. The iodo arabinose **55** was applied for metabolic labeling of Mtb bacteria and labeling efficiency was subsequently detected by CyTOF analysis.

#### Synthesis

The synthesis of 5Aral (**55**) started from the tosylated arabinofuranose derivative **50**, which was prepared as described before in the synthesis pathway of 5AraAz (**40**) (Scheme 7). A nucleophilic substitution reaction using sodium iodide gave the iodo derivative **54**<sup>286</sup> in 79% yield. Deprotection according to Zemplén's method<sup>183</sup> resulted in the desired 5Aral (**55**).



**Scheme 9. Synthesis of iodo arabinofuranose 55 (5Aral).** a) NaI, DMF, 80°C, 5 h, 79%; b) NaOMe, MeOH, rt, 1 h, 89%.

Metabolic labeling and CyTOF analysis was performed by Dr. Rajiv Lochan Gaur from the group of Prof Dr. Niaz Banaei. Mtb bacteria were cultured in the presence of 5Aral (**55**, 5 mM) for three days and subsequently analyzed by CyTOF. At least 44% of the mycobacteria were detected as positive for the iodo atom (graph not shown). Further experiments are currently carried out including labeling and detection of Mtb bacteria within macrophages.

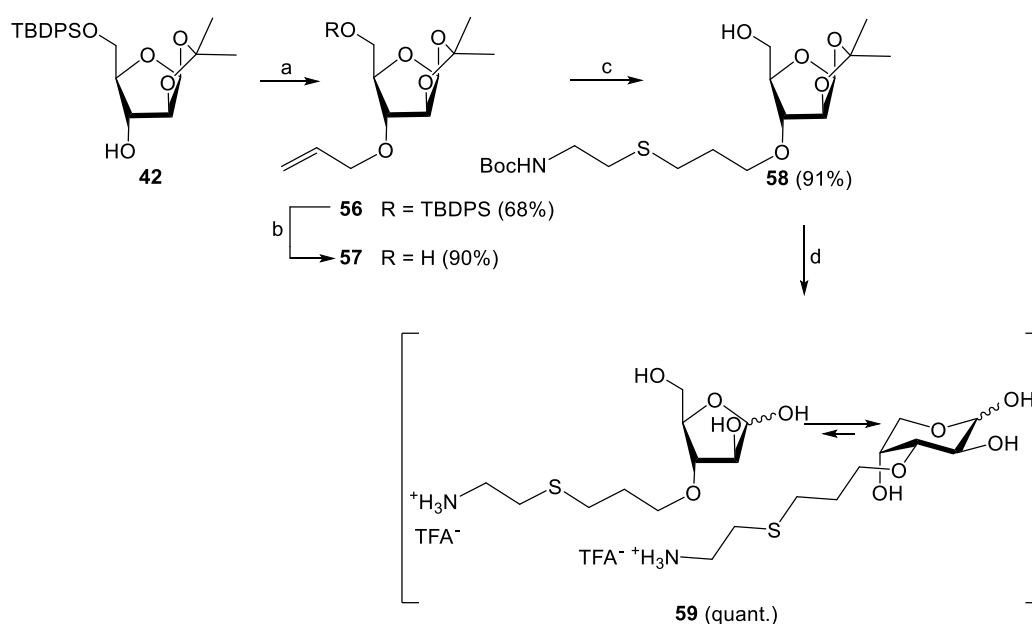
These results indicate that metabolic labeling of Mtb bacteria with the arabinose derivative 5Aral (**55**) offers the opportunity to detect Mtb bacteria by CyTOF analysis.

### 3.3.13 Cysteamine derivatives and their influence on mycobacterial growth

Successful metabolic labeling is associated with an effective uptake of the sugar derivatives. Thus, the sugar part may be used as a “shuttle” for molecules, such as antibiotics, to overcome the critical permeability of the Mtb cell envelope. For first insights into targeted antibiotic transport, cysteamine derivatives were synthesized (Scheme 10-12) in analogy to the azido pentoses **38**, **39** and **40** and tested in a mycobacterial growth assay. Cysteamine was chosen due to its antibacterial activity, as previously detected,<sup>296</sup> and its small size, which might be favorable in order to allow carbohydrate-based transport activity.

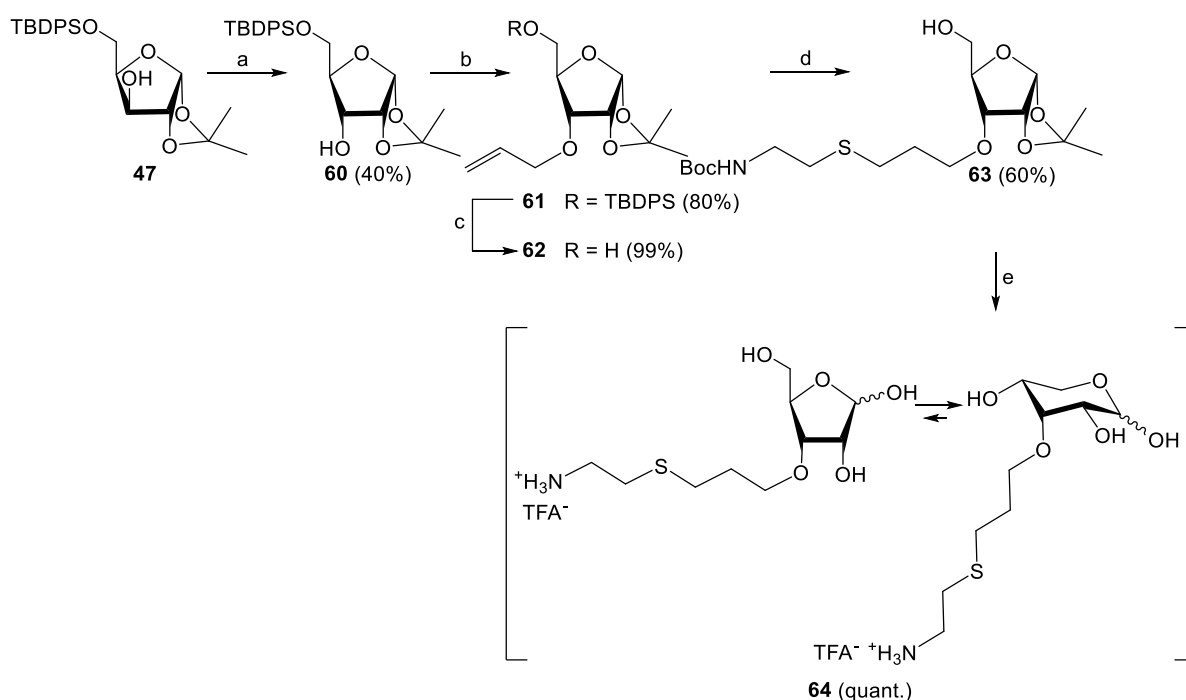
#### Syntheses

The 3AraAz-analog cysteamine derivative **59** was synthesized over four reaction steps with the arabinofuranose derivative **42** as starting material (Scheme 10). The unprotected hydroxyl group was deprotonated under basic conditions to increase the reactivity and enable the nucleophilic substitution reaction with allyl bromide giving the allylated derivative **56** in 68% yield. The TBDPS-protecting group was selectively cleaved with TBAF to give the 5-OH free derivative **57**. *tert*-Butyloxycarbonyl (Boc)-protected cysteamine **72**<sup>297</sup> was introduced by a photoinduced thiol-ene coupling. This radical addition reaction occurred at room temperature by irradiation at  $\lambda_{\max}$  365 nm and in the presence of 2,2-dimethoxy-2-phenyl-acetophenone (DPAP) as the sensitizer. The thiahexyl derivative **58** was obtained in 91% yield. Isopropylidene- and Boc-protecting groups were removed under acidic conditions, which led to the product **59** in an overall yield of 48%.



**Scheme 10. Synthesis of thiahexyl arabinose 59.** a) NaH, DMF, 0°C, 30 min, allyl bromide, rt, 3.5 h, 68%; b) TBAF, THF, rt, 1 h, 90%; c) molecule **72**, DPAP, MeOH, rt, 1 h, hv, 91%; d) TFA, H<sub>2</sub>O, DCM, 0°C, 2 h, quant..

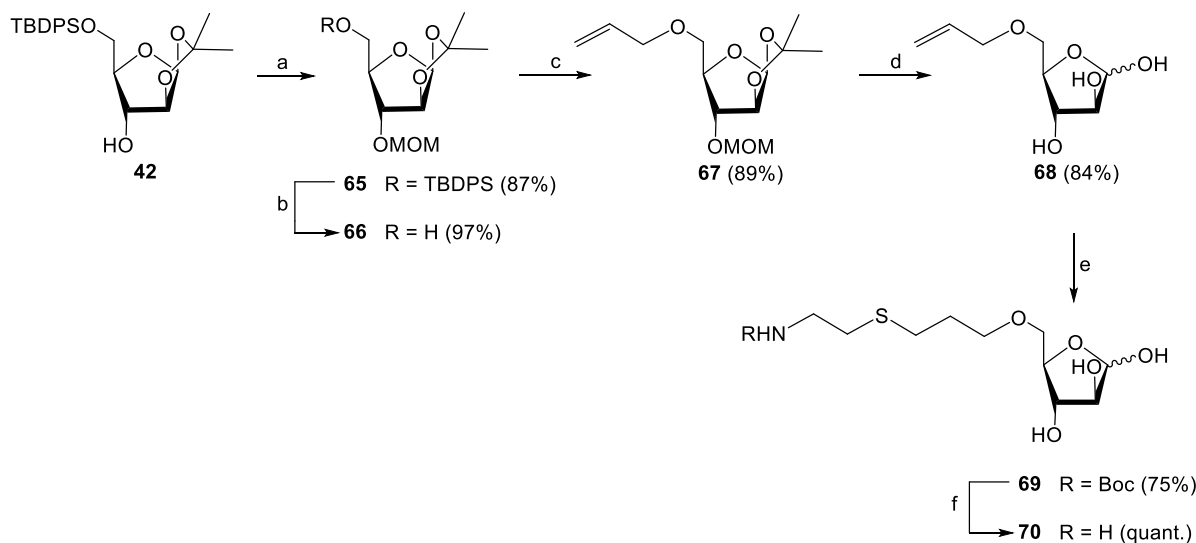
The synthesis of the 3RiboAz-analog cysteamine derivative **64** started from the arabinofuranose derivative **47**, which was prepared as described before (Scheme 6). The hydroxyl group at the 3-position was activated by  $\text{Tf}_2\text{O}$  under basic conditions and subsequently reacted with sodium nitrite giving the epimerized product **60**<sup>298</sup> in a yield of 40%. After allylation with sodium hydride and allyl bromide the fully protected arabinofuranose **61** was obtained in 80% yield. The TBDPS group was removed with TBAF to provide **62** in almost quantitative yield. Boc-protected cysteamine **72**<sup>297</sup> was introduced in a radical addition reaction with azobisisobutyronitrile (AIBN) as radical initiator, which led to the derivative **63** in a yield of 60%. In a final step the thiahexyl derivative **63** was deprotected under acidic conditions giving the desired product **64** (Scheme 11).



**Scheme 11. Synthesis of thiahexyl ribose **64**.** a) 1.  $\text{Tf}_2\text{O}$ , pyridine, DCM,  $0^\circ\text{C}$ , 3 h; 2.  $\text{NaNO}_2$ , DMF,  $70^\circ\text{C}$ , overnight, 40%; b) NaH, DMF,  $0^\circ\text{C}$ , 30 min, allyl bromide, rt, 3.5 h, 80%; c) TBAF, THF, rt, 1 h, 99%; d) molecule **72**, AIBN, MeOH,  $70^\circ\text{C}$ , 6 h, 60%; e) TFA,  $\text{H}_2\text{O}$ , DCM,  $0^\circ\text{C}$ , 2 h, quant..

Arabinose derivative **42**, the same starting material as used for the synthesis of the thiahexyl derivative **59** (Scheme 10), was applied for the synthesis of the 5AraAz-analog cysteamine derivative **70**. The hydroxyl group at the 3-position was protected under basic conditions with chloromethyl methyl ether (MOMCl) giving the fully protected arabinofuranose **65** in 87% yield. The primary hydroxyl group was selectively deprotected with TBAF and subsequently allylated under basic conditions with allyl bromide. Isopropylidene- and MOM-protecting groups were removed under acidic conditions giving the allyl arabinofuranose derivative **68** in 84% yield. Boc-protected cysteamine<sup>297</sup> was introduced by a photoinduced thiol-ene coupling in analogy to the synthesis of the thiahexyl derivative **59**

(Scheme 10). The Boc-protecting group was subsequently removed under acidic conditions, which led to the desired product **70** in an overall yield of 47% over six steps (Scheme 12).



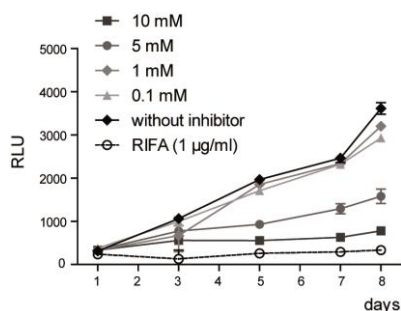
**Scheme 12. Synthesis of thiahexyl arabinofuranose 70.** a) MOMCl, TBAI, DIPEA, 60°C, 2 h, 87%; b) TBAF, THF, rt, 1 h, 97%; c) NaH, DMF, 0°C, 30 min, allyl bromide, rt, overnight, 89%; d) TFA, H<sub>2</sub>O, DCM, 0°C, 1 h → 40°C, 1 h, 84%; e) molecule **72**, DPAP, MeOH, rt, 1 h, hv, 75%; f) TFA, H<sub>2</sub>O, DCM, 0°C, 2 h, quant..

### Influence of cysteamine on mycobacterial growth

Anti-microbial activity of cysteamine and cysteamine derivatives was previously shown.<sup>296,299</sup> Cysteamine was active against several bacterial pathogens detected within the lung of patients with cystic fibrosis, such as *Pseudomonas aeruginosa*.<sup>296</sup> In addition, different aminothiahexyl glycosides showed antibacterial activity against *E. coli*.<sup>299</sup> However, the impact of cysteamine and cysteamine derivatives on mycobacteria replication was not studied so far. Therefore, bacterial growth analysis performed in 96-well microtiter plates using GFP-expressing Mtb bacteria<sup>288</sup> was carried out with cysteamine at different concentrations for eight days (Figure 52).

Increase of fluorescence intensity over eight days was detected for mycobacteria cultured in the presence of lower concentrations (0.1 mM and 1 mM) of cysteamine similar to the increase measured for untreated bacteria cultures. Addition of cysteamine in higher concentrations (5 mM) led to a reduced increase by half and no change in fluorescence intensity was detected at a cysteamine concentration of 10 mM.

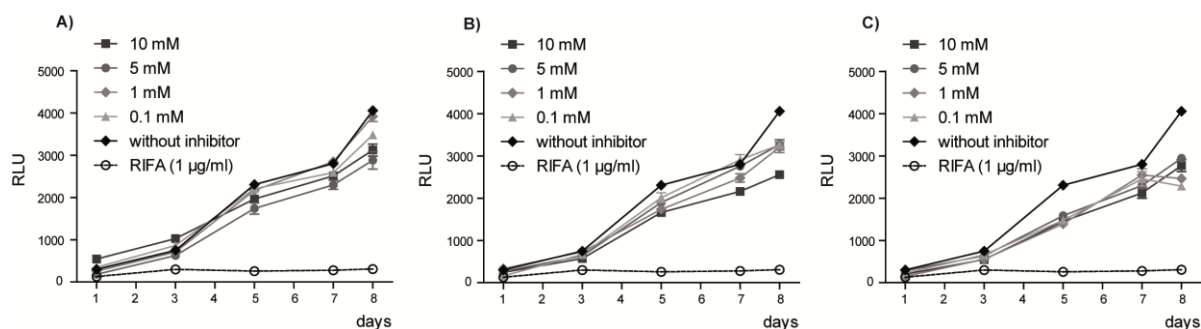
Fluorescence intensities correlate with mycobacteria quantity. Thus, the results indicate that cysteamine has a negative impact on bacteria replication at concentrations over 1 mM and leads to complete growth arrest at a concentration of 10 mM.



**Figure 52. Influence of cysteamine on mycobacterial growth.** Mtb growth analysis was performed as described elsewhere.<sup>288</sup> Cysteamine was tested regarding the antibacterial effect in different concentrations (0.1 mM, 1 mM, 5 mM, 10 mM). Rifampicin (RIFA, 1 µg/ml) was used as positive control. Data represent means (+/-SD) of three technical replicates. One of two independent experiments shown. (RLU: relative light units)

### Influence of the thiahexyl derivatives 59, 64 and 70 on mycobacterial growth

Thiahexyl sugars **59**, **64** and **70** were analyzed regarding their influence on mycobacterial growth using the same assay as applied for bacterial growth analysis before.



**Figure 53. Influence of thiahexyl derivatives 59 (A), 64 (B) and 70 (C) on mycobacterial growth.** Mtb growth analysis was performed as described elsewhere.<sup>288</sup> The thiahexyl pentoses **59**, **64** and **70** were tested regarding their antibacterial effect in different concentrations (0.1 mM, 1 mM, 5 mM, 10 mM). Rifampicin (RIFA, 1 µg/ml) was used as positive control. Data represent means (+/-SD) of three technical replicates. One of at least two independent experiments shown. (RLU: relative light units)

Increase of fluorescence intensity over eight days was detected for mycobacteria cultured in the presence of the thiahexyl derivatives **59**, **64** or **70** similar to the increase measured for untreated bacteria cultures. In cultures supplemented with rifampicin no change in fluorescence intensity was detected.

The data indicate that none of the synthesized thiahexyl derivatives **59**, **64** or **70** has a mycobacterial growth-limiting effect at concentrations up to 10 mM.





The results indicate that the acetylated cysteamine derivatives **74** and **75** have a negative impact on bacterial replication at concentrations of 5 mM and 10 mM. The effect is not as strong as measured for unprotected cysteamine, but clearly detectable.

#### **Results 3.3.12 and Results 3.3.13: Summary**

- Four new carbohydrate derivatives, 5Aral (**55**) and the thiahexyl derivatives **59**, **64** and **70**, were synthesized.
- 5Aral (**55**) was successfully used for first CyTOF analysis.
- While cysteamine showed mycobacterial growth-limiting effects in high concentrations (5 mM and 10 mM), the cysteamine-modified carbohydrate derivatives **59**, **64** and **70** had no antibacterial activity.

### 3.4 Discussion

The structures of the mycobacterial cell envelope and the related biosynthetic pathways represent targets of many diagnostic tools and therapeutic agents. For example, the lipoglycan LAM was discovered as a specific biomarker in Tb infection being measurable in sputum and urine.<sup>17,300</sup> Furthermore, several anti-Tb drugs, including the first-line drugs isoniazid and ethambutol, act as inhibitors of the cell envelope biosynthesis.<sup>30,301</sup> Recently, first efforts have been made not only to detect or inhibit unique cell wall structures, but to specifically modify them using MOE.<sup>88,192,302</sup> Based on the absence of D-arabinose in many organisms and the high amounts of D-arabinofuranosides in the mycobacterial cell envelope, D-arabinose derivatives were identified in this study as potential candidates to target Mtb bacteria by MOE. The Mtb bacteria were successfully labeled using the synthesized azido pentoses 3AraAz (**38**), 3RiboAz (**39**) and 5AraAz (**40**). Therefore, the azido pentoses had to be (i) taken up, (ii) metabolized and subsequently (iii) be introduced into the mycobacterial cell envelope.

#### 3.4.1 Arabinose uptake mechanisms

The initial critical process for a successful metabolic labeling is the transport of the carbohydrate derivative into the cytoplasm. Since the azido pentoses used in this study for metabolic labeling of Mtb bacteria were not acetylated, they were hydrophilic and had to be actively transported across the hydrophobic cell envelope of Mtb. The presence of carbohydrate transporters in the cell envelope is often connected to the nutrition requirements of the organism. For mycobacteria nutrition requirements have been intensively studied. Already 1951 the utilization of several carbohydrates, fatty acids and amino acids by mycobacteria was examined by measuring oxygen consumption, which is connected to an active aerobic respiration. Glycerol, lactate and fatty acids were proven to be the most effective stimulants of respiration. Glucose caused a weaker stimulation and arabinose had no significant effects.<sup>303</sup> Furthermore, growth analysis of Mtb bacteria on various sugars as a sole carbon source for seven days revealed that L-arabinose but not D-arabinose can be utilized.<sup>304</sup> However, after a long time lag of eight to ten days, growth of mycobacteria was observed also in media containing D-arabinose.<sup>99</sup> D-Arabinose uptake activity was further analyzed by the use of radioactive <sup>14</sup>C-D-arabinose, verifying the transport of this rare pentose through the mycobacterial cell envelope.<sup>99</sup> D-Arabinose might not be a preferred carbon source of mycobacteria, but can verifiably pass through the mycobacterial cell envelope.

While carbohydrate uptake mechanisms of Mtb have been widely studied and eight putative pentose transporters were identified, transport systems of Mtb are poorly characterized.<sup>100</sup> Analysis of the genome of Mtb H37Rv bacteria predicts four ABC (ATP-binding cassette)-type transporters and one permease for carbohydrates.<sup>305,306</sup> Two of the ABC-type transporters are

similar (62% and 80% similar amino acids) to those described for Msg but the substrate specificity was only recently solved for one of them. The SugABC-LpqY transporter exhibits a high specificity for trehalose and is used as a recycling system for this disaccharide, which may be extracellularly released by TDM hydrolases or as a byproduct of cell envelope biosynthesis (Figure 10).<sup>87</sup> Genetic similarities of the other three ABC systems to known transporters outside the genus *Mycobacterium* are so low that potential substrates cannot be predicted by comparative analyses.<sup>305</sup> Another possible candidate as a pentose uptake system may be the permease SugI, because of its sequence similarities to the arabinose transporter (AraE, 24%) of *E. coli*. However, also in this case the substrate has not been identified to date.<sup>100</sup>

Although it is still unclear by which mechanism the synthesized azido sugars (3AraAz (**38**), 3RiboAz (**39**), 5AraAz (**40**)) were taken up, the successful metabolic labeling strongly suggests that pentose transporters are present in the Mtb cell envelope.

The azido pentose-based metabolic labeling strategy can now be used to study the widely unknown pentose transport mechanisms of Mtb bacteria in further detail.

### 3.4.2 Arabinose metabolism

For metabolic labeling the carbohydrate derivatives do not only have to enter the bacterium, but also have to pass through the natural carbohydrate metabolism. 3AraAz (**38**) and 3RiboAz (**39**) were designed to be incorporated as arabinofuranoside derivatives into the mycobacterial cell envelope. The only known donor of D-arabinofuranosides in mycobacteria is decaprenyl-phospho-arabinose, which was isolated from Msg and characterized by mass spectrometry and NMR spectroscopy.<sup>307</sup> Further activated forms of D-arabinose, such as D-arabinose phosphate and D-arabinose nucleotides, have not been demonstrated in mycobacteria to date.<sup>97</sup> Thus, the azido pentoses **38** and **39** have to be included into the decaprenyl-phospho-arabinose biosynthesis pathway, as described in the introduction (Figure 11).

3AraAz (**38**) might pass the whole metabolism starting with a reduction to D-arabinitol. However, the subsequent conversion to D-xylulose derivatives cannot take place, because this requires an epimerization at the 3-position. This isomerization is excluded since the 3-position is functionalized by the azido group. The formation of xylulose intermediates, however, might be important, because the phosphorylation of the primary hydroxyl group, which might be essential for the following metabolic steps, is mediated by a D-xylulose kinase.<sup>97</sup> Alternative enzymes converting D-arabinose directly into further downstream D-ribose derivatives have not been identified to date. Thus, it is still unclear, how 3AraAz (**38**) is included.

3RiboAz (**39**) might enter the biosynthesis pathway as a D-ribose 5-phosphate derivative. This would require the activity of a ribose kinase. The adenosine kinase (ADK) of Mtb typically

catalyzes the phosphorylation of adenosine to adenosine monophosphate (AMP).<sup>34,308</sup> However, Mtb ADK has a very low sequence similarity with other ADKs, which are mainly present in eukaryotic organisms, but is genetically more closely related to the ribokinase (RK) from *E. coli*. 25% identity was detected based on the amino acid sequence.<sup>309,310</sup> Moreover, both Mtb ADK and *E. coli* RK are dimers, whereas all other known ADKs are monomers.<sup>310</sup> In *E. coli* RK catalyzes the phosphorylation of ribose to ribose 5-phosphate. RK activity of the Mtb ADK would explain the entry of 3RiboAz (**39**) into the arabinan metabolism as 3-azido-3-deoxy-5-phospho-D-ribose. However, this activity has not been demonstrated so far. While the introduction of 3RiboAz (**39**) into the mycobacterial cell envelope by the decaprenyl-phospho-arabinose biosynthesis pathway is feasible, the entry of 5AraAz (**40**) is unlikely.

5AraAz (**40**) was synthesized as a negative control compound, since intermediates of the arabinan metabolism are phosphorylated at the 5-position and this phosphorylation is not removed until the pre-final synthetic step.<sup>97</sup> Enzymes catalyzing the functionalization of the phosphorylated substrates with decaprenyl phosphate are essential as determined by transposon mutagenesis.<sup>311</sup> If these enzymes might also transfer decaprenyl-phosphate to non-phosphorylated ribose or arabinose has not been studied to date. The improbability of the incorporation of 5AraAz (**40**) into the polysaccharides of the mycobacterial cell envelope is further supported by the fact that arabinofuranosides in AG and LAM are mainly connected by (1→5) linkage and terminally functionalized with mycolic acids and mannosides, respectively. The structural details of AG and LAM result in only a few putative positions to be modified by 5AraAz (**40**). However, in the current study isolation of cell envelope structures, followed by detection of azido functions revealed that 5AraAz (**40**) is incorporated into the Mtb cell envelope. The azide-containing structure was detected on a SDS-gel with a molecular weight roughly 10 kDa larger than ManLAM. This shift could be explained by an enhanced size due to functionalization with DIBO-biotin. On the other hand, an intercalation into a novel unknown glycoconjugate larger than ManLAM is also likely, since bands in the same molecular range were visualized by PAS and silver staining even in non DIBO-biotin treated samples. Although no bands were detected by coomassie staining, protein origin cannot be fully excluded and has to be analyzed more precisely, since the used coomassie imaging method is less sensitive.<sup>312</sup> More intense signals in the silver staining compared to the PAS staining indicate that the main part of the unknown compound may not consist of carbohydrates, but rather of highly negative charged molecules. While lipids are mainly neutral even after oxidation, proteins containing amino acids with a carboxyl group in the side chain can increase the negative charge. Thus, the unknown structure might be a glycoprotein, although it was not detected by coomassie staining. Mycobacterial glycoproteins have been detected earlier, but full extent and nature of glycosylation as well as the glycosylation pathway remain poorly characterized.<sup>313–315</sup> Carbohydrate analysis by capillary zone electrophoresis combined with

laser induced fluorescence detection of 1-aminopyrene-3,6,8-trisulfonate derivatives revealed the presence of glucose, mannose and arabinose in mycobacterial cell surface proteins (CSP).<sup>313</sup> These observations support the possibility that 5AraAz (**40**) may be included into the carbohydrate part of mycobacterial glycoproteins. However, further studies are needed to prove this hypothesis.

In future experiments, the cell envelope preparations containing the 5AraAz (**40**)-labeled cell envelope structure should be incubated with DIBO-biotin and biotin-tagged molecules separated by magnetic beads functionalized with streptavidin. Subsequently, the captured compound might be released and analyzed by mass spectrometry. Furthermore, not only the LAM/LM/PIM fraction should be examined, but the whole cell lysate, since 5AraAz (**40**) might be incorporated into yet unknown cell envelope structures. The method bears further the chance to identify the intermediates of the metabolism, whereby 5AraAz (**40**) was incorporated into the mycobacterial cell envelope, and will give new insights into the biosynthetic pathways of Mtb. Finally, characterizing 3AraAz (**38**) and 3RiboAz (**39**)-labeled structures will help to identify how these derivatives entered the arabinan metabolism and confirm or confute predictions.

Taken together, MOE with the azido pentoses **38**, **39** and **40** can not only be used to target Mtb bacteria, but moreover enables novel insights into the carbohydrate composition of the Mtb cell envelope and into the biosynthetic pathways of pathogenic mycobacteria.

### 3.4.3 Arabinose derivatives used for MOE

MOE is a powerful tool to target not only eukaryotic but also prokaryotic cells. To date, only a few studies have addressed metabolic labeling of Mtb bacteria. Recently, trehalose derivatives were identified as potent compounds to label mycobacteria.<sup>88,192,316</sup> These molecules were either taken up by the SugABC-LpqY transporter and proceeded through the trehalose recycling pathway or were directly anchored into the mycobacterial cell envelope by the extracellular proteins Ag85A, Ag85B and Ag85C, which catalyze esterification of the trehalose derivatives and the formation of TMM and TDM derivatives (for details of the TDM metabolism see Figure 10).<sup>88,192</sup> K. M. Backus et al. revealed strong specificity of all Ag85 isoforms for trehalose-like disaccharides but a striking variety of trehalose derivatives that were converted. Modifications on every position of the sugar scaffold were tolerated and even the large FITC-trehalose derivative was processed. Labeling experiments with an Ag85C mutant strain verified the significance of this extracellular protein for incorporation of FITC-trehalose into the mycobacterial cell envelope.<sup>192</sup> However, 2-, 4- and 6TreAz labeling required uptake into the cytoplasm by the ABC transporter, as shown by B. M. Swarts et al..<sup>88</sup> For these labeling strategies not only the biosynthetic pathway, but also the modified cell envelope structures were identified. Trehalose derivatives were mainly incorporated into TMM and TDM.<sup>88,192</sup>

Efficiency and required concentrations (between 2.5  $\mu\text{M}$  and 250  $\mu\text{M}$ ) varied dependent on the used trehalose derivative.<sup>88</sup> Furthermore, trehalose dependent labeling is highly specific: FITC-trehalose led to high fluorescence in Mtb bacteria, whereas neither *Staphylococcus aureus*, *Pseudomonas aeruginosa* nor *Haemophilus influenza* showed appreciable labeling after incubation with the trehalose derivative.<sup>192</sup> Strikingly, FITC-trehalose could also be applied for targeting Mtb bacteria within macrophages. In contrast to the uniform staining of bacilli observed *in vitro*, mycobacterial labeling *in vivo* varied between different macrophages or even within a single macrophage.<sup>192</sup> This heterogeneity might be explained by the metabolic status of the bacterium and the maturation status of the phagosomal compartment. Beside this well studied carbohydrate-based labeling method, D-amino acid derivatives were developed to label peptidoglycan structures of the mycobacterial cell envelope.<sup>302</sup> Azide and alkyne-functionalized D-alanine, respectively, was successfully used for staining of Mtb bacteria, but required much higher concentrations (at least 200  $\mu\text{M}$ ) compared to the trehalose derivatives. Furthermore, this metabolic method is not specific and leads to cell envelope modification of Gram-positive bacteria (e.g. *Listeria monocytogenes*, *Corynebacterium glutamicum*), Gram-negative bacteria (e.g. *E. coli*) and mycobacteria (e.g. Mtb).<sup>302</sup>

In the current study, the azido pentoses **38**, **39** and **40** were successfully applied as new compounds for MOE of Mtb. D-Arabinose and D-ribose derivatives have never been used for metabolic labeling before. Labeling efficiency differed between the applied azido derivatives. Whereas 3AraAz (**38**) and 3RiboAz (**39**) led to similar low labeling intensities, 5AraAz (**40**) resulted in as strong signals as detected with the known trehalose derivative 6TreAz (**28**). However, five times higher concentrations were required. The applied concentrations were similar to those used for D-amino acid labeling.

That MOE with the azido pentoses **38**, **39** and **40** was only detected at sugar concentrations of at least 100  $\mu\text{M}$  might be explained by a limited uptake of those derivatives. Recently, R. Lowery et al. used deuterated carbohydrates to analyze sugar transport of Msc and revealed that trehalose is taken up in three times higher amounts compared to L-arabinopyranose.<sup>317</sup> Although D-arabinose was not tested, these results indicate that the uptake efficiency might vary between different carbohydrates. The more intense labeling by 5AraAz (**40**) compared to 3AraAz (**38**) might also be explained by uptake mechanisms. It is conceivable that arabinofuranoses have a preferred entry compared to arabinopyranoses. While 5AraAz (**40**) is fixed in the furanose form 3AraAz (**38**) is mainly present as a pyranose. Furthermore, intracellular degradation or competitive processes during the metabolism can influence the amount of cell envelope modifications. Decaprenyl-phospho-arabinose is not only synthesized from external D-arabinose, but also from glucose, which is highly present in the used 7H9/OADC-culture medium. Thus, the azido pentoses, especially 3AraAz (**38**) and 3RiboAz (**39**), which are assumed to pass through the decaprenyl-phospho-arabinose

biosynthesis pathway, might compete with glucose for cell envelope incorporation. This might also explain the low labeling efficiency of 3AraAz (**38**) and 3RiboAz (**39**) compared to 5AraAz (**40**).

Finally, also the accessibility of the azido function for the click reaction can have a strong impact on the detected fluorescence intensity. Therefore, it might be speculated that 3AraAz (**38**), 3RiboAz (**39**) and 5AraAz (**40**) were present in much higher amounts in the mycobacteria envelope, but more closely located to the cell membrane and therefore shielded by the “outer layer”. In contrast labeling with trehalose derivatives leads to modifications of TMM and TDM, which are mainly components of the “outer layer”. Therefore, azido modification of these glycolipids might be easily accessible for applied cyclooctynes.

The disadvantage of the required higher concentrations is offset by a highly favorable toxicity profile. None of the azido pentoses **38**, **39** and **40** had any impact on bacterial replication up to concentrations of 10 mM. Thus, they can be used as potent agents for metabolic labeling of Mtb bacteria in a millimolar range. Moreover, required concentrations might even be lower under a changed experimental set-up. As detected for FITC-trehalose, labeling efficiency of Mtb bacteria is strongly influenced by the composition of the bacterial environment and the metabolic status of Mtb. It is known that Mtb bacteria respond to environmental conditions and adjust their metabolism for example by switching their main carbon source from carbohydrates to lipids.<sup>318</sup> To address whether labeling with the new azido derivatives **38**, **39** and **40** is influenced by the metabolic status of Mtb, labeling experiments should be carried out not only in glucose-rich 7H9/OADC-medium, but also in medium exclusively containing a non-carbohydrate carbon source, such as acetate.

Beside low toxicity and high labeling efficiency the degree of specificity is important for a good metabolic labeling tool. Therefore, the new azido derivatives **38**, **39** and **40** should label all strains of the MTBC, but should not be incorporated into cell envelopes of other bacteria or host cells.

MOE experiments with four different strains of the MTBC (H37Rv, Haarlem, Beijing and EAI) led to a successful labeling of all strains with the three azido pentoses **38**, **39** and **40**, but with different efficiency dependent on the used strain. Varying labeling intensities might be explained by different glycolipid and lipoglycan compositions of the cell envelope. While these particular strains were instrumental in the identification of clade-specific virulence patterns,<sup>46</sup> divergences of their cell envelope composition have never been addressed. However, differences in this respect were shown for other Mtb strains.<sup>292</sup> Thus, it is feasible that the obtained labeling results were based on cell envelope diversity. On the other hand the optical density (OD) was only measured and adjusted before carbohydrate supplementation. After three days of cultivation the OD was not further controlled. Therefore, it cannot be excluded that labeling diversity relies on varying bacterial replication rates. However, it seems rather

unlikely, since similar replication rates were previously detected for the investigated strains.<sup>319</sup> The new azido pentoses **38**, **39** and **40** can be used as fast and easy tools to label different Mtb clinical isolates and might also give deeper insights into the structural heterogeneity of the MTBC strains.

Labeling experiments with other bacteria, which do not belong to the MTBC, have not been carried out so far. Since arabinofuranosides are present in the cell envelopes of different genera of *Actinomycetales* and a similar arabinan metabolism was described for several bacteria of this order,<sup>97</sup> one might expect that these bacteria can also be labeled by the new azido derivatives **38**, **39** and **40**. However, 5AraAz (**40**) labeling seems not to be based on the known metabolism and might not be incorporated into the common arabinan heteropolysaccharides LAM and AG. Thus, this sugar derivative might be even more specific than expected. To finally analyze specificity, other bacteria belonging to the *Actinomycetales* order, such as the non-tuberculosis mycobacteria *M. avium*, *M. leprae* and *M. marinum* or other non-mycobacterial human colonizing bacteria (e.g. *Rhodococcus equi*, *Nocardia araoensis*, *Actinomyces israelii*), should be examined. Furthermore, Gram-negative bacteria, like *E. coli* or the lung pathogens *Pseudomonas aeruginosa*, *Legionella pneumophila* and *Haemophilus influenza*, should be addressed using this metabolic labeling method. In the cell envelope of Gram-negative bacteria the monosaccharide Kdo is present as a constituent of LPS. This eight-carbon sugar is synthesized based on arabinose-5-phosphate (Ara5P). Ara5P is converted with phosphoenolpyruvate (PEP) catalyzed by Kdo synthase to give Kdo-8-phosphate. This activated Kdo is subsequently transformed into free Kdo and further activated to form the cytidine monophosphate (CMP-Kdo) donor prior to its incorporation into LPS.<sup>320,321</sup> Thus, labeling of Gram-negative bacteria might be possible by 3AraAz (**38**), but not 5AraAz (**40**). 3RiboAz (**39**) might also be incorporated as azido Kdo into the cell envelope, because it is known that ribose 5-phosphate is converted to ribulose 5-phosphate (Ru5P), which is subsequently isomerized to the Kdo precursor Ara5P.<sup>322,323</sup>

In addition, labeling with 3AraAz (**38**) and 3RiboAz (**39**) might not be limited to prokaryotes, since a few eukaryotic pathogens like the trypanosomatid parasite *L. major* have arabinopyranosides in their cell envelope.<sup>90–93,324</sup> In *L. major* these pentoses are part of the lipophosphoglycan (LPG). The galactoside residues of LPG are capped by (1→2) linkage with β-D-arabinopyranosides, which are strongly associated with parasite release from midgut of the sand fly and thus important virulence factors.<sup>325,326</sup> It would be highly fascinating to apply the synthesized pentose derivative **38** to modify those arabinose structures. *L. major* has never been stained by MOE before. However, radioactive D-arabinose was successfully incorporated into LPG and glycosylphosphatidylinositol lipids (GPIL) as shown by N. M. Novozhilova et al.<sup>327</sup> These results make it reasonable that 3AraAz (**38**) can be used for



metabolic labeling of *L. major*. To address this question, a cooperation with Prof. Dr. Ger van Zandbergen of the Paul Ehrlich Institute, Germany was started.

To target pathogens within host cells, the azido pentoses **38**, **39** and **40** should not be incorporated into the glycocalyx of mammalian cells. Therefore, a human epithelial cell line was incubated with the new azido sugars and incorporation analyzed by click reaction with DIBO-Alexa 647. No labeling was obtained. Thus, all three derivatives have the capability to be used as intracellular labeling tools. This was further supported by the fact that none of the synthesized sugars **38**, **39** and **40** showed any cytotoxic effect up to concentrations of at least 5 mM.

Taken together, the applied azido pentoses **38**, **39** and **40** represent a new tool to label different mycobacterial strains and address their structural heterogeneity. While 5AraAz (**40**) might specifically label mycobacteria, 3AraAz (**38**) and 3RiboAz (**39**) might further be applied to target Gram-negative bacteria or the trypanosomatid parasite *L. major*. However, additional studies are necessary to prove the assumed labeling specificity of the three azido pentoses **38**, **39** and **40**.

#### 3.4.4 Applications of MOE

MOE has the potential to develop new strategies to study, image or treat Mtb bacteria:

Trehalose analogs were recently used to localize new cell envelope formation and to identify the involved enzymes.<sup>328</sup> Both K. M. Backus et al. and B. M. Swarts et al. revealed high levels of trehalose derivative incorporation particular at the bacterial poles.<sup>88,192</sup> This observation was consistent with the polar growth model of mycobacteria.<sup>328-330</sup> An irregular distribution of the pentose derivative **40** within the cell envelope was not further quantified. However, partial higher fluorescence intensity at the mycobacterial poles was visualized by microscopy (Figure 37).

In the current study metabolic labeling was used to get deeper insights into cell envelope dynamics. Labeling degradation was time and temperature dependent. While a fast fluorescence reduction was observed at 37°C, fluorescence intensity remained nearly constant at 4°C. These findings suggest that enzyme-catalyzed cellular processes may be involved in either shedding of cell surface structures or turnover mechanisms. The results are similar to previous observations with Msp, where the radioactive labeling with *N*-acetyl-glucosamine (<sup>14</sup>C-GlcNAc) was reduced to 20% within twelve hours.<sup>331</sup> Our results on the time-dependent reduction of fluorescent intensity suggest a complete cell envelope turnover within less than 18 hours. Thus, the half-life of cell envelope constitution may be shorter than previously anticipated. Nevertheless, these experiments were carried out in nutrient-rich medium. Natural nutrient supply differs and depends on bacterial location within the host,<sup>318</sup> thus cell wall turnover might also be completely different *in vivo*.

Beside the use of MOE as a method to study biochemical processes, it can also be applied as a new tool for fast and easy staining of clinical isolates evading time-consuming genetic modifications. Therefore, metabolic labeling should not influence the virulence characteristics of the pathogen. To analyze the impact of surface modifications on Mtb pathogenicity, human macrophages were infected with 5AraAz (**40**)-labeled and untreated mycobacteria, respectively, for three hours. Fluorescence derived from metabolic labeling was stable under early infection conditions and was clearly detectable within the macrophage. The best characterized virulence mechanism of Mtb bacteria is the inhibition of phagosome maturation.<sup>332,333</sup> Thus, antibodies recognizing endosomal or lysosomal marker proteins were applied to characterize the phagosomal status. Both, labeled and untreated Mtb bacteria, mainly resided in phagosomes positive for the endosome associated protein Rab5 but negative for the lysosomal-associated protein LAMP-1.<sup>334,335</sup> Thus, also labeled Mtb bacteria seemed to be able to inhibit phagosome maturation. These results indicate that MOE does not influence Mtb virulence characteristics in primary macrophages during early phase of infection. However, only two phagosomal markers were analyzed so far. To get more reliable information further marker proteins should be examined.<sup>127</sup> For example increased EEA1<sup>293</sup> concentrations and the appearance of Rab7<sup>335</sup> would indicate a late endosomal status, whereas Rab14<sup>133</sup> and the uncleaved lysosomal aspartyl protease procathepsin D<sup>336</sup> would refer to early endosomes. Despite the wide use of antibodies to document the degree of maturation, this method provides only a static measurement of a dynamic process and provides limited information about the environment within the phagosomes. Inhibition of phagosome maturation is connected with a reduced acidification.<sup>294</sup> This could be visualized by the lack of fluorescence imaging with the hydrophobic and acidotropic fluorescent dye LysoTracker.<sup>337</sup> So far the stability of the introduced label and the influence of MOE on Mtb pathogenicity were investigated during the early phase of infection. In a time period of three hours mycobacteria are phagocytosed and first host-pathogen interactions, including inhibition of the phagosomal maturation,<sup>127</sup> take place. To address whether the introduced label might also withstand intracellular mycobacterial replication and later stages of infection, the infection studies should be carried out for at least 24 hours.

Beside visualization of Mtb bacteria within macrophages, as shown in the current study, MOE might also be applied to investigate the bacterial environment within the phagosome. Metabolic labeling might be used to functionalize mycobacteria with biosensors. Molecules detecting phagosomal maturation by pH measurement, identification of  $\beta$ -galactosidase, protease or lipase activity or directly determine lysosomal fusion are conceivable. Specific host immune stresses could be detected via measurements of hypoxia, reactive nitrogen species (RNS) or reactive oxygen species (ROS). Furthermore, ion concentrations ( $\text{Ca}^{2+}$  or  $\text{Fe}^{3+}$ ), nutrient supply or the release of specific signaling or virulence factors could be addressed. While the Russell

group already genetically developed a panel of reporter strains to analyze the physiology of the phagosomes,<sup>338,339</sup> introduction of biosensors via MOE would have several advantages. This carbohydrate based strategy might enable to easily compare the virulence characteristics of different Mtb clinical isolates without time consuming genetic modifications, can be introduced even after a normal infection at a specific time point and might also be applicable within monkeys. To study the environmental composition of mycobacteria within a macaques's lung is of special interest, since it is known that some bacteria or even whole infected regions do not respond to therapy, while others are easily cured.<sup>340</sup>

First efforts to use MOE to detect therapeutic outcome have been done by the Barry group.<sup>21</sup> They applied the radiolabeled tracer 2-deoxy-2-(<sup>18</sup>F)fluoro-D-glucose (FDG) to illuminate areas of inflammation within the lung.<sup>20</sup> While the radioactivity is detected by positron emission tomography (PET), morphological information is added by computed tomography (CT) high-resolution X-ray images. These PET/CT scans (Figure 1) can monitor infections over time. Since FDG is mainly taken up by activated inflammatory cells, which have a high glycolytic rate, this imaging method detects inflammation but not the mycobacterium itself within the lung.<sup>21</sup> To directly visualize Mtb bacteria 2-deoxy-2-(<sup>18</sup>F)fluoro-trehalose (FDT) is currently under investigation in the group of Prof. Dr. Clifton E. Barry 3rd.

Beside radioactive fluorine derivatives, carbohydrates carrying iodine isotopes could be applied. These molecules might also enable Mtb imaging, but can further be used as therapeutic tools. For iodine-based PET/CT imaging the  $\gamma$ -emitting isotopes iodine-123 (<sup>123</sup>I) with a half-life of 13 hours could be chosen, while the  $\beta$ -emitting isotope iodine-131 (<sup>131</sup>I) with a half-life of eight days would be suitable for radiotherapy. In the current work the iodo arabinofuranose 5Aral (**55**) was successfully used for metabolic labeling of Mtb bacteria. Although a non-radioactive derivative was synthesized, the results demonstrate that iodine-functionalized arabinose can be introduced into mycobacteria. Moreover, 5Aral (**55**) was applied in cooperation with Prof. Dr. Niaz Banaei of Stanford University, USA for first CyTOF analysis of Mtb bacteria. To analyze and quantify metabolically labeled bacteria at a single-cell level often fluorescent flow cytometry is used. However, there are several limitations of this technique including photobleaching of the fluorescent dye and spectral overlap, when using several different fluorescent molecules in the same sample. CyTOF analysis, combining flow cytometry and mass spectrometry (MS), facilitates multiparametric analysis. Therefore, bacteria have to be labeled with heavy and good ionizable atoms. Labeled bacteria, solely or within a host-cell, can be separated by flow cytometry. Subsequently, the introduced heavy atoms, rarely present in the non-labeled bacteria, can be specifically detected after plasma treatment by mass spectrometry, such as TOF-MS. Here we used an iodine analog (5Aral, **55**) of 5AraAz (**40**) to verify metabolic incorporation of arabinofuranose derivatives into Mtb bacteria by CyTOF analysis. In contrast to the azide-cyclooctyne-based labeling method,

CyTOF enables detection of metabolic modifications by a one-step approach, excluding the biorthogonal reaction. Furthermore, the small iodine group might also be an advantage for labeling of Mtb bacteria within macrophages in comparison to large and hydrophobic fluorescent dyes like fluorescein.

MOE might not only be used as an imaging or diagnostic tool, but can also enable the development of novel therapeutic strategies. Since metabolic labeling is associated with an effective uptake of sugar derivatives, MOE can be used to “smuggle” carbohydrate-linked molecules through the highly impermeable cell envelope of Mtb. Here, we used the cysteamine derivatives **59**, **64** and **70** to get first insights into targeted antibiotic transport. Although cysteamine had only Mtb growth limiting effects in high concentrations, this molecule was chosen for first experiments. The small size seemed to be an advantage in order to allow carbohydrate-based transport activity. Additionally, antibacterial effects of thiahexyl derivatives were previously reported by the Lindhorst group.<sup>299</sup> A low anti-Mtb activity of the original molecule would further allow to easily detect carbohydrate-dependent increase of bacteriostatic activity. However, none of the cysteamine-functionalized sugars **59**, **64** and **70** synthesized in analogy to 3AraAz (**38**), 3RiboAz (**39**) and 5AraAz (**40**) had any effect on mycobacterial growth even at very high concentrations. These results might be explained by an absent uptake of the new thiahexyl derivatives **59**, **64** and **70** or a loss of activity due to functionalization of the thiol group. To address the question whether a free thiol is responsible for the growth limiting effect of cysteamine, the *N*- and *S*-acetylated cysteamine **75** and **74**, respectively, were also tested in the bacterial growth assay. Both had minor, but similar bacteriostatic activity, thus functionalization of the thiol seemed not to be responsible for the negative results obtained with the sugar derivatives **59**, **64** and **70**. However, acetyl-protecting groups can migrate from the thiol to the amine and thereby re-generate a free thiol. Nevertheless, cysteamine derivatives appeared not to be the ideal molecules to study targeted antibiotic transport. Thus, further experiments should be carried out with other antibacterial agents linked to arabinose or trehalose. Cycloserin, a second-line drug of Mtb, ethambutol or other small but maybe less active molecules could be glycosylated and utilized. Furthermore, trehalose derivatives of penicillin are conceivable. Although penicillin was reported to be not active against Mtb bacteria, recent studies revealed that penicillin can be used for Tb therapy, but only in combination with  $\beta$ -lactamase inhibitors.<sup>341</sup> It might also be possible to avoid  $\beta$ -lactam cleavage by a fast and targeted transport of penicillin through the mycobacterial cell envelope. It is tempting to speculate that this transport might be achieved by carbohydrate-functionalization.

While cycloserin, ethambutol or penicillin would directly inhibit the cell envelope biosynthesis,<sup>30,341,342</sup> other molecules could be incorporated by MOE and then subsequently be activated to exhibit antibacterial characteristics in a second step. This two-step approach

might reduce resistance formation, which would be a great benefit since MDR and XDR strains are the main challenge in the fight against Tb. Up to now only two examples for incorporating therapeutics by MOE into bacterial glycans have been published.<sup>343–345</sup> However, huge inspiration can be obtained from the area of cancer research.<sup>346,347</sup> Novel classes of therapeutics such as carbohydrate-linked photosensitizers, NO sensitizer or activatable nanoparticles could be developed to catalyze damage to mycobacteria.<sup>240</sup> These molecules are either activated by light, pH or in a magnetic field. In photodynamic therapy ROS are generated by photosensitizers when excited by light.<sup>348,349</sup> Formation of singlet oxygen species, for example, can result in oxidation and thereby inactivation of essential biomolecules followed by cell death. These destructing oxygen species have an incredibly short life span in water,<sup>350</sup> with the result that toxicity is localized and targeted bacteria would be killed with high selectivity. Several porphyrin-based photosensitizers are clinically approved in cancer therapy<sup>348,349</sup> and were already applied for treatment of bacterial infections.<sup>351–353</sup> Although glycosylated photosensitizers hold a great potential for MOE-based therapy and excitation with light is feasible within the lung,<sup>348</sup> Mtb might be able to survive this treatment. Pathogenic mycobacteria utilize a wide range of mechanisms to defend against ROS and RNS using enzymes like catalase and superoxide dismutase (SOD) or the NO detoxifying truncated hemoglobin (trHbN). However, the Misra group showed that inhalable microparticles, which contain the three nitric oxide donors isosorbide mononitrate (ISMN), sodium nitroprusside (SNP) and diethylenetriamine nitric oxide (DETA/NO), significantly reduced Mtb colony forming units (cfu) by up to 4-log within a mouse lung.<sup>354,355</sup> Carbohydrates could be easily functionalized with the small DETA/NO molecule via peptide coupling or thiourea formation. After cell envelope incorporation NO would then spontaneously dissociate activated by pH reduction (pH < 6). Alternatively, carbohydrates could also be connected to microparticles, which might be activated by light or in a magnetic field to dissipate heat. Localized thermal changes can disturb biochemical processes and induce cellular lysis.<sup>356</sup> First successful applications were shown by R. S. Norman et al. using antibody-conjugated gold nanorods to trigger targeted photothermal lysis of Gram-negative *Pseudomonas aeruginosa*.<sup>357</sup> Beside gold nanoparticles incorporation of magnetic nanostructures could be of interest to induce thermal lysis after positioning in a magnetic field.<sup>356</sup> Carbohydrate functionalized magnetic beads could be used not only for Mtb therapy, but also for mycobacteria detection via magnetic resonance tomography (MRT).

Taken together, MOE opens up the possibility to develop novel, specific and local diagnostic and therapeutic tools, which might completely change Mtb therapy in future.

### 3.5 Concluding remarks

In the current study azido pentoses, especially 5AraAz (**40**), were identified as new molecules to efficiently label *Mycobacterium tuberculosis*. This metabolic strategy verified the presence of D-arabinose and D-ribose transporters in the Mtb cell envelope and disclosed putative novel biosynthetic pathways for arabinose derivatives. Moreover, the azido sugars **38**, **39** and **40** represent a new tool to identify these widely unknown uptake and metabolic mechanisms in further detail. Beside biochemical applications, the new azido derivatives **38**, **39** and **40** served as powerful reagents to fluorescently label different Mtb clinical isolates without any time consuming genetic modifications. Neither mycobacterial growth nor the typical virulence characteristics of the pathogen were influenced by this carbohydrate-based strategy. Thus, metabolic labeled Mtb strains can be perfectly applied for infection studies. Absence of metabolic labeling of epithelial cells and low cytotoxicity indicate that the azido pentoses **38**, **39** and **40** might even be used to target Mtb bacteria within host cells. Furthermore, these new molecules form the basis for a potential investigation of targeted antibiotic transport or anti-Mtb radiotherapy. Two examples of the huge amount of new potential antibacterial or diagnostic strategies that might prospectively be developed based on MOE.

### 3.6 Materials and methods

Reagents, buffer and media, which are listed in part 1 of this thesis, are excluded in the following register.

#### 3.6.1 Reagents

<i>N</i> -Acetylcysteamine	Sigma-Aldrich, St. Louis, USA
Allyl bromide	Sigma-Aldrich, St. Louis, USA
Ammonia solution (25%)	Merck KGaA, Darmstadt, Germany
Ammonium persulfate	Sigma-Aldrich, St. Louis, USA
Azobisisobutyronitrile (AIBN)	Sigma-Aldrich, St. Louis, USA
Bovine serum albumin (BSA)	AppliChem GmbH, Darmstadt, Germany
Bromophenol blue	Sigma-Aldrich, St. Louis, USA
Calcein AM	Sigma-Aldrich, St. Louis, USA
Chloromethyl methyl ether (MOMCl)	Sigma-Aldrich, St. Louis, USA
Click-IT Alexa Fluor 488 DIBO Alkyne (DIBO-Alexa 488)	Thermo Fisher Scientific, Waltham, USA
Click-IT Alexa Fluor 647 DIBO Alkyne (DIBO-Alexa 647)	Thermo Fisher Scientific, Waltham, USA
Click-IT Biotin DIBO Alkyne (DIBO-Biotin)	Thermo Fisher Scientific, Waltham, USA
Coomassie Brilliant Blue R-250	Thermo Fisher Scientific, Waltham, USA
Cysteamine hydrochloride	Sigma-Aldrich, St. Louis, USA
4',6-Diamidino-2-phenylindole (DAPI)	Roche Diagnostics, Rotkreuz, Switzerland
<i>N,N</i> -Diisopropylethylamine (DIPEA)	Sigma-Aldrich, St. Louis, USA
2,2-Dimethoxy-2-phenylacetophenone (DPAP)	TOKYO CHEMICAL INDUSTRY CO., Tokyo, Japan
2,2-Dimethoxypropane	Sigma-Aldrich, St. Louis, USA
Di- <i>tert</i> -butyl dicarbonate	Sigma-Aldrich, St. Louis, USA
Dulbecco's phosphate-buffered saline	Thermo Fisher Scientific, Waltham, USA
Ethidium homodimer	Thermo Fisher Scientific, Waltham, USA
Fetal calf serum (FCS)	Merck KGaA, Darmstadt, Germany
GlutaMAX	Thermo Fisher Scientific, Waltham, USA
Hank's balanced salt solution (HBSS)	Merck KGaA, Darmstadt, Germany
Human epidermal growth factor (hEGF)	Thermo Fisher Scientific, Waltham, USA
Hydrocortisone	Sigma-Aldrich, St. Louis, USA
Isopropanol	Merck KGaA, Darmstadt, Germany
MCDB-131 medium	Thermo Fisher Scientific, Waltham, USA
Macrophage colony stimulating factor (M-CSF)	R&D Systems Inc., Minneapolis, USA
Mercaptoethanol	Sigma-Aldrich, St. Louis, USA
Normal goat serum (NGS)	Merck KGaA, Darmstadt, Germany
Pancoll, human	PAN-Biotech GmbH, Aidenbach, Germany
Paraformaldehyde (PFA)	Merck KGaA, Darmstadt, Germany
Penicillin/streptomycin	Merck KGaA, Darmstadt, Germany
Periodic acid	Sigma-Aldrich, St. Louis, USA
Phenol	Sigma-Aldrich, St. Louis, USA
ProLong Gold antifade Reagent	Thermo Fisher Scientific, Waltham, USA
Roti-Immunoblock	Carl Roth GmbH & Co. KG, Karlsruhe, Germany

RPMI 1640 (without L-glutamine)	GE Healthcare, Little Chalfont, UK
Silver nitrate	Sigma-Aldrich, St. Louis, USA
Sodium citrate	Sigma-Aldrich, St. Louis, USA
Sodium dodecyl sulfate (SDS)	Sigma-Aldrich, St. Louis, USA
Sodium hydride	Sigma-Aldrich, St. Louis, USA
Sodium hydroxide	Sigma-Aldrich, St. Louis, USA
Sodium iodine	Sigma-Aldrich, St. Louis, USA
Sodium metabisulfite	Sigma-Aldrich, St. Louis, USA
Sodium nitrite	Sigma-Aldrich, St. Louis, USA
Streptavidin-horseradish peroxidase (HRP)	Thermo Fisher Scientific, Waltham, USA
Sulfuric acid	Sigma-Aldrich, St. Louis, USA
<i>tert</i> -Butyldiphenylsilyl chloride (TBDPSCI)	Sigma-Aldrich, St. Louis, USA
<i>N,N,N,N</i> -Tetramethylethylenediamine (TEMED)	Thermo Fisher Scientific, Waltham, USA
Tetra- <i>N</i> -butylammonium fluoride solution in THF (1 M)	Sigma-Aldrich, St. Louis, USA
<i>p</i> -Toluenesulfonic acid ( <i>p</i> -TsOH)	Sigma-Aldrich, St. Louis, USA
Trifluoroacetic acid (TFA)	Sigma-Aldrich, St. Louis, USA
Trifluoromethanesulfonic anhydride (Tf <sub>2</sub> O)	Sigma-Aldrich, St. Louis, USA
Triton X-100	Sigma-Aldrich, St. Louis, USA

### 3.6.2 Buffer and media

pH-Values were adjusted with aqueous HCl (100 mM) or NaOH (100 mM) solutions, respectively, unless otherwise described. All buffer and media were autoclaved prior use.

APS solution (10%)	Ammonium persulfate (100 mg, 438 μmol) was dissolved in double dist. water (1.00 ml).
Blocking buffer (blot)	Skim milk powder (5.00 g) was suspended in T-TBS (100 ml).
Blocking buffer (fluorescence microscopy)	NGS (100 μl) and Triton X-100 (10.0 μl, 16.5 μmol) were added to PBS (10.0 ml).
Coomassie solution	Coomassie Brilliant Blue R-250 (50.0 mg, 60.5 μmol) was dissolved in methanol (11.5 ml) and supplemented with double dist. water (11.5 ml) and glacial acetic acid (2.50 ml). The solution was filtered before use.
Destaining solution (Coomassie staining)	Isopropanol (4.50 ml) and glacial acetic acid (2.00 ml) were added to double dist. water (18.5 ml).
Fixative/destaining solution (PAS)	Methanol (17.5 ml) and acetic acid (5.00 ml) were added to double dist. water (27.5 ml).



Fixative/destaining solution (silver staining)	Ethanol (20.0 ml) and acetic acid (2.50 ml) were added to double dist. water (27.5 ml).
Human macrophage medium (HMM, culturing)	RPMI 1640 (450 ml) was supplemented with FCS (50.0 ml) and L-glutamine (292 mg, 2.00 mmol)
Human monocyte medium (HMM, differentiation)	RPMI 1640 (435 ml) was supplemented with L-glutamine (292 mg, 2.00 mmol), M-CSF (1 µg), human serum (10.0 ml) and penicillin/streptomycin (10000 U/ml / 10000 µg/ml, 5.00 ml)
2 x Lysis buffer , pH 6.8	Tris (15.1 mg, 125 µmol) and SDS (40.0 mg, 139 µmol) were dissolved in double dist. water (800 µl). The Solution was supplemented with glycerol (200 µl, 2.74 mmol) and the pH was adjusted. Mercaptoethanol (4.0 µl, 56.8 µmol) was added.
MDCB-131 medium	MDCB-131 (445 ml) was supplemented with GlutaMAX (5.00 ml), FCS (50.0 ml), hEGF (5 µg) and hydrocortisone (500 µg).
PFA solution, pH 7.2 (4%)	PFA (4.00 g) was suspended in PBS (100 ml) and concentrated sodium hydroxide solution (few drops) was added. The mixture was heated in order to dissolve PFA. Subsequently the pH was adjusted.
PBSB	BSA (250 mg) was dissolved in PBS (50.0 ml)
Periodic acid solution	Periodic acid (175 mg, 768 µmol) was dissolved in acetic acid (5%, 25.0 ml).
Reaction buffer	NGS (10.0 µl) and Triton X-100 (10.0 µl, 16.5 µmol) were added to PBS (10.0 ml).
Running buffer, pH 8.3	Tris (3.03 g, 25.0 mmol), SDS (1.00 g, 3.47 mmol) and glycine (14.4 g, 192 mmol) were dissolved in double dist. water (1.00 l). pH was adjusted.
SDS solution (10%)	SDS (1.00 g) was dissolved in double dist. water (10.0 ml).
Silver nitrate solution	Silver nitrate (500 mg, 2.94 mmol) was dissolved in double dist. water (73.5 ml) and sodium hydroxide

Sodium citrate solution	<p>solution (1 M, 1.40 ml) and ammonia solution (25%, 1.00 ml) were added.</p> <p>Sodium citrate (1.25 mg, 5.84 mmol) was dissolved in double dist. water (25.0 ml) and formaldehyde (37%, 12.5 µl, 120 µmol) was added.</p>
Sodium metabisulfite solution	<p>Sodium metabisulfite (50.0 mg, 263 µmol) was dissolved in acetic acid (5%, 25.0 ml).</p>
Sodium periodate solution	<p>Sodium periodate (17.5 mg, 81.8 µmol) was dissolved in double dist. water (25.0 ml).</p>
TBS, pH 8.0 (blot)	<p>Tris (1.21 g, 10.0 mmol) and sodium chloride (8.76 g, 150 mmol) were dissolved in double dist. water (1.00 l) with subsequent pH adjustment.</p>
Transfer buffer, pH 8.3 (blot)	<p>Tris (3.03 g, 25.0 mmol), SDS (200 mg, 693 µmol) and glycine (14.4 g, 192 mmol) were dissolved in double dist. water (800 ml) and the pH was adjusted. Methanol (200 ml) was added.</p>
Tris/HCl solution, pH 6.8 (0.5 M) (SDS-PAGE)	<p>Tris (6.05 g, 50.0 mmol) was dissolve in double dist. water (100 ml) with subsequent pH adjustment.</p>
Tris/HCl solution, pH 8.8 (1.5 M) (SDS-PAGE)	<p>Tris (18.2 g, 150 mmol) was dissolve in double dist. water (100 ml) with subsequent pH adjustment.</p>
T-TBS (blot)	<p>Tween 20 (1.00 ml, 896 µmol) was added to TBS (1.00 l)</p>

### 3.6.3 Biological assays

#### Mtb strains used in this study

Clinical isolates (Table 6) were initially cultured from clinical samples on Löwenstein/Jensen medium at the National Reference Center for Mycobacteria in Borstel, Germany. Further characterization by genotyping methods and susceptibility testing are described elsewhere.<sup>358</sup>

All strains (Table 6 and 7) were grown in Middlebrook 7H9 medium containing oleic acid-albumin-dextrose-catalase (OADC, 10%), Tween 80 (0.05%) and glycerol (0.2%). At mid-log phase ( $OD_{600} = 0.4$ ) cultures were harvested and frozen at  $-80^{\circ}\text{C}$  as described previously.<sup>288</sup>

**Table 6. Clinical strains used in this study.**

<u>Sample name</u>	<u>Species</u>	<u>Superlineage</u>	<u>Lineage</u>
1934/03 <sup>358</sup>	Mtb	Clade I	Beijing
2336/02 <sup>358</sup>	Mtb	Clade I/Euro-American	Haarlem
1797/03 <sup>358</sup>	Mtb	Clade II	EAI

**Table 7. Laboratory strains used in this study.**

<u>Sample name</u>	<u>Description</u>	<u>Source</u>
GFP-expressing Mtb H37Rv	In order to obtain stable GFP expression in Mtb H37Rv, codon usage, fluorescence and folding optimized <i>gfpm2+</i> from pMN437 <sup>234</sup> was cloned into the integrative mycobacterial plasmid pMV306 <sup>235</sup> giving pSvM4 which was used to transform Mtb H37Rv (ATCC 27294).	Plasmid (pMN437) <sup>234</sup> kindly provided by Prof. Dr. M. Niederweis, University of Alabama at Birmingham, USA
mCherry-expressing Mtb (Cherry 10) <sup>359</sup>	Strain carrying a mCherry-expressing plasmid (pCherry10), <sup>360</sup> derived from H37Rv (ATCC 25618)	Prof. Dr. U. E. Schaible, Research Center Borstel, Germany

#### Bacterial culture conditions

All bacterial cultures used were derived from frozen stocks ( $2.5 \cdot 10^8$  bacteria/ml). Homogenous bacterial suspensions were prepared in 7H9 medium (50.0 ml) supplemented with OADC (10%), Tween 80 (0.05%) and glycerol (0.2%). 25.0 ml each were incubated in 30 ml square medium bottles (Nalgene) at  $37^{\circ}\text{C}$  without shaking (preculture). Growth ( $\sim 3$  d) to mid-log phase was monitored by measuring the optical density at 600 nm ( $OD_{600} = 0.4$ ) (Bio-Tek Synergy).

### Labeling of Mtb bacteria

Precultured bacteria (5.00 ml/batch) were mixed with the azido sugars **28**, **38**, **39** and **40**, respectively, in the desired concentration and cultured 3 d at 37°C without shaking. The samples (2.00 ml each) were washed twice with PBSB (1.00 ml). Subsequently, bacteria were incubated with DIBO-Alexa 488 (1:250 dilution of 1 mM stock solution in DMSO into PBSB, 1.00 ml) in the dark for 1 h at 37°C gently shaking. The samples were washed (one time PBSB, one time PBS, 1.00 ml each) and fixed with PFA (4%, 1.00 ml) in the dark for 1 h at rt without shaking. After centrifugation (3629 x g, 10 min, 4°C) the pellet was suspended in PBS (400 µl) and fluorescence intensity was analyzed on a FACS Cantoll flow cytometer (BD Biosciences) using the 488 nm and 633 nm laser, respectively. The analysis was performed using the FCSEXPRESS4 program (DeNovo Software).

### Labeling stability

Bioorthogonal labeling was performed with 5AraAz (**40**) as described in method “Labeling of Mtb bacteria”. Before fixation bacteria were re-cultured (7H9 medium (50.0 ml) supplemented with OADC (10%), Tween 80 (0.05%) and glycerol (0.2%), 1.125 ml/batch) for desired time points (1 h, 2 h, 5 h, 18 h) at 4°C or 37°C. The samples (1.00 ml each) were centrifuged (3629 x g, 4°C, 10 min) and fixed with PFA (4%, 1.00 ml) in the dark for 1 h at rt without shaking. After centrifugation (3629 x g, 10 min, 4°C) the pellet was suspended in PBS (400 µl) and fluorescence intensity was analyzed on a FACS Cantoll flow cytometer (BD Biosciences) using the 488 nm laser. The analysis was performed using the FCSEXPRESS4 program (DeNovo Software).

### Microscopic analysis of 5AraAz (**40**)-labeled Cherry 10

Bioorthogonal labeling of Mtb Cherry 10 bacteria was performed with 5AraAz (**40**, 5 mM) as described in method “Labeling of Mtb bacteria”. Labeled (with 5AraAz (**40**)) and unlabeled (without 5AraAz (**40**)) mycobacteria were not fixed in PFA (4%) as described before, instead were re-suspended in PFA (1% in PBS; 1.00 ml), transferred to µ-slides (µ-slide VI, ibidi; 100 µl/channel) and incubated overnight at 4°C. The slides were washed three times with PBS (100 µl/channel) and mounted with ProLong Gold Antifade Reagent. Bacteria were analyzed by use of an Axio Observer microscope, equipped with an ApoTome and the AxioVision Software 4.8 (Carl Zeiss AG). Used excitation and emission filters: for Alexa 488 (excitation: BP 470/40 nm, emission: BP 525/50 nm) and for mCherry (excitation: BP 565/30 nm, emission: BP 620/60 nm).

### Mtb growth analysis<sup>288</sup>

GFP-expressing Mtb H37Rv bacteria ( $1 \cdot 10^6$  bacteria) were cultured in 7H9 medium (supplemented with OADC (10%), Tween 80 (0.05%) and glycerol (0.2%)) and mixed with the azido sugars **28**, **38**, **39** and **40**, respectively, in different concentrations (total volume 100  $\mu$ l). The experiments were performed in black 96-well plates with a clear bottom (Corning Inc) sealed with an air-permeable membrane (Porvair Sciences). Growth was measured as relative light units at 528 nm after excitation at 485 nm in a fluorescence microplate reader (Synergy 2, Biotek) at different time points.

### Glycolipid and lipoglycan isolation<sup>289</sup>

Precultured Mtb H37Rv bacteria (300 ml) were mixed with 5AraAz (**40**, final concentration: 1 mM) and incubated 3 d at 37°C without shaking. Bacteria were washed twice with PBS (30.0 ml each) and suspended in PBS (300 ml). The suspension was autoclaved and the solvent was reduced in vacuo to 15.0 ml. The residue was lyophilized, re-suspended in PBS (15.0 ml) supplemented with Triton X-100 (0.5%) and sonicated. Bacteria were disrupted by three passages through a cell disruption system (40.000 psi; 1psi = 6.89 kPa) (Constant Systems Ltd) and centrifuged (17000 x g, 60 min, 4°C). The supernatant was precipitated with cold acetone (135 ml) over night at -20°C, centrifuged (3500 x g, 20 min, 4°C) and the obtained sediment was washed twice with acetone (30.0 ml each) and dried under a stream of nitrogen. The residue was dissolved in dist. water and lyophilized. The lyophilisate was dissolved in dist. water (36.0 ml) supplemented with Triton X-114 (10%) and stirred 1 h at rt. Phase separation was obtained after 2 h at 37°C and centrifugation (3500 x g, 30 min, 30°C). Triton X-114 (1.4 ml) was added to the aqueous layer and the solution was stirred overnight at rt. Phase separation was obtained after 2 h at 37°C and centrifugation (3500 x g, 20 min, 30°C). The two Triton X layers were precipitated with cold acetone (150 ml) for 2 d at -20°C and centrifuged (12000 x g, 30 min, 4°C). The combined sediments were washed twice with acetone (15.0 ml each) and dried under a stream of nitrogen. The residue was dissolved in dist. water and lyophilized. The lyophilisate was dissolved in dist. water (8.00 ml), mixed with aqueous phenol (80% w/v phenol/PBS, 8.00 ml) and stirred 25 min at 80°C. Phase separation was obtained after 20 min on ice and centrifugation (3500 x g, 60 min, 4°C). The extraction was repeated. To remove phenol and low-molecular mass components the aqueous layer was dialyzed against dist. water using 3500 MWCO membrane ( $d_i = 29$  mm) (Spectrum Laboratories, 1 d, rt and 1 d, 4°C) and lyophilized. The residue was dissolved in dist. water (5.00 ml), precipitated with cold acetone (60.0 ml) for 1 d at -20°C and centrifuged (12000 x g, 30 min, 4°C). The sediment was lyophilized and re-suspended in dist. water (1.00 ml) resulting in the desired isolated glycolipid fraction A (concentration: 2.00 mg/ml).

### Analysis of the glycolipid and lipoglycan fractions

Glycolipids and lipoglycans were denaturated and separated by sodium dodecyl sulfate polyacrylamide gel electrophoresis (SDS-PAGE). SDS-gels were directly used for Periodic acid-Schiff reaction (PAS), silver or coomassie staining.

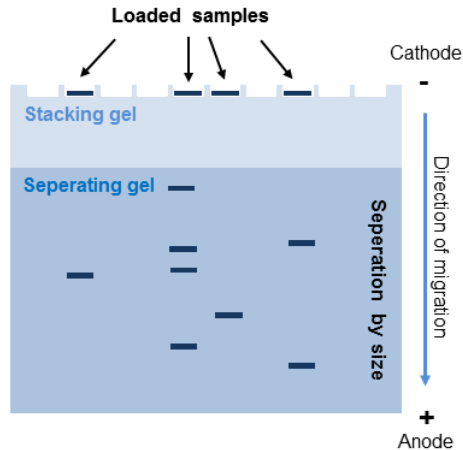
### SDS-PAGE

For the SDS-PAGE (Figure 55) a SDS polyacrylamide gel was used composed of a stacking gel and a separating gel. The stacking gel with a larger pore size allows the loaded samples to be concentrated into a tight band during electrophoresis before entering the resolving portion of the gel.

**Table 8. Ingredients of the solutions for the stacking gel and the separating gel.**

Buffer and reagents	Stacking gel	Separating gel	
	5%	15%	17%
Double dist. water	6.15 ml	6.02 ml	5.175 ml
Tris/HCl solution, pH 6.8 (0.5 M)	2.50 ml		
Tris/HCl solution, pH 8.8 (1.5 M)		4.25 ml	4.25 ml
Acrylamide	1.25 ml	6.38 ml	7.225 ml
SDS solution (10%)	100 µl	170 µl	170 µl
TEMED	10.0 µl	20.0 µl	20.0 µl
APS solution (10%)	50.0 µl	100 µl	100 µl

The separating gel solution (7.50 ml) was pipetted into the gap between the glass plates of the casting frame (BioRad) and overlaid with ethanol, which led to a straight edge of the gel. The gel polymerized within 30 min. Ethanol was removed and the stacking gel solution (4.00 ml) was pipetted on top of the polymerized separating gel. A comb was inserted resulting in gel pockets in the stacking gel. The stacking gel polymerized within 30 to 45 min. The polymerized gel was mounted to the gel electrophoresis chamber (Mini-Protean IV, BioRad), running buffer was added, the comb removed and the samples of the cell envelope preparation (20.0 µl each) and a protein standard (low range marker (LRM), 14.4 97.4 kDa, BioRad or ColoPlus Prestained Protein Marker, broad range 7 175 kDa, New England Biolabs) or  $\alpha$ -1-acid-glycoprotein (Sigma Aldrich)) as a marker (5.0 µl) loaded into the gel pockets. Prior to gel electrophoresis the samples were supplemented with the same amount of 2 x lysis buffer and incubated for 15 min at 95°C. Thus, the compounds were denaturated and coated with SDS. These negative charged and linearized molecules were separated by size in the electric field during gel electrophoresis (20 min, 70 V and 1 h, 180 V).



**Figure 55. Illustration of an SDS-PAGE.**

Denaturated and SDS-coated compounds were loaded into the gel pockets of the stacking gel. These negative charged and linearized molecules were separated by size in the electric field during gel electrophoresis.

### Periodic acid-Schiff reaction (PAS)<sup>361</sup>

The SDS-gel was incubated in fixative/destaining solution (20.0 ml) for 2 h at rt under gentle agitation. Fixative was removed and carbohydrates were oxidized by addition of periodic acid solution (20.0 ml) for 1 h at rt under gentle agitation. Oxidized gel was washed five times with double dist. water (1 min each, 20.0 ml each) and sodium metabisulfite solution (20.0 ml) was added. The gel turned from colorless to yellow and back to colorless. Sodium metabisulfite solution was replaced by Schiff reagent (20.0 ml, Microscopy PAS Kit, Merck) and gel was incubated for 2 h at 4°C under gentle agitation. The gel was placed into fixative/destaining solution (20.0 ml) overnight at 4°C under gentle agitation. The gel was washed (two times fixative/destaining solution, 30 min each, 20.0 ml each; two times dist. water, 10 min each, 20.0 ml each) and scanned.

### Silver staining<sup>362</sup>

The SDS-gel was incubated in fixative (20.0 ml) for 1 h at rt under gentle agitation. After washing with double dist. water carbohydrates were oxidized by addition of sodium periodate solution (20.0 ml) for 10 min at rt under gentle agitation. Oxidized gel was washed four times with double dist. water (5 min each, 20.0 ml each), silver nitrate solution (20.0 ml) was added and gel incubated for 10 min at rt under gentle agitation. The gel was washed four times with double dist. water (5 min each, 20.0 ml each) and developed by sodium citrate solution (20.0 ml) for 5 min. Sodium citrate solution was replaced by acetic acid (7%, 20.0 ml) and gel incubated 30 min at rt under gentle agitation. The gel was stored in dist. water and scanned.

### Coomassie

SDS-gel was incubated in coomassie solution (20.0 ml) for 1 h at rt under gentle agitation. After washing with double dist. water gel was placed into destaining solution (20.0 ml) and finally scanned.

### Azide detection in isolated glycolipid/lipoglycan fractions

Glycolipid/lipoglycan isolate A (2.00 mg/ml; 10.0  $\mu$ l), prepared from 5AraAz (**40**)-labeled Mtb H37Rv bacterial cultures, and glycolipid/lipoglycan isolate B (5.00 mg/ml; 1.5  $\mu$ l) prepared from unlabeled Mtb H37Rv bacterial cultures, (used concentrations based on previous PAS staining) were mixed with DIBO-biotin (1:6 dilution of 25  $\mu$ M stock solution in DMSO into water, final volume 12.0  $\mu$ l) and incubated 1.5 h at rt and 100 rpm. Reaction mixtures were treated with 2 x lysis buffer (12.0  $\mu$ l) for 15 min at 95°C. The samples (20.0  $\mu$ l/slot) were separated by 15% SDS-PAGE as described before with protein standards (ColoPlus Prestained Protein Marker, broad range 7-175 kDa, New England Biolabs) as a marker. The SDS-Gel was stored in TBS overnight at 4°C. Glycolipids/lipoglycans were transferred to a polyvinylidene fluoride (PVDF) membrane (Millipore) at 75 V for 85 min using a wet blot system (Mini Protean II, BioRad) under ice cooling. The membrane was blocked in milk (5%) in T-TBS (TBS, Tween 20 (0.1%)) for 1 h at rt, washed three times in T-TBS (10 min each) and incubated with streptavidin-horseradish peroxidase (HRP, 1:6000 dilution of 1.00 mg/ml stock solution in dist. water into Roti-Immunoblock (Carl Roth, 10% in T-TBS, 12.0 ml)) for 1 h, at rt and under gentle agitation. After three washing steps with T-TBS (10 min each) the blot was developed using Amersham ECL Western blotting Detection Reagent (GE Healthcare, 1.00 ml) and Amersham Hyperfilm ECL (GE Healthcare) and analyzed with the X-Omat M35 film processor (Kodak).

### Eukaryotic cells used in this study

For metabolic labeling experiments and cytotoxicity analysis a human epithelial cell line (human mammary epithelial cells, HMEC-1, Centers for Disease Control and Prevention (CDC)) was used. Infection studies and immunofluorescence analysis were carried out with human monocyte-derived macrophages (hMDMs) isolated from venous blood of healthy volunteers at the Research Center Borstel, Germany.

### Cell culture conditions HMEC-1

HMEC-1 cells were cultured in MDCB-131 medium containing GlutaMAX (1%), fetal bovine serum (FCS, 10%), human epidermal growth factor (hEGF, 10 ng/ml) and hydrocortisone (1  $\mu$ g/ml). Cells were kept at 37°C in a 5% humidified CO<sub>2</sub>-atmosphere.

### Isolation, differentiation and cultivation of hMDMs<sup>46</sup>

#### *Ethics statement*

Experiments with hMDMs were approved by the Ethics Committee of the University of Lübeck, Lübeck, Germany (14-032, March 2014).



Mononuclear cells were isolated from peripheral blood mononuclear cells (PBMC) of healthy volunteers by density gradient centrifugation. Heparinized peripheral blood was collected and diluted in PBS (1:1), slowly transferred on top of a polysucrose solution (Pancoll, 10.0 ml) and centrifuged in a swing bucket rotor (403 x g, 40 min, rt; without break). The upper layer was discarded and the interface transferred to a new 50 ml tube. Cells were washed with PBS (50.0 ml) and re-suspended in Hank's Balanced Salt Solution (HBSS) containing 0.1% BSA. Cell numbers were adjusted ( $5 \cdot 10^6$  cells/ml) using a cell counter (Casy2, Schärfe System). Isolated PBMCs, containing lymphocytes, monocytes and thrombocytes, were separated by counterflow elutriation using a centrifuge equipped with an elutriation rotor (JE-5-B rotor, Beckman), tubing systems and a peristaltic pump (RTC) (purity consistently greater than 92%). Prior to elutriation, the rotor was disinfected with ethanol (70%), washed twice with dH<sub>2</sub>O and equilibrated (BSA (0.1%) in HBSS). PBMCs were loaded and separated under centrifugation by stepwise increase of the flow rate (24 up to 44 ml/min, Table 9). Received fractions were analyzed with a cell counter (Casy2, Schärfe System). Isolated monocytes were centrifuged (258 x g, 10 min, 4°C) and cell density was adjusted to  $2 \cdot 10^7$  cells/ml by addition of RPMI 1640 containing human serum (2%) and recombinant human macrophage colony-stimulating factor (M-CSF, 10 ng/ml). For differentiation of monocytes into macrophage, cells were seeded into teflon-coated cell culture bags (VueLife™ 72, Celgenix) and incubated for 7 d at 37°C in a 5% humidified CO<sub>2</sub>-atmosphere. To detach macrophages, cell culture bags were placed on ice for 1 h and subsequently pulled over the edge of a bench. Cells were counted in a counting chamber (Neubauer, Brand) using trypan blue vital staining.

**Table 9. Elutriation protocol.**

<u>Flow rate (ml/min)</u>	<u>Volume (ml)</u>	<u>Fraction</u>
24	200	Loading of PBMC
26	50	Thrombocytes
28	50	Washing
30	50	Small lymphocytes
32	50	Lymphocytes
33	50	Lymphocytes
34	50	Lymphocytes
35	50	Lymphocytes
36	50	Large lymphocytes
37	50	Washing
38	50	Washing
39	50	Washing
40	50	Washing
41	50	Washing
42	50	Washing
43	50	Monocytes
44 (stop)	50	Pure Monocytes

For infection studies macrophages ( $2 \cdot 10^5$  cells/chamber) were seeded on chamber slides (Lab Tek II, 8 well, Thermo Fischer Scientific) and allowed to attach for 2 h at 37°C in a 5% humidified CO<sub>2</sub>-atmosphere.

#### Infection of hMDMs and immunofluorescence analysis

Bioorthogonal labeling of Mtb Cherry 10 bacteria was performed with 5AraAz (**40**, 5 mM) as described in method “Labeling of Mtb bacteria” (bacteria were not fixed with PFA).

hMDMs were infected with Cherry 10 (5AraAz (**40**)-labeled or unlabeled) with a multiplicity of infection (MOI) of 10 for 3 h. Subsequently cells were washed twice with PBS (500 µl/chamber) and fixed with PFA (1%, 300 µl/chamber) at 4°C overnight. After washing with PBS (500 µl/chamber), cells were permeabilized with Triton X in PBS (0.1%, 300 µl/chamber) for 10 min at rt. Cells were washed with PBS (500 µl/chamber) three times and blocked with blocking buffer (300 µl/chamber) for 1 h at rt. To visualize lysosomal-associated membrane protein 1 (LAMP-1) or ras-related protein (Rab5) slides were partly incubated with anti-LAMP-1 IgG mouse antibody (Abcam, 1:100 in reaction buffer, 100 µl/chamber) or anti-Rab5 polyclonal rabbit IgG antibody (Santa Cruz Biotechnology, 200 µg/ml, 1:100 in reaction buffer, 100 µl/chamber) for 1 h at rt. After three washing steps with PBS (500 µl/chamber) the secondary antibody, Cy5-conjugated anti-mouse IgG antibody (Jackson, ImmunoResearch, 1:200 in reaction buffer, 100 µl/chamber) and DyLight 680-conjugated goat anti-rabbit IgG antibody (Thermo Scientific, 1 mg/ml, 1:200 in reaction buffer, 100 µl/chamber), respectively, was added and slides incubated 1.5 h at rt. Cells were washed three times with PBS (500 µl/chamber) and once with dist. water (500 µl/chamber). Nuclei were stained with 4',6-diamidino-2-phenylindole (DAPI, Roche Diagnostics; 1:2000 dist. water, 100 µl/well) 10 min at rt. Slides were washed twice with dist. water (500 µl/chamber) and mounted with ProLong Gold Antifade Reagent, covered with glass coverslips (R. Langenbrink) and analyzed by use of an Axio Observed microscope, equipped with an ApoTome and the AxioVision Software 4.8 (Carl Zeiss AG). Used excitation and emission filters: for DAPI (excitation: 365 nm, emission: BP 445/50 nm), for Alexa 488 (excitation: BP 470/40 nm, emission: BP 525/50 nm), for mCherry (excitation: BP 565/30 nm, emission: BP 620/60 nm) and for Cy5 (excitation: BP 640/30 nm, emission: BP 690/50 nm).

#### Metabolic labeling of eukaryotic cells

HMEC-1 cells were seeded in collagen coated LabTek I 8-well slides (Nunc) with a density of  $0.75 \cdot 10^4$ . After 6 h cell medium was supplemented with azido sugar (Ac5AraAz (**51**), Ac3AraAz (**52**), Ac3RiboAz (**53**), Ac6TreAz (**27**), 5AraAz (**40**), 3AraAz (**38**), 3RiboAz (**39**) or 6TreAz (**28**); dissolved in DMSO (acetylated sugars) or dist. water (non-acetylated sugars)) to a final sugar concentration of 5 mM in the growth medium. Acetylated *N*-azidoacetyl-

mannosamine (AcManNAz, 100  $\mu\text{M}$  final concentration) was used as a positive control. After 3 d of incubation at 37°C in a 5% humidified CO<sub>2</sub>-atmosphere, cells were washed three times with growth medium, stained for 15 min with DIBO-Alexa 647 (5  $\mu\text{M}$ ), and washed twice with growth medium. Cells were investigated by use of a Cell Observer SD microscope and the ZEN Software (Carl Zeiss AG).

#### Cytotoxicity measurements

HMEC-1 cells were seeded in collagen coated LabTek II 8-well slides (Nunc) with a density of  $0.5 \cdot 10^4$ . After 6 h cell medium was supplemented with azido sugar (5AraAz (**40**), 3AraAz (**38**), 3RiboAz (**39**) or 6TreAz (**28**)) in different concentrations (final sugar concentration: 10  $\mu\text{M}$ , 100  $\mu\text{M}$ , 1 mM or 10 mM). After 2 d of incubation, the cells were washed three times with growth medium and treated with phosphate-buffered saline (PBS)+Ca<sup>2+</sup>/Mg<sup>2+</sup> containing calcein AM (0.5  $\mu\text{M}$ ) and ethidium homodimer (3  $\mu\text{M}$ ). Upon excitation with 488 nm, the 515 nm fluorescence of calcein AM displays living cells whereas the 635 nm fluorescence of ethidium homodimer indicates dead cells. Confocal images were taken of more than 1000 cells per condition with a Cell Observer SD microscope and the ZEN Software (Carl Zeiss AG). After applying a threshold, the number of cells fluorescing in each channel was counted using the Objects Counter Plugin of ImageJ. The viability was defined as the number of living cells divided by the total number of cells.

### 3.6.4 Syntheses

#### General methods for synthesis

(as described in part 1)

#### 3-Azido-3-deoxy- $\alpha,\beta$ -D-arabinose (38)

The arabinofuranose derivative **45** (400 mg, 1.86 mmol) was dissolved in DCM (30.0 ml), cooled with ice and supplemented with dist. water (4.00 ml) and trifluoroacetic acid (TFA, 14.0 ml, 183 mmol, 100 eq.). The reaction mixture was stirred for 2 h and concentrated in vacuo. The crude product was chromatographed on silica gel (cyclohexane/ethyl acetate/methanol, 1:1:0.25) and lyophilized to give the product **38** (318 mg, 1.82 mmol, 98%) as a colorless oil ( $\alpha$ -pyranose:  $\beta$ -pyranose: furanose ratio = 7:5:1 by integration of the  $^1\text{H}$  NMR spectrum). TLC (cyclohexane/ethyl acetate/methanol, 1:1:0.25):  $R_f$  = 0.2 and 0.15; rotation value:  $[\alpha]_D^{22} = -74.6^\circ$  ( $c = 0.24$ , MeOH);  $^1\text{H}$  NMR (only resonances of  $\alpha$ - and  $\beta$ -pyranose are listed, not the resonances of the minor furanose) (500 MHz,  $\text{D}_2\text{O}$ , 300 K):  $\delta$  = 5.18 (d,  $^3J_{1,2} = 3.6$  Hz, 1H, H-1 ( $\beta$ )), 4.51 (d,  $^3J_{1,2} = 7.5$  Hz, 1H, H-1 ( $\alpha$ )), 4.07-4.05 (m, 1H, H-4( $\beta$ )), 4.01 (ddd,  $^3J_{3,4} = 3.2$  Hz,  $^3J_{4,5a} = 2.0$  Hz,  $^3J_{4,5b} = 1.4$  Hz, 1H, H-4 ( $\alpha$ )), 3.98 (dd,  $^3J_{4,5a} = 1.3$  Hz,  $^2J_{5a,5b} = 12.9$  Hz, 1H, H-5a ( $\beta$ )), 3.88 (dd,  $^3J_{1,2} = 3.6$  Hz,  $^3J_{2,3} = 10.5$  Hz, 1H, H-2 ( $\beta$ )), 3.84 (dd,  $^3J_{4,5a} = 2.1$  Hz,  $^2J_{5a,5b} = 13.1$  Hz, 1H, H-5a ( $\alpha$ )), 3.73 (dd,  $^3J_{2,3} = 10.5$  Hz,  $^3J_{3,4} = 3.2$  Hz, 1H, H-3 ( $\beta$ )), 3.64 (dd,  $^3J_{4,5b} = 1.2$  Hz,  $^2J_{5a,5b} = 13.1$  Hz, 1H, H-5b ( $\alpha$ )), 3.57 (dd,  $^3J_{1,2} = 7.4$  Hz,  $^3J_{2,3} = 10.3$  Hz, 1H, H-2 ( $\alpha$ )), 3.56 (dd,  $^3J_{4,5b} = 2.4$  Hz,  $^2J_{5a,5b} = 12.9$  Hz, 1H, H-5b ( $\beta$ )), 3.50 (dd,  $^3J_{2,3} = 10.4$  Hz,  $^3J_{3,4} = 3.2$  Hz, 1H, H-3 ( $\alpha$ )) ppm;  $^{13}\text{C}$  NMR (only resonances of  $\alpha$ - and  $\beta$ -pyranose are listed, not the resonances of the minor furanose) (125 MHz,  $\text{D}_2\text{O}$ , 300 K):  $\delta$  = 96.8 (C-1 ( $\alpha$ )), 92.1 (C-1 ( $\beta$ )), 70.4 (C-2 ( $\alpha$ )), 67.7 (C-4 ( $\beta$ )), 67.5 (C-4 ( $\alpha$ )), 67.1 (C-2 ( $\beta$ ), C-5 ( $\alpha$ )), 64.7 (C-3 ( $\alpha$ )), 62.4 (C-5 ( $\beta$ )), 61.2 (C-3 ( $\beta$ )) ppm; IR (ATR-IR):  $\tilde{\nu}$  = 3335, 2927, 2104, 1674, 1305, 1251, 1134, 1060, 998, 945, 923, 870, 849, 785, 643, 595, 570, 552; HRMS (ESI-MS):  $m/z$  = 198.0486,  $[\text{M}+\text{Na}]^+$  (calc. 198.0491 for  $\text{C}_5\text{H}_9\text{N}_3\text{O}_4 + \text{Na}$ ).

#### 3-Azido-3-deoxy- $\alpha,\beta$ -D-ribose (39)

The ribofuranose derivative **49** (300 mg, 1.39 mmol) was dissolved in DCM (30.0 ml), cooled with an ice bath and supplemented with TFA (12.0 ml, 157 mmol, 113 eq.) and dist. water (2.50 ml). The reaction mixture was stirred for 2 h and concentrated in vacuo. The crude product was chromatographed on silica gel (cyclohexane/ethyl acetate/methanol, 1:1:0.25) and lyophilized to give the product **39** (220 mg, 1.26 mmol, 91%) as a colorless oil ( $\alpha$ -pyranose:  $\beta$ -pyranose:  $\alpha$ -furanose:  $\beta$ -furanose ratio = 1.3:8:1:1.3 by integration of the  $^1\text{H}$  NMR spectrum). TLC (cyclohexane/ethyl acetate/methanol, 1:1:0.25):  $R_f$  = 0.22 and 0.20; rotation value:  $[\alpha]_D^{22} = -6.00^\circ$  ( $c = 0.4$ , MeOH);  $^1\text{H}$  NMR (only resonances of  $\beta$ -pyranose are listed, minor  $\alpha$ -pyranose and furanose resonances are not shown) (500 MHz,  $\text{D}_2\text{O}$ , 300 K):  $\delta$  = 4.85 (d,  $^3J_{1,2} = 7.1$  Hz, 1H, H-1 ( $\beta$ )), 4.21 (ddd~dt,  $^3J_{2,3} = 3.3$  Hz,  $^3J_{3,4} = 3.3$  Hz,  $^4J_{3,5a} = 1.0$  Hz,

1H, H-3 ( $\beta$ ), 4.07 (ddd,  $^3J_{3,4} = 3.4$  Hz,  $^3J_{4,5a} = 4.6$  Hz,  $^3J_{4,5b} = 9.4$  Hz, 1H, H-4 ( $\beta$ ), 3.84 (ddd,  $^4J_{3,5a} = 1.0$  Hz,  $^3J_{4,5a} = 4.7$  Hz,  $^2J_{5a,5b} = 11.5$  Hz, 1H, H-5a ( $\beta$ )) 3.57 (dd,  $^3J_{1,2} = 7.2$  Hz,  $^3J_{2,3} = 3.3$  Hz, 1H, H-2 ( $\beta$ )), 3.65 (dd,  $^3J_{4,5b} = 9.3$  Hz,  $^2J_{5a,5b} = 11.6$  Hz, 1H, H-5b ( $\beta$ )) ppm;  $^{13}\text{C}$  NMR (only resonances of  $\beta$ -pyranose are listed, minor  $\alpha$ -pyranose and furanose resonances are not shown) (125 MHz,  $\text{D}_2\text{O}$ , 300 K):  $\delta = 93.6$  (C-1), 70.2 (C-2), 66.3 (C-4), 64.6 (C-3), 63.4 (C-5) ppm; IR (ATR-IR):  $\tilde{\nu} = 3342, 2927, 2103, 1674, 1422, 1262, 1203, 1081, 1038, 991, 954, 915, 870, 802, 711, 611, 552$ ; HRMS (ESI-MS):  $m/z = 198.0483$ ,  $[\text{M}+\text{Na}]^+$  (calc. 198.0491 for  $\text{C}_5\text{H}_9\text{N}_3\text{O}_4 + \text{Na}$ ).

#### 5-Azido-5-deoxy- $\alpha,\beta$ -D-arabinofuranose (**40**)<sup>286</sup>

The reported synthesis<sup>286</sup> was modified according to the following procedure: Triacetate **51** (1.00 g, 3.32 mmol) was dissolved in dry methanol (10.0 ml). Sodium methoxide (a spatula tip) was added and the reaction mixture was stirred overnight at rt under a nitrogen atmosphere. After neutralization with Amberlite IR120 ion exchange resin and concentration in vacuo, the crude product was chromatographed on silica gel (cyclohexane/ethyl acetate/methanol, 1:1:0.25) and lyophilized to give the product **40** (557 mg, 3.18 mmol, 96%) as a colorless oil ( $\alpha:\beta$  ratio = 2:1 by integration of the  $^1\text{H}$  NMR spectrum). TLC (cyclohexane/ethyl acetate/methanol, 1:1:0.5):  $R_f = 0.44$ ;  $^1\text{H}$  NMR (500 MHz,  $\text{D}_2\text{O}$ , 300 K):  $\delta = 5.26$  (dd,  $^3J_{1,2} = 3.2$  Hz,  $^4J = 0.8$  Hz, 1H, H-1 ( $\beta$ )), 5.22 (d,  $^3J_{1,2} = 2.8$  Hz, 1H, H-1 ( $\alpha$ )), 4.15 (dt,  $^3J_{3,4} = 6.1$  Hz,  $^3J_{4,5a} = 3.5$  Hz,  $^3J_{4,5b} = 6.1$  Hz, 1H, H-4 ( $\alpha$ )), 4.07-4.03 (m, 2H, H-2 ( $\beta$ ), H-3 ( $\beta$ )), 3.99 (dd,  $^3J_{1,2} = 2.8$  Hz,  $^3J_{2,3} = 4.7$  Hz, 1H, H-2 ( $\alpha$ )), 3.95 (dd,  $^3J_{2,3} = 4.7$  Hz,  $^3J_{3,4} = 6.3$  Hz, 1H, H-3 ( $\alpha$ )), 3.86 (dt,  $^3J_{3,4} = 6.4$  Hz,  $^3J_{4,5a} = 3.6$  Hz,  $^3J_{4,5b} = 6.5$  Hz, 1H, H-4 ( $\beta$ )), 3.62 (dd,  $^3J_{4,5a} = 3.5$  Hz,  $^2J_{5a,5b} = 13.5$  Hz, 1H, H-5a ( $\alpha$ )), 3.57 (dd,  $^3J_{4,5a} = 3.5$  Hz,  $^2J_{5a,5b} = 13.5$  Hz, 1H, H-5a ( $\beta$ )), 3.42 (dd,  $^3J_{4,5b} = 5.9$  Hz,  $^2J_{5a,5b} = 13.6$  Hz, 1H, H-5b ( $\alpha$ )), 3.40 (dd,  $^3J_{4,5b} = 6.5$  Hz,  $^2J_{5a,5b} = 13.5$  Hz, 1H, H-5b ( $\beta$ )) ppm.

#### 5-O-*tert*-Butyldiphenylsilyl- $\alpha,\beta$ -D-arabinofuranose (**41**)<sup>281</sup>

The reported synthesis<sup>281</sup> was modified according to the following procedure: D-Arabinose (6.50 g, 43.3 mmol) was suspended in dry pyridine (50.0 ml). *tert*-Butyl-diphenylsilyl chloride (TBDPSCI, 11.0 ml, 42.3 mmol, 1 eq.) was added and the reaction was stirred overnight at rt under a nitrogen atmosphere. The reaction mixture was concentrated in vacuo. The crude product was chromatographed on silica gel (cyclohexane/ethyl acetate, 2:1) to give arabinofuranose **41** (11.8 g, 30.4 mmol, 70%) as a colorless oil ( $\alpha:\beta$  ratio = 2:1 by integration of the  $^1\text{H}$  NMR spectrum). TLC (cyclohexane/ethyl acetate, 1:1):  $R_f = 0.36$ ;  $^1\text{H}$  NMR (only resonances of  $\alpha$ -anomer are listed) (500 MHz,  $\text{CDCl}_3$ , 300 K, TMS):  $\delta = 7.70$ -7.65 (m, 4H, aryl- $\text{H}_{\text{ortho}}$  ( $\alpha$ )), 7.47-7.38 (m, 6H, aryl- $\text{H}_{\text{meta}}$ , aryl- $\text{H}_{\text{para}}$  ( $\alpha$ )), 5.43 (d~s, 1H, H-1 ( $\alpha$ )), 4.27 (dd,  $^3J_{1,2} = 3.9$  Hz,  $^3J_{2,3} = 1.8$  Hz, 1H, H-2 ( $\alpha$ )), 4.22 (dd~s, 1H, H-3 ( $\alpha$ )), 4.05 (ddd~s, 1 H, H-4 ( $\alpha$ )),

3.83 (dd,  $^3J_{4,5a} = 2.5$  Hz,  $^2J_{5a,5b} = 11.4$  Hz, 1H, H-5a ( $\alpha$ )), 3.73 (dd,  $^3J_{4,5b} = 1.7$  Hz,  $^2J_{5a,5b} = 11.5$  Hz, 1H, H-5b ( $\alpha$ )), 1.05 (s, 9H, C(CH<sub>3</sub>)<sub>3</sub> ( $\alpha$ )) ppm.

#### 5-O-*tert*-Butyldiphenylsilyl-1,2-O-isopropylidene- $\beta$ -D-arabinofuranose (**42**)<sup>281</sup>

The reported synthesis<sup>281</sup> was modified according to the following procedure: The arabinofuranose derivative **41** (8.00 g, 20.6 mmol) was dissolved in dry acetone (50.0 ml) and supplemented with 2,2-dimethoxypropane (25.0 ml, 204 mmol, 10 eq.) and *p*-toluenesulfonic acid (*p*-TsOH, 350 mg, 2.03 mmol, 2 eq.). The reaction mixture was stirred for 3 h at rt under a nitrogen atmosphere. The reaction was cooled with ice and quenched by addition of dist. water. The resulting mixture was extracted with DCM. The combined organic layer was dried over MgSO<sub>4</sub>, filtered and concentrated in vacuo. The crude product was chromatographed on silica gel (cyclohexane/ethyl acetate, 4:1) to give **42** (7.77 g, 18.1 mmol, 87%) as a colorless oil. TLC (cyclohexane/ethyl acetate, 2:1): R<sub>f</sub> = 0.23; <sup>1</sup>H NMR (200 MHz, CDCl<sub>3</sub>, 300 K, TMS):  $\delta = 7.70$ -7.64 (m, 4H, aryl-H<sub>ortho</sub>), 7.45-7.34 (m, 6H, aryl-H<sub>meta</sub>, aryl-H<sub>para</sub>), 5.88 (d,  $^3J_{1,2} = 4.1$  Hz, 1H, H-1), 4.55 (dd~d,  $^3J_{1,2} = 4.1$  Hz, 1H, H-2), 4.43 (dd~d,  $^3J_{3,4} = 2.6$  Hz, 1H, H-3), 4.05 (ddd~dt,  $^3J_{3,4} = 2.5$  Hz,  $^3J_{4,5a} = 6.7$  Hz,  $^3J_{4,5b} = 6.8$  Hz, 1H, H-4), 3.90-3.80 (m, 2H, H-5a, H-5b), 1.81 (s, 1H, OH), 1.34, 1.29 (s each, 3H each, O<sub>2</sub>C(CH<sub>3</sub>)<sub>2</sub>), 1.07 (s, 9H, C(CH<sub>3</sub>)<sub>3</sub>) ppm.

#### 5-O-*tert*-Butyldiphenylsilyl-1,2-O-isopropylidene- $\beta$ -D-lyxofuranose (**43**)<sup>282</sup>

The reported synthesis<sup>282</sup> was modified according to the following procedure: The arabinofuranose derivative **42** (5.00 g, 11.7 mmol) was dissolved in dry DCM (50.0 ml). The solution was cooled with an ice bath and supplemented with dry pyridine (3.00 ml, 37.2 mmol, 3 eq.) and trifluoromethanesulfonic anhydride (Tf<sub>2</sub>O, 4.00 ml, 23.8 mmol, 2 eq.). The reaction mixture was stirred for 2 h under a nitrogen atmosphere. The reaction was quenched by addition of a saturated aqueous NaHCO<sub>3</sub> solution and extracted with DCM. The combined organic layers were washed with dist. water, dried over MgSO<sub>4</sub>, filtered and concentrated in vacuo. The crude residue was dissolved in dry DMF (50.0 ml) and sodium nitrite (8.00 g, 116 mmol, 10 eq.) was added. The reaction mixture was stirred overnight at 70°C under a nitrogen atmosphere. Diethyl ether was added and the organic layer was washed with brine and dist. water, dried over MgSO<sub>4</sub>, filtered and concentrated in vacuo. The crude product was chromatographed on silica gel (cyclohexane/ethyl acetate, 7:1 → 5:1) to give lyxofuranose derivative **43** (2.51 g, 5.86 mmol, 50%) as a white solid. TLC (cyclohexane/ethyl acetate, 4:1): R<sub>f</sub> = 0.22; <sup>1</sup>H NMR (500 MHz, CDCl<sub>3</sub>, 300 K):  $\delta = 7.72$ -7.68 (m, 4H, aryl-H<sub>ortho</sub>), 4.45-7.35 (m, 6H, aryl-H<sub>meta</sub>, aryl-H<sub>para</sub>), 5.72 (d,  $^3J_{1,2} = 4.1$  Hz, 1H, H-1), 4.62 (dd,  $^3J_{1,2} = 4.1$  Hz,  $^3J_{2,3} = 5.9$  Hz, 1H, H-2), 4.34 (ddd~q,  $^3J_{2,3} = 5.9$  Hz,  $^3J_{3,4} = 5.9$  Hz,  $^3J_{3,OH} = 5.9$  Hz, 1H, H-3),

4.19-4.12 (m, 2H, H-4, H-5a), 3.89 (dd,  $^3J_{4,5b} = 5.1$  Hz,  $^2J_{5a,5b} = 9.5$  Hz, 1H, H-5b), 3.06 (d,  $^3J_{3,OH} = 6.4$  Hz, 1H, OH), 1.43, 1.36 (s each, 3H each,  $O_2C(CH_3)_2$ ), 1.07 (s, 9H,  $C(CH_3)_3$ ) ppm.

### 3-Azido-5-O-tert-butylidiphenylsilyl-3-deoxy-1,2-O-isopropylidene- $\beta$ -D-arabinofuranose (**44**)<sup>282</sup>

The reported synthesis<sup>282</sup> was modified according to the following procedure: The lyxofuranose derivative **43** (1.50 g, 3.50 mmol) was dissolved in dry DCM (15.0 ml). The solution was cooled with an ice bath and supplemented with dry pyridine (900  $\mu$ l, 11.2 mmol, 3 eq.) and  $Tf_2O$  (1.20 ml, 7.14 mmol, 2 eq.). The reaction mixture was stirred for 4.5 h under a nitrogen atmosphere. The reaction was quenched by addition of a saturated aqueous  $NaHCO_3$  solution and extracted with DCM. The combined organic layers were washed with dist. water, dried over  $MgSO_4$ , filtered, concentrated in vacuo and co-evaporated with toluene. The crude residue was dissolved in dry DMF (50.0 ml) and sodium azide (1.20 g, 18.5 mmol, 5 eq.) was added. It was stirred for 5 h at 80°C and overnight at rt under a nitrogen atmosphere. Diethyl ether was added and the organic layer was washed with brine and dist. water, dried over  $MgSO_4$ , filtered and concentrated in vacuo. Silica gel chromatography (cyclohexane/ethyl acetate, 20:1) gave the azido derivative **44** (1.19 g, 2.63 mmol, 75%) as a colorless oil. TLC (cyclohexane/ethyl acetate, 18:1):  $R_f = 0.27$ ;  $^1H$  NMR (500 MHz,  $CDCl_3$ , 300 K):  $\delta = 7.69$ -7.65 (m, 4H, aryl- $H_{ortho}$ ), 7.46-7.37 (m, 6H, aryl- $H_{meta}$ , aryl- $H_{para}$ ), 5.84 (d,  $^3J_{1,2} = 4.0$  Hz, 1H, H-1), 4.56 (dd~d,  $^3J_{1,2} = 4.0$  Hz, 1H, H-2), 4.25 (dd~d,  $^3J_{3,4} = 2.7$  Hz, 1H, H-3), 4.11 (ddd,  $^3J_{3,4} = 2.9$  Hz,  $^3J_{4,5a} = 8.0$  Hz,  $^3J_{4,5b} = 5.0$  Hz, 1H, H-4), 3.84 (dd,  $^3J_{4,5a} = 8.1$  Hz,  $^2J_{5a,5b} = 10.3$  Hz, 1H, H-5a), 3.79 (dd,  $^3J_{4,5b} = 5.0$  Hz,  $^2J_{5a,5b} = 10.4$  Hz, 1H, H-5b), 1.35, 1.29 (s each, 3H each,  $O_2C(CH_3)_2$ ), 1.08 (s, 9H,  $C(CH_3)_3$ ) ppm.

### 3-Azido-3-deoxy-1,2-O-isopropylidene- $\beta$ -D-arabinofuranose (**45**)

The azido sugar **44** (1.30 g, 2.86 mmol) was dissolved in dry THF (25.0 ml) and supplemented with tetra-*N*-butylammonium fluoride (TBAF, 1 M solution in THF, 6.00 ml, 6.00 mmol, 2 eq.). The reaction mixture was stirred for 45 min at rt under a nitrogen atmosphere and concentrated in vacuo. The crude product was chromatographed on silica gel (cyclohexane/ethyl acetate, 3:1  $\rightarrow$  2:1) to give **45** (549 mg, 2.56 mmol, 90%) as a white solid. TLC (cyclohexane/ethyl acetate, 3:1):  $R_f = 0.14$ ; rotation value:  $[\alpha]_D^{22} = -0.79$  ( $c = 0.5$ ,  $CH_2Cl_2$ );  $^1H$  NMR (500 MHz,  $CDCl_3$ , 300 K):  $\delta = 5.87$  (d,  $^3J_{1,2} = 4.1$  Hz, 1H, H-1), 4.64 (dd,  $^3J_{1,2} = 4.1$  Hz,  $^3J_{2,3} = 1.5$  Hz, 1H, H-2), 4.06 (ddd~dt,  $^3J_{3,4} = 3.9$  Hz,  $^3J_{4,5a} = 5.4$  Hz,  $^3J_{4,5b} = 5.4$  Hz, 1H, H-4), 4.03 (dd,  $^3J_{2,3} = 1.4$  Hz,  $^3J_{3,4} = 3.8$  Hz, 1H, H-3), 3.80 (dd,  $^3J_{4,5a} = 5.6$  Hz,  $^2J_{5a,5b} = 11.8$  Hz, 1H, H-5a), 3.78 (dd,  $^3J_{4,5b} = 5.1$  Hz,  $^2J_{5a,5b} = 11.8$  Hz, 1H, H-5b), 2.06 (s, 1H, OH), 1.55, 1.35 (s each, 3H each,  $O_2C(CH_3)_2$ ) ppm;  $^{13}C$  NMR (125 MHz,  $CDCl_3$ , 300 K):  $\delta = 113.5$  ( $O_2C(CH_3)_2$ ), 105.4 (C-1), 85.5 (C-2), 85.0 (C-4), 65.5 (C-3), 62.3 (C-5), 27.1, 26.4 ( $O_2C(CH_3)_2$  each) ppm; IR (ATR-IR):  $\tilde{\nu} = 3440, 2988, 2941, 2100, 1458, 1379, 1313, 1247, 1211, 1162, 1083, 1060,$

1014, 949, 857, 837, 812, 780, 693, 615, 552, 519; ESI-MS: $m/z$  = 238.082,  $[M+Na]^+$  (calc. 238.127 for  $C_8H_{13}O_5+Na$ ).

#### 1,2-O-Isopropylidene- $\alpha$ -D-xylofuranose (**46**)<sup>283</sup>

D-Xylose (4.00 g, 26.7 mmol) was dissolved in dry acetone (100 ml) and concentrated sulphuric acid (4.00 ml) was added. The reaction was stirred for 30 min at rt under a nitrogen atmosphere. A solution of  $Na_2CO_3$  (5.20 g) in dist. water (44.8 ml) was added dropwise under cooling with an ice bath and the mixture was stirred for further 3 h. Solid  $Na_2CO_3$  (2.80 g) was added,  $Na_2SO_4$  was filtered off and washed with acetone. The combined filtrates were evaporated. Silica gel chromatography (cyclohexane/ethyl acetate, 1:1) gave the xylofuranose **46** (3.70 g, 19.5 mmol, 73%) as colorless crystals. TLC (cyclohexane/ethyl acetate, 1:1):  $R_f$  = 0.13;  $^1H$  NMR (500 MHz,  $CDCl_3$ , 300 K, TMS):  $\delta$  = 5.98 (d,  $^3J_{1,2}$  = 3.7 Hz, 1H, H-1), 4.52 (dd~d,  $^3J_{1,2}$  = 3.7 Hz, 1H, H-2), 4.32 (dd~d,  $^3J_{3,4}$  = 2.8 Hz, 1H, H-3), 4.18-4.15 (m, 1H, H-4), 4.12 (dd,  $^3J_{4,5a}$  = 3.9 Hz,  $^2J_{5a,5b}$  = 12.5 Hz, 1H, H-5a), 4.03 (dd,  $^3J_{4,5b}$  = 2.8 Hz,  $^2J_{5a,5b}$  = 12.5 Hz, 1H, H-5b), 3.25 (s, 1H, OH), 1.48, 1.32 (s each, 3H each,  $O_2C(CH_3)_2$ ) ppm.

#### 5-O-*tert*-Butyldiphenylsilyl-1,2-O-isopropylidene- $\alpha$ -D-xylofuranose (**47**)<sup>284,285</sup>

The reported synthesis<sup>284,285</sup> was modified according to the following procedure: The arabinofuranose derivative **46** (3.00 g, 15.8 mmol) was dissolved in dry pyridine (25.0 ml) and TBDPSCI (4.00 ml, 15.4 mmol, 1 eq.) was added. The reaction was stirred for 3.5 h at rt under a nitrogen atmosphere. After neutralization with a saturated aqueous  $NaHCO_3$  solution the resulting mixture was extracted with DCM. The combined organic layers were dried over  $MgSO_4$ , filtered and concentrated in vacuo. The crude product was chromatographed on silica gel (cyclohexane/ethyl acetate, 1:1) to give **47** (6.47 g, 15.1 mmol, 96%) as a white solid. TLC (cyclohexane/ethyl acetate, 1:1):  $R_f$  = 0.55;  $^1H$  NMR (500 MHz,  $CDCl_3$ , 300 K, TMS):  $\delta$  = 7.73-7.71 (m, 2H, aryl- $H_{ortho}$ ), 7.69-7.67 (m, 2H, aryl- $H_{ortho}$ ), 7.47-7.38 (m, 6H, aryl- $H_{meta}$ , aryl- $H_{para}$ ), 6.01 (d,  $^3J_{1,2}$  = 3.7 Hz, 1H, H-1), 4.55 (dd~d,  $^3J_{1,2}$  = 3.7 Hz, 1H, H-2), 4.37 (dd~d,  $^3J_{3,4}$  = 2.2 Hz, 1H, H-3), 4.15-4.13 (m, 1H, H-4), 4.12-4.09 (m, 2H, H-5a, H-5b), 4.02 (s, 1H, OH), 1.47, 1.33 (s each, 3H each,  $O_2C(CH_3)_2$ ), 1.05 (s, 9H,  $C(CH_3)_3$ ) ppm.

#### 3-Azido-5-O-*tert*-butyldiphenylsilyl-3-deoxy-1,2-O-isopropylidene- $\alpha$ -D-ribofuranose (**48**)<sup>284,285</sup>

The reported synthesis<sup>284,285</sup> was modified according to the following procedure: The arabinofuranose derivative **47** (4.00 g, 9.33 mmol) was dissolved in dry DCM (30.0 ml). The solution was cooled with an ice bath and supplemented with dry pyridine (2.70 ml, 33.3 mmol, 3.6 eq.) and  $Tf_2O$  (4.00 ml, 23.3 mmol, 2.5 eq.). The reaction mixture was stirred for 5 h under a nitrogen atmosphere. The reaction was quenched by addition of a saturated aqueous  $NaHCO_3$  solution and extracted with DCM. The combined organic layers were washed with



dist. water, dried over  $\text{MgSO}_4$ , filtered, concentrated in vacuo and co-evaporated with toluene. The crude residue was dissolved in dry DMF (50.0 ml) and supplemented with sodium azide (3.00 g, 46.3 mmol, 5 eq.). The reaction mixture was stirred for 5 h at  $80^\circ\text{C}$  and overnight at rt under a nitrogen atmosphere. Diethyl ether was added and the organic layer was washed with brine and dist. water, dried over  $\text{MgSO}_4$ , filtered and concentrated in vacuo. Silica gel chromatography (cyclohexane/ethyl acetate, 18:1) gave the azido derivative **48** (1.93 g, 4.25 mmol, 46%) as a white solid. TLC (cyclohexane/ethyl acetate, 18:1):  $R_f = 0.17$ ;  $^1\text{H NMR}$  (500 MHz,  $\text{CDCl}_3$ , 300 K, TMS):  $\delta = 7.71\text{--}7.67$  (m, 4H, aryl- $\text{H}_{\text{ortho}}$ ),  $7.45\text{--}7.37$  (m, 6H, aryl- $\text{H}_{\text{meta}}$ , aryl- $\text{H}_{\text{para}}$ ), 5.84 (d,  $^3J_{1,2} = 3.7$  Hz, 1H, H-1), 4.78-4.75 (m, 1H, H-2), 4.15 (ddd~dt,  $^3J_{3,4} = 9.4$  Hz,  $^3J_{4,5a} = 2.8$  Hz,  $^3J_{4,5b} = 2.8$  Hz, 1H, H-4), 3.99 (dd,  $^3J_{4,5a} = 2.6$  Hz,  $^2J_{5a,5b} = 11.9$  Hz, 1H, H-5a), 3.79 (dd,  $^3J_{4,5b} = 3.0$  Hz,  $^2J_{5a,5b} = 11.9$  Hz, 1H, H-5b), 3.74 (dd,  $^3J_{2,3} = 4.7$  Hz,  $^3J_{3,4} = 9.4$  Hz, 1H, H-3), 1.58, 1.39 (s each, 3H each,  $\text{O}_2\text{C}(\text{CH}_3)_2$ ), 1.08 (s, 9H,  $\text{C}(\text{CH}_3)_3$ ) ppm.

### 3-Azido-3-deoxy-1,2-O-isopropylidene- $\alpha$ -D-ribofuranose (**49**)<sup>284,285</sup>

The reported synthesis<sup>284,285</sup> was modified according to the following procedure: The azido sugar **48** (1.70 g, 3.75 mmol) was dissolved in dry THF (25.0 ml) and supplemented with TBAF (1 M solution in THF, 7.80 ml, 7.80 mmol, 2 eq.). The reaction mixture was stirred for 45 min at rt under a nitrogen atmosphere and concentrated in vacuo. The crude product was chromatographed (cyclohexane/ethyl acetate, 3:1  $\rightarrow$  2:1) to give **49** (765 mg, 3.56 mmol, 95%) as a white solid. TLC (cyclohexane/ethyl acetate, 3:1):  $R_f = 0.08$ ;  $^1\text{H NMR}$  (500 MHz,  $\text{CDCl}_3$ , 300 K, TMS):  $\delta = 5.81$  (d,  $^3J_{1,2} = 3.7$  Hz, 1H, H-1), 4.75 (dd~t,  $^3J_{1,2} = 4.1$  Hz,  $^3J_{2,3} = 4.1$  Hz, 1H, H-2), 4.13 (ddd~dt,  $^3J_{3,4} = 9.6$  Hz,  $^3J_{4,5a} = 2.7$  Hz,  $^3J_{4,5b} = 2.7$  Hz, 1H, H-4), 4.00 (dd,  $^3J_{4,5a} = 2.4$  Hz,  $^2J_{5a,5b} = 12.7$  Hz, 1H, H-5a), 3.71 (dd,  $^3J_{4,5b} = 3.0$  Hz,  $^2J_{5a,5b} = 12.7$  Hz, 1H, H-5b), 3.60 (dd,  $^3J_{2,3} = 4.7$  Hz,  $^3J_{3,4} = 9.6$  Hz, 1H, H-3), 1.89 (s, 1H, OH), 1.58, 1.37 (s each, 3H each,  $\text{O}_2\text{C}(\text{CH}_3)_2$ ) ppm.

### 5-O-Tosyl-1,2,3-tri-O-acetyl- $\alpha,\beta$ -D-arabinofuranose (**50**)<sup>286</sup>

The reported synthesis<sup>286</sup> was modified according to the following procedure: The arabinofuranose derivative **14** (2.00 g, 7.25 mmol) was dissolved in dry pyridine (20.0 ml). The reaction was cooled with an ice bath and tosyl chloride (TsCl, 3.00 g, 15.6 mmol, 2 eq.) was added slowly. The reaction was warmed to rt and stirred overnight under a nitrogen atmosphere. After addition of a saturated aqueous  $\text{NaHCO}_3$  solution the resulting mixture was extracted with DCM. The combined organic layer was dried over  $\text{MgSO}_4$ , filtered and concentrated in vacuo. The crude product was chromatographed on silica gel (cyclohexane/ethyl acetate, 3:1  $\rightarrow$  2:1) to give **50** (3.00 g, 6.98 mmol, 96%) as a colorless oil ( $\alpha:\beta$  ratio = 2:1 by integration of the  $^1\text{H NMR}$  spectrum). TLC (cyclohexane/ethyl acetate, 2:1):  $R_f = 0.13$ ;  $^1\text{H NMR}$  (500 MHz,  $\text{CDCl}_3$ , 300 K, TMS):  $\delta = 7.79$  (qd,  $^3J_{\text{meta,ortho}} = 8.4$  Hz,

$^4J_{\text{meta,CH}_3} = 1.9$  Hz, 2H, aryl-H<sub>meta</sub> ( $\alpha,\beta$ ), 7.34 (d,  $^3J_{\text{meta,ortho}} = 8.0$  Hz, 2H, aryl-H<sub>ortho</sub> ( $\alpha,\beta$ )), 6.33 (d,  $^3J_{1,2} = 3.9$  Hz, 1H, H-1 ( $\beta$ )), 6.11 (d~s, 1H, H-1 ( $\alpha$ )), 5.31-5.29 (m, 2H, H-2 ( $\beta$ ), H-3 ( $\beta$ )), 5.15 (dd~d,  $^3J_{2,3} = 1.4$  Hz, 1H, H-2 ( $\alpha$ )), 5.00-4.98 (m, 1H, H-3 ( $\alpha$ )), 4.30 (ddd~q,  $^3J_{3,4} = 4.2$  Hz,  $^3J_{4,5a} = 4.2$  Hz,  $^3J_{4,5b} = 4.2$  Hz, 1H, H-4 ( $\alpha$ )), 4.28 (dd,  $^3J_{4,5a} = 6.3$  Hz,  $^2J_{5a,5b} = 10.0$  Hz, 1H, H-5a ( $\beta$ )), 4.27 (dd,  $^3J_{4,5a} = 4.2$  Hz,  $^2J_{5a,5b} = 11.2$  Hz, 1H, H-5a ( $\alpha$ )), 4.24 (dd,  $^3J_{4,5b} = 4.0$  Hz,  $^2J_{5a,5b} = 11.0$  Hz, 1H, H-5b ( $\alpha$ )), 4.19 (dd,  $^3J_{4,5b} = 6.3$  Hz,  $^2J_{5a,5b} = 10.4$  Hz, 1H, H-5b ( $\beta$ )), 4.17-4.14 (m, 1H, H-4 ( $\beta$ )), 2.44 (s, 6H, aryl-CH<sub>3</sub> ( $\alpha,\beta$ )) 2.10, 2.09, 2.08 (s each, 3H each, COCH<sub>3</sub> ( $\alpha$ )), 2.07, 2.06, 2.04 (s each, 3H each, COCH<sub>3</sub> ( $\beta$ )) ppm.

### 5-Azido-5-deoxy-1,2,3-tri-O-acetyl- $\alpha,\beta$ -D-arabinofuranose (**51**)<sup>286</sup>

The reported synthesis<sup>286</sup> was modified according to the following procedure: To a stirring solution of the tosylated molecule **50** (2.50 g, 5.81 mmol) in dry DMF (50.0 ml) sodium azide (1.50 g, 23.3 mmol, 4 eq.) was added. The reaction mixture was heated to 70°C and stirred for 5 h under a nitrogen atmosphere. Dist. water was added and the reaction mixture was extracted with diethyl ether. The combined organic layer was dried over MgSO<sub>4</sub>, filtered and concentrated in vacuo. The crude product was chromatographed on silica gel (cyclohexane/ethyl acetate, 2:1) to give the azido sugar **51** (1.48 g, 4.92 mmol, 85%) as a colorless oil ( $\alpha:\beta$  ratio = 2.5:1 by integration of the <sup>1</sup>H NMR spectrum). TLC (cyclohexane/ethyl acetate, 2:1): R<sub>f</sub> = 0.28; <sup>1</sup>H NMR (500 MHz, CDCl<sub>3</sub>, 300 K, TMS):  $\delta$  = 6.41-6.39 (m, 1H, H-1 ( $\beta$ )), 6.22 (d~s, 1H, H-1 ( $\alpha$ )), 5.39-5.35 (m, 2H, H-2 ( $\beta$ ), H-3 ( $\beta$ )), 5.22 (dd~d,  $^3J_{2,3} = 1.5$  Hz, 1H, H-2 ( $\alpha$ )), 5.04 (ddd,  $^3J_{2,3} = 1.4$  Hz,  $^3J_{3,4} = 4.7$  Hz,  $^4J = 0.7$  Hz, 1H, H-3 ( $\alpha$ )), 4.23 (ddd~dt,  $^3J_{3,4} = 4.7$  Hz,  $^3J_{4,5a} = 3.3$  Hz,  $^3J_{4,5b} = 4.7$  Hz, 1H, H-4 ( $\alpha$ )), 4.12 (ddd~dt,  $^3J_{3,4} = 3.6$  Hz,  $^3J_{4,5a} = 3.6$  Hz,  $^3J_{4,5b} = 6.2$  Hz, 1H, H-4 ( $\beta$ )), 3.68 (dd,  $^3J_{4,5a} = 3.3$  Hz,  $^2J_{5a,5b} = 13.4$  Hz, 1H, H-5a ( $\alpha$ )), 3.60 (dd,  $^3J_{4,5a} = 3.7$  Hz,  $^2J_{5a,5b} = 13.3$  Hz, 1H, H-5a ( $\beta$ )), 3.46 (dd,  $^3J_{4,5b} = 6.3$  Hz,  $^2J_{5a,5b} = 13.3$  Hz, 1H, H-5b ( $\beta$ )), 3.45 (dd,  $^3J_{4,5b} = 4.8$  Hz,  $^2J_{5a,5b} = 13.4$  Hz, 1H, H-5b ( $\alpha$ )), 2.14, 2.12, 2.11 (s each, 3H each, COCH<sub>3</sub> ( $\alpha$ )), 2.11, 2.10, 2.08 (s each, 3H each, COCH<sub>3</sub> ( $\beta$ )) ppm.

### 3-Azido-3-deoxy-1,2,5-tri-O-acetyl- $\alpha,\beta$ -D-arabinose (**52**)

The azido arabinose **38** (50.0 mg, 290  $\mu$ mol) was dissolved in dry pyridine (4.00 ml) and Ac<sub>2</sub>O (1.30 ml, 13.8 mmol, 48 eq.) was added. The reaction mixture was stirred for 2 h at rt under a nitrogen atmosphere and concentrated in vacuo. The crude product was chromatographed on silica gel (cyclohexane/ethyl acetate, 4:1) to give the acetylated azido sugar **52** (69.0 mg, 230  $\mu$ mol, 82%) as a colorless oil ( $\alpha$ -pyranose:  $\beta$ -pyranose: furanose ratio = 3:3:1 according to integration of the <sup>1</sup>H NMR spectrum). TLC (cyclohexane/ethyl acetate/methanol, 1:1:0.25): R<sub>f</sub> = 0.62; rotation value:  $[\alpha]_D^{22} = -83.0^\circ$  (c = 0.42, CH<sub>2</sub>Cl<sub>2</sub>); <sup>1</sup>H NMR (only resonances of  $\alpha$ - and  $\beta$ -pyranose are listed, not the resonances of the minor furanose) (500 MHz, CDCl<sub>3</sub>, 300 K):  $\delta$

= 6.33 (d,  $^3J_{1,2} = 3.5$  Hz, 1H, H-1 ( $\beta$ )), 5.65 (d,  $^3J_{1,2} = 6.6$  Hz, 1H, H-1 ( $\alpha$ )), 5.34 (dd,  $^3J_{1,2} = 3.5$  Hz,  $^3J_{2,3} = 10.9$  Hz, 1H, H-2 ( $\beta$ )), 5.29-5.25 (m, 2H, H-2 ( $\alpha$ ), H-4 ( $\beta$ )), 5.23 (ddd~dt,  $^3J_{3,4} = 2.2$  Hz,  $^3J_{4,5a} = 3.7$  Hz,  $^3J_{4,5b} = 3.7$  Hz, 1H, H-4 ( $\alpha$ )), 4.07 (dd,  $^3J_{4,5a} = 3.9$  Hz,  $^2J_{5a,5b} = 12.9$  Hz, 1H, H-5a ( $\alpha$ )), 3.97 (dd,  $^3J_{4,5a} = 1.5$  Hz,  $^2J_{5a,5b} = 13.2$  Hz, 1H, H-5a ( $\beta$ )), 3.94 (dd,  $^3J_{2,3} = 10.9$  Hz,  $^3J_{3,4} = 3.2$  Hz, 1H, H-3 ( $\beta$ )), 3.85 (dd,  $^3J_{4,5b} = 2.0$  Hz,  $^2J_{5a,5b} = 13.3$  Hz, 1H, H-5b ( $\beta$ )), 3.72 (dd,  $^3J_{4,5b} = 2.2$  Hz,  $^2J_{5a,5b} = 13.1$  Hz, 1H, H-5b ( $\alpha$ )), 3.69 (dd,  $^3J_{2,3} = 9.2$  Hz,  $^3J_{3,4} = 3.8$  Hz, 1H, H-3 ( $\alpha$ )), 2.17, 2.16, 2.15, 2.13, 2.12, 2.10 (s each, 3H each, COCH<sub>3</sub> ( $\alpha,\beta$ )) ppm;  $^{13}\text{C}$  NMR (only resonances of  $\alpha$ - and  $\beta$ -pyranose are listed, not the resonances of the minor furanose) (125 MHz, CDCl<sub>3</sub>, 300 K):  $\delta = 170.1, 169.7, 169.7, 169.2, 169.1, 168.9$  (6 COCH<sub>3</sub>), 92.0 (C-1 ( $\alpha$ )), 89.6 (C-1 ( $\beta$ )), 69.3 (C-4 ( $\beta$ )), 68.7 (C-4 ( $\alpha$ )), 68.4 (C-2 ( $\alpha$ )), 68.0 (C-2 ( $\beta$ )), 64.0 (C-5 ( $\alpha$ )), 62.7 (C-5 ( $\beta$ )), 60.2 (C-3 ( $\alpha$ )), 56.8 (C-3 ( $\beta$ )), 20.9, 20.9, 20.8, 20.7, 20.6 (6 COCH<sub>3</sub>) ppm; IR (ATR-IR):  $\tilde{\nu} = 2099.41, 1738.74, 1436.54, 1371.97, 1210.01, 1054.11, 1031.92, 1002.80, 937.11, 760.29, 731.76, 645.27, 600.70, 551.32, 502.02, 460.37$ ; HRMS (ESI-MS):  $m/z = 324.0802$ , [M+Na]<sup>+</sup> (calc. 324.0808 for C<sub>11</sub>H<sub>15</sub>N<sub>3</sub>O<sub>7</sub>+Na).

### 3-Azido-3-deoxy-1,2,5-tri-O-acetyl- $\alpha,\beta$ -D-ribose (53)

The azido ribose **39** (48.0 mg, 270  $\mu\text{mol}$ ) was dissolved in dry pyridine (4.00 ml) and Ac<sub>2</sub>O (1.30 ml, 13.8 mmol, 50 eq.) was added. The reaction mixture was stirred for 2 h at rt and concentrated in vacuo. Silica gel chromatography (cyclohexane/ethyl acetate, 4:1) gave the acetylated azido sugar **53** (52.0 mg, 170  $\mu\text{mol}$ , 98%) as a colorless oil ( $\alpha$ -pyranose:  $\beta$ -pyranose:  $\beta$ -furanose ratio = 1:6:1 by integration of the  $^1\text{H}$  NMR spectrum). TLC (cyclohexane/ethyl acetate/methanol, 1:1:0.25):  $R_f = 0.64$ ; rotation value:  $[\alpha]_D^{22} = -2.38^\circ$  ( $c = 0.33$ , CH<sub>2</sub>Cl<sub>2</sub>);  $^1\text{H}$  NMR (only resonances of  $\beta$ -pyranose are listed, minor  $\alpha$ -pyranose and furanose resonances are not shown) (500 MHz, CDCl<sub>3</sub>, 300 K):  $\delta = 5.97$  (d,  $^3J_{1,2} = 5.5$  Hz, 1H, H-1 ( $\beta$ )), 5.11 (ddd~dt,  $^3J_{3,4} = 3.9$  Hz,  $^3J_{4,5a} = 3.9$  Hz,  $^3J_{4,5b} = 6.4$  Hz, 1H, H-4 ( $\beta$ )), 5.01 (dd,  $^3J_{1,2} = 5.5$  Hz,  $^3J_{2,3} = 3.6$  Hz, 1H, H-2 ( $\beta$ )), 4.09 (dd~t,  $^3J_{2,3} = 3.5$  Hz,  $^3J_{3,4} = 3.5$  Hz, 1H, H-3 ( $\beta$ )), 3.92 (dd,  $^3J_{4,5a} = 4.1$  Hz,  $^2J_{5a,5b} = 12.3$  Hz, 1H, H-5a ( $\beta$ )) 3.89 (dd,  $^3J_{4,5b} = 6.4$  Hz,  $^2J_{5a,5b} = 12.2$  Hz, 1H, H-5b ( $\beta$ )), 2.16, 2.15, 2.11 (s each, 3H each, COCH<sub>3</sub> ( $\beta$ )) ppm;  $^{13}\text{C}$  NMR (only resonances of  $\beta$ -pyranose are listed, minor  $\alpha$ -pyranose and furanose resonances are not shown) (125 MHz, CDCl<sub>3</sub>, 300 K):  $\delta = 169.9, 169.6, 168.7$  (3 COCH<sub>3</sub> ( $\beta$ )), 90.2 (C-1 ( $\beta$ )), 68.7 (C-2 ( $\beta$ )), 67.4 (C-4 ( $\beta$ )), 62.4 (C-5 ( $\beta$ )), 57.4 (C-3 ( $\beta$ )) 20.8, 20.8, 20.7 (3 COCH<sub>3</sub> ( $\beta$ )) ppm; IR (ATR-IR):  $\tilde{\nu} = 3473, 2936, 2108, 1741, 1432, 1369, 1208, 1138, 1043, 1013, 952, 882, 723, 601, 550, 438$ ; HRMS (ESI-MS):  $m/z = 324.0795$ , [M+Na]<sup>+</sup> (calc. 324.0808 for C<sub>11</sub>H<sub>15</sub>N<sub>3</sub>O<sub>7</sub>+Na).

### 5-Deoxy-5-iodo-1,2,3-tri-O-acetyl- $\alpha,\beta$ -D-arabinofuranose (54)<sup>286</sup>

The reported synthesis<sup>286</sup> was modified according to the following procedure: To a stirring solution of the tosylated molecule **50** (1.00 g, 2.33 mmol) in dry DMF (20.0 ml) sodium iodine

(1.40 g, 9.6 mmol, 4. eq.) was added. The reaction mixture was heated to 80°C and stirred for 5 h under a nitrogen atmosphere. Dist. water was added and the reaction mixture was extracted with diethyl ether. The combined organic layers were dried over MgSO<sub>4</sub>, filtered and concentrated in vacuo. The crude product was chromatographed on silica gel (cyclohexane/ethyl acetate, 2:1) to give the azido sugar **54** (709 mg, 1.84 mmol, 79%) as a colorless oil ( $\alpha$ : $\beta$  ratio = 2:1 by integration of the <sup>1</sup>H NMR spectrum). TLC (cyclohexane/ethyl acetate, 2:1): R<sub>f</sub> = 0.28; <sup>1</sup>H NMR (500 MHz, CDCl<sub>3</sub>, 300 K):  $\delta$  = 6.40 (d, <sup>3</sup>J<sub>1,2</sub> = 4.2 Hz, 1H, H-1 ( $\beta$ )), 6.21 (d-s, 1H, H-1 ( $\alpha$ )), 5.36 (dd, <sup>3</sup>J<sub>1,2</sub> = 4.8 Hz, <sup>3</sup>J<sub>2,3</sub> = 6.6 Hz, 1H, H-2 ( $\beta$ )), 5.34 (dd, <sup>3</sup>J<sub>2,3</sub> = 6.5 Hz, <sup>3</sup>J<sub>3,4</sub> = 4.3 Hz, 1H, H-3 ( $\beta$ )), 5.21 (dd~d, <sup>3</sup>J<sub>2,3</sub> = 1.7 Hz, 1H, H-2 ( $\alpha$ )), 5.00 (dd, <sup>3</sup>J<sub>2,3</sub> = 1.7 Hz, <sup>3</sup>J<sub>3,4</sub> = 4.7 Hz, 1H, H-3 ( $\alpha$ )), 4.25-4.17 (m, 2H, H-4 ( $\alpha,\beta$ )), 3.47-3.34 (m, 4H, H-5a ( $\alpha,\beta$ ), H-5b ( $\alpha,\beta$ )), 2.13, 2.12, 2.11 (s each, 3H each, COCH<sub>3</sub> ( $\alpha$ )), 2.11, 2.10, 2.08 (s each, 3H each, COCH<sub>3</sub> ( $\beta$ )) ppm.

#### 5-Deoxy-5-iodo- $\alpha,\beta$ -D-arabinofuranose (**55**)

The iodo derivative **58** (250 mg, 650  $\mu$ mol) was dissolved in a sodium methoxide/methanol solution (10 mM, 5 ml) and stirred for 1 h at rt under a nitrogen atmosphere. After neutralization with Amberlite IR120 ion exchange resin and concentration in vacuo at a low heat (max. 30°C), the crude product was chromatographed on silica gel (cyclohexane/ethyl acetate/methanol, 1:1:0.25) and lyophilized to give the product **41** (150 mg, 580  $\mu$ mol, 89%) as a white solid ( $\alpha$ : $\beta$  ratio = 1.5:1 by integration of the <sup>1</sup>H NMR spectrum). TLC (cyclohexane/ethyl acetate/methanol, 1:1:0.25): R<sub>f</sub> = 0.3; rotation value:  $[\alpha]_D^{22} = +17.5^\circ$  (c = 0.21, MeOH); <sup>1</sup>H NMR (500 MHz, D<sub>2</sub>O, 300 K):  $\delta$  = 5.27 (d, <sup>3</sup>J<sub>1,2</sub> = 4.7 Hz, 1H, H-1 ( $\beta$ )), 5.23 (d, <sup>3</sup>J<sub>1,2</sub> = 3.0 Hz, 1H, H-1 ( $\alpha$ )), 4.06 (dd, <sup>3</sup>J<sub>1,2</sub> = 4.7 Hz, <sup>3</sup>J<sub>2,3</sub> = 7.2 Hz, 1H, H-2 ( $\beta$ )), 4.03 (dd, <sup>3</sup>J<sub>1,2</sub> = 3.0 Hz, <sup>3</sup>J<sub>2,3</sub> = 4.8 Hz, 1H, H-2 ( $\alpha$ )), 3.99-3.95 (m, 2H, H-3 ( $\beta$ ), H-4 ( $\alpha$ )), 3.90 (dd, <sup>3</sup>J<sub>2,3</sub> = 4.8 Hz, <sup>3</sup>J<sub>3,4</sub> = 6.2 Hz, 1H, H-3 ( $\alpha$ )), 3.82 (ddd~dt, <sup>3</sup>J<sub>3,4</sub> = 6.7 Hz, <sup>3</sup>J<sub>4,5a</sub> = 5.4 Hz, <sup>3</sup>J<sub>4,5b</sub> = 6.9 Hz, 1H, H-4 ( $\beta$ )), 3.45 (dd, <sup>3</sup>J<sub>4,5a</sub> = 4.8 Hz, <sup>2</sup>J<sub>5a,5b</sub> = 11.0 Hz, 1H, H-5a ( $\alpha$ )), 3.44 (dd, <sup>3</sup>J<sub>4,5a</sub> = 5.3 Hz, <sup>2</sup>J<sub>5a,5b</sub> = 10.6 Hz, 1H, H-5a ( $\beta$ )), 3.34 (dd, <sup>3</sup>J<sub>4,5b</sub> = 5.8 Hz, <sup>2</sup>J<sub>5a,5b</sub> = 11.0 Hz, 1H, H-5b ( $\alpha$ )), 3.31 (dd, <sup>3</sup>J<sub>4,5b</sub> = 7.1 Hz, <sup>2</sup>J<sub>5a,5b</sub> = 10.6 Hz, 1H, H-5b ( $\beta$ )) ppm; <sup>13</sup>C NMR (125 MHz, D<sub>2</sub>O, 300 K):  $\delta$  = 101.1 (C-1 ( $\alpha$ )), 95.3 (C-1 ( $\beta$ )), 81.6 (C-4 ( $\alpha$ )), 81.4 (C-2 ( $\alpha$ )), 80.7 (C-4 ( $\beta$ )), 79.2 (C-3 ( $\alpha$ )), 77.9 (C-3 ( $\beta$ )), 76.4 (C-2 ( $\beta$ )), 7.1 (C-5 ( $\beta$ )), 6.5 (C-5 ( $\alpha$ )) ppm.

#### 3-O-Allyl-5-O-*tert*-butyldiphenylsilyl-1,2-O-isopropylidene- $\beta$ -D-arabinofuranose (**56**)

The arabinofuranose derivative **42** (1.00 g, 2.33 mmol) was dissolved in dry DMF (40.0 ml). The solution was cooled with an ice bath and sodium hydride (NaH, 108 mg, 4.50 mmol, 2 eq.) was slowly added. The reaction was stirred for 30 min under ice cooling and a nitrogen atmosphere. Allyl bromide (650  $\mu$ l, 7.52 mmol, 3 eq.) was added and the reaction stirred for 3.5 h at rt. After addition of dist. water the resulting mixture was extracted with diethyl ether.

The combined organic layers were dried over  $\text{MgSO}_4$ , filtered and concentrated in vacuo. The crude product was chromatographed on silica gel (cyclohexane/ethyl acetate, 6:1) to give the fully protected sugar **56** (741 mg, 1.58 mmol, 64%) as a colorless oil. TLC (cyclohexane/ethyl acetate, 4:1):  $R_f = 0.55$ ; rotation value:  $[\alpha]_D^{25} = -0.30^\circ$  ( $c = 0.5$ ,  $\text{CH}_2\text{Cl}_2$ );  $^1\text{H}$  NMR (500 MHz,  $\text{CDCl}_3$ , 300 K):  $\delta = 7.69$ -7.65 (m, 6H, aryl-H<sub>meta</sub>, aryl-H<sub>para</sub>), 7.45-7.35 (m, 4H, aryl-H<sub>ortho</sub>), 5.92 (ddt,  $^3J_{\text{OCHa,CH=CH}_2} = 5.5$  Hz,  $^3J_{\text{OCHb,CH=CH}_2} = 5.5$  Hz,  $^3J_{\text{CH=CH}_2,\text{CH=CH}_2\text{cis}} = 10.5$  Hz,  $^3J_{\text{CH=CH}_2,\text{CH=CH}_2\text{trans}} = 17.2$  Hz, 1H,  $\text{CH=CH}_2$ ), 5.87 (d,  $^3J_{1,2} = 4.1$  Hz, 1H, H-1), 5.32 (dq,  $^4J_{\text{OCHa,CH=CH}_2\text{trans}} = 1.6$  Hz,  $^4J_{\text{OCHb,CH=CH}_2\text{trans}} = 1.6$  Hz,  $^3J_{\text{CH=CH}_2,\text{CH=CH}_2\text{trans}} = 17.2$  Hz,  $^2J_{\text{CH=CH}_2\text{cis,CH=CH}_2\text{trans}} = 1.6$  Hz, 1H,  $\text{CH=CH}_2$ ,trans), 5.22 (ddd,  $^4J_{\text{OCH}_2,\text{CH=CH}_2\text{cis}} = 2.9$  Hz,  $^3J_{\text{CH=CH}_2,\text{CH=CH}_2\text{cis}} = 10.4$  Hz,  $^2J_{\text{CH=CH}_2\text{cis,CH=CH}_2\text{trans}} = 1.3$  Hz, 1H,  $\text{CH=CH}_2$ ,cis), 4.60 (dd-d,  $^3J_{1,2} = 4.1$  Hz, 1H, H-2), 4.18-4.14 (m, 2H, H-3, H-4), 4.13-4.05 (m, 2H, OCHa, OCHb), 3.84-4.05 (m, 2H, H-5a, H-5b), 1.34, 1.29 (s each, 3H each,  $\text{O}_2\text{C}(\text{CH}_3)_2$ ), 1.07 (s, 9H,  $\text{C}(\text{CH}_3)_3$ ) ppm;  $^{13}\text{C}$  NMR (125 MHz,  $\text{CDCl}_3$ , 300 K):  $\delta = 135.6$  (aryl-C<sub>ortho</sub>), 134.0 ( $\text{CH=CH}_2$ ), 133.3, 133.2 (aryl-C<sub>ipso</sub>), 129.7 (aryl-C<sub>para</sub>), 127.7 (aryl-C<sub>meta</sub>), 117.5 ( $\text{CH=CH}_2$ ), 112.4 ( $\text{O}_2\text{C}(\text{CH}_3)_2$ ), 105.7 (C-1), 85.3 (C-4), 85.1 (C-2), 82.7 (C-3), 70.6 ( $\text{OCH}_2$ ), 63.5 (C-5), 27.0, 26.1 ( $\text{O}_2\text{C}(\text{CH}_3)_2$ ), 26.8 ( $\text{OSi}(\text{C}_6\text{H}_5)_2\text{C}(\text{CH}_3)_3$ ), 19.2 ( $\text{OSi}(\text{C}_6\text{H}_5)_2\text{C}(\text{CH}_3)_3$ ) ppm; ESI-MS:  $m/z = 491.4$ ,  $[\text{M}+\text{Na}]^+$  (calc. 491.2 for  $\text{C}_{27}\text{H}_{36}\text{O}_5\text{Si}+\text{Na}$ ).

### 3-O-Allyl-1,2-O-isopropylidene- $\beta$ -D-arabinofuranose (57)

The product **57** was obtained by a different synthetic route as described in literature.<sup>363</sup> The arabinofuranose derivative **56** (500 mg, 1.07 mmol) was dissolved in dry THF (20.0 ml) and supplemented with TBAF (1 M solution in THF, 3.50 ml, 3.50 mmol, 3.3 eq.). The reaction mixture was stirred for 1 h at rt under a nitrogen atmosphere and concentrated in vacuo. The crude product was chromatographed on silica gel (cyclohexane/ethyl acetate, 2:1  $\rightarrow$  1:1) to give **57** (220 mg, 960  $\mu\text{mol}$ , 90%) as a colorless oil. TLC (cyclohexane/ethyl acetate, 4:1):  $R_f = 0.04$ ;  $^1\text{H}$  NMR (500 MHz,  $\text{CDCl}_3$ , 300 K):  $\delta = 5.94$ -5.85 (m, 1H,  $\text{CH=CH}_2$ ), 5.90 (d,  $^3J_{1,2} = 4.3$  Hz, 1H, H-1), 5.31 (dq,  $^4J_{\text{OCHa,CH=CH}_2\text{trans}} = 1.6$  Hz,  $^4J_{\text{OCHb,CH=CH}_2\text{trans}} = 1.6$  Hz,  $^3J_{\text{CH=CH}_2,\text{CH=CH}_2\text{trans}} = 17.2$  Hz,  $^2J_{\text{CH=CH}_2\text{cis,CH=CH}_2\text{trans}} = 1.6$  Hz, 1H,  $\text{CH=CH}_2$ ,trans), 5.23 (ddd,  $^4J_{\text{OCH}_2,\text{CH=CH}_2\text{cis}} = 2.8$  Hz,  $^3J_{\text{CH=CH}_2,\text{CH=CH}_2\text{cis}} = 10.4$  Hz,  $^2J_{\text{CH=CH}_2\text{cis,CH=CH}_2\text{trans}} = 1.3$  Hz, 1H,  $\text{CH=CH}_2$ ,cis), 4.62 (dd,  $^3J_{1,2} = 4.1$  Hz,  $^3J_{2,3} = 0.8$  Hz, 1H, H-2), 4.17-4.13 (m, 1H, H-4), 4.10 (ddt,  $^2J_{\text{OCHa,OCHb}} = 12.7$  Hz,  $^3J_{\text{OCHa,CH=CH}_2} = 5.5$  Hz,  $^4J_{\text{OCHa,CH=CH}_2\text{cis}} = 1.4$  Hz,  $^4J_{\text{OCHa,CH=CH}_2\text{trans}} = 1.4$  Hz, 1H, OCHa), 4.04 (ddt,  $^2J_{\text{OCHa,OCHb}} = 12.7$  Hz,  $^3J_{\text{OCHb,CH=CH}_2} = 5.7$  Hz,  $^4J_{\text{OCHb,CH=CH}_2\text{cis}} = 1.4$  Hz,  $^4J_{\text{OCHb,CH=CH}_2\text{trans}} = 1.4$  Hz, 1H, OCHb), 3.92 (dd,  $^3J_{2,3} = 0.7$  Hz,  $^3J_{3,4} = 3.4$  Hz, 1H, H-3), 3.77-3.75 (m, 2H, H-5a, H-5b), 2.06 (s, 1H, OH), 1.53, 1.34 (s each, 3H each,  $\text{O}_2\text{C}(\text{CH}_3)_2$ ) ppm.

3-O-[6'-N-(tert-Butoxycarbonyl)amino-4'-thiahexyl]-1,2-O-isopropylidene-β-D-arabinofuranose (58)

The arabinofuranose derivative **57** (100 mg, 430 μmol) and Boc protected cysteamine **72** (300 mg, 2.00 mmol, 4.7 eq.) were dissolved in dry methanol (23.0 ml) and 2,2-dimethoxy-2-phenylacetophenone (DPAP, 33.0 mg, 130 μmol, 0.3 eq.) was added. The reaction mixture was degassed with nitrogen and stirred for 1 h at rt under a nitrogen atmosphere while irradiating at  $\lambda_{\max}$  365 nm. After concentration in vacuo, the crude product was chromatographed on silica gel (cyclohexane/ethyl acetate, 2:1 → 1:1) to give **58** (159 mg, 390 μmol, 91%) as a colorless oil. TLC (cyclohexane/ethyl acetate, 1:1):  $R_f$  = 0.29; rotation value:  $[\alpha]_D^{25} = +6.90^\circ$  ( $c = 0.5$ ,  $\text{CH}_2\text{Cl}_2$ );  $^1\text{H}$  NMR (500 MHz,  $\text{CDCl}_3$ , 300 K):  $\delta = 5.88$  (d,  $^3J_{1,2} = 4.1$  Hz, 1H, H-1), 4.92 (s, 1H, NH), 4.59 (dd,  $^3J_{1,2} = 4.1$  Hz,  $^3J_{2,3} = 0.8$  Hz, 1H, H-2), 4.14-4.08 (m, 1H, H-4), 3.86 (dd,  $^3J_{2,3} = 0.7$  Hz,  $^3J_{3,4} = 3.3$  Hz, 1H, H-3), 3.75 (dd,  $^3J_{4,5} = 5.6$  Hz,  $^3J_{5,\text{OH}} = 1.5$  Hz, 2H, H-5a, H-5b), 3.66 (dt,  $^2J_{\text{OCHa},\text{OCHb}} = 9.4$  Hz,  $^3J_{\text{OCHa},\text{OCH}_2\text{CHa}} = 6.0$  Hz,  $^3J_{\text{OCHa},\text{OCH}_2\text{CHb}} = 6.0$  Hz, 1H, OCHa), 3.57 (dt,  $^2J_{\text{OCHa},\text{OCHb}} = 9.4$  Hz,  $^3J_{\text{OCHb},\text{OCH}_2\text{CHa}} = 6.0$  Hz,  $^3J_{\text{OCHb},\text{OCH}_2\text{CHb}} = 6.0$  Hz, 1H, OCHb), 3.30 (d,  $^3J_{\text{SCH}_2,\text{CH}_2\text{NHBoc}} = 4.2$  Hz, 2H,  $\text{CH}_2\text{NHBoc}$ ), 2.62 (dt,  $^2J_{\text{SCHa}/\text{CHaS}}$ ,  $^2J_{\text{SCHb}/\text{CHbS}} = 11.9$  Hz,  $^3J_{\text{SCHa,b}/\text{CHa,bS},\text{CHaNHBoc}/\text{OCH}_2\text{CHa}} = 6.9$  Hz,  $^3J_{\text{SCHa,b}/\text{CHa,bS},\text{CHbNHBoc}/\text{OCH}_2\text{CHb}} = 6.9$  Hz, 4H,  $\text{SCH}_2$ ,  $\text{CH}_2\text{S}$ ), 1.97 (s, 1H, OH), 1.88-1.82 (m, 2H,  $\text{OCH}_2\text{CH}_2$ ) 1.53, 1.33 (s each, 3H each,  $\text{O}_2\text{C}(\text{CH}_3)_2$ ), 1.44 (s, 9H,  $\text{COOC}(\text{CH}_3)_3$ ) ppm;  $^{13}\text{C}$  NMR (125 MHz,  $\text{CDCl}_3$ , 300 K):  $\delta = 155.8$  ( $\text{COOC}(\text{CH}_3)_3$ ), 112.8 ( $\text{O}_2\text{C}(\text{CH}_3)_2$ ), 105.5 (C-1), 85.6 (C-4), 85.1 (C-2), 83.5 (C-3), 79.5 ( $\text{COOC}(\text{CH}_3)_3$ ), 68.0 ( $\text{OCH}_2$ ), 62.7 (C-5), 39.8 ( $\text{CH}_2\text{NHBoc}$ ), 32.2 ( $\text{CH}_2\text{S}$ ), 29.5 ( $\text{OCH}_2\text{CH}_2$ ), 28.4 ( $\text{COOC}(\text{CH}_3)_3$ ), 28.3 ( $\text{SCH}_2$ ), 27.1, 26.3 ( $\text{O}_2\text{C}(\text{CH}_3)_2$ ) ppm; ESI-MS:  $m/z = 430.1$ ,  $[\text{M}+\text{Na}]^+$  (calc. 430.2 for  $\text{C}_{18}\text{H}_{33}\text{NO}_7\text{S}+\text{Na}$ ).

3-O-(6'-Amino-4'-thiahexyl)-α,β-D-arabinose (59)

Thiahexyl derivative **58** (75.0 mg, 180 μmol) was dissolved in DCM (15.0 ml), cooled with ice and supplemented with dist. water (2.00 ml) and TFA (7.00 ml, 91.5 mmol, 500 eq.). The reaction mixture was stirred for 2 h and concentrated in vacuo. The product **59** was co-evaporated with toluene and lyophilized to give a light yellow oil (68.0 mg, 180 μmol, quant.) ( $\alpha$ -pyranose:  $\beta$ -pyranose: furanose ratio = 6:3:1 by integration of the  $^1\text{H}$  NMR spectrum); TLC (methylene chloride/methanol, 4:1):  $R_f = 0.22$ ; rotation value:  $[\alpha]_D^{25} = -35.8^\circ$  ( $c = 0.6$ , MeOH);  $^1\text{H}$  NMR (only resonances of  $\alpha$ - and  $\beta$ -pyranose are listed, not the resonances of the minor furanose): (500 MHz,  $\text{D}_2\text{O}$ , 300 K):  $\delta = 5.18$  (d,  $^3J_{1,2} = 3.7$  Hz, 1H, H-1 ( $\beta$ )), 4.46 (d,  $^3J_{1,2} = 7.8$  Hz, 1H, H-1 ( $\alpha$ )), 4.15-4.13 (m, 1H, H-4 ( $\beta$ )), 4.12-4.08 (m, 1H, H-4 ( $\alpha$ )), 3.95 (dd,  $^3J_{4,5a} = 1.4$  Hz,  $^2J_{5a,5b} = 12.8$  Hz, 1H, H-5a ( $\beta$ )), 3.87 (dd,  $^3J_{4,5a} = 2.2$  Hz,  $^2J_{5a,5b} = 13.1$  Hz, 1H, H-5a ( $\alpha$ )), 3.80 (dd,  $^3J_{1,2} = 3.7$  Hz,  $^3J_{2,3} = 10.0$  Hz, 1H, H-2 ( $\beta$ )), 3.78-3.65 (m, 3H, OCHa ( $\alpha$ ), OCH<sub>2</sub> ( $\beta$ )), 3.63-3.54 (m, 4H, H-3 ( $\beta$ ), H-5b ( $\alpha$ ), H-5b ( $\beta$ ), OCHb ( $\alpha$ )), 3.47 (dd,  $^3J_{1,2} = 7.8$  Hz,  $^3J_{2,3} = 9.8$  Hz, 1H, H-2 ( $\alpha$ )), 3.38 (dd,  $^3J_{2,3} = 10.1$  Hz,  $^3J_{3,4} = 3.7$  Hz, 1H, H-3 ( $\alpha$ )), 3.18 (t,

$^3J_{\text{SCHa,CH}_2\text{NH}_2} = 6.6$  Hz,  $^3J_{\text{SCHb,CH}_2\text{NH}_2} = 6.6$  Hz, 4H, CH<sub>2</sub>NH<sub>2</sub> ( $\alpha,\beta$ ), 2.81 (t,  $^3J_{\text{SCHa,CH}_2\text{NH}_2} = 6.6$  Hz,  $^3J_{\text{SCHb,CH}_2\text{NH}_2} = 6.6$  Hz, 4H, SCH<sub>2</sub> ( $\alpha,\beta$ )), 2.65 (t,  $^3J_{\text{OCH}_2\text{CH}_a,\text{CH}_2\text{S}} = 7.3$  Hz,  $^3J_{\text{OCH}_2\text{CH}_b,\text{CH}_2\text{S}} = 7.3$  Hz, 2H, CH<sub>2</sub>S ( $\alpha$ )), 2.60 (t,  $^3J_{\text{OCH}_2\text{CH}_a,\text{CH}_2\text{S}} = 7.2$  Hz,  $^3J_{\text{OCH}_2\text{CH}_b,\text{CH}_2\text{S}} = 7.2$  Hz, 2H, CH<sub>2</sub>S ( $\beta$ )), 1.89-1.81 (m, 1H, 4H, OCH<sub>2</sub>CH<sub>2</sub> ( $\alpha,\beta$ )) ppm;  $^{13}\text{C}$  NMR (125 MHz, D<sub>2</sub>O, 300 K):  $\delta = 96.8$  (C-1 ( $\beta$ )), 92.6 (C-1 ( $\alpha$ )), 80.4 (C-3 ( $\alpha$ )), 76.6 (C-3 ( $\beta$ )), 70.9 (C-2 ( $\alpha$ )), 67.7, 67.5 (OCH<sub>2</sub> ( $\alpha,\beta$ )), 67.4 (C-2 ( $\beta$ )), 66.3 (C-5 ( $\alpha$ )), 65.6 (C-4 ( $\beta$ )), 65.0 (C-4 ( $\alpha$ )), 62.4 (C-5 ( $\beta$ )), 38.9, 38.3 (CH<sub>2</sub>NH<sub>2</sub> ( $\alpha,\beta$ )), 28.7, 28.6 (SCH<sub>2</sub> ( $\alpha,\beta$ )), 28.2 (OCH<sub>2</sub>CH<sub>2</sub> ( $\alpha,\beta$ )), 27.3 (CH<sub>2</sub>S ( $\alpha,\beta$ )) ppm; HRMS (ESI-MS):  $m/z = 268.1221$ ,  $[\text{M}+\text{H}]^+$  (calc. 268.1213 for C<sub>10</sub>H<sub>22</sub>NO<sub>5</sub>S+H).

#### 5-O-tert-Butyldiphenylsilyl-1,2-O-isopropylidene- $\alpha$ -D-ribofuranose (60)

The product **60** was obtained by a different synthetic route as described in literature.<sup>298</sup> The xylofuranose derivative **47** (4.00 g, 9.32 mmol) was dissolved in dry DCM (40.0 ml). The solution was cooled with an ice bath and supplemented with dry pyridine (2.40 ml, 29.8 mmol, 3 eq.) and Tf<sub>2</sub>O (4.00 ml, 23.8 mmol, 2.5 eq.). The reaction mixture was stirred for 3 h under a nitrogen atmosphere. The reaction was quenched by addition of a saturated aqueous NaHCO<sub>3</sub> solution and extracted with DCM. The combined organic layers were washed with dist. water, dried over MgSO<sub>4</sub>, filtered and concentrated in vacuo. The crude residue was dissolved in dry DMF (50.0 ml) and sodium nitrite (9.00 g, 131 mmol, 14 eq.) was added. The reaction mixture was stirred overnight at 70°C under a nitrogen atmosphere. Diethyl ether was added and the organic layer was washed with brine and dist. water, dried over MgSO<sub>4</sub>, filtered and concentrated in vacuo. The crude product was chromatographed on silica gel (cyclohexane/ethyl acetate, 6:1 → 5:1) to give ribofuranose derivative **60** (1.60 g, 3.73 mmol, 40%) as a colorless solid. TLC (cyclohexane/ethyl acetate, 4:1): R<sub>f</sub> = 0.30;  $^1\text{H}$  NMR (500 MHz, CDCl<sub>3</sub>, 300 K, TMS):  $\delta = 7.71$ -7.68 (m, 4H, aryl-H<sub>ortho</sub>), 7.44-7.36 (m, 6H, aryl-H<sub>meta</sub>, aryl-H<sub>para</sub>), 5.85 (d,  $^3J_{1,2} = 3.8$  Hz, 1H, H-1), 4.60 (dd,  $^3J_{1,2} = 3.9$  Hz,  $^3J_{2,3} = 5.2$  Hz, 1H, H-2), 4.14 (dd,  $^3J_{2,3} = 5.2$  Hz,  $^3J_{3,4} = 8.3$  Hz, 1H, H-3), 3.98-3.94 (m, 1H, H-4), 3.88-3.83 (m, 2H, H-5a, H-5b), 2.11 (s, 1H, OH), 1.56, 1.39 (s each, 3H each, O<sub>2</sub>C(CH<sub>3</sub>)<sub>2</sub>), 1.05 (s, 9H, C(CH<sub>3</sub>)<sub>3</sub>) ppm.

#### 3-O-Allyl-5-O-tert-butylidiphenylsilyl-1,2-O-isopropylidene- $\alpha$ -D-ribofuranose (61)

The ribofuranose derivative **60** (1.00 g, 2.33 mmol) was dissolved in dry DMF (40.0 ml). The solution was cooled with an ice bath and sodium hydride (NaH, 108 mg, 4.50 mmol, 2 eq.) was slowly added. The reaction was stirred for 30 min under ice cooling and a nitrogen atmosphere. Allyl bromide (650  $\mu\text{l}$ , 7.52 mmol, 3 eq.) was added and the reaction stirred for 3.5 h at rt. After addition of dist. water the resulting mixture was extracted with diethyl ether. The combined organic layers were dried over MgSO<sub>4</sub>, filtered and concentrated in vacuo. The crude product was chromatographed on silica gel (cyclohexane/ethyl acetate, 6:1) to give the fully protected sugar **61** (873 mg, 1.87 mmol, 80%) as a colorless oil. TLC (cyclohexane/ethyl acetate, 4:1):

$R_f = 0.55$ ; rotation value:  $[\alpha]_D^{23} = +68.3^\circ$  ( $c = 0.4$ ,  $\text{CH}_2\text{Cl}_2$ );  $^1\text{H NMR}$  (500 MHz,  $\text{CDCl}_3$ , 300 K):  $\delta = 7.73$ -7.66 (m, 4H, aryl- $\text{H}_{\text{ortho}}$ ), 7.45-7.35 (m, 6H, aryl- $\text{H}_{\text{meta}}$ , aryl- $\text{H}_{\text{para}}$ ), 5.96 (ddt,  $^3J_{\text{OCHa,CH=CH}_2} = 5.9$  Hz,  $^3J_{\text{OCHb,CH=CH}_2} = 5.9$  Hz,  $^3J_{\text{CH=CH}_2,\text{CH=CH}_2\text{cis}} = 10.4$  Hz,  $^3J_{\text{CH=CH}_2,\text{CH=CH}_2\text{trans}} = 16.2$  Hz, 1H,  $\text{CH=CH}_2$ ), 5.79 (d,  $^3J_{1,2} = 3.6$  Hz, 1H, H-1), 5.31 (ddd,  $^4J_{\text{OCH}_2,\text{CH=CH}_2\text{trans}} = 3.1$  Hz,  $^3J_{\text{CH=CH}_2,\text{CH=CH}_2\text{trans}} = 17.2$  Hz,  $^2J_{\text{CH=CH}_2\text{cis},\text{CH=CH}_2\text{trans}} = 1.5$  Hz, 1H,  $\text{CH=CH}_2$ ,trans), 5.22 (ddd,  $^4J_{\text{OCH}_2,\text{CH=CH}_2\text{cis}} = 2.6$  Hz,  $^3J_{\text{CH=CH}_2,\text{CH=CH}_2\text{cis}} = 17.2$  Hz,  $^2J_{\text{CH=CH}_2\text{cis},\text{CH=CH}_2\text{trans}} = 1.2$  Hz, 1H,  $\text{CH=CH}_2$ ,cis), 4.65 (dd,  $^3J_{1,2} = 3.6$  Hz,  $^3J_{2,3} = 3.6$  Hz, 1H, H-2), 4.21 (ddt,  $^2J_{\text{OCHa,OCHb}} = 12.8$  Hz,  $^3J_{\text{OCHa,CH=CH}_2} = 5.8$  Hz,  $^4J_{\text{OCHa,CH=CH}_2\text{cis}} = 1.3$  Hz,  $^4J_{\text{OCHa,CH=CH}_2\text{trans}} = 1.3$  Hz, 1H, OCHa), 4.11 (ddt,  $^2J_{\text{OCHa,OCHb}} = 12.8$  Hz,  $^3J_{\text{OCHb,CH=CH}_2} = 5.8$  Hz,  $^4J_{\text{OCHb,CH=CH}_2\text{cis}} = 1.3$  Hz,  $^4J_{\text{OCHb,CH=CH}_2\text{trans}} = 1.3$  Hz, 1H, OCHb), 4.14-4.04 (m, 2H, H-3, H-4), 4.02-3.98 (m, 1H, H-5a), 3.82 (dd,  $^3J_{4,5b} = 2.4$  Hz,  $^2J_{5a,5b} = 11.8$  Hz, 1H, H-5b), 1.58, 1.38 (s each, 3H each,  $\text{O}_2\text{C}(\text{CH}_3)_2$ ), 1.05 (s, 9H,  $\text{C}(\text{CH}_3)_3$ ) ppm;  $^{13}\text{C NMR}$  (125 MHz,  $\text{CDCl}_3$ , 300 K):  $\delta = 135.7$ , 135.6 (aryl- $\text{C}_{\text{ortho}}$ ), 134.8, 134.6 ( $\text{CH=CH}_2$ ), 133.6, 133.2 (aryl- $\text{C}_{\text{ipso}}$ ), 129.7, 129.6 (aryl- $\text{C}_{\text{para}}$ ), 127.7, 127.6 (aryl- $\text{C}_{\text{meta}}$ ), 117.9 ( $\text{CH=CH}_2$ ), 112.9 ( $\text{O}_2\text{C}(\text{CH}_3)_2$ ), 104.0 (C-1), 79.4 (C-4), 77.8 (C-2), 76.8 (C-3), 71.7 (OCH<sub>2</sub>), 61.7 (C-5), 26.9, 26.6 ( $\text{O}_2\text{C}(\text{CH}_3)_2$ ), 26.8 ( $\text{OSi}(\text{C}_6\text{H}_5)_2\text{C}(\text{CH}_3)_3$ ), 19.4 ( $\text{OSi}(\text{C}_6\text{H}_5)_2\text{C}(\text{CH}_3)_3$ ) ppm; ESI-MS:  $m/z = 491.3$ ,  $[\text{M}+\text{Na}]^+$  (calc. 491.2 for  $\text{C}_{27}\text{H}_{36}\text{O}_5\text{Si}+\text{Na}$ ).

### 3-O-Allyl-1,2-O-isopropylidene- $\alpha$ -D-ribofuranose (62)

The product **62** was obtained by a different synthetic route as described in literature.<sup>364</sup> The ribofuranose derivative **61** (800 mg, 1.71 mmol) was dissolved in dry THF (20.0 ml) and supplemented with TBAF (1 M solution in THF, 3.50 ml, 3.50 mmol, 2.0 eq.). The reaction mixture was stirred for 1 h at rt under a nitrogen atmosphere and concentrated in vacuo. The crude product was chromatographed on silica gel (cyclohexane/ethyl acetate, 2:1  $\rightarrow$  1:1) to give **62** (390 mg, 1.70 mmol, 99%) as a colorless oil. TLC (cyclohexane/ethyl acetate, 4:1):  $R_f = 0.04$ ;  $^1\text{H NMR}$  (500 MHz,  $\text{CDCl}_3$ , 300 K):  $\delta = 5.95$  (ddt,  $^3J_{\text{OCHa,CH=CH}_2} = 5.9$  Hz,  $^3J_{\text{OCHb,CH=CH}_2} = 5.9$  Hz,  $^3J_{\text{CH=CH}_2,\text{CH=CH}_2\text{cis}} = 10.3$  Hz,  $^3J_{\text{CH=CH}_2,\text{CH=CH}_2\text{trans}} = 17.2$  Hz, 1H,  $\text{CH=CH}_2$ ), 5.74 (d,  $^3J_{1,2} = 3.6$  Hz, 1H, H-1), 5.32 (dq,  $^4J_{\text{OCHa,CH=CH}_2\text{trans}} = 1.6$  Hz,  $^4J_{\text{OCHb,CH=CH}_2\text{trans}} = 1.6$  Hz,  $^3J_{\text{CH=CH}_2,\text{CH=CH}_2\text{trans}} = 17.2$  Hz,  $^2J_{\text{CH=CH}_2\text{cis},\text{CH=CH}_2\text{trans}} = 1.6$  Hz, 1H,  $\text{CH=CH}_2$ ,trans), 5.23 (ddd,  $^4J_{\text{OCH}_2,\text{CH=CH}_2\text{cis}} = 2.8$  Hz,  $^3J_{\text{CH=CH}_2,\text{CH=CH}_2\text{cis}} = 10.3$  Hz,  $^2J_{\text{CH=CH}_2\text{cis},\text{CH=CH}_2\text{trans}} = 1.2$  Hz, 1H,  $\text{CH=CH}_2$ ,cis), 4.62 (dd~t,  $^3J_{1,2} = 4.0$  Hz,  $^3J_{2,3} = 4.0$  Hz, 1H, H-2), 4.20 (ddt,  $^2J_{\text{OCHa,OCHb}} = 12.7$  Hz,  $^3J_{\text{OCHa,CH=CH}_2} = 5.7$  Hz,  $^4J_{\text{OCHa,CH=CH}_2\text{cis}} = 1.4$  Hz,  $^4J_{\text{OCHa,CH=CH}_2\text{trans}} = 1.4$  Hz, 1H, OCHa), 4.12-4.05 (m, 2H, H-4, OCHb), 3.94 (dd,  $^3J_{4,5a} = 2.5$  Hz,  $^2J_{5a,5b} = 12.5$  Hz, 1H, H-5a), 3.83 (dd,  $^3J_{2,3} = 4.3$  Hz,  $^3J_{3,4} = 9.1$  Hz, 1H, H-3), 3.67 (dd,  $^3J_{4,5b} = 3.0$  Hz,  $^2J_{5a,5b} = 12.5$  Hz, 1H, H-5b), 1.84 (s, 1H, OH), 1.57, 1.36 (s each, 3H each,  $\text{O}_2\text{C}(\text{CH}_3)_2$ ) ppm.



### 3-O-[6'-N-(tert-Butoxycarbonyl)amino-4'-thiahexyl]-1,2-O-isopropylidene- $\alpha$ -D-ribofuranose (63)

The ribofuranose derivative **62** (150 mg, 650  $\mu$ mol) and Boc protected cysteamine **72** (460 mg, 3.07 mmol, 4.7 eq.) were dissolved in dry methanol (23.0 ml) and catalytic amounts of azobisisobutyronitrile (AIBN) were added. The reaction mixture was stirred for 6 h at 70°C under a nitrogen atmosphere. After addition of DCM the organic layer was washed with brine and dist. water, dried over MgSO<sub>4</sub>, filtered and concentrated in vacuo. The crude product was chromatographed on silica gel (cyclohexane/ethyl acetate, 1:1) to give thiahexyl derivative **63** (160 mg, 390  $\mu$ mol, 60%) as a colorless oil. TLC (cyclohexane/ethyl acetate, 1:1): R<sub>f</sub> = 0.09; rotation value:  $[\alpha]_D^{23} = +59.0^\circ$  (c = 0.3, CH<sub>2</sub>Cl<sub>2</sub>); <sup>1</sup>H NMR (500 MHz, CDCl<sub>3</sub>, 300 K):  $\delta$  = 5.76 (d, <sup>3</sup>J<sub>1,2</sub> = 3.7 Hz, 1H, H-1), 4.96 (s, 1H, NH), 4.64 (dd~t, <sup>3</sup>J<sub>1,2</sub> = 4.0 Hz, <sup>3</sup>J<sub>2,3</sub> = 4.0 Hz, 1H, H-2), 4.04 (ddd~dt, <sup>3</sup>J<sub>3,4</sub> = 9.1 Hz, <sup>3</sup>J<sub>4,5a</sub> = 2.7 Hz, <sup>3</sup>J<sub>4,5b</sub> = 2.7 Hz, 1H, H-4), 3.94 (dd, <sup>3</sup>J<sub>4,5a</sub> = 2.5 Hz, <sup>2</sup>J<sub>5a,5b</sub> = 12.4 Hz, 1H, H-5a), 3.80 (dd, <sup>3</sup>J<sub>2,3</sub> = 4.4 Hz, <sup>3</sup>J<sub>3,4</sub> = 9.0 Hz, 1H, H-3), 3.81-3.76 (m, 1H, OCHa), 3.68 (dd, <sup>3</sup>J<sub>4,5b</sub> = 2.9 Hz, <sup>2</sup>J<sub>5a,5b</sub> = 12.4 Hz, 1H, H-5b), 3.57 (dt, <sup>2</sup>J<sub>OCHa,OCHb</sub> = 9.5 Hz, <sup>3</sup>J<sub>OCHb,OCH<sub>2</sub>CHa</sub> = 5.7 Hz, <sup>3</sup>J<sub>OCHb,OCH<sub>2</sub>CHb</sub> = 6.8 Hz, 1H, OCHb), 3.32-3.27 (m, 2H, CH<sub>2</sub>NHBoc), 2.62 (t, <sup>3</sup>J<sub>SCHa,b/CHa,bS,CHaNH<sub>2</sub>Boc/OCH<sub>2</sub>CHa</sub> = 7.1 Hz, <sup>3</sup>J<sub>SCHa,b/CHa,bS,CHbNH<sub>2</sub>Boc/OCH<sub>2</sub>CHb</sub> = 7.1 Hz, 4H, SCH<sub>2</sub>, CH<sub>2</sub>S), 1.84 (s, 1H, OH), 1.93-1.84 (m, 2H, OCH<sub>2</sub>CH<sub>2</sub>) 1.56, 1.35 (s each, 3H each, O<sub>2</sub>C(CH<sub>3</sub>)<sub>2</sub>), 1.44 (s, 9H, COOC(CH<sub>3</sub>)<sub>3</sub>) ppm; <sup>13</sup>C NMR (125 MHz, CDCl<sub>3</sub>, 300 K):  $\delta$  = 155.8 (COOC(CH<sub>3</sub>)<sub>3</sub>), 113.1 (O<sub>2</sub>C(CH<sub>3</sub>)<sub>2</sub>), 104.1 (C-1), 79.5 (COOC(CH<sub>3</sub>)<sub>3</sub>), 78.6 (C-4), 77.8 (C-2), 77.5 (C-3), 68.7 (OCH<sub>2</sub>), 60.5 (C-5), 39.9 (CH<sub>2</sub>NHBoc), 32.3 (CH<sub>2</sub>S), 29.7 (OCH<sub>2</sub>CH<sub>2</sub>), 28.4 (COOC(CH<sub>3</sub>)<sub>3</sub>), 28.2 (SCH<sub>2</sub>), 26.8, 26.5 (O<sub>2</sub>C(CH<sub>3</sub>)<sub>2</sub>) ppm; ESI-MS: m/z = 430.2, [M+Na]<sup>+</sup> (calc. 430.2 for C<sub>18</sub>H<sub>33</sub>NO<sub>7</sub>S+Na).

### 3-O-(6'-Amino-4'-thiahexyl)- $\alpha,\beta$ -D-ribose (64)

Thiahexyl derivative **63** (90.0 mg, 220  $\mu$ mol) was dissolved in DCM (15.0 ml), cooled with ice and supplemented with dist. water (2.00 ml) and TFA (7.00 ml, 91.5 mmol, 400 eq.). The reaction mixture was stirred for 2 h and concentrated in vacuo. The product **64** was co-evaporated with toluene and lyophilized to give a light yellow oil (83.0 mg, 220  $\mu$ mol, quant.) ( $\alpha$ -pyranose:  $\beta$ -pyranose:  $\alpha$ -furanose:  $\beta$ -furanose ratio = 4:4:1:2 by integration of the <sup>1</sup>H NMR spectrum). TLC (methylene chloride/methanol, 4:1): R<sub>f</sub> = 0.25; rotation value:  $[\alpha]_D^{23} = -3.37^\circ$  (c = 0.2, MeOH); <sup>1</sup>H NMR (500 MHz, D<sub>2</sub>O, 300 K):  $\delta$  = 5.29 (d, <sup>3</sup>J<sub>1,2</sub> = 4.1 Hz, 1H, H-1<sub>f</sub> ( $\alpha$ )), 5.20 (d, <sup>3</sup>J<sub>1,2</sub> = 1.6 Hz, 1H, H-1<sub>f</sub> ( $\beta$ )), 4.99 (d, <sup>3</sup>J<sub>1,2</sub> = 4.7 Hz, 1H, H-1<sub>py</sub> ( $\alpha$ )), 4.71 (1H, H-1<sub>py</sub> ( $\beta$ )), 4.16 (dd, <sup>3</sup>J<sub>1,2</sub> = 4.1 Hz, <sup>3</sup>J<sub>2,3</sub> = 5.6 Hz, 1H, H-2<sub>f</sub> ( $\alpha$ )), 4.13-4.07 (m, 2H, H-2<sub>f</sub> ( $\beta$ ), H-4<sub>f</sub> ( $\beta$ )), 3.99-3.92 (m, 4H, H-2<sub>py</sub> ( $\alpha$ ), H-2<sub>py</sub> ( $\beta$ ), H-4<sub>f</sub> ( $\alpha$ ), H-4<sub>py</sub> ( $\alpha$ )), 3.89 (dd, <sup>3</sup>J<sub>4,5a</sub> = 3.7 Hz, <sup>2</sup>J<sub>5a,5b</sub> = 12.8 Hz, 1H, H-5a<sub>py</sub> ( $\alpha$ )), 3.87 (dd, <sup>3</sup>J<sub>4,5a</sub> = 3.4 Hz, <sup>2</sup>J<sub>5a,5b</sub> = 12.2 Hz, 1H, H-5a<sub>py</sub> ( $\beta$ )), 3.83 (t, <sup>3</sup>J<sub>2,3</sub> = 5.4 Hz, <sup>3</sup>J<sub>3,4</sub> = 5.4 Hz, 1H, H-3<sub>f</sub> ( $\beta$ )), 3.76-3.53 (m, 18H, H-3<sub>f</sub> ( $\alpha$ ), H-3<sub>py</sub> ( $\alpha,\beta$ ), H-4<sub>py</sub> ( $\beta$ )), H-5a<sub>f</sub> ( $\alpha,\beta$ ), H-5b<sub>f</sub> ( $\alpha,\beta$ ), H-5b<sub>py</sub> ( $\alpha,\beta$ ), OCH<sub>2,f</sub> ( $\alpha,\beta$ ), OCH<sub>2,py</sub> ( $\alpha,\beta$ )), 2.83-2.79 (m, 8H, CH<sub>2</sub>NH<sub>2,f</sub> ( $\alpha,\beta$ ),

$\text{CH}_2\text{NH}_{2,\text{py}}$  ( $\alpha,\beta$ ), 2.65 (t,  $^3J_{\text{OCH}_2\text{CH}_a,\text{CH}_2\text{S}} = 6.5$  Hz,  $^3J_{\text{OCH}_2\text{CH}_b,\text{CH}_2\text{S}} = 6.5$  Hz, 8H,  $\text{SCH}_{2,\text{f}}$  ( $\alpha,\beta$ ),  $\text{SCH}_{2,\text{py}}$  ( $\alpha,\beta$ ), 2.68-2.61 (m, 8H,  $\text{CH}_2\text{S}_\text{f}$  ( $\alpha,\beta$ ),  $\text{CH}_2\text{S}_{\text{py}}$  ( $\alpha,\beta$ )), 1.91-1.82 (m, 8H,  $\text{OCH}_2\text{CH}_{2,\text{f}}$  ( $\alpha,\beta$ ),  $\text{OCH}_2\text{CH}_{2,\text{py}}$  ( $\alpha,\beta$ )) ppm;  $^{13}\text{C}$  NMR (125 MHz,  $\text{D}_2\text{O}$ , 300 K):  $\delta = 163.0, 162.7$  ( $\text{CF}_3\text{COO}^-$ ), 117.4, 115.2 ( $\text{CF}_3\text{COO}^-$ ), 101.3 (C-1<sub>f</sub> ( $\beta$ )), 96.3 (C-1<sub>f</sub> ( $\alpha$ )), 94.3 (C-1<sub>py</sub> ( $\alpha$ )), 93.9 (C-1<sub>py</sub> ( $\beta$ )), 81.3 (C-4<sub>f</sub> ( $\beta$ )), 80.9, 78.3, 77.7, 76.3, 75.2 (C-4<sub>f</sub> ( $\alpha$ ), C-4<sub>py</sub> ( $\alpha,\beta$ ), C-3<sub>f</sub> ( $\alpha,\beta$ ), C-3<sub>py</sub> ( $\beta$ )), 73.2 (C-2<sub>f</sub> ( $\beta$ )), 70.1 (C-3<sub>py</sub> ( $\alpha$ )), 70.0 (C-2<sub>f</sub> ( $\alpha$ )), 69.4, 69.2, 69.1, 69.0, 67.8 ((C-2<sub>py</sub> ( $\beta$ ),  $\text{OCH}_{2,\text{f}}$  ( $\alpha,\beta$ ),  $\text{OCH}_{2,\text{py}}$  ( $\alpha,\beta$ )), 67.1 (C-2<sub>py</sub> ( $\alpha$ )), 66.1 (C-5<sub>f</sub> ( $\beta$ )), 63.3 (C-5<sub>py</sub> ( $\alpha$ )), 62.6 (C-5<sub>py</sub> ( $\beta$ )), 61.5 (C-5<sub>f</sub> ( $\alpha$ )), 38.3 ( $\text{CH}_2\text{NH}_{2,\text{f}}$  ( $\alpha,\beta$ ),  $\text{CH}_2\text{NH}_{2,\text{py}}$  ( $\alpha,\beta$ )), 28.8, 28.6 ( $\text{SCH}_{2,\text{f}}$  ( $\alpha,\beta$ ),  $\text{SCH}_{2,\text{py}}$  ( $\alpha,\beta$ )), 28.5, 28.2 ( $\text{OCH}_2\text{CH}_{2,\text{f}}$  ( $\alpha,\beta$ ),  $\text{OCH}_2\text{CH}_{2,\text{py}}$  ( $\alpha,\beta$ )), 27.4, 27.3 ( $\text{CH}_2\text{S}_\text{f}$  ( $\alpha,\beta$ ),  $\text{CH}_2\text{S}_{\text{py}}$  ( $\alpha,\beta$ )) ppm; HRMS (ESI-MS):  $m/z = 268.1221$ ,  $[\text{M}+\text{H}]^+$  (calc. 268.1213 for  $\text{C}_{10}\text{H}_{22}\text{NO}_5\text{S}+\text{H}$ ).

### 5-O-tert-Butyldiphenylsilyl-1,2-O-isopropylidene-3-O-methoxymethyl- $\beta$ -D-arabinofuranose

#### (65)

The arabinofuranose derivative **42** (2.00 g, 4.66 mmol) was dissolved in *N,N*-diisopropylethylamine (DIPEA, 30.0 ml) and TBAI (3.50 g, 9.48 mmol, 2 eq.) and chloromethyl methyl ether (MOMCl, 5.20 ml, 68.5 mmol, 15 eq.) were added. The reaction mixture was stirred under a nitrogen atmosphere for 2 h at 60°C and concentrated in vacuo. Ethyl acetate was added and the organic layer was washed with dist. water, dried over  $\text{MgSO}_4$ , filtered and concentrated in vacuo. The crude product was chromatographed on silica gel (cyclohexane/ethyl acetate, 4:1) to give the fully protected sugar **65** (1.91 g, 4.05 mmol, 87%) as colorless oil. TLC (cyclohexane/ethyl acetate, 4:1):  $R_f = 0.36$ ; rotation value:  $[\alpha]_D^{25} = +7.30^\circ$  ( $c = 0.5$ ,  $\text{CH}_2\text{Cl}_2$ );  $^1\text{H}$  NMR (600 MHz,  $\text{CDCl}_3$ , 300 K):  $\delta = 7.72$ -7.63 (m, 4H, aryl-H<sub>ortho</sub>), 7.47-7.31 (m, 6H, aryl-H<sub>meta</sub>, aryl-H<sub>para</sub>), 5.88 (d,  $^3J_{1,2} = 4.0$  Hz, 1H, H-1), 4.74, 4.70 (d each,  $^2J_{\text{OCH}_a\text{OCH}_3,\text{OCH}_b\text{OCH}_3} = 6.7$  Hz, 1H each,  $\text{OCH}_2\text{OCH}_3$ ), 4.60 (dd~d,  $^3J_{1,2} = 4.0$  Hz, 1H, H-2), 4.41 (dd~d,  $^3J_{3,4} = 2.2$  Hz, 1H, H-3), 4.17 (ddd,  $^3J_{3,4} = 2.2$  Hz,  $^3J_{4,5a} = 6.0$  Hz,  $^3J_{4,5b} = 7.9$  Hz, 1H, H-4), 3.83 (dd,  $^3J_{4,5a} = 5.5$  Hz,  $^2J_{5a,5b} = 12.3$  Hz, 1H, H-5a), 3.78 (dd,  $^3J_{4,5b} = 7.3$  Hz,  $^2J_{5a,5b} = 13.2$  Hz, 1H, H-5b), 3.39 (s, 3H,  $\text{OCH}_2\text{OCH}_3$ ), 1.33, 1.29 (s each, 3H each,  $\text{O}_2\text{C}(\text{CH}_3)_2$ ), 1.07 (s, 9H,  $\text{C}(\text{CH}_3)_3$ ) ppm;  $^{13}\text{C}$  NMR (125 MHz,  $\text{CDCl}_3$ , 300 K):  $\delta = 135.6, 135.5$  (aryl-C<sub>ortho</sub>), 133.2, 133.1 (aryl-C<sub>ipso</sub>), 129.7, 129.6 (aryl-C<sub>para</sub>), 127.7, 127.6 (aryl-C<sub>meta</sub>), 112.4 ( $\text{O}_2\text{C}(\text{CH}_3)_2$ ), 105.8 (C-1), 95.5 ( $\text{OCH}_2\text{OCH}_3$ ), 86.0 (C-4), 85.3 (C-2), 80.0 (C-3), 63.4 (C-5), 55.7 ( $\text{OCH}_2\text{OCH}_3$ ), 26.9, 26.0 ( $\text{O}_2\text{C}(\text{CH}_3)_2$ ), 26.8 ( $\text{OSi}(\text{C}_6\text{H}_5)_2\text{C}(\text{CH}_3)_3$ ), 19.2 ( $\text{OSi}(\text{C}_6\text{H}_5)_2\text{C}(\text{CH}_3)_3$ ) ppm; ESI-MS:  $m/z = 495.5$ ,  $[\text{M}+\text{Na}]^+$  (calc. 495.2 for  $\text{C}_{26}\text{H}_{36}\text{O}_6\text{Si}+\text{Na}$ ).

#### 1,2-O-Isopropylidene-3-O-methoxymethyl- $\beta$ -D-arabinofuranose (66)

The arabinofuranose derivative **65** (3.00 g, 6.36 mmol) was dissolved in dry THF (50.0 ml) and supplemented with TBAF (1 M solution in THF, 14.0 ml, 14.0 mmol, 2 eq.). The reaction mixture was stirred for 1 h at rt under a nitrogen atmosphere and concentrated in vacuo. The

crude product was chromatographed on silica gel (cyclohexane/ethyl acetate, 2:1 → 1:2) to give the product **66** (1.45 g, 6.20 mmol, 97%) as a colorless oil. TLC (cyclohexane/ethyl acetate, 4:1):  $R_f = 0.07$ ; rotation value:  $[\alpha]_D^{25} = +33.2^\circ$  ( $c = 0.5$ ,  $\text{CH}_2\text{Cl}_2$ );  $^1\text{H NMR}$  (500 MHz,  $\text{CDCl}_3$ , 300 K):  $\delta = 5.88$  (d,  $^3J_{1,2} = 4.0$  Hz, 1H, H-1), 4.72, 4.67 (d each,  $^2J_{\text{OCH}_a\text{OCH}_3, \text{OCH}_b\text{OCH}_3} = 6.8$  Hz, 1H each,  $\text{OCH}_2\text{OCH}_3$ ), 4.62 (dd,  $^3J_{1,2} = 4.0$  Hz,  $^3J_{2,3} = 0.6$  Hz, 1H, H-2), 4.14-4.10 (m, 2H, H-3, H-4), 3.77 (dd,  $^3J_{4,5a} = 6.2$  Hz,  $^2J_{5a,5b} = 11.7$  Hz, 1H, H-5a), 3.73 (dd,  $^3J_{4,5b} = 4.8$  Hz,  $^2J_{5a,5b} = 11.7$  Hz, 1H, H-5b), 3.38 (s, 3H,  $\text{OCH}_2\text{OCH}_3$ ), 2.24 (s, 1H, OH), 1.52, 1.32 (s each, 3H each,  $\text{O}_2\text{C}(\text{CH}_3)_2$ ) ppm;  $^{13}\text{C NMR}$  (125 MHz,  $\text{CDCl}_3$ , 300 K):  $\delta = 112.9$  ( $\text{O}_2\text{C}(\text{CH}_3)_2$ ), 105.5 (C-1), 95.5 ( $\text{OCH}_2\text{OCH}_3$ ), 85.9 (C-3), 85.7 (C-2), 80.7 (C-4), 62.7 (C-5), 55.8 ( $\text{OCH}_2\text{OCH}_3$ ), 27.1, 26.3 ( $\text{O}_2\text{C}(\text{CH}_3)_2$ ) ppm; ESI-MS:  $m/z = 257.2$ ,  $[\text{M}+\text{Na}]^+$  (calc. 257.1 for  $\text{C}_{10}\text{H}_{18}\text{O}_6+\text{Na}$ ).

#### 5-O-Allyl-1,2-O-isopropylidene-3-O-methoxymethyl- $\beta$ -D-arabinofuranose (**67**)

The arabinofuranose derivative **66** (500 mg, 2.14 mmol) was dissolved in dry DMF (40.0 ml). The solution was cooled with an ice bath and sodium hydride (NaH, 100 mg, 4.17 mmol, 2 eq.) was slowly added. The reaction was stirred for 30 min under ice cooling and a nitrogen atmosphere. Allyl bromide (580  $\mu\text{l}$ , 6.71 mmol, 3 eq.) was added and the reaction stirred overnight at rt. After addition of dist. water the resulting mixture was extracted with diethyl ether. The combined organic layers were dried over  $\text{MgSO}_4$ , filtered and concentrated in vacuo. The crude product was chromatographed on silica gel (cyclohexane/ethyl acetate, 4:1) to give the fully protected sugar **67** (520 mg, 1.90 mmol, 89%) as a colorless liquid. TLC (cyclohexane/ethyl acetate, 4:1):  $R_f = 0.45$ ; rotation value:  $[\alpha]_D^{25} = +16.3^\circ$  ( $c = 0.5$ ,  $\text{CH}_2\text{Cl}_2$ );  $^1\text{H NMR}$  (500 MHz,  $\text{CDCl}_3$ , 300 K):  $\delta = 5.94$ -5.85 (m, 1H,  $\text{CH}=\text{CH}_2$ ), 5.88 (d,  $^3J_{1,2} = 3.9$  Hz, 1H, H-1), 5.27 (dq,  $^4J_{\text{OCH}_a, \text{CH}=\text{CH}_2\text{trans}} = 1.6$  Hz,  $^4J_{\text{OCH}_b, \text{CH}=\text{CH}_2\text{trans}} = 1.6$  Hz,  $^3J_{\text{CH}=\text{CH}_2, \text{CH}=\text{CH}_2\text{trans}} = 17.3$  Hz,  $^2J_{\text{CH}=\text{CH}_2\text{cis}, \text{CH}=\text{CH}_2\text{trans}} = 1.6$  Hz, 1H,  $\text{CH}=\text{CH}_2(\text{trans})$ ), 5.17 (ddd,  $^4J_{\text{OCH}_2, \text{CH}=\text{CH}_2\text{cis}} = 2.9$  Hz,  $^3J_{\text{CH}=\text{CH}_2, \text{CH}=\text{CH}_2\text{cis}} = 10.4$  Hz,  $^2J_{\text{CH}=\text{CH}_2\text{cis}, \text{CH}=\text{CH}_2\text{trans}} = 1.3$  Hz, 1H,  $\text{CH}=\text{CH}_2(\text{cis})$ ), 4.71, 4.68 (d each,  $^2J_{\text{OCH}_a\text{OCH}_3, \text{OCH}_b\text{OCH}_3} = 6.8$  Hz, 1H each,  $\text{OCH}_2\text{OCH}_3$ ), 4.60 (dd~d,  $^3J_{1,2} = 4.0$  Hz, 1H, H-2), 4.18-4.13 (m, 2H, H-3, H-4), 4.04 (ddt,  $^2J_{\text{OCH}_a, \text{OCH}_b} = 6.0$  Hz,  $^3J_{\text{OCH}_a, \text{CH}=\text{CH}_2} = 4.7$  Hz,  $^4J_{\text{OCH}_a, \text{CH}=\text{CH}_2\text{cis}} = 1.4$  Hz,  $^4J_{\text{OCH}_a, \text{CH}=\text{CH}_2\text{trans}} = 1.4$  Hz, 2H, OCH<sub>a</sub>, OCH<sub>b</sub>), 3.62 (dd~d,  $^3J_{4,5} = 6.1$  Hz, 2H, H-5a, H-5b), 3.38 (s, 3H,  $\text{OCH}_2\text{OCH}_3$ ), 1.52, 1.33 (s each, 3H each,  $\text{O}_2\text{C}(\text{CH}_3)_2$ ) ppm;  $^{13}\text{C NMR}$  (125 MHz,  $\text{CDCl}_3$ , 300 K):  $\delta = 134.6$  ( $\text{CH}=\text{CH}_2$ ), 117.1 ( $\text{CH}=\text{CH}_2$ ), 112.9 ( $\text{O}_2\text{C}(\text{CH}_3)_2$ ), 105.6 (C-1), 95.7 ( $\text{OCH}_2\text{OCH}_3$ ), 85.5 (C-2), 84.1 (C-3), 80.6 (C-4), 72.3 ( $\text{OCH}_2$ ), 70.1 (C-5), 55.7 ( $\text{OCH}_2\text{OCH}_3$ ), 27.1, 26.3 ( $\text{O}_2\text{C}(\text{CH}_3)_2$ ) ppm; ESI-MS:  $m/z = 297.3$ ,  $[\text{M}+\text{Na}]^+$  (calc. 297.1 for  $\text{C}_{13}\text{H}_{22}\text{O}_6+\text{Na}$ ).

#### 5-O-Allyl- $\alpha,\beta$ -D-arabinofuranose (**68**)

The fully protected sugar **67** (900 mg, 3.28 mmol) was dissolved in DCM (30.0 ml), cooled with ice and supplemented with dist. water (3.00 ml) and TFA (15.0 ml, 196 mmol, 60 eq.). The

reaction mixture was stirred for 1 h under ice cooling and for 1 h at 40°C while concentrating in vacuo. The crude product was chromatographed on silica gel (cyclohexane/ethyl acetate/methanol, 4:4:1) to give the arabinofuranose derivative **68** (520 mg, 2.74 mmol, 84%) as a colorless oil ( $\alpha$ -furanose:  $\beta$ -furanose = 3:2 by integration of the  $^1\text{H}$  NMR spectrum). TLC (cyclohexane/ethyl acetate/methanol, 4:4:1):  $R_f = 0.20, 0.14$ ; rotation value:  $[\alpha]_D^{23} = +25.8^\circ$  ( $c = 0.5$ , MeOH);  $^1\text{H}$  NMR (500 MHz, MeOH- $d_4$ , 300 K):  $\delta = 6.00$ -5.91 (m, 2H,  $\text{CH}=\text{CH}_2$  ( $\alpha, \beta$ )), 5.32 (ddd,  $^4J_{\text{OCH}_2, \text{CH}=\text{CH}_2\text{trans}} = 3.5$  Hz,  $^3J_{\text{CH}=\text{CH}_2, \text{CH}=\text{CH}_2\text{trans}} = 17.3$  Hz,  $^2J_{\text{CH}=\text{CH}_2\text{cis}, \text{CH}=\text{CH}_2\text{trans}} = 1.7$  Hz, 2H,  $\text{CH}=\text{CH}_2$ ,trans ( $\alpha, \beta$ )), 5.21 (d,  $^3J_{1,2} = 3.7$  Hz, 1H, H-1 ( $\beta$ )), 5.22-5.18 (m, 2H,  $\text{CH}=\text{CH}_2$ ,cis ( $\alpha, \beta$ )), 5.15 (d,  $^3J_{1,2} = 2.3$  Hz, 1H, H-1 ( $\alpha$ )), 4.14 (ddd~dt,  $^3J_{3,4} = 6.0$  Hz,  $^3J_{4,5a} = 3.4$  Hz,  $^3J_{4,5b} = 5.9$  Hz, 1H, H-4 ( $\alpha$ )), 4.10-4.06 (m, 5H, H-4 ( $\beta$ ),  $\text{OCH}_2$  ( $\alpha, \beta$ )), 3.98 (dd~t,  $^3J_{2,3} = 6.1$  Hz,  $^3J_{3,4} = 6.1$  Hz, 1H, H-3 ( $\beta$ )), 3.98-3.80 (m, 3H, H-2 ( $\alpha, \beta$ ), H-3 ( $\alpha$ )), 3.68 (dd,  $^3J_{4,5a} = 3.4$  Hz,  $^2J_{5a,5b} = 10.7$  Hz, 2H, H-5a ( $\alpha, \beta$ )), 3.59 (dd,  $^3J_{4,5b} = 5.7$  Hz,  $^2J_{5a,5b} = 10.7$  Hz, 2H, H-5b ( $\alpha, \beta$ )) ppm;  $^{13}\text{C}$  NMR (125 MHz, MeOH- $d_4$ , 300 K):  $\delta = 136.0$  ( $\text{CH}=\text{CH}_2$  ( $\beta$ )), 135.9 ( $\text{CH}=\text{CH}_2$  ( $\alpha$ )), 117.4 ( $\text{CH}=\text{CH}_2$  ( $\alpha, \beta$ )), 103.6 (C-1 ( $\alpha$ )), 97.6 (C-1 ( $\beta$ )), 83.7 (C-4 ( $\alpha, \beta$ )), 83.6 (C-2 ( $\alpha$ )), 82.4 (C-2 ( $\beta$ )), 78.6 (C-3 ( $\alpha$ )), 77.3 (C-3 ( $\beta$ )), 73.3 ( $\text{OCH}_2$  ( $\alpha, \beta$ )), 71.6 (C-5 ( $\alpha, \beta$ )) ppm.

#### 5-O-[6'-N-(tert-Butoxycarbonyl)amino-4'-thiahexyl]- $\alpha, \beta$ -D-arabinofuranose (**69**)

The arabinofuranose derivative **68** (130 mg, 680  $\mu\text{mol}$ ) and Boc protected cysteamine **72** (475 mg, 3.17 mmol, 4.7 eq.) were dissolved in dry methanol (35.0 ml) and 2,2-dimethoxy-2-phenylacetophenone (DPAP, 52.0 mg, 200  $\mu\text{mol}$ , 0.3 eq.) was added. The reaction mixture was degassed with nitrogen and stirred 1 h at rt under a nitrogen atmosphere while irradiating at  $\lambda_{\text{max}}$  365 nm. After concentration in vacuo, the crude product was chromatographed on silica gel (methylene chloride/methanol, 18:1  $\rightarrow$  15:1) to give **69** (187 mg, 510  $\mu\text{mol}$ , 75%) as a colorless oil ( $\alpha$ -furanose:  $\beta$ -furanose = 2:1 by integration of the  $^1\text{H}$  NMR spectrum). TLC (cyclohexane/ethyl acetate/methanol, 4:4:1):  $R_f = 0.125$ ; rotation value:  $[\alpha]_D^{25} = +17.5^\circ$  ( $c = 0.3$ , MeOH);  $^1\text{H}$  NMR (500 MHz, MeOH- $d_4$ , 300 K):  $\delta = 5.21$  (d,  $^3J_{1,2} = 4.4$  Hz, 1H, H-1 ( $\beta$ )), 5.15 (d~dd,  $^3J_{1,2} = 2.4$  Hz,  $^4J_{1,3} = 0.4$  Hz, 1H, H-1 ( $\alpha$ )), 4.13 (ddd~dt,  $^3J_{3,4} = 5.8$  Hz,  $^3J_{4,5a} = 3.4$  Hz,  $^3J_{4,5b} = 3.4$  Hz, 1H, H-4 ( $\alpha$ )), 3.98 (dd~t,  $^3J_{2,3} = 6.2$  Hz,  $^3J_{3,4} = 6.2$  Hz, 1H, H-3 ( $\beta$ )), 3.93 (dd,  $^3J_{1,2} = 2.4$  Hz,  $^3J_{2,3} = 4.2$  Hz, 1H, H-2 ( $\alpha$ )), 3.91 (dd,  $^3J_{1,2} = 4.4$  Hz,  $^3J_{2,3} = 6.4$  Hz, 1H, H-2 ( $\beta$ )), 3.88 (dd,  $^3J_{2,3} = 4.3$  Hz,  $^3J_{3,4} = 6.0$  Hz, 1H, H-3 ( $\alpha$ )), 3.85-3.81 (m, 1H, H-4 ( $\beta$ )), 3.67-3.56 (m, 8H, H-5a,b ( $\alpha, \beta$ ),  $\text{OCH}_2$  ( $\alpha, \beta$ )), 3.24 (t,  $^3J_{\text{SCH}_a, \text{CH}_2\text{NHBoc}} = 7.1$  Hz,  $^3J_{\text{SCH}_b, \text{CH}_2\text{NHBoc}} = 7.1$  Hz, 4H,  $\text{CH}_2\text{NHBoc}$  ( $\alpha, \beta$ )), 2.68-2.60 (m, 8H,  $\text{SCH}_2$  ( $\alpha, \beta$ ),  $\text{CH}_2\text{S}$  ( $\alpha, \beta$ )), 1.91-1.84 (m, 4H,  $\text{OCH}_2\text{CH}_2$  ( $\alpha, \beta$ )), 1.47 (s, 18H,  $\text{COOC}(\text{CH}_3)_3$  ( $\alpha, \beta$ )) ppm;  $^{13}\text{C}$  NMR (125 MHz,  $\text{CDCl}_3$ , 300 K):  $\delta = 158.4$  ( $\text{COOC}(\text{CH}_3)_3$  ( $\alpha, \beta$ )), 103.6 (C-1 ( $\alpha$ )), 97.6 (C-1 ( $\beta$ )), 83.7 (C-4 ( $\alpha$ )), 83.6 (C-2 ( $\alpha$ )), 82.4 (C-4 ( $\beta$ )), 801 (C-2 ( $\beta$ )), 78.6 (C-3 ( $\alpha$ )), 77.3 (C-3 ( $\beta$ )), 74.0 (C-5 ( $\alpha$ )), 72.2 (C-5 ( $\beta$ )), 70.9 ( $\text{OCH}_2$  ( $\alpha, \beta$ )), 70.8 ( $\text{COOC}(\text{CH}_3)_3$  ( $\alpha, \beta$ )), 41.4 ( $\text{CH}_2\text{NHBoc}$  ( $\alpha, \beta$ )), 32.6 ( $\text{CH}_2\text{S}$  ( $\alpha, \beta$ )), 30.9 ( $\text{OCH}_2\text{CH}_2$

( $\alpha,\beta$ ), 29.3 (SCH<sub>2</sub> ( $\alpha,\beta$ )), 28.8 (COOC(CH<sub>3</sub>)<sub>3</sub> ( $\alpha,\beta$ )) ppm; ESI-MS:  $m/z$  = 390.1, [M+Na]<sup>+</sup> (calc. 390.2 for C<sub>15</sub>H<sub>29</sub>NO<sub>7</sub>S+Na).

#### 5-O-(6'-Amino-4'-thiahexyl)- $\alpha,\beta$ -D-arabinofuranose (70)

Thiahexyl derivative **69** (75.0 mg, 200  $\mu$ mol) was dissolved in DCM (15.0 ml), cooled with ice and supplemented with dist. water (2.00 ml) and TFA (7.00 ml, 91.5 mmol, 460 eq.). The reaction mixture was stirred for 7 h under ice cooling and concentrated in vacuo. The product **70** was co-evaporated with toluene and lyophilized to give a colorless oil (76.0 mg, 200  $\mu$ mol, quant.) ( $\alpha$ -furanose:  $\beta$ -furanose = 3:2 by integration of the <sup>1</sup>H NMR spectrum). TLC (methylene chloride/methanol, 4:1): R<sub>f</sub> = 0.29; rotation value:  $[\alpha]_D^{23} = +7.71^\circ$  (c = 0.2, MeOH); <sup>1</sup>H NMR (500 MHz, D<sub>2</sub>O, 300 K):  $\delta$  = 5.23 (d, <sup>3</sup>J<sub>1,2</sub> = 4.6 Hz, 1H, H-1 ( $\beta$ )), 5.18 (d, <sup>3</sup>J<sub>1,2</sub> = 2.7 Hz, 1H, H-1 ( $\alpha$ )), 4.14 (ddd~dt, <sup>3</sup>J<sub>3,4</sub> = 6.4 Hz, <sup>3</sup>J<sub>4,5a</sub> = 3.0 Hz, <sup>3</sup>J<sub>4,5b</sub> = 6.4 Hz, 1H, H-4 ( $\alpha$ )), 4.02 (dd, <sup>3</sup>J<sub>1,2</sub> = 4.6 Hz, <sup>3</sup>J<sub>2,3</sub> = 7.3 Hz, 1H, H-2 ( $\beta$ )), 3.97 (dd, <sup>3</sup>J<sub>1,2</sub> = 2.7 Hz, <sup>3</sup>J<sub>2,3</sub> = 4.4 Hz, 1H, H-2 ( $\alpha$ )), 3.95 (dd~t, <sup>3</sup>J<sub>2,3</sub> = 7.3 Hz, <sup>3</sup>J<sub>3,4</sub> = 7.3 Hz, 1H, H-3 ( $\beta$ )), 3.89 (dd, <sup>3</sup>J<sub>2,3</sub> = 4.4 Hz, <sup>3</sup>J<sub>3,4</sub> = 6.4 Hz, 1H, H-3 ( $\alpha$ )), 3.85 (ddd~dt, <sup>3</sup>J<sub>3,4</sub> = 7.2 Hz, <sup>3</sup>J<sub>4,5a</sub> = 3.1 Hz, <sup>3</sup>J<sub>4,5b</sub> = 7.1 Hz, 1H, H-4 ( $\beta$ )), 3.70-3.54 (m, 8H, H-5a,b ( $\alpha,\beta$ ), OCH<sub>2</sub> ( $\alpha,\beta$ )), 3.17 (t, <sup>3</sup>J<sub>OCH<sub>2</sub>CH<sub>a</sub>,CH<sub>2</sub>S</sub> = 6.1 Hz, <sup>3</sup>J<sub>OCH<sub>2</sub>CH<sub>b</sub>,CH<sub>2</sub>S</sub> = 6.7 Hz, 4H, CH<sub>2</sub>NH<sub>2</sub> ( $\alpha,\beta$ )), 2.81 (t, <sup>3</sup>J<sub>OCH<sub>2</sub>CH<sub>a</sub>,CH<sub>2</sub>S</sub> = 6.7 Hz, <sup>3</sup>J<sub>OCH<sub>2</sub>CH<sub>b</sub>,CH<sub>2</sub>S</sub> = 6.7 Hz, 4H, SCH<sub>2</sub> ( $\alpha,\beta$ )), 2.61 (t, <sup>3</sup>J<sub>OCH<sub>2</sub>CH<sub>a</sub>,CH<sub>2</sub>S</sub> = 7.3 Hz, <sup>3</sup>J<sub>OCH<sub>2</sub>CH<sub>b</sub>,CH<sub>2</sub>S</sub> = 7.3 Hz, 4H, CH<sub>2</sub>S ( $\alpha,\beta$ )), 1.88-1.80 (m, 4H, OCH<sub>2</sub>CH<sub>2</sub> ( $\alpha,\beta$ )) ppm; <sup>13</sup>C NMR (125 MHz, D<sub>2</sub>O, 300 K):  $\delta$  = 101.2 (C-1 ( $\alpha$ )), 95.4 (C-1 ( $\beta$ )), 81.6 (C-4 ( $\alpha$ )), 81.3 (C-2 ( $\alpha$ )), 79.6 (C-4 ( $\beta$ )), 76.1 (C-3 ( $\alpha$ )), 76.0 (C-2 ( $\beta$ )), 74.7 (C-3 ( $\beta$ )), 71.8 (C-5 ( $\beta$ )), 70.2 (C-5 ( $\alpha$ )), 69.7 (OCH<sub>2</sub> ( $\alpha$ )), 69.6 (OCH<sub>2</sub> ( $\beta$ )), 38.3 (CH<sub>2</sub>NH<sub>2</sub> ( $\alpha,\beta$ )), 28.4 (SCH<sub>2</sub> ( $\alpha,\beta$ )), 28.2 (OCH<sub>2</sub>CH<sub>2</sub> ( $\alpha,\beta$ )), 27.3 (CH<sub>2</sub>S<sub>f</sub> ( $\alpha,\beta$ )) ppm;

#### 2-N-(tert-Butoxycarbonyl)amino-ethanethiol (72)<sup>297</sup>

Cysteamine hydrochloride (10.0 g, 87.7 mmol) was suspended in DCM (800 ml) and supplemented with di-*tert*-butyl dicarbonate (19.2 g, 88.0 mmol, 1 eq.). Triethylamine (22.0 ml, 158 mmol, 1.8 eq.) was slowly added and the reaction mixture was stirred 6 h at rt. The crude product was washed with hydrochloric acid (0.5 M), brine and dist. water, dried over MgSO<sub>4</sub>, filtered and concentrated in vacuo. The Boc-protected cysteamine **72** (10.1 g, 87.8 mmol, quant.) was obtained as a colorless liquid. TLC (cyclohexane/ethyl acetate/methanol, 4:4:1): R<sub>f</sub> = 0.75; <sup>1</sup>H NMR (200 MHz, CDCl<sub>3</sub>, 300 K):  $\delta$  = 4.94 (s, 1H, NH<sub>2</sub>Boc), 3.35-3.20 (m, 2H, CH<sub>2</sub>NHBoc), 2.62 (dt, <sup>3</sup>J<sub>H<sub>2</sub>SCH<sub>2</sub>,HSCH<sub>2</sub></sub> = 8.3 Hz, <sup>3</sup>J<sub>H<sub>2</sub>SCH<sub>2</sub>,CH<sub>a</sub>NHBoc</sub> = 6.5 Hz, <sup>3</sup>J<sub>H<sub>2</sub>SCH<sub>2</sub>,CH<sub>b</sub>NHBoc</sub> = 6.5 Hz, 2H, HSCH<sub>2</sub>), 1.43 (s, 9H, COOC(CH<sub>3</sub>)<sub>3</sub>), 2.62 (t, <sup>3</sup>J<sub>H<sub>2</sub>SCH<sub>2</sub>,HSC<sub>H<sub>a</sub></sub></sub> = 8.5 Hz, <sup>3</sup>J<sub>H<sub>2</sub>SCH<sub>2</sub>,HSC<sub>H<sub>b</sub></sub></sub> = 8.5 Hz, 2H, HSCH<sub>2</sub>) ppm.

S-Acetyl-2-N-(tert-butylcarbonyl)amino-ethanethiol (73)

The product **73** was obtained by a different synthetic route as described in literature.<sup>365</sup> The Boc-protected cysteamine **72** (3.00 g, 26.1 mmol) was dissolved in dry pyridine (40.0 ml) and Ac<sub>2</sub>O (4.00 ml, 42.5 mmol, 1.6 eq.) was added. The reaction mixture was stirred for 4 h at rt and concentrated in vacuo. Silica gel chromatography (cyclohexane/ethyl acetate, 4:1) gave the fully protected cysteamine derivative **73** (4.06 g, 23.5 mmol, 90%) as a colorless solid. TLC (cyclohexane/ethyl acetate, 4:1): R<sub>f</sub> = 0.4; <sup>1</sup>H NMR (500 MHz, CDCl<sub>3</sub>, 300 K): δ = 4.80 (s, 1H, NH<sub>2</sub>Boc), 3.29 (s, 2H, CH<sub>2</sub>NHBoc), 2.99 (t, <sup>3</sup>J<sub>AcSCH<sub>2</sub>,CH<sub>2</sub>NHBoc</sub> = 6.6 Hz, <sup>3</sup>J<sub>AcSCH<sub>2</sub>,CH<sub>2</sub>NHBoc</sub> = 6.6 Hz, 2H, AcSCH<sub>2</sub>), 2.34 (s, 3H, COCH<sub>3</sub>), 2.34 (s, 9H, COOC(CH<sub>3</sub>)<sub>3</sub>) ppm.

S-Acetyl-2-amino-ethanethiol (74)<sup>366</sup>

The fully protected cysteamine derivative **73** (1.00 g, 5.78 mmol) was dissolved in DCM (100 ml) and supplemented with TFA (15.0 ml, 196 mmol, 34 eq.). The reaction mixture was stirred for 1 h at rt and concentrated in vacuo. The product **74** was co-evaporated with toluene and a colorless oil was obtained (1.34 g, 5.75 mmol, 99%). TLC (methylene chloride/methanol, 4:1): R<sub>f</sub> = 0.64; <sup>1</sup>H NMR (500 MHz, MeOH-*d*<sub>4</sub>, 300 K): δ = 3.20-3.13 (m, 4H, NH<sub>2</sub>C<sub>2</sub>H<sub>4</sub>SAc), 2.42 (s, 3H, COCH<sub>3</sub>) ppm.

## 4 References

1. World Health Organization. Global tuberculosis report 2015 (2015).
2. World Health Organization. Implementing the WHO Stop TB strategy. A handbook for national tuberculosis control programmes (2008).
3. Nyendak, M. R., Lewinsohn, D. A., Lewinsohn, D. M. New diagnostic methods for tuberculosis. *Curr Opin Infect Dis* **22**, 174-182 (2009).
4. Parsons, L. M. *et al.* Laboratory diagnosis of tuberculosis in resource-poor countries: challenges and opportunities *Clin Microbiol Rev* **24**, 314-350 (2011).
5. Greco, S., Girardi, E., Navarra, A., Saltini, C. Current evidence on diagnostic accuracy of commercially based nucleic acid amplification tests for the diagnosis of pulmonary tuberculosis *Thorax* **61**, 783-790 (2006).
6. Ling, D. I., Flores, L. L., Riley, L. W., Pai, M. Commercial nucleic-acid amplification tests for diagnosis of pulmonary tuberculosis in respiratory specimens: meta-analysis and meta-regression *PLoS One* **3**, e1536 (2008).
7. Boehme, C. C. *et al.* Rapid molecular detection of tuberculosis and rifampin resistance. *N Eng J Med* **363**, 1005-1015 (2010).
8. Lacombe, A. *et al.* GenoType MTBDRplus assay for molecular detection of rifampin and isoniazid resistance in *Mycobacterium tuberculosis* strains and clinical samples. *J Clin Microbiol* **46**, 3660-3667 (2008).
9. Arnold, C. *et al.* Single-nucleotide polymorphism-based differentiation and drug resistance detection in *Mycobacterium tuberculosis* from isolates or directly from sputum. *Clin Microbiol Infect* **11**, 122-130 (2005).
10. Andersen, P., Munk, M. E., Pollock, J. M., Doherty, T. M. Specific immune-based diagnosis of tuberculosis. *Lancet* **356**, 1099-1104 (2000).
11. Huebner, R. E., Schein, M. F., Bass, J. B. The tuberculin skin test. *Clin Infect Dis* **17**, 968-975 (1993).
12. Van Pinxteren, L. A. H., Ravn, P., Agger, E. M., Pollock, J., Andersen, P. Diagnosis of tuberculosis based on the two specific antigens ESAT-6 and CFP10. *Clin Diagn Lab Immunol* **7**, 155-160 (2000).
13. Ravn, P. *et al.* Prospective evaluation of a whole-blood test using *Mycobacterium tuberculosis*-specific antigens ESAT-6 and CFP-10 for diagnosis of active tuberculosis. *Clin Diagn Lab Immunol* **12**, 491-496 (2005).
14. Walzl, G., Ronacher, K., Djoba Siawaya, J. F., Dockrell, H. M. Biomarkers for TB treatment response: challenges and future strategies. *J Infect* **57**, 103-109 (2008).
15. Wallis, R. S. *et al.* Induction of the antigen 85 complex of *Mycobacterium tuberculosis* in sputum: a determinant of outcome in pulmonary tuberculosis treatment. *J Infect Dis* **178**, 1115-1121 (1998).
16. Pereira Arias-Bouda, L. M. *et al.* Development of antigen detection assay for diagnosis of tuberculosis using sputum samples. *J Clin Microbiol* **38**, 2278-2283 (2000).
17. Hamasur, B. *et al.* Rapid diagnosis of tuberculosis by detection of mycobacterial lipoarabinomannan in urine. *J Microbiol Methods* **45**, 41-52 (2001).
18. Boehme, C. *et al.* Detection of mycobacterial lipoarabinomannan with an antigen-capture ELISA in unprocessed urine of Tanzanian patients with suspected tuberculosis. *Trans R Soc Trop Med Hyg* **99**, 893-900 (2005).

19. Minion, J. *et al.* Diagnosing tuberculosis with urine lipoarabinomannan: systematic review and meta-analysis. *Eur Respir J* **38**, 1398-1405 (2011).
20. Yang, C. M., Hsu, C. H., Lee, C. M., Wang, F. C. Intense uptake of [F-18]-fluoro-2 deoxy-D-glucose in active pulmonary tuberculosis. *Ann Nucl Med* **17**, 407-410 (2003).
21. Chen, R. Y. *et al.* PET/CT imaging correlates with treatment outcome in patients with multidrug-resistant tuberculosis. *Sci Transl Med.* **6**, 265ra166 (2014).
22. Russell, D. G., Barry, C. E. 3rd, Flynn, J. L. Tuberculosis: what we don't know can, and does, hurt us. *Science* **328**, 852-856 (2010).
23. Capon, A. W. Streptomycin, PAS and isoniazid in the treatment of pulmonary tuberculosis. *Can Med Assoc J* **70**, 62-67 (1954).
24. Falzon, D. *et al.* WHO guidelines for the programmatic management of drug-resistant tuberculosis: 2011 update. *Eur Respir J* **38**, 516-528 (2011).
25. Ling, L. L. *et al.* A new antibiotic kills pathogens without detectable resistance. *Nature* **517**, 455-459 (2015).
26. Gomez, J. E., McKinney, J. D. *M. tuberculosis* persistence, latency, and drug tolerance. *Tuberculosis* **84**, 29-44 (2004).
27. Nathan, C., Barry, C. E. 3rd TB drug development: immunology at the table. *Immunol Rev* **264**, 308-318 (2015).
28. Kremer, L. S., Besra, G. S. Current status and future development of antitubercular chemotherapy. *Expert Opin Investig Drugs* **11**, 1033-1049 (2002).
29. Suarez, J. *et al.* An oxyferrous heme/protein-based radical intermediate is catalytically competent in the catalase reaction of *Mycobacterium tuberculosis* catalase-peroxidase (KatG). *J Biol Chem* **284**, 7017-7029 (2009).
30. Lee, R. E., Mikusova, K., Brennan, P. J., Besra, G. S. Synthesis of the arabinose donor  $\beta$ -D-arabinofuranosyl-1-monophosphoryldecaprenol, development of a basic arabinosyl-transferase assay, and identification of ethambutol as an arabinosyl transferase inhibitor. *J Am Chem Soc* **117**, 11829-11832 (1995).
31. Calvori, C., Frontali, L., Leoni, L., Tecce, G. Effect of rifamycin on protein synthesis. *Nature* **207**, 417-418 (1965).
32. Shi, W. *et al.* Pyrazinamide inhibits trans-translation in *Mycobacterium tuberculosis*. *Science* **333**, 1630-1632 (2011).
33. Koch, R. Die Ätiologie der Tuberkulose. *Berliner Klinische Wochenschrift*, 428-445 (1882).
34. Cole, S. T. *et al.* Deciphering the biology of *Mycobacterium tuberculosis* from the complete genome sequence. *Nature* **393**, 537-544 (1998).
35. de Jong, B. C., Antonio, M. & Gagneux, S. *Mycobacterium africanum*-review of an important cause of human tuberculosis in West Africa. *PLoS Negl Trop Dis* **4**, e744 (2010).
36. Fabre, M. *et al.* Molecular characteristics of "*Mycobacterium canettii*" the smooth *Mycobacterium tuberculosis* bacilli. *Infect Genet Evol* **10**, 1165-1173 (2010).
37. Koeck, J. L. *et al.* Clinical characteristics of the smooth tubercle bacilli '*Mycobacterium canettii*' infection suggest the existence of an environmental reservoir. *Clin Microbiol Infect* **17**, 1013-1019 (2011).



38. Smith, N. H. *et al.* Ecotypes of the *Mycobacterium tuberculosis* complex. *J Theor Biol* **239**, 220-225 (2006).
39. Grange, J. M. *Mycobacterium bovis* infection in human beings. *Tuberculosis* **81**, 71-77 (2001).
40. Smith, N. H., Gordon, S. V., de la Rúa-Domenech, R., Clifton-Hadley, R. S., Hewinson, R. G. Bottlenecks and broomsticks: the molecular evolution of *Mycobacterium bovis*. *Nat Rev Microbiol* **4**, 670-681 (2006).
41. Gagneux, S., Small, P. M. Global phylogeography of *Mycobacterium tuberculosis* and implications for tuberculosis product development. *Lancet Infect Dis* **7**, 328-337 (2007).
42. Brosch, R. *et al.* A new evolutionary scenario for the *Mycobacterium tuberculosis* complex. *Proc Natl Acad Sci USA* **99**, 3684-3689 (2002).
43. Gagneux, S. Host-pathogen coevolution in human tuberculosis. *Phil Trans R Soc B* **367**, 850-859 (2012).
44. Brudey, K. *et al.* *Mycobacterium tuberculosis* complex genetic diversity: mining the fourth international spoligotyping database (SpolDB4) for classification, population genetics and epidemiology. *BMC Microbiol* **6**, 23 (2006).
45. Gagneux, S. *et al.* Variable host-pathogen compatibility in *Mycobacterium tuberculosis*. *Proc Natl Acad Sci USA* **103**, 2869-2873 (2006).
46. Reiling, N. *et al.* Clade-specific virulence patterns of *Mycobacterium tuberculosis* complex strains in human primary macrophages and aerogenically infected mice. *mBio* **4**, e00250-13 (2013).
47. Homolka, S., Niemann, S., Russell, D. G., Rohde, K. H. Functional genetic diversity among *Mycobacterium tuberculosis* complex clinical isolates: delineation of conserved core and lineage-specific transcriptomes during intracellular survival. *PLoS Pathog* **6**, e1000988 (2010).
48. Comas, I. *et al.* Out-of-Africa migration and Neolithic coexpansion of *Mycobacterium tuberculosis* with modern humans. *Nat Genet* **45**, 1176-1182 (2013).
49. Barry, C. E. 3rd Interpreting cell wall 'virulence factors' of *Mycobacterium tuberculosis*. *Trends Microbiol* **9**, 237-241 (2001).
50. Olsen, G. J., Woese, C. R. Ribosomal RNA: a key to phylogeny. *FASEB J* **7**, 113-123 (1993).
51. Woese, C. R. Bacterial evolution. *Microbiol Rev* **51**, 221-271 (1987).
52. Fu, L. M., Fu-Liu, C. S. Is *Mycobacterium tuberculosis* a closer relative to Gram-positive or Gram-negative bacterial pathogens? *Tuberculosis* **82**, 85-90 (2002).
53. Hoffmann, C., Leis, A., Niederweis, M., Plitzko, J. M., Engelhardt, H. Disclosure of the mycobacterial outer membrane: cryo-electron tomography and vitreous sections reveal the lipid bilayer structure. *Proc Natl Acad Sci USA* **105**, 3963-3967 (2008).
54. Zuber, B. *et al.* Direct visualization of the outer membrane of mycobacteria and corynebacteria in their native state. *J Bacteriol* **190**, 5672-5680 (2008).
55. Brennan, P. J., Crick, D. C. The cell-wall core of *Mycobacterium tuberculosis* in the context of drug Discovery. *Curr Top Med Chem* **7**, 475-488 (2007).
56. Wietzerbin, J. *et al.* Occurrence of D-alanyl-D-meso-diaminopimelic acid and meso-diaminopimelyl-meso-diaminopimelic acid interpeptide linkages in the peptidoglycan of mycobacteria. *Biochemistry* **13**, 3471-3476 (1974).

57. Schleifer, K. H., Kandler, O. Peptidoglycan types of bacterial cell walls and their taxonomic implications. *Bacteriol Rev* **36**, 407-477 (1972).
58. McNeil, M., Daffe, M., Brennan, P. J. Evidence of the nature of the link between the arabinogalactan and peptidoglycan of the mycobacterial cell wall. *J Biol Chem* **265**, 18200-18206 (1990).
59. Daffe, M., Brennan, P. J., McNeil, M. Predominant structural features of the cell wall arabinogalactan of *Mycobacterium tuberculosis* as revealed through characterization of oligoglycosyl alditol fragments by gas chromatography/mass spectrometry and by <sup>1</sup>H and <sup>13</sup>C NMR analyses. *J Biol Chem* **265**, 6734-6743 (1990).
60. McNeil, M., Daffe, M., Brennan, P. J. Location of the mycolyl ester substituents in the cell walls of mycobacteria. *J Biol Chem* **266**, 13217-13223 (1991).
61. Hong, S. *et al.* Ultralong C100 mycolic acids support the assignment of *Segniliparus* as a new bacterial genus. *PLoS One* **7**, e39017 (2012).
62. Barry, C. E. 3rd *et al.* Mycolic acids: structure, biosynthesis and physiological functions. *Prog Lipid Res* **37**, 143-179 (1998).
63. Besra, G. S., Brennan, P. J. The mycobacterial cell wall: biosynthesis of arabinogalactan and lipoarabinomannan. *Biochem Soc Trans* **25**, 845-850 (1997).
64. Marrakchi, H., Lanéelle, M. A., Daffé, M. Mycolic acids: structures, biosynthesis, and beyond. *Chem Biol* **21**, 67-85 (2014).
65. Hunter, S. W., Brennan, P. J. Evidence for the presence of a phosphatidylinositol anchor on the lipoarabinomannan and lipomannan of *Mycobacterium tuberculosis*. *J Biol Chem* **265**, 9272-9279 (1990).
66. Korduláková, J. *et al.* Identification of the required acyltransferase step in the biosynthesis of the phosphatidylinositol mannosides of mycobacterium species. *J Biol Chem* **278**, 36285-36295 (2003).
67. Hsu, F. F., Turk, J., Owens, R. M., Rhoades, E. R., Russell, D. G. Structural characterization of phosphatidylmyo-inositol mannosides from *Mycobacterium bovis* *Bacillus Calmette Guérin* by multiple-stage quadrupole ion-trap mass spectrometry with electrospray ionization. II. Monoacyl- and diacyl-PIMs. *J Am Soc Mass Spectrom* **18**, 479-492 (2007).
68. Briken, V., Porcelli, S. A., Besra, G. S., Kremer, L. Mycobacterial lipoarabinomannan and related lipoglycans: from biogenesis to modulation of the immune response. *Mol Microbiol* **53**, 391-403 (2004).
69. Nigou, J., Gilleron, M., Puzo, G. Lipoarabinomannans: from structure to biosynthesis. *Biochimie* **85**, 153-166 (2003).
70. Chatterjee, D., Khoo, K. H. The surface glycopeptidolipids of mycobacteria: structures and biological properties. *Cell Mol Life Sci* **58**, 2018-2042 (2001).
71. Khoo, K. H., Dell, A., Morris, H. R., Brennan, P. J., Chatterjee, D. Inositol phosphate capping of the nonreducing termini of lipoarabinomannan from rapidly growing strains of *Mycobacterium*. *J Biol Chem* **270**, 12380-12389 (1995).
72. Guerardel, Y. *et al.* Structural study of lipomannan and lipoarabinomannan from *Mycobacterium chelonae*. Presence of unusual components with alpha 1,3-mannopyranose side chains. *J Biol Chem* **277**, 30635-30648 (2002).
73. Fujiwara, N. Distribution of antigenic glycolipids among *Mycobacterium tuberculosis* strains and their contribution to virulence. *Kekkaku* **72**, 193-205 (1997).

74. Sarathy, J. P., Dartois, V., Lee, E. J. D. The role of transport mechanisms in *Mycobacterium tuberculosis* drug resistance and tolerance. *Pharmaceuticals* **5**, 1210-1235 (2012).
75. Elbein, A. D., Pan, Y. T., Pastuszak, I., Carroll, D. New insights on trehalose: a multifunctional molecule. *Glycobiology* **13**, 17R-27R (2003).
76. Berg, S., Kaur, D., Jackson, M., Brennan, P. J. The glycosyltransferases of *Mycobacterium tuberculosis* - roles in the synthesis of arabinogalactan, lipoarabinomannan, and other glycoconjugates. *Glycobiology* **17**, 35-56R (2007).
77. Webb, K. M., DiRuggiero, J. Role of Mn<sup>2+</sup> and compatible solutes in the radiation resistance of thermophilic bacteria and archaea. *Archaea* **2012**, 845756 (2012).
78. Lee, J. *et al.* Trehalose glycopolymers as excipients for protein stabilization. *Biomacromolecules* **14**, 2561-2569 (2013).
79. Iturriaga, G., Suárez, R., Nova-Franco, B. Trehalose metabolism: from osmoprotection to signaling. *Int J Mol Sci* **10**, 3793-3810 (2009).
80. Lang, R. Recognition of the mycobacterial cord factor by Mincle: relevance for granuloma formation and resistance to tuberculosis. *Front Immunol* **4**, 5 (2013).
81. Billi, D., Potts, M. Life and death of dried prokaryotes. *Res Microbiol* **153**, 7-12 (2002).
82. Nobre, A., Alarico, S., Maranhã, A., Mendes, V., Empadinhas, N. The molecular biology of mycobacterial trehalose in the quest for advanced tuberculosis therapies. *Microbiology* **160**, 1547-1570 (2014).
83. De Smet, K. A., Weston, A., Brown, I. N., Young, D. B., Robertson, B. D. Three pathways for trehalose biosynthesis in mycobacteria. *Microbiology* **146**, 199-208 (2000).
84. Tahlan, K. *et al.* SQ109 targets MmpL3, a membrane transporter of trehalose monomycolate involved in mycolic acid donation to the cell wall core of *Mycobacterium tuberculosis*. *Antimicrob Agents Chemother* **56**, 1797-1809 (2012).
85. Grzegorzewicz, A. E. *et al.* Inhibition of mycolic acid transport across the *Mycobacterium tuberculosis* plasma membrane. *Nat Chem Biol* **8**, 334-341 (2012).
86. Sathyamoorthy, N., Takayama, K. Purification and characterization of a novel mycolic acid exchange enzyme from *Mycobacterium smegmatis*. *J Biol Chem* **262**, 13417-13423 (1987).
87. Kalscheuer, R., Weinrick, B., Veeraraghavan, U., Besra, G. S., Jacobs, W. R. Trehalose-recycling ABC transporter LpqY-SugA-SugB-SugC is essential for virulence of *Mycobacterium tuberculosis*. *Proc Natl Acad Sci USA* **107**, 21761-21766 (2010).
88. Swarts, B. M. *et al.* Probing the mycobacterial trehalome with bioorthogonal chemistry. *J Am Chem Soc* **134**, 16123-16126 (2012).
89. Fincher, G. B., Stone, B. A., Clarke, A. E. Arabinogalactan-Proteins: Structure, Biosynthesis, and Function. *Ann Rev Plant Physiol* **34**, 47-70 (1983).
90. Dobson, D. E. *et al.* Identification of genes encoding arabinosyltransferases (SCA) mediating developmental modifications of lipophosphoglycan required for sand fly transmission of *Leishmania major*. *J Biol Chem* **278**, 28840-28848 (2003).
91. Goswami, M., Dobson, D. E., Beverley, S. M., Turco, S. J. Demonstration by heterologous expression that the *Leishmania* SCA1 gene encodes an arabinopyranosyltransferase. *Glycobiology* **16**, 230-236 (2006).

92. Guha-Niyogi, A., Sullivan, D. R., Turco, S. J. Glycoconjugate structures of parasitic protozoa. *Glycobiology* **11**, 45R-59R (2001).
93. Previato, J. O., Mendonca-Previato, L., Lewanczuk, R. Z., Travassos, L. R., Gorin, P. A. J. *Crithidia* spp.: structural comparison of polysaccharides for taxonomic significance. *Exp Parasitol* **53**, 170-178 (1982).
94. Xavier Da Dilveira, E., Jones, C., Wait, R., Previato, J. O., Mendonca-Previato, L. Glycoinositol phospholipids from *Endotrypanum* species express epitopes in common with saccharide side chains of the lipophosphoglycan from *Leishmania major*. *Biochem J* **329**, 665-673 (1998).
95. Levin, D. H., Racker, E. Condensation of Arabinose 5-Phosphate and Phosphorylenol Pyrovate by 2-Keto-3-deoxy-8-phosphooctonic Acid Synthetase. *J Biol Chem* **234**, 2532-2539 (1959).
96. McNeil, M., Wallner, S. J., Hunter, S. W., Brennan, P. J. Demonstration that the galactosyl and arabinosyl residues in the cell-wall arabinogalactan of *Mycobacterium leprae* and *Mycobacterium tuberculosis* are furanoid. *Carbohydr Res* **166**, 299-308 (1987).
97. Wolucka, B. A. Biosynthesis of D-arabinose in mycobacteria - a novel bacterial pathway with implications for antimycobacterial therapy. *FEBS J* **275**, 2691-2711 (2008).
98. Wojtkiewicz, B., Szmidszinski, R., Jezierska, A., Cocito, C. Identification of a salvage pathway for D-arabinose in *Mycobacterium smegmatis*. *Eur J Biochem* **172**, 197-203 (1988).
99. Izumori, K., Waltanabe, Y., Sugimoto, S. Evolution of D-arabinose, L-xylose and L-ribose utilization in *Mycobacterium smegmatis*: mutants with a novel enzyme "pentose reductase". *Agric Bioi Chem* **44**, 1443-1446 (1980).
100. Niederweis, M. Nutrient acquisition by mycobacteria. *Microbiology* **154**, 679-692 (2008).
101. Schlesinger, L. S. *et al.* Determinants of phagocytosis, phagosome biogenesis and autophagy for *Mycobacterium tuberculosis*. In *Handbook of Tuberculosis: Immunology and Cell Biology* Edn 2 Vol. **2** (eds Kaufmann, S. H. E., Rubin, E.), 1-22 (WILEY-VCH, Weinheim, 2008).
102. Vergne, I., Gilleron, M., Nigou, J. Manipulation of the endocytic pathway and phagocyte functions by *Mycobacterium tuberculosis* lipoarabinomannan. *Front Cell Infect Microbiol* **4**, 187 (2015).
103. Kleinnijenhuis, J., Oosting, M., Joosten, L. A., Netea, M. G., van Crevel, R. Innate immune recognition of *Mycobacterium tuberculosis*. *Clin Dev Immunol* **2011**, 405310 (2011).
104. Hossain, M. M., Norazmi, M.N. Pattern recognition receptors and cytokines in *Mycobacterium tuberculosis* infection - the double-edged sword? *Biomed Res Int* **2013**, 179174 (2013).
105. Gaynor, C. D., McCormack, F. X., Voelker, D. R., McGowan, S. E., Schlesinger, L. S. Pulmonary surfactant protein A mediates enhanced phagocytosis of *Mycobacterium tuberculosis* by a direct interaction with human macrophages. *J Immunol* **155**, 5343-5351 (1995).
106. Garred, P., Harboe, M., Oettinger, T., Koch, C., Svejgaard, A. Dual role of mannan-binding protein in infections: another case of heterosis? *Eur J Immunogenet* **21**, 125-131 (1994).
107. Tailleux, L. *et al.* DC-SIGN induction in alveolar macrophages defines privileged target host cells for mycobacteria in patients with tuberculosis. *PLoS Med* **2**, e381 (2005).
108. Tailleux, L. *et al.* DC-SIGN is the major *Mycobacterium tuberculosis* receptor on human dendritic cells. *J Exp Med* **197**, 121-127 (2003).

109. van de Veerdonk, F. L. *et al.* *Mycobacterium tuberculosis* induces IL-17A responses through TLR4 and dectin-1 and is critically dependent on endogenous IL-1. *J Leukoc Biol* **88**, 227-232 (2010).
110. Yadav, M., Schorey, J. S. The beta-glucan receptor dectin-1 functions together with TLR2 to mediate macrophage activation by mycobacteria. *Blood* **108**, 3168-3175 (2006).
111. Yonekawa, A. *et al.* Dectin-2 is a direct receptor for mannose-capped lipoarabinomannan of mycobacteria. *Immunity* **41**, 402-413 (2014).
112. Ishikawa, E. *et al.* Direct recognition of the mycobacterial glycolipid, trehalose dimycolate, by C-type lectin Mincle. *J Exp Med* **206**, 2879-2888 (2009).
113. Lobato-Pascual, A., Saether, P. C., Fossum, S., Dissen, E., Daws, M. R. Mincle, the receptor for mycobacterial cord factor, forms a functional receptor complex with MCL and FcεRI-γ. *Eur J Immunol* **43**, 3167-3174 (2013).
114. Richardson, M. B., Williams, S. J. MCL and Mincle: C-type lectin receptors that sense damaged self and pathogen-associated molecular patterns. *Front Immunol* **5**, 288 (2014).
115. Schlesinger, L. S., Hull, S. R., Kaufman, T. M. Binding of the terminal mannosyl units of lipoarabinomannan from a virulent strain of *Mycobacterium tuberculosis* to human macrophages. *J Immunol* **152**, 4070-4079 (1994).
116. Schlesinger, L. S. Macrophage phagocytosis of virulent but not attenuated strains of *Mycobacterium tuberculosis* is mediated by mannose receptors in addition to complement receptors. *J Immunol* **150**, 2920-2930 (1993).
117. Schlesinger, L. S., Kaufman, T. M., Iyer, S., Hull, S. R., Marchiando, L. K. Differences in mannose receptor-mediated uptake of lipoarabinomannan from virulent and attenuated strains of *Mycobacterium tuberculosis* by human macrophages. *J Immunol* **157**, 4568-4575 (1996).
118. Torrelles, J. B., Azad, A. K., Schlesinger, L. S. Fine discrimination in the recognition of individual species of phosphatidyl-myo-inositol mannosides from *Mycobacterium tuberculosis* by C-type lectin pattern recognition receptors. *J Immunol* **177**, 1805-1816 (2006).
119. Torrelles, J. B., Schlesinger, L. S. Diversity in *Mycobacterium tuberculosis* mannosylated cell wall determinants impacts adaptation to the host. *Tuberculosis* **90**, 84-93 (2010).
120. Nigou, J. *et al.* Mannan chain length controls lipoglycans signaling via and binding to TLR2. *J Immunol* **180**, 6696-6702 (2008).
121. Quesniaux, V. J. *et al.* Toll-like receptor 2 (TLR2)-dependent-positive and TLR2-independent-negative regulation of proinflammatory cytokines by mycobacterial lipomannans. *J Immunol* **172**, 4425-4434 (2004).
122. Reiling, N., Ehlers, S., Hölscher, C. MyDths and un-TOLled truths: sensor, instructive and effector immunity to tuberculosis. *Immunol Lett* **116**, 15-23 (2008).
123. Geurtsen, J. *et al.* Identification of mycobacterial alpha-glucan as a novel ligand for DC-SIGN: involvement of mycobacterial capsular polysaccharides in host immune modulation. *J Immunol* **183**, 5221-5231 (2009).
124. Geijtenbeek, T. B. *et al.* Mycobacteria target DC-SIGN to suppress dendritic cell function. *J Exp Med* **197**, 7-17 (2002).
125. Pitarque, S. *et al.* Deciphering the molecular bases of *Mycobacterium tuberculosis* binding to the lectin DC-SIGN reveals an underestimated complexity. *Biochem J* **392**, 615-624 (2005).

126. Dinadayala, P. *et al.* Revisiting the structure of the anti-neoplastic glucans of *Mycobacterium bovis* Bacille Calmette-Guerin. Structural analysis of the extracellular and boiling water extract-derived glucans of the vaccine substrains. *J Biol Chem* **279**, 12369-12378 (2004).
127. Russell, D. G., Purdy, G. E., Owens, R. M., Rohde, K. H., Yates, R. M. *Mycobacterium tuberculosis* and the four-minute phagosome. *ASM News* **71**, 459-463 (2005).
128. Mishra, A. K., Driessen, N. N., Appelmek, B. J. & Besra, G. S. Lipoarabinomannan and related glycoconjugates: structure, biogenesis and role in *Mycobacterium tuberculosis* physiology and host-pathogen interaction. *FEMS Microbiol Rev* **35**, 1126-1157 (2011).
129. Kang, P. B. *et al.* The human macrophage mannose receptor directs *Mycobacterium tuberculosis* lipoarabinomannan-mediated phagosome biogenesis. *J Exp Med* **202**, 987-999 (2005).
130. Malik, Z. A., Iyer, S. S., Kusner, D. J. *Mycobacterium tuberculosis* phagosomes exhibit altered calmodulin-dependent signal transduction. Contribution to inhibition of phagosome-lysosome fusion and intracellular survival in human macrophages. *J Immunol* **166**, 3392-3401 (2001).
131. Malik, Z. A., Denning, G. M., Kusner, D. J. Inhibition of Ca<sup>2+</sup> signaling by *Mycobacterium tuberculosis* is associated with reduced phagosome-lysosome fusion and increased survival within human macrophages. *J Exp Med* **191**, 287-302 (2000).
132. Vergne, I., Chua, J. & Deretic, V. Tuberculosis toxin blocking phagosome maturation inhibits a novel Ca<sup>2+</sup>/calmodulin-PI3K hVPS34 cascade. *J Exp Med* **198**, 653-659 (2003).
133. Kyei, G. B. *et al.* Rab14 is critical for maintenance of *Mycobacterium tuberculosis* phagosome maturation arrest. *EMBO J* **25**, 5250-5259 (2006).
134. Axelrod, S. *et al.* Delay of phagosome maturation by a mycobacterial lipid is reversed by nitric oxide. *Cell Microbiol* **10**, 1530-1545 (2008).
135. Seto, S., Tsujimura, K., Koide, Y. Rab GTPases regulating phagosome maturation are differentially recruited to mycobacterial phagosomes. *Traffic* **12**, 407-420 (2011).
136. Steinhäuser, C. *et al.* Lipid-labeling facilitates a novel magnetic isolation procedure to characterize pathogen-containing phagosomes. *Traffic* **14**, 321-336 (2013).
137. Rojas, M., Garcia, L. F., Nigou, J., Puzo, G. & Olivier, M. Mannosylated lipoarabinomannan antagonizes *Mycobacterium tuberculosis*-induced macrophage apoptosis by altering Ca<sup>2+</sup>-dependent cell signaling. *J Infect Dis* **182**, 240-251 (2000).
138. Maiti, D., Bhattacharyya, A., Basu, J. Lipoarabinomannan from *Mycobacterium tuberculosis* promotes macrophage survival by phosphorylating Bad through a phosphatidylinositol 3-kinase/Akt pathway. *J Biol Chem* **276**, 329-333 (2001).
139. Dao, D. N. *et al.* *Mycobacterium tuberculosis* lipomannan induces apoptosis and interleukin-12 production in macrophages. *Infect Immun* **72**, 2067-2074 (2004).
140. Vignal, C. *et al.* Lipomannans, but not lipoarabinomannans, purified from *Mycobacterium chelonae* and *Mycobacterium kansasii* induce TNF- and IL-8 secretion by a CD14-Toll-like receptor 2-dependent mechanism. *J Immunol* **171**, 2014-2023 (2003).
141. Torrelles, J. B. *et al.* Identification of *Mycobacterium tuberculosis* clinical isolates with altered phagocytosis by human macrophages due to a truncated lipoarabinomannan. *J Biol Chem* **283**, 31417-31428 (2008).

142. Amin, A. G. *et al.* EmbA is an essential arabinosyltransferase in *Mycobacterium tuberculosis*. *Microbiology* **154**, 240-248 (2008).
143. Goude, R., Amin, A. G., Chatterjee, D., Parish, T. The critical role of embC in *Mycobacterium tuberculosis*. *J Bacteriol* **190**, 4335-4341 (2008).
144. Esko, J. D., Sharon, N. Microbial lectins: hemagglutinins, adhesins, and toxins. In *Essentials of Glycobiology*. Edn 2 (eds. Varki *et al.*), 489-500 (Cold Spring Harbor (NY): Cold Spring Harbor Laboratory Press, 2009).
145. Kundu, M., Basu, J., Chakrabarti, P. Purification and characterization of an extracellular lectin from *Mycobacterium smegmatis*. *FEBS Lett* **256**, 207-210 (1989).
146. Goswami, S., Sarkar, S., Basu, J., Kundu, M., Chakrabarti, P. Mycotin. A lectin involved in the adherence of mycobacteria to macrophages. *FEBS Lett* **355**, 183-186 (1994).
147. Anton, V., Roug, P., Daffé, M. Identification of the sugars involved in mycobacterial cell aggregation. *FEMS Microbiol Lett* **144**, 167-170 (1996).
148. Singh, D. D., Chandran, D., Jeyakani, J., Chandran, N. Scanning the genome of *Mycobacterium tuberculosis* to identify potential lectins. *Protein Pept Lett* **14**, 683-691 (2007).
149. Abhinav, K. V., Sharma, A., Vijayan, M. Identification of mycobacterial lectins from genomic data. *Proteins* **81**, 644-657 (2013).
150. Steingart, K. R. *et al.* Sputum processing methods to improve the sensitivity of smear microscopy for tuberculosis: a systematic review. *Lancet Infect Dis* **6**, 664-674 (2006).
151. Yeager, H. Jr., Lacy, J., Smith, L. R., Lemaistre, C. A. Quantitative studies of mycobacterial populations in sputum and saliva. *Am Rev Respir Dis* **95**, 998-1004 (1967).
152. Zar, H. J. *et al.* Sputum induction for the diagnosis of pulmonary tuberculosis in infants and young children in an urban setting in South Africa. *Arch Dis Child* **82**, 305-308 (2000).
153. Owens, S. *et al.* Nasopharyngeal aspiration for diagnosis of pulmonary tuberculosis. *Arch Dis Child* **92**, 693-696 (2007).
154. Marais, B. J., Pai, M. Specimen collection methods in the diagnosis of childhood tuberculosis. *Indian J Med Microbiol* **24**, 249-251 (2006).
155. Lunawat, P. P. *et al.* Detection of acid fast bacilli in saliva using papanicolaou stain induced fluorescence method versus fluorochrome staining: an evaluative study. *J Int Oral Health* **7**, 115-120 (2015).
156. Holani, A. G. *et al.* Demonstration of *Mycobacterium tuberculosis* in sputum and saliva smears of tuberculosis patients using Ziehl Neelsen and fluoro-chrome staining - a comparative study. *J Clin Diagn Res* **8**, ZC42-ZC45 (2014).
157. Mediero, G. G., Gallardo, R. V., Del Molino, M. L. P., Dios, P. D. Evaluation of two commercial nucleic acid amplification kits for detecting *Mycobacterium tuberculosis* in saliva samples. *Oral Dis* **21**, 451-455 (2015).
158. Yassen, G., Noori, J., Yas, N. S. Detection of acid fast bacilli in the saliva of patients having pulmonary tuberculosis. *J Bagh College Dentistry* **24**, 59-62 (2012).
159. Neild, N., Dunkley, E. V. The role of the saliva in the transmission of tubercle. *Lancet* **173**, 1096-1098 (1909).
160. Stratmann, J., Strommenger, B., Stevenson, K., Gerlach, G. F. Development of a peptide-mediated capture PCR for detection of *Mycobacterium avium* subsp. paratuberculosis in milk. *J Clin Microbiol* **40**, 4244-4250 (2002).

161. Garbaccio, S. G., Cataldi, A. A. Evaluation of an immunomagnetic capture method followed by PCR to detect *Mycobacterium bovis* in tissue samples from cattle. *Rev Argent Microbiol* **42**, 247-253 (2010).
162. Arutyunov, D. *et al.* Mycobacteriophage cell binding proteins for the capture of mycobacteria. *Bacteriophage* **4**, e960346 (2014).
163. Hunter, D. M., Lim, D. V. An IMS/ATP assay for the detection of *Mycobacterium tuberculosis* in urine. *Tuberc Res Treat* **2012**, 292605 (2012).
164. Sweeney, F. P. *et al.* Immunomagnetic recovery of *Mycobacterium bovis* from naturally infected environmental samples. *Lett Appl Microbiol* **43**, 364-369 (2006).
165. Grant, I. R., Ball, H. J., Rowe, M. T. Isolation of *Mycobacterium paratuberculosis* from milk by immunomagnetic separation. *Appl Environ Microbiol* **64**, 3153-3158 (1998).
166. Wilson, S., Lane, A., Rosedale, R., Stanley, C. Concentration of *Mycobacterium tuberculosis* from sputum using ligand-coated magnetic beads. *Int J Tuberc Lung Dis* **14**, 1164-1168 (2010).
167. Wang, X. *et al.* Bead capture increases the sensitivity of sputum microscopy for the diagnosis of tuberculosis in Beijing, China. *Trans R Soc Trop Med Hyg* **107**, 741-743 (2013).
168. Ghodbane, R., Drancourt, M. Magnetic bead protocol for culturing *Mycobacterium tuberculosis* from sputum specimens. *J Clin Microbiol* **51**, 1578-1579 (2013).
169. Kang, J. H. *et al.* An extracorporeal blood-cleansing device for sepsis therapy. *Nat Med* **20**, 1211-1216 (2014).
170. Hartmann, M. *et al.* Saccharide-modified nanodiamond conjugates for the efficient detection and removal of pathogenic bacteria. *Chemistry* **18**, 6485-6492 (2012).
171. Qi, Z. *et al.* Multivalency at interfaces: supramolecular carbohydrate-functionalized graphene derivatives for bacterial capture, release, and disinfection. *Nano Lett* **15**, 6051-6057 (2015).
172. Carr, S. W., Pickup, K. M., Smith, P. M., Schilling, K. M. Oral care compositions. US Patent 5824292 filed 12 Apr. 1996, and issued 20 Oct. 1998.
173. Lau, A., Eason, R., Brevnow, M., Li, H., Hacker, K. Magnetic beads having surface glycoconjugates and use thereof. US Patent PCT/US2011/048693 filed 22 Aug. 2011, and issued 23 Feb. 2012.
174. Wang, H., Ng, T. B. First report of an arabinose-specific fungal lectin. *Biochem Biophys Res Commun* **337**, 621-625 (2005).
175. Sudakevitz, D., Imberty, A., Gilbos-Garber, N. Production, properties and specificity of a new bacterial L-fucose- and D-arabinose-binding lectin of the plant aggressive pathogen *Ralstonia solanacearum*, and its comparison to related plant and microbial lectins. *J Biochem* **132**, 353-358 (2002).
176. Adam, J. *et al.* Engineering of PA-IIL lectin from *Pseudomonas aeruginosa* - Unravelling the role of the specificity loop for sugar preference. *BMC Struct Biol* **7**, 36 (2007).
177. Stanley, P., Schachter, H., Taniguchi, N. N-Glycans. In *Essentials of Glycobiology*. Edn 2 (eds. Varki *et al.*), 101-114 (Cold Spring Harbor (NY): Cold Spring Harbor Laboratory Press, 2009).
178. Knight, S. D., Bouckaert, J. Structure, function, and assembly of type 1 fimbriae. *Top Curr Chem* **288**, 67-107 (2009).
179. Hartmann, M., Lindhorst, T. K. The bacterial lectin FimH, a target for drug discovery - Carbohydrate inhibitors of type-1 fimbriae-mediated bacterial adhesion. *Eur J Org Chem* **2011**, 3583-3609 (2011).



180. Lindhorst, T. K., Kötter, S., Krallmann-Wenzel, U., Ehlers, S. Trivalent  $\alpha$ -D-mannoside clusters as inhibitors of type-1 fimbriae-mediated adhesion of *Escherichia coli*. Structural variation and biotinylation. *J Chem Soc* **1**, 823-831 (2001).
181. Bonner, W. Isomers of tetra-O-acetyl-D-mannopyranose. *J Am Chem Soc* **80**, 3372-3378 (1958).
182. Dahmén, J. *et al.* 2-Bromoethyl glycosides: synthesis and characterisation. *Carbohydr Res* **116**, 303-307 (1983).
183. Zemplén, G., Pacsu, E. Über die Verseifung acetylierter Zucker und verwandter Substanzen. *Ber Dtsch Chem Ges* **62**, 1613-1614 (1929).
184. Lindhorst, T. K. *Essentials of Carbohydrate Chemistry and Biochemistry*. Edn 3 (WILEY-VCH, Weinheim, 2007).
185. Kam, B. L., Barascut, J. L., Imbach, J. L. A general method of synthesis and isolation, and an NMR-spectroscopic study, of tetra-O-acetyl-D-aldopento-furanoses. *Carbohydr Res* **69**, 135-142 (1979).
186. Pathak, A. K., Pathak, V., Bansal, N., Maddry, J. A., Reynolds, R. C. Synthesis of a fluorescent arabinofuranosyl disaccharide: a probe for arabinosyltransferase activity in *Mycobacterium tuberculosis*. *Tetrahedron Lett* **42**, 979-982 (2001).
187. Westphal, O., Feier, H. Darstellung künstlicher Antigene mit determinanten Zuckergruppen, II. Mitteil.: Synthese der *p*-Aminophenyl-O- $\alpha$ -glykoside von L-Fucose, L-Rhamnose, D-galaktose und D-Mannose. *Eur J Inorg Chem* **89**, 582-588 (1956).
188. Legler, G., Stiitz, A. E., Immich, H. Synthesis of 1,5-dideoxy-1,5-imino-D-arabinitol (5-nor-L-fuco-1-deoxynojirimycin) and its application for the affinity purification and characterisation of  $\alpha$ -L-fucosidase. *Carbohydr Res* **272**, 17-30 (1995).
189. Koenigs, W., Knorr, E. Über einige Derivate des Traubenzuckers und der Galaktose. *Ber Dtsch Chem Ges* **34**, 957-981 (1901).
190. Bloch, H., Sorkin, E., Erlenmeyer, H. A toxic lipid component of the tubercle bacillus (cord factor). I. Isolation from petroleum ether extracts of young bacterial cultures. *Am Rev Tuberc* **67**, 629-643 (1953).
191. Glickman, M. S., Cox, J. S., Jacobs, W. R. Jr. A novel mycolic acid cyclopropane synthetase is required for cording, persistence, and virulence of *Mycobacterium tuberculosis*. *Mol Cell* **5**, 717-727 (2000).
192. Backus, K. M. *et al.* Uptake of unnatural trehalose analogs as a reporter for *Mycobacterium tuberculosis*. *Nat Chem Biol* **7**, 228-235 (2011).
193. Wang, M., Tu, P. F., Xu, Z. D., Yu, X. L., Yang, M. Design and synthesis of guanidinoglycosides directed against the TAR RNA of HIV-1. *Helv Chim Acta* **86**, 2637-2644 (2003).
194. Jezo, I. Aminoderivate der Saccharose und der  $\alpha$ , $\alpha$ -Trehalose. I. Herstellung von 6-Desoxy-6-amino- und 6,6'-Dideoxy-6,6'-diaminoderivaten. *Chem zvesti* **25**, 364-368 (1971).
195. Sizovs, A. *et al.* Poly(trehalose): sugar-coated nanocomplexes promote stabilization and effective polyplex-mediated siRNA delivery. *J Am Chem Soc* **135**, 15417-15424 (2013).
196. Hartmann, M., Horst, A. K., Klemm, P., Lindhorst, T. K. A kit for the investigation of live *Escherichia coli* cell adhesion to glycosylated surfaces. *Chem Commun* **46**, 330-332 (2010).
197. Calmette, A., Plotz, H. Protective inoculation against tuberculosis with BCG. *Am Rev Tuberc* **19**, 567-572 (1929).

198. Sumner, J. B., Howell, S. F. The identification of the hemagglutinin of the jack bean with Concanavalin A. *J Bacteriol* **32**, 227–237 (1936).
199. Nogueira, L. *et al.* *Mycobacterium tuberculosis* Rv1419 encodes a secreted 13 kDa lectin with immunological reactivity during human tuberculosis. *Eur J Immunol* **40**, 744–753 (2010).
200. Patra, D. *et al.* Cloning, expression, purification, crystallization and preliminary X-ray studies of a secreted lectin (Rv1419) from *Mycobacterium tuberculosis*. *Acta Crystallogr Sect F Struct Biol Cryst Commun* **66**, 1662–1665 (2010).
201. Patra, D., Sharma, A., Chandran, D., Vijayan, M. Cloning, expression, purification, crystallization and preliminary X-ray studies of the mannose-binding lectin domain of MSMEG\_3662 from *Mycobacterium smegmatis*. *Acta Crystallogr Sect F Struct Biol Cryst Commun* **67**, 596–599 (2011).
202. Sewón, L. A., Karjalainen, S. M., Söderling, E., Lapinleimu, H., Simell, O. Associations between salivary calcium and oral health. *J Clin Periodontol* **25**, 913–919 (1998).
203. Smith, E., Collins, I. Photoaffinity labeling in target- and binding-site identification. *Future Med Chem* **7**, 159–183 (2015).
204. Vodovozova, E. L. Photoaffinity labeling and its application in structural biology. *Biochemistry* **72**, 1–20 (2007).
205. Sumranjit, J., Chung, S. J. Recent advances in target characterization and identification by photoaffinity probes. *Molecules* **18**, 10425–10451 (2013).
206. Pham, N. D., Parker, R. B., Kohler, J. J. Photocrosslinking approaches to interactome mapping. *Curr Opin Chem Biol* **17**, 90–101 (2013).
207. Dubinsky, L., Krom, B. P., Meijler, M. M. Diazirine based photoaffinity labeling. *Bioorg Med Chem* **20**, 554–570 (2012).
208. Yu, S. H. *et al.* Metabolic labeling enables selective photocrosslinking of O-GlcNAc-modified proteins to their binding partners. *Proc Natl Acad Sci USA* **109**, 4834–4839 (2012).
209. Hashimoto, M., Hatanaka, Y. Recent progress in diazirine-based photoaffinity labeling. *Eur J Org Chem* **2008**, 2513–2523 (2008).
210. Yu, S. H., Wands, A. M., Kohler, J. J. Photoaffinity probes for studying carbohydrate biology. *J Carbohydr Chem* **31**, 325–352 (2012).
211. Bond, M. R., Whitman, C. M., Kohler, J. J. Metabolically incorporated photocrosslinking sialic acid covalently captures a ganglioside-protein complex. *Mol Biosyst* **6**, 1796–1799 (2010).
212. Bond, M. R. *et al.* Metabolism of diazirine-modified *N*-acetylmannosamine analogues to photo-cross-linking sialosides. *Bioconjug Chem* **22**, 1811–1823 (2011).
213. Tanaka, Y., Kohler, J. J. Photoactivatable crosslinking sugars for capturing glycoprotein interactions. *J Am Chem Soc* **130**, 3278–3279 (2008).
214. Robinette, D., Neamati, N., Tomer, K. B., Borchers, C. H. Photoaffinity labeling combined with mass spectrometric approaches as a tool for structural proteomics. *Expert Rev Proteomics* **3**, 399–408 (2006).
215. Sokurenko, E. V., Vogel, V., Thomas, W. E. Catch-bond mechanism of force-enhanced adhesion: counterintuitive, elusive, but ... widespread? *Cell Host Microbe* **4**, 314–323 (2008).

216. Thomas, W. E., Trintchina, E., Forero, M., Vogel, V., Sokurenko, E. V. Bacterial Adhesion to Target Cells Enhanced by Shear Force. *Cell* **109**, 913-923 (2002).
217. Interlandi, G., Thomas, W. E. The catch bond mechanism between von Willebrand factor and platelet surface receptors investigated by molecular dynamics simulations. *Proteins* **78**, 2506-2522 (2010).
218. Rakshit, S., Zhang, Y., Manibog, K., Shafraz, O., Sivasankar, S. Ideal, catch, and slip bonds in cadherin adhesion. *Proc Natl Acad Sci USA* **109**, 18815-18820 (2012).
219. Dvir, O., Kansas, G. S., Alon, R. An activated L-selectin mutant with conserved equilibrium binding properties but enhanced ligand recognition under shear flow. *J Biol Chem* **275**, 18682-18691 (2000).
220. Thomas, W. E., Nilsson, L. M., Forero, M., Sokurenko, E. V., Vogel, V. Shear-dependent 'stick-and-roll' adhesion of type-1 fimbriated *Escherichia coli*. *Mol Microbiol* **53**, 1545-1557 (2004).
221. Thielbeer, F., Donaldson, K., Bradley, M. Zeta potential mediated reaction monitoring on nano and microparticles. *Bioconjugate Chem* **22**, 144-150 (2011).
222. Kang, E. T., Tan, K. L., Kato, K., Uyama, Y., Ikada, Y. Surface modification and functionalization of polytetrafluoroethylene films. *Macromolecules* **29**, 6872-6879 (1996).
223. Stanley, C. J., Wilson, S. M. Capture of micro-organisms. US Patent EP2588863 A1 filed 29 Jun. 2011, and issued 8 Mai. 2013.
224. Feinberg, H. *et al.* Mechanism for recognition of an unusual mycobacterial glycolipid by the macrophage receptor Mincle. *J Biol Chem* **288**, 28457-28465 (2013).
225. Behra, M. *et al.* Magnetic porous sugar-functionalized PEG microgels for efficient isolation and removal of bacteria from solution. *Biomacromolecules* **14**, 1927-1935 (2013).
226. Sanares, A. M. E., King, N. M., Itthagarun, A., Wong, H. M. Chewing gum as a medium for the delivery of anticariogenic therapeutic agents: a review. *Hong Kong Dent J* **6**, 13-22 (2009).
227. Imfeld, T. Chewing gum - facts and fiction: A review of gum-chewing and oral health. *Crit Rev Oral Biol Med* **10**, 405-419 (1999).
228. Meinel, L., Schnabelrauch, M., Schlottig, F. Diagnostic chewing gum for pathogens. Patent WO2013132058 filed 8 Mar. 2012, and issued 12 Sep. 2013.
229. Allen, N. Microsoft's Bill Gates invests in chewing gum and chocolate in fight against malaria. *The Telegraph* (2009).
230. Beatty, W. L. *et al.* Trafficking and release of mycobacterial lipids from infected macrophages. *Traffic* **1**, 235-247 (2000).
231. Kong, Y. *et al.* Imaging tuberculosis with endogenous beta-lactamase reporter enzyme fluorescence in live mice. *Proc Natl Acad Sci USA* **107**, 12239-12244 (2010).
232. Xie, H. *et al.* Rapid point-of-care detection of the tuberculosis pathogen using a BlaC-specific fluorogenic probe. *Nat Chem* **4**, 802-809 (2012).
233. Cheng, Y. *et al.* Fluorogenic probes with substitutions at the 2 and 7 positions of cephalosporin are highly BlaC-specific for rapid *Mycobacterium tuberculosis* detection. *Angew Chem Int Ed* **53**, 9360-9364 (2014).
234. Song, H., Sandie, R., Wang, Y., Andrade-Navarro, M. A., Niederweis, M. Identification of outer membrane proteins of *Mycobacterium tuberculosis*. *Tuberculosis* **88**, 526-544 (2008).

235. Stover, C. K. *et al.* New use of BCG for recombinant vaccines. *Nature* **351**, 456-460 (1991).
236. Hillemann, D., Warren, R., Kubica, T., Rüsche-Gerdes, S., Niemann, S. Rapid detection of *Mycobacterium tuberculosis* Beijing genotype strains by real-time PCR. *J Clin Microbiol* **44**, 302-306 (2006).
237. Amaike, M., Kobayashi, H., Shinkai, S. New organogelators bearing both sugar and cholesterol units: an approach toward molecular design of universal gelators. *Bull Chem Soc Jpn* **73**, 2553-2558 (2000).
238. Dumont, A., Malleron, A., Awwad, M., Dukan, S., Vauzeilles, B. Click-mediated labeling of bacterial membranes through metabolic modification of the lipopolysaccharide inner core. *Angew Chem* **124**, 3197-3200 (2012).
239. Sadamoto, R. *et al.* Cell-wall engineering of living bacteria. *J Am Chem Soc* **124**, 9018-9019 (2002).
240. Tra, V. N., Dube, D. H. Glycans in pathogenic bacteria - potential for targeted covalent therapeutics and imaging agents. *Chem Commun* **50**, 4659-4673 (2014).
241. Dube, D. Metabolic oligosaccharide engineering as a tool for glycobiology. *Curr Opin Chem Biol* **7**, 616-625 (2003).
242. Laughlin, S. T., Bertozzi, C. R. Metabolic labeling of glycans with azido sugars and subsequent glycan-profiling and visualization via Staudinger ligation. *Nat Protoc* **2**, 2930-2944 (2007).
243. Mahal, L. K., Yarema, K. J., Bertozzi, C. R. Engineering chemical reactivity on cell surfaces through oligosaccharide biosynthesis. *Science* **276**, 1125-1128 (1997).
244. Saxon, E., Bertozzi, C. R. Cell surface engineering by a modified Staudinger reaction. *Science* **287**, 2007-2010 (2000).
245. Keppler, O. T., Horstkorte, R., Pawlita, M., Schmidt, C., Reutter, W. Biochemical engineering of the *N*-acetyl side chain of sialic acid: biological implications. *Glycobiology* **11**, 11R-18R (2001).
246. Keppler, O. T. *et al.* Biosynthetic modulations of sialic acid dependent virus-receptor Interactions of two primate polyoma viruses. *J Biol Chem* **270**, 1308-1314 (1995).
247. Sletten, E. M., Bertozzi, C. R. From mechanism to mouse: a tale of two bioorthogonal reactions. *Acc Chem Res* **44**, 666-676 (2011).
248. Prescher, J. A., Bertozzi, C. R. Chemistry in living systems. *Nat Chem Biol* **1**, 12-21 (2005).
249. Sletten, E. M., Bertozzi, C. R. Bioorthogonal chemistry: fishing for selectivity in a sea of functionality. *Angew Chem Int Ed* **48**, 6974-6998 (2009).
250. Ramil, C. P., Lin, Q. Bioorthogonal chemistry: strategies and recent developments. *Chem Commun* **49**, 11007-11022 (2013).
251. Lim, R. K. V., Lin, Q. Bioorthogonal chemistry: recent progress and future directions. *Chem Commun* **46**, 1589-1600 (2010).
252. Hangauer, M. J., Bertozzi, C. R. A FRET-based fluorogenic phosphine for live-cell imaging with the Staudinger ligation. *Angew Chem Int Ed* **47**, 2394-2397 (2008).
253. Rostovtsev, V. V., Green, L. G., Fokin, V. V., Sharpless, K. B. A Stepwise Huisgen cycloaddition process: Copper(I)-catalyzed regioselective "ligation" of azides and terminal alkynes. *Angew Chem* **114**, 2708-2711 (2002).

254. Tornøe, C. W., Christensen, C., Meldal, M. Peptidotriazoles on Solid Phase. [1,2,3]-Triazoles by regioselective copper(I)-catalyzed 1,3-dipolar cycloadditions of terminal alkynes to azides. *J Org Chem* **67**, 3057-3064 (2002).
255. Presolski, S. I., Hong, V., Cho, S.-H., Finn, M. G. Tailored ligand acceleration of the Cu-catalyzed azide-alkyne cycloaddition reaction: practical and mechanistic implications. *J Am Chem Soc* **132**, 14570-14576 (2010).
256. Gaetke, L., Chow, C. K. Copper toxicity, oxidative stress, and antioxidant nutrients. *Toxicology* **189**, 147-163 (2003).
257. Zödl, B., Zeiner, M., Marktl, W., Steffan, I., Ekmekcioglu, C. Pharmacological levels of copper exert toxic effects in Caco-2 cells. *Biol Trace Elem Res* **96**, 143-152 (2003).
258. Kennedy, D. C. *et al.* Cellular consequences of copper complexes used to catalyze bioorthogonal click reactions. *J Am Chem Soc* **133**, 17993-18001 (2011).
259. Hong, V., Steinmetz, N. F., Manchester, M., Finn, M. G. Labeling live cells by copper-catalyzed alkyne-azide click chemistry. *Bioconjug Chem* **21**, 1912-1916 (2010).
260. Chan, T. R., Hilgraf, R., Sharpless, K. B., Fokin, V. V. Polytriazoles as copper(I)-stabilizing ligands in catalysis. *Org Lett* **6**, 2853-2855 (2004).
261. Besanceney-Webler, C. *et al.* Increasing the efficacy of bioorthogonal click reactions for bioconjugation: a comparative study. *Angew Chem* **50**, 8051-8056 (2011).
262. Michaels, H. A., Zhu, L. Ligand-assisted, copper(II) acetate-accelerated azide-alkyne cycloaddition. *Chem Asian J* **6**, 2825-2834 (2011).
263. Wang, W. *et al.* Sulfated ligands for the copper(I)-catalyzed azide-alkyne cycloaddition. *Chem Asian J* **6**, 2796-2802 (2011).
264. Agard, N. J., Prescher, J. A. & Bertozzi, C. R. A strain-promoted [3 + 2] azide-alkyne cycloaddition for covalent modification of biomolecules in living systems. *J Am Chem Soc* **126**, 15046-15047 (2004).
265. Baskin, J. M. *et al.* Copper-free click chemistry for dynamic in vivo imaging. *Proc Natl Acad Sci USA* **104**, 16793-16797 (2007).
266. Wittig, G., Krebs, A. Zur Existenz niedergliedriger Cycloalkyne, I. *Eur J Inorg Chem* **94**, 3260-3275 (1961).
267. de Almeida, G., Townsend, L. C., Bertozzi, C. R. Synthesis and reactivity of dibenzoselenacycloheptynes. *Org Lett* **15**, 3038-3041 (2013).
268. Debets, M. F. *et al.* Aza-dibenzocyclooctynes for fast and efficient enzyme PEGylation via copper-free (3+2) cycloaddition. *Chem Commun* **46**, 97-99 (2010).
269. Chigrinova, M. *et al.* Rearrangements and addition reactions of biarylazacyclooctynones and the implications to copper-free click chemistry. *Org Biomol Chem* **11**, 3436-3441 (2013).
270. Dehnert, K. W. *et al.* Imaging the sialome during zebrafish development with copper-free click chemistry. *Chembiochem* **13**, 353-357 (2012).
271. Dehnert, K. W. *et al.* Metabolic labeling of fucosylated glycans in developing zebrafish. *ACS Chem Biol* **6**, 547-552 (2011).
272. Laughlin, S. T., Baskin, J. M., Amacher, S. L., Bertozzi, C. R. In vivo imaging of membrane-associated glycans in developing zebrafish. *Science* **320**, 664-667 (2008).

273. Laughlin, S. T., Bertozzi, C. R. In vivo imaging of *Caenorhabditis elegans* glycans. *ACS Chem Biol* **4**, 1068-1072 (2009).
274. Chang, P. V. *et al.* Copper-free click chemistry in living animals. *Proc Natl Acad Sci USA* **107**, 1821-1826 (2010).
275. Nauman, D. A., Bertozzi, C. R. Kinetic parameters for small-molecule drug delivery by covalent cell surface targeting. *Biochim Biophys Acta*. **1568**, 147-154 (2001).
276. Dirksen, A., Hackeng, T. M., Dawson, P. E. Nucleophilic catalysis of oxime ligation. *Angew Chem Int Ed* **45**, 7581-7584 (2006).
277. Li, J. *et al.* Ligand-free palladium-mediated site-specific protein labeling inside Gram-negative bacterial pathogens. *J Am Chem Soc* **135**, 7330-7338 (2013).
278. Patterson, D. M., Nazarova, L. A., Xie, B., Kamber, D. N., Prescher, J. A. Functionalized cyclopropenes as bioorthogonal chemical reporters. *J Am Chem Soc* **134**, 18638-18643 (2012).
279. Song, W. *et al.* A metabolic alkene reporter for spatiotemporally controlled imaging of newly synthesized proteins in mammalian cells. *ACS Chem Biol* **5**, 875-885 (2010).
280. Li, Q., Dong, T., Liu, X., Lei, X. A bioorthogonal ligation enabled by click cycloaddition of o-quinolinone quinone methide and vinyl thioether. *J Am Chem Soc* **135**, 4996-4999 (2013).
281. Doboszewski, B., Herdewijn, P. Carbohydrate chiral-pool approach to four enantiomerically pure 2-naphthylmethyl 3-hydroxy-2-methylbutanoates. *Tetrahedron* **64**, 5551-5562 (2008).
282. Elliott, R. P. *et al.* Attempted ring contraction of  $\alpha$ -triflates of 3-azido- and 3-fluoro- $\gamma$ -lactones to oxetanes. *Tetrahedron* **1**, 715-718 (1990).
283. Moravcov, J., Capkova, J., Stanek, J. One-pot synthesis of 1,2-O-isopropylidene- $\alpha$ -D-xylofuranose. *Carbohydr Res* **263**, 61-66 (1994).
284. Botta, O., Moyroud, E., Lobato, C., Strazewski, P. Synthesis of 3'-azido- and 3'-amino-3'-deoxyadenosine in both enantiomeric forms. *Tetrahedron* **54**, 13529-13546 (1998).
285. McDevitt, J. P., Lansbury, P. T. Glycosamino acids. New building blocks for combinatorial synthesis. *J Am Chem Soc* **118**, 3818-3828 (1996).
286. Smellie, I. A., Bhakta, S., Sim, E., Fairbanks, A. J. Synthesis of putative chain terminators of mycobacterial arabinan biosynthesis. *Org Biomol Chem* **5**, 2257-2266 (2007).
287. Tracy, B. P., Gaida, S. M., Papoutsakis, E. T. Flow cytometry for bacteria. Enabling metabolic engineering, synthetic biology and the elucidation of complex phenotypes. *Curr Opin Biotechnol* **21**, 85-99 (2010).
288. Michelucci, A. *et al.* Immune-responsive gene 1 protein links metabolism to immunity by catalyzing itaconic acid production. *Proc Natl Acad Sci USA* **110**, 7820-7825 (2013).
289. Khoo, K. H., Tang, J. B., Chatterjee, D. Variation in mannose-capped terminal arabinan motifs of lipoarabinomannans from clinical isolates of *Mycobacterium tuberculosis* and *Mycobacterium avium* complex. *J Biol Chem* **276**, 3863-3871 (2001).
290. Chatterjee, D., Lowell, K., Rivoire, B., McNeil, M. R., Brennan, P. J. Lipoarabinomannan of *Mycobacterium tuberculosis*. *J Biol Chem* **267**, 6234-6239 (1992).
291. Venisse, A., Berjeaud, J. M., Chaurand, P., Gilleron, M., Puzo, G. Structural features of lipoarabinomannan from *Mycobacterium bovis* BCG. *J Biol Chem* **268**, 12401-12411 (1993).

292. Ortalo-Magné, A., Andersen, A. B., Daffé, M. The outermost capsular arabinomannans and other mannoconjugates of virulent and avirulent tubercle bacilli. *Microbiology* **142**, 927-935 (1996).
293. Fratti, R. A., Backer, J. M., Gruenberg, J., Corvera, S., Deretic, V. Role of phosphatidylinositol 3-kinase and Rab5 effectors in phagosomal biogenesis and mycobacterial phagosome maturation arrest. *J Cell Biol* **154**, 631-644 (2001).
294. Sturgill-Koszycki, S. *et al.* Lack of acidification in *Mycobacterium* phagosomes produced by exclusion of the visicular proton-ATPase. *Science* **263**, 678-681 (1994).
295. Bozyczko-Coyne, D., McKenna, B. W., Connors, T. J., Neff, N. T. A rapid fluorometric assay to measure neuronal survival in vitro. *J Neurosci Methods* **50**, 205-216 (1993).
296. Charrier, C. *et al.* Cysteamine (Lynovex), a novel mucoactive antimicrobial & antibiofilm agent for the treatment of cystic fibrosis. *Orphanet J Rare Dis* **9**, 189-200 (2014).
297. Suzuki, T. *et al.* Design, synthesis, and biological activity of folate receptor-targeted prodrugs of thiolate histone deacetylase inhibitors. *Bioorg Med Chem Lett* **17**, 4208-4212 (2007).
298. Straten, N. C. R., van der Marel, G. A., van Boom, J. H. An Expeditious Route to the Synthesis of Adenophostin A. *Tetrahedron Lett* **37**, 3599-3602 (1996).
299. Fessele, C., Lindhorst, T. K. Effect of aminophenyl and aminothiahexyl  $\alpha$ -D-glycosides of the manno-, gluco-, and galacto-series on type-1 fimbriae-mediated adhesion of *Escherichia coli*. *Biology* **2**, 1135-1149 (2013).
300. Dheda, K. *et al.* Clinical utility of a commercial LAM-ELISA assay for TB diagnosis in HIV-infected patients using urine and sputum samples. *PloS One* **5**, e9848 (2010).
301. Slayden, R. A., Lee, R. E., Barry, C. E. 3rd Isoniazid affects multiple components of the type II fatty acid synthase system of *Mycobacterium tuberculosis*. *Mol Microbiol* **38**, 514-525 (2000).
302. Siegrist, M. S. *et al.* D-Amino acid chemical reporters reveal peptidoglycan dynamics of an intracellular pathogen. *ACS Chem Biol* **8**, 500-505 (2013).
303. Edson, N. L. The intermediary metabolism of the mycobacteria. *Bacteriol Rev.* **15**, 147-182 (1951).
304. Izumori, K., Yamanaka, K., Elbein, D. Pentose metabolism in *Mycobacterium smegmatis*: Specificity of induction of pentose isomerases. *J Bacteriol* **128**, 587-591 (1976).
305. Titgemeyer, F. *et al.* A genomic view of sugar transport in *Mycobacterium smegmatis* and *Mycobacterium tuberculosis*. *J Bacteriol* **189**, 5903-5915 (2007).
306. Braibant, M., Gilot, P., Content, J. The ATP binding cassette (ABC) transport systems of *Mycobacterium tuberculosis*. *FEMS Microbiol Rev* **24**, 449-467 (2000).
307. Wolucka, B. A., McNeil, M. R., de Hoffmann, E., Chojnacki, T., Brennan, P. J. Recognition of the lipid intermediate for arabinogalactadkabinomannan biosynthesis and its relation to the mode of action of ethambutol on mycobacteria. *J Biol Chem* **269**, 23328-23335 (1994).
308. Basso, L. A. *et al.* Purine nucleoside phosphorylase from *Mycobacterium tuberculosis*. Analysis of inhibition by a transition-state analogue and dissection by parts. *Biochemistry* **40**, 8196-8203 (2001).
309. Sigrell, J. A., Cameron, A. D., Jones, T. A., Mowbray, S. L. Purification, characterization, and crystallization of *Escherichia coli* ribokinase. *Protein Sci* **6**, 2474-2476 (1997).

- 310.Reddy, M. C. *et al.* High resolution crystal structures of *Mycobacterium tuberculosis* adenosine kinase: insights into the mechanism and specificity of this novel prokaryotic enzyme. *J Biol Chem* **282**, 27334-27342 (2007).
- 311.Sasseti, C. M., Boyd, D. H., Rubin, E. J. Genes required for mycobacterial growth defined by high density mutagenesis. *Mol Microbiol* **48**, 77-84 (2003).
- 312.Winkler, C., Denker, K., Wortelkamp, S., Sickmann, A. Silver- and Coomassie-staining protocols: detection limits and compatibility with ESI MS. *Electrophoresis* **28**, 2095-2099 (2007).
- 313.Ragas, A., Roussel, L., Puzo, G., Rivière, M. The *Mycobacterium tuberculosis* cell-surface glycoprotein apa as a potential adhesin to colonize target cells via the innate immune system pulmonary C-type lectin surfactant protein A. *J Biol Chem* **282**, 5133-5142 (2007).
- 314.Dobos, K. M., Khoo, K. H., Swiderek, K. M., Brennan, P. J., Belisle, J. T. Definition of the full extent of glycosylation of the 45-kilodalton glycoprotein of *Mycobacterium tuberculosis*. *J Bacteriol* **178**, 2498-2506 (1996).
- 315.Smith, G. T., Sweredoski, M. J., Hess, S. O-linked glycosylation sites profiling in *Mycobacterium tuberculosis* culture filtrate proteins. *J Proteomics* **97**, 296-306 (2014).
- 316.Foley, H. N., Stewart, J. A., Kavunja, H. W., Rundell, S. R., Swarts, B. M. Bioorthogonal chemical reporters for selective in situ probing of mycomembrane components in mycobacteria. *Angew Chem* **128**, 2093-2097 (2016).
- 317.Lowery, R., Gibson, M. I., Thompson, R. L., Fullam, E. Deuterated carbohydrate probes as 'label-free' substrates for probing nutrient uptake in mycobacteria by nuclear reaction analysis. *Chem Commun* **51**, 4838-4841 (2015).
- 318.Russell, D. G. *et al.* *Mycobacterium tuberculosis* wears what it eats. *Cell Host Microbe* **8**, 68-76 (2010).
- 319.Homolka, S., Niemann, S., Russell, D. G., Rohde, K. H., Deretic, V. Functional genetic diversity among *Mycobacterium tuberculosis* complex clinical isolates. Delineation of conserved core and lineage-specific transcriptomes during intracellular survival. *PLoS Pathog* **6**, e1000988 (2010).
- 320.Meredith, T. C., Aggarwal, P., Mamat, U., Lindner, B., Woodard, R. W. Redefining the requisite lipopolysaccharide structure in *Escherichia coli*. *ACS Chem Biol* **1**, 33-42 (2006).
- 321.Ray, P. H. Purification and characterization of 3-deoxy-D-manno-octulosonate 8-phosphate synthetase from *Escherichia coli*. *J Bacteriol* **141**, 635-644 (1980).
- 322.Cech, D., Wang, P. F., Holler, T. P., Woodard, R. W. Analysis of the arabinose-5-phosphate isomerase of *Bacteroides fragilis* provides insight into regulation of single-domain arabinose phosphate isomerases. *J Bacteriol* **196**, 2861-2868 (2014).
- 323.Horecker, B. L. The pentose phosphate pathway. *J Biol Chem* **277**, 47965-47971 (2002).
- 324.Xavier Da Silveira, E., Jones, C., Wait, R., Previato, J. O., Mendonca-Previato, L. Glycoinositol phospholipids from *Endotrypanum* species express epitopes in common with saccharide side chains of the lipophosphoglycan from *Leishmania major*. *Biochem J* **329**, 665-673 (1998).
- 325.Pimenta, P. F. *et al.* Stage-specific adhesion of *Leishmania* promastigotes to the sandfly midgut. *Science* **256**, 1812-1815 (1992).
- 326.Kamhawi, S. *et al.* A role for insect galectins in parasite survival. *Cell* **119**, 329-341 (2004).



327. Novozhilova, N. M., Bovin, N. V. D-Arabinose metabolism: characterization of bifunctional arabinokinase/pyrophosphorylase of *Leishmania major*. *Acta Naturae*, 81-83 (2009).
328. Meniche, X. *et al.* Subpolar addition of new cell wall is directed by DivIVA in mycobacteria. *Proc Natl Acad Sci USA* **111**, E3243-51 (2014).
329. Hett, E. C., Rubin, E. J. Bacterial growth and cell division: a mycobacterial perspective. *Microbiol Mol Biol Rev* **72**, 126-156 (2008).
330. Thanky, N. R., Young, D. B., Robertson, B. D. Unusual features of the cell cycle in mycobacteria: polar-restricted growth and the snapping-model of cell division. *Tuberculosis* **87**, 231-236 (2007).
331. Plocinski, P. *et al.* *Mycobacterium tuberculosis* CwsA interacts with CrgA and Wag31, and the CrgA-CwsA complex is involved in peptidoglycan synthesis and cell shape determination. *J Bacteriol.* **194**, 6398-6409 (2012).
332. Vergne, I., Chua, J., Singh, S. B., Deretic, V. Cell biology of *Mycobacterium tuberculosis* phagosome. *AnnuRev Cell Dev Biol* **20**, 367-394 (2004).
333. Russell, D. G. *Mycobacterium tuberculosis*: here today, and here tomorrow. *Nat Rev Mol Cell Biol* **2**, 569-577 (2001).
334. Clemens, D. L., Lee, B. Y., Horwitz, M. A. Deviant expression of Rab5 on phagosomes containing the intracellular pathogens *Mycobacterium tuberculosis* and *Legionella pneumophila* is associated with altered phagosomal fate. *Infect Immun* **68**, 2671-2684 (2000).
335. Via, L. E. *et al.* Arrest of mycobacterial phagosome maturation is caused by a block in vesicle fusion between stages controlled by Rab5 and Rab7. *J Biol Chem* **272**, 13326-13331 (1997).
336. Ullrich, H. J., Beatty, W. L., Russell, D. G. Direct delivery of procathepsin D to phagosomes. Implications for phagosome biogenesis and parasitism by *Mycobacterium*. *Eur J Cell Biol* **78**, 739-748 (1999).
337. Via, L. E. *et al.* Effects of cytokines on mycobacterial phagosome maturation. *J Cell Sci* **111**, 897-905 (1998).
338. Sukumar, N., Tan, S., Aldridge, B. B., Russell, D. G., Salgame, P. Exploitation of *Mycobacterium tuberculosis* reporter strains to probe the impact of vaccination at sites of infection. *PLoS Pathog* **10**, e1004394 (2014).
339. Tan, S., Sukumar, N., Abramovitch, R. B., Parish, T., Russell, D. G. *Mycobacterium tuberculosis* responds to chloride and pH as synergistic cues to the immune status of its host cell. *PLoS Pathog* **9**, e1003282 (2013).
340. Kaplan, G. *et al.* *Mycobacterium tuberculosis* growth at the cavity surface: a microenvironment with failed immunity. *Infect Immun* **71**, 7099-7108 (2003).
341. Keener, A. B. Oldie but goodie: Repurposing penicillin for tuberculosis. *Nat Med* **20**, 976-978 (2014).
342. Prosser, G. A., de Carvalho, L. P. Kinetic mechanism and inhibition of *Mycobacterium tuberculosis* D-alanine: D-alanine ligase by the antibiotic D-cycloserine. *FEBS J* **280**, 1150-1166 (2013).
343. Kaewsapsak, P., Esonu, O., Dube, D. H. Recruiting the host's immune system to target *Helicobacter pylori*'s surface glycans. *Chembiochem* **14**, 721-726 (2013).
344. Memmel, E., Homann, A., Oelschlaeger, T. A., Seibel, J. Metabolic glycoengineering of *Staphylococcus aureus* reduces its adherence to human T24 bladder carcinoma cells. *Chem Commun* **49**, 7301-7303 (2013).
345. McEnaney, P. J., Parker, C. G., Zhang, A. X., Spiegel, D. A. Antibody-recruiting molecules: an emerging paradigm for engaging immune function in treating human disease. *ACS Chem Biol* **7**, 1139-1151 (2012).

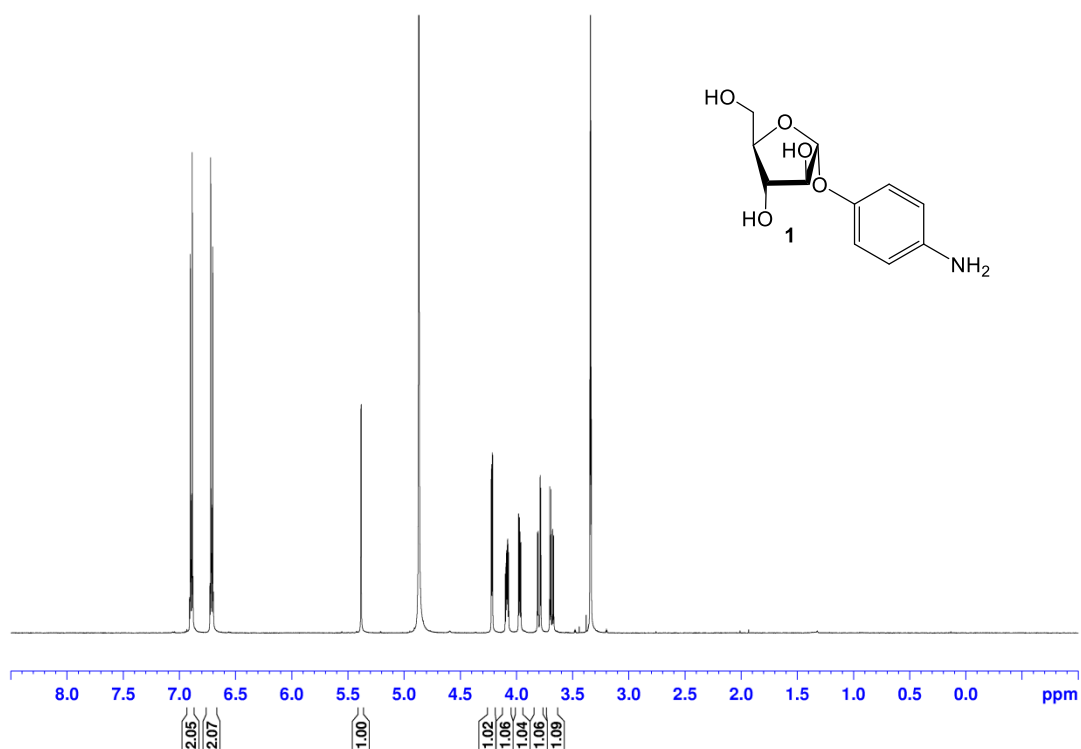
346. Brown, S. B., Brown, E. A., Walker, I. The present and future role of photodynamic therapy in cancer treatment. *Lancet Oncol* **5**, 497-508 (2004).
347. Davis, M. E., Chen, Z. G., Shin, D. M. Nanoparticle therapeutics: an emerging treatment modality for cancer. *Nat Rev Drug Discov* **7**, 771-782 (2008).
348. O'Connor, A. E., Gallagher, W. M., Byrne, A. T. Porphyrin and nonporphyrin photosensitizers in oncology. Preclinical and clinical advances in photodynamic therapy. *Photochem Photobiol* **85**, 1053-1074 (2009).
349. Josefsen, L. B., Boyle, R. W. Unique diagnostic and therapeutic roles of porphyrins and phthalocyanines in photodynamic therapy, imaging and theranostics. *Theranostics* **2**, 916-966 (2012).
350. Moan, J., Berg, K. The photodegradation of porphyrins in cells can be used to estimate the lifetime of singlet oxygen. *Photochem Photobiol* **53**, 549-553 (1991).
351. Sharma, S. K. *et al.* Drug discovery of antimicrobial photosensitizers using animal models. *Curr Pharm Des* **17**, 1303-1319 (2011).
352. Sperandio, F. F., Huang, Y. Y., Hamblin, M. R. Antimicrobial photodynamic therapy to kill Gram-negative bacteria. *Recent Pat Antiinfect Drug Discov* **8**, 108-120 (2013).
353. Wardlaw, J. L., Sullivan, T. J., Lux, C. N., Austin, F. W. Photodynamic therapy against common bacteria causing wound and skin infections. *Vet J* **192**, 374-377 (2012).
354. Verma, R. K. *et al.* Inhalable microparticles containing nitric oxide donors: saying NO to intracellular *Mycobacterium tuberculosis*. *Mol Pharm* **9**, 3183-3189 (2012).
355. Verma, R. K. *et al.* Inhalable microparticles of nitric oxide donors induce phagosome maturation and kill *Mycobacterium tuberculosis*. *Tuberculosis* **93**, 412-417 (2013).
356. Doane, T. L., Burda, C. The unique role of nanoparticles in nanomedicine: imaging, drug delivery and therapy. *Chem Soc Rev* **41**, 2885-2911 (2012).
357. Norman, R. S., Stone, J. W., Gole, A., Murphy, C. J., Sabo-Attwood, T. L. Targeted photothermal lysis of the pathogenic bacteria, *Pseudomonas aeruginosa*, with gold nanorods. *Nano Lett* **8**, 302-306 (2008).
358. Wirth, T. *et al.* Origin, spread and demography of the *Mycobacterium tuberculosis* complex. *PLoS Pathog* **4**, e1000160 (2008).
359. Zelmer, A. *et al.* A new in vivo model to test anti-tuberculosis drugs using fluorescence imaging. *J Antimicrob Chemother* **67**, 1948-1960 (2012).
360. Carroll, P. *et al.* Sensitive detection of gene expression in mycobacteria under replicating and non-replicating conditions using optimized far-red reporters. *PLoS One* **5**, e9823 (2010).
361. Dubray, G., Bezar, G. A Highly sensitive periodic acid-silver stain for 1,2-diol groups of glycoproteins and polysaccharides in polyacrylamide gels. *Anal Biochem* **119**, 325-329 (1982).
362. Tsai, C. M., Frasch, C. E. A Sensitive Silver Stain for Detecting Lipopolysaccharides in Polyacrylamide Gels. *Anal Biochem* **119**, 115-119 (1982).
363. Hashimoto, H., Izumi, M. A Facile synthesis of 5-thio-L-fucose and 3-O-allyl-L-fucose triacetate from D-arabinose. *Chem Lett* **21**, 25-28 (1992).
364. Machado, I. C., Alonso, O. M. & Bencomo, V. V. A new approach to the ribosylribitol intermediate for the synthesis of *Haemophilus influenzae* type B oligosaccharides. *J Carbohydr Chem* **13**, 465-474 (1994).

365. Vedejs, E., Stults, J. S. Synthesis of azocine derivatives from thio aldehyde Diels-Alder adducts. *J Org Chem* **53**, 2226-2232 (1988).
366. Roy, B. C., Mallik, S. Synthesis of conjugated diacetylene, metal-chelating monomers for polymerizable monolayer assemblies. *Org Lett* **3**, 1877-1879 (2001).

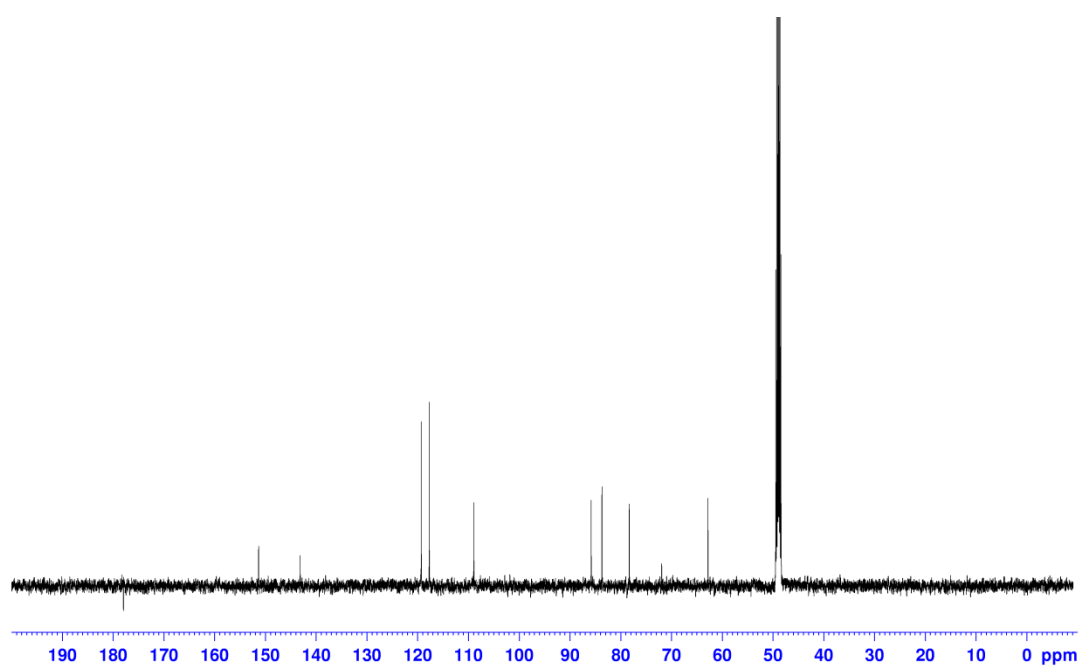
## 5 Appendix

### 5.1 NMR spectra

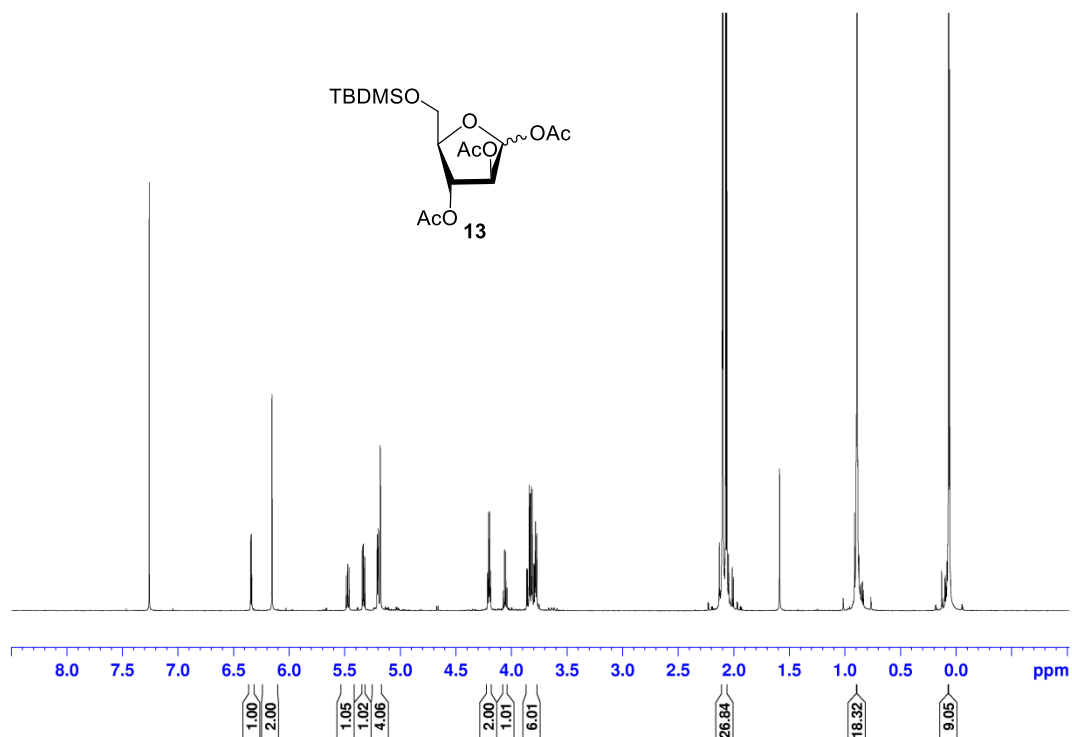
$^1\text{H}$  and  $^{13}\text{C}$  NMR spectra of new compounds and  $^1\text{H}$  NMR of known molecules, which were used for metabolic labeling:



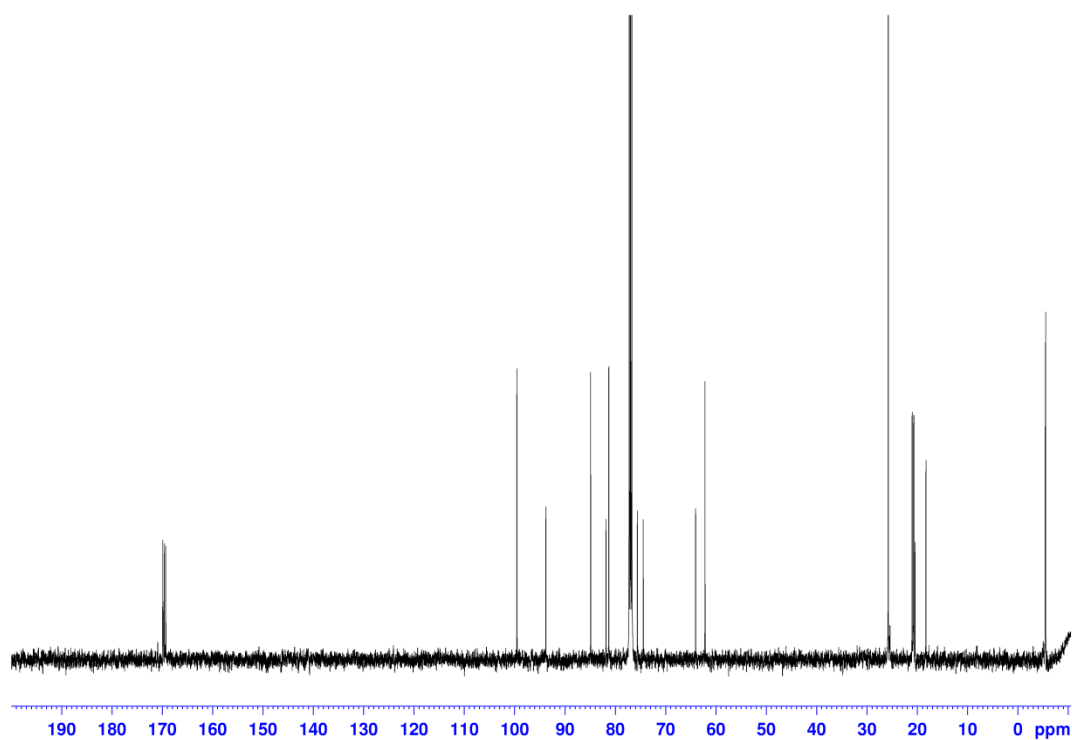
**Figure 56.**  $^1\text{H}$  NMR spectrum (500 MHz,  $\text{MeOH-}d_4$ , 300 K) of *p*-aminophenyl  $\alpha$ -D-arabinofuranoside (1).



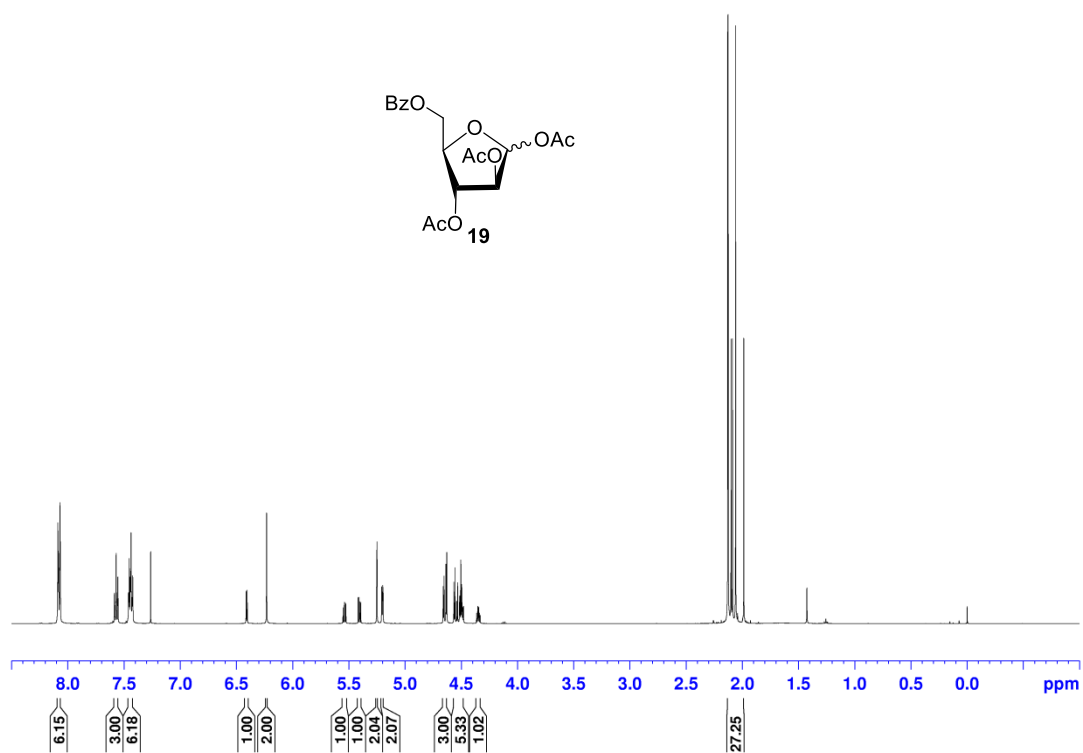
**Figure 57.**  $^{13}\text{C}$  NMR spectrum (125 MHz,  $\text{MeOH-}d_4$ , 300 K) of *p*-aminophenyl  $\alpha$ -D-arabinofuranoside (1).



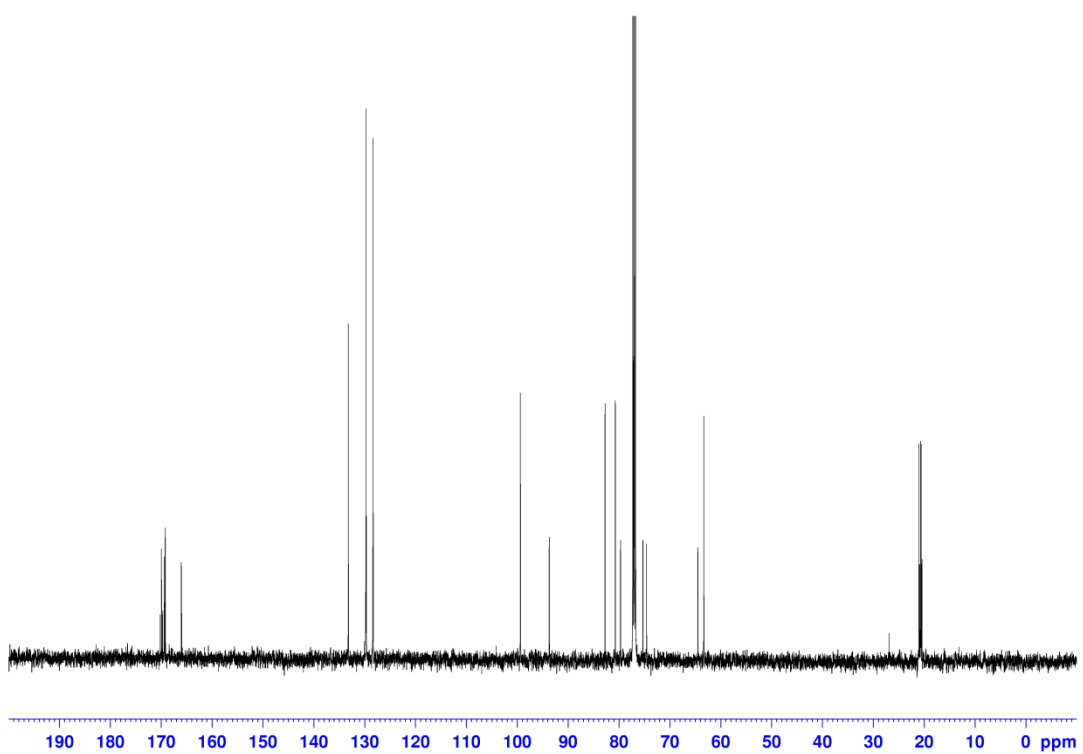
**Figure 58.** <sup>1</sup>H NMR spectrum (500 MHz, CDCl<sub>3</sub>, 300 K) of 5-*O*-*tert*-butyldimethylsilyl-1,2,3-tri-*O*-acetyl- $\alpha,\beta$ -D-arabinofuranose (**13**).



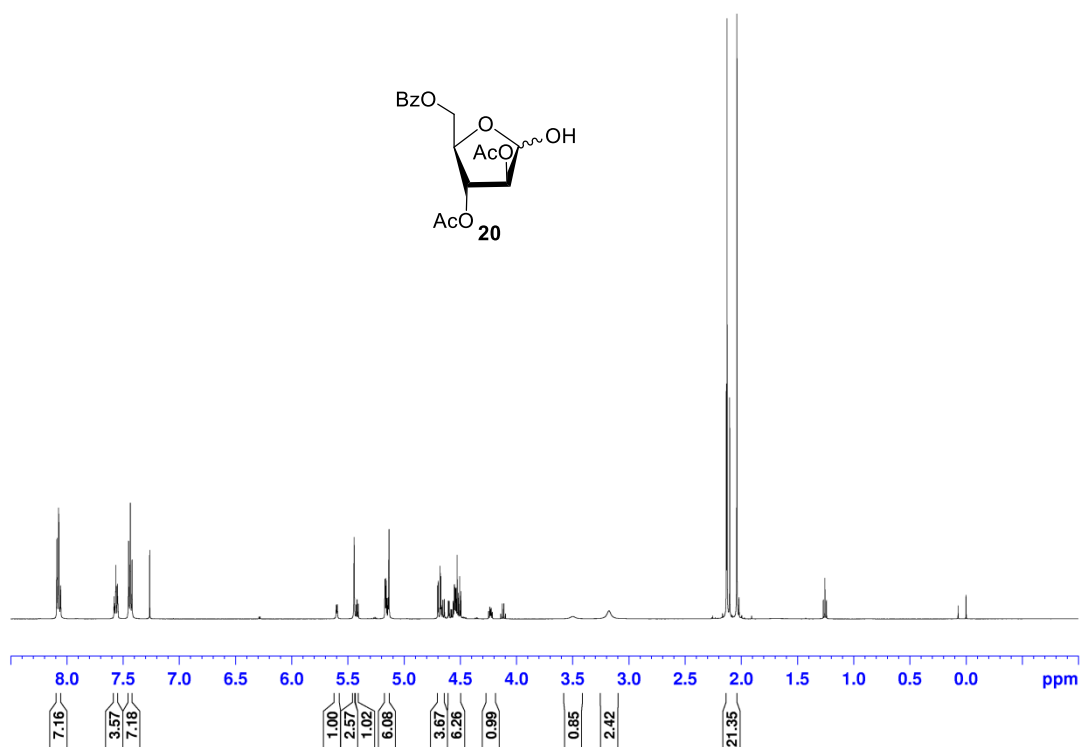
**Figure 59.** <sup>13</sup>C NMR spectrum (125 MHz, CDCl<sub>3</sub>, 300 K) of 5-*O*-*tert*-butyldimethylsilyl-1,2,3-tri-*O*-acetyl- $\alpha,\beta$ -D-arabinofuranose (**13**).



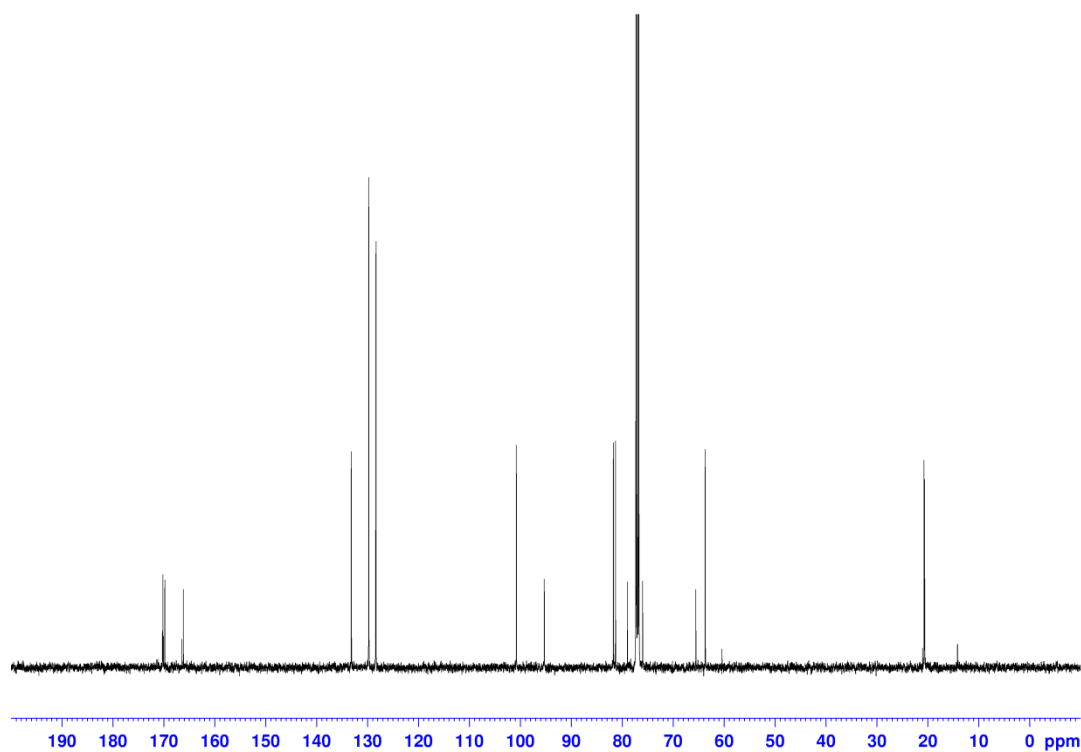
**Figure 60.**  $^1\text{H NMR}$  spectrum (500 MHz,  $\text{CDCl}_3$ , 300 K) of 5-O-benzoyl-1,2,3-tri-O-acetyl- $\alpha,\beta$ -D-arabinofuranose (19).



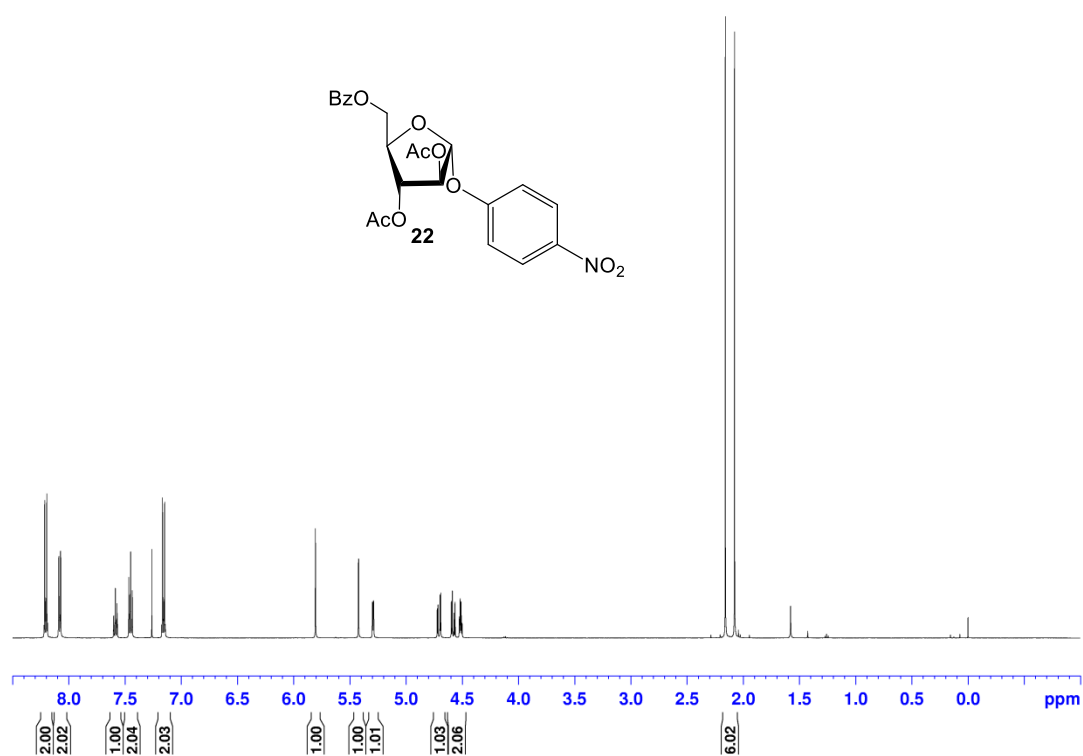
**Figure 61.**  $^{13}\text{C NMR}$  spectrum (125 MHz,  $\text{CDCl}_3$ , 300 K) of 5-O-benzoyl-1,2,3-tri-O-acetyl- $\alpha,\beta$ -D-arabinofuranose (19).



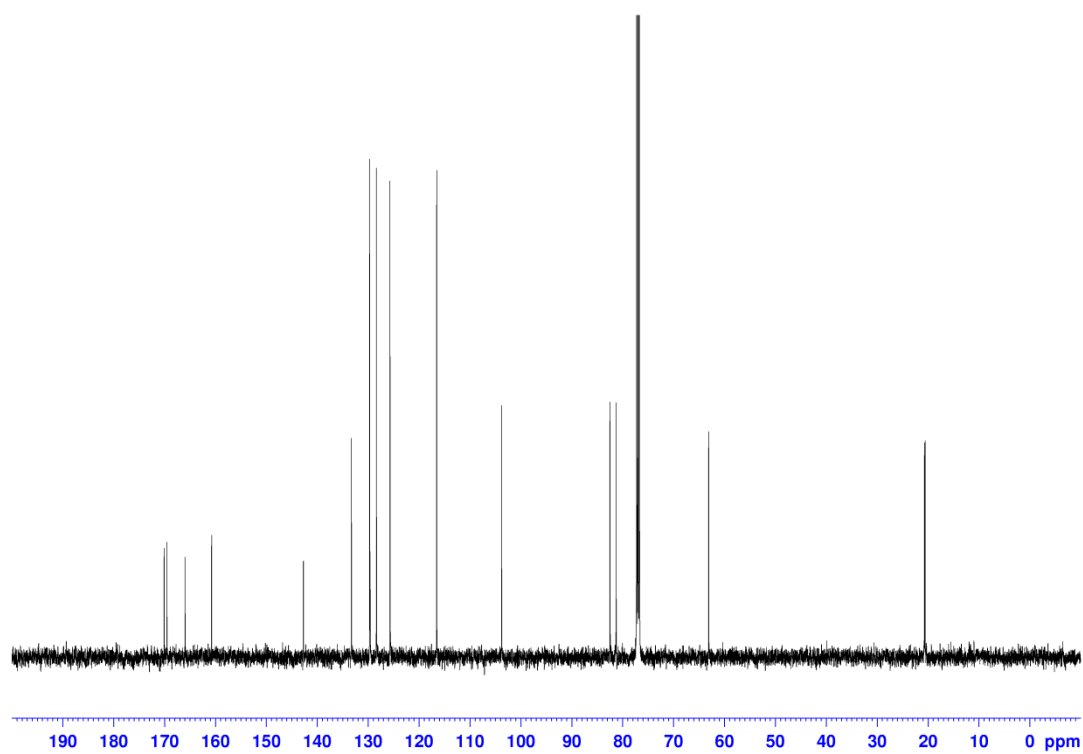
**Figure 62.**  $^1\text{H NMR}$  spectrum (500 MHz,  $\text{CDCl}_3$ , 300 K) of 5-O-benzoyl-2,3-di-O-acetyl- $\alpha,\beta$ -D-arabinofuranose (20).



**Figure 63.**  $^{13}\text{C NMR}$  spectrum (125 MHz,  $\text{CDCl}_3$ , 300 K) of 5-O-benzoyl-2,3-di-O-acetyl- $\alpha,\beta$ -D-arabinofuranose (20).

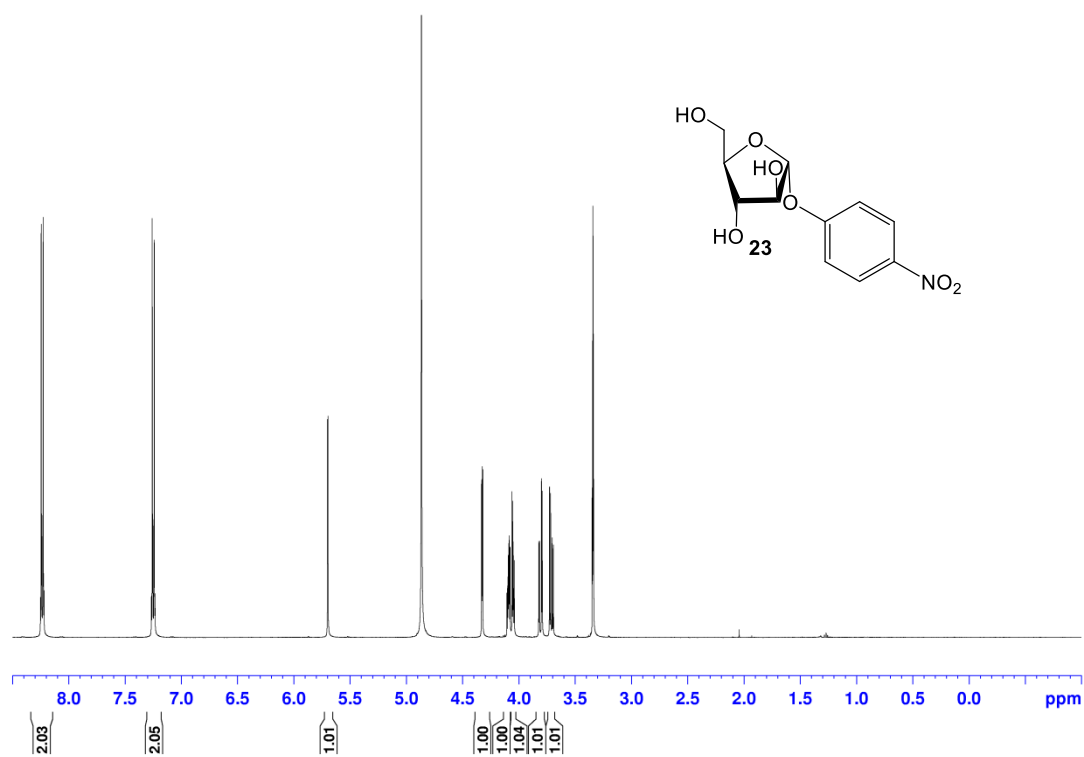


**Figure 64.**  $^1\text{H}$  NMR spectrum (500 MHz,  $\text{CDCl}_3$ , 300 K) of *p*-nitrophenyl 5-*O*-benzoyl-2,3-di-*O*-acetyl- $\alpha$ -D-arabinofuranoside (**22**).

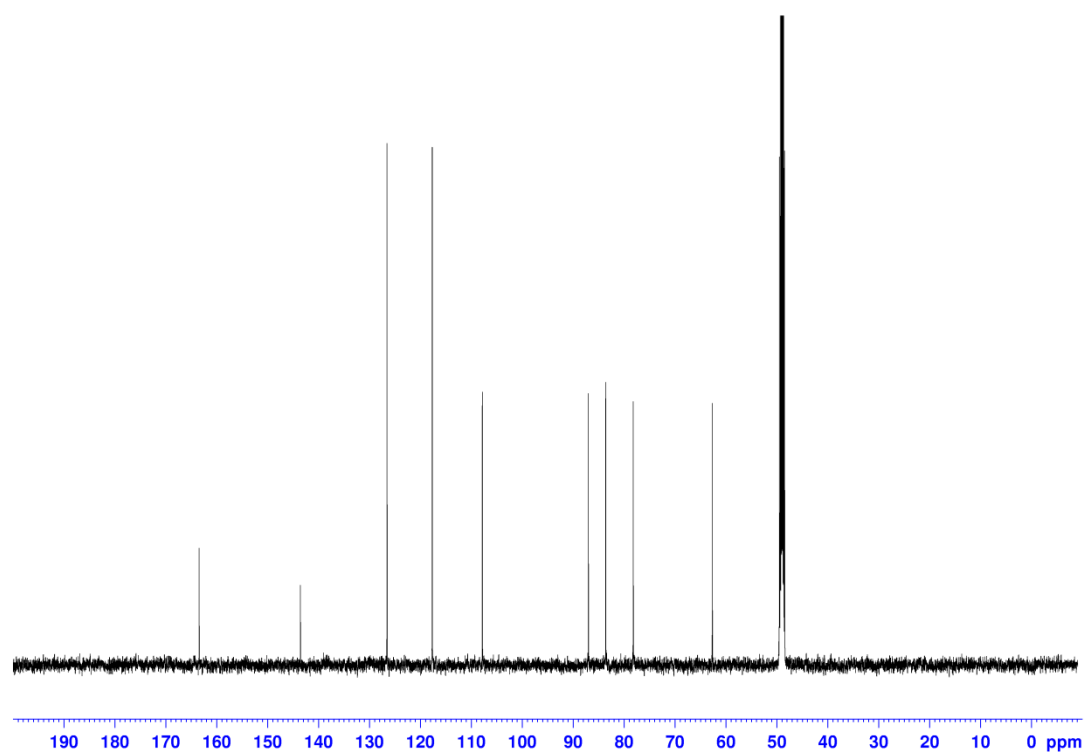


**Figure 65.**  $^{13}\text{C}$  NMR spectrum (125 MHz,  $\text{CDCl}_3$ , 300 K) of *p*-nitrophenyl 5-*O*-benzoyl-2,3-di-*O*-acetyl- $\alpha$ -D-arabinofuranoside (**22**).

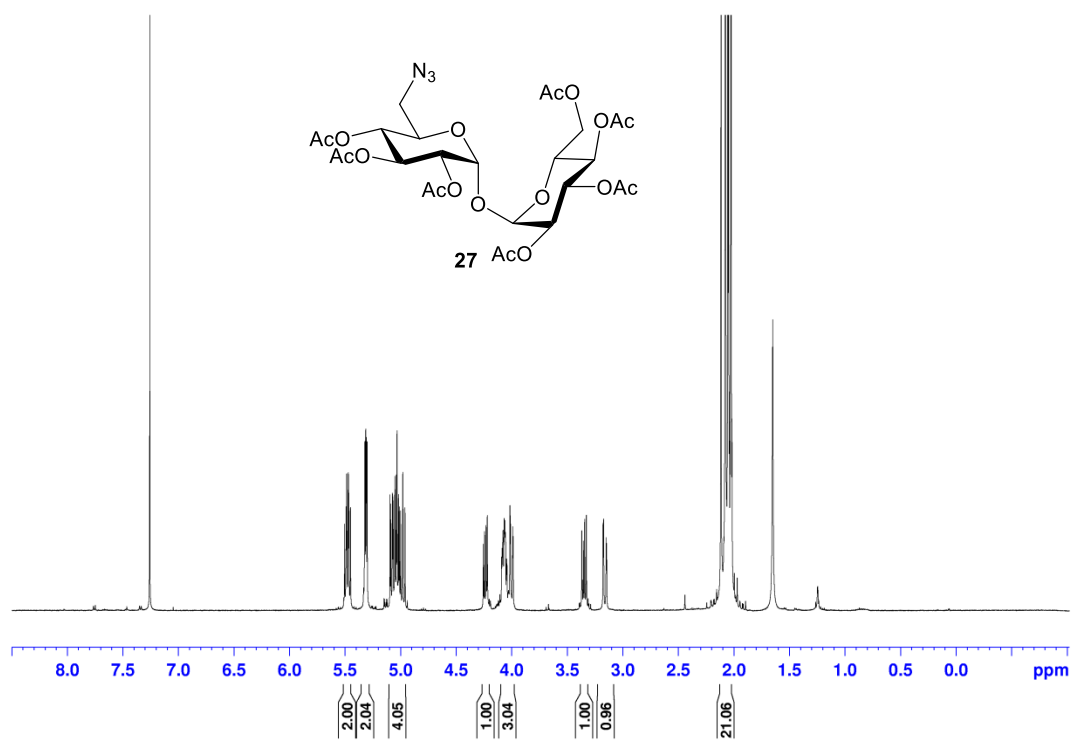




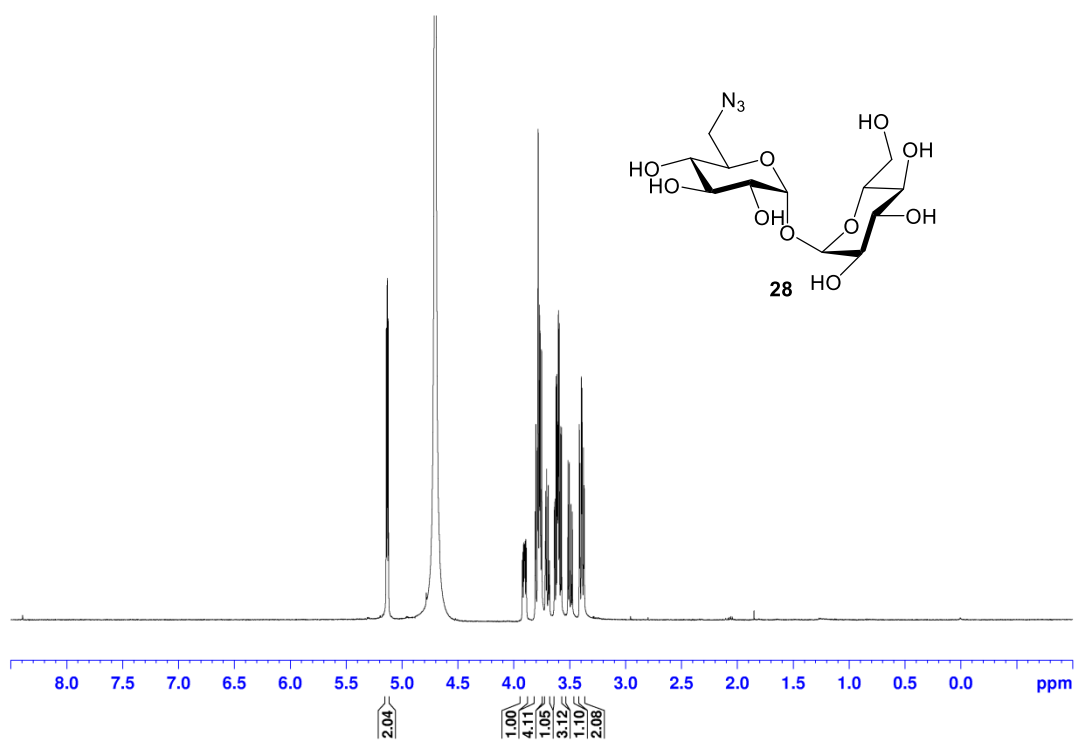
**Figure 66.** <sup>1</sup>H NMR spectrum (500 MHz, MeOH-*d*<sub>4</sub>, 300 K) of *p*-nitrophenyl α-D-arabinofuranoside (**23**).



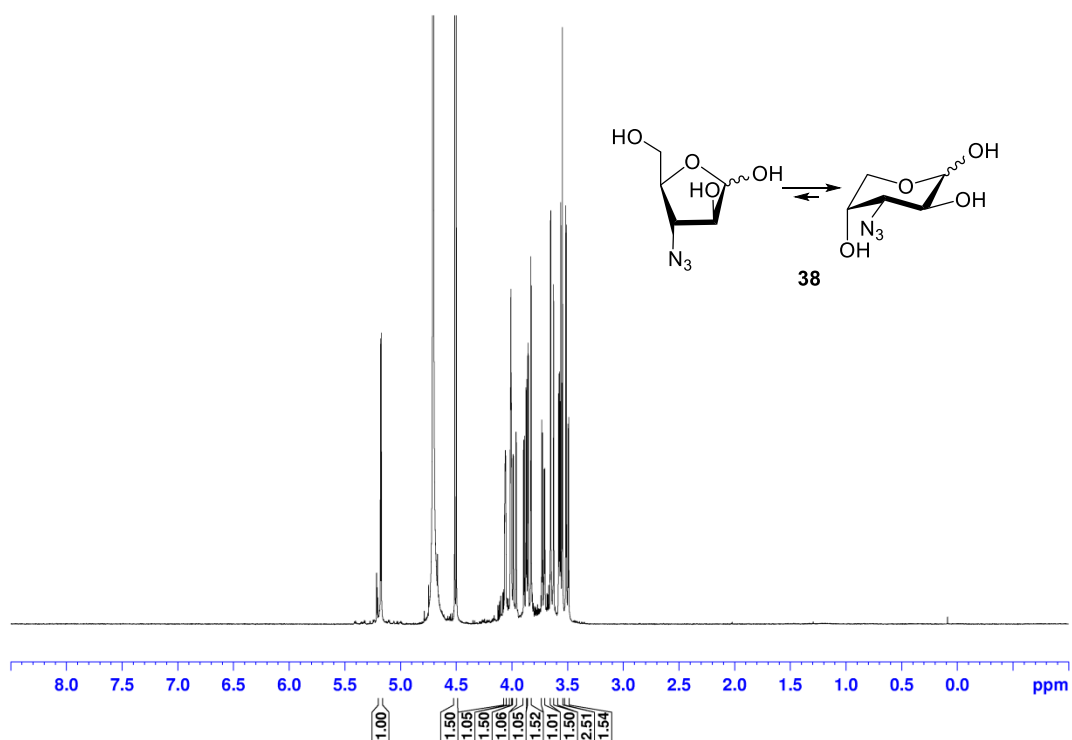
**Figure 67.** <sup>13</sup>C NMR spectrum (125 MHz, MeOH-*d*<sub>4</sub>, 300 K) of *p*-nitrophenyl α-D-arabinofuranoside (**23**).



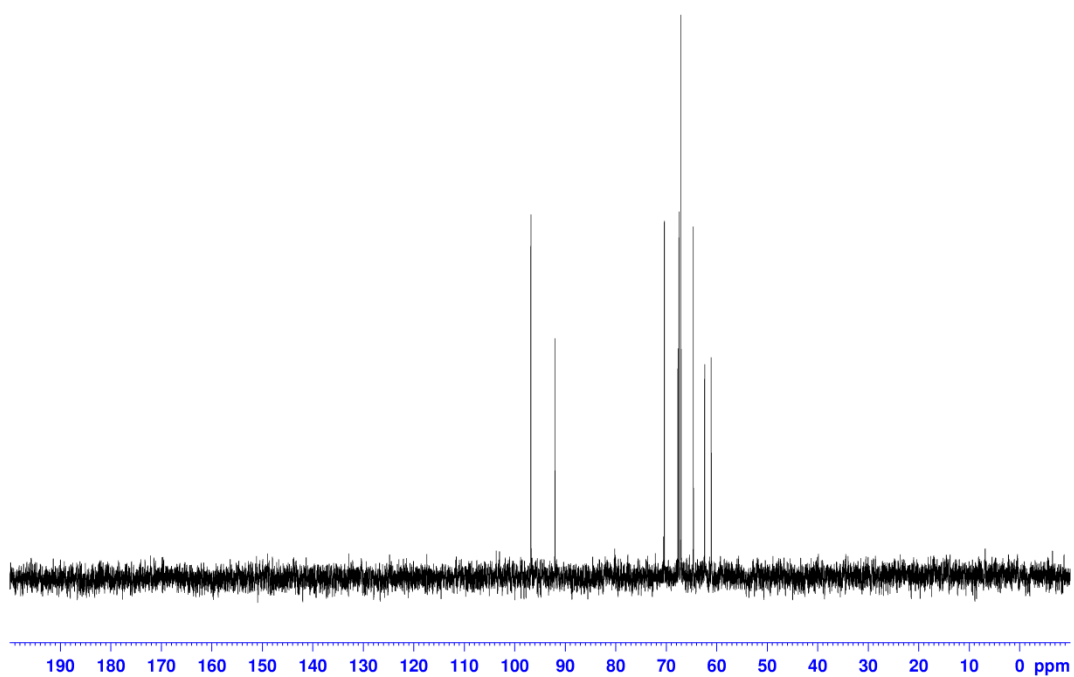
**Figure 68.** <sup>1</sup>H NMR spectrum (500 MHz, CDCl<sub>3</sub>, 300 K) of 6-azido-6-deoxy-2,3,4,2',3',4',6'-hepta-O-acetyl- $\alpha,\alpha$ -D-trehalose (**27**).



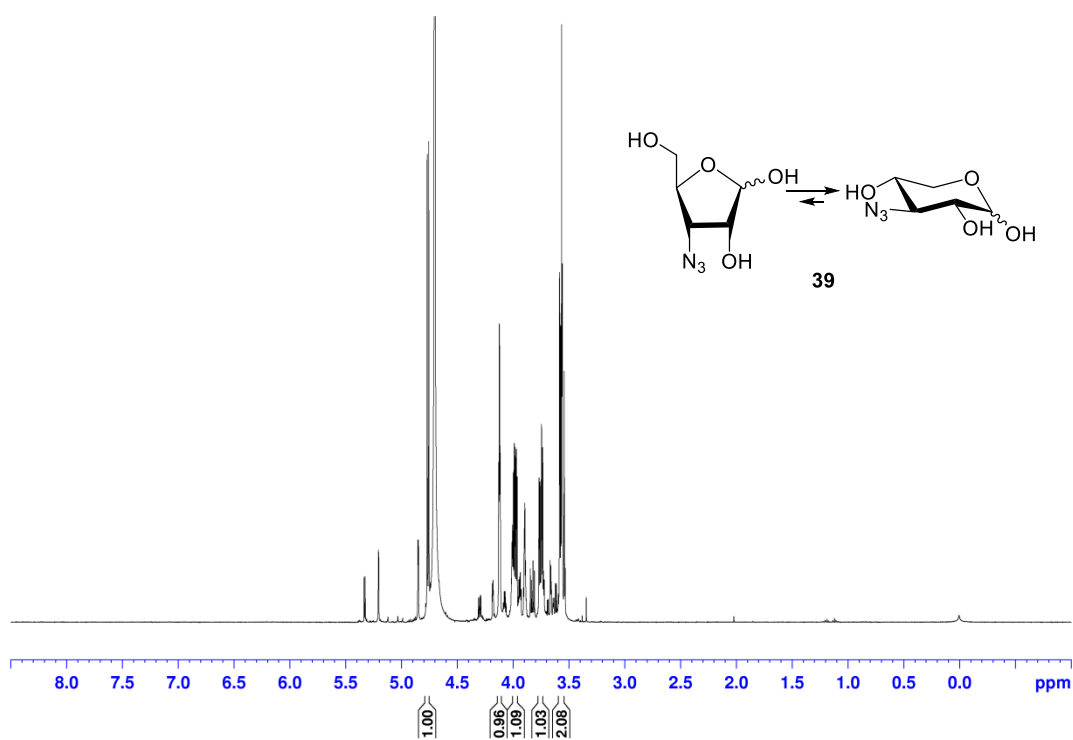
**Figure 69.** <sup>1</sup>H NMR spectrum (500 MHz, D<sub>2</sub>O, 300 K) of 6-azido-6-deoxy-α,α-D-trehalose (**28**).



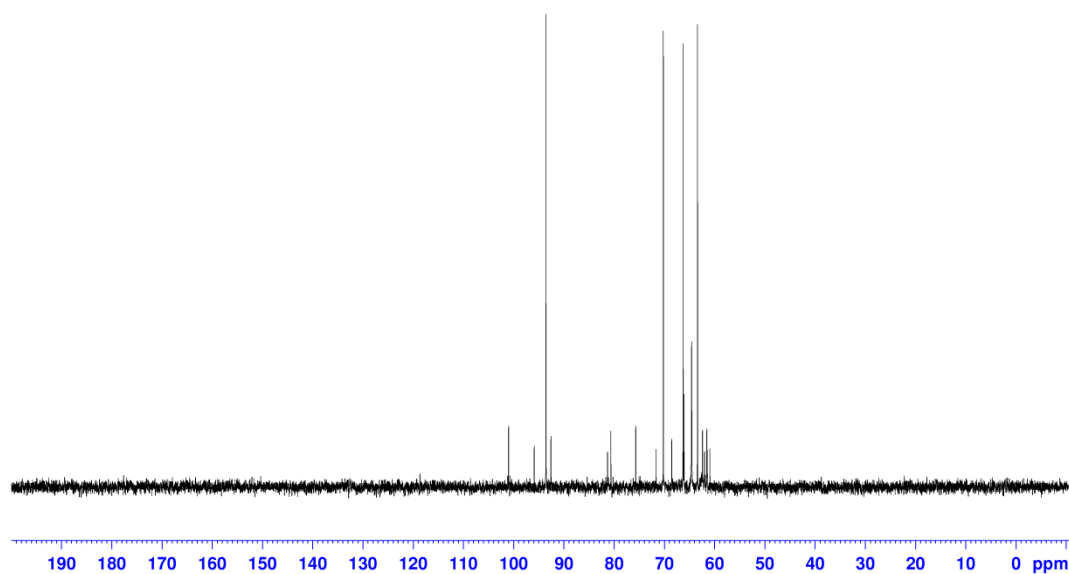
**Figure 70.**  $^1\text{H}$  NMR spectrum (500 MHz,  $\text{D}_2\text{O}$ , 300 K) of 3-azido-3-deoxy- $\alpha,\beta$ -D-arabinose (38).



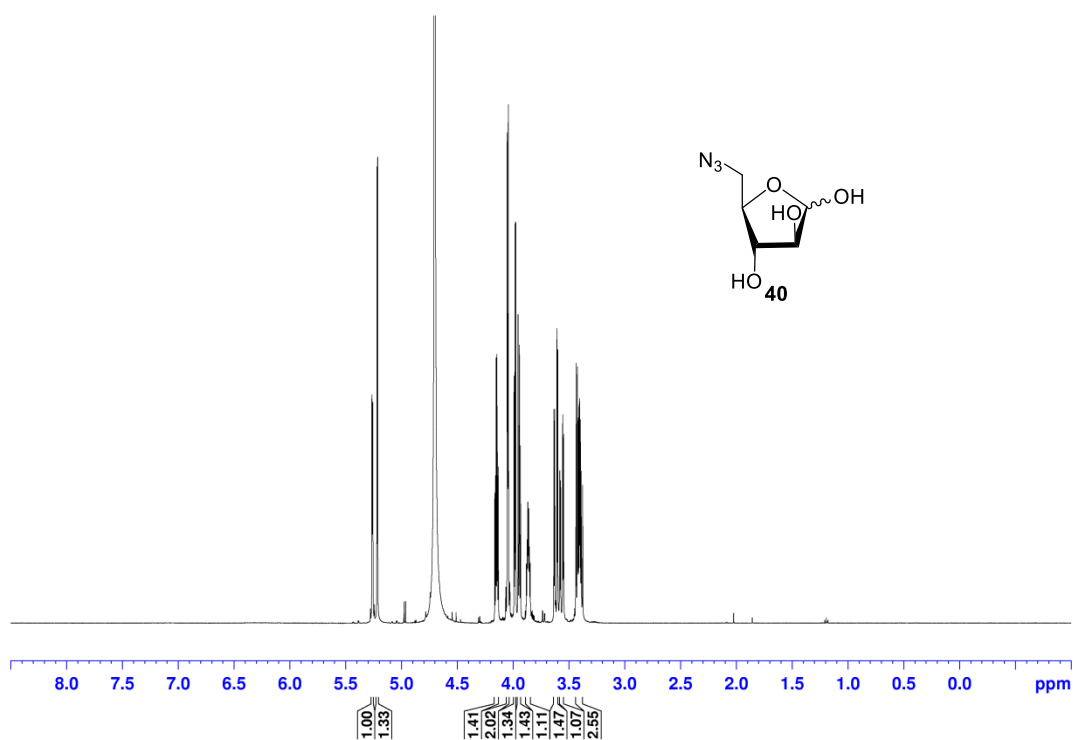
**Figure 71.**  $^{13}\text{C}$  NMR spectrum (125 MHz,  $\text{D}_2\text{O}$ , 300 K) of 3-azido-3-deoxy- $\alpha,\beta$ -D-arabinose (38).



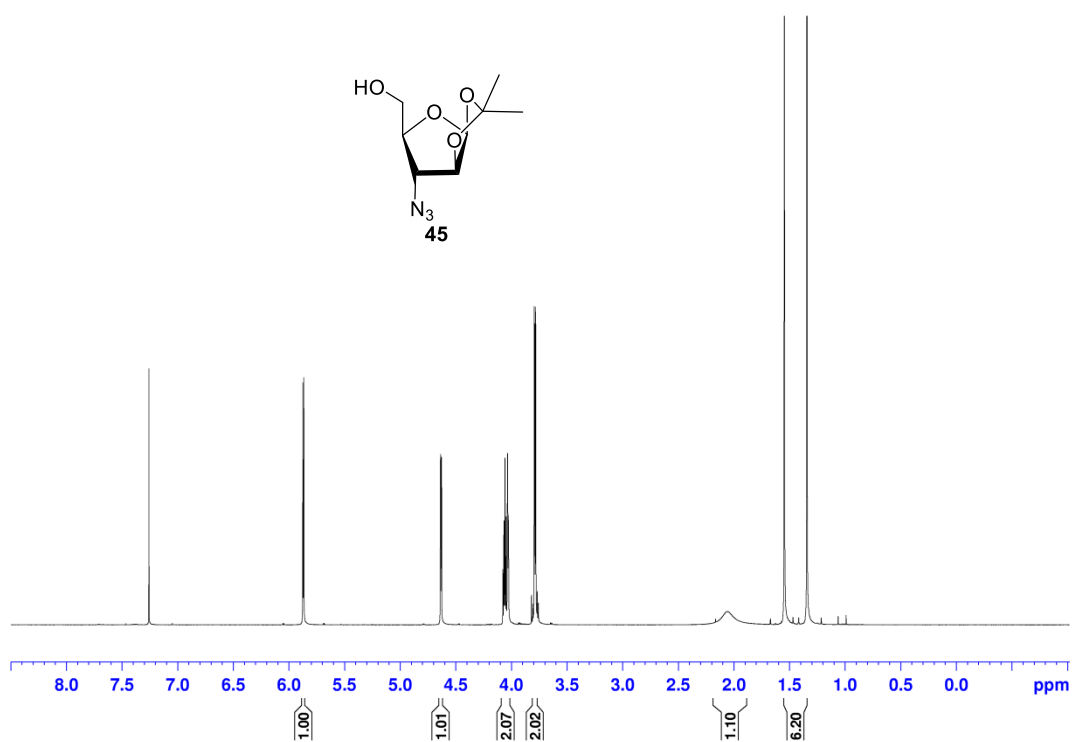
**Figure 72.** <sup>1</sup>H NMR spectrum (500 MHz, D<sub>2</sub>O, 300 K) of 3-azido-3-deoxy-α,β-D-ribose (**39**).



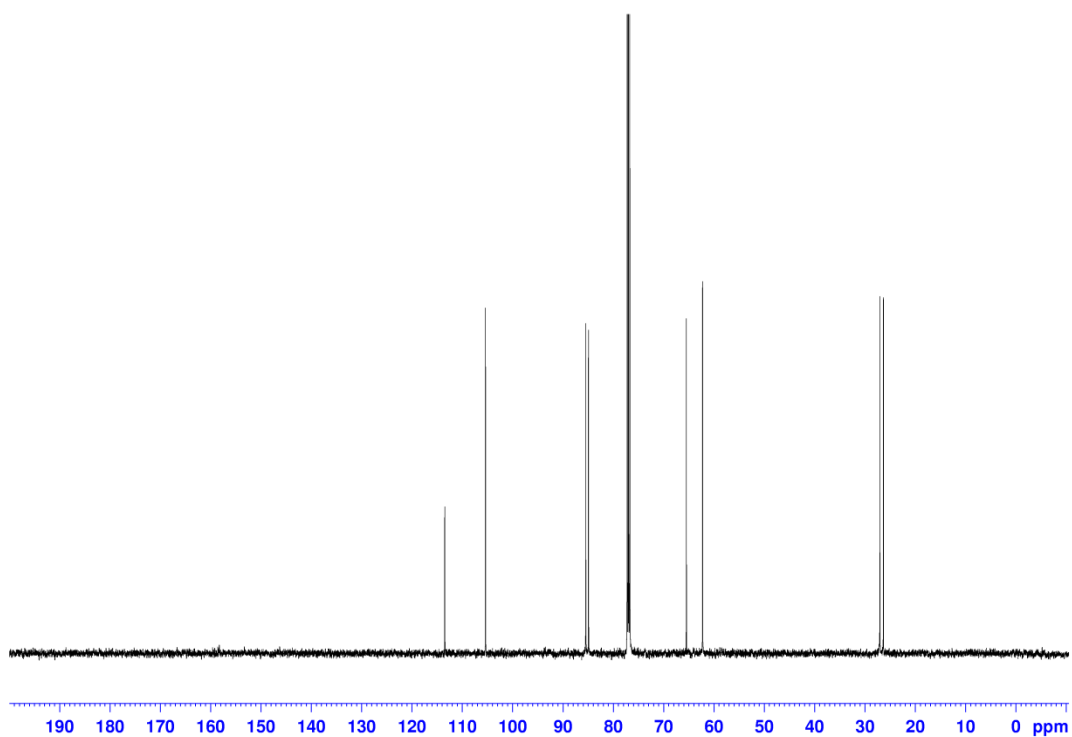
**Figure 73.** <sup>13</sup>C NMR spectrum (125 MHz, D<sub>2</sub>O, 300 K) of 3-azido-3-deoxy-α,β-D-ribose (**39**).



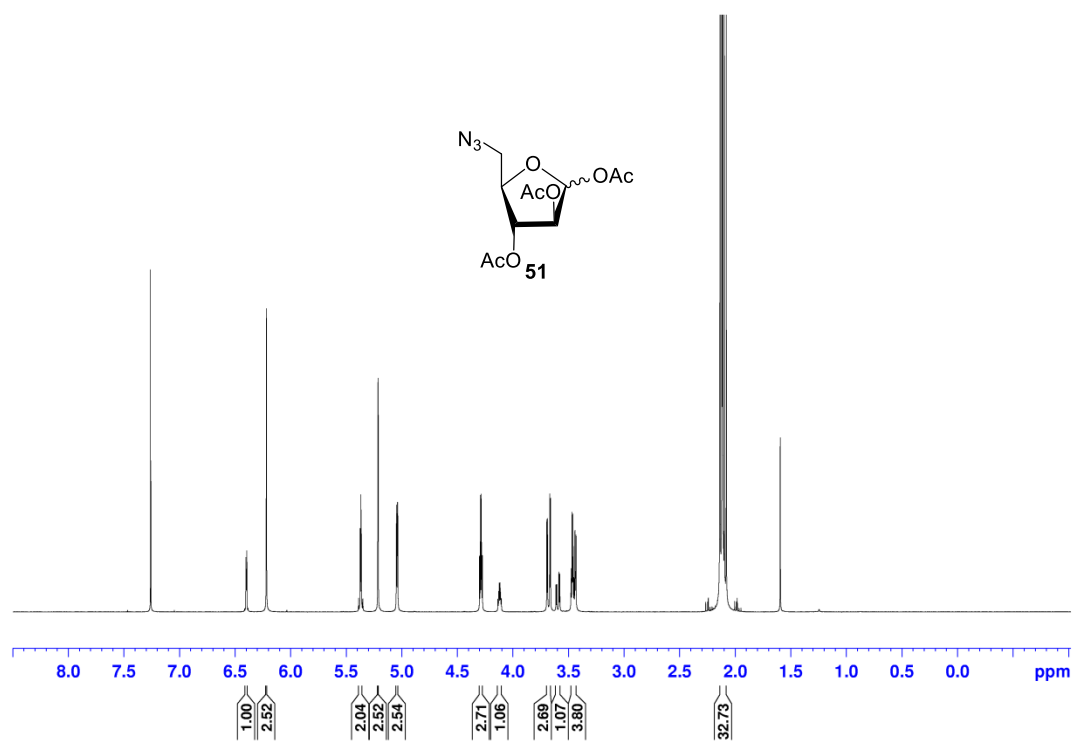
**Figure 74.** <sup>1</sup>H NMR spectrum (500 MHz, D<sub>2</sub>O, 300 K) of 5-azido-5-deoxy- $\alpha,\beta$ -D-arabinofuranose (**40**).



**Figure 75.** <sup>1</sup>H NMR spectrum (500 MHz, CDCl<sub>3</sub>, 300 K) of 3-azido-3-deoxy-1,2-O-isopropylidene-β-D-arabinofuranose (**45**).

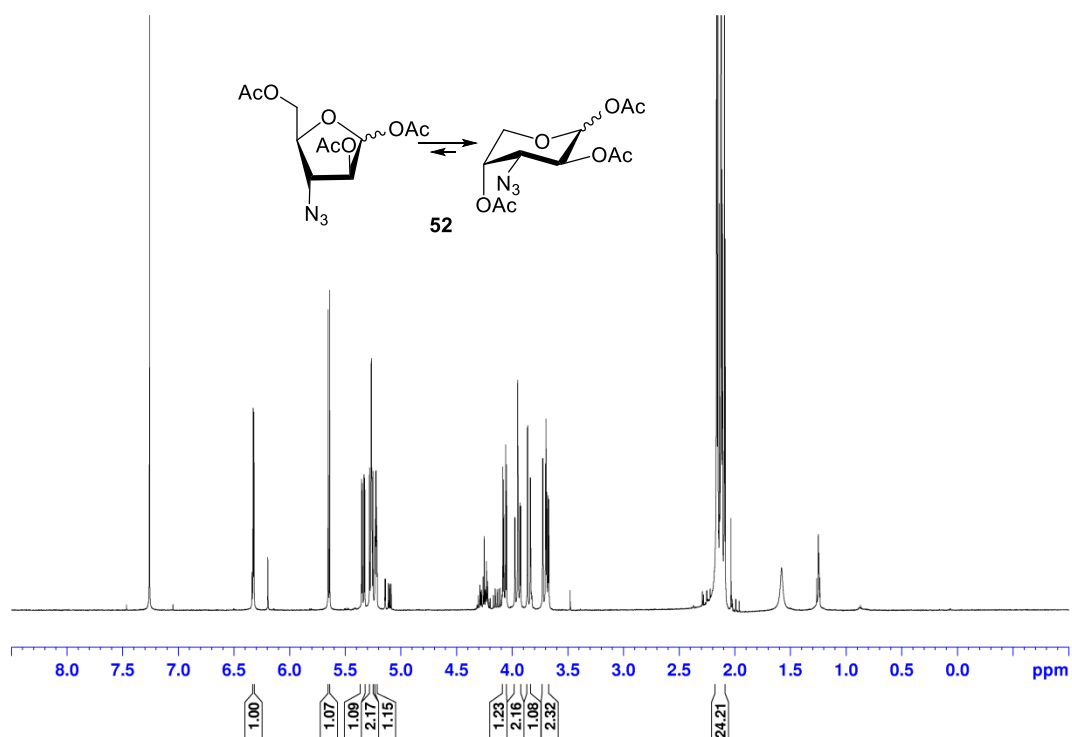


**Figure 76.** <sup>13</sup>C NMR spectrum (125 MHz, CDCl<sub>3</sub>, 300 K) of 3-azido-3-deoxy-1,2-O-isopropylidene-β-D-arabinofuranose (**45**).

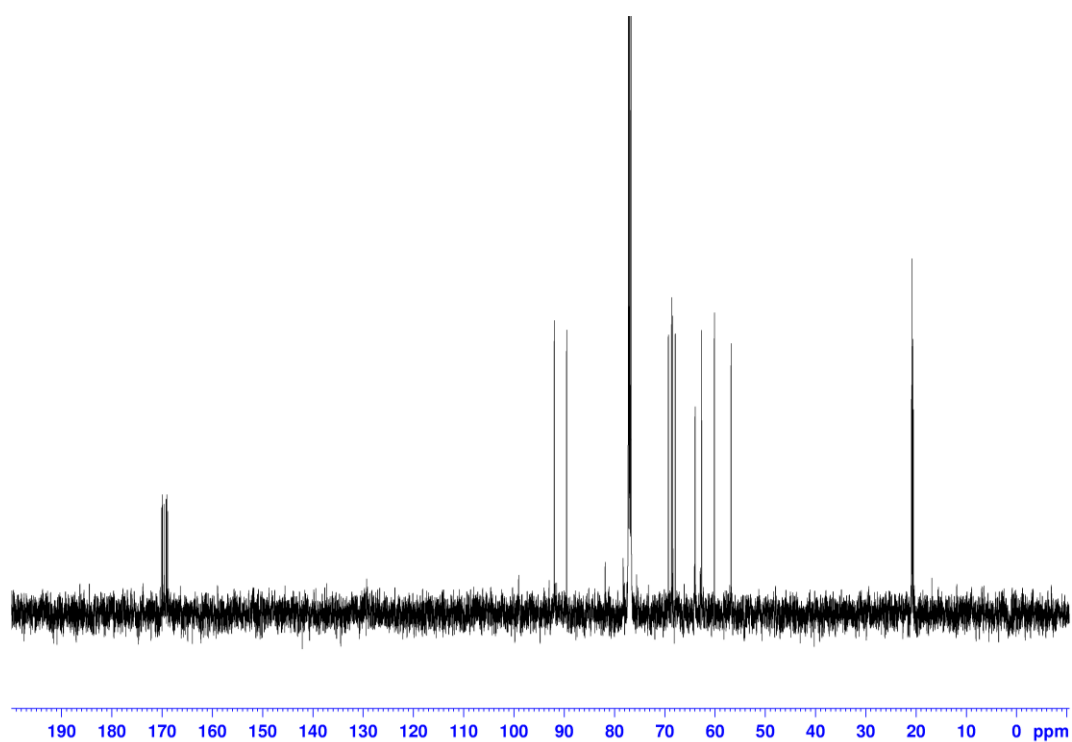


**Figure 77.** <sup>1</sup>H NMR spectrum (500 MHz, CDCl<sub>3</sub>, 300 K) of 5-azido-5-deoxy-1,2,3-tri-O-acetyl- $\alpha,\beta$ -D-arabinofuranose (**51**).

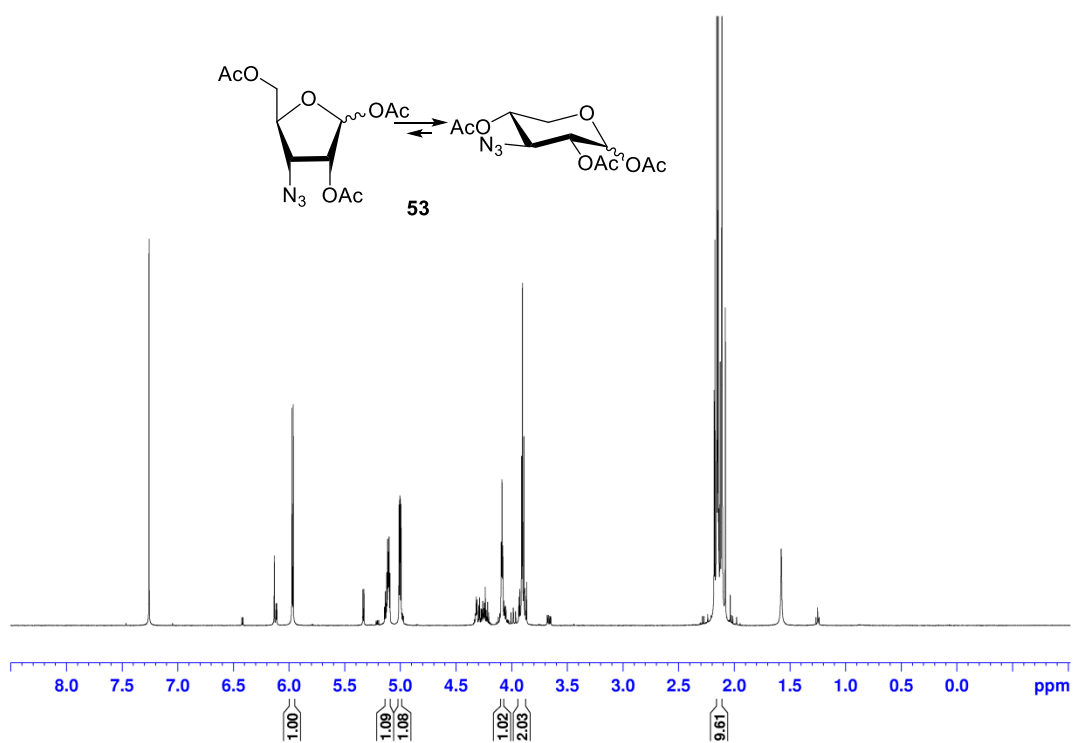




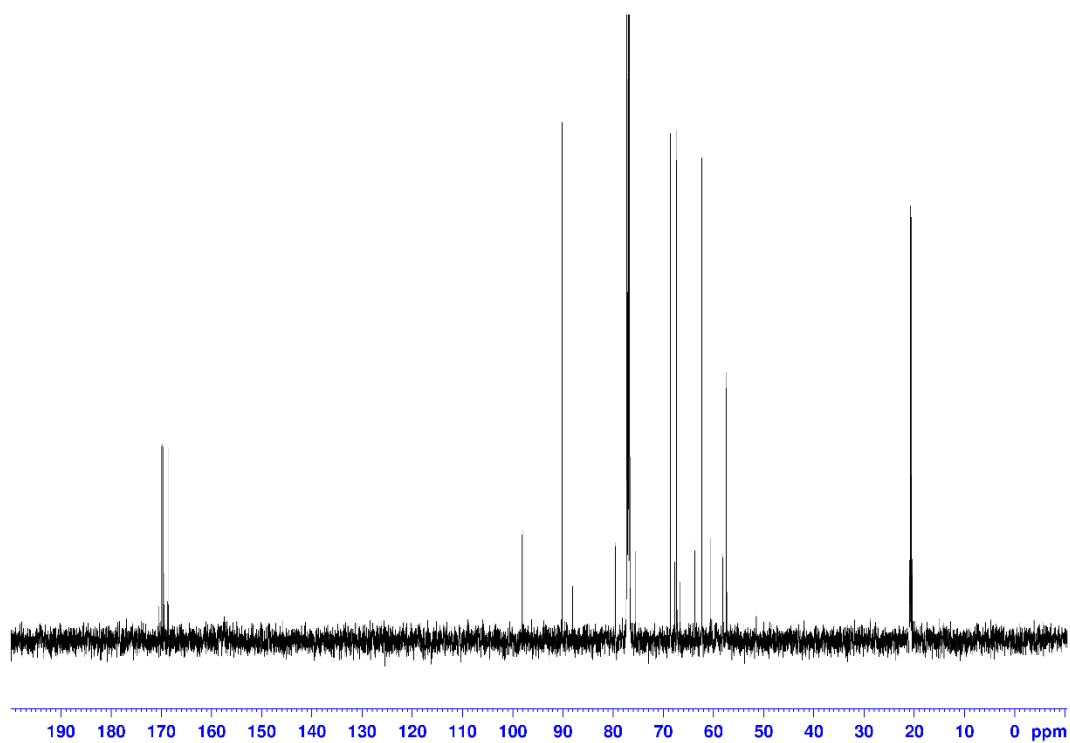
**Figure 78.** <sup>1</sup>H NMR spectrum (500 MHz, CDCl<sub>3</sub>, 300 K) of 3-azido-3-deoxy-1,2,5-tri-O-acetyl- $\alpha,\beta$ -D-arabinose (52).



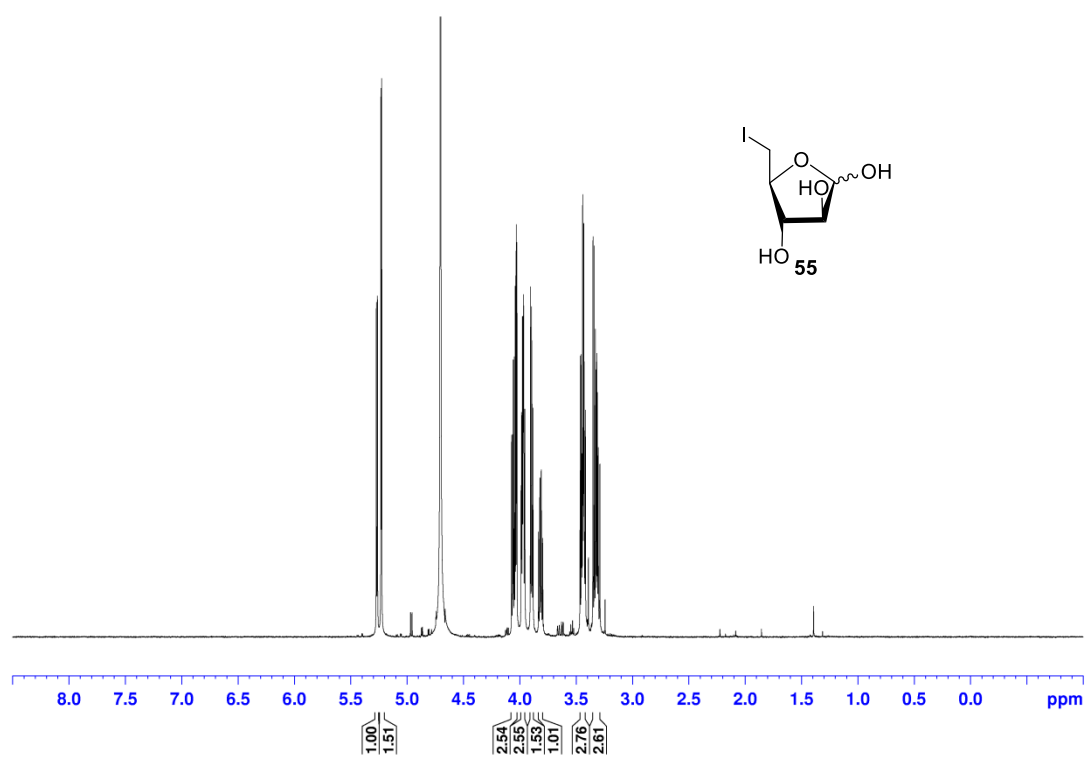
**Figure 79.** <sup>13</sup>C NMR spectrum (125 MHz, CDCl<sub>3</sub>, 300 K) of 3-azido-3-deoxy-1,2,5-tri-O-acetyl- $\alpha,\beta$ -D-arabinose (52).



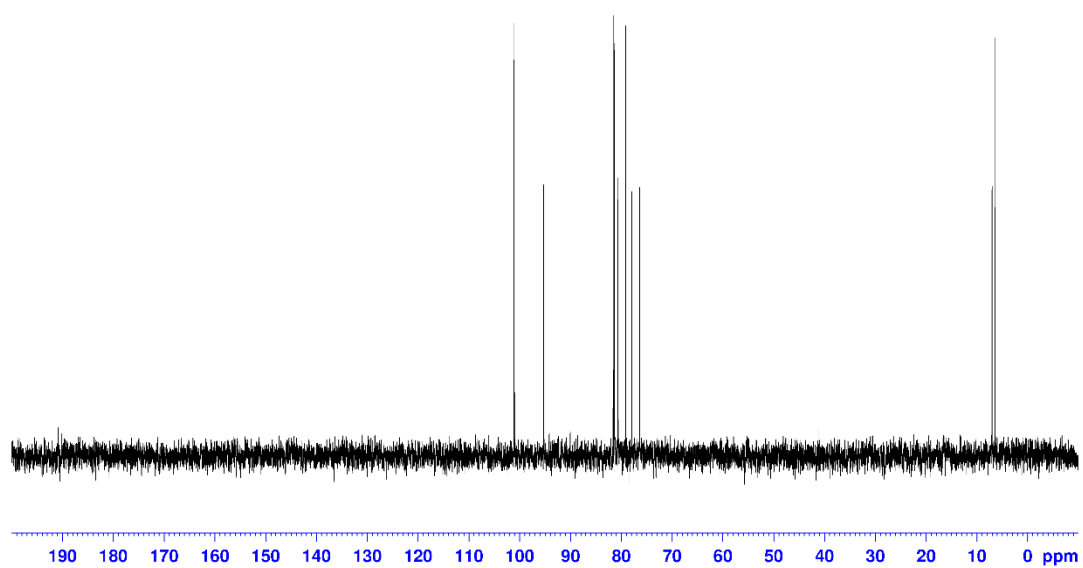
**Figure 80.**  $^1H$  NMR spectrum (500 MHz,  $CDCl_3$ , 300 K) of 3-azido-3-deoxy-1,2,5-tri-O-acetyl- $\alpha,\beta$ -D-ribose (**53**).



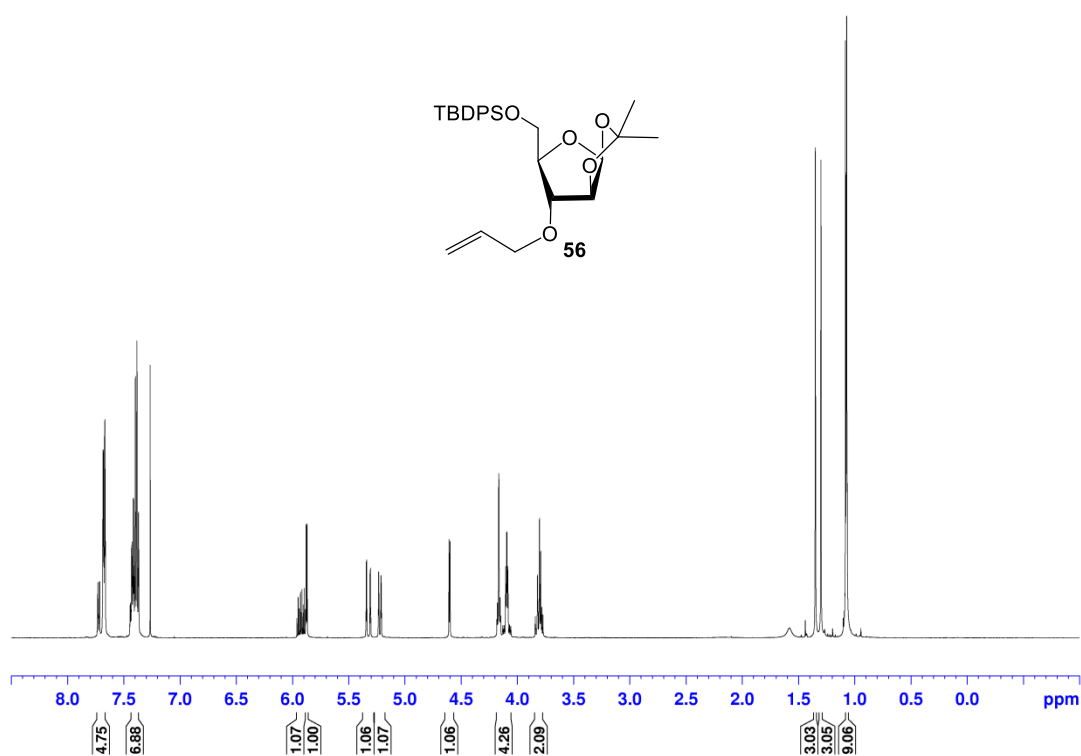
**Figure 81.**  $^{13}C$  NMR spectrum (125 MHz,  $CDCl_3$ , 300 K) of 3-azido-3-deoxy-1,2,5-tri-O-acetyl- $\alpha,\beta$ -D-ribose (**53**).



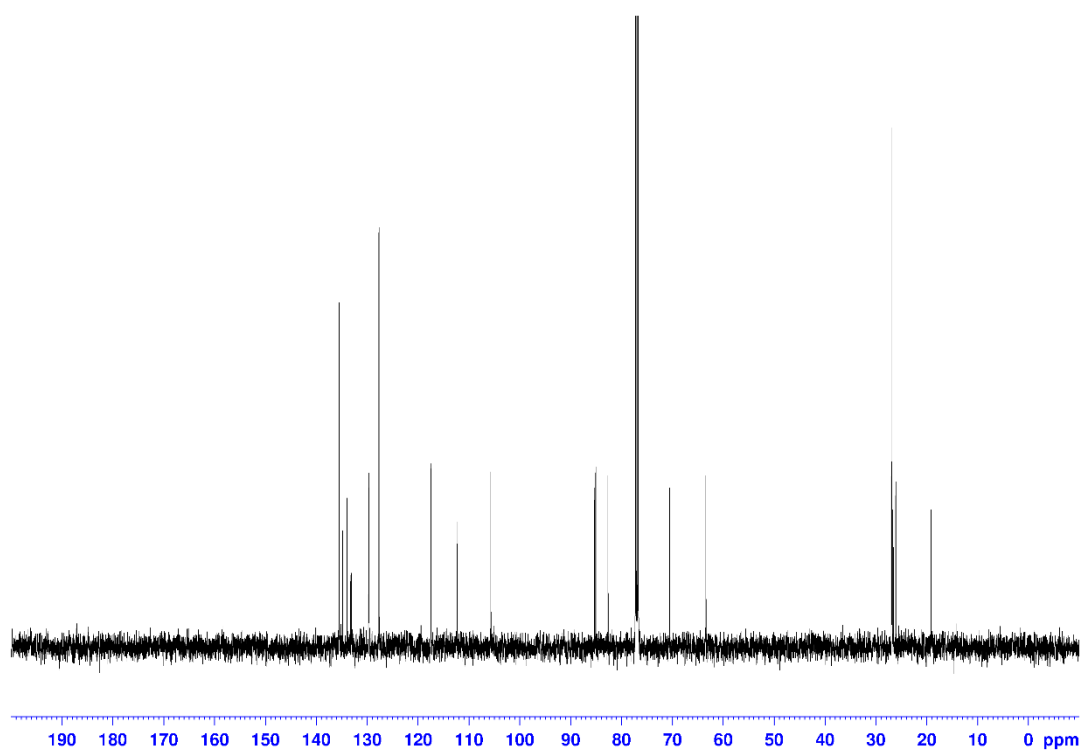
**Figure 82.**  $^1\text{H}$  NMR spectrum (500 MHz,  $\text{D}_2\text{O}$ , 300 K) of 5-deoxy-5-iodo- $\alpha,\beta$ -D-arabinofuranose (55).



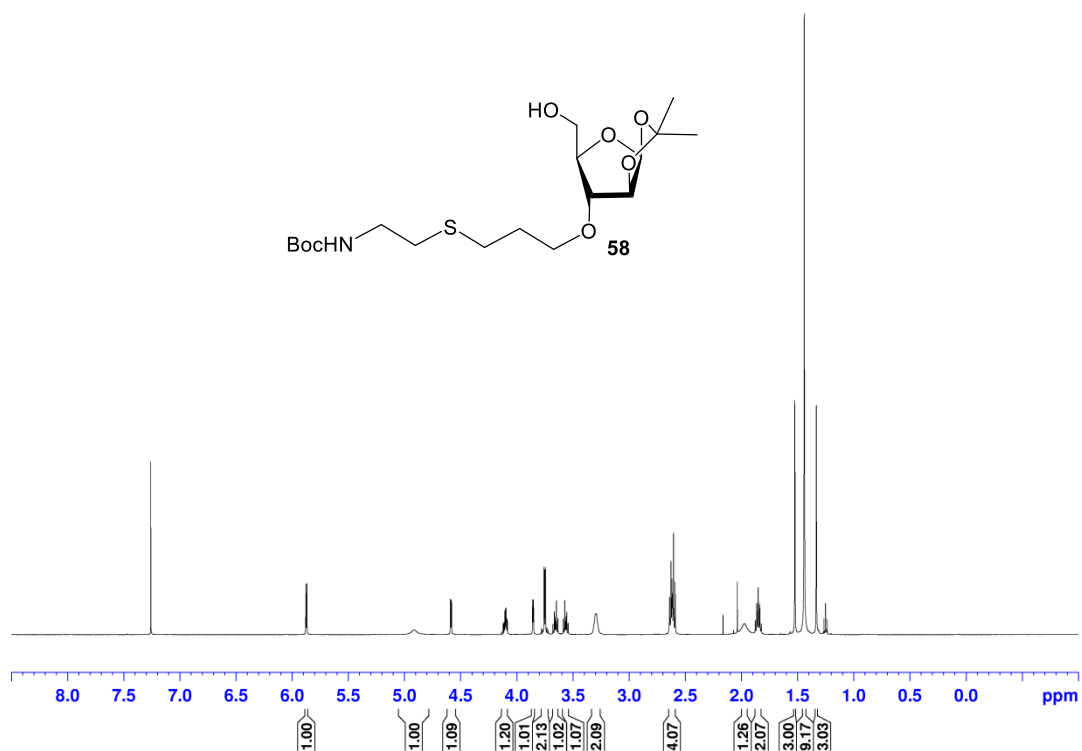
**Figure 83.**  $^{13}\text{C}$  NMR spectrum (125 MHz,  $\text{D}_2\text{O}$ , 300 K) of 5-deoxy-5-iodo- $\alpha,\beta$ -D-arabinofuranose (55).



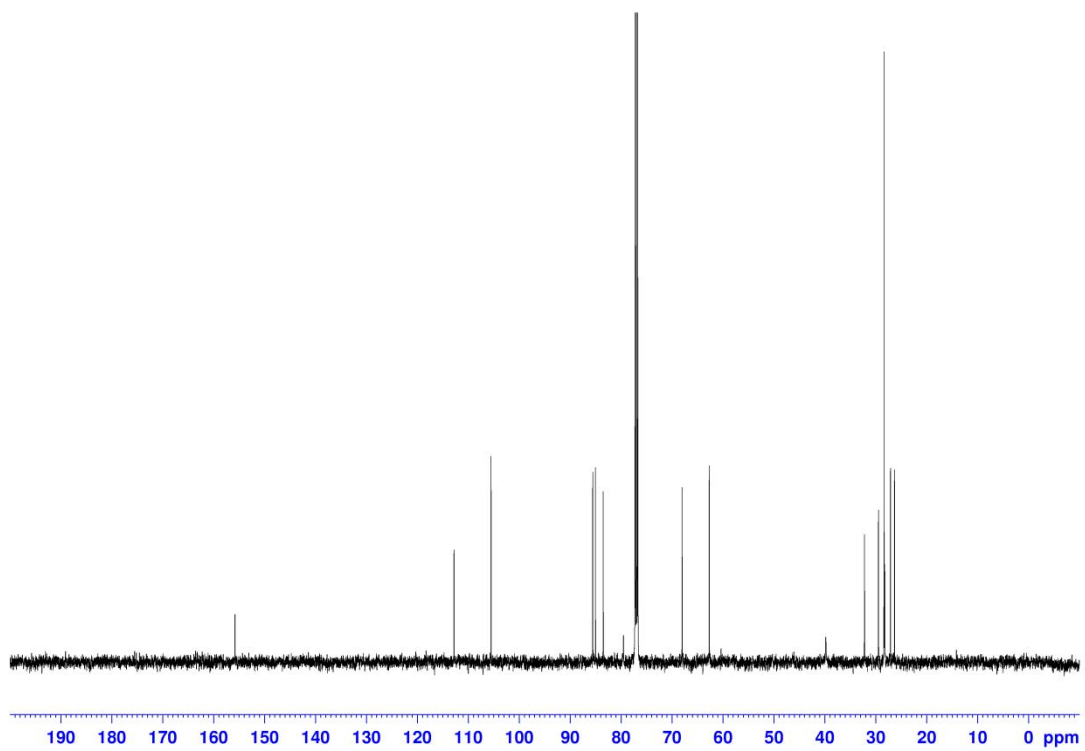
**Figure 84.** <sup>1</sup>H NMR spectrum (500 MHz, CDCl<sub>3</sub>, 300 K) of 3-*O*-allyl-5-*O*-*tert*-butyldiphenylsilyl-1,2-*O*-isopropylidene-β-D-arabinofuranose (**56**).



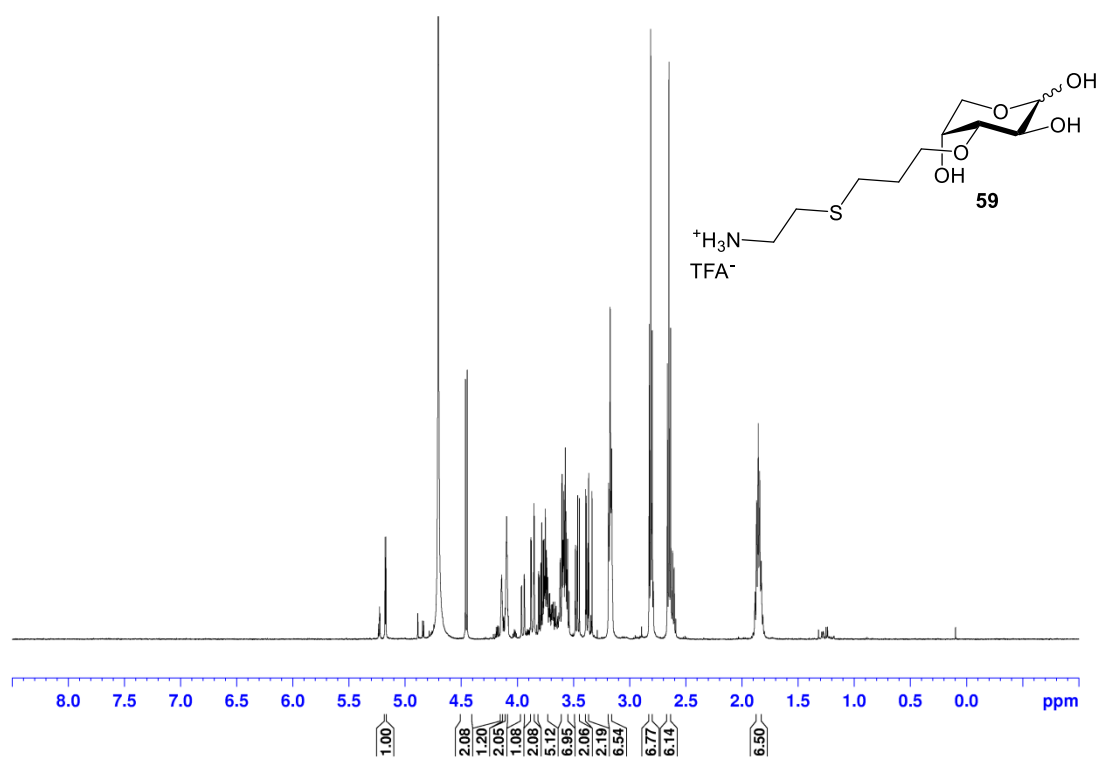
**Figure 85.** <sup>13</sup>C NMR spectrum (125 MHz, CDCl<sub>3</sub>, 300 K) of 3-*O*-allyl-5-*O*-*tert*-butyldiphenylsilyl-1,2-*O*-isopropylidene-β-D-arabinofuranose (**56**).



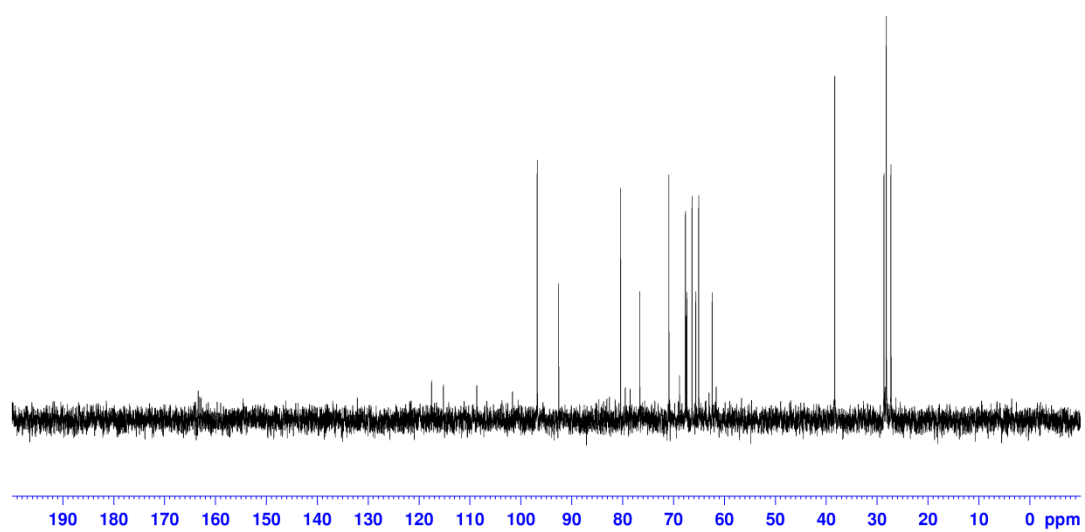
**Figure 86.** <sup>1</sup>H NMR spectrum (500 MHz, CDCl<sub>3</sub>, 300 K) of 3-O-[6'-N-(*tert*-butoxycarbonyl)amino-4'-thiahexyl]-1,2-O-isopropylidene-β-D-arabinofuranose (**58**).



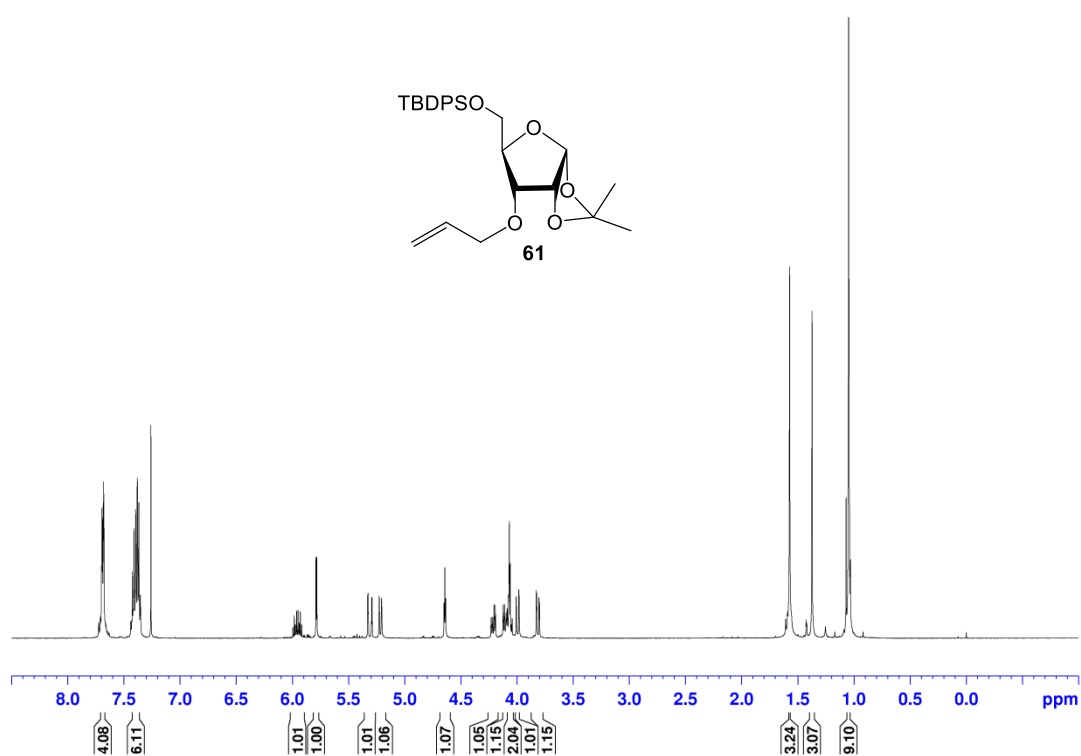
**Figure 87.** <sup>13</sup>C NMR spectrum (125 MHz, CDCl<sub>3</sub>, 300 K) of 3-O-[6'-N-(*tert*-butoxycarbonyl)amino-4'-thiahexyl]-1,2-O-isopropylidene-β-D-arabinofuranose (**58**).



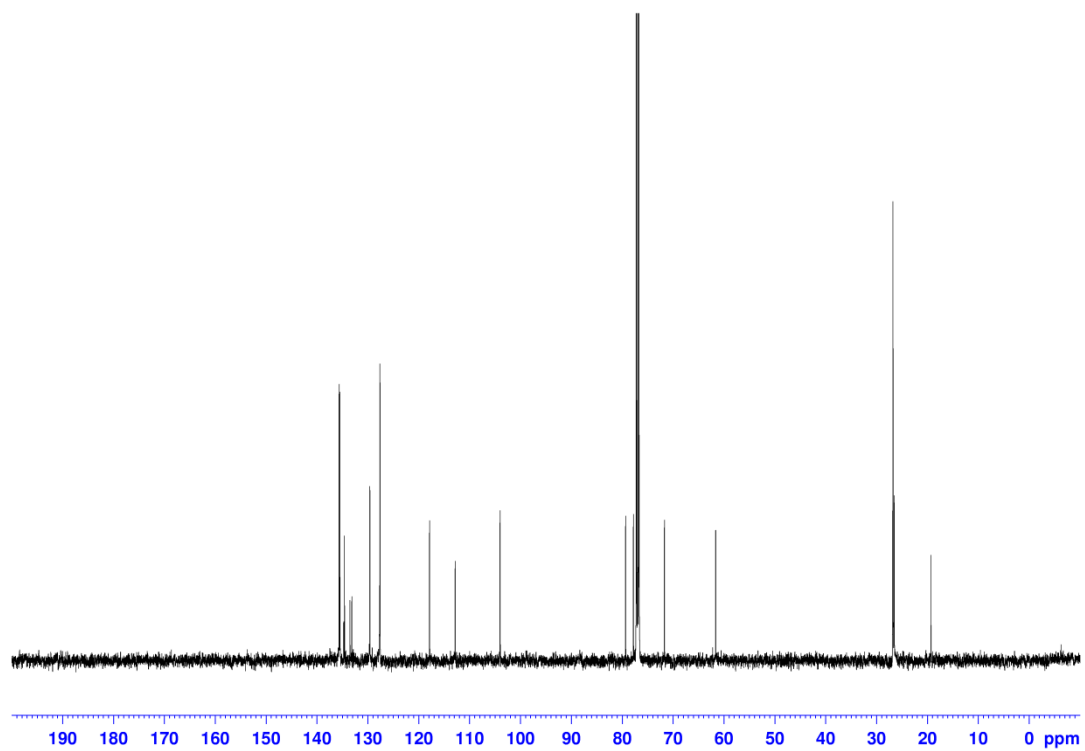
**Figure 88.**  $^1\text{H}$  NMR spectrum (500 MHz,  $\text{D}_2\text{O}$ , 300 K) of 3-O-(6'-amino-4'-thiahexyl)- $\alpha,\beta$ -D-arabinose (**59**).



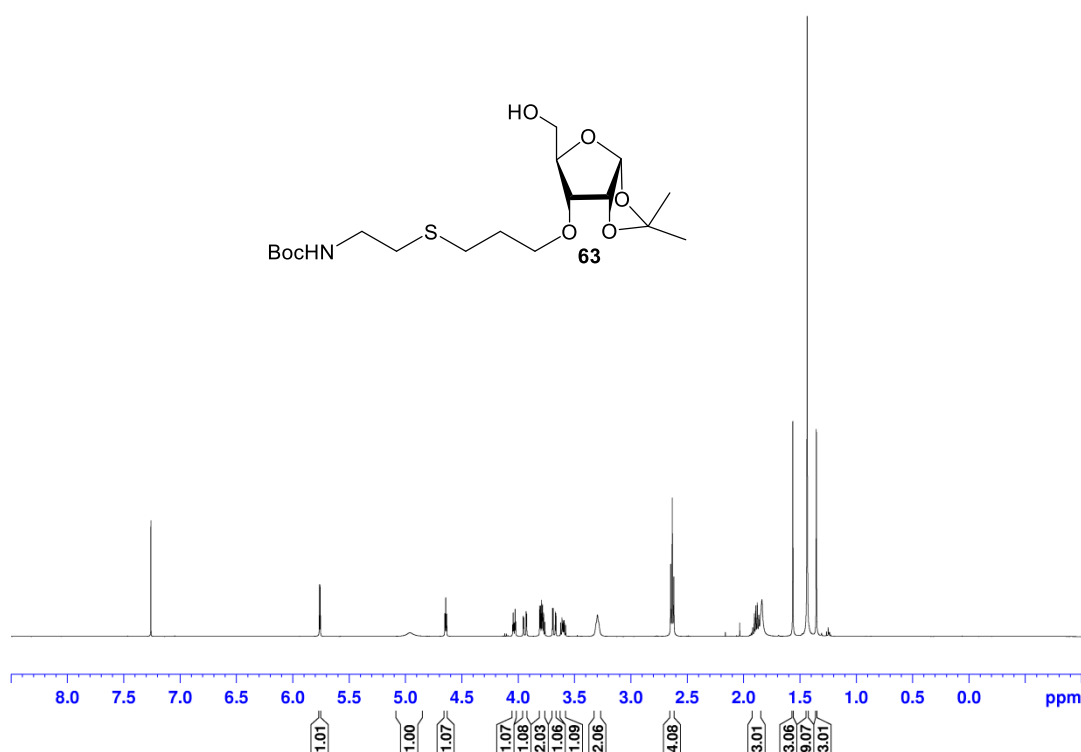
**Figure 89.**  $^{13}\text{C}$  NMR spectrum (125 MHz,  $\text{D}_2\text{O}$ , 300 K) of 3-O-(6'-amino-4'-thiahexyl)- $\alpha,\beta$ -D-arabinose (**59**).



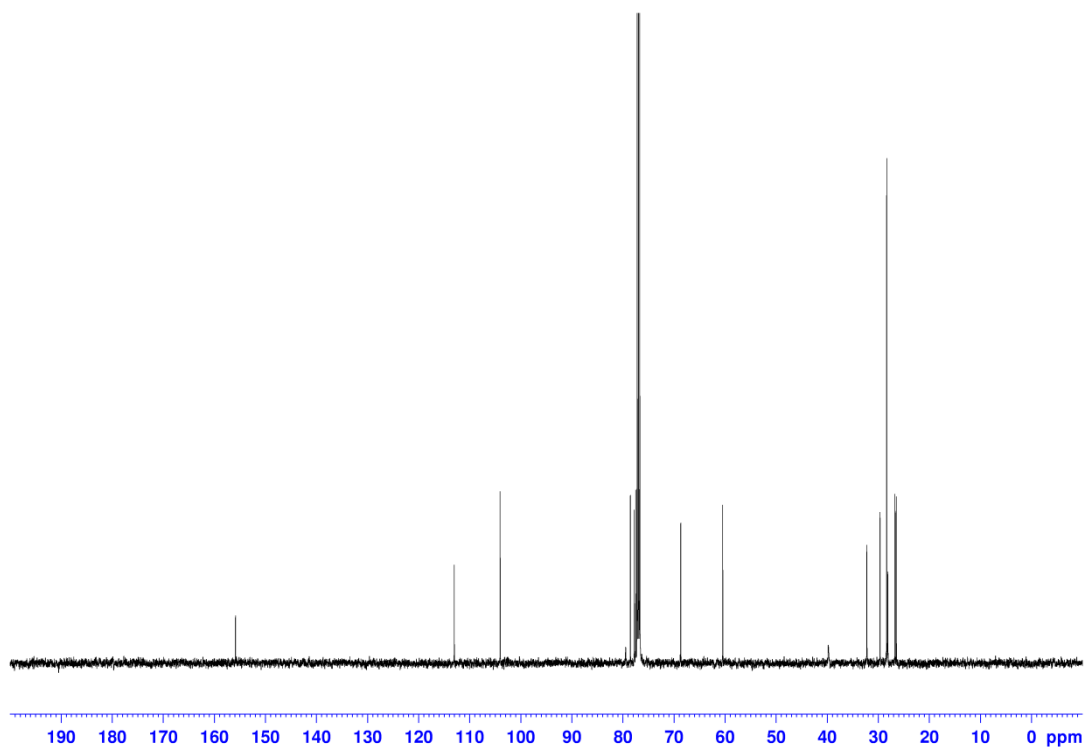
**Figure 90.**  $^1\text{H}$  NMR spectrum (500 MHz,  $\text{CDCl}_3$ , 300 K) of 3-O-allyl-5-O-*tert*-butyldiphenylsilyl-1,2-O-isopropylidene- $\alpha$ -D-ribofuranose (**61**).



**Figure 91.**  $^{13}\text{C}$  NMR spectrum (125 MHz,  $\text{CDCl}_3$ , 300 K) of 3-O-allyl-5-O-*tert*-butyldiphenylsilyl-1,2-O-isopropylidene- $\alpha$ -D-ribofuranose (**61**).

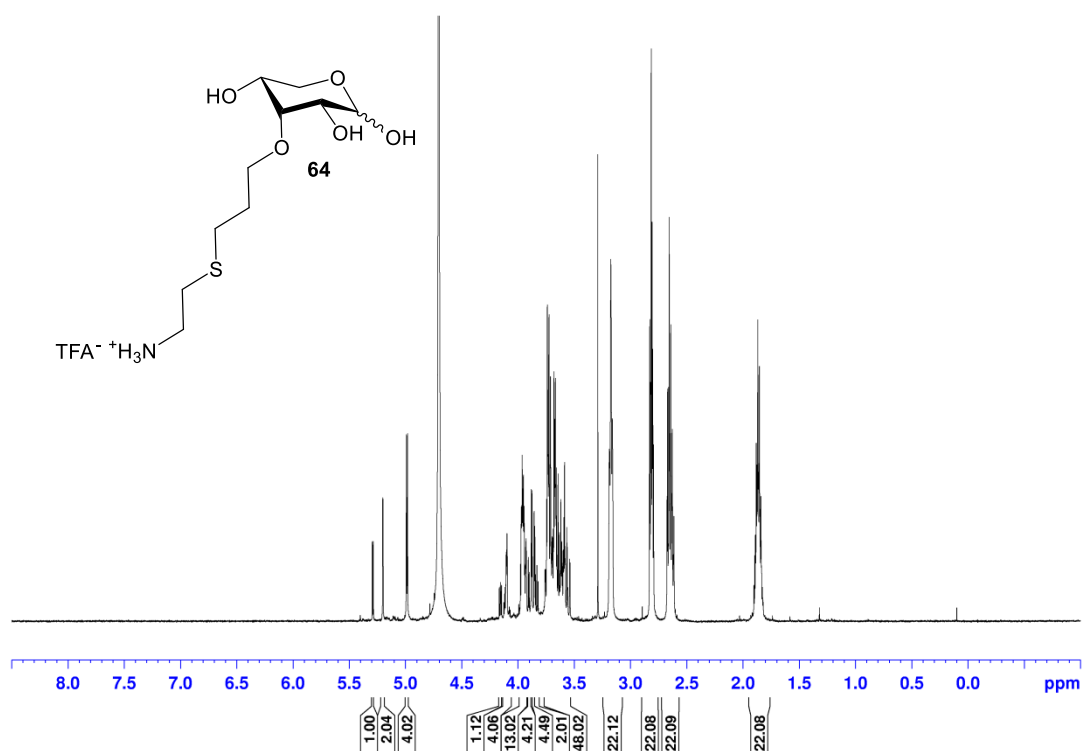


**Figure 92.**  $^1\text{H}$  NMR spectrum (500 MHz,  $\text{CDCl}_3$ , 300 K) of 3-O-[6'-N-(*tert*-butoxycarbonyl)amino-4'-thiahexyl]-1,2-O-isopropylidene- $\alpha$ -D-ribofuranose (**63**).

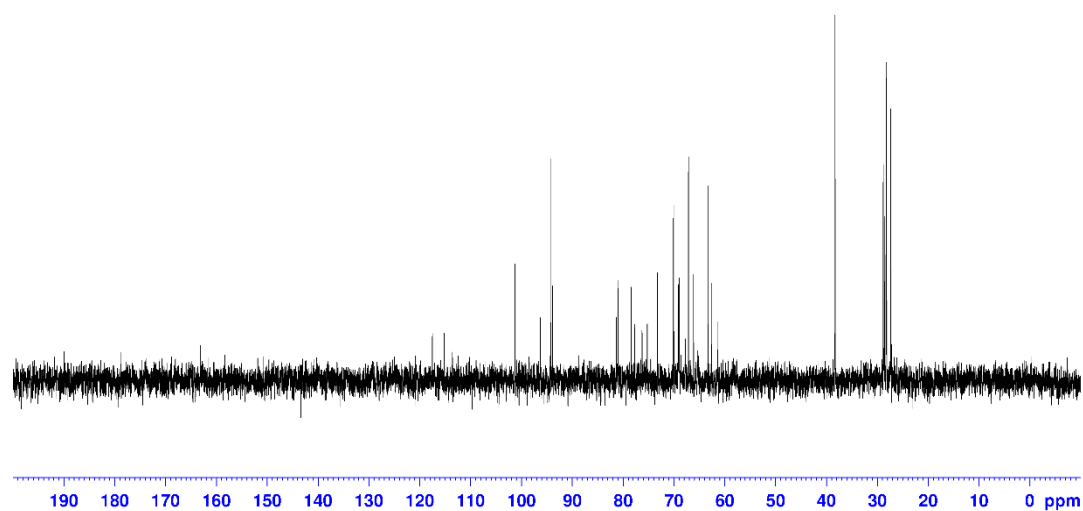


**Figure 93.**  $^{13}\text{C}$  NMR spectrum (125 MHz,  $\text{CDCl}_3$ , 300 K) of 3-O-[6'-N-(*tert*-butoxycarbonyl)amino-4'-thiahexyl]-1,2-O-isopropylidene- $\alpha$ -D-ribofuranose (**63**).

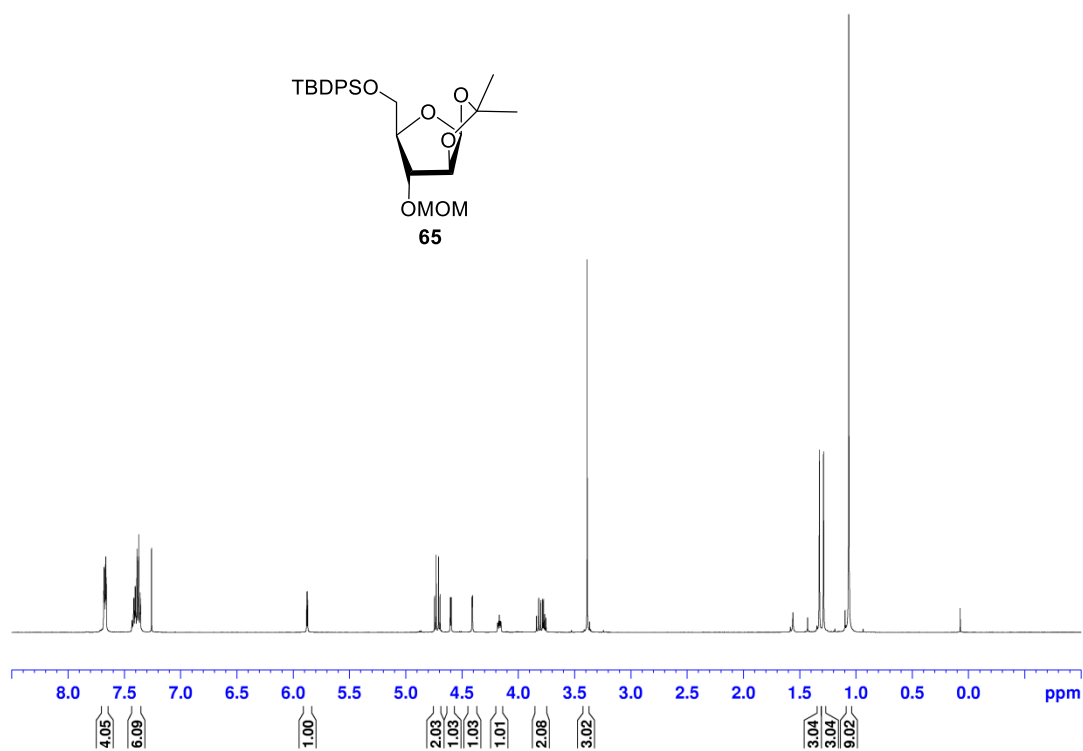




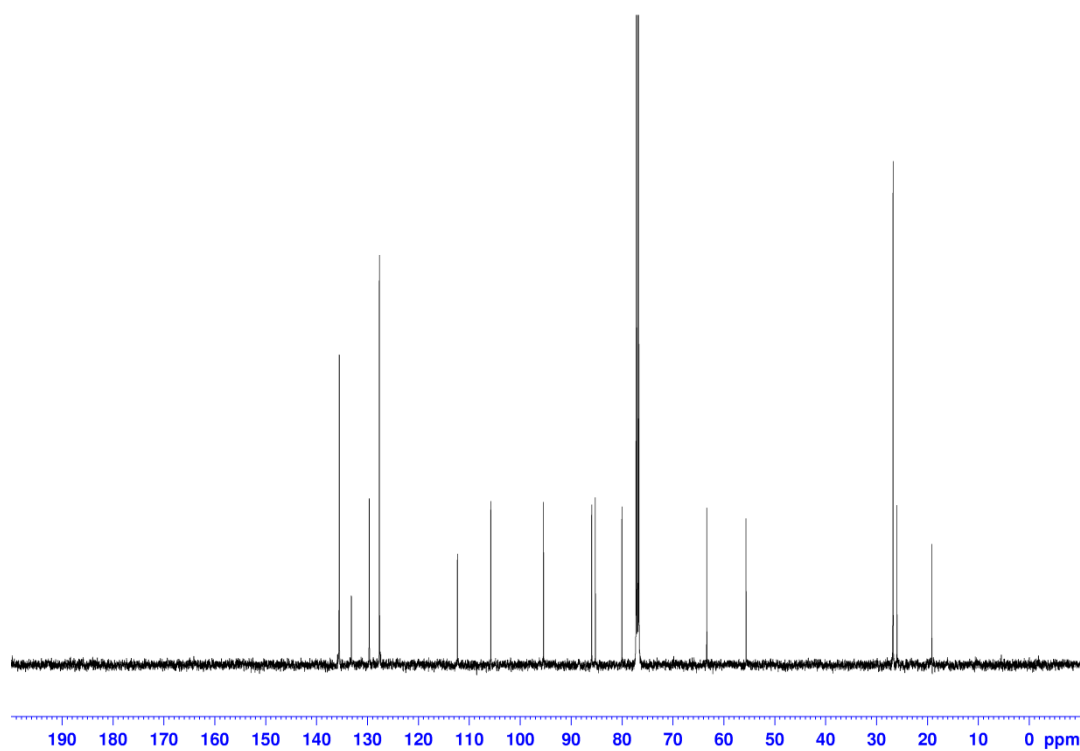
**Figure 94.**  $^1\text{H}$  NMR spectrum (500 MHz,  $\text{D}_2\text{O}$ , 300 K) of 3-O-(6'-amino-4'-thiahexyl)- $\alpha,\beta$ -D-ribose (**64**).



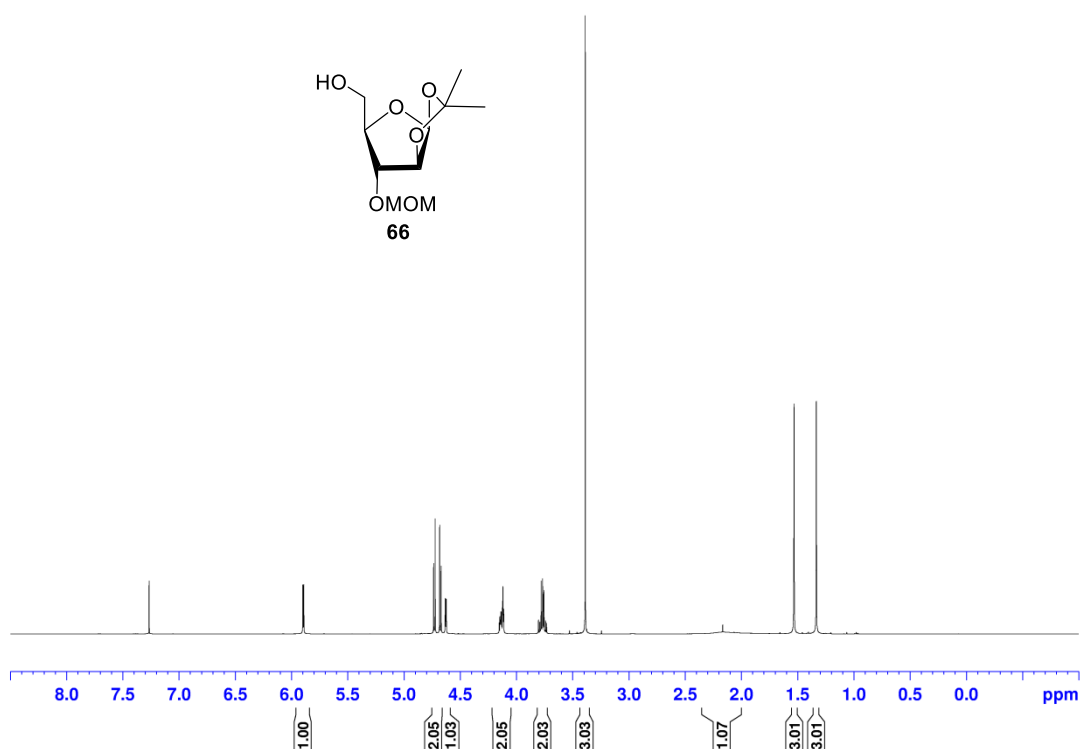
**Figure 95.**  $^{13}\text{C}$  NMR spectrum (125 MHz,  $\text{D}_2\text{O}$ , 300 K) of 3-O-(6'-amino-4'-thiahexyl)- $\alpha,\beta$ -D-ribose (**64**).



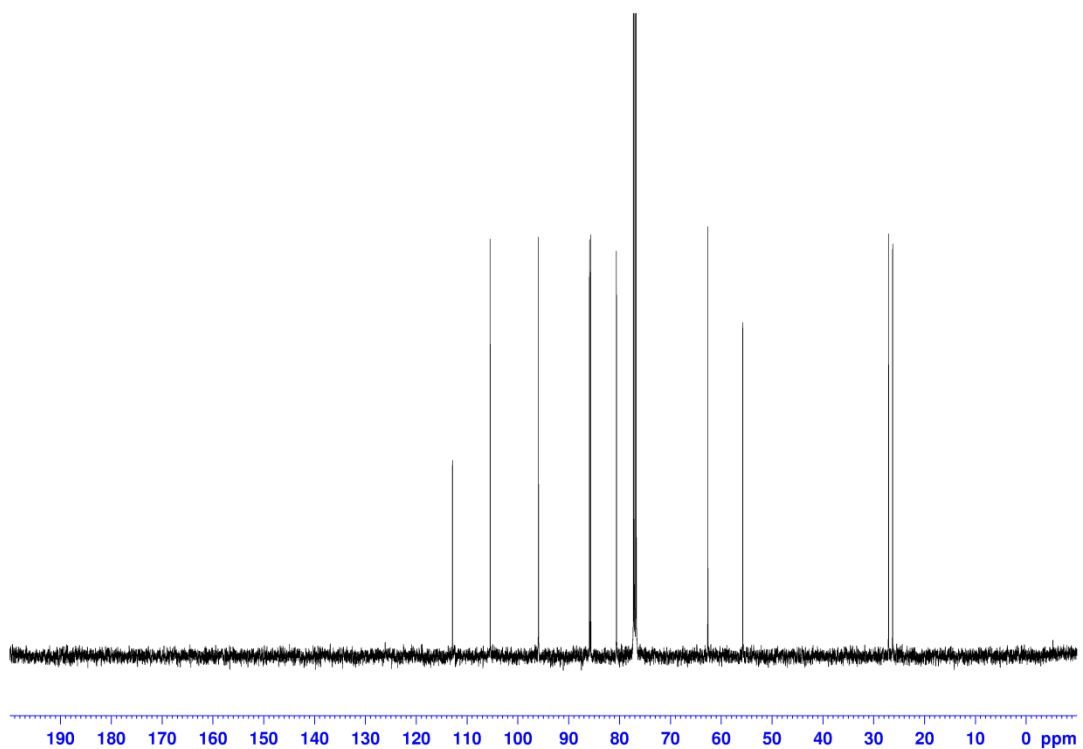
**Figure 96.** <sup>1</sup>H NMR spectrum (500 MHz, CDCl<sub>3</sub>, 300 K) of 5-*O*-*tert*-butyldiphenylsilyl-1,2-*O*-isopropylidene-3-*O*-methoxymethyl-β-D-arabinofuranose (**65**).



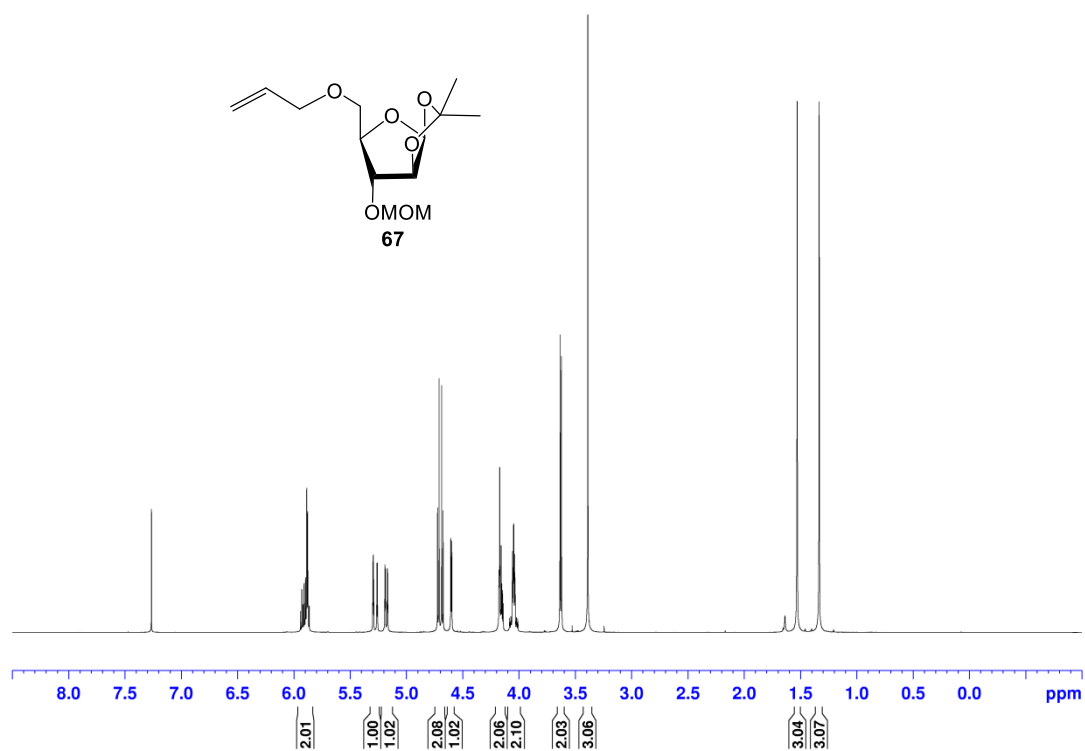
**Figure 97.** <sup>13</sup>C NMR spectrum (125 MHz, CDCl<sub>3</sub>, 300 K) of 5-*O*-*tert*-butyldiphenylsilyl-1,2-*O*-isopropylidene-3-*O*-methoxymethyl-β-D-arabinofuranose (**65**).



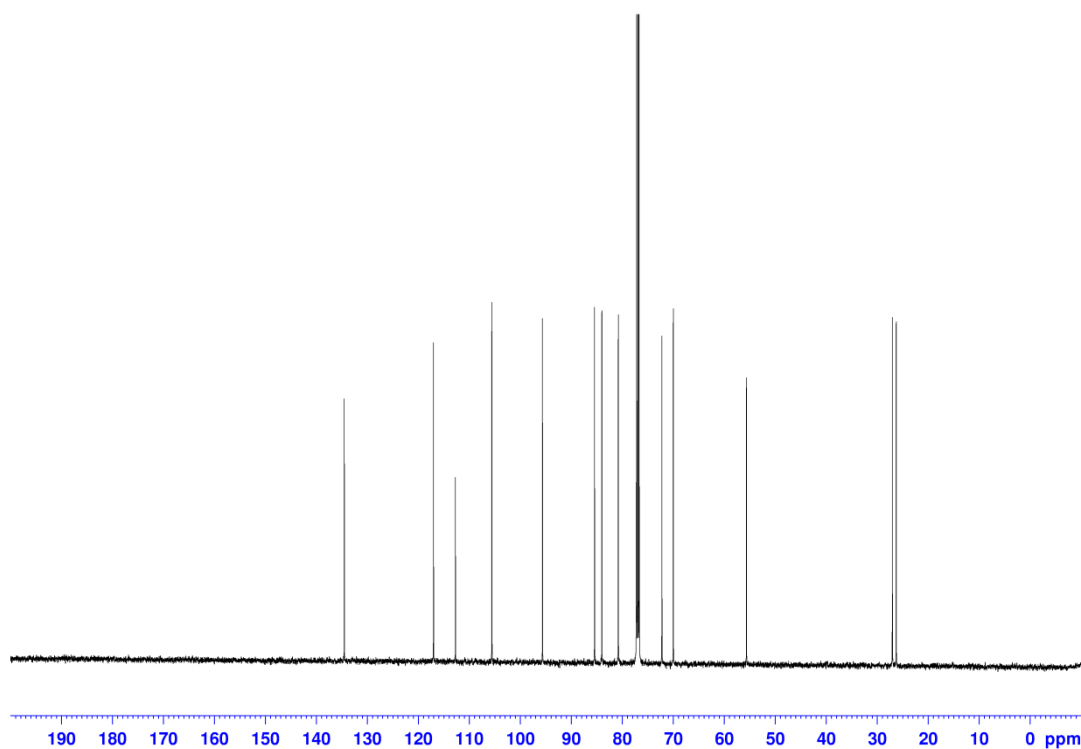
**Figure 98.** <sup>1</sup>H NMR spectrum (500 MHz, CDCl<sub>3</sub>, 300 K) of 1,2-O-isopropylidene-3-O-methoxymethyl-β-D-arabinofuranose (**66**).



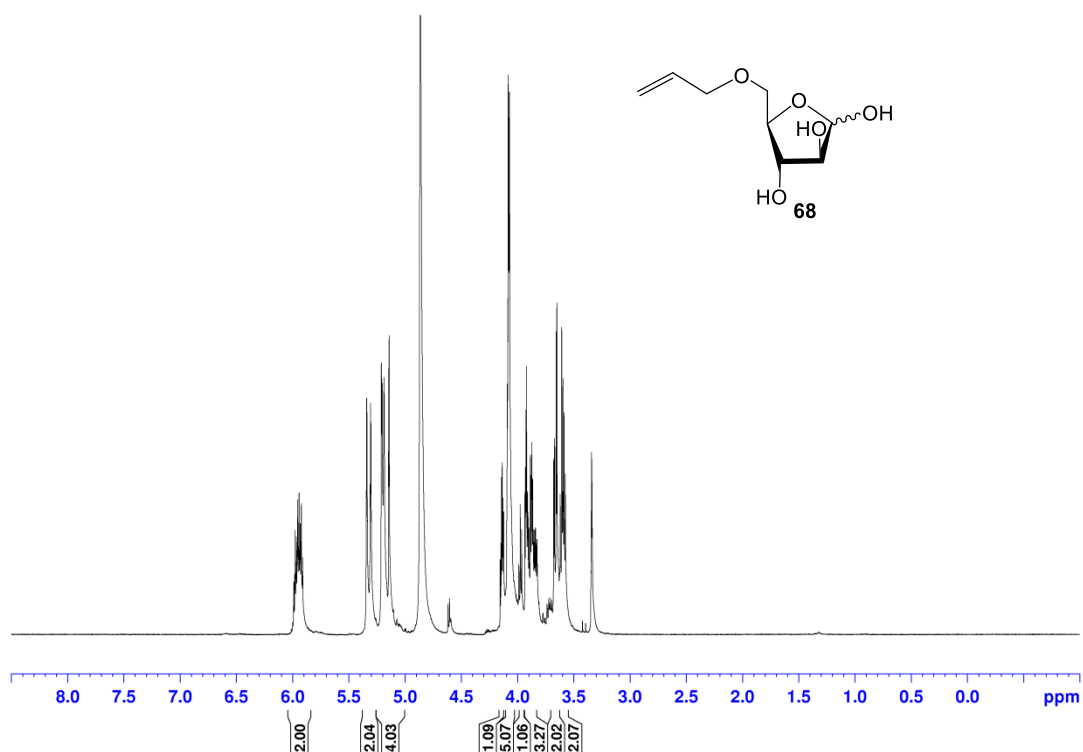
**Figure 99.** <sup>13</sup>C NMR spectrum (125 MHz, CDCl<sub>3</sub>, 300 K) of 1,2-O-isopropylidene-3-O-methoxymethyl-β-D-arabinofuranose (**66**).



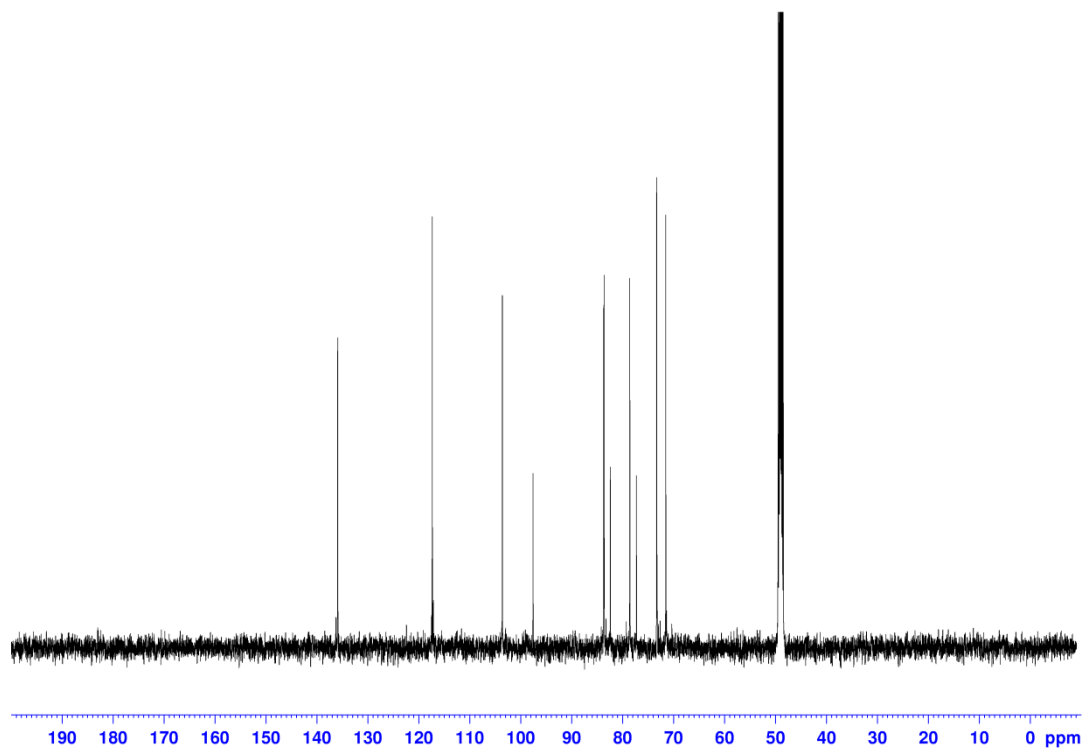
**Figure 100.** <sup>1</sup>H NMR spectrum (500 MHz, CDCl<sub>3</sub>, 300 K) of 5-O-allyl-1,2-O-isopropylidene-3-O-methoxymethyl-β-D-arabinofuranose (**67**).



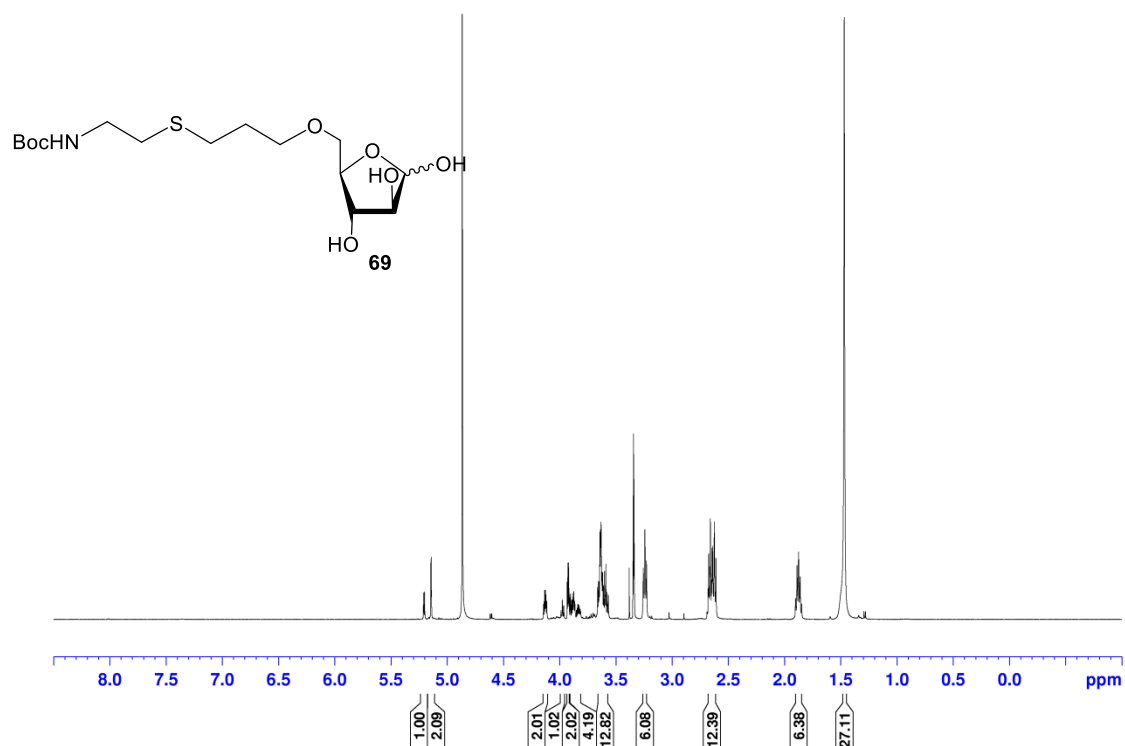
**Figure 101.** <sup>13</sup>C NMR spectrum (125 MHz, CDCl<sub>3</sub>, 300 K) of 5-O-allyl-1,2-O-isopropylidene-3-O-methoxymethyl-β-D-arabinofuranose (**67**).



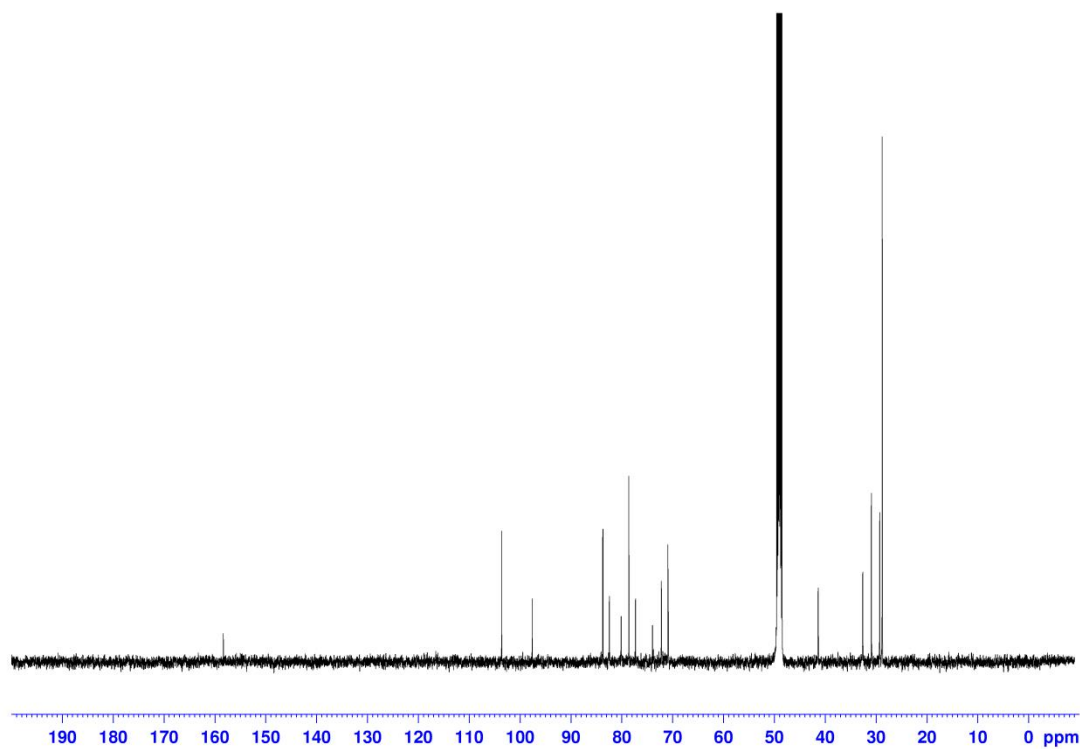
**Figure 102.** <sup>1</sup>H NMR spectrum (500 MHz, MeOH-*d*<sub>4</sub>, 300 K) of 5-O-allyl-α,β-D-arabinofuranose (**68**).



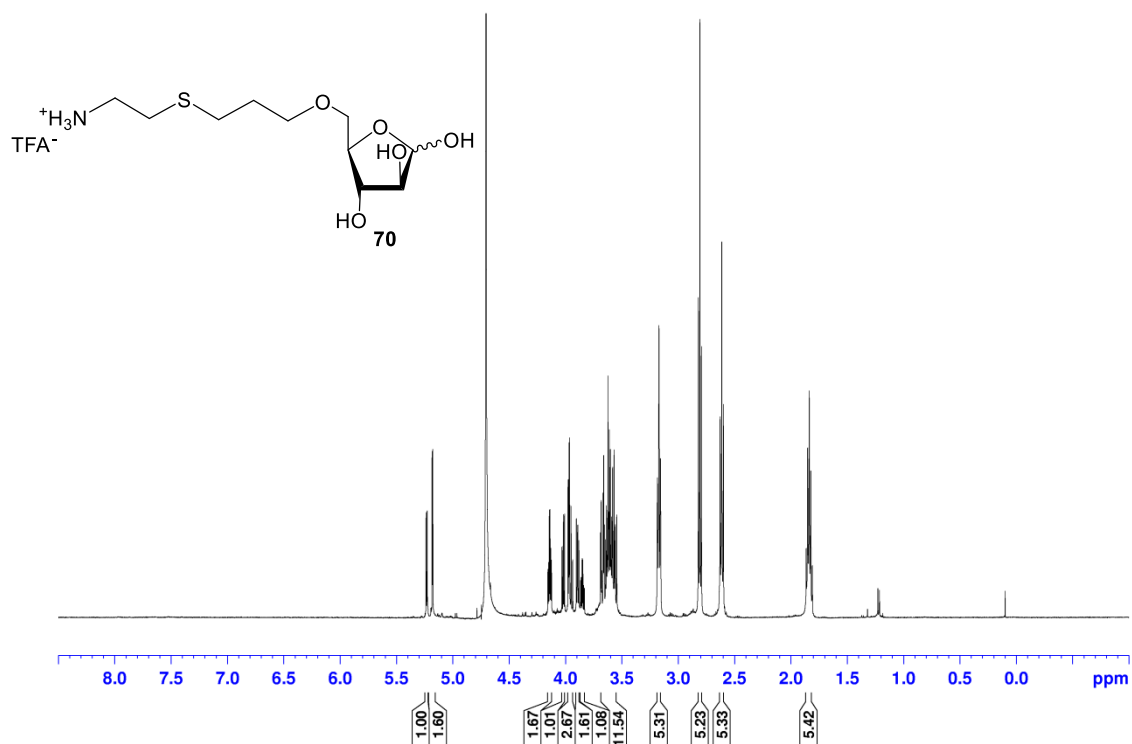
**Figure 103.** <sup>13</sup>C NMR spectrum (125 MHz, MeOH-*d*<sub>4</sub>, 300 K) of 5-O-allyl-α,β-D-arabinofuranose (**68**).



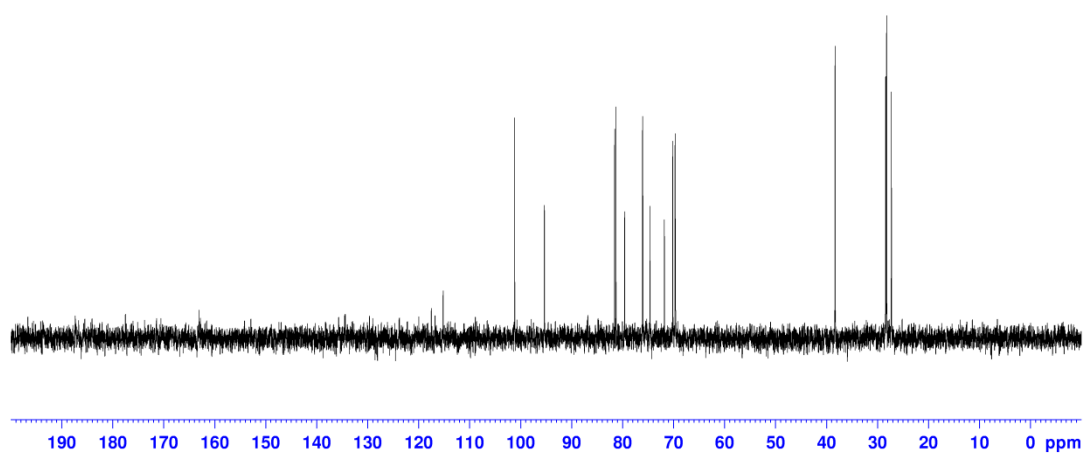
**Figure 104.** <sup>1</sup>H NMR spectrum (500 MHz, MeOH-*d*<sub>4</sub>, 300 K) of 5-O-[6'-*N*-(*tert*-butoxycarbonyl)amino-4'-thiahexyl]-α,β-D-arabinofuranose (**69**).



**Figure 105.** <sup>13</sup>C NMR spectrum (125 MHz, MeOH-*d*<sub>4</sub>, 300 K) of 5-O-[6'-*N*-(*tert*-butoxycarbonyl)amino-4'-thiahexyl]-α,β-D-arabinofuranose (**69**).



**Figure 106.**  $^1\text{H}$  NMR spectrum (500 MHz,  $\text{D}_2\text{O}$ , 300 K) of 5-O-(6'-amino-4'-thiahexyl)- $\alpha,\beta$ -D-arabinofuranose (70).



**Figure 107.**  $^{13}\text{C}$  NMR spectrum (125 MHz,  $\text{D}_2\text{O}$ , 300 K) of 5-O-(6'-amino-4'-thiahexyl)- $\alpha,\beta$ -D-arabinofuranose (70).

## 5.2 Abbreviations

Ab 1	Primary antibody
Ab 2	Secondary antibody
ABC	ATP-binding cassette
Ac	Acetyl
Ac3AraAz	3-Azido-3-deoxy-1,2,5-tri- <i>O</i> -acetyl- $\alpha,\beta$ -D-arabinose
Ac5AraAz	5-Azido-5-deoxy-1,2,3-tri- <i>O</i> -acetyl- $\alpha,\beta$ -D-arabinofuranose
AcManNAz	Acetylated <i>N</i> -azidoacetyl-mannosamine
Ac3RiboAz	3-Azido-3-deoxy-1,2,5-tri- <i>O</i> -acetyl- $\alpha,\beta$ -D-ribose
Ac6TreAz	2,3,4,2',3',4',6'-Hepta- <i>O</i> -acetyl-6-azido- $\alpha,\alpha$ -D-trehalose
Ac <sub>2</sub> O	Acetic anhydride
AcOH	Acetic acid
ADK	Adenosine kinase
AG	Arabinogalactan
Ag85	Antigen 85
AIBN	Azobisisobutyronitrile
D-Ala	D-Alanine
L-Ala	L-Alanine
AMP	Adenosine monophosphate
APS	Ammonium persulfate
3AraAz	3-azido-3-deoxy- $\alpha,\beta$ -D-arabinose
5AraAz	5-azido-5-deoxy- $\alpha,\beta$ -D-arabinofuranose
$\alpha$ -D-Araf	$\alpha$ -D-Arabinofuranoside
5Aral	5-Deoxy-5-iodo- $\alpha,\beta$ -D-arabinofuranose
AraLAM	Non-capped LAM
Arap	D-Arabinopyranose
Ara5P	Arabinose-5-phosphate
ATP	Adenosine triphosphate
Bad	Bcl-2-associated death promoter
BBQ	BlackBerry
Bcl-2	B-cell lymphoma 2
BCG	<i>Bacillus Calmette-Guérin</i>
BlaC	$\beta$ -Lactamase C
Boc	<i>tert</i> -Butyloxycarbonyl
Boc <sub>2</sub> O	di- <i>tert</i> -Butyl dicarbonate
BP filter	Band-pass filter
BSA	Bovine serum albumin
calc.	Calculated
Calcein AM	Acetomethoxy derivate of calcein
CAMK II	Ca <sup>2+</sup> /calmodulin-dependent protein kinase II
CAS	<i>Central Asian</i>
CDC	Centers for Disease Control and Prevention
CDCl <sub>3</sub> , Chloroform- <i>d</i> <sub>1</sub>	Deuterated chloroform
cfu	Colony forming units



CMP	Cytidine monophosphate
ConA	Concanavalin A
COSY	Correlation spectroscopy
CSP	Cell surface proteins
CT	Computed tomography
ct (RT-PCR)	Cycle threshold
C-type	Calcium-dependent
CyTOF	Cytometry by time of flight
d (NMR)	Doublet
pDADMAC	poly-Diallyldimethyl ammonium chloride
DAP	meso-Diaminopimelate
DAPI	4',6-Diamidino-2-phenylindole
DBU	1,8-Diazabicycloundec-7-ene
DC	Dendritic cell
DCM	Dichloromethane
DC-SIGN	DC-specific intercellular adhesion molecule 3-grabbing nonintegrin
Dectin	Dendritic cell-specific C-type lectin
dest.	Distilled
DETA/NO	Diethylenetriamine nitric oxide
DIBO	Dibenzocyclooctyne
DIPEA	<i>N,N</i> -Diisopropylethylamine
DMF	Dimethylformamide
DMSO	Dimethylsulfoxide
DNA	Deoxyribonucleic acid
dNTPs	Deoxynucleoside triphosphates
DPAP	2,2-Dimethoxy-2-phenyl-acetophenone
D <sub>2</sub> O	Deuterium oxide
EAI	<i>East African Indian</i>
ECL	Enhanced chemiluminescence
<i>E. coli</i>	<i>Escherichia coli</i>
EDC	1-Ethyl-3-(3-dimethylaminopropyl)-carbodiimide
EDTA	Ethylenediaminetetraacetate
EEA1	Early endosome antigen 1
ELISA	Enzyme-linked immunosorbent
ESI-MS	Electrospray ionization mass spectrometry
Et <sub>2</sub> O	Diethyl ether
FAM	Fluorescein
FDG	2-Deoxy-2-( <sup>18</sup> F)fluoro-D-glucose
FDT	2-Deoxy-2-( <sup>18</sup> F)fluoro-D-trehalose
FCS	Fetal calf serum
FI	Fluorescence intensity
FITC	Fluorescein isothiocyanate
FRET	Fluorescence resonance energy transfer
FSC	Forward scatter
β-D-Galf	β-D-Galactofuranoside

Gc	Glycolyl
GFP	Green fluorescent protein
$\alpha$ -D-Glcp	$\alpha$ -D-Glucopyranoside
$\alpha/\beta$ -D-GlcNAc	<i>N</i> -Acetyl- $\alpha/\beta$ -D-glucosamine
GPIL	Glycosylphosphatidylinositol lipids
GTPase	Enzyme, which binds and hydrolyzes guanosine triphosphate (GTP)
HBSS	Hank's balanced salt solution
hEGF	Human epidermal growth factor
HEPES	4-(2-Hydroxyethyl)-1-piperazineethanesulfonic acid
hMDM	Human monocyte-derived macrophages
HMEC	Human mammary epithelial cells
HMBC	Heteronuclear multiple-bond correlation spectroscopy
HMM	Human macrophage medium
HOEtBr	2-Bromoethanol
HOEtCl	2-Chloroethanol
HRMS	High-resolution mass spectrometry
HSQC	Heteronuclear single-quantum correlation spectroscopy
IFN- $\gamma$	Interferon- $\gamma$
IgA	Immunoglobulins A
IgG	Immunoglobulins G
IGRA	Interferon- $\gamma$ release assay
IR	Infrared
ISMN	Isosorbide mononitrate
D-IsoGln	D-Isoglutamine
<i>J</i>	Coupling constant (in hertz (Hz))
<i>k</i>	Reaction rate constant
Kdo	3-Deoxy-D-manno-octulosonic acid
KdoAz	Azide-modified Kdo
LAM (lipoglycan)	Lipoarabinomannan
LAM (Mtb family)	<i>Latin American Mediterranean</i>
LAMP-1	Lysosome-associated membrane protein 1
LBB	Lectin binding buffer
LM	Lipomannan
<i>L. major</i>	<i>Leishmania major</i>
LPG	Lipophosphoglycan
LPS	Lipopolysaccharide
LRM	Low range marker
<i>m</i> (NMR)	Multiplet
<i>M.</i>	<i>Mycobacterium</i>
<i>m.p.</i>	Melting points
MA	Mycolic acids
ManLAM	Mannosylated LAM
$\alpha$ -D-Manp	$\alpha$ -D-Mannopyranoside
mAGP	Mycolyl-arabinogalactan-peptidoglycan
MBL	Mannose-binding lectin

MCL	Macrophage C-type lectin
M-CSF	Macrophage colony stimulating factor
MDR	Multi-drug resistant
MeOH	Methanol
MES	2-( <i>N</i> -morpholino)ethanesulfonic acid
Methanol- <i>d</i> <sub>4</sub>	Deuterated methanol
MFI	Mean fluorescence intensity
Mid-log phase	Middle logarithmic phase
Mincle	Macrophage inducible C-type lectin
MmpL3	Mycobacterial membrane protein large 3
MOE	Metabolic oligosaccharide engineering
MOI	Multiplicity of infection
MOMCI	Chloromethyl methyl ether
MR	Mannose receptor
MRT	Magnetic resonance tomography
Msg	<i>Mycobacterium smegmatis</i>
Mtb	<i>Mycobacterium tuberculosis</i>
MTBC	<i>Mycobacterium tuberculosis</i> complex
β-D-MurNAc/Gc	<i>N</i> -Acetyl-/ <i>N</i> -glycolyl-β-D-muramic acid
<i>m/z</i>	Mass-to-charge ratio
MVL	<i>Microcystis viridis</i> lectin
MWCO	Molecular weight cut-off
NAD	Nicotinamide adenine dinucleotide
NaOAc	Sodium acetate
NaOMe	Sodium methoxide
NGS	Normal goat serum
NHS	<i>N</i> -Hydroxysuccinimide
NMR	Nuclear magnetic resonance
pNO <sub>2</sub> PhOH	<i>p</i> -Nitrophenol
NRC	National Reference Center
OADC	Oleic acid, albumin, dextrose, catalase
OD	Optical density
OtsA	Trehalose-6-phosphate synthase
OtsB	Trehalose-6-phosphate phosphatase
PAL	Photoaffinity labeling
PAS	Periodic acid-Schiff reaction
PBMC	Peripheral blood mononuclear cells
PBS	Phosphate buffered saline
PBSB	PBS supplemented with BSA
PCR	Polymerase chain reaction
Pd/C	Palladium on charcoal
PEG	Polyethylene glycol
PEP	Phosphoenolpyruvate
PET	Positron emission tomography
PFA	Paraformaldehyde

PG	Peptidoglycan
PGL	Phenolic glycolipids
PI	Phosphatidylinositol
PI3K	Phosphatidylinositol 3 kinase
PILAM	Phosphate-capped LAM
PIM	Phosphatidylinositol mannosides
PI3P	Phosphatidylinositol 3-phosphate
ppm	Parts per million
PRRs	Pattern recognition receptors
PVDF	Polyvinylidene fluoride
q (NMR)	Quartet
QD	Quantum dots
quant.	Quantitative
Rab5	Ras-related in brain 5
R <sub>f</sub>	Retention factor
RFI	Relative fluorescence intensity
α-D-Rhap	α-D-Rhamnopyranoside
3RiboAz	3-Azido-3-deoxy-α,β-D-ribose
RIFA	Rifampicin
RK	Ribokinase
RLU	Relative light units
RNA	Ribonucleic acid
RNS	Reactive nitrogen species
ROS	Reactive oxygen species
rt	Room temperature
RT-PCR	Real-time PCR
R-type	Ricin-type
Ru5P	Ribulose 5-phosphate
s (NMR)	Singlet
SD	Standard deviation
SDS	Sodium dodecyl sulfate
SDS-PAGE	Sodium dodecyl sulfate polyacrylamide gel electrophoresis
SEM	Standard error of the mean
S-HRP	Streptavidin-horseradish peroxidase
SL	Sulfolipids
sMTL-13	13 kDa large lectin from Mtb
SNP	Sodium nitroprusside
SOD	Superoxide dismutase
SP-A	Surfactant proteins A
SPAAC	Strain promoted azide-alkyne cycloaddition
SSC	Sideward scatter
SugABC	ATP-dependent sugar transporter
t (NMR)	Triplet
Taq	<i>Thermus aquaticus</i>
Tb	Tuberculosis

TBAI	Tetrabutylammonium iodide
TBAF	tetra- <i>N</i> -Butylammonium fluoride
TBDMSCI	<i>tert</i> -Butyl-dimethylsilyl chloride
TBDPSCI	<i>tert</i> -Butyl-diphenylsilyl chloride
TBO	Toluidine blue O
TBS	Tris-buffered saline
TDM	Trehalose 6,6'-dimycolate
TEMED	<i>N,N,N',N'</i> -Tetramethylethylenediamine
TFA	Trifluoroacetic acid
Tf <sub>2</sub> O	Trifluoromethanesulfonic anhydride
TGN	trans-Golgi network
THF	Tetrahydrofuran
TLC	Thin layer chromatography
TLRs	Toll-like receptors
TMM	Trehalose 6-monomycolate
TMS	Tetramethylsilane
TOF-MS	Time-of-flight mass spectrometry
T6P	Trehalose-6-phosphate
trHbN	NO detoxifying truncated hemoglobin
6TreAz	6-Azido-6-deoxy-D-trehalose
Tris	Tris(hydroxymethyl)aminomethane
TreY	Maltooligosyltrehalose synthase
TreZ	Maltooligosyltrehalose trehalohydrolase
TsCl	Tosyl chloride
p-TsOH	<i>p</i> -Toluenesulfonic acid
TST	Tuberculin skin test
T-TBS	TBS supplemented with Tween 20
UDP	Uracil-diphosphate
UDP-MurNAc	uridine diphosphate <i>N</i> -acetylmuramic acid
UK	United Kingdom
USA	United States of America
UV	Ultraviolet
WHO	World Health Organization
XDR	Extensively-drug resistant
YAK	YakimaYellow

## 6 Curriculum vitae

Born in December, 21<sup>th</sup> 1986

**German** Citizenship

Herrenstraße 8, 24214 Gettorf, Germany  
kkolbe@oc.uni-kiel.de, kkolbe@fz-borstel.de  
+49 (0)4346 413787, +49 (0)162 2056968



---

### **Education:**

#### Since March 2012: **PhD thesis in Organic Chemistry and Microbiology**

research groups:

- a) T. K. Lindhorst, Organic Chemistry, Christiana Albertina University, Kiel, Germany
- b) N. Reiling, Microbial Interface Biology, Research Center Borstel, Leibniz-Center for Medicine and Bioscience, Borstel, Germany

March 2012-February 2014: VCI (Verband der Chemischen Industrie) PhD grant

#### October 2006-May 2011: **Study of Biochemistry and Molecular Biology**

University: Christiana Albertina University, Kiel, Germany

May 2011                      Diploma examinations                      (grade: excellent, 1.0)

Nov. 2010-May 2011: Diploma thesis in Organic Chemistry

research group: T. K. Lindhorst, Organic Chemistry, Christiana Albertina University, Kiel, Germany

thesis title: Functionalization of surfaces to study mannose-specific adhesion of bacteria under static and flow conditions.

October 2008                      Intermediate diploma examination                      (grade: excellent, 1.0)

#### summer 1993-summer 2006: **School**

June 2006                      Abitur                      (grade: very good, 1.3)

1997-2006                      secondary school

Gymnasium Kronshagen, Kronshagen, Germany

during the school year 2003 King's School, Bruton, Great Britain

1993-1997                      primary school

Grundschule Gettorf, Gettorf, Germany

## Honors and Awards

---

- March 2014: Award for an excellent talk:  
*Modifying the cell wall of Mycobacterium tuberculosis with azido pentoses and bioorthogonal "click"-reaction.*  
18<sup>th</sup> Symposium "infection and immune defense", Burg Rothenfels, Germany
- July 2013: Selected as participant in the 63<sup>th</sup> Lindau Meeting of Nobel Laureates, Lindau, Germany
- October 2012: Poster prize  
*Functional multivalent glycomimetics in the glycosciences*  
2<sup>nd</sup> International SFB 765-Symposium, Berlin, Germany
- March 2012-February 2014: VCI (Verband der Chemischen Industrie) PhD grant
- October 2008: Best intermediate diploma of the year award
- June 2006: GDCH-award for the best high school graduate in the subject Chemistry

## Publications, talks, poster

---

### Paper:

- Möckl, L., Horst, A. K., Kolbe, K., Lindhorst, Th. K., Bräuchle, C. Microdomain formation controls spatiotemporal dynamics of cell surface glycoproteins. *ChemBiochem.* **16**, 2023-2028 (2015).
- Chandrasekaran, V., Kolbe, K., Beiroth, F., Lindhorst, Th. K. Synthesis and testing of the first azobenzene mannobioside as photoswitchable ligand for the bacterial lectin FimH, *Beilstein J. Org. Chem.* **9**, 223-233 (2013).
- Grabosch, C., Kolbe, K., Lindhorst, Th. K. Glycoarrays by a new tandem noncovalent-covalent modification of polystyrene microtiter plates and their interrogation with live cells. *ChemBiochem.* **13**, 1874-1879 (2012).

### Manuscripts in preparation:

Kolbe, K., Möckl, L., Sohst, V., Brandenburg, J., Engel, R., Malm, S., Bräuchle, C., Holst, O., Lindhorst, Th. K., Reiling, N. Entering unknown territory: specific labeling of *Mycobacterium tuberculosis* with azido pentoses.

Kolbe, K., Reiling, N., Lindhorst, Th. K. Carbohydrate-binding characteristics of mycobacteria.

**Talks:**

- February 2015: *Azido pentoses, a novel tool to label the cell wall of Mycobacterium tuberculosis*, Oberjoch-Seminar, Oberjoch, Germany
- November 2014: *Metabolic labeling of the cell wall of Mycobacterium tuberculosis*, 18<sup>th</sup> Joint Meeting of the Signal Transduction Society (STS), Weimar, Germany
- October 2014: *Cell wall modification with azido pentoses of Mycobacterium tuberculosis*, 37<sup>th</sup> Symposium of the North German Immunologists, Borstel, Germany
- March 2014: *Modifying the cell wall of Mycobacterium tuberculosis with azido pentoses and bioorthogonal "click"-reaction*, 18<sup>th</sup> Symposium "infection and immune defense", Burg Rothenfels, Germany
- February 2014: *From mycobacterial carbohydrates and lectins to tuberculosis therapy and diagnostics: A novel approach*, VCI-scholarship holder meeting, Berlin, Germany

**Poster:**

- January 2015: *Azido pentoses, a novel tool to modify the cell wall of Mycobacterium tuberculosis*, Keystone Symposium: Host Response in Tuberculosis, Santa Fe, New Mexico, USA
- September 2014: *"Click"-mediated modification of the cell wall of Mycobacterium tuberculosis with azido pentoses*, 44<sup>rd</sup> Annual Meeting of the German Society for Immunology, Bonn, Germany
- September 2014: *"Click"-mediated labeling of the cell wall of Mycobacterium tuberculosis with azido-modified sugars*, 19. Organic Chemistry (ORCHEM) Conference, Weimar, Germany
- October 2012: *Functional multivalent glycomimetics in the glycosciences*, 2<sup>nd</sup> International SFB 765-Symposium, Berlin, Germany
- September 2012: *Lectins of Mycobacterium tuberculosis - a point of application?*, EMBO Conference, Chemical Biology, Heidelberg, Germany
- July 2012: *Are bacterial lectins important for tuberculosis? Investigation of the carbohydrate-binding specificity of Mycobacterium tuberculosis*, 26<sup>th</sup> International Carbohydrate Symposium, Madrid, Spain



## 7 Danksagung

Mein besonderer Dank gilt meiner Doktormutter Prof. Dr. Thisbe K. Lindhorst, die immer an mich geglaubt hat und mir ermöglichte, meine eigenen Projektideen zu verwirklichen. Durch ihre Unterstützung durfte ich nicht nur in der Organischen Chemie in Kiel, sondern auch in der Mikrobiologie in Borstel forschen. Sie hat mir mit dieser interdisziplinären Arbeit einen großen Wunsch erfüllt.

Die Arbeit wäre aber nicht möglich gewesen ohne die große Unterstützung meines Doktorvaters PD Dr. Norbert Reiling. Er hat mich in seinem Arbeitskreis wie seine eigene Doktorandin aufgenommen. Ich danke ihm für seine Begeisterung an der Forschung, dem großen Interesse an meinem Thema, den vielen hilfreichen Ratschlägen und dem stets offenen Ohr.

Die Ergebnisse wären jedoch auch ohne eine Vielzahl an Kooperationen nie so entstanden. Mein Dank gilt Daniela Sievert für die Messung der zahlreichen Proben mittels RT-PCR, Regina Engel für die zeitaufwendige Isolation der Glykolipide und Lipoglykane aus der Mtb-Zellwand, Dr. Leonhard Möckl für die begeisterte Hilfe bei der metabolischen Markierung der humanen Epithelzellen, Prof. Dr. Niaz Banai für den interessanten Vorschlag Iod-Arabinose für die CyTOF-Analytik zu nutzen, Prof. Dr. Karl-Heinz Wiesmüller und Prof. Dr. Mark S. Baird für die schnelle Bereitstellung der Lipid-Liganden. Ich bedanke mich bei meinen Kooperationspartnern für die immer sehr freundliche Zusammenarbeit und die zahlreichen Ideen.

Ein weiterer besonderer Dank gilt Prof. Dr. Frank Sönnichsen und den Mitarbeitern der Spektroskopischen Abteilung Holger Franzen, Gitta Kohlmeyer-Yilmaz, Marion Höftmann, Dirk Meyer, Silke Rühl und Rolf Schmied für die Unterstützung bei der Analytik der synthetisierten Substanzen.

Zudem danke ich Victoria Sohst, Dr. Julius Brandenburg, Anne Müller, Katrin Seeger, Carolin Golin und Elwira Klima-Bartczak für die Hilfe bei dem einen oder anderen Versuch im Labor und für die zahlreichen Tipps.

Meine Arbeit wurde zudem tatkräftig und mit viel Motivation von meinen Bachelor-, Masterstudentinnen und F-Praktikantinnen Anna Maria Volquardsen, Karolina-Theresa Neumann und Jana Brehmer unterstützt. Es hat mir sehr viel Spaß gemacht mit euch zusammenzuarbeiten. Danke!

Ich bedanke mich auch bei Dr. Christian Herzmann für die Möglichkeit, bei der Entwicklung eines diagnostischen Kaugummis mithelfen zu dürfen. Auch möchte ich mich bei Dr. Doris Hillemann und PD Dr. Sven Müller-Loennies für die vielen Ideen während der „Kaugummi-Besprechungen“ bedanken.

Für die spontane Hilfe, wenn das Durchflusszytometer mal wieder nicht so wollte wie ich, danke ich Dr. Jochen Behrends und für die Unterstützung im S3-Labor Silvia Maaß.

Für die besonders nette Hilfe in allen organisatorischen Dingen danke ich Christine Haug.

Die Fertigstellung der Doktorarbeit wurde gerade in den letzten Monaten tatkräftig von Christina Hopf, Victoria Sohst, Anne Müller und Dr. Femke Beiroth unterstützt. Hierfür möchte ich mich ganz besonders bedanken. Auch für jedes aufmunternde Gespräche bei so mancher Kaffeepause und der einen oder anderen motivierenden Postkarte.

Die letzten vier Jahre wären natürlich niemals so schön gewesen ohne die lieben Kollegen und Freunde im Arbeitskreis Lindhorst. Vielen Dank für die netten Frühstücksrunden, Grillmitage und Kaffeepausen. Ganz besonders danke ich Dr. Vijayanand Chandrasekaran, Oksana Sereda, Anne Müller und meiner Geburtstagspartnerin Elwira Klima-Bartczak.

Eine super schöne Zeit hatte ich auch in Borstel. Dafür danke ich Victoria Sohst, Dr. Julius Brandenburg, Katrin Seeger, Svenja Goldenbaum, Lisa Niwinski, Carolin Golin, Anna Stubbe, Anna C. Geffken, Maïke Burmeister, Dr. Tobias Dallenga und noch vielen mehr. Ich werde euch nie vergessen.

Schließlich und vor allem danke ich meiner Familie für die liebevolle Unterstützung.

Danke!